Journal of Mathematics

Methods in Dynamical Systems and Applications in Engineering

Lead Guest Editor: Fairouz Tchier
Guest Editors: Ioannis Dassios and Lakhdar Ragoub

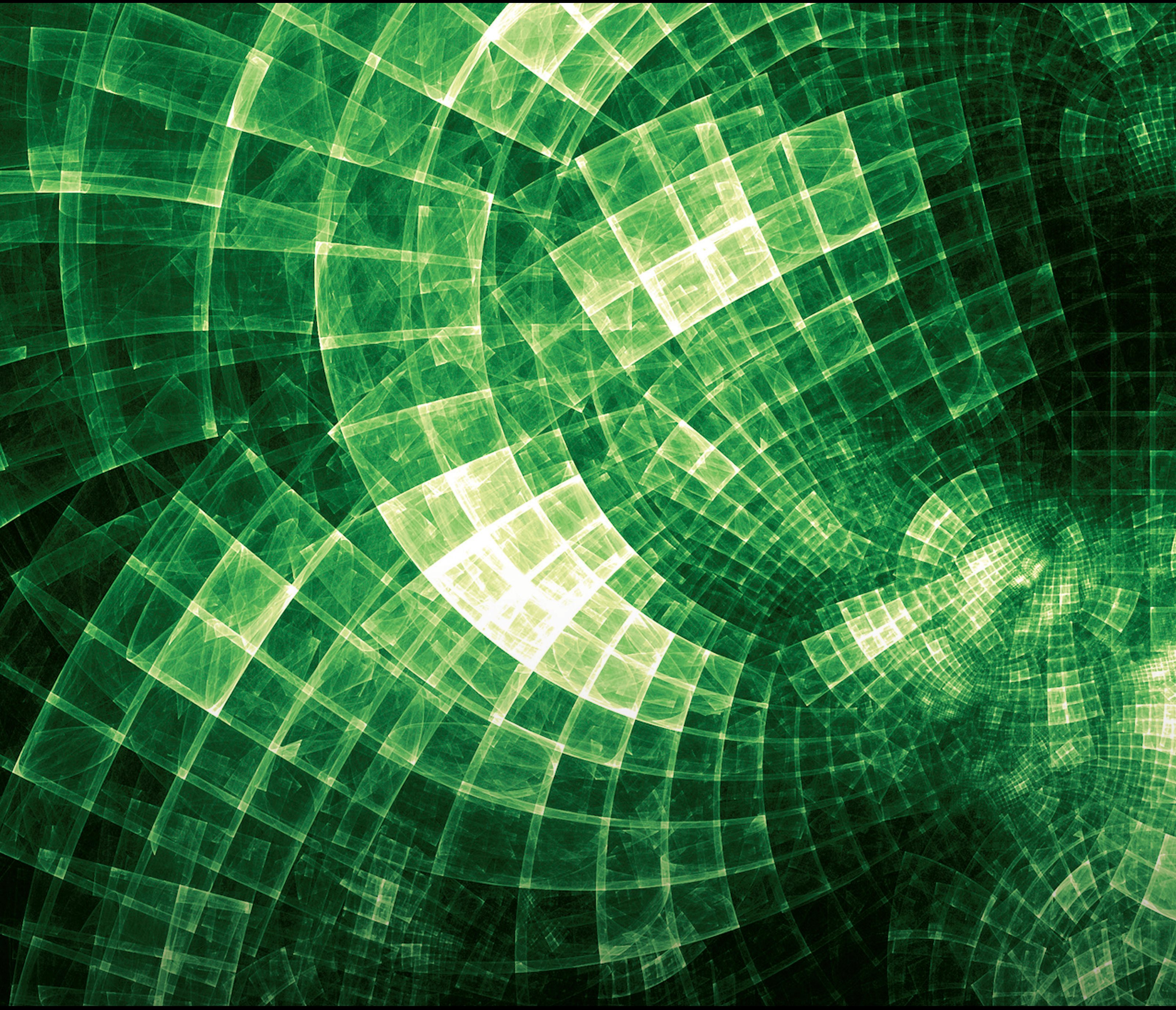

Methods in Dynamical Systems and Applications in Engineering

Journal of Mathematics

Methods in Dynamical Systems and Applications in Engineering

Lead Guest Editor: Fairouz Tchier
Guest Editors: Ioannis Dassios and Lakhdar Ragoub

Contents

Hindawi
Journal of Mathematics
Volume 2022, Article ID 2771854, 11 pages
https://doi.org/10.1155/2022/2771854

Research Article

Time-Scale Integral Inequalities of Copson with Steklov Operator in High Dimension

Wedad Albalawi

Department of Mathematical Sciences, College of Science, Princess Nourah bint Abdulrahman University, P.O. Box 84428, Riyadh 11671, Saudi Arabia

Correspondence should be addressed to Wedad Albalawi; wsalbalawi@pnu.edu.sa

Received 23 December 2021; Accepted 15 February 2022; Published 12 October 2022

Academic Editor: Fairouz Tchier

The paper derives some new time-scale (TS) dynamic inequalities for multiple integrals. The obtained inequalities are special cases of Copson integral using Steklov operator in (TS) version with high dimension. We prove the inequalities with several formulas for the operator and in different cases $m > \mu + 1$ and $m < \mu + 1$ for every $\mu \geq 1$, using time-scales (TSs) setting for integral properties, chain rules, Fubini's theorem, and Hölder's inequality.

1. Introduction

Equations and inequalities are the core of scientific study and have a great influence on a huge number of applications. A large number of physical phenomena and engineering studies have been analyzed and explained through equations and inequalities. For this reason, the study in this field developed rapidly and many types of inequalities and equations appeared. Dynamic inequalities on (TS) are some of the important inequalities that were extended by a lot of researchers and have interesting applications. Furthermore, dynamic inequalities are used to study the behaviour of dynamic equations.

Mathematical analysis has been the most important study in mathematics for the past three decades. Integral inequalities are one of the main studies and the core of mathematical analysis. In the 20th century, a significant part of science was numerical inequalities as the first composition to be released in 1934, through the published study by P'olya et al. [1]. This framework of inequalities played a vital role in the improvement processes and various applications of mathematics.

A large number of essential studies of integral inequalities appeared in the twentieth century, including pure and applied mathematics study. In 1920, Hardy produced the discrete Hardy inequality [2]. This inequality was also proved by himself in [3] (see also [4]), using the variations calculus to obtain the following inequality that is very valuable across both technological sciences and mathematics. If $p > 1$ and $h \geq 0$ in $(0, \infty)$ and

$$H(x) = \int_0^x h(t)\mathrm{d}t < \infty,$$

then

$$\int_0^\infty \left(\frac{H}{x}\right)^p \mathrm{d}x < \Lambda^p \int_0^\infty h^p(x)\mathrm{d}x, \tag{1}$$

where $\Lambda = p(p-1)^{-1}$ is the best possible constant (BPC). Several important assessments and their implementation are done by inequality (1). Furthermore, the inequality is true in case $0 < a < b < \infty$,

$$\int_a^b \left(\frac{H}{x}\right)^p \mathrm{d}x < \Lambda^p \int_a^b h^p(x)\mathrm{d}x, \tag{2}$$

where $0 < \int_0^b h^p(x)\mathrm{d}x < \infty$. The classical inequality of Hardy declares that if $p > 1$ and h is nonnegative and measurable on (a, b), then (2) is valid except $h \equiv 0$ a.e. in (a, b), considering the (BPC).

Integral inequalities (3) and (4) are established in 1928 by Hardy [5].

Let f be a nonnegative measurable function on $(0, \infty)$:

$$(Hh)(x) \leq \begin{cases} \int_0^x h(t)\mathrm{d}t, & \text{for } a < p-1, \\ \int_x^\infty h(t)\mathrm{d}t, & \text{for } a > p-1. \end{cases} \tag{3}$$

Then,

$$\int_0^\infty x^{a-p}(Hh)^p(x)\mathrm{d}x \leq \left(\frac{p}{|p-a-1|}\right)^p \int_0^\infty x^a h^p(x)\mathrm{d}x, \quad \text{for } p > 1. \tag{4}$$

Later, in 1976, Copson studied the integral inequalities ([6], Theorem 1, Theorem 3) as follows.

Let h and v be functions such that they are nonnegative measurable on $(0,\infty)$;

$$V(x) = \int_0^x v(t)\mathrm{d}t,$$

$$(Ch)(x) \leq \begin{cases} \int_0^x h(t)v(t)\mathrm{d}t, & \text{for } c > 1, \\ \int_x^\infty h(t)v(t)\mathrm{d}t, & \text{for } c < 1. \end{cases}$$

Then,

$$\int_0^\infty V^{-c}(x)v(x)(Ch)^p(x)\mathrm{d}x \leq \left(\frac{p}{|c-1|}\right)^p \int_0^\infty V^{p-c}(x)v(x)\mathrm{d}x, \quad \text{for } p \geq 1.$$

Many papers included new extensions and generalizations for the inequalities above in more general settings. For instance, in 1979, some generalizations of Hardy-type inequality were proved by Chan [7]. Then, in 1992, Pachpatte [8] generalized the inequalities that were produced by Chan [7]. In 2005, P. Rehak used (TS) setting to extend Hardy's inequalities [9]. In 2015, Pachpatte's inequalities [8] were extended by Saker and O'Regan [10], with setting of (TSs). Later, some extensions of (TSs) Hardy inequalities were done for functions with high dimensions (see, for example, [11–14]).

In 2021, Albalawi and Khan generalized the main integral of Hardy and Copson inequalities, using the Steklov operator. The operator is defined in the following formulas with considering conditions in two cases (for more details, see [15]).

The aim of this paper is extending the study in [16] that was used for some new Hardy-type inequalities to obtain new special Copson inequalities with the Steklov operator (see [15]) in (TS) versions with high dimension. The results below are proved in two cases $m > \mu + 1$ and $m < \mu + 1$ by considering some general conditions that can be applied for any variable in the integral. To achieve this paper, we use (TSs) settings in integrals properties, chain rules, Hölder's inequality, and Fubini's theorem.

The paper takes the following structure: After introduction, the main concepts of (TSs) are presented in Section 2. Then, in Section 3, we generalized a class of Copson inequalities pertaining the Steklov operator with (TS) in high dimension. Lastly, conclusion of our results is presented.

2. Preliminaries and Lemmas on Time Scales

We state the main concepts of (TSs) that are used in this paper (for more details about (TS) calculus, see [17, 18]).

(TS) calculus in continuous case and discrete analysis was introduced by Hilger [19] in 1988. We denote to a subset (TS) of the real numbers $\mathbb{R}$ by $\mathbb{T}$. Hence, the sets of numbers $\mathbb{R}$, $\mathbb{Z}$, and $\mathbb{N}$ can be considered as (TSs).

Let $\sigma\colon \mathbb{T} \longrightarrow \mathbb{T}$ be a forward jump operator, such that $\sigma(t) \coloneqq \inf\{s \in \mathbb{T}\colon s > t\}$, while $\varsigma\colon \mathbb{T} \longrightarrow \mathbb{T}$ is the backward jump operator, given by $\varsigma(t) = \sup\{s \in \mathbb{T}\colon s < t\}$ for all $t \in \mathbb{T}$.

If $\sigma(t) > t$, then t is right-scattered, and if $\varsigma(t) < t$, t is left-scatted. In the case if points are right-scattered and left-scattered at the same time, then they will be isolated. The point t is right-dense if $t < \sup\mathbb{T}$ and $\sigma(t) = t$, while t is left-dense if $t > \inf\mathbb{T}$ and $\varsigma(t) = t$.

Let $g\colon \mathbb{T} \longrightarrow \mathbb{R}$ be a continuous function and if it satisfied the continuity at all right-dense points in $\mathbb{T}$ and the limits of the left-sided exist (finite) at all left-dense points in $\mathbb{T}$, then g is known rd-continuous. We use $C_r(\mathbb{T},\mathbb{R})$ to denote the space of all rd-continuous.

A function $g\colon \mathbb{T} \longrightarrow \mathbb{R}$ is Δ-differentiable at $t \in \mathbb{T}$, if there is a real number $\beta = g^\Delta(t)$ and for all $\varepsilon > 0$, there exists a neighbor. U of t satisfies

$$|g(\sigma(t)) - g(s) - \beta(\sigma(t) - s)| \leq \varepsilon|\sigma(t) - s|, \quad \text{for all } s \in U.$$

The Δ-derivative of a function g in high order $n \in N$ is given by

$$g^{\Delta^n}(t) = \left(g^{\Delta^{n-1}}(t)\right)^\Delta.$$

If the Δ-derivative of $g^{\Delta^{n-1}}(t)$ exists, the following examples show that the delta derivative for every number set of (TSs).

If $\mathbb{T} = \mathbb{R}$, then

$$g^\Delta(t) = g' = \lim_{\Delta t \longrightarrow 0} \frac{g(t+\Delta t) - g(t)}{\Delta t}, \quad \text{for all } t \in \mathbb{T}.$$

If $\mathbb{T} = \mathbb{N}$, then

$$g^\Delta(t) = g(t+1) - g(t), \quad \text{for all } t \in \mathbb{T}.$$

Let $g\colon \mathbb{T} \longrightarrow \mathbb{R}$; if g is continuous at right-scattered t, then it is delta-derivative of the function g, given by

$$g^\Delta(t) = \frac{g(\sigma(t)) - g(t)}{\sigma(t) - t}.$$

In the case of t is not right-scattered, then the derivative of g is given by

$$g^{\Delta}(t) = \lim_{s\longrightarrow t} \frac{g(\sigma(t)) - g(s)}{t-s}$$
$$= \lim_{s\longrightarrow\infty} \frac{g(t) - g(s)}{t-s}.$$

Here, the limit exists. Note that if $\mathbb{T} = \mathbb{R}$, we have

$$\sigma(t) = t,$$
$$g^{\Delta}(t) = g'(t).$$

If $\mathbb{T} = \mathbb{Z}$, we have

$$\sigma(t) = t+1,$$
$$g^{\Delta}(t) = \Delta g(t),$$
$$\int_a^b g(t)\Delta t = \sum_{t=a}^{b-1} g(t).$$

Lemma 1. *Let $h; g$: $\mathbb{T} \longrightarrow \mathbb{R}$ be delta-differentiable. Then,*

$$\begin{aligned}(hg)^{\Delta} &= h^{\Delta} g + h^{\sigma} h^{\Delta} \\ &= f g^{\Delta} + f^{\Delta} g^{\sigma}, \\ \left(\frac{h}{g}\right)^{\Delta} &= \frac{h^{\Delta} g - h g^{\Delta}}{g g^{\sigma}}.\end{aligned} \tag{5}$$

The Cauchy integral of a delta-differential function of $g(g^{\Delta})$ is defined by

$$\int_a^d g^{\Delta}(t)\Delta t = g(d) - g(a), \quad \text{for } a, d \in \mathbb{T}.$$

The time-scale integration by parts formula is given by

$$\int_a^d h(t) g^{\Delta}(t)\Delta t = h(t)g(t)]_a^d - \int_a^d h^{\Delta}(t) g^{\sigma()}\Delta t, \quad a, d \in \mathbb{T}. \tag{6}$$

The infinite integrals are defined by

$$\int_a^{\infty} g(t)\Delta t = \lim_{d\longrightarrow\infty} \int_a^d g(t)\Delta t.$$

If $\mathbb{T} = \mathbb{R}$, we have

$$\int_a^d g(t)\Delta t = \int_a^d g(t)\mathrm{d}t.$$

If $\mathbb{T} = \mathbb{Z}$, we get

$$\int_a^d g(t)\Delta t = \sum_{t=a}^{d-1} g(t).$$

Lemma 2 (chain rule [16]). *Assume a continuous function, w: $\mathbb{R} \longrightarrow \mathbb{R}$, a delta-differentiable, and w: $\mathbb{T} \longrightarrow \mathbb{R}$, on $\mathbb{T}^c$ and a continuous differentiable h: $\mathbb{R} \longrightarrow \mathbb{R}$. Then, there exists $c \in [t, \sigma(t)]$ with*

$$(h \circ w)^{\Delta}(t) = h'(w(c)) w^{\Delta}(t). \tag{7}$$

Lemma 3 (dynamic Hölder inequality). *Let $a, d \in \mathbb{T}$ and $h, w \in C_{r\,d}([a,d]_T), [0,\infty))$. If $p_1, p_2 > 1$ with $1/p_1 + 1/p_2 = 1$, then*

$$\int_a^d h(t) w(t)\Delta t \leq \left(\int_a^d h^{p_1}(t)\Delta t\right)^{1/p_1} \left(\int_a^d w^{p_2}(t)\Delta t\right)^{1/p_2}. \tag{8}$$

Theorem 4 (Fubini's theorem [20]). *Let $(\Upsilon, N, \mu_{\Delta})$ and $(\Sigma, L, \gamma_{\Delta})$ be (TS) measure spaces with finite dimension. Consider $(\Upsilon \times \Sigma, N \times L, \mu_{\Delta} \times \gamma_{\Delta})$ as the measure space, where $N \times L$ is the $\sigma-$algebra product that is generated by $\{E \times F\colon E \in N, F \in L\}$ and*

$$(\mu_{\Delta} \times \gamma_{\Delta})(E \times F) = \mu_{\Delta}(E)\gamma_{\Delta}(F).$$

Then, Fubini's theorem satisfied.

To be more accurate, if ξ: $\Upsilon \times \Sigma \longrightarrow \mathbb{R}$ is $(\mu_{\Delta} \times \gamma_{\Delta})$—integrable,

$$\Psi(\gamma) = \int_{\Sigma} \xi(\gamma, \Pi)\Delta\Pi, \quad \text{exists for } \Pi \in \Upsilon,$$

and

$$\Psi(\Pi) = \int_{\Upsilon} \xi(\gamma, \Pi)\Delta\gamma, \quad \text{exists for } \gamma \in \Sigma.$$

Then,

$$\int_{\Upsilon} \Delta\gamma \int_{\Sigma} \xi(\gamma, \Pi)\Delta\Pi = \int_{\Sigma} \Delta\Pi \int_{\Upsilon} \xi(\gamma, \Pi)\Delta\gamma.$$

3. Main Results

A new (TS) version of Copson-type inequality with Steklov operator for multiple integrals is obtained in this section. We consider the nonnegative rd-continuous functions w_l, f_l, g_l, and v_l are Δ-integrable and defined integrals. Throughout this paper, we set $K(t_1, \ldots, t_k)$ as the Copson–Steklov-type operator considering the existence of the integral and also finite.

Theorem 5. *Let $\mathbb{T}_l$ be a (TS) and $a \in [0,\infty)_{\mathbb{T}_l}$, for $1 \leq l \leq k$ with $l, k \in \mathbb{N}$. In addition, let w_l, f_l, g_l, and v_l be nonnegative and rd-continuous functions on $[a,\infty)_{\mathbb{T}_l}$. Furthermore, assume there exist $\mu, \lambda \geq 1$ such that*

$$\frac{w_l^{\Delta_l}(t_l)}{w_l^{\sigma}(t_l)} \leq \mu \frac{V_l^{\Delta_l}(t_l)}{V_l(t_l)},$$

and

$$\frac{g_l^{\Delta_l}(t_l)}{g_l^{\sigma}(t_l)} \leq \lambda \frac{F^{\Delta_l}(t_1, \ldots, t_k)}{F(t_1, \ldots, t_k)},$$

where $\Delta_l = \partial/\partial t_l$ *for every* l,

$$V_l(t_l) = \int_a^{t_l} v_l(s_l)\Delta s_l, \quad \text{with } V_l(\infty) = \infty, \text{ and } w_l(a) = 0,$$

and

$$F(t_1,\ldots,t_k) := \int_a^{t_1}\cdots\int_a^{t_k}\prod_{l=1}^{k}\frac{1}{g_l(s_l)}\frac{v_l(s_l)}{V_l(s_l)} f \cdot (s_1,\ldots,s_k)\Delta s_1,\ldots,\Delta s_k.$$

Define the operator

$$K(t_1,\ldots,t_k) = \prod_{l=1}^{k} g_l(t_l)F(t_1,\ldots,t_k), \tag{9}$$

Then

$$\int_a^{\infty}\cdots\int_a^{\infty}\prod_{l=1}^{k} w_l^{\sigma}(t_l)\frac{v_l(t_l)}{V_l^m(t_l)}\left(K^{\sigma}(t_1,\ldots,t_k)\right)^p\Delta t_1,\ldots,\Delta t_k \le \left(\frac{p(\lambda+1)}{m-(\mu+1)}\right)^p\int_a^{\infty}\frac{v_k(t_k)}{V_k^m(t_k)}\frac{w_k^p(t_k)}{(w_k^{\sigma}(t_k))^{p-1}}\left(\frac{g_k^{\sigma}(t_k)}{g_k(t_k)}\right)^p\left(\int_a^{\infty}\cdots\int_a^{\infty}\prod_{l=1}^{k-1} w_l^{\sigma}(t_l)\frac{v_l(t_l)}{V_l^m(t_l)}f^p(t_1,\ldots,t_k)\Delta t_1,\ldots,\Delta t_{k-1}\right)\Delta t_k, \tag{10}$$

where $p \ge 1$ *and* $m > \mu + 1$.

Proof. We write the left side of (10) as follows:

$$\int_a^{\infty}\cdots\int_a^{\infty}\prod_{l=1}^{k-1} w_l^{\sigma}(t_l)\frac{v_l(t_l)}{V_l^m(t_l)}\Gamma_k\Delta t_1,\ldots,\Delta t_{k-1}, \tag{11}$$

where Γ_k is the k-term

$$\Gamma_k = \int_a^{\infty} w_k^{\sigma}(t_k)\frac{v_k(t_k)}{V_k^m(t_k)}\left(K^{\sigma}(t_1,\ldots,t_k)\right)^p\Delta t_k.$$

Using formula (6) for integration by parts to compute Γ_k, we have

$$\Gamma_k = \int_a^{\infty} w_k^{\sigma}(t_k)\frac{v_k(t_k)}{V_k^m(t_k)}\left(K^{\sigma}(t_1,\ldots t_k)\right)^p\Delta t_k = \left[z(t_k)u(t_k)\right]_a^{\infty} - \int_a^{\infty} u(t_k)\left(z(t_k)\right)^{\Delta_k}\Delta t_k, \tag{12}$$

where $u^{\Delta_k}(t_k) = (v_k(t_k)/V_k^m(t_k))$ and then $u(t_k) = (-m+1)V_k^{-m+1}(t_k)$ and $z^{\sigma}(t_k) = w_k^{\sigma}(t_k)(K^{\sigma}(t_1,\ldots,t_k))^p$, implying that $z(t_k) = w_k(t_k)(K(t_1,\ldots,t_k))^p$, and hence,

$$z^{\Delta_k}(t_k)$$

&9; $\cdot\left[g_k^{\Delta_k}(t_k)F(t_1,\ldots,t_k) + g_k^{\sigma}(t_k)F^{\Delta_k}(t_1,\ldots,t_k)\right].$

Assume $\lambda \ge 1$ such that

$$\frac{g_k^{\Delta_k}(t_k)}{g_k^{\sigma}(t_k)} \le \lambda\frac{F^{\Delta_k}(t_1,\ldots,t_k)}{F(t_1,\ldots,t_k)},$$

where $F^{\Delta_k} = (\partial F/\partial t_k)$, and since $c_l \in [t_l, \sigma(t_l)]$, we have

$$z^{\Delta_k}(t_k) \le w_k^{\Delta_k}(t_k)\left(K^{\sigma}(t_1,\ldots,t_k)\right)^p + p(\lambda+1)w_k(t_k) \cdot \left(K^{\sigma}(t_1,\ldots,t_k)\right)^{p-1}g_k^{\sigma}(t_k)F^{\Delta_k}(t_1,\ldots t_k).$$

Substituting the previous quantities in (12) and since $V_l(\infty) = \infty$ and $w_l(a) = 0$, then we have

$$\int_a^{\infty} w_k^{\sigma}(t_k)\frac{v_k(t_k)}{V_k^m(t_k)}\left(K^{\sigma}(t_1,\ldots,t_k)\right)^p\Delta t_k = \frac{1}{m-1}\int_a^{\infty}\frac{1}{V_k^{m-1}(t_k)}w_k^{\Delta_k}(t_k)\left(K^{\sigma}(t_1,\ldots,t_k)\right)^p\Delta t_k + \frac{p(\lambda+1)}{m-1}\int_a^{\infty}\frac{1}{V_k^{m-1}(t_k)}w_k(t_k)\left(K^{\sigma}(t_1,\ldots,t_k)\right)^{p-1}g_k^{\sigma}(t_k)F^{\Delta_k}(t_1,\ldots,t_k)\Big)\Delta t_k.$$

Assume $\mu \ge 1$ such that

$$\frac{w_l^{\Delta_l}(t_l)}{w_l^{\sigma}(t_l)} \le \mu \frac{V_l^{\Delta_l}(t_l)}{V_l(t_l)}.$$

Then, we obtain

$$\int_a^\infty w_k^\sigma(t_k)\frac{v_k(t_k)}{V_k^m(t_k)}(K^\sigma(t_1,\ldots,t_k))^p\Delta t_k = \frac{\mu}{m-1}\int_a^\infty w_k^\sigma(t_k)\frac{v_k(t_k)}{V_k^m(t_k)}(K^\sigma(t_1,\ldots,t_k))^p\Delta t_k$$
$$+\frac{p(\lambda+1)}{m-1}\int_a^\infty \frac{1}{V_k^{m-1}(t_k)} w_k(t_k)(K^\sigma(t_1,\ldots,t_k))^{p-1} g_k^\sigma(t_k)F^{\Delta_k}(t_1,\ldots,t_k)\big)\Delta t_k.$$

Since $F^{\Delta_k}(t_1,\ldots,t_k) = (f(t_1,\ldots,t_k)/g_k(t_k))\ (v_k(t_k)/V_k(t_k))$, then we have

$$\int_a^\infty w_k^\sigma(t_k)\frac{v_k(t_k)}{V_k^m(t_k)}(K^\sigma(t_1,\ldots,t_k))^p\Delta t_k \le \frac{p(\lambda+1)}{m-1-\mu}\int_a^\infty \frac{v_k(t_k)}{V_k^m(t_k)} w_k(t_k)(K^\sigma(t_1,\ldots,t_k))^{p-1} g_k^\sigma(t_k)\frac{f(t_1,\ldots,t_k)}{g_k(t_k)}\Delta t_k.$$

Then, Hölder's inequality (8) with indices p and $p/(p-1)$ can be applied:

$$\Gamma_k = \int_a^\infty w_k^\sigma(t_k)\frac{v_k(t_k)}{V_k^m(t_k)}(K^\sigma(t_1,\ldots,t_k))^p\Delta t_k \le \left(\frac{p(\lambda+1)}{m-1-\mu}\right)^p \int_a^\infty \frac{v_k(t_k)}{V_k^m(t_k)}\frac{w_k^p(t_k)}{(w_k^\sigma(t_k))^{p-1}} f^p(t_1,\ldots,t_k)\left(\frac{g_k^\sigma(t_k)}{g_k(t_k)}\right)^p\Delta t_k. \quad (13)$$

Substituting Γ_k in (11) and applying Fubini's Theorem 4, then we obtain the inequality

$$\int_a^\infty\cdots\int_a^\infty \prod_{l=1}^k w_l^\sigma(t_l)\frac{v_l(t_l)}{V_l^m(t_l)}(K^\sigma(t_1,\ldots t_k))^p\Delta t_1\ldots\Delta t_k$$
$$\le\left(\frac{p(\lambda+1)}{m-(\mu+1)}\right)^p\int_a^\infty \frac{v_k(t_k)}{V_k^m(t_k)}\frac{w_k^p(t_k)}{(w_k^\sigma(t_k))^{p-1}}\left(\frac{g_k^\sigma(t_k)}{g_k(t_k)}\right)^p\left(\int_a^\infty\cdots\int_a^\infty\prod_{l=1}^{k-1} w_l^\sigma(t_l)\frac{v_l(t_l)}{V_l^m(t_l)} f^p(t_1,\ldots,t_k)\Delta t_1\ldots\Delta t_{k-1}\right)\Delta t_k.$$

□

Corollary 6. *If $l=1$ in Theorem 5, inequality (10) becomes*

$$\int_a^\infty w^\sigma(t)\frac{v(t)}{V^m(t)}(K^\sigma(t))^p\Delta t \le \left(\frac{p(\lambda+1)}{m-(\mu+1)}\right)^p\int_a^\infty \frac{v(t)}{V^m(t)}\frac{w^p(t)}{(w^\sigma(t))^{p-1}}\left(\frac{g^\sigma(t)}{g(t)}\right)^p f^p(t)\Delta t. \quad (14)$$

Corollary 7. *If $\mathbb{T}=\mathbb{R}$ in Corollary 6, we obtain*

$$\int_a^\infty w(t)\frac{v(t)}{V^m(t)}K^p(t)\mathrm{d}t \le \left(\frac{p(\lambda+1)}{m-(\mu+1)}\right)^p \int_a^\infty \frac{v(t)}{V^m(t)} w(t) f^p(t)\mathrm{d}t. \tag{15}$$

Remark 8. Assume $\mu = 0$ and $\beta > \lambda$ in Corollary 7; then, we have Corollary 3 in [15]

$$\begin{aligned}&\int_a^\infty w(t)\frac{v(t)}{V^m(t)}K^p(t)\mathrm{d}t\\ &\le \left(\frac{\beta p}{m-1}\right)^p \int_a^\infty w(t)\frac{v(t)}{V^m(t)} f^p(t)\mathrm{d}t.\end{aligned} \tag{16}$$

Theorem 9. *Let $\mathbb{T}_l$ be (TS) and $a \in [0,\infty)_{\mathbb{T}_l}$, for $1 \le l \le k$ with $l,k \in \mathbb{N}$. In addition, let w_l, f_l, g_l, and v_l be nonnegative and rd-continuous functions on $[a,\infty)_{\mathbb{T}_l}$. Furthermore, assume there exist $\lambda, \mu \ge 1$ such that*

$$\frac{w_l^{\Delta_l}(t_l)}{w_l^\sigma(t_l)} \ge \mu \frac{V_l^{\Delta_l}(t_l)}{V_l(t_l)},$$

and

$$\frac{g_l^{\Delta_l}(t_l)}{g_l^\sigma(t_l)} \ge \lambda \frac{F^{\Delta_l}(t_1,\ldots,t_k)}{F(t_1,\ldots,t_k)},$$

where $F^{\Delta_l} = (\partial F/\partial t_l)$; for every l,

$$V_l(t_l) = \int_a^{t_l} v_l(s_l)\Delta s_l, \quad \text{with } V_l(\infty) = \infty, \text{ and } w_l(a) = 0,$$

and

$$F(t_1,\ldots,t_k) := \int_{t_1}^\infty \cdots \int_{t_k}^\infty \prod_{l=1}^k \frac{1}{g_l(s_l)} \frac{v_l(s_l)}{V_l(s_l)} f(s_1,\ldots s_k)\Delta s_1 \ldots \Delta s_k.$$

Define the operator

$$K(t_1,\ldots,t_k) = \prod_{l=1}^k g_l(t_l) F(t_1,\ldots,t_k).$$

Then,

$$\begin{aligned}&\int_a^\infty \cdots \int_a^\infty \prod_{l=1}^k w_l^\sigma(t_l)\frac{v_l(t_l)}{V_l^m(t_l)}\left(K^\sigma(t_1,\ldots t_k)\right)^p \Delta t_1 \ldots \Delta t_k\\ &\le \left(\frac{p(\lambda+1)}{\mu+1-m}\right)^p \int_a^\infty \frac{v_k(t_k)}{V_k^m(t_k)} \frac{w_k^p(t_k)}{(w_k^\sigma(t_k))^{p-1}}\left(\frac{g_k^\sigma(t_k)}{g_k(t_k)}\right)^p \left(\int_a^\infty \cdots \int_a^\infty \prod_{l=1}^{k-1} w_l^\sigma(t_l)\frac{v_l(t_l)}{V_l^m(t_l)} f^p(t_1,\ldots,t_k)\Delta t_1 \ldots \Delta t_{k-1}\right)\Delta t_k,\end{aligned} \tag{17}$$

%

where $p \ge 1$ and $0 \le m < \mu+1$.

Proof. We write the left side of (17) as follows:

$$\int_a^\infty \cdots \int_a^\infty \prod_{l=1}^{k-1} w_l^\sigma(t_l)\frac{v_l(t_l)}{V_l^m(t_l)}\Gamma_k \Delta t_1 \ldots \Delta t_{k-1}. \tag{18}$$

Use formula (6) to calculate the following k–term:

$$\begin{aligned}\Gamma_k &= \int_a^\infty w_k^\sigma(t_k)\frac{v_k(t_k)}{V_k^m(t_k)}\left(K^\sigma(t_1,\ldots,t_k)\right)^p \Delta t_k\\ &= \left[u(t_k) z(t_k)\right]_a^\infty + \int_a^\infty (u(t_k))(-z(t_k))^{\Delta_k}\Delta t_k,\end{aligned} \tag{19}$$

where $u^{\Delta_k}(t_k) = w_k^\sigma(t_k)(v_k(t_k)/(V_k(t_k))^m)$ and $z^\sigma(t_k) = (K^\sigma(t_1,\ldots,t_k))^p$.

Using (7) and the product rule (5), there exists $c_k \in [s_k, \sigma(s_k)]$ such that

$$\begin{aligned}\left(w_k(s_k)V_k^{1-m}(s_k)\right)^{\Delta_k} &= w_k^{\Delta_k}(s_k)V_k^{1-m}(s_k)\\ &+ w_k^\sigma(1-m)(V_k^{-m}(c_k))V_k^{\Delta_k}(s_k).\end{aligned}$$

Assume $\mu \ge 1$ such that

$$\frac{w_k^{\Delta_k}(t_k)}{w_k^\sigma(t_k)} \ge \mu \frac{V_k^{\Delta_k}(t_k)}{V_k(t_k)}.$$

Since $V_k^{\Delta_k}(s_k) = v_k(s_k) \ge 0$, $s_k \le c_k \le \sigma(s_k)$, and $0 \le m < 1$, then

$$w_k^{\sigma}V_k^{-m}(s_k)v_k(s_k) \leq \frac{1}{1-m+\mu}\left(w_k(s_k)V_k^{1-m}(s_k)\right)^{\Delta_k}. \quad (20)$$

By integration, we have

$$u(t_k) \leq \frac{1}{1-m+\mu}\int_a^{\infty}\left(w_k(s_k)V_k^{1-m}(s_k)\right)^{\Delta_k}\Delta s_k.$$

Now, we calculate $(-K^p(t_1,\ldots,t_k))^{\Delta_k}$ and we obtain

$$(K^p(t_1,\ldots,t_k))^{\Delta_k} \cdot \left[g_k^{\Delta_k}(t_k)F(t_1,\ldots t_k) + g_k^{\sigma}(t_k)F^{\Delta_k}(t_1,\ldots,t_k)\right].$$

Assume $\lambda \geq 1$ such that

$$\frac{g_k^{\Delta_k}(t_k)}{g_k^{\sigma}(t_k)} \geq \lambda\frac{F^{\Delta_k}(t_1,\ldots,t_k)}{F(t_1,\ldots,t_k)},$$

where

$$F(t_1,\ldots,t_k) := g_k(t_k)\int_{t_k}^{\infty}\frac{1}{g_k(s_k)}\frac{v_k(s_k)}{V_k(s_k)}f(s_1,\ldots,s_k)\Delta s_k, \quad (21)$$

and since $V_k(\infty) = \infty$ and $c_k \geq s_k$, then we have

$$(K^p(t_1,\ldots,t_k))^{\Delta_k} \geq pK^{p-1}(t_1,\ldots,t_k)(\lambda+1)g_k^{\sigma}(t_k)F^{\Delta_k}(t_1,\ldots,t_k)$$
$$\geq p(\lambda+1)K^{p-1}(t_1,\ldots,t_k)\left(-\frac{g_k^{\sigma}(t_k)}{g_k(t_k)}\frac{v_k(t_k)}{V_k(t_k)}f(t_1,\ldots,t_k)\right).$$

Then,

$$(-K^p(t_1,\ldots,t_k))^{\Delta_k} \leq p(\lambda+1)K^{p-1}(t_1,\ldots,t_k)\frac{g_k^{\sigma}(t_k)}{g_k(t_k)}\frac{v_k(t_k)}{V_k(t_k)}f(t_1,\ldots,t_k).$$

Hence, we have

$$\int_a^{\infty}w_k^{\sigma}(t_k)\frac{v_k(t_k)}{V_k^m(t_k)}(K^{\sigma}(t_1,\ldots,t_k))^p\Delta t \leq \frac{p(\lambda+1)}{\mu+1-m}\int_a^{\infty}w_k(t_k)\frac{v_k(t_k)}{V_k^m(t_k)}f(t_1,\ldots,t_k)\frac{g_k^{\sigma}(t_k)}{g_k(t_k)}(K^{\sigma}(t_1,\ldots,t_k))^{p-1}\Delta t_k.$$

Using Hölder's inequality, where $p_1 = p$ and $p_2 = (p/(p-1))$, we obtain

$$\int_a^{\infty}w_k^{\sigma}(t_k)\frac{v_k(t_k)}{V_k^m(t_k)}(K^{\sigma}(t_1,\ldots,t_k))^p\Delta t_k \leq \left(\frac{p(\lambda+1)}{\mu+1-m}\right)^p\int_a^{\infty}\frac{v_k(t_k)}{V_k^m(t_k)}\frac{w_k^p(t_k)}{(w_k^{\sigma}(t_k))^{p-1}}f^p(t_1,\ldots,t_k)\left(\frac{g_k^{\sigma}(t_k)}{g_k(t_k)}\right)^p\Delta t_k. \quad (22)$$

Substituting (22) in (17), we have

$$\int_a^\infty \cdots \int_a^\infty \prod_{l=1}^{k} w_l^\sigma(t_l) \frac{v_l(t_l)}{V_l^m(t_l)} (K^\sigma(t_1, \dots t_k))^p \Delta t_1 \dots \Delta t_k$$
$$\leq \left(\frac{p(\lambda+1)}{\mu+1-m}\right)^p \int_a^\infty \frac{v_k(t_k)}{V_k^m(t_k)} \frac{w_k^p(t_k)}{(w_k^\sigma(t_k))^{p-1}} \left(\frac{g_k^\sigma(t_k)}{g_k(t_k)}\right)^p \left(\int_a^\infty \cdots \int_a^\infty \prod_{l=1}^{k-1} w_l^\sigma(t_l) \frac{v_l(t_l)}{V_l^m(t_l)} f^p(t_1, \dots, t_k) \Delta t_1 \dots \Delta t_{k-1}\right) \Delta t_k.$$

□

Corollary 10. *If $l = 1$ and $\mathbb{T} = \mathbb{R}$ in Theorem 9, we get*

$$\int_a^\infty w(t) \frac{v(t)}{V^m(t)} K^p(t) \mathrm{d}t \leq \left(\frac{p(\lambda+1)}{\mu+1-m}\right)^p \int_a^\infty \frac{v(t)}{V^m(t)} w(t) f^p(t) \mathrm{d}t, \tag{23}$$

where

$$K(t) = g(t) \int_t^\infty \frac{1}{g(s)} \frac{v(s)}{V(s)} f(s) \mathrm{d}s.$$

Remark 11. Assume $\mu = 0$ and $\theta > \lambda$ in Corollary 10; we have Corollary 5 in [15].

Theorem 12. *Let $\mathbb{T}_l$ be (TS) and $a \in [0, \infty)_{\mathbb{T}_l}$, for $1 \leq l \leq k$ with $l, k \in \mathbb{N}$. In addition, let w_l, f_l, g_l, and v_l be nonnegative rd-continuous functions on $[a, \infty)_{\mathbb{T}_l}$. Furthermore, assume there exist $\lambda, \mu \geq 1$ such that*

$$\frac{w_l^{\Delta_l}(t_l)}{w_l^\sigma(t_l)} \geq \mu \frac{V_l^{\Delta_l}(t_l)}{V_l(t_l)},$$

and

$$\frac{g_l^{\Delta_l}(t)}{g_l^\sigma(t)} \geq \lambda \frac{F^{\Delta_l}(t_1, \dots, t_k)}{F(t_1, \dots, t_k)},$$

where for every l,

$$V_l(t_l) = \int_a^{t_l} v_l(s_l) \Delta s_l, \quad \text{with } V_l(\infty) = \infty, \text{ and } w_l(a) = 0,$$

and

$$F(t_1, \dots, t_k) := \int_{t_1}^\infty \cdots \int_{t_k}^\infty \prod_{l=1}^{k} g_l(s_l) \frac{v_l(s_l)}{V_l(s_l)} f(s_1, \dots s_k) \Delta s_1 \dots \Delta s_k.$$

Define the operator

$$K(t_1, \dots, t_k) := \prod_{l=1}^{k} \frac{1}{g_l(t_l)} F(t_1, \dots, t_k).$$

Then,

$$\int_a^\infty \cdots \int_a^\infty \prod_{l=1}^{k} w_l^\sigma(t_l) \frac{v_l(t_l)}{V_l^m(t_l)} (K^\sigma(t_1, \dots t_k))^p \Delta t_1 \dots \Delta t_k$$
$$\leq \left(\frac{p(\lambda-1)}{\mu+1-m}\right)^p \int_a^\infty \frac{v_k(t_k)}{V_k^m(t_k)} \frac{w_k^p(t_k)}{(w_k^\sigma(t_k))^{p-1}} \left(\frac{g_k(t_k)}{g_k^\sigma(t_k)}\right)^p \left(\int_a^\infty \cdots \int_a^\infty \prod_{l=1}^{k-1} w_l^\sigma(t_l) \frac{v_l(t_l)}{V_l^m(t_l)} f^p(t_1, \dots, t_k) \Delta t_1, \dots, \Delta t_{k-1}\right) \Delta t_k, \tag{24}$$

where $p \geq 1$ and $0 \leq m < \mu + 1$.

Proof. We write the left side of (24) as follows:

$$\int_a^\infty \cdots \int_a^\infty \prod_{l=1}^{k-1} w_l^\sigma(t_l) \frac{v_l(t_l)}{V_l^m(t_l)} \Gamma_k \Delta t_1 \dots \Delta t_{k-1}. \tag{25}$$

Apply (6) to calculate the following k−term:

$$\Gamma_k = \int_a^\infty w_k^\sigma(t_k) \frac{v_k(t_k)}{V_k^m(t_k)} (K^\sigma(t_1, \dots, t_k))^p \Delta t_k = [u(t_k) z(t_k)]_a^\infty + \int_a^\infty (u(t_k)) \left(-(z(t_k))^{\Delta_k} \Delta t_k, \right. \tag{26}$$

where $u^{\Delta_k}(t_k) = w_k^\sigma(t_k)(v_k(t_k)/V_k^m(t_k))$. Using the chain rule on (TS) (7) and product rule (5), there exist $c_k \in [s_k, \sigma(s_k)]$ such that

$$\left(w_k(s_k)V_k^{1-m}(s_k)\right)^{\Delta_k}$$
$$+(1-m)w^{\sigma}(s_k)V_k^{-m}(c_k)V_k^{\Delta_k}(s_k).$$

Assume $\mu \geq 1$ such that

$$\frac{w_k^{\Delta_k}(t_k)}{w_k^{\sigma}(t_k)} \geq \mu \frac{V_k^{\Delta_k}(t_k)}{V_k(t_k)}.$$

Since $V_k^{\Delta_k}(s_k) = v_k(s_k) \geq 0$, $s_k \leq c_k \leq \sigma(s_k)$, and $0 \leq m < \mu + 1$, then

$$\left(w_k(s_k)V_k^{1-m}(s_k)\right)^{\Delta_k} \geq (1-m+\mu)w_k^{\sigma}V_k^{-m}(s_k)v_k(s_k),$$

implying

$$u(t_k)$$
$$\leq \frac{1}{1-m+\mu}\int_a^{t_k}\left(w_k(s_k)V_k^{1-m}(s_k)\right)^{\Delta_k}\Delta s_k$$
$$\leq \frac{1}{1-m+\mu}w_k(t_k)V_k^{1-m}(t_k).$$

We calculate $(-(K^p(t_1,\ldots,t_k))^{\Delta_k}$, and we obtain

$$\left(K^p(t_1,\ldots,t_k)\right)^{\Delta_k} = pK^{p-1}(t_1,\ldots,c_k)\left[\frac{-g_k^{\Delta}}{g_k^{\sigma}(t_k)g(t_k)}F(t_1,\ldots,t_k) + \frac{1}{g_k^{\sigma}(t_k)}F^{\Delta_k}(t_1,\ldots,t_k)\right].$$

Assume $\lambda \geq 1$ such that

$$\frac{g_k^{\Delta_{t_k}}(t_k)}{g_k(t_k)} \geq \lambda \frac{F^{\Delta_k}(t_1,\ldots,t_k)}{F(t_1,\ldots,t_k)},$$

where

$$F(t_1,\ldots,t_k) := \frac{1}{g_k(t_k)}\int_a^{t_k} g_k(s_k)\frac{v_k(s_k)}{V_k(s_k)}f(s_1,\ldots,s_k)\Delta s_k, \tag{27}$$

and since $c_k \geq t_k$, then we have

$$\begin{aligned}\left(K^p(t_1,\ldots,t_k)\right)^{\Delta_k} &\geq pK^{p-1}(t_1,\ldots,t_k)(1-\lambda)\frac{1}{g_k^{\sigma}(t_k)}F^{\Delta_k}(t_1,\ldots,t_k)\\ &\geq p(\lambda-1)K^{p-1}(t_1,\ldots,t_k)\frac{1}{g_k^{\sigma}(t_k)}g_k(t_k)\frac{v_k(t_k)}{V_k(t_k)}f(t_1,\ldots,t_k).\end{aligned}$$

Since $V(\infty) = \infty$, then

$$\begin{aligned}\left(-K^p(t_1,\ldots,t_k)\right)^{\Delta_k} &\leq -p(\lambda-1)K^{p-1}(t_1,\ldots,t_k)\frac{g_k(t_k)}{g_k^{\sigma}(t_k)}\frac{v_k(t_k)}{V_k(t_k)}f(t_1,\ldots,t_k)\\ &\leq p(\lambda-1)K^{\sigma(p-1)}(t_1,\ldots,t_k)\frac{g_k(t_k)}{g_k^{\sigma}(t_k)}\frac{v_k(t_k)}{V_k(t_k)}f(t_1,\ldots,t_k).\end{aligned}$$

Hence, we have

$$\int_a^\infty w_k^\sigma(t_k)\frac{v_k(t_k)}{V_k^m(t_k)}(K^\sigma(t_1,\ldots,t_k))^p\Delta t_k$$

$$\leq [u(\infty)z(\infty)-u(a)z(a)]+\frac{p(\lambda-1)}{\mu+1-m}\int_a^\infty w_k(t_k)\frac{v_k(t_k)}{V_k^m(t_k)}f(t_1,\ldots,t_k)\frac{g_k(t_k)}{g_k^\sigma(t_k)}(K^\sigma(t_1,\ldots,t_k))^{p-1}\Delta t_k$$

$$\leq\frac{p(\lambda-1)}{\mu+1-m}\int_a^\infty w_k(t_k)\frac{v_k(t_k)}{V_k^m(t_k)}f(t_1,\ldots,t_k)\frac{g_k(t_k)}{g_k^\sigma(t_k)}(K_k^\sigma(t_1,\ldots,t_k))^{p-1}\Delta t_k.$$

Then, Hölder's inequality (8) can be applied with indices p and $p/(p-1)$:

$$\int_a^\infty w_k^\sigma(t_k)\frac{v_k(t_k)}{V_k^m(t_k)}(K^\sigma(t_1,\ldots,t_k))^p\Delta t_k\leq\left(\frac{p(\lambda-1)}{\mu+1-m}\right)^p\int_a^\infty\frac{v_k(t_k)}{V_k^m(t_k)}\frac{w_k^p(t_k)}{(w_k^\sigma)^{p-1}}f^p(t_1,\ldots,t_k)\left(\frac{g_k(t_k)}{g_k^\sigma(t_k)}\right)^p\Delta t_k. \tag{28}$$

Substituting (28) in (26), we have

$$\int_a^\infty\cdots\int_a^\infty\prod_{l=1}^k w_l^\sigma(t_l)\frac{v_l(t_l)}{V_l^m(t_l)}(K^\sigma(t_1,\ldots t_k))^p\Delta t_1\ldots\Delta t_k$$

$$\leq\left(\frac{p(\lambda-1)}{\mu+1-m}\right)^p\int_a^\infty\frac{v_k(t_k)}{V_k^m(t_k)}\frac{w_k^p(t_k)}{(w_k^\sigma(t_k))^{p-1}}\left(\frac{g_k(t_k)}{g_k^\sigma(t_k)}\right)^p\left(\int_a^\infty\cdots\int_a^\infty\prod_{l=1}^{k-1}w_l^\sigma(t_l)\frac{v_l(t_l)}{V_l^m(t_l)}f^p(t_1,\ldots,t_k)\Delta t_1\ldots\Delta t_{k-1}\right)\Delta t_k.$$

□

Corollary 13. *If $l=1$ and $\mathbb{T}=\mathbb{R}$ in Theorem 12, we obtain*

$$\int_a^\infty w(t)\frac{v(t)}{V^m(t)}K^p(t)dt\leq\left(\frac{p(\lambda-1)}{\mu+1-m}\right)^p\int_a^\infty\frac{v(t)}{V^m(t)}w(t)f^p(t)dt, \tag{29}$$

where

$$K(t)=\frac{1}{g(s)}\int_a^t g(t)\frac{v(s)}{V(s)}f(s)ds.$$

Example 14. Choose $\mu=m,\lambda=2$, and $p=1$ in Theorem 12. Hence, we get

$$\int_a^\infty\cdots\int_a^\infty\prod_{l=1}^k w_l^\sigma(t_l)\frac{v_l(t_l)}{V_l^m(t_l)}K^\sigma(t_1,\ldots t_k)\Delta t_1\ldots\Delta t_k$$
$$\leq\int_a^\infty\frac{v_k(t_k)}{V_k^m(t_k)}\frac{g_k(t_k)}{g_k^\sigma(t_k)}w_k(t_k)\left(\int_a^\infty\cdots\int_a^\infty\prod_{l=1}^{k-1}w_l^\sigma(t_l)\frac{v_l(t_l)}{V_l^m(t_l)}f(t_1,\ldots,t_k)\Delta t_1\ldots\Delta t_{k-1}\right)\Delta t_k. \tag{30}$$

4. Conclusions

(TSs) calculus is used in this paper to prove special cases of (TS) Copson–Steklov-type inequalities with several variables. The obtained inequalities would be interesting to apply in different fields of mathematics (functional spaces, partial differential equations, mathematical modeling). Furthermore, the inequalities can be discussed in calculus, discrete calculus, and quantum calculus. As a perspective, we propose to study these results for other kinds of operators and solve the singularity that appeared in Theorem 12 with case $m > \mu + 1$.

Data Availability

All data that support the findings of this study are included within the article.

Conflicts of Interest

The author declares no conflicts of interest.

Acknowledgments

This work was supported by Princess Nourah bint Abdulrahman University Researchers Supporting Project number (PNURSP2022R157), Princess Nourah bint Abdulrahman University, Riyadh, Saudi Arabia.

References

[1] G. Hardy, J. Littlewood, and G. Plya, *Inequalities*, Cambridge University Press, Cambridge, UK, 1934.

[2] G. H. Hardy, “Note on a theorem of hilbert,” *Mathematische Zeitschrift*, vol. 6, no. 3-4, pp. 314–317, 1920.

[3] G. H. Hardy, “Notes on some points in the integral calculus (LX). an inequality between integrals,” *Messenger Math*, vol. 54, pp. 150–156, 1925.

[4] G. H. Hardy and J. E. Littlewood, “Notes on the theory of series (XII): on certain inequalities connected with the calculus of variations,” *Journal of the London Mathematical Society*, vol. s1-5, pp. 283–290, 1930.

[5] G. H. Hardy, “Notes on some points in the integral calculus,” *Messenger Math*, vol. 57, pp. 12–16, 1928.

[6] E. T. Copson, “13.-Some integral inequalities,” *Proceedings of the Royal Society of Edinburgh: Section A Mathematics*, vol. 75, no. 2, pp. 157–164, 1976.

[7] L.-Y. Chan, “Some extensions of hardy’s inequality,” *Canadian Mathematical Bulletin*, vol. 22, no. 2, pp. 165–169, 1979.

[8] B. G. Pachpatte, “A note on certain inequalities related to Hardy’s inequality,” *Indian Journal of Pure and Applied Mathematics*, vol. 23, pp. 773–776, 1992.

[9] P. Rehak, “Hardy inequality on time scales and its application to half-linear dynamic equations,” *Journal of Inequalities and Applications*, vol. 2005, Article ID 942973, 507 pages, 2005.

[10] S. H. Saker and D. O’Regan, “Extensions of dynamic inequalities of hardy’s type on time scales,” *Mathematica Slovaca*, vol. 65, no. 5, pp. 993–1012, 2015.

[11] M. S. Ashraf, K. A. Khan, and A. Nosheen, “Hardy-copson type inequalities on time scales for the functions of *n* independent variables,” *International Journal of Analysis and Applications*, vol. 17, pp. 244–259, 2019.

[12] W. Ahmad, K. A. Khan, A. Nosheen, and M. A. Sultan, “CopsonLeindler type inequalities for function of several variables on time scales,” *Punjab University Journal of Mathematics*, vol. 51, pp. 157–168, 2019.

[13] T. Donchev, A. Nosheen, and J. Pečarić, “Hardy-type inequalities on time scale via convexity in several variables,” *International Scholarly Research Notices*, vol. 2013, Article ID 903196, 9 pages, 2013.

[14] A. Nosheen, A. Nawaz, K. A. Khan, and K. M. Awan, “Multivariate Hardy and Littlewood inequalities on time scales,” *Arab Journal of Mathematical Sciences*, vol. 26, no. 1/2, pp. 245–263, 2019.

[15] W. Albalawi and Z. A. Khan, “Synchronization analysis of multiple integral inequalities driven by steklov operator,” *Fractal Fractional*, vol. 5, p. 97, 2021.

[16] A. A. El-Deeb, H. A. Elsennary, and D. Baleanu, “Some new Hardy-type inequalities on time scales,” *Advances in Difference Equations*, vol. 2020, pp. 1–21, 2020.

[17] M. Bohner and A. Peterson, *Dynamic Equations on Time Scales: An Introduction with Applications*, Springer Science and Business Media, Berlin, Germany, 2001.

[18] M. Bohner and A. Peterson, *Advanced in Dynamic Equations on Time Scales*, Birkhuser Boston. Inc., Boston, MA, USA, 2003.

[19] S. Hilger, *Ein Makettenkalkl mit Anwendung auf Zentrumsmannigfaltigkeiten*, Wurzburg Universtat, Würzburg, Germany, 1988.

[20] M. J. Bohner, A. Nosheen, J. Pečarić, and A. Younus, “Some dynamic Hardy-type inequalities with general kernel,” *Journal of Mathematical Inequalities*, vol. 8, no. 1, pp. 185–199, 2014.

Hindawi
Journal of Mathematics
Volume 2022, Article ID 5454685, 13 pages
https://doi.org/10.1155/2022/5454685

Research Article

Novel Analytical and Numerical Approximations to the Forced Damped Parametric Driven Pendulum Oscillator: Chebyshev Collocation Method

M.R. Alharthi,[1] Alvaro H. Salas ,[2] Wedad Albalawi,[3] and S.A. El-Tantawy [4,5]

[1]*Department of Mathematics and Statistics, College of Science, Taif University, P.O.Box 11099, Taif 21944, Saudi Arabia*
[2]*Department of Mathematics and Statistics, Universidad Nacional de Colombia, FIZMAKO Research Group, Bogota, Colombia*
[3]*Department of Mathematical Sciences, College of Science, Princess Nourah bint Abdulrahman University, P.O. Box 84428, Riyadh 11671, Saudi Arabia*
[4]*Department of Physics, Faculty of Science, Port Said University, Port Said 42521, Egypt*
[5]*Research Center for Physics (RCP), Department of Physics, Faculty of Science and Arts, Al-Mikhwah, Al-Baha University, Al-Bahah, Saudi Arabia*

Correspondence should be addressed to S.A. El-Tantawy; tantawy@sci.psu.edu.eg

Received 20 December 2021; Revised 16 February 2022; Accepted 24 February 2022; Published 22 June 2022

Academic Editor: Fairouz Tchier

In this work, some novel approximate analytical and numerical solutions to the forced damped driven nonlinear (FDDN) pendulum equation and some relation equations of motion on the pivot vertically for arbitrary angles are obtained. The analytical approximation is derived in terms of the Jacobi elliptic functions with arbitrary elliptic modulus. For the numerical approximations, the Chebyshev collocation numerical method is introduced for analyzing the equation of motion. Moreover, the analytical approximation and numerical approximation using the Chebyshev collocation numerical method and the MATHEMATICA command Fit are compared with the Runge–Kutta (RK) numerical solution. Also, the maximum distance error to all obtained approximations is estimated with respect to the RK numerical solution. The obtained results help many authors to understand the mechanism of many phenomena related to the plasma physics, classical mechanics, quantum mechanics, optical fiber, and electronic circuits.

1. Introduction

The pendulum oscillator and some related equation have been used as a physical model to solve several natural problems related to bifurcations, oscillations, and chaos such as nonlinear plasma oscillations [1–9], Duffing oscillators [10–14], and Helmholtz oscillations [12], and many other applications can be found in [15–24]. There are few attempts for analyzing the equation of motion of the nonlinear damped pendulum taking the friction forces into account [25]. The approximate solution was obtained in form of the Jacobi elliptic functions. However, there are many others forces in addition to the friction force that affect the motion of the pendulum such as perturbed and periodic forces. These forces appear in different dynamic systems and cannot be neglected due to their great impact on the behavior of the oscillator. For instance, the unforced damped driven nonlinear pendulum equation/or the unforced damped parametric driven pendulum equation

$$\ddot{\varphi} + 2\beta\dot{\varphi} + \phi(t)\sin\varphi = 0, \tag{1}$$

has been derived in detail in [26], where $\phi(t) = \omega_0^2 - \varepsilon\omega_2\cos(\gamma t)$, $\omega_0^2 = g/l$, $\beta = \mu/2ml$, $\omega_1 = \gamma/ml$, $\omega_2 = \gamma^2/l$, $\varepsilon \ll 1$ is a small parameter, and $\varphi \equiv \varphi(t)$ denotes the angular displacement. In (1), ω_0 indicates the eigenfrequency of the system and β represents the damping coefficient. Here, the pendulum is modeled by a sphere of mass m, hanging at the end of a massless wire with length l and fixed to a supporting point "O," swinging to and from in a vertical plane under the gravity acceleration "g.". For $(\beta, \omega_2, F) = (0, 0, 0)$, the unforced undamped nonlinear pendulum oscillation/the unforced undamped Duffing oscillator is recovered [5]. (1) has only been analyzed numerically via the midpoint scheme, and based on our comprehensive survey, we did not find any attempt to find a semi-analytical solution to this equation. Motivated by the potential applications of the nonlinear oscillators, the forced damped driven nonlinear (FDDN) pendulum equation or sometimes called the forced damped parametric driven pendulum equation will be studied:

$$\ddot{\varphi} + 2\beta\dot{\varphi} + \phi(t)\sin\varphi = F\cos(\Omega t). \tag{2}$$

Also, some analytical approximations to (2) and some related equations will be derived for the first time and will be compared with the Runge–Kutta (RK) numerical solution. Moreover, the Chebyshev collocation numerical method [27–29] is introduced for analyzing both (1) and (2). Furthermore, the MATHEMATICA command Fit is devoted for analyzing the equation of motion. We graphically make a comparison between the analytical and numerical approximations, and the maximum distance error in the whole time domain is estimated.

2. Analytical Approximations to the FDDN Pendulum Equation

Let us now write the evolution equation in the form of the initial value problem (i.v.p.):

$$\begin{cases} c\ddot{\varphi} + 2\beta\dot{\varphi} + \phi(t)\sin\varphi = F\cos(\Omega t), \\ \varphi(0) = \varphi_0 \text{ and } \varphi'(0) = \dot{\varphi}_0. \\ 0 \le t \le T, \end{cases} \tag{3}$$

where $\varphi(t = 0) = \varphi_0$ indicates the oscillation amplitude.

Using Chebyshev polynomial approximation, we can approximate $\sin\varphi$ as

$$\sin\varphi \approx \varphi - \lambda\varphi^3 \text{ for } -M \le \varphi \le M, \tag{4}$$

where

$$\lambda \equiv \lambda_M = \frac{1}{6} + \frac{M}{5569} - \frac{M^2}{112} + \frac{M^3}{1883}. \tag{5}$$

The error E_M of this approximation may be estimated via the following formula:

$$E_M = \frac{3}{298}M^3 - \frac{5}{378}M^2 + \frac{1}{203}M - \frac{1}{2837} \text{ for } \frac{2\pi}{180} \le M \le \frac{\pi}{2}. \tag{6}$$

For example, at the angle $M = 30^\circ$, the exact error equals $E_{ex} = 0.0000608542$ while the error according to formula (6) equals $E_M = 0.0000455313$ and the difference between them is given by $E = E_{ex} - E_M = 0.0000153229$. The respective approximation for $-30^\circ \le \varphi \le 30^\circ$ reads as

$$\sin\varphi \approx \varphi - 0.164389\varphi^3 \approx \varphi - \frac{9}{55}\varphi^3. \tag{7}$$

Also, for $M = 75^\circ$, we obtain $\lambda = 2/13$ which will be used as the default value in the present study. Consequently, i.v.p. (3) can be reduced to the following variable coefficient forced damped Duffing i.v.p.

$$\begin{cases} c\mathbb{Q} \equiv \ddot{\varphi} + 2\beta\dot{\varphi} + \phi(t)\left(\varphi - \frac{2}{13}\varphi^3\right) - F\cos(\Omega t) = 0, \\ \varphi(0) = \varphi_0 \text{ and } \varphi'(0) = \dot{\varphi}_0. \end{cases} \tag{8}$$

Suppose the solution of this problem is given by

$$\begin{cases} c\varphi = \theta + c_1\cos(\Omega t) + c_2\sin(\Omega t), \\ \theta(0) \equiv \theta_0 = \varphi_0 - c_1 \text{ and } \varphi'(0) \equiv \theta_1 = \dot{\varphi}_0 - c_2\Omega. \end{cases} \tag{9}$$

The function $\theta \equiv \theta(t)$ is a solution to the following ode:

$$\ddot{\theta} + 2\beta\dot{\theta} + \phi(t)\left(\theta - \frac{2}{13}\theta^3\right) = 0. \tag{10}$$

Accordingly, we get

$$\mathbb{Q} = -\frac{1}{26}\cos(\Omega t)A_1 - \frac{1}{26}\sin(\Omega t)A_2 - \frac{1}{26}\left(12\theta^2 A_3 + 6\theta A_4 + A_5\right)\phi(t), \tag{11}$$

where the coefficients $A_1 - A_5$ are given in Appendix 1.

Now, for small γ, we can define $\phi(t) = \omega_0^2 - \varepsilon\omega_2\cos(\gamma t) \approx \omega_0^2 - \varepsilon\omega_2 = \kappa$ which leads to

$$\mathbb{Q} \approx -\frac{1}{26}\cos(\Omega t)B_1 - \frac{1}{26}\sin(\Omega t)B_2 - \frac{\kappa}{26}\left(12\theta^2 A_3 + 6\theta A_4 + A_5\right), \tag{12}$$

where the coefficients $A_1 - A_3$ have the same values given in Appendix 1 while the values of coefficients of B_1 and B_2 are given in Appendix 2.

The constants c_1 and c_2 could be determined from the following system:

$$\begin{cases} c3\left(c_1^3 + 3c_2^2c_1 - 26c_1\right)\kappa - 52c_2\beta\Omega + 26c_1\Omega^2 + 26F = 0, \\ \left(3c_2^3 + 3c_1^2c_2 - 26c_2\right)\kappa + 52c_1\beta\Omega + 26c_2\Omega^2 = 0. \end{cases} \tag{13}$$

Eliminating c_2 from system (13), we have the following cubic equation:

$$-26c_1\begin{pmatrix} 3F^2\kappa^2 - 3F^2\kappa\Omega^2 - 416\beta^4\Omega^4 \\ -104\beta^2\kappa^2\Omega^2 + 208\beta^2\kappa\Omega^4 - 104\beta^2\Omega^6 \end{pmatrix} + 9F^2\kappa^2c_1^3$$
$$\left(-624F\beta^2\Omega^2c_1^2 + 78F^3 - 2704F\beta^2\Omega^2\right)\kappa + 2704F\beta^2\Omega^4 = 0. \tag{14}$$

Also, by eliminating c_1 from system (13), we get

$$\left(10816\beta^4\Omega^4 + 2704\beta^2\kappa^2\Omega^2 - 5408\beta^2\kappa\Omega^4 + 2704\beta^2\Omega^6\right)c_2$$
$$+9F^2\kappa^2c_2^3 + \left(312F\beta\kappa\Omega^3 - 312F\beta\kappa^2\Omega\right)c_2^2 - 5408F\beta^3\Omega^3 = 0. \tag{15}$$

We choose the least in magnitude pair of real roots (c_1, c_2) in (14) and (15). Accordingly, the final form of the analytical approximation to i.v.p. (3) is given by

$$\varphi_{\text{approx}}(t) = \theta(t) + c_1 \cos(t\Omega) + c_2 \sin(t\Omega), \tag{16}$$

with

$$\begin{aligned} \theta(t) &= \frac{e^{-\beta t}}{1 + b_2 sn(f(t)\sqrt{\omega}\,|m)^2}\begin{pmatrix} b_1 dn(f(t)\sqrt{\omega}\,|m) sn(f(t)\sqrt{\omega}\,|m) \\ +\theta_0 cn(f(t)\sqrt{\omega}\,|m) \end{pmatrix}, \\ f(t) &= \frac{2\sqrt{-330\beta^2 - 329\kappa/\kappa\%}}{\sqrt{329}\gamma} E\left(\frac{t\gamma}{2}\,|\,\frac{658\varepsilon\omega_2}{330\beta^2 - 329\kappa}\right), \end{aligned} \tag{17}$$

where

$$\begin{aligned} \omega &= -\frac{p}{2m-1}, \\ m &= \frac{1}{2}\left(1 - \frac{p}{\sqrt{\left(p + q\varphi_0^2\right)^2 + 2\theta_1^2 q}}\right), \\ b_1 &= \frac{\delta\theta_1\sqrt{1-2m}}{\sqrt{p}}, \\ b_2 &= \frac{p + q\varphi_0^2 - \omega}{2\omega}, \\ p &= \kappa,\ q = -\frac{2}{13}\kappa. \end{aligned} \tag{18}$$

3. Chebyshev Collocation Numerical Scheme for Analyzing FDDN Pendulum Equation

Now, the Chebyshev interpolation collocation method is introduced for analyzing i.v.p. (3) on the time interval $[0, T]$. To do that, we first solve numerically the ode. Let $\widehat{\varphi}$ be the RK numerical solution to the i.v.p. described by (3). Then, we assume that the solution is given in terms of Chebyshev polynomials:

$$\varphi(t) = \sum_{k=0}^{n} c_k T_k\left(\frac{2t}{T} - 1\right), \tag{19}$$

where $T_k(t)$ stands for the Chebyshev polynomial of the first kind and n denotes the highest degree of the Chebyshev polynomials involved in the linear combination.

The collocation points t_k are defined as

$$t_k = \frac{1}{2}T\left[1 + \cos\left(\frac{4k+1}{2(n+1)}\pi\right)\right], \tag{20}$$

for $k = 1, 2, 3, \ldots, n$.

The additional equations are required for determining the values of c_k. Thus, the values of the coefficients c_k are found from the following linear system:

$$\begin{aligned} \varphi(0) &= \varphi_0, \\ \varphi'(0) &= \dot{\varphi}_0, \\ \varphi''(0) &= \widehat{\varphi}''(0). \\ \varphi(T) &= \widehat{\varphi}(T), \\ \varphi'(T) &= \widehat{\varphi}'(T), \\ \varphi''(T) &= \widehat{\varphi}''(T). \\ \varphi(t_k) &= \widehat{\varphi}(t_k)\ for\ k = 5, 6, \ldots, n. \end{aligned} \tag{21}$$

In general, increasing the value of n will not guarantee good approximations. Thus, we must choose some optimal value for n to our approximations. To this end, we define a range for possible n values, say

$$7 \le n_{\min} \le n \le n_{\max}. \tag{22}$$

We then find the optimal value for n within this range. Let $\varphi_n(t)$ be the solution using formula (19) and let $\varphi_{\text{RK}}(t)$ be the RK numerical solution to i.v.p. (3) on the interval $0 \le t \le T$. The following maximum distance error with respect to the RK numerical solution is defined:

$$E_{T,n} = \max_{0\le t\le T}\left|\varphi_n(t) - \varphi_{\text{RK}}(t)\right|. \tag{23}$$

The optimal value for n on the range $n_{\min} \le n \le n_{\max}$ will then be that for which the error $E_{T,n}$ is as small as possible. *o* verifies the validity of this claim. Let us use the following data: $(\beta, \gamma, \omega_0, \omega_2, \varepsilon, \Omega, F, \varphi_0, \dot{\varphi}_0) = (0.2, 0.2, 1, 1, 0.2, 1, 0.1, 0, 0)$, as an example in i.v.p. (3). By solving this problem via both RK and Chebyshev collocation numerical methods in the interval $0 \le t \le 50$ and estimating the error $E_{T,n}$ based on relation (23) for $7 \le n \le 60$, we finally get the error $E_{T,n}$ associated with each number n as shown in Table 1. The results in Table 1 illustrate that the optimal value of n based on the mention data for $(\beta, \gamma, \omega_0, \omega_2, \varepsilon, \Omega, F, \varphi_0, \dot{\varphi}_0)$ equals $n = 45$ and the error value corresponding to $n = 45$ equals

$E_{50,45} = 0.000964248$. Also, the optimal polynomial according to the mentioned data reads as

$$\begin{aligned}\varphi_{45}(t) = {} & 0.0511403t^2 - 0.0177057t^3 \\ & + 0.0340205t^4 - 0.0823837t^5 + 0.109124t^6 - 0.0998239t^7 + 0.0677353t^8 \\ & - 0.0353909t^9 + 0.0146451t^{10} - 0.00490664t^{11} + 0.00135445t^{12} - 0.000312451t^{13} \\ & + 0.0000609427t^{14} - 0.0000101493t^{15} + 1.45518\times 10^{-6}t^{16} - 1.80894\times 10^{-7}t^{17} \\ & + 1.96141\times 10^{-8}t^{18} - 1.86462\times 10^{-9}t^{19} + 1.561\times 10^{-10}t^{20} - 1.15515\times 10^{-11}t^{21} \\ & + 7.57989\times 10^{-13}t^{22} - 4.42193\times 10^{-14}t^{23} + 2.29822\times 10^{-15}t^{24} - 1.06583\times 10^{-16}t^{25} \\ & + 4.41541\times 10^{-18}t^{26} - 1.63491\times 10^{-19}t^{27} + 5.41107\times 10^{-21}t^{28} - 1.6\times 10^{-22}t^{29} \\ & + 4.22221\times 10^{-24}t^{30} - 9.92634\times 10^{-26}t^{31} + 2.07398\times 10^{-27}t^{32} - 3.83854\times 10^{-29}t^{33} \\ & + 6.26651\times 10^{-31}t^{34} - 8.97497\times 10^{-33}t^{35} + 1.11996\times 10^{-34}t^{36} - 1.2071\times 10^{-36}t^{37} \\ & + 1.1112\times 10^{-38}t^{38} - 8.60994\times 10^{-41}t^{39} + 5.50647\times 10^{-43}t^{40} - 2.82885\times 10^{-45}t^{41} \\ & + 1.12172\times 10^{-47}t^{42} - 3.22145\times 10^{-50}t^{43} + 5.96106\times 10^{-53}t^{44} - 5.33464\times 10^{-56}t^{45}.\end{aligned} \tag{24}$$

Polynomial (24) allows us to estimate the cuts with the horizontal axis as well as the maxima and minima to the crest and the trough, respectively, as shown in Figure 1 and Table 2. Using the MATHEMATICA command Fit gives the following solution $\varphi_{\text{Math}}(t) \equiv \varphi_{\text{Mathematica}}(t)$ for $(\beta, \gamma, \omega_0, \omega_2, \varepsilon, \Omega, F, \varphi_0, \dot{\varphi}_0) = (0.2, 0.2, 1, 1, 0.2, 1, 0.1, 0, 0)$:

$$\begin{aligned}\varphi_{\text{Math}}(t) = {} & e^{-t/5}\left(\frac{t^6}{365} - \frac{2t^5}{23} + \frac{125t^4}{94} - \frac{229t^3}{32} - \frac{21045t^2}{619} + \frac{33029t}{74} - \frac{63445}{76}\right)\sin(t) \\ & + \frac{e^{-t/5}}{787321464}\left(\begin{array}{c} 2193096t^6 - 17115684t^5 - 426465793t^4 + 10891280252t^3 \\ -83720431296t^2 + 147163503646t + 393199198728 \end{array}\right)\cos(t) \\ & + \frac{e^{-t/5}}{1544400}\left(\begin{array}{c} -3575t^7 + 93600t^6 - 1480050t^5 + 12725856t^4 \\ -38075400t^3 - 118006200t^2 + 1213821180t + 294883875 \end{array}\right) - \frac{11736}{17},\end{aligned} \tag{25}$$

with error $E = 0.000213725$. Figure 2 demonstrates the comparison between the approximations of i.v.p. (3) using RK numerical solution with MATHEMATICA command Fit (here, polynomial (25)) and Chebyshev collocation numerical solution (24). It is noted that all used techniques give highly accurate approximations with low errors as compared to the RK numerical solutions.

The semi-analytical solution (16) to i.v.p. (3) could be recovered as follows.

Case (1). For $(\beta, \omega_2, F) = (0, 0, 0.1)$, the different approximations to the forced undamped Duffing oscillator with constant coefficients are introduced in Figure 3 with $(\gamma, \omega_0, \varepsilon, \Omega, \varphi_0, \dot{\varphi}_0) = (0.1, 1, 0.1, 2, 0, 0)$. The comparison between the RK method and the analytical approximation (15) is presented in Figure 3(a). The approximate solutions using the MATHEMATICA command Fit and RK method are displayed in Figure 3(b). In Figure 3(c), both RK and Chebyshev collocation numerical approximations are presented. Also, the maximum error for the analytical approximation (15) and MATHEMATICA command Fit and Chebyshev collocation numerical solutions as compared to the RK numerical approximation is estimated based on the following relation:

$$E_\infty\big|_{\text{Type-solution}} = \max_{0\le t\le 30}\left|\varphi_{\text{Type-solution}} - \varphi_{\text{RK}}\right|. \tag{26}$$

Accordingly, the maximum error of the three approximations for the present case is estimated as

Table 1

N	ET;n
7	12:7318
8	8:18709
9	5:34902
10	3:73001
11	2:47806
12	5:99151
13	15:6472
14	19:1789
15	11:4247
16	12:9725
17	44:5793
N	ET;n
18	56:0277
19	22:7408
20	45:8666
21	86:0102
22	41:4478
23	54:48:00
24	81:8262
25	9:2908
26	50:9774
27	35:2609
28	7:88678
N	ET;n
29	24:0096
30	11:8633
31	11:9267
32	13:0699
33	16:4155
34	160:44:00
35	1021:51:00
36	455:30:00
37	293:27:00
38	62:37:00
39	594:34:00
N	ET;n
40	1011:59:00
41	1016:07:00
42	193:44:00
43	978:08:00
44	154:12:00
45	779:04:00
46	584:21:00
47	655:31:00
48	1042:34:00
49	04:05:00
50	1060:25:00
N	ET;n
51	135:10:00
52	626:08:00
53	401:51:00
54	666:50:00
55	999:51:00
56	893:24:00
57	622:23:00
58	199:58:00
59	7:1974
60	30:729

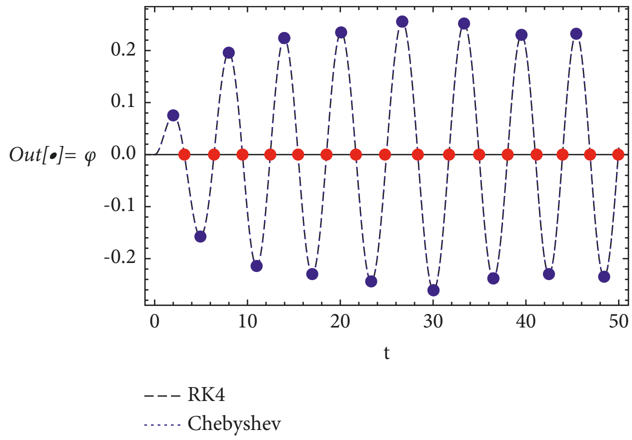

FIGURE 1: The Chebyshev collocation and RK numerical approximations to i.v.p. (3) for $(\beta, \gamma, \omega_0, \omega_2, \varepsilon, \Omega, \varphi_0, \dot{\varphi}_0) = (0.2, 0.2, 1, 1, 0.2, 1, 0.1, 0, 0)$ and with $n = 45$ is plotted in the (φ, t) plane and the cuts with the horizontal axis as well as the maxima and minima to the crest and the trough is determined.

TABLE 2

Zeros of the polynomial solution '45(t)				Zeros of the derivative '045(t)			
K	Tk	k	tk	k	tk	k	tk
1	3:1993	11	34:9609	1	1:99978	11	26:6741
2	6:39594	12	38:0328	2	4:93036	12	30:43:00
3	9:46288	13	41:1493	3	7:98259	13	30:43:00
4	12:4583	14	43:9479	4	10:9844	14	33:3364
5	15:4562	15	46:912	5	13:9641	15	36:4941
6	18:5134	16	49:9492	6	13:9645	16	36:4941
7	21:6812			7	16:98	17	39:5245
8	24:8139			8	20:0903	18	42:4811
9	28:3547			9	23:3291	19	45:4226
10	31:7165			10	26:674	20	48:4281

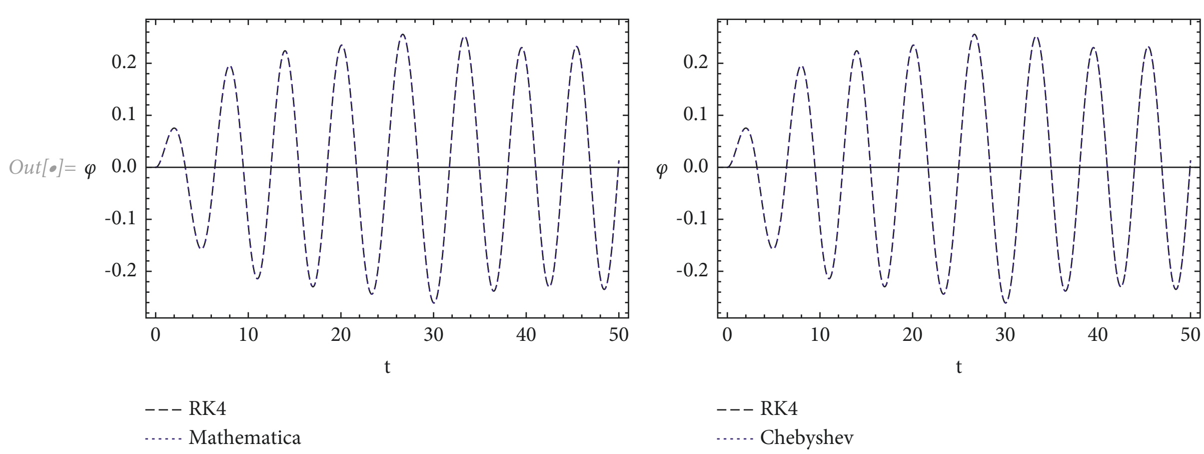

(a) (b)

FIGURE 2: The comparison between the approximations of i.v.p. (3) using RK numerical solution with MATHEMATICA command Fit (here, polynomial (25)) and Chebyshev collocation numerical solution (24) for $(\beta, \gamma, \omega_0, \omega_2, \varepsilon, \Omega, \varphi_0, \dot{\varphi}_0) = (0.2, 0.2, 1, 1, 0.2, 1, 0.1, 0, 0)$ and $n = 45$.

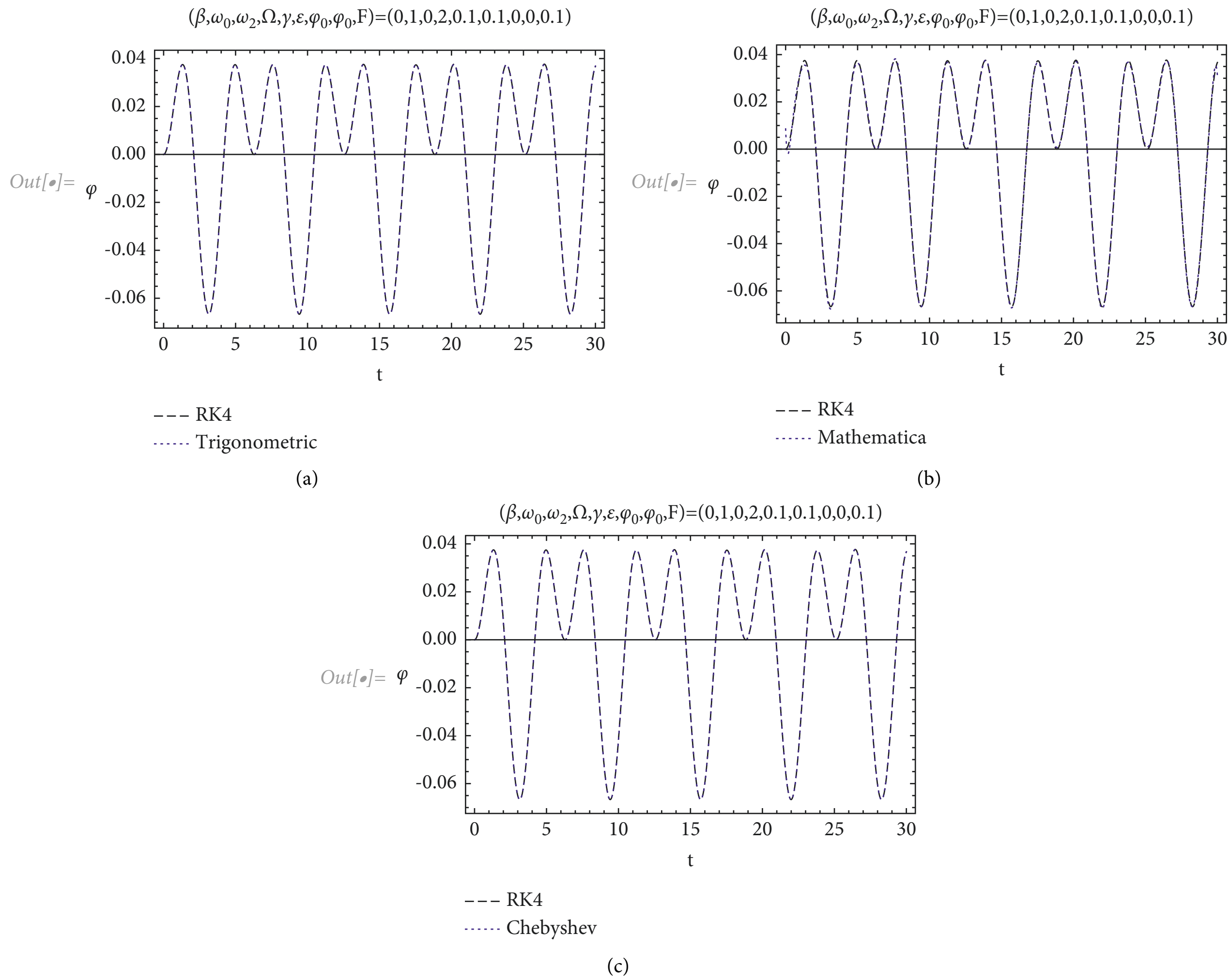

Figure 3: The comparison between the semi-analytical solution (analytical approximation) (16) and the numerical approximations using the Chebyshev collocation method and RK numerical method as well as the MATHEMATICA command Fit to i.v.p. (3) for case (1): $(\beta, \omega_2, F) = (0, 0, 0.1)$.

$$\begin{aligned} E|_{semi-analy} &= 0.000214826, \\ E|_{Mathematica} &= 0.00856153, \\ E_{n=47}|_{Chebyshev} &= 0.0000389093. \end{aligned} \tag{27}$$

Case (2). For $(\beta, \omega_2, F) = (0, 1, 0.1)$, the comparison between the analytical approximation (16) and the numerical approximations using the RK, MATHEMATICA command Fit, and Chebyshev collocation numerical methods to the forced undamped Duffing equation with variable coefficients is considered as shown in Figure 4 with $(\gamma, \omega_0, \varepsilon, \Omega, \varphi_0, \dot{\varphi}_0) = (0.1, 1, 0.1, 2, 0, 0)$. The maximum error of the three approximations to the present case is calculated as

$$\begin{aligned} E|_{semi-analy} &= 0.00344896, \\ E|_{Mathematica} &= 0.0100608, \\ E_{n=47}|_{Chebyshev} &= 0.0000237867. \end{aligned} \tag{28}$$

Case (3). For $(\beta, \omega_2, F) = (0.1, 1, 0)$, the unforced damped Duffing equation with variable coefficients is recovered and its semi-analytical solution (16) is compared with the numerical approximations using RK, MATHEMATICA command Fit, and Chebyshev collocation numerical methods as demonstrated in Figure 5 with $(\gamma, \omega_0, \varepsilon, \Omega, \varphi_0, \dot{\varphi}_0) = (0.1, 1, 0.1, 2, 0, 0.1)$. In addition, the maximum error to the three approximations as compared to RK numerical approximation is estimated as

$$\begin{aligned} E|_{semi-analy} &= 0.000447172, \\ E|_{Mathematica} &= 0.00133459, \\ E_{n=47}|_{Chebyshev} &= 2.05447 \times 10^{-6}. \end{aligned} \tag{29}$$

The MATHEMATICA code for the RK and Chebyshev collocation numerical approximations with the maximum error is given in Appendix 3.

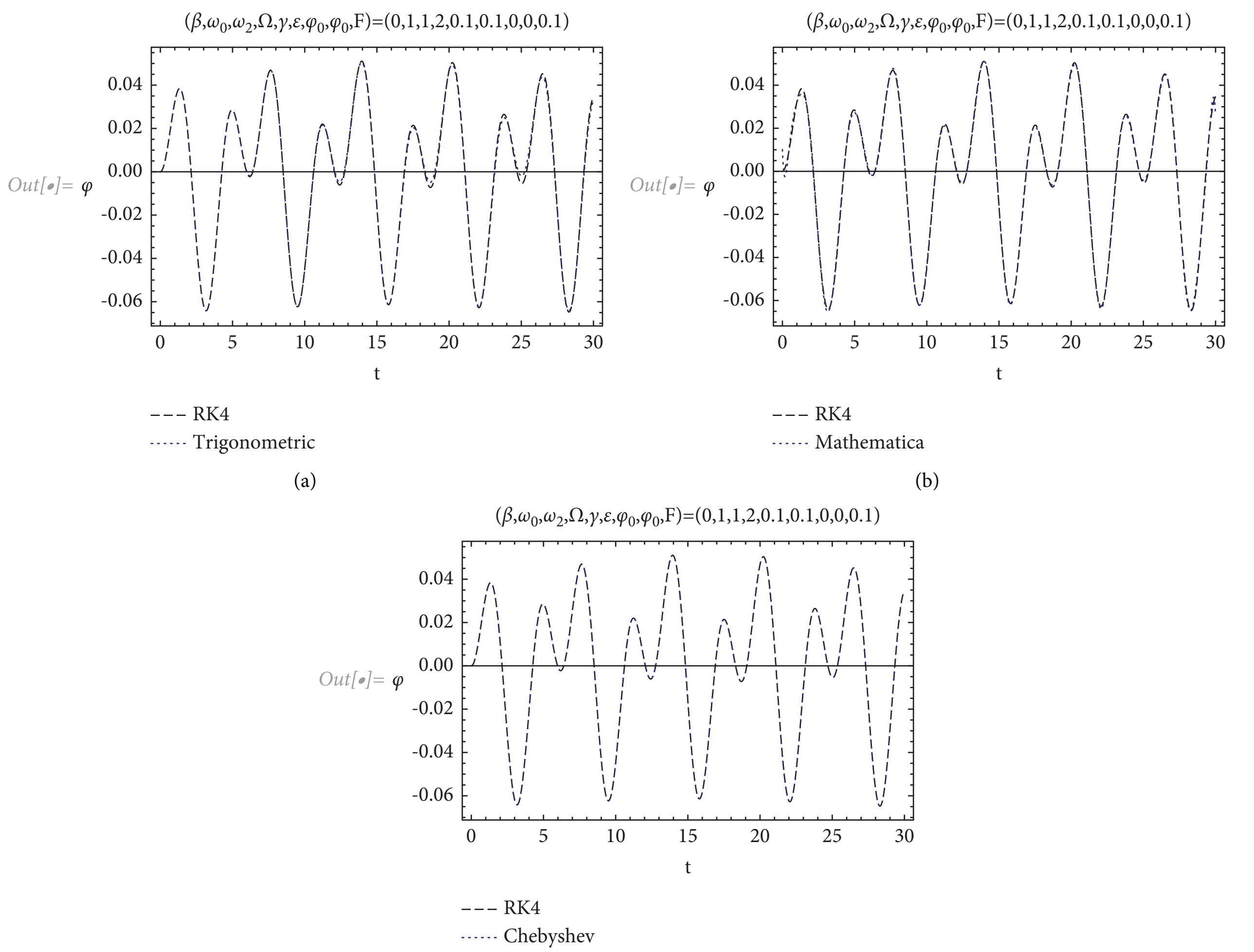

(a) (b) (c)

Figure 4: The comparison between the analytical approximation (16) and the numerical approximations using the Chebyshev collocation method and RK numerical method as well as the MATHEMATICA command Fit to i.v.p. (3) for case (2): $(\beta, \omega_2, F) = (0, 1, 0.1)$.

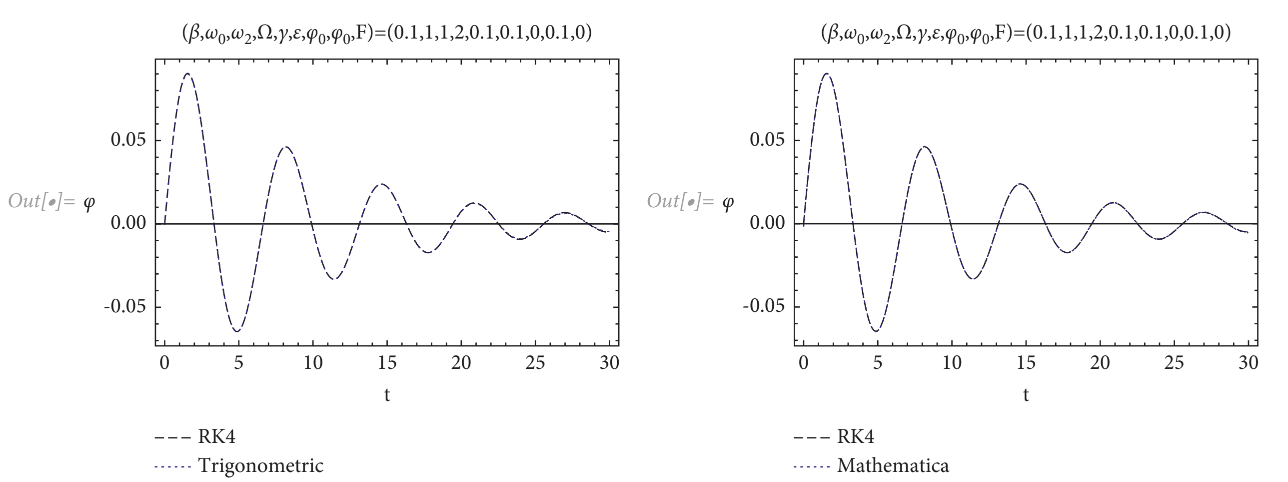

(a) (b)

Figure 5: Continued.

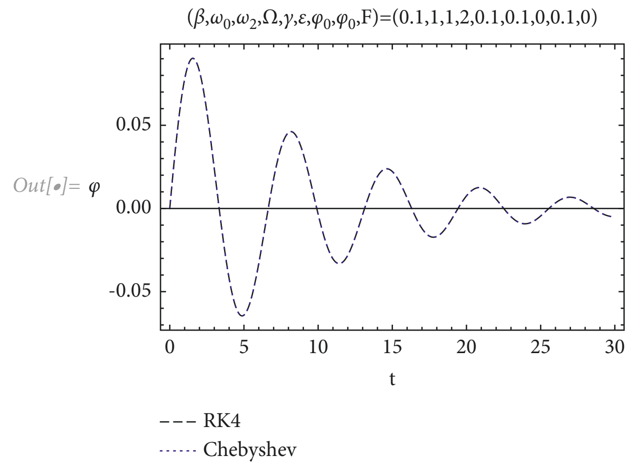

(c)

Figure 5: The comparison between the analytical approximation (16) and the numerical approximations using the Chebyshev collocation method and RK numerical method as well as the MATHEMATICA command Fit to i.v.p. (3) for case (3): $(\beta, \omega_2, F) = (0.1, 1, 0)$.

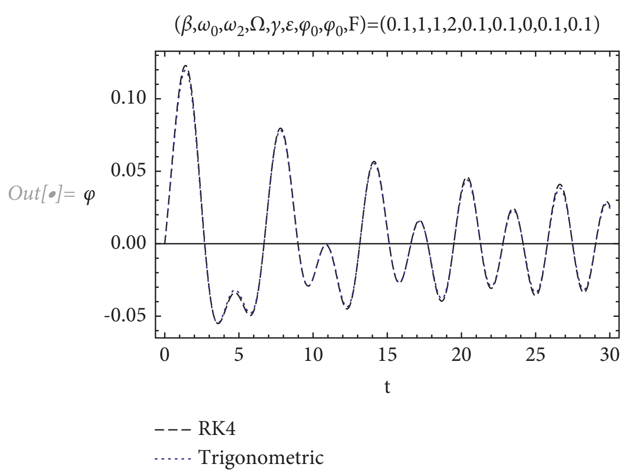

(a)

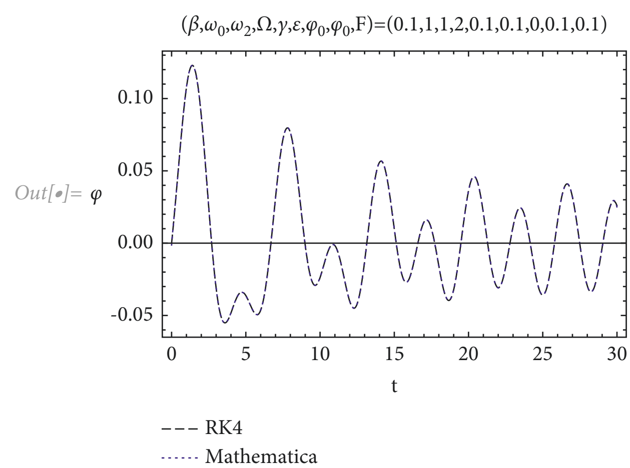

(b)

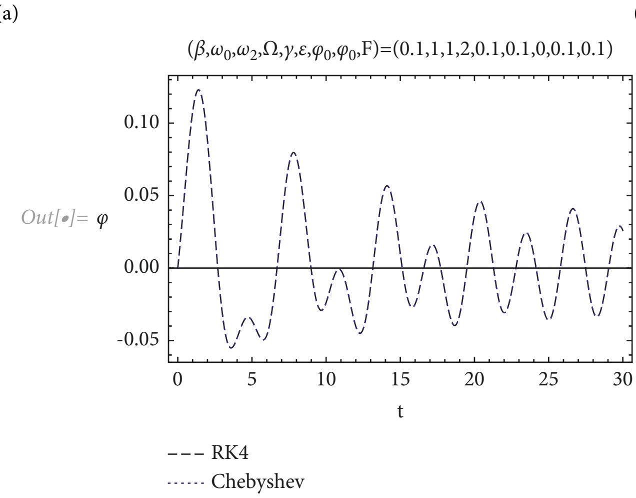

(c)

Figure 6: The comparison between the analytical approximation (16) and the numerical approximations using the Chebyshev collocation method and RK numerical method as well as the MATHEMATICA command Fit to i.v.p. (3) for case (4): $(\beta, \omega_2, F) = (0.1, 1, 0.1)$.

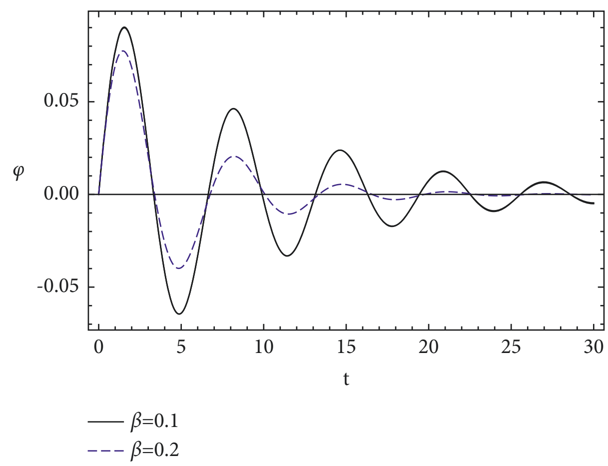

FIGURE 7: The analytical approximation (16) to i.v.p. (3) plotted in the (φ, t)plane for different values to the coefficient of the damping term β.

Case (4). For $(\beta, \omega_2, F) = (0.1, 1, 0.1)$, the general analytical approximation (16) to the forced damped parametric driven pendulum i.v.p. (3) is compared with the RK, MATHEMATICA command Fit, and Chebyshev collocation numerical solutions as elucidated in Figure 6. The influence of β on the amplitude of the semi-analytical solution (16) is investigated as shown in Figure 7. It is noted that the amplitude of the analytical approximation (15) decreases with the increase of β. Also, the maximum error according to relation (23) to the analytical approximation (16) and MATHEMATICA command Fit, and Chebyshev collocation numerical solutions as compared to the RK numerical solution is estimated as follows:

$$\begin{aligned} E|_{semi-analy} &= 0.00326255, \\ E|_{Mathematica} &= 0.0128206, \\ E_{n=47}|_{Chebyshev} &= 0.000155082. \end{aligned} \tag{30}$$

In all mentioned cases, it is observed that analytical approximation (16) to i.v.p. (3) and its related equations (here we mean the four mentioned cases) give highly accurate results as compared to the numerical approximations. It is observed that analytical approximation (16) is better than the MATHEMATICA approximation but less than the Chebyshev collocation numerical solution for all mentioned cases. However, in the fourth case, i.e., the forced damped parametric driven pendulum i.v.p. (3), the MATHEMATICA approximation is better than the analytical approximation (16). In general, all obtained approximations are characterized by their high accuracy. However, semi-analytical solution (16) is more stable than the Chebyshev collocation numerical solution against all relevant physical variables.

4. Conclusions

In this work, some effective and accurate analytical and numerical approximations to the forced damped parametric driven pendulum equation have been derived and investigated. The mentioned equation of motion has been reduced to the forced damped Duffing equation with variable coefficients in order to find its analytical solution. In terms of the Jacobi elliptic functions, the analytical approximation has been derived. For the numerical approximations, the Chebyshev collocation method has been used for analyzing the equation of motion and some related equations. It was noted that the analytical approximation could recover some special cases to the nonlinear pendulum oscillators. For instance, for undamping case, i.e., for $\beta = 0$, the solution to the forced undamped Duffing equation with variable coefficients has been recovered and examined. Also, for $(\beta, \omega_2) = (0, 0)$, the solution to the forced undamped Duffing equation with constant coefficients has been recovered and discussed. The obtained approximations were compared with the RK numerical approximation and the MATHEMATICA command Fit approximation. Also, the maximum distance error has been estimated for all approximations as compared to the RK numerical approximation. It was found that the analytical approximation gives good results with high accuracy as compared to the numerical approximations. Furthermore, it was observed that the analytical approximation is better than the MATHEMATICA approximation but less than the Chebyshev collocation numerical solution for all mentioned cases except the case of the forced damped parametric driven pendulum i.v.p. (3), the MATHEMATICA approximation is slowly better than the analytical approximation (16). The methods used in this study could be extended to solve many nonlinear equations that control the different cases of pendulum oscillations [30–33]. In addition, the obtained results/solutions are useful for investigating several physical problems related to the oscillations in plasma physics, fluid mechanics, field theory, engineering science, solid state physics, and quantum mechanics.

Appendices

Appendix A

The coefficients $A_1 - A_5$ of equation (11):

$$
\begin{aligned}
A_1 &= \begin{bmatrix} \phi(t)\left(3c_1^3 + 3c_2^2 c_1 - 26c_1\right) \\ -52c_2\beta\Omega + 26c_1\Omega^2 + 26F \end{bmatrix}, \\
A_2 &= \begin{bmatrix} \phi(t)\left(3c_2^3 + 3c_1^2 c_2 - 26c_2\right) \\ +\left(52c_1\beta\Omega + 26c_2\Omega^2\right) \end{bmatrix}, \\
A_3 &= \left(c_2 \sin(\Omega t) + c_1 \cos(\Omega t)\right), \\
A_4 &= \begin{bmatrix} \left(c_1^2 - c_2^2\right)\cos(2\Omega t) \\ +c_1^2 + c_2^2 + 2c_2 c_1 \sin(2\Omega t) \end{bmatrix}, \\
A_5 &= \left[c_2\left(3c_1^2 - c_2^2\right)\sin(3\Omega t) + c_1\left(c_1^2 - 3c_2^2\right)\cos(3\Omega t)\right].
\end{aligned}
\tag{A.1}
$$

Appendix B

The coefficients B_1 and B_2 of equation (12):

$$
\begin{aligned}
B_1 &= \begin{bmatrix} \kappa\left(3c_1^3 + 3c_2^2 c_1 - 26c_1\right) \\ -52c_2\beta\Omega + 26c_1\Omega^2 + 26F \end{bmatrix}, \\
B_2 &= \begin{bmatrix} \kappa\left(3c_2^3 + 3c_1^2 c_2 - 26c_2\right) \\ +\left(52c_1\beta\Omega + 26c_2\Omega^2\right) \end{bmatrix}.
\end{aligned}
\tag{B.1}
$$

Appendix C

MATHEMATICA Code for Chebyshev Collocation Numerical Method to Figure 5(c). Note that this is general code which can be used and applied for analyzing many oscillators related to the present evolution equation.

```
Clear[a, b, m, h, x, \ [CurlyPhi], n, \ [Chi]]; \{a = 0,
b = 30, m = 45\};
\ [Beta] = 0.1; [CapitalOmega] = 2; \ [Omega]0 = 1; \
[Omega]2 = 1; \\ [CurlyEpsilon] = 0.1; \ [Gamma] = 0.1;
x0 = 0; x1 = 0.1;
\ [Phi][t_]: = \ [Omega]0ˆ2 - \ [CurlyEpsilon] \ [Omega]
2 Cos[ \ [Gamma] \
t]; F = 0;
rk = NDSolve[
y"[t] + 2 \ [Beta] y'[t] + \ [Phi][t] Sin[y[t]] = =
F Cos[ \ [CapitalOmega] t] && y[a] = = x0 && y'[a] = =
x1,
y, \{t, 0, 100\}][[1, 1, 2]];
Plot[Evaluate[\{rk[t]\}], \{t, a, b - 10\}, PlotRange - >rbin
All.
PlotStyle - >rbin \{\{Black, Thin\}\}]
h = (b - a)/m;
x[t_]:= Sum[
Subscript[c, k] ChebyshevT[k, (a + b - 2 t)/(a - b)], \{k, 0,
m\}];
R[t_]: = x"[t] + 2 \ [Beta] x'[t] + \ [Phi][t]*Sin[x[t]] -
F Cos[ \ [CapitalOmega] t];
\ [Xi][j_]: = 1/2 (a + b + (-a + (b) Cos[( \ [Pi] + 4 j \ [Pi])/
(2 + 2 m)])
solc = Flatten[Solve[sys0]];
x[t_]:= Sum[
Subscript[c, k] ChebyshevT[k, (a + b - 2 t)/(a - b)]//. solc,
\{k.
0, m\}];
\ [Chi][m_][t_]: =
Sum[Subscript[c, k] ChebyshevT[k, (a + b - 2 t)/(a - b)]//
.
solc, \{k, 0, m\}];
er[m_]: = Max[Table[Abs[rk[t] - \ [Chi][m][t]], \{t, a, b,
0.1\}]];
error[m_]:= Module[\{ \ [Xi], \ [Chi], R, sys, solc, err\},
\{ \ [Xi][j_]: =
1/2 (a + b + (-a + (b) Cos[( \ [Pi] + 4 j \ [Pi])/(2 + 2 m)]); \
[Chi][tt_]: =
Sum[Subscript[c, k] ChebyshevT[k, (a + b - 2 tt)/(a - b)],
\{k, 0,
m\}]; R[t_]: = \ [Chi]"[tt] +
2 \ [Beta] \ [Chi]'[tt] + \ [Phi][tt]∗Sin[ \ [Chi][tt]] -
F Cos[ \ [CapitalOmega] tt];
sys =
Flatten[Join[
Table[rk[ \ [Xi][j]] = = \ [Chi][ \ [Xi][j]], \{j, 5,
m\}], \{\{ \ [Chi][a] - x0 = = 0, \ [Chi]'[a] - x1 = = 0, \
[Chi][b] - rk[b] = = 0, \ [Chi]'[b] - rk'[b] = =
0, \ [Chi]"[b] - rk"[b] = = 0\}\}]];
solc = Flatten[NSolve[sys]]; \ [Chi][tt_]: =
Sum[Subscript[c, k] ChebyshevT[k, (a + b - 2 t)/(a - b)],
\{k, 0,
m\}]//. solc;
err = Maximize[\{Abs[rk[t] -[Chi][t]], 0 = t = b\}, t][[1]];
\};
\{err, \ [Chi][t]\}
];
nmin = 7; nmax = 60;
opt = Sort[Table[\{error[jj][[1]], jj\}, \{jj, nmin, nmax\}]]
[[1]];
n = opt[[2]];
OPtimalnValue = = n
errx = error[n];
Error = = errx[[1]]
poly = errx[[2]];
Cheb = Plot[Evaluate[\{rk[t], poly\}], \{t, a, b\}, Plo-
tRange - > All.
PlotStyle - > \{\{Dashing[0.05], Thick, Black\}, \{Dotted,
Thick, Blue\}\},
PlotLegends - > Placed[\{"RK4″, "Chebyshev"\}, Frame
- > True].
```

Data Availability

All data generated or analyzed during this study are included within the article (more details can be requested from the corresponding author).

Disclosure

This paper was only published as a preprint entitled Approximate Solutions to the Forced Damped Parametric Driven Pendulum Oscillator: Chebyshev Collocation Numerical Solution [34].

Conflicts of Interest

The authors declare that they have no conflicts of interest.

Authors' Contributions

All authors contributed equally and approved the final version of the manuscript.

Acknowledgments

The authors express their gratitude to Princess Nourah bint Abdulrahman University Researchers Supporting Project number (PNURSP2022R157), Princess Nourah bint Abdulrahman University, Riyadh, Saudi Arabia. Taif University Researchers supporting project number (TURSP-2020/275), Taif University, Taif, Saudi Arabia.

References

[1] N. Nayfeth and D. T. Mook, *Non-linear Oscillations*, John Wiley, New York, NY, USA, 1973.
[2] T. O'Neil, "Collisionless damping of nonlinear plasma oscillations," *Physics of Fluids*, vol. 8, p. 2255, 1965.
[3] A. H. Salas S, S. A. El-Tantawy, and M. R. Alharthi, "Novel solutions to the (un) damped Helmholtz-Duffing oscillator and its application to plasma physics: moving boundary method," *Physica Scripta*, vol. 96, no. 10, p. 104003, 2021.
[4] Haifa A. Alyousef, Alvaro H. Salas, Sadah A. Alkhateeb, and S. A. El-Tantawy, "Some Novel Analytical Approximations to the (Un)damped Duffing–Mathieu Oscillators," *Journal of Mathematics*, vol. 2022, p. 2715767, 2022.
[5] A. Beléndez, C. Pascual, D. I. Méndez, T. Beléndez, and C. Neipp, "Exact solution for the nonlinear pendulum," *Revista Brasileira de Ensino de Física*, vol. 29, no. 4, pp. 645–648, 2007.
[6] A. H. Salas, S. A. El-Tantawy, and E. Jairo, "On the approximate and analytical solutions to the fifth-order Duffing oscillator and its physical applications," *Waves in Random and Complex Media*, pp. 1–21, 2021.
[7] S. A. El-Tantawy, A. H. Salas, and M. R. Alharthi, "A new approach for modelling the damped Helmholtz oscillator: applications to plasma physics and electronic circuits," *Communications in Theoretical Physics*, vol. 73, no. 3, p. 035501, 2021.
[8] A. H. Salas, S. A. El-Tantawy, and H. Noufe, "An exact solution to the quadratic damping strong nonlinearity Duffing oscillator," *Mathematical Problems in Engineering*, vol. 2021, Article ID 8875589, 8 pages, 2021.
[9] W. Albalawi, A. H. Salas, S. A. El-Tantawy, and A. Youssef, "Approximate analytical and numerical solutions to the damped pendulum oscillator: Newton-Raphson and moving boundary methods," *Journal of Taibah University for Science*, vol. 15, no. 1, pp. 479–485, 2021.
[10] P. G. D. Barkham and A. C. Soudack, "An extension to the method of Kryloff and Bogoliuboff†," *International Journal of Control*, vol. 10, no. 4, pp. 377–392, 1969.
[11] N. H. Aljahdaly and S. A. El-Tantawy, "On the multistage differential transformation method for analyzing damping Duffing oscillator and its applications to plasma physics," *Mathematics*, vol. 9, no. 4, p. 432, 2021.
[12] A. Elías-Zúñiga, O. Martínez-Romero, D. Olvera-Trejo, and L. M. Palacios-Pineda, "Determination of the frequency-amplitude response curves of undamped forced Duffing's oscillators using an ancient Chinese algorithm," *Results in Physics*, vol. 24, p. 104085, 2021.
[13] M. Turkyilmazoglu, "An effective approach for approximate analytical solutions of the damped Duffing equation," *Physica Scripta*, vol. 86, no. 1, p. 015301, 2012.
[14] H. G. Kadji Enjieu, O. J. B. Chabi, and P. Woafo, "Regular and chaotic behaviors of plasma oscillations modeled by a modified Duffing equation," *Phys. Scr.*vol. 77, p. 025503, 2008.
[15] I. F. Collins, "On the theory of rigid/perfectly plastic plates under uniformly distributed loads," *Acta Mechanica*, vol. 18, no. 3-4, pp. 233–254, 1973.
[16] B. M. Karmakar, "Nonlinear vibrations of orthotropic plates carrying concentrated mass," *Journal of Engineering for Industry*, vol. 100, no. 2, pp. 293-294, 1978.
[17] J. Zajaczkowski, "Destabilizing effect of Coulomb friction on vibration of a beam supported at an axially oscillating mount," *Journal of Sound and Vibration*, vol. 79, no. 4, pp. 575–580, 1981.
[18] S. S. Chang, "The general solutions of the doubly periodic cracks," *Engineering Fracture Mechanics*, vol. 18, no. 4, pp. 887–893, 1983.
[19] D. Grozev, A. Shivarova, and A. D. Boardman, "Envelope solitons of surface waves in a plasma column," *Journal of Plasma Physics*, vol. 38, no. 3, pp. 427–437, 1987.
[20] A. I. J. Manevich, "Approximate solutions to the forced damped parametric driven pendulum oscillator: Chebyshev collocation numerical solution," *Applied Mathematics and Mechanics*, vol. 58, p. 1061, 1994.
[21] R. H. Rand, R. J. Kinsey, and D. L. Mingori, "Dynamics of spinup through resonance," *International Journal of Non-linear Mechanics*, vol. 27, no. 3, pp. 489–502, 1992.
[22] W. Hu and D. J. Scheeres, "Spacecraft motion about slowly rotating asteroids," *Adv. Astronaut. Sci.*vol. 105, p. 839, 2000.
[23] W. Lestari and S. Hanagud, "Nonlinear vibration of buckled beams: some exact solutions," *International Journal of Solids and Structures*, vol. 38, no. 26-27, pp. 4741–4757, 2001.
[24] S. Liu, Z. Fu, S. Liu, and Q. Zhao, "Jacobi elliptic function expansion method and periodic wave solutions of nonlinear wave equations," *Physics Letters A*, vol. 289, no. 1-2, pp. 69–74, 2001.
[25] K. Johannessen, "An analytical solution to the equation of motion for the damped nonlinear pendulum," *European Journal of Physics*, vol. 35, no. 3, p. 035014, 2014.
[26] Y. Guo, A. C. J. Luo, and J. Luo, "Bifurcation dynamics of a damped parametric pendulum," *Synthesis Lectures on Mechanical Engineering*, vol. 3, no. 5, pp. 1–98, 2019.
[27] Y. H. Youssri and R. M. Hafez, "Chebyshev collocation treatment of Volterra-Fredholm integral equation with error analysis," *Arabian Journal of Mathematics*, vol. 9, no. 2, pp. 471–480, 2020.
[28] E. H. Doha, W. M. Abd-Elhameed, N. A. Elkot, and Y. H. Youssri, "Integral spectral Tchebyshev approach for solving space Riemann-Liouville and Riesz fractional

advection-dispersion problems," *Advances in Difference Equations*, p. 284, 2017.

[29] W. M. Abd-Elhameed, E. H. Doha, Y. H. Youssri, and M. A. Bassuony, "New Tchebyshev-Galerkin operational matrix method for solving linear and nonlinear hyperbolic telegraph type equations," *Numerical Methods for Partial Differential Equations*, vol. 32, no. 6, pp. 1553–1571, 2016.

[30] S. A. El-Tantawy, A. H. Salas, and M. R. Alharthi, "On the analytical solutions of the forced damping duffing equation in the form of weierstrass elliptic function and its applications," *Mathematical Problems in Engineering*, vol. 2021, Article ID 6678102, 9 pages, 2021.

[31] J. Ángel Cid, "On the existence of periodic oscillations for pendulum-type equations," *Advance in Nonlinear Analysis*, vol. 10, p. 121, 2021.

[32] G. I. Depetri, F. A. C. Pereira, B. Marin, M. S. Baptista, and J. C. Sartorelli, "Dynamics of a parametrically excited simple pendulum," *Chaos: An Interdisciplinary Journal of Nonlinear Science*, vol. 28, no. 3, p. 033103, 2018.

[33] A. Ugulava, Z. Toklikishvili, and S. Chkhaidze, "On the dynamics of the angular momentum of a quantum pendulum," *Chaos: An Interdisciplinary Journal of Nonlinear Science*, vol. 30, no. 6, p. 063104, 2020.

[34] W. Albalawi, A. H. Salas, and S. A. El-Tantawy, "Approximate solutions to the forced damped parametric driven pendulum oscillator: chebyshev collocation numerical solution," , 2021.

Hindawi
Journal of Mathematics
Volume 2022, Article ID 2871511, 12 pages
https://doi.org/10.1155/2022/2871511

Research Article

Fourth-Order Hankel Determinants and Toeplitz Determinants for Convex Functions Connected with Sine Functions

Farah Zulfiqar,[1] **Sarfraz Nawaz Malik**,[1] **Mohsan Raza**,[2] **and Md. Shajib Ali**[3]

[1]*Department of Mathematics, COMSATS University Islamabad, Wah Campus, Wah Cantt, Pakistan*
[2]*Department of Mathematics, Government College University, Faisalabad, Pakistan*
[3]*Department of Mathematics, Islamic University, Kushtia 7003, Bangladesh*

Correspondence should be addressed to Md. Shajib Ali; shajib_301@yahoo.co.in

Received 24 December 2021; Revised 6 February 2022; Accepted 6 April 2022; Published 25 May 2022

Academic Editor: Fairouz Tchier

This article deals with the upper bound of fourth-order Hankel and Toeplitz determinants for the convex functions which are defined by using the sine function. The main tools in this study are the coefficient inequalities for the class P of functions with positive real parts. Also, the investigation of the upper bound of the fourth-order Hankel determinant for 3-fold symmetric convex functions associated with the sine function is included.

1. Introduction

Let the family of all functions f be denoted by A which are analytic in an open unit disc $D = \{z \in \mathbb{C}: |z| < 1\}$ with Taylor series expansion:

$$f(z) = z + \sum_{n=2}^{\infty} a_n z^n, \ (z \in D), \tag{1}$$

and S represent a family of functions $f \in A$ which are univalent in D. Let S^*, C, and K_g denote the families of starlike, convex, and close-to-convex functions, respectively, and they are defined as

$$S^* = \left\{ f \in S: \Re\left(\frac{zf'(z)}{f(z)}\right) > 0, \ (z \in D) \right\},$$

$$C = \left\{ f \in S: \Re\left(1 + \frac{zf''(z)}{f'(z)}\right) > 0, \ (z \in D) \right\}, \tag{2}$$

$$K_g = \left\{ f \in S: \Re\left(\frac{zf'(z)}{g(z)}\right) > 0, \quad \text{for } g \in S^*, \ (z \in D) \right\}.$$

Let P denote the family of all analytic functions p of the form

$$p(z) = 1 + \sum_{n=1}^{\infty} c_n z^n, \ z \in \mathrm{D}, \tag{3}$$

with the positive real parts in D. As the n^{th} coefficient for the functions belonging to the family is bounded by n, this bound helps in the study of geometric properties of functions $f \in S$. Specifically, the second coefficient a_2 helps in finding the distortion and growth properties of a normalized univalent function. Likewise, the problems involving power series with integral coefficients and investigating the singularities are successfully handled by using Hankel determinants. Pommerenke [1, 2] introduced the idea of Hankel determinants, and he defined those for univalent functions $f \in S$ of form (7) as follows:

$$H_{q,n}(f) = \begin{vmatrix} a_n & a_{n+1} & \cdots & a_{n+q-1} \\ a_{n+1} & a_{n+2} & \cdots & a_{n+q} \\ \vdots & \vdots & \cdots & \vdots \\ a_{n+q-1} & a_{n+q} & \cdots & a_{n+2q-2} \end{vmatrix}. \tag{4}$$

In the theory of analytic functions, finding the upper bound of $|H_{q,n}(f)|$ is one of the most studied problems. Several researchers found the above-mentioned bound for different subfamilies of univalent functions for fixed values of q and n. A few remarkable contributions in this regard are included here for reference. For the subfamilies S^*, C, and $K_z = R$ (the class of functions with bounded turnings) of the set S, the sharp bounds of $|H_{(2,2)}(f)|$ were investigated by Janteng et al. [3, 4]. They proved the bounds as follows:

$$|H_{(2,2)}(f)| \le \begin{cases} 1 \text{ for } f \in S^*, \\ \dfrac{1}{8} \text{ for } f \in C, \\ \dfrac{4}{9} \text{ for } f \in R. \end{cases} \quad (5)$$

The accurate estimate of $|H_{(2,2)}(f)|$ was obtained by Krishna et al. [5] for the family of Bazilevic functions. For subfamilies of S, more studies regarding $H_{(2,2)}(f)$ can be seen in [6–12]. According to Thomas' conjecture [13], if $f \in S$, then $|H_{(q,2)}(f)| \le 1$, but it was shown by Li and Srivastava in [14] that this conjecture is not true for $n \ge 4$. Also, Raducanu and Zaprawa [15] showed that it is false for $n = 2$. Rather, they showed that $\max\{|H_{(2,2)}(f)|: f \in S\} \ge 1.175$. As compared to $|H_{(2,2)}(f)|$, estimation of $|H_{(3,1)}(f)|$ is much more difficult. Babalola [16] published the first paper on $H_{(3,1)}(f)$ in 2010 in which he obtained the upper bound of $|H_{(3,1)}(f)|$ for subfamilies of S^*, C, and R. After that, for different subfamilies of analytic and univalent functions, few other authors [17–25] also published their work regarding $|H_{(3,1)}(f)|$. Zaprawa [26] improved the results of Babalola [16] recently in 2017, by showing

$$|H_{(3,1)}(f)| \le \begin{cases} 1 \text{ for } f \in S^*, \\ \dfrac{49}{540} \text{ for } f \in C, \\ \dfrac{41}{60} \text{ for } f \in R. \end{cases} \quad (6)$$

He claimed that these bounds are not sharp. Furthermore, he considered the subfamilies of S^*, C, and R for sharpness, having functions with m-fold symmetry, and obtained the sharp bounds. Arif et al. [27–30] made a remarkable contribution in studying the fourth- and fifth-order Hankel determinants $H_{(4,1)}(f)$ and $H_{(5,1)}(f)$ for certain subfamilies of univalent functions. Mashwani et al. [31] have studied the fourth-order Hankel determinant for starlike functions related to sigmoid functions, whereas Kaur et al. [32] studied the same problem for a subclass of bounded turning functions. Wang et al. [33] studied the problem for bounded turning functions related to the lemniscate of Bernoulli. Recently, Zhang and Tang [34] have studied the fourth-order Hankel determinant for the class of starlike functions related to sine functions. Motivated by the above-mentioned work, we intend to add some contributions to the fourth-order Hankel determinant for the class of convex functions associated with sine functions. Recently, the following class C_s of convex functions was introduced, which is associated with the sine function:

$$C_s = \left\{ f \in A: \frac{(zf'(z))'}{f'(z)} \prec 1 + \sin z \ (z \in D) \right\}, \quad (7)$$

where $\prec$ is a subordination symbol and it also implies that the region defined by $(zf'(D))'/f'(D)$ lies in the eight-shaped region in the right-half plane. For different subfamilies of univalent functions, growth of $H_{q,n}(f)$ has been studied for fixed values of q and n. Particularly, we have

$$H_{4,1}(f) = \begin{vmatrix} a_1 & a_2 & a_3 & a_4 \\ a_2 & a_3 & a_4 & a_5 \\ a_3 & a_4 & a_5 & a_6 \\ a_4 & a_5 & a_6 & a_7 \end{vmatrix} (n = 1, q = 4). \quad (8)$$

Also, Thomas and Halim defined the symmetric Toeplitz determinant $T_q(n)$ as follows:

$$T_{q,n}(f) = \begin{vmatrix} a_n & a_{n+1} & \cdots & a_{n+q-1} \\ a_{n+1} & a_n & \cdots & a_{n+q} \\ \vdots & \vdots & \cdots & \vdots \\ a_{n+q-1} & a_{n+q} & \cdots & a_n \end{vmatrix} (n \ge 1, q \ge 1). \quad (9)$$

The Toeplitz determinants are closely related to Hankel determinants. As Hankel matrices consist of constant entries along the reverse diagonal, the Toeplitz matrices consist of constant entries along the diagonal.

As a special case, when $n = 1$ and $q = 4$, we have

$$T_{4,2}(f) = \begin{vmatrix} a_1 & a_2 & a_3 & a_4 \\ a_2 & a_1 & a_4 & a_3 \\ a_3 & a_4 & a_1 & a_2 \\ a_4 & a_3 & a_2 & a_1 \end{vmatrix}. \quad (10)$$

In this paper, we intend to find the upper bound of $|H_{4,1}(f)|$ and $|T_{4,2}(f)|$ for the class of functions defined by (6). The following sharp results would be useful for investigating our main results.

Lemma 1. *If $p \in P$ and p is of form (2), then for each $n, k, m, l \in \mathbb{N} = \{1, 2, \ldots\}$, the following sharp inequalities hold:*

$$|c_n| \le 2,$$

$$|c_{n+k} - \mu c_n c_k| \le \begin{cases} 2, \text{ for } 0 \le \mu \le 1 \\ 2|2\mu - 1|, \text{ elsewhere} \end{cases}, \quad (11)$$

$$c_{n+2k} - c_n c_k^2 \le 6, \quad (12)$$

$$|c_n c_k - c_m c_l| \le 4, \quad \text{for } n + k = m + l. \quad (13)$$

Inequalities (10)–(12) are proved in [26, 35, 36], respectively. Inequality (13) is obvious.

Libera and Złotkiewicz proved the following result [37].

Lemma 2. *Let $p \in P$ be of form (2). Then, the modulus of the expressions*

$$\begin{aligned} A_3 &= c_1^3 - 2c_1c_2 + c_3, \\ A_4 &= c_1^4 + c_2^2 + 2c_1c_3 - 3c_1^2c_2 - c_4, \\ A_5 &= c_1^5 + 3c_1c_2^2 + 3c_1^2c_3 - 4c_1^3c_2 - 2c_1c_4 - 2c_2c_3 + c_5, \\ A_6 &= c_1^6 + 6c_1^2c_2^2 + 4c_1^3c_3 + 2c_1c_5 + 2c_2c_4 + c_3^2 \\ &\quad - c_2^3 - 5c_1^4c_2 - 3c_1^2c_4 - 6c_1c_2c_3 - c_6 \end{aligned} \tag{14}$$

are all bounded by 2.

2. Main Results

2.1. Bounds of $|H_{4,1}(f)|$ and $|T_{4,2}(f)|$ for the Set C_s Connected with the Sine Function. Following (7), we can write $H_{4,1}(f)$, where $f \in S$ and $a_1 = 1$, as

$$H_{4,1}(f) = a_7 H_{3,1}(f) - a_6 R_1 + a_5 R_2 - a_4 R_3, \tag{15}$$

where

$$H_{3,1}(f) = \left(a_3a_5 - a_4^2\right) - a_2\left(a_2a_5 - a_3a_4\right) + a_3\left(a_2a_4 - a_3^2\right) \tag{16}$$

and R_1, R_2, and R_3 are determinants of order 3, given by

$$R_1 = \left(a_3a_6 - a_4a_5\right) - a_2\left(a_2a_6 - a_3a_5\right) + a_4\left(a_2a_4 - a_3^2\right), \tag{17}$$

$$R_2 = \left(a_4a_6 - a_5^2\right) - a_2\left(a_3a_6 - a_4a\right)_5 + a_3\left(a_3a_5 - a_4^2\right), \tag{18}$$

$$R_3 = a_2\left(a_4a_6 - a_5^2\right) - a_3\left(a_3a_6 - a_4a_5\right) + a_4\left(a_3a_5 - a_4^2\right). \tag{19}$$

Also,

$$T_{4,1}(f) = a_1C_1 - a_2C_2 + a_3C_3 - a_4C_4, \tag{20}$$

where

$$C_1 = a_1\left(a_1^2 - a_2^2\right) - a_4\left(a_1a_4 - a_2a_3\right) + a_3\left(a_4a_2 - a_1a_3\right), \tag{21}$$

$$\begin{aligned} C_2 &= a_2\left(a_1^2 - a_2^2\right) - a_4\left(a_1a_3 - a_2a_4\right) + a_3\left(a_2a_3 - a_1a_4\right), \\ C_3 &= a_2\left(a_1a_4 - a_2a_3\right) - a_3\left(a_1^2 - a_3^2\right) + a_4\left(a_1a_2 - a_3a_4\right), \\ C_4 &= a_2\left(a_2a_4 - a_1a_3\right) - a_3\left(a_1a_2 - a_3a_4\right) + a_4\left(a_1^2 - a_4^2\right). \end{aligned} \tag{22}$$

As, from (7), $H_{4,1}(f)$ is a polynomial of six coefficients of function f of the given class, these coefficients are taken as a_2, a_3, a_4, a_5, a_6, and a_7. However, there is a connection between these coefficients and the coefficients of function p in the class P in many problems. Consider that $f \in C_s$ has form (1); then, there is a Schwartz function $w(z)$ with $w(0) = 0$ and $|w(z)| < 1$, such that

$$\frac{(zf'(z))'}{f'(z)} = 1 + \sin(w(z)). \tag{23}$$

Now,

$$\begin{aligned} \frac{(zf'(z))'}{f'(z)} &= \frac{1 + \sum_{n=2}^{\infty} n^2 a_n z^{n-1}}{1 + \sum_{n=2}^{\infty} n a_n z^{n-1}} \\ &= 1 + 2a_2 z + \left(6a_3 - 4a_2^2\right)z^2 \\ &\quad + \left(-18a_2a_3 + 12a_4 + 8a_2^3\right)z^3 \\ &\quad + \left(-32a_2a_4 + 20a_5 - 18a_3^2 + 48a_3a_2^2 - 16a_2^4\right)z^4 \\ &\quad + \left(-50a_2a_5 + 30a_6 - 60a_4a_3 \right. \\ &\quad \left. + 80a_4a_2^2 + 90a_2a_3^2 - 120a_3a_2^3 + 32a_2^5\right)z^5 + \ldots \end{aligned} \tag{24}$$

Consider

$$p(z) = \frac{1 + w(z)}{1 - w(z)} = 1 + c_1 z + c_2 z^2 + c_3 z^3 + \cdots. \tag{25}$$

Since we have $p \in P$,

$$w(z) = \frac{p(z) - 1}{1 + p(z)} = \frac{c_1 z + c_2 z^2 + c_3 z^3 + \cdots}{2 + c_1 z + c_2 z^2 + c_3 z^3 + \cdots}. \tag{26}$$

Also,

$$\begin{aligned} 1 + \sin(w(z)) &= 1 + \frac{1}{2}c_1 z + \left(\frac{1}{2}c_2 - \frac{1}{4}c_1^2\right)z^2 + \left(\frac{1}{2}c_3 - \frac{1}{2}c_1c_2 + \frac{5}{48}c_1^3\right)z^3 \\ &\quad + \left(\frac{5}{16}c_2c_1^2 - \frac{1}{32}c_1^4 + \frac{1}{2}c_4 - \frac{1}{2}c_1c_3 - \frac{1}{4}c_2^2\right)z^4 \\ &\quad + \left(\frac{1}{3840}c_1^5 + \frac{5}{16}c_1c_2^2 - \frac{1}{8}c_2c_1^3 - \frac{1}{2}c_2c_3 + \frac{5}{16}c_3c_1^2 \right. \\ &\quad \left. - \frac{1}{2}c_1c_4 + \frac{1}{2}c_5\right)z^5 + \cdots. \end{aligned} \tag{27}$$

On comparing coefficients between (25) and (28), we get

$$\begin{aligned} a_2 &= \frac{1}{4}c_1, \\ a_3 &= \frac{1}{12}c_2, \\ a_4 &= -\frac{1}{96}c_1c_2 - \frac{1}{576}c_1^3 + \frac{1}{24}c_3, \\ a_5 &= -\frac{1}{960}c_2c_1^2 + \frac{1}{1152}c_1^4 - \frac{1}{120}c_1c_3 - \frac{1}{160}c_2^2 + \frac{1}{40}c_4, \\ a_6 &= -\frac{11}{28800}c_1^5 + \frac{71}{34560}c_2c_1^3 + \left(\frac{1}{1152}c_2^2 - \frac{1}{160}c_4\right)c_1 - \frac{7}{720}c_2c_3 + \frac{1}{60}c_5, \end{aligned} \tag{28}$$

and

$$\begin{aligned}a_7 = {} & \frac{2399}{14515200}c_1^6 - \frac{347}{241920}c_2c_1^4 + \frac{1}{756}c_3c_1^3 + \left(\frac{1}{3360}c_4 + \frac{29}{16128}c_2^2\right)c_1^2 \\ & + \left(-\frac{1}{210}c_5 + \frac{23}{10080}c_2c_3\right)c_1 + \frac{1}{84}c_6 - \frac{1}{252}c_3^2 + \frac{5}{8064}c_2^3 - \frac{5}{672}c_4c_2.\end{aligned} \tag{29}$$

By using these coefficients, we can write (16)–(19) in the following way:

$$\begin{aligned}H_{3,1}(f) = {} & -\frac{19}{331776}c_1^6 + \frac{1}{34560}c_2c_1^4 + \frac{23}{34560}c_3c_1^3 + \left(-\frac{11}{46080}c_2^2 - \frac{1}{640}c_4\right)c_1^2 \\ & + \frac{11}{5760}c_3c_1c_2 + \frac{1}{12}c_2\left(\frac{1}{40}c_4 - \frac{1}{160}c_2^2\right) - \frac{1}{1728}c_2^3 - \frac{1}{576}c_3^2,\end{aligned} \tag{30}$$

$$\begin{aligned}R_1 = {} & \frac{289}{11059200}c_1^7 - \frac{29}{230400}c_2c_1^5 - \frac{1}{11520}c_3c_1^4 + \left(\frac{187}{1658880}c_2^2 + \frac{1}{2304}c_4\right)c_1^3 \\ & + \left(\frac{1}{5760}c_2c_3 - \frac{1}{960}c_5\right)c_1^2 + \frac{1}{12}c_2\left(\frac{1}{1152}c_2^2 - \frac{1}{160}c_4\right) + \frac{1}{1280}c_3^2 + \frac{1}{32}c_2\left(\frac{1}{40}c_4 - \frac{1}{160}c_2^2\right) + \frac{1}{13824}c_2^3c_1 \\ & + \frac{1}{12}c_2\left(-\frac{7}{720}c_2c_3 + \frac{1}{60}c_5\right) - \frac{1}{3456}c_3c_2^2 - \frac{1}{24}c_3\left(\frac{1}{40}c_4 - \frac{1}{160}c_2^2\right), \\ & + \frac{1}{12}c_2\left(-\frac{7}{720}c_2c_3 + \frac{1}{60}c_5\right) - \frac{1}{3456}c_3c_2^2 - \frac{1}{24}c_3\left(\frac{1}{40}c_4 - \frac{1}{160}c_2^2\right),\end{aligned} \tag{31}$$

$$\begin{aligned}R_2 = {} & -\frac{31}{66355200}c_1^8 + \frac{101}{12441600}c_2c_1^6 + \frac{31}{2764800}c_3c_1^5 + \left(-\frac{197}{4147200}c_2^2 - \frac{1}{23040}c_4\right)c_1^4 \\ & + \left(\frac{7}{64800}c_2c_3 - \frac{1}{34560}c_5\right)c_1^3 + \left(-\frac{1}{6400}c_3^2 + \frac{7}{38400}c_2c_4 - \frac{37}{921600}c_2^3\right)c_1^2 \\ & + \left(\frac{1}{5400}c_2^2c_3 - \frac{1}{1920}c_2c_5 + \frac{1}{2400}c_3c_4\right)c_1 + \frac{1}{1440}c_3c_5 + \frac{7}{14400}c_2^2c_4 - \frac{1}{1600}c_4^2 \\ & - \frac{19}{230400}c_2^4 - \frac{19}{34560}c_2c_2^3,\end{aligned} \tag{32}$$

and

$$\begin{aligned}R_3 = {} & -\frac{83}{4777574400}c_1^9 + \frac{317}{796262400}c_2c_1^7 - \frac{49}{66355200}c_3c_1^6 \\ & + \left(-\frac{1}{122880}c_4\right. \\ & \left.-\frac{169}{132710400}c_2^2\right)c_1^5\left(-\frac{1}{138240}c_5 + \frac{209}{8294400}c_2c_3\right)c_1^4 + \frac{61}{2764800} \\ & c_2c_4 - \frac{23}{2764800}c_3^2 - \frac{2993}{199065600}c_2^3\Big)c_1^3 \\ & + \left(-\frac{1}{23040}c_2c_5 + \frac{11}{5529600}c_2^2c_3\right) \\ & + \frac{1}{25600}c_3c_4\Big)c_1^2 + \left(\frac{1}{12800}c_2^2c_4 - \frac{41}{8294400}c_2^4\right. \\ & + \frac{1}{5760}c_3c_5 - \frac{1}{6400}c_4^2 - \\ & \left.\frac{29}{276480}c_2c_3^2\right)c_1 - \frac{1}{8640}c_2^2c_5 + \frac{1}{41472}c_2^3c_3 \\ & - \frac{1}{13824}c_3^3 + \frac{1}{5760}c_2c_3c_4.\end{aligned} \tag{33}$$

Similarly, in case of Toeplitz determinants,

$$\begin{aligned}C_1 = {} & -\frac{1}{331776}c_1^6 - \frac{1}{9216}c_1^4c_2 + \frac{1}{6912}c_1^3c_3 + \left(-\frac{1}{16} - \frac{5}{9216}c_2^2\right)c_1^2 \\ & + \frac{1}{384}c_1c_2c_3 + 1 - \frac{1}{576}c_3^2 - \frac{1}{144}c_2^2,\end{aligned} \tag{34}$$

$$\begin{aligned}C_2 = {} & \frac{1}{1327104}c_1^7 + \frac{1}{110592}c_1^5c_2 - \frac{1}{27648}c_1^4c_3 + \left(\frac{1}{36864}c_2^2 - \frac{1}{64}\right. \\ & \left.+\frac{1}{3456}c_2\right)c_1^3 - \frac{1}{4608}c_1^2c_2c_3 + \left(\frac{1}{4} + \frac{1}{288}c_2^2 + \frac{1}{2304}c_3^2\right)c_1 \\ & - \frac{1}{144}c_3c_2,\end{aligned} \tag{35}$$

$$\begin{aligned}C_3 = {} & -\frac{1}{3981312}c_1^6c_2 + \left(-\frac{1}{1152} - \frac{1}{331776}c_2^2\right)c_1^4 \\ & + \frac{1}{82944}c_1^3c_3c_2 + \\ & \left(-\frac{1}{110592}c_2^3 - \frac{1}{96}c_2\right)c_1^2 + \left(\frac{1}{48}c_3 + \frac{1}{13824}c_2^2c_3\right)c_1 + \frac{1}{1728} \\ & c_2^3 - \frac{1}{6912}c_3^2c_2 - \frac{1}{12}c_2,\end{aligned} \tag{36}$$

$$C_4 = \frac{1}{191102976}c_1^9 + \frac{1}{10616832}c_1^7c_2 - \frac{1}{2654208}c_1^6c_3 + \left(\frac{1}{1769472}c_2^2 - \frac{1}{9216}\right)c_1^5 - \frac{1}{221184}c_1^4c_2c_3 + \left(\frac{1}{884736}c_2^3 - \frac{1}{1536}c_2 - \frac{1}{82944}c_2^2 + \frac{1}{110592}c_3^2 - \frac{1}{576}\right)c_1^3 + \left(\frac{1}{384}c_3 - \frac{1}{73728}c_2^2c_3\right)c_1^2 + \left(-\frac{15}{96}c_2 + \frac{1}{18432}c_3^2c_2 - \frac{1}{13824}c_2^3\right)c_1 + \frac{1}{24}c_3 - \frac{1}{13824}c_3^3 + \frac{1}{3456}c_2^2c_3. \tag{37}$$

By using the previous computations, we prove the following.

Theorem 1. *If the function $f \in C_s$ and is of form (1), then*

$$\left|H_{4,1}(f)\right| \le \frac{112267159597}{15049359360000} \approx 0.0074599\cdots. \tag{38}$$

Proof. As $f \in C_s$, then by using (30)–(33) in (15), we get

$$\begin{aligned} H_{4,1}(f) = {} & \frac{38723}{481579499520000}c_1^{12} + \frac{23}{2322432}c_3^4 - \frac{1159}{6967296000}c_2^6 \\ & - \frac{4169}{6967296000}c_1^7c_5 - \frac{19}{27869184}c_6c_1^6 \\ & - \frac{19}{1451520}c_6c_2^3 - \frac{1}{48384}c_6c_3^2 - \frac{17}{6967296}c_3^2c_2^3 + \frac{2539}{580608000}c_2^4c_4 + \frac{1}{1792000}c_2^2c_4^2 \\ & + \frac{1}{57600}c_1^2c_5^2 - \frac{1}{43200}c_2c_5^2 - \frac{1}{64000}c_4^3 + \frac{1619}{580608000}c_1^3c_3c_2c_4 - \frac{1}{67200}c_1^2c_5c_2c_3 - \frac{1}{53760}c_1c_5c_2c_4 \\ & - \frac{713}{48384000}c_2^2c_1c_3c_4 + \frac{11}{483840}c_6c_2c_1c_3 + \frac{247}{58060800}c_2c_1c_3^3 + \frac{589}{145152000}c_1^5c_5c_2 \\ & + \frac{53}{36864000}c_2c_1^4c_3^2 + \frac{23}{2903040}c_6c_1^3c_3 + \frac{563}{32256000}c_1^2c_4^2c_2 + \frac{1}{64000}c_1c_4^2c_3 + \frac{29}{1036800}c_2^2c_3c_5 \\ & + \frac{1}{28800}c_5c_3c_4 - \frac{913}{348364800}c_1^3c_5c_2^2 - \frac{43}{2419200}c_1c_5c_3^2 - \frac{3019}{1032192000}c_2^2c_1^5c_3 \\ & - \frac{11}{3870720}c_6c_1^2c_2^2 + \frac{67}{9676800}c_1c_5c_2^3 + \frac{1}{2903040}c_6c_2c_1^4 + \frac{151}{96768000}c_1^2c_4c_3^2 + \frac{251}{139345920}c_1^6c_2c_4 \\ & + \frac{1073}{580608000}c_1^2c_4c_2^3 - \frac{11077}{55738368000}c_1^7c_2c_3 + \frac{1}{40320}c_6c_2c_4 - \frac{1}{3628800}c_1^4c_5c_3 \\ & - \frac{1919}{1741824000}c_2^4c_1c_3 - \frac{29}{20736000}c_1^5c_3c_4 - \frac{1}{53760}c_6c_1^2c_4 - \frac{30703}{4644864000}c_2^2c_1^4c_4 \\ & + \frac{195313}{41803776000}c_1^3c_3c_2^3 + \frac{4699}{2322432000}c_1^2c_2^2c_3^2 - \frac{17}{2419200}c_1^3c_5c_4 - \frac{1}{37800}c_3^2c_2c_4 \\ & - \frac{136291}{20065812480000}c_1^{10}c_2 + \frac{14201}{1003290624000}c_1^9c_3 + \frac{67139}{1337720832000}c_1^8c_2^2 - \frac{77}{7962624000}c_1^8c_4 \\ & - \frac{40073}{1003290624000}c_1^6c_2^3 + \frac{8419}{9289728000}c_1^6c_3^2 + \frac{852083}{668860416000}c_2^4c_1^4 \\ & - \frac{5947}{1741824000}c_1^3c_3^3 + \frac{1}{2867200}c_1^4c_4^2 - \frac{391}{217728000}c_1^2c_2^5. \end{aligned} \tag{39}$$

$$
\begin{aligned}
H_{4,1}(f) = \frac{1}{481579499520000}\{&38723c_1^{12} - 3270984c_1^{10}c_2 + 6816480c_1^9c_3 \\
&+\big(24170040c_2^2 \\
&- 4656960c_4\big)c_1^8 + (-288161280c_5 - 95705280c_2c_3)c_1^7 + (-328320000c_6 \\
&+ 436440960c_2^2 - 19235040c_2^3 + 867456000c_4c_2)c_1^6 + (-673505280c_3c_4 \\
&-1408544640c_3c_2^2 + 1954160640c_2c_5)c_1^5 + \big(613499760c_2^4 + 165888000c_6c_2 \\
&- 3183287040c_2^2c_4 + 167961600c_4^2 - 132710400c_3c_5 + 692375040c_2c_3^2\big)c_1^4 \\
&+\big(-1644226560c_3^3 + 1342863360c_2c_3c_4 + 2250005760c_2^3c_3 \\
&+3815424000c_6c_3 - 3384115200c_5c_4 - 1262131200c_2^2c_5\big)c_1^3 \\
&+\big(8360755200c_5^2 - 8957952000c_6c_4 - 7166361600c_5c_2c_3 - 1368576000c_6c_2^2 \\
&+ 8405544960c_4^2c_2 + 751472640c_4c_3^2 - 864829440c_2^5 + 974384640c_2^2c_3^2 \\
&+889989120c_4c_2^3\big)c_1^2 + \big(3334348800c_5c_2^3 + 7524679680c_4^2c_3 \\
&+ 10948608000c_6c_2c_3 + 2048716800c_2c_3^3 - 7096688640c_2^2c_3c_4 \\
&-8957952000c_5c_2c_4 - 530565120c_2^4c_3 - 8559820800c_5c_3^2\big)c_1 \\
&- 1175040000c_3^2c_2^3 + 2105948160c_2^4c_4 - 12740198400c_3^2c_2c_4 \\
&+ 11943936000c_6c_2c_4 + 16721510400c_5c_3c_4 - 7524679680c_4^3 + 4769280000c_3^4 \\
&- 80110080c_2^6 - 9953280000c_6c_3^2 - 11147673600c_2c_5^2 + 13470105600c_2^2c_3c_5 \\
&- 6303744000c_6c_2^3 + 268738560c_2^2c_4^2\}.
\end{aligned}
\tag{40}
$$

After rearranging the terms, we get

$$
\begin{aligned}
H_{4,1}(f) = {} & \frac{1}{481579499520000} \\
&\cdot \big\{-38723A_6\big(c_2 - c_1^2\big)^3 - 2961200c_2A_5^2 + 6661588c_3A_3A_6 \\
&- 448912A_6(c_3 - c_1c_2)^2 - 45407915c_4A_3A_5 - 288238726c_1 \\
&A_6\left(c_5 - \frac{1}{288238726}c_2c_3\right) - 328281275A_6\left(c_6 - \frac{403543209}{328281275}c_3^2\right) - A_6(c_6 - 827940501c_2c_4) - A_6 \\
&\cdot\big(c_6 - 45022105c_2^3\big) + 519121748c_2A_5\left(c_5 - \frac{1592920565}{519121748}c_2c_3\right) + 635357352 \\
&\cdot c_3A_4(c_5 - c_1c_4) - 1475634554c_2A_4\left(c_6 - \frac{2857592366}{1475634554}c_3^2\right) - 371563976c_5A_3 \\
&\cdot (c_4 - c_1c_3) + 158880018c_4^2A_3c_1 + 769228159c_2^4A_3c_1 + 1052977475c_2^2c_4A_3c_1 \\
&+ 5135210696\big(c_2 - c_1^2\big)(c_4 - c_1c_3)\left(c_6 - \frac{3289911688}{5135210696}c_3^2\right) - 3872726611\big(c_2 - c_1^2\big) \\
&\cdot\left(c_4 - \frac{2520764034}{3872726611}c_2^2\right)(c_6 - c_1c_5) - 4015593821A_3c_2c_4c_3 - 4121711992A_3c_3c_2^3 \\
&- 8680311746c_4c_1^2\left(c_6 - \frac{11237134463}{8680311746}c_2c_4\right) - 24834316c_3^2c_1^2
\end{aligned}
$$

$$
\begin{aligned}
&\cdot\left(c_4-\frac{11757634360}{24834316}c_2^2\right)-8937232652c_5\left(c_2-c_1^2\right)\left(c_5-\frac{7761341290}{8937232652}c_2c_3\right)\\
&-1898862450c_2^3c_1^2\left(c_4-\frac{430044643}{1898862450}c_2^2\right)-1305360709c_2^2c_1^2c_6+17052974791\\
&\cdot c_3c_2c_1\left(c_6-\frac{13683368690}{17052974791}c_2c_4\right)-13635892999c_5c_2c_1\left(c_4-\frac{3937309300}{13635892999}c_2^2\right)\\
&+\left(-4485418959c_2c_3^3-4542515027c_2^4c_3+6721360728c_4^2c_3\right)c_1+368323828c_5c_1\\
&\cdot\left(c_6-\frac{10733372524}{368323828}c_3^2\right)-2726601496c_2c_5\left(c_5-\frac{7692726219}{2726601496}c_2c_3\right)+10690320416\\
&\cdot c_2c_4\left(c_6-\frac{4233634378}{10690320416}c_3^2\right)+2843921897c_2^4\left(c_4-\frac{35126698}{2843921897}c_2^2\right)-9215242838\\
&\cdot c_3^2\left(c_6-\frac{4359524115}{9215242838}c_3^2\right)-7632171375c_6c_2^3-2720144201c_3^2c_2^3+17732972519\\
&\cdot c_5c_3c_4-328281277c_6^2-7524679680c_4^3-31507775c_2c_1^7c_3-1387142442c_2^2c_4^2.
\end{aligned}
\tag{41}
$$

After using triangular inequalities and lemmas, we get the following expression:

$$
\begin{aligned}
\left|H_{4,1}(f)\right|=&\frac{1}{481579499520000}\\
&\left\{(38723\times 2)\times 2^3+4(2961200\times 2)+4\times(6661588\times 2)+(448912\times 2)\times\right.\\
&2^2+2\times(45407915\times 2)\times 2+2(288238726\times 2)\times 2+\frac{957610286}{328281275}\times(328281275\times 2)+2\times\\
&3311762002+2\times 3311762002+2\times(519121748\times 2)\times\frac{1333359691}{129780437}+2\times(635357352\times 2)\\
&\times 2+2\times(1475634554\times 2)\times\frac{4239550178}{737817277}+371563976\times(2)\times(2)\times(2)+158880018\times(4)\\
&\times(2)\times(2)+769228159\times(16)\times(2)\times(2)+1052977475\times(4)\times(2)\times(2)\times(2)\\
&+5135210696\times(2)\times(2)\times\frac{51593310}{91700191}+872726611\times(2)\times(2)\times(2)+4015593821\times(16)\\
&+4121711992\times(32)+8680311746\times(8)\times\frac{13793957180}{4340155873}+24834316\times(16)\times\frac{11745217202}{6208579}\\
&+8937232652\times(2)\times(2)\times(2)+1898862450\times(32)\times(2)+1305360709\times(32)\\
&+17052974791\times(8)\times(2)++13635892999\times(8)\times(2)+(4485418959\\
&+6721360728\times(8)\times(2)+368323828\times(4)\times\frac{10549210610}{92080957}+2726601496\times(4)\times\frac{6329425471}{681650374}\\
&+10690320416\times(4)\times(2)+2843921897\times(16)\times(2)+9215242838\times(4)\times(2)\\
&+7632171375\times(16)+2720144201\times(32)+17732972519\times(8)+328281277\times(4)\\
&\left.+7524679680\times(8)+31507775\times(512)+1387142442\times(16)\right\}.
\end{aligned}
\tag{42}
$$

Hence,

$$\left|H_{4,1}(f)\right| \le \frac{3592549107104}{481579499520000} \approx 0.0074599, \tag{43}$$

which completes the proof. □

Theorem 2. *If the function $f \in C_s$ and is of form (1), then*

$$\left|T_{4,1}(f)\right| \le \frac{501434459}{286654464} \approx 1.7493. \tag{44}$$

Proof. As $f \in C_s$, using (34)–(37) in (20), we get

$$\begin{aligned}
T_{4,1}(f) = {} & 1 + \frac{1}{256}c_1^4 - \frac{1}{288}c_3^2 - \frac{1}{165888}c_1^6 - \frac{1}{8}c_1^2 - \frac{1}{72}c_2^2 + \frac{5}{576}c_1c_2c_3 + \frac{1}{9216}c_1^3c_3c_2 \\
& + \frac{1}{3456}c_1^3c_3 - \frac{1}{221184}c_1^6c_2 + \frac{1}{497664}c_1^3c_3c_2^2 - \frac{1}{5308416}c_1^3c_2^3c_3 \\
& + \frac{1}{82944}c_1c_2^3c_3 - \frac{1}{331776}c_1c_2c_3^3 + \frac{1}{884736}c_1^2c_2^2c_3^2 - \frac{1}{10616832}c_1^5c_2^2c_3 \\
& - \frac{1}{63700992}c_1^7c_2c_3 + \frac{1}{2654208}c_1^4c_2c_3^2 - \frac{13}{4608}c_1^2c_2^2 + \frac{1}{55296}c_1^5c_3 \\
& - \frac{1}{73728}c_1^4c_2^2 - \frac{1}{4608}c_1^2c_3^2 - \frac{1}{23887872}c_1^6c_2^2 - \frac{1}{1990656}c_1^4c_2^3 \\
& - \frac{1}{663552}c_1^2c_2^4 - \frac{1}{41472}c_2^2c_3^2 + \frac{1}{84934656}c_1^4c_2^4 + \frac{1}{127401984}c_1^6c_2^3 \\
& + \frac{1}{509607936}c_1^8c_2^2 + \frac{1}{4586471424}c_1^{10}c_2 - \frac{1}{1146617856}c_1^9c_3 + \frac{1}{31850496}c_1^6c_3^2 \\
& - \frac{1}{1990656}c_1^3c_3^3 - \frac{1}{2654208}c_1^8 + \frac{1}{20736}c_2^4 + \frac{1}{110075314176}c_1^{12}.
\end{aligned} \tag{45}$$

Rearranging the terms, we may write

$$\begin{aligned}
T_{4,1}(f) = {} & \frac{1}{110075314176}\Big\{c_1^{12} + 24c_1^{10}c_2 - 96c_1^9c_3 + \left(-41472 + 216c_2^2\right)c_1^8 - 1728c_1^7c_2c_3 \\
& + \left(-663552 + 3456c_3^2 - 497664c_2 + 864c_2^3 - 4608c_2^2\right)c_1^6 \\
& + \left(-10368c_2^2c_3 + 1990656c_3\right)c_1^5 \\
& + \left(-1492992c_2^2 + 41472c_3^2c_2 - 55296c_2^3 - 39813120c_2 + 1296c_2^4 + 429981696\right)c_1^4 \\
& + \left(11943936c_2c_3 + 31850496c_3 - 55296c_3^3 - 20736c_2^3c_3 + 221184c_3c_2^2\right)c_1^3 \\
& + \left(-310542336c_2^2 - 13759414272 + 124416c_2^2c_3^2 - 165888c_2^4 - 23887872c_3^2\right)c_1^2 \\
& + \left(1327104c_2^3c_3 + 955514880c_2c_3 - 331776c_2c_3^3\right)c_1 \\
& - 1528823808c_2^2 - 382205952c_3^2 + 331776c_3^4 + 5308416c_2^4 \\
& + 110075314176 - 2654208c_2^2c_3^2\Big\}.
\end{aligned} \tag{46}$$

After rearranging the terms, we get

$$
\begin{aligned}
T_{4,1}(f) = {} & \frac{1}{110075314176}\Big\{-A_6\big(c_2-c_1^2\big)^3-100A_3A_6\Big(c_3-\frac{32}{100}c_1c_2\Big)-2c_1A_6\Big(c_5-\frac{3}{2}c_1c_4\Big)\\
& -2570c_1c_2A_6\Big(c_3-\frac{416}{2570}c_1c_2\Big)-41472A_3A_5+2156544A_5\Big(c_3-\frac{746496}{2156544}c_1c_2\Big)\\
& -22704c_2^2A_5\Big(c_3-\frac{2467}{22704}c_1c_2\Big)-312c_4A_5\Big(c_3-\frac{100}{312}c_1c_2\Big)+29c_2A_4\Big(c_6-\frac{68}{29}c_1c_5\Big)\\
& +\big(-663552+c_6-4608c_2^2+3955c_3^2\big)A_6+22311936c_2A_3\Big(c_3-\frac{4022784}{22311936}c_1c_2\Big)\\
& -902c_2^2A_3\Big(c_5-\frac{1389}{902}c_1c_4\Big)-12A_3c_4\Big(c_5-\frac{9}{12}c_1c_4\Big)-104c_3A_3\Big(c_6-\frac{208}{104}c_1c_5\Big)\\
& -70616c_3^2A_3\Big(c_3-\frac{69470}{70616}c_1c_2\Big)-102891c_2^3A_3\Big(c_3-\frac{9058}{102891}c_1c_2\Big)+239616c_2^2A_3\\
& \Big(c_3-\frac{78336}{239616}c_1c_2\Big)+41472A_3\Big(c_5-\frac{82944}{41472}c_1c_4\Big)+12498c_3c_4c_1^2\Big(c_3-\frac{8344}{12498}c_1c_2\Big)\\
& +\big(5c_6c_2-4313088c_2+429981696\big)A_4+34504704c_3A_3-633c_4^2c_1\Big(c_3-\frac{212}{633}c_1c_2\Big)\\
& +4313088c_3c_1\Big(c_4-\frac{30233088}{4313088}c_1c_3\Big)-188c_5c_2c_1\Big(c_4-\frac{5216}{188}c_1c_3\Big)+1857024\\
& c_2^3c_1\Big(c_3-\frac{294912}{1857024}c_1c_2\Big)-144138c_2^4c_1\Big(c_3-\frac{11076}{144138}c_1c_2\Big)-859963392c_1.
\end{aligned}
\tag{47}
$$

$$
\begin{aligned}
& \Big(c_3-\frac{1289945088}{859963392}c_1c_2\Big)-4c_6c_1\Big(c_5-\frac{6}{4}c_1c_4\Big)-517010c_2c_3^2c_1\Big(c_3-\frac{293955}{517010}c_1c_2\Big)\\
& +746496c_2c_1\Big(c_5-\frac{1492992}{746496}c_1c_4\Big)+9216c_2^2c_1\Big(c_5-\frac{13824}{9216}c_1c_4\Big)-2608c_6c_2c_1\\
& \Big(c_3-\frac{451}{2608}c_1c_2\Big)+40974336c_2^2c_1\Big(c_3-\frac{6054912}{40974336}c_1c_2\Big)-40985c_2^2c_4c_1\\
& \Big(c_3-\frac{6702}{40985}c_1c_2\Big)+1106804736c_2c_1\Big(c_3-\frac{435953664}{1106804736}c_1c_2\Big)\\
& +\big(4c_5^2-1990656c_4-13759414272\big)c_1^2+23606c_2^2c_5\Big(c_3-\frac{4203}{23606}c_1c_2\Big)+3958c_3^2\\
& \Big(c_6-\frac{7916}{3958}c_1c_5\Big)-41803776c_2\Big(c_4-\frac{42467328}{41803776}c_2^2\Big)+429981696\\
& \Big(c_4-\frac{1958805504}{429981696}c_2^2\Big)+9216c_2^3\Big(c_4-\frac{4608}{9216}c_2^2\Big)+32c_2c_6\Big(c_4-\frac{34}{32}c_2^2\Big)\\
& +2c_2^4\Big(c_4-\frac{1}{2}c_2^2\Big)-8334c_3^2c_2\Big(c_4-\frac{61339}{8334}c_2^2\Big)-663552\Big(c_6-\frac{1327104}{663552}c_1c_5\Big)\\
& -4608c_6c_2^2+398537c_3^4+5308416c_2^4+110075314176-416047104c_3^2\\
& +324c_4c_5c_3+c_6^2-18081792c_2c_3^2-2889216c_2^2c_3^2-2156544c_5c_3\Big\}.
\end{aligned}
\tag{48}
$$

After using the triangular inequality and above-stated lemmas, we get

$$\begin{aligned}|T_{4,1}(f)| = {} & \frac{1}{110075314176} \\ & \{2\times(2)^3+100\times(2)\times(2)\times(2)+2\times(2)\times(2)\times(4)+2570\times(2)\times(2)\times \\ & (2)\times(2)+41472\times(2)\times(2)+2156544\times(2)\times(2)+22704\times(4)\times(2)\times(2)+312\times(2)\times \\ & (2)\times(2)+29\times(2)\times(2)\times\frac{214}{29}+(663552+2+4608\times(4)+3955\times4)\times(2)+22311936\times \\ & (2)\times(2)\times(2)+902\times(4)\times(2)\times\frac{1876}{451}+12\times(2)\times(2)(2)+104\times(2)\times(2)\times(6)+ \\ & 70616\times(4)\times(2)\times(2)+102891\times(8)\times(2)\times(2)+2\times(239616\times4)\times2+6\times(41472\times2) \\ & +2\times(2\times(12498\times2)\times4)+(5\times4+43130880\times2+429981696)\times2+34504704\times(2)\times \\ & (2)+2\times(633\times4)\times2+2\times(4313088\times2)\times\frac{677}{26}+\frac{5122}{47}\times(2\times(188\times2)\times2)+2\times \\ & (1857024\times8)\times2+2\times(144138\times16)\times2+4\times(859963392\times2)+2\times(4\times2)\times4+2\times \\ & (4\times(517010\times2)\times2)+2\times(746496\times2)\times6+2\times(9216\times4)\times4+2\times(2\times(2608\times2)) \\ & \times(2)+2\times(40974336\times4)\times2+2\times(2\times(40985\times4)\times2)+2\times((1106804736\times2)\times2)+ \\ & (4\times4+1990656\times2+13759414272)\times4+23606\times(4)\times(2)\times(2)+3958\times(4)\times(6)+ \\ & 41803776\times(2)\times\frac{130}{63}+429981696\times\frac{146}{9}+9216\times(8)\times(2)+32\times(2)\times(2)\times\frac{9}{4}+2 \\ & \times(16)\times(2)+8334\times(4)\times(2)\times\frac{114344}{4167}+663552\times(6)+4608\times(2)\times(4)+398537 \\ & \times(16)+5308416\times(16)+110075314176+416047104\times(4)+324\times(2)\times(2)\times(2)+ \\ & (4)+18081792\times(2)\times(4)+2889216\times(4)\times(4)+2156544\times(2)\times(2)\}.\end{aligned} \tag{49}$$

This reduces to

$$|T_{4,1}(f)| \leq \frac{192550832256}{110075314176} = \frac{501434459}{286654464} \approx 1.7493\cdots, \tag{50}$$

which completes the proof. □

2.2. Bounds of $|H_{4,1}|$ *for the Set* $C_s^{(3)}$. Let $n \in \mathbb{N} = \{1, 2, 3, \ldots\}$. Rotation of a domain $\mathcal{D}$ about the origin through an angle of $2\pi/n$ containing $\mathcal{D}$ onto itself is said to be n-fold symmetric. An analytic function f is n-fold symmetric in D if

$$f\left(e^{2\pi i/n}z\right) = e^{2\pi i/n} f(z) \tag{51}$$

holds for any $z \in D$. Denote $S^{(n)}$ as the set of n-fold univalent functions which have the following Taylor series form:

$$f(z) = z + \sum_{k=1}^{\infty} a_{nk+1} z^{nk+1} \, (z \in D). \tag{52}$$

Denote $C^{(n)}$ as the subfamily of $S^{(n)}$ of n-fold symmetric convex functions. We can see that an analytic function f of form (52) belongs to the family $C^{(n)}$, if and only if

$$\frac{(zf'(z))'}{f'(z)} = p(z), \tag{53}$$

where $p \in P^{(n)}$. The family $P^{(n)}$ is defined as

$$P^{(n)} = \left\{ p \in P\colon\, p(z) = 1 + \sum_{k=1}^{\infty} c_{nk} z^{nk}, \, (z \in D) \right\}. \tag{54}$$

Now, consider the following.

Theorem 3. *Let* $f \in C_s^{(3)}$ *be of form (52). Then,*

$$|H_{4,1}(f)| \leq \frac{1}{6048} \approx 0.00016534. \tag{55}$$

Proof. Let $f \in C_s^{(3)}$ of form (52). Consider the function $p \in P^{(3)}$ as

$$p(z) = \frac{1 + w(z)}{1 - w(z)} = 1 + c_3 z^3 + c_6 z^6 + c_9 z^9 + \cdots. \quad (56)$$

Now,

$$w(z) = \frac{p(z) - 1}{p(z) + 1}. \quad (57)$$

The class $C_s^{(3)}$ which is associated with the sine functions can be written in the following form:

$$\frac{(zf'(z))}{f'(z)} = 1 + \sin(w(z)), \ (z \in D). \quad (58)$$

By expanding and equating them, we get the following expression:

$$1 + 12a_4 z^3 + \left(42a_7 - 48a_4^2\right)z^6 + \cdots = 1 + \frac{1}{2}c_3 z^3 + \left(\frac{1}{2}c_6 - \frac{1}{4}c_3^2\right)z^6 + \cdots. \quad (59)$$

This implies

$$a_4 = \frac{1}{24}c_3, \quad a_7 = -\frac{1}{252}c_3^2 + \frac{1}{84}c_6. \quad (60)$$

By using these coefficients, we can get $H_{3,1}(f)$, R_1, R_2, and R_3 as

$$H_{3,1} = -\frac{1}{576}c_3^2, \quad R_1 = 0, \ R_2 = 0, \quad R_3 = -\frac{1}{13824}c_3^3. \quad (61)$$

By using these values in $H_{4,1}(f)$, we get

$$\begin{aligned} H_{4,1}(f) &= a_7 H_{3,1}(f) - a_6 R_1 + a_5 R_2 - a_4 R_3 \\ &= \left(-\frac{1}{252}c_3^2 + \frac{1}{84}c_6\right)\left(-\frac{1}{576}c_3^2\right) - \left(\frac{1}{24}c_3\right)\left(-\frac{1}{13824}c_3^3\right) \\ &= \frac{23}{2322432}c_3^4 - \frac{1}{48384}c_3^2 c_6 \\ &= -\frac{1}{48384}c_3^2\left(c_6 - \frac{23}{48}c_3^2\right). \end{aligned} \quad (62)$$

The triangle inequality and the application of Lemma 1 lead us to

$$\left|H_{4,1}(f)\right| = \frac{1}{6048} \approx 0.00016534, \quad (63)$$

which completes the proof. □

3. Conclusion

In this paper, we have found the upper bounds of fourth-order Hankel and Toeplitz determinants, followed by a review of such findings obtained so far for certain analytic functions. We have studied them for the convex functions associated with the function $1 + \sin z$. A similar bound of the fourth-order Hankel determinant for 3-fold symmetric convex functions associated with $1 + \sin z$ has also been investigated.

Data Availability

No data were used to support this study.

Conflicts of Interest

The authors declare that there are no conflicts of interest regarding the publication of this article.

Authors' Contributions

All authors contributed equally to this study and approved the final manuscript.

References

[1] C. Pommerenke, "On the coefficients and Hankel determinants of univalent functions," *Journal of the London Mathematical Society*, vol. s1-41, no. 1, pp. 111–122, 1966.

[2] C. Pommerenke, "On the Hankel determinants of univalent functions," *Mathematika*, vol. 14, no. 1, pp. 108–112, 1967.

[3] A. Janteng, S. A. Halim, and M. Darus, "Hankel determinant for starlike and convex functions," *Iernational Journal of Mathematics and Analysisl*, vol. 1, no. 13, pp. 619–625, 2007.

[4] A. Janteng, S. A. Halim, and M. Darus, "Coefficient inequality for a function whose derivative has a positive real part," *Journal of Inequalities in Pure and Applied Mathematicsh*, vol. 7, no. 2, p. 50, 2006.

[5] D. Vamshee Krishna and T. RamReddy, "Second Hankel determinant for the class of Bazilevic functions," *Stud. Univ. Babeş-Bolyai Math.*vol. 60, no. 3, pp. 413–420, 2015.

[6] D. Bansal, "Upper bound of second Hankel determinant for a new class of analytic functions," *Applied Mathematics Letters*, vol. 26, no. 1, pp. 103–107, 2013.

[7] W. K. Hayman, "On the second Hankel determinant of mean univalent functions," *Proceedings of the London Mathematical Society*, vol. s3, no. 1, pp. 77–94, 1968.

[8] D. V. Krishna and T. Ramreddy, "Hankel determinant for starlike and convex functions of order alpha," *Tbilisi Maematical Journal*, vol. 5, pp. 65–76, 2012.

[9] S. K. Lee, V. Ravichandran, and S. Supramaniam, "Bounds for the second Hankel determinant of certain univalent functions," *Journal of Inequalities and Applications*, vol. 2013, no. 1, p. 281, 2013.

[10] M.-S. Liu, J.-F. Xu, and M. Yang, "Upper bound of second Hankel determinant for certain subclasses of analytic functions," *Absact and Applied Analysis*, vol. 2014, Article ID 603180, 10 pages, 2014.

[11] J. W. Noonan and D. K. Thomas, "On the second Hankel determinant of areally mean ?-valent functions," *Transactions of the American Mathematical Society*, vol. 223, pp. 337–346, 1976.

[12] H. Orhan, N. Magesh, and J. Yamini, "Bounds for the second Hankel determinant of certain bi-univalent functions," *Turkish Journal of Mathematics*, vol. 40, no. 3, pp. 679–687, 2016.

[13] R. Parvatham and S. Ponnusamy, *New Trends in Geometric Function Theory and Application*, World Scientific Publishing Company, London, UK, 1981.

[14] J.-L. Li and H. M. Srivastava, "Some questions and conjectures in the theory of univalent functions," *Rocky Mountain Journal of Mathematicsh*, vol. 28, no. 3, pp. 1035–1041, 1998.

[15] D. Raducanu and P. Zaprawa, "Second Hankel determinant for close-to-convex functions," *Comptes Rendus de l'Académie des Sciences*, vol. 355, no. 10, pp. 1063–1071, 2017.

[16] K. O. Babalola, "On H3(1) Hankel determinant for some classes of univalent functions," *Ineq. Theory Appl.*vol. 6, pp. 1–7, 2007.

[17] S. Altinkaya and S. Yalçin, "Third Hankel determinant for Bazilevic functions," *Advances in Mathematics*, vol. 5, no. 2, pp. 91–96, 2016.

[18] S. Banga and S. Sivaprasad Kumar, "The sharp bounds of the second and third Hankel determinants for the class SL∗," *Mathematica Slovaca*, vol. 70, no. 4, pp. 849–862, 2020.

[19] D. Bansal, S. Maharana, and J. K. Prajapat, "Third order Hankel determinant for certain univalent functions," *Journal of the Korean Mathematical Society*, vol. 52, no. 6, pp. 1139–1148, 2015.

[20] O. Barukab, M. Arif, M. Abbas, and S. K. Khan, "Sharp bounds of the coefficient results for the family of bounded turning functions associated with petal shaped domain," *Journal of Function Spaces*, vol. 2021, Article ID 5535629, 2021.

[21] N. E. Cho, B. Kowalczyk, O. S. Kwon, A. Lecko, and Y. J. Sim, "Some coefficient inequalities related to the Hankel determinant for strongly starlike functions of order alpha," *Journal of Mathematical Inequalities*, vol. 11, no. 2, pp. 429–439, 2017.

[22] B. Kowalczyk, A. Lecko, M. Lecko, and Y. J. Sim, "The sharp bound of the third Hankel determinant for some classes of analytic functions," *Bulletin of the Korean Mathematical Society*, vol. 55, no. 6, pp. 1859–1868, 2018.

[23] M. Raza and S. N. Malik, "Upper bound of the third Hankel determinant for a class of analytic functions related with lemniscate of Bernoulli," *Journal of Inequalities and Application*, vol. 412, p. 8, 2013.

[24] G. Shanmugam, B. A. Stephen, and K. O. Babalola, "Third Hankel determinant for α-starlike functions," *Gulf Journal of Mathematics*, vol. 2, no. 2, pp. 107–113, 2014.

[25] D. Vamshee Krishna, B. Venkateswarlu, and T. RamReddy, "Third Hankel determinant for bounded turning functions of order alpha," *Journal of the Nigerian Mathematical Society*, vol. 34, no. 2, pp. 121–127, 2015.

[26] P. Zaprawa, "Third Hankel determinants for subclasses of univalent functions," *Mediterranean Journal of Mathematics*, vol. 14, no. 1, p. 19, 2017.

[27] M. Arif, R. Rani, M. Raza, and P. Zaprawa, "Fourth Hankel determinant for a family of functions with bounded turning," *Bulletin of the Korean Mathematical Society*, vol. 55, no. 6, pp. 1703–1711, 2018.

[28] M. Arif, L. Rani, M. Raza, and P. Zaprawa, "Fourth Hankel determinant for the set of starlike functions," *Mathematical Problems in Engineering*, vol. 2021, Article ID 6674010, 8 pages, 2021.

[29] M. Arif, I. Ullah, M. Raza, and P. Zaprawa, "Investigation of the fifth Hankel determinant for a family of functions with bounded turnings," *Mathematica Slovaca*, vol. 70, no. 2, pp. 319–328, 2020.

[30] M. Arif, S. Umer, M. Raza, T. Bulboaca, M. U. Farooq, and H. Khan, "On fourth Hankel determinant for functions associated with Bernoulli's lemniscate," *Hacettepe Journal of Mathematics and Statistics*, vol. 49, pp. 1777–1780, 2020.

[31] W. K. Mashwani, B. Ahmad, N. Khan et al., "Fourth Hankel determinant for a subclass of starlike functions based on modified sigmoid," *Journal of Function Spaces*, vol. 2021, Article ID 6116172, 10 pages, 2021.

[32] G. Kaur, G. Singh, M. Arif, R. Chinram, and J. Iqbal, "A study of third and fourth Hankel determinant problem for a particular class of bounded turning functions," *Mathematical Problems in Engineeringi*, vol. 2021, Article ID 6687805, 8 pages, 2021.

[33] Z.-G. Wang, M. Raza, M. Arif, and K. Ahmad, "On the third and fourth Hankel determinants for a subclass of analytic functions," *Bull. Malays. Math. Sci. Soc.*vol. 45, pp. 323–359, 2022.

[34] H.-Y. Zhang and H. Tang, "A study of fourth-order Hankel determinants for starlike functions connected with the sine function," *Journal of Function Spaces*, vol. 2021, p. 8, Article ID 9991460, 2021.

[35] C. Carathéodory, "Über den variabilitätsbereich der fourier'schen konstanten von positiven harmonischen funktionen," *Rendiconti del Circolo Matematico di Palermo*, vol. 32, no. 1, pp. 193–217, 1911.

[36] A. E. Livingston, "The coefficients of multivalent close-to-convex functions," *Proceedings of the American Mathematical Society*, vol. 21, no. 3, p. 545, 1969.

[37] R. J. Libera and E. J. Złotkiewicz, "Early coefficients of the inverse of a regular convex function," *Proceedings of the American Mathematical Society*, vol. 85, no. 2, pp. 225–230, 1982.

Hindawi
Journal of Mathematics
Volume 2022, Article ID 1883268, 11 pages
https://doi.org/10.1155/2022/1883268

Research Article

Novel Analysis of Fractional-Order Fifth-Order Korteweg–de Vries Equations

Ahmed B. Khoshaim,[1] Muhammad Naeem ,[2] Ali Akgul,[3] Nejib Ghanmi,[4] and Shamsullah Zaland [5]

[1]*Department of Mechanical Engineering, King Abdulaziz University, Jeddah, Saudi Arabia*
[2]*Deanship of Joint First Year Umm Al-Qura University, Makkah, Saudi Arabia*
[3]*Department of Mathematics, Art and Science Faculty, Siirt University, Siirt, Turkey*
[4]*Higher Institute of Applied Sciences and Technologies Campus Universitaire Route Peripherique Dar El Amen Kairouan, Kairouan 3100, Tunisia*
[5]*Department of Mathematics, Kabul Polytechnic University, Kabul, Afghanistan*

Correspondence should be addressed to Muhammad Naeem; mfaridoon@uqu.edu.sa and Shamsullah Zaland; shamszaland@kpu.edu.af

Received 12 December 2021; Revised 14 January 2022; Accepted 9 April 2022; Published 23 May 2022

Academic Editor: Lakhdar Ragoub

In this paper, the ρ-homotopy perturbation transformation method was applied to analysis of fifth-order nonlinear fractional Korteweg–de Vries (KdV) equations. This technique is the mixture form of the ρ-Laplace transformation with the homotopy perturbation method. The purpose of this study is to demonstrate the validity and efficiency of this method. Furthermore, it is demonstrated that the fractional and integer-order solutions close in on the exact result. The suggested technique was effectively utilized and was accurate and simple to use for a number of related engineering and science models.

1. Introduction

A number of researchers have recently become interested in fractional calculus, which was first developed during Newton's period. Within the fractional calculus structure, many interesting and significant steps have been discovered within the last thirty decades. A fractional derivative was invented as a result of the complexity of a heterogeneous phenomenon. The fractional derivative operators, by incorporating diffusion methods, are capable of capturing the attitudes of multidimensional media [1–4]. The use of differential equations of any scale has proved useful in showing a number of problems more quickly and accurately. Increasingly, scholars turned to generalized calculus to convey their viewpoints while analyzing complex phenomena in the context of mathematical methods using software [5–10].

Nonlinear impacts occur in several implemented scientific fields, such as fluid, mathematical biology, nonlinear image sensors, quantum field theory, kinetics, thermodynamics, and fluid dynamics. It is based on nonlinear partial differential equations of various degrees of complexity to model these processes. Partial differential equations are generally applied in the description of physical processes [11–15]. Most of the essential physical systems do not exhibit linear behavior. There is no way to determine the exact result of such nonlinear phenomena. Only techniques that are appropriate for solving nonlinear equations can be used to investigate this phenomenon [16–22].

In 1895, Korteweg and de Vries proposed a KdV equation to design Russell's soliton phenomenon, such as small and huge water waves. Solitons are steady solitary waves, which mean that these solitary waves are a particle. KdV equations are applied in different applied fields such as quantam mechanics, fluid dynamics, optics, and plasma physics. Fifth-order KdV form equations were utilized to analyze many nonlinear phenomena in particle physics [23–25]. It plays a vital role in the distribution of waves [26]. In their analysis, the KdV form equation has dispersive terms of the third and fifth-order relevant to the magnetoacoustic wave problem in cold plasma free collision plasma and dispersive terms appear near-critical angle propagation [27]. Plasma is a dynamic, quasineutral, and electrically conductive fluid. It consists of neutral particles, electrons, and ions. It consists of magnetic and electric areas due to the electrically conducting behavior of plasma. The mixture of particles and areas supports plasma waves of various forms. A magnetic lock is a less longitudinal ion dispersion. The magnetoacoustic wave behaves as an ion-acoustic wave in the low magnetic field range, while in the low-temperature capacity, it acts as an Alfven wave [28, 29].

The general model for the analysis of magnetic properties-acoustic waves in plasma and shallow water waves with surface tension is equated with the fifth order of KdV. Recent study reveals that the solutions to this equation for travelling waves do not vanish at infinity [30, 31]. Consider the well-known three types of the fifth-order KdV equations as follows [32, 33]:

$$D_{\tau}^{\gamma}\mathscr{V} + \mathscr{V}_{\zeta} + \mathscr{V}^2\mathscr{V}_{2\zeta} + \mathscr{V}_{\zeta}\mathscr{V}_{2\zeta} - 20\mathscr{V}^2\mathscr{V}_{3\zeta} + \mathscr{V}_{5\zeta} = 0, \quad 0 < \beta \leq 1, \tag{1}$$

with initial condition $\mathscr{V}(\zeta, 0) = 1/\zeta$,

$$D_{\tau}^{\beta}\mathscr{V} + \mathscr{V}\mathscr{V}_{\zeta} - \mathscr{V}\mathscr{V}_{3\zeta} + \mathscr{V}_{5\zeta} = 0, \quad 0 < \beta \leq 1, \tag{2}$$

with initial condition $\mathscr{V}(\zeta, 0) = e^{\zeta}$, and

$$D_{\tau}^{\beta}\mathscr{V} + \mathscr{V}\mathscr{V}_{\zeta} + \mathscr{V}_{3\zeta} - \mathscr{V}_{5\zeta} = 0, \quad 0 < \beta \leq 1, \tag{3}$$

with initial condition $\mathscr{V}(\zeta, 0) = 105/169\text{sech}^4(\zeta - \phi/2\sqrt{13})$.

(1) and (2) are called fifth-order KdV equations and (3) is called the Kawahara equation. Analytic techniques for these mathematical model are particularly difficult to come across due to their severe nonlinearity. Several researchers have employed various analytical and computational strategies to the solution of linear and nonlinear KdV equations throughout the last decade, such as the multisymplectic method [34], variational iteration method [33], He's homotopy perturbation method [35], and Exp-function method [36].

Recently, Fahd and Abdeljawad [37] developed the Laplace transform of the generalized fractional Caputo derivatives. We established a novel methodology with ρ-Laplace transform for solving fractional differential equations with a generalized fractional Caputo derivative. The homotopy perturbation method is merged with the Laplace transform method to create a highly effective method for handling nonlinear terms which is known as the homotopy perturbation transformation technique. This technique can provide the result in quick convergent series. Ghorbani pioneered the use of He's polynomials in nonlinear terms [38–40]. Later on, many scholars utilized the homotopy perturbation transformation method for linear and nonlinear differential equations such as heat-like equations [41], Navier–Stokes equations [42], hyperbolic equation and Fisher's equation [43], and gas dynamic equation [44].

2. Basic Definitions

2.1. Definition. The fractional generalized integral of order β of a continuous function (CF) g: $[0, +\infty] \longrightarrow R$ is defined as [37]

$$\left(I^{\beta,\rho} g\right)(\zeta) = \frac{1}{\Gamma(\beta)} \int_0^{\zeta} \left(\frac{\zeta^{\rho} - s^{\rho}}{\rho}\right)^{\beta-1} \frac{g(s)ds}{s^{1-\rho}}, \quad \rho > 0,\ \zeta > 0,\ 0 < \beta < 1. \tag{4}$$

2.2. Definition. The order β fractional generalized derivative of a CF g: $[0, +\infty] \longrightarrow R$ is given as [37]

$$\begin{aligned}\left(D^{\beta,\rho} g\right)(\zeta) &= \left(I^{1-\beta,\rho} g\right)(\zeta) \\ &= \frac{1}{\Gamma(1-\beta)} \left(\frac{d}{d\zeta}\right) \int_0^{\zeta} \left(\frac{\zeta^{\rho} - s^{\rho}}{\rho}\right)^{-\beta-1} \frac{g(s)ds}{s^{1-\rho}}, \\ &\rho > 0,\ \zeta > 0 \text{ and } 0 < \beta < 1.\end{aligned} \tag{5}$$

2.3. Definition. The Caputo derivative of fractional-order β of a CF g: $[0, +\infty] \longrightarrow R$ is defined as [37]

$$\left(D^{\beta,\rho} g\right)(\zeta) = \frac{1}{\Gamma(1-\beta)} \left(\frac{d}{d\zeta}\right) \int_0^{\zeta} \left(\frac{\zeta^{\rho} - s^{\rho}}{\rho}\right)^{-\beta-1} \beta^n \frac{g(s)\text{ds}}{s^{1-\rho}}, \tag{6}$$

where $\rho > 0$, $\zeta > 0$, $\beta = \zeta^{1-\beta} d/d\zeta$, and $0 < \beta < 1$.

2.4. Definition. The ρ-Laplace transform of a CF g: $[0, +\infty] \longrightarrow R$ is defined as [37]

$$L_{\rho}\{g(\zeta)\}(s) = \int_0^{\infty} e^{-s\zeta^{\rho}/\rho} g(\zeta) \frac{d\zeta}{\zeta^{1-\rho}}. \tag{7}$$

The fractional generalized Caputo derivative of ρ-Laplace transformation of a CF g is given by [37]

$$L_{\rho}\left\{D^{\beta,\rho} g(\zeta)\right\}(s) = s^{\beta} L_{\rho}\{g(\zeta)\} - \sum_{k=0}^{n-1} s^{\beta-k-1}\left(I^{\beta,\rho} \beta^n g\right)(0). \tag{8}$$

2.5. Definition. The generalized Mittag-Leffler function is defined by

$$E_{\beta,\rho}(z) = \sum_{k=0}^{\infty} \frac{z^{\beta}}{\Gamma(\beta k + \gamma)}, \tag{9}$$

where $\beta > 0$, $\gamma > 0$, and $E_{\beta}(z) = E_{\beta,1}(z)$.

3. The Rod Map of the Proposed Method

Consider the general partial differential equation given as

$$D_\tau^\gamma \mathscr{V}(\zeta,\tau) + M\mathscr{V}(\zeta,\tau) + N\mathscr{V}(\zeta,\tau) = h(\zeta,\tau), \quad \tau>0,\ 0<\gamma\le 1,$$
$$\mathscr{V}(\zeta,0) = g(\zeta), \quad \nu \in \mathfrak{R}. \tag{10}$$

Applying ρ-Laplace transformation of (10), we get

$$L_\rho\left[D_\tau^\gamma \mathscr{V}(\zeta,\tau) + M\mathscr{V}(\zeta,\tau) + N\mathscr{V}(\zeta,\tau)\right] = L_\rho[h(\zeta,\tau)], \quad \tau>0,\ 0<\gamma\le 1,$$
$$\mu(\zeta,\tau) = \frac{1}{s}g(\zeta) + \frac{1}{s^\beta}L_\rho[h(\zeta,\tau)] - \frac{1}{s^\beta}L_\rho[M\mathscr{V}(\zeta,\tau) + N\mathscr{V}(\zeta,\tau)]. \tag{11}$$

Now, applying the inverse ρ-Laplace transform, we get

$$\mathscr{V}(\zeta,\tau) = F(\zeta,\tau) - L_\rho^{-1}\left[\frac{1}{s^\beta}L_\rho\{M\mathscr{V}(\zeta,\tau) + N\mathscr{V}(\zeta,\tau)\}\right], \tag{12}$$

where

$$F(\zeta,\tau) = L_\rho^{-1}\left[\frac{1}{s}g(\zeta) + \frac{1}{s^\beta}L_\rho[h(\zeta,\tau)]\right]$$
$$= g(\nu) + L_\rho^{-1}\left[\frac{1}{s^\beta}L_\rho[h(\zeta,\tau)]\right]. \tag{13}$$

Now, the perturbation procedure in terms of power series with parameter p is presented as

$$\mathscr{V}(\zeta,\tau) = \sum_{\kappa=0}^{\infty} p^\kappa \mathscr{V}_\kappa(\zeta,\tau), \tag{14}$$

where p is the perturbation parameter and $p \in [0,1]$.

The nonlinear term can be defined as

$$N\mathscr{V}(\zeta,\tau) = \sum_{\kappa=0}^{\infty} p^\kappa H_\kappa(\mathscr{V}_\kappa), \tag{15}$$

where H_n are He's polynomials in terms of $\mathscr{V}_0, \mathscr{V}_1, \mathscr{V}_2, \ldots, \mathscr{V}_n$ and can be calculated as

$$H_n(\mathscr{V}_0, \mathscr{V}_1, \ldots, \mathscr{V}_n) = \frac{1}{\gamma(n+1)} D_p^\kappa\left[N\left(\sum_{\kappa=0}^{\infty} p^\kappa \mathscr{V}_\kappa\right)\right]_{p=0}, \tag{16}$$

where $D_p^\kappa = \partial^\kappa/\partial p^\kappa$.

Substituting (15) and (16) in (12), we get

$$\sum_{\kappa=0}^{\infty} p^\kappa \mathscr{V}_\kappa(\zeta,\tau) = F(\zeta,\tau) - p \times \left[L_\rho^{-1}\left\{\frac{1}{s^\beta}L_\rho\left\{M\sum_{\kappa=0}^{\infty} p^\kappa \mathscr{V}_\kappa(\zeta,\tau) + \sum_{\kappa=0}^{\infty} p^\kappa H_\kappa(\mathscr{V}_\kappa)\right\}\right\}\right]. \tag{17}$$

The coefficients comparison on both sides of p, we have

$$p^0\colon \mathscr{V}_0(\zeta,\tau) = F(\zeta,\tau),$$
$$p^1\colon \mathscr{V}_1(\zeta,\tau) = L_\rho^{-1}\left[\frac{1}{s^\beta}L_\rho\left(M\mathscr{V}_0(\zeta,\tau) + H_0(\mathscr{V})\right)\right],$$
$$p^2\colon \mathscr{V}_2(\zeta,\tau) = L_\rho^{-1}\left[\frac{1}{s^\beta}L_\rho\left(M\mathscr{V}_1(\zeta,\tau) + H_1(\mathscr{V})\right)\right],$$
$$\vdots$$
$$p^\kappa\colon \mathscr{V}_\kappa(\zeta,\tau) = L_\rho^{-1}\left[\frac{1}{s^\beta}L_\rho\left(M\mathscr{V}_{\kappa-1}(\zeta,\tau) + H_{\kappa-1}(\mathscr{V})\right)\right],$$
$$\kappa>0,\ \kappa \in N. \tag{18}$$

The $\mathscr{V}\kappa(\zeta,\tau)$ component can be determined easily which quickly leads us to the convergent series. We can get $p \longrightarrow 1$:

$$\mathscr{V}(\zeta,\tau) = \lim_{M\longrightarrow\infty} \sum_{\kappa=1}^{M} \mathscr{V}_\kappa(\zeta,\tau). \tag{19}$$

4. Numerical Implementations

Example 1. Consider the fifth-order nonlinear KdV equation

$$D_\tau^\beta \mathscr{V} + \mathscr{V}_\zeta + \mathscr{V}^2\mathscr{V}_{2\zeta} - \mathscr{V}_\zeta\mathscr{V}_{2\zeta}$$
$$- 20\mathscr{V}^2\mathscr{V}_{3\zeta} + \mathscr{V}_{5\zeta} = 0, \quad 0<\beta\le 1, \tag{20}$$

with the IC

$$\mathscr{V}(\zeta,\tau) = \frac{1}{\zeta}. \tag{21}$$

Applying the ρ-Laplace transform on (20), we get

$$L_\rho \mathscr{V}(\zeta,\tau)] = \frac{1}{s\zeta} - \frac{1}{s^\beta} L_\rho \mathscr{V}_\zeta + \mathscr{V}^2\mathscr{V}_{2\zeta} + \mathscr{V}_\zeta \mathscr{V}_{2\zeta} - 20\mathscr{V}^2\mathscr{V}_{3\zeta} + \mathscr{V}_{5\zeta}]. \tag{22}$$

Next, using the inverse of ρ-Laplace transform of (22),

$$[\mathscr{V}(\zeta,\tau)] = \frac{1}{\zeta} - L_\rho^{-1}\left[\frac{1}{s^\beta} L_\rho \left[\mathscr{V}_\zeta + \mathscr{V}^2\mathscr{V}_{2\zeta} + \mathscr{V}_\zeta \mathscr{V}_{2\zeta} - 20\mathscr{V}^2\mathscr{V}_{3\zeta} + \mathscr{V}_{5\zeta}\right]\right]. \tag{23}$$

Now, we apply HPM

$$\sum_{n=0}^{\infty} p^n \mathscr{V}_n(\zeta,\tau) = \frac{1}{\zeta} - p\left[L_\rho^{-1}\left[\frac{1}{s^\beta} L_\rho \left[\left(\sum_{n=0}^{\infty} p^n H_n(\mathscr{V})\right) + \left(\sum_{n=0}^{\infty} p^n \mathscr{V}_n(\zeta,\tau)\right)_\zeta + \left(\sum_{n=0}^{\infty} p^n \mathscr{V}_n(\zeta,\tau)\right)_{5\zeta}\right]\right]\right], \tag{24}$$

where $H_n(x)$ represents the nonlinear function of He's polynomial. For the first few components, we present He's polynomials

$$\begin{aligned}
H_0(\mathscr{V}) &= \mathscr{V}_0^2(\mathscr{V}_0)_{2\zeta} + (\mathscr{V}_0)_\zeta(\mathscr{V}_0)_{2\zeta} - 20\mathscr{V}_0^2(\mathscr{V}_0)_{3\zeta},\\
H_1(\mathscr{V}) &= \mathscr{V}_0^2(\mathscr{V}_1)_{2\zeta} + 2\mathscr{V}_0\mathscr{V}_1(\mathscr{V}_o)_{2\zeta} + (\mathscr{V}_o)_\zeta(\mathscr{V}_1)_{2\zeta} + (\mathscr{V}_o)_{2\zeta}(\mathscr{V}_1)_\zeta - 20\mathscr{V}_0^2(\mathscr{V}_1)_{3\zeta} - 40\mathscr{V}_0\mathscr{V}_1(\mathscr{V}_o)_{3\zeta},\\
H_2(\mathscr{V}) &= \mathscr{V}_0^2(\mathscr{V}_2)_{2\zeta} + 2\mathscr{V}_0\mathscr{V}_1(\mathscr{V}_1)_{2\zeta} + 2\mathscr{V}_0\mathscr{V}_2(\mathscr{V}_o)_{2\zeta} + \mathscr{V}_1^2(\mathscr{V}_o)_{2\zeta} + (\mathscr{V}_o)_\zeta(\mathscr{V}_2)_{2\zeta} + (\mathscr{V}_1)_\zeta(\mathscr{V}_1)_{2\zeta}\\
&\quad + (\mathscr{V}_o)_{2\zeta}(\mathscr{V}_2)_\zeta - 20\mathscr{V}_0^2(\mathscr{V}_2)_{3\zeta} - 40\mathscr{V}_0\mathscr{V}_1(\mathscr{V}_1)_{3\zeta} - 40\mathscr{V}_0\mathscr{V}_2(\mathscr{V}_o)_{3\zeta} - 20\mathscr{V}_1^2(\mathscr{V}_o)_{3\zeta},\\
H_3(\mathscr{V}) &= \mathscr{V}_0^2(\mathscr{V}_3)_{2\zeta} + 2\mathscr{V}_0\mathscr{V}_1(\mathscr{V}_2)_{2\zeta} + 2\mathscr{V}_0\mathscr{V}_2(\mathscr{V}_1)_{2\zeta} + 2\mathscr{V}_0\mathscr{V}_3(\mathscr{V}_o)_{2\zeta} + \mathscr{V}_1^2(\mathscr{V}_1)_{2\zeta} + 2\mathscr{V}_1\mathscr{V}_2(\mathscr{V}_o)_{2\zeta}\\
&\quad + (\mathscr{V}_o)_\zeta(\mathscr{V}_3)_{2\zeta} + (\mathscr{V}_1)_\zeta(\mathscr{V}_2)_{2\zeta} + (\mathscr{V}_1)_{2\zeta}(\mathscr{V}_2)_\zeta + (\mathscr{V}_0)_{2\zeta}(\mathscr{V}_3)_\zeta - 20\mathscr{V}_0^2(\mathscr{V}_3)_{3\zeta} - 40\mathscr{V}_0\mathscr{V}_1(\mathscr{V}_2)_{3\zeta}\\
&\quad - 40\mathscr{V}_0\mathscr{V}_2(\mathscr{V}_1)_{3\zeta} - 40\mathscr{V}_0\mathscr{V}_3(\mathscr{V}_o)_{3\zeta} - 20\mathscr{V}_1^2(\mathscr{V}_1)_{3\zeta} - 40\mathscr{V}_1\mathscr{V}_2(\mathscr{V}_o)_{3\zeta},\\
H_4(\mathscr{V}) &= \mathscr{V}_0^2(\mathscr{V})_{2\zeta} + 2\mathscr{V}_0\mathscr{V}_1(\mathscr{V}_3)_{2\zeta} + 2\mathscr{V}_0\mathscr{V}_2(\mathscr{V}_2)_{2\zeta} + 2\mathscr{V}_0\mathscr{V}_3(\mathscr{V}_1)_{2\zeta} + 2\mathscr{V}_0\mathscr{V}_4(\mathscr{V}_o)_{2\zeta} + \mathscr{V}_1^2(\mathscr{V}_2)_{2\zeta}\\
&\quad + 2\mathscr{V}_1\mathscr{V}_2(\mathscr{V}_1)_{2\zeta} + 2\mathscr{V}_1\mathscr{V}_3(\mathscr{V}_o)_{2\zeta} + \mathscr{V}_2^2(\mathscr{V}_o)_{2\zeta} + (\mathscr{V}_o)_\zeta(\mathscr{V}_4)_{2\zeta} + (\mathscr{V}_1)_\zeta(\mathscr{V}_3)_{2\zeta} + (\mathscr{V}_2)_{2\zeta}(\mathscr{V}_2)_\zeta\\
&\quad + (\mathscr{V}_1)_{2\zeta}(\mathscr{V}_3)_\zeta + (\mathscr{V}_o)_{2\zeta}(\mathscr{V}_4)_\zeta - 20\mathscr{V}_0^2(\mathscr{V}_4)_{3\zeta} - 40\mathscr{V}_0\mathscr{V}_1(\mathscr{V}_3)_{3\zeta} - 40\mathscr{V}_0\mathscr{V}_2(\mathscr{V}_2)_{3\zeta} - 40\mathscr{V}_0\mathscr{V}_3(\mathscr{V}_1)_{3\zeta}\\
&\quad - 40\mathscr{V}_0\mathscr{V}_4(\mathscr{V}_o)_{3\zeta} - 20\mathscr{V}_1^2(\mathscr{V}_2)_{3\zeta} - 40\mathscr{V}_1\mathscr{V}_2(\mathscr{V}_1)_{3\zeta} - 40\mathscr{V}_1\mathscr{V}_3(\mathscr{V}_o)_{3\zeta} - 20\mathscr{V}_2^2(\mathscr{V}_o)_{2\zeta},\\
&\vdots
\end{aligned} \tag{25}$$

Comparing the P-like coefficients, we have

$$\begin{aligned}
P^0&: \mathscr{V}_0(\zeta,\tau) = \frac{1}{\zeta},\\
P^1&: \mathscr{V}_1(\zeta,\tau) = -L_\rho^{-1}\left[\frac{1}{s^\beta}L_\rho\left[H_0(\mathscr{V}) + (\mathscr{V}_0)_\zeta + (\mathscr{V}_0)_{5\zeta}\right]\right] = \frac{(\tau^\rho/\rho)^\beta}{\zeta^2\Gamma(\beta+1)},\\
P^2&: \mathscr{V}_2(\zeta,\tau) = -L_\rho^{-1}\left[\frac{1}{s^\beta}L_\rho\left[H_1(\mathscr{V}) + (\mathscr{V}_1)_\zeta + (\mathscr{V}_1)_{5\zeta}\right]\right] = \frac{(\tau^\rho/\rho)^{2\beta}}{\zeta^3\Gamma(2\beta+1)},\\
P^3&: \mathscr{V}_3(\zeta,\tau) = -L_\rho^{-1}\left[\frac{1}{s^\beta}L_\rho\left[H_2(\mathscr{V}) + (\mathscr{V}_2)_\zeta + (\mathscr{V}_2)_{5\zeta}\right]\right] = \frac{(\tau^\rho/\rho)^{3\beta}}{\zeta^4\Gamma(3\beta+1)},\\
P^4&: \mathscr{V}_4(\zeta,\tau) = -L_\rho^{-1}\left[\frac{1}{s^\beta}L_\rho\left[H_3(\mathscr{V}) + (\mathscr{V}_3)_\zeta + (\mathscr{V}_3)_{5\zeta}\right]\right] = \frac{(\tau^\rho/\rho)^{4\beta}}{\zeta^5\Gamma(4\beta+1)},\\
P^5&: \mathscr{V}_5(\zeta,\tau) = -L_\rho^{-1}\left[\frac{1}{s^\beta}L_\rho\left[H_4(\mathscr{V}) + (\mathscr{V}_4)_\zeta + (\mathscr{V}_4)_{5\zeta}\right]\right] = \frac{(\tau^\rho/\rho)^{5\beta}}{\zeta^6\Gamma(5\beta+1)}.\\
&\vdots
\end{aligned} \tag{26}$$

The analytical solution of $\mathscr{V}(\zeta,\tau)$ is defined as

$$\mathscr{V}(\zeta,\tau) = \sum_{i=0}^{\infty}\mathscr{V}(\zeta,\tau)_i = \frac{1}{\zeta} + \frac{(\tau^\rho/\rho)^\beta}{\zeta^2\Gamma(\beta+1)} + \frac{(\tau^\rho/\rho)^{2\beta}}{\zeta^3\Gamma(2\beta+1)} + \frac{(\tau^\rho/\rho)^{3\beta}}{\zeta^4\Gamma(3\beta+1)} + \frac{(\tau^\rho/\rho)^{4\beta}}{\zeta^5\Gamma(4\beta+1)} + \frac{(\tau^\rho/\rho)^{5\beta}}{\zeta^6\Gamma(5\beta+1)} + \cdots. \tag{27}$$

Then, put $\beta = 1$ in (27):

$$\mathscr{V}(\zeta,\tau) = \sum_{i=0}^{\infty}\mathscr{V}_i(\zeta,\tau) = \frac{1}{\zeta} + \frac{\tau}{\zeta^2} + \frac{\tau^2}{\zeta^3} + \frac{\tau^3}{\zeta^4} + \cdots. \tag{28}$$

The exact result is $\mathscr{V}(\zeta,\tau) = 1/\zeta - \tau$.

In Figure 1, the three-dimensional figures of ρ-HPTM and exact results in graphs (a) and (b) respectively at $\beta = 1$ and the close contact of the exact and ρ-HPTM solutions are investigated. In Figure 2, represent that various fractional

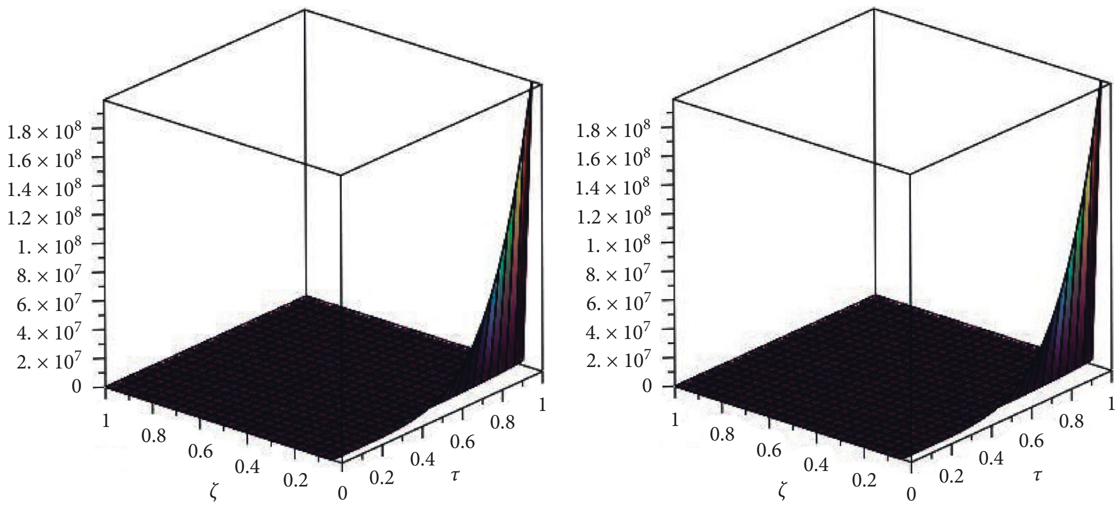

(a) (b)

Figure 1: Graph of (a) exact and (b) analytic solutions of $\beta = 1$ of Example 1.

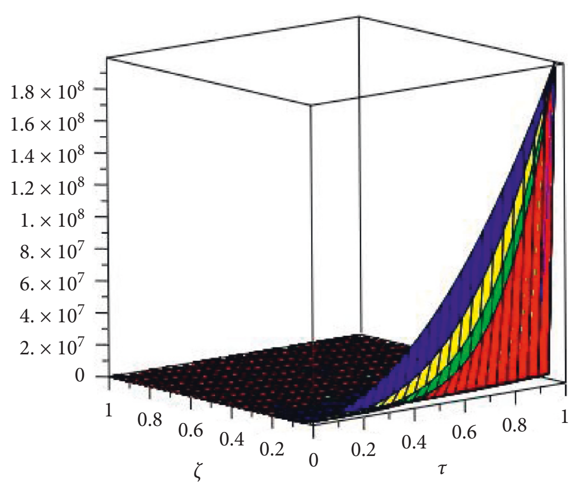

Figure 2: Figure of various fractional orders of Example 1.

order of ρ-HPTM results at $\beta = 1, 0.8, 0.6, 0.4$. The non-classical results are investigated to be converge to an integer-order result of the given problem.

Example 2. Consider the fifth-order nonlinear fraction KdV equation

$$D_\tau^\beta \mathscr{V} + \mathscr{V}\mathscr{V}_\zeta - \mathscr{V}\mathscr{V}_{3\zeta} + \mathscr{V}_{5\zeta} = 0, \quad 0 < \beta \leq 1, \tag{29}$$

with the IC

$$\mathscr{V}(\zeta, \tau) = e^\zeta. \tag{30}$$

Applying the ρ-Laplace transform on (29), we get

$$L_\rho[\mathscr{V}(\zeta, \tau)] = \frac{1}{s}e^\zeta + \frac{1}{s^\beta}L_\rho\left[\mathscr{V}\mathscr{V}_{3\zeta} - \mathscr{V}\mathscr{V}_\zeta - \mathscr{V}_{5\zeta}\right]. \tag{31}$$

Next, using the inverse of ρ-Laplace transform of (31),

$$\mathscr{V}(\zeta, \tau) = e^\zeta + L_\rho^{-1}\left[\frac{1}{s^\beta}L_\rho\left\{\mathscr{V}\mathscr{V}_{3\zeta} - \mathscr{V}\mathscr{V}_\zeta - \mathscr{V}_{5\zeta}\right\}\right]. \tag{32}$$

Now, we apply HPM

$$\sum_{n=0}^{\infty} p^n \mathscr{V}_n(\zeta, \tau) = e^\zeta + p\left[L_\rho^{-1}\left\{\frac{1}{s^\beta}L_\rho\left(\left(\sum_{n=0}^{\infty} p^n H_n(\mathscr{V})\right) - \left(\sum_{n=0}^{\infty} p^n \mathscr{V}_n(\zeta, \tau)\right)\right)_{5\zeta}\right\}\right], \tag{33}$$

where $H_n(x)$ represents the nonlinear term of He's polynomial. For the first few components, we present He's polynomials

$$\begin{aligned}
H_0(\mathscr{V}) &= \mathscr{V}_o(\mathscr{V}_0)_{3\zeta} - \mathscr{V}_0(\mathscr{V}_0)_{\zeta},\\
H_1(\mathscr{V}) &= \mathscr{V}_1(\mathscr{V}_0)_{3\zeta} + \mathscr{V}_0(\mathscr{V}_1)_{3\zeta} - \mathscr{V}_1(\mathscr{V}_0)_{\zeta} - \mathscr{V}_0(\mathscr{V}_1)_{\zeta},\\
H_2(\mathscr{V}) &= \mathscr{V}_2(\mathscr{V}_0)_{3\zeta} + \mathscr{V}_1(\mathscr{V}_1)_{3\zeta} + \mathscr{V}_0(\mathscr{V}_2)_{3\zeta}\\
&\quad - \mathscr{V}_2(\mathscr{V}_0)_{\zeta} - \mathscr{V}_1(\mathscr{V}_1)_{\zeta} - \mathscr{V}_0(\mathscr{V}_2)_{\zeta},\\
H_3(\mathscr{V}) &= \mathscr{V}_3(\mathscr{V}_0)_{3\zeta} + \mathscr{V}_2(\mathscr{V}_1)_{3\zeta} + \mathscr{V}_1(\mathscr{V}_2)_{3\zeta}\\
&\quad + \mathscr{V}_0(\mathscr{V}_3)_{3\zeta} - \mathscr{V}_3(\mathscr{V}_0)_{\zeta} - \mathscr{V}_2(\mathscr{V}_1)_{\zeta}\\
&\quad - \mathscr{V}_1(\mathscr{V}_2)_{\zeta} - \mathscr{V}_0(\mathscr{V}_3)_{\zeta},\\
H_4(\mathscr{V}) &= \mathscr{V}_4(\mathscr{V}_0)_{3\zeta} + \mathscr{V}_3(\mathscr{V}_1)_{3\zeta} + \mathscr{V}_2(\mathscr{V}_2)_{3\zeta}\\
&\quad + \mathscr{V}_1(\mathscr{V}_3)_{3\zeta} + \mathscr{V}_0(\mathscr{V}_4)_{3\zeta} - \mathscr{V}_4(\mathscr{V}_0)_{\zeta}\\
&\quad - \mathscr{V}_3(\mathscr{V}_1)_{\zeta} - \mathscr{V}_2(\mathscr{V}_2)_{\zeta} - \mathscr{V}_1(\mathscr{V}_3)_{\zeta} - \mathscr{V}_0(\mathscr{V}_4)_{\zeta},\\
&\ \vdots
\end{aligned} \tag{34}$$

Comparing the P-like coefficients, we have

$$\begin{aligned}
p^0&: \mathscr{V}_0(\zeta,\tau) = e^{\zeta},\\
p^1&: \mathscr{V}_1(\zeta,\tau) = L_\rho^{-1}\left[\frac{1}{s^\beta}L_\rho\{H_0(\mathscr{V}) - (\mathscr{V}_0)_{5\zeta}\}\right] = -\frac{(\tau^\rho/\rho)^\beta}{\Gamma(\beta+1)}e^{\zeta},\\
p^2&: \mathscr{V}_2(\zeta,\tau) = L_\rho^{-1}\left[\frac{1}{s^\beta}L_\rho\{H_1(\mathscr{V}) - (\mathscr{V}_1)_{5\zeta}\}\right] = \frac{(\tau^\rho/\rho)^{2\beta}}{\Gamma(2\beta+1)}e^{\zeta},\\
p^3&: \mathscr{V}_3(\zeta,\tau) = L_\rho^{-1}\left[\frac{1}{s^\beta}L_\rho\{H_2(\mathscr{V}) - (\mathscr{V}_2)_{5\zeta}\}\right] = -\frac{(\tau^\rho/\rho)^{3\beta}}{\Gamma(3\beta+1)}e^{\zeta},\\
p^4&: \mathscr{V}_4(\zeta,\tau) = L_\rho^{-1}\left[\frac{1}{s^\beta}L_\rho\{H_3(\mathscr{V}) - (\mathscr{V}_3)_{5\zeta}\}\right] = \frac{(\tau^\rho/\rho)^{4\beta}}{\Gamma(4\beta+1)}e^{\zeta},\\
p^5&: \mathscr{V}_5(\zeta,\tau) = L_\rho^{-1}\left[\frac{1}{s^\beta}L_\rho\{H_4(\mathscr{V}) - (\mathscr{V}_4)_{5\zeta}\}\right] = -\frac{(\tau^\rho/\rho)^{5\beta}}{\Gamma(5\beta+1)}e^{\zeta}.\\
&\ \vdots
\end{aligned} \tag{35}$$

Therefore, the analytic solution of $\mathscr{V}(\zeta,\tau)$ is defined as

$$\mathscr{V}(\zeta,\tau) = \sum_{i=0}^{\infty}\mathscr{V}_i(\zeta,\tau) = e^{\zeta}\left(1 - \frac{(\tau^\rho/\rho)^\beta}{\Gamma(\beta+1)} + \frac{(\tau^\rho/\rho)^{2\beta}}{\Gamma(2\beta+1)} - \frac{(\tau^\rho/\rho)^{3\beta}}{\Gamma(3\beta+1)} + \frac{(\tau^\rho/\rho)^{4\beta}}{\Gamma(4\beta+1)} - \frac{(\tau^\rho/\rho)^{5\beta}}{\Gamma(5\beta+1)} + \cdots\right). \tag{36}$$

Then, $\beta = 1$ for (36), and we get

$$\mathscr{V}(\zeta,\tau) = \sum_{i=0}^{\infty}\mathscr{V}_i(\zeta,\tau) = e^{\zeta}\left(1 - \tau + \frac{\tau^2}{2!} - \frac{\tau^3}{3!} + \frac{\tau^4}{4!} - \frac{\tau^5}{5!} + \cdots\right). \tag{37}$$

The exact solution is $\mathscr{V}(\zeta,\tau) = e^{\zeta-\tau}$.

In Figure 3, the three-dimensional figures of ρ-HPTM and exact results in graphs (a) and (b) respectively at $\beta = 1$ and the close contact of the exact and ρ-HPTM solutions are investigated. In Figure 4, represent that various fractional order of ρ-HPTM results at $\beta = 1, 0.8, 0.6, 0.4$. The non-classical results are investigated to be converge to an integer-order result of the given problem.

Example 3. Consider nonlinear fractional-order Kawahara equation

$$D_\tau^\beta\mathscr{V} + \mathscr{V}\mathscr{V}_\zeta + \mathscr{V}_{3\zeta} - \mathscr{V}_{5\zeta} = 0, \quad 0 < \beta \le 1, \tag{38}$$

with the IC

$$\mathscr{V}(\zeta,\tau) = \frac{105}{169}\operatorname{sech}^4\left(\frac{\zeta-\phi}{2\sqrt{13}}\right). \tag{39}$$

Applying the ρ-Laplace transform on (38), we get

$$L_\rho\mathscr{V}(\zeta,\tau)] = \frac{1}{s}\frac{105}{169}\operatorname{sech}^4\left(\frac{\zeta-\phi}{2\sqrt{13}}\right) + \frac{1}{s^\beta}L_\rho\left[\mathscr{V}_{5\zeta} - \mathscr{V}_{3\zeta} - \mathscr{V}\mathscr{V}_\zeta\right]. \tag{40}$$

Next, using the inverse of ρ-Laplace transform of (40),

$$\mathscr{V}(\zeta,\tau) = \frac{105}{169}\operatorname{sech}^4\left(\frac{\zeta-\phi}{2\sqrt{13}}\right) + L_\rho^{-1}\left[\frac{1}{s^\beta}L_\rho\left[\mathscr{V}_{5\zeta} - \mathscr{V}_{3\zeta} - \mathscr{V}\mathscr{V}_\zeta\right]\right]. \tag{41}$$

Now, we apply HPM

$$\sum_{n=0}^{\infty}p^n\mathscr{V}_n(\zeta,\tau) = \frac{105}{169}\operatorname{sech}^4\left(\frac{\zeta-\phi}{2\sqrt{13}}\right) + p\left[L_\rho^{-1}\left\{\frac{1}{s^\beta}L_\rho\left(\left(\sum_{n=0}^{\infty}p^n\mathscr{V}_n(\zeta,\tau)\right)_{5\zeta} - \left(\sum_{n=0}^{\infty}p^n\mathscr{V}_n(\zeta,\tau)\right)_{3\zeta} - \left(\sum_{n=0}^{\infty}p^nH_n(\mathscr{V})\right)\right)\right\}\right], \tag{42}$$

where $H_n(\mathscr{V})$ represent the nonlinear terms of He's polynomial. For the first few components, we present He's polynomials

$$\begin{aligned}
H_0(\mathscr{V}) &= \mathscr{V}_0(\mathscr{V}_0)_\zeta,\\
H_1(\mathscr{V}) &= \mathscr{V}_0(\mathscr{V}_1)_\zeta + \mathscr{V}_1(\mathscr{V}_0)_\zeta,\\
H_2(\mathscr{V}) &= \mathscr{V}_0(\mathscr{V}_2)_\zeta + \mathscr{V}_1(\mathscr{V}_1)_\zeta + \mathscr{V}_2(\mathscr{V}_0)_\zeta,\\
H_3(\mathscr{V}) &= \mathscr{V}_0(\mathscr{V}_3)_\zeta + \mathscr{V}_1(\mathscr{V}_2)_\zeta + \mathscr{V}_2(\mathscr{V}_1)_\zeta + \mathscr{V}_3(\mathscr{V}_0)_\zeta,\\
H_4(\mathscr{V}) &= \mathscr{V}_0(\mathscr{V}_4)_\zeta + \mathscr{V}_1(\mathscr{V}_3)_\zeta + \mathscr{V}_2(\mathscr{V}_2)_\zeta\\
&\quad + \mathscr{V}_3(\mathscr{V}_1)_\zeta + \mathscr{V}_4(\mathscr{V}_0)_\zeta,\\
&\ \vdots
\end{aligned} \tag{43}$$

Comparing the P-like coefficients, we get

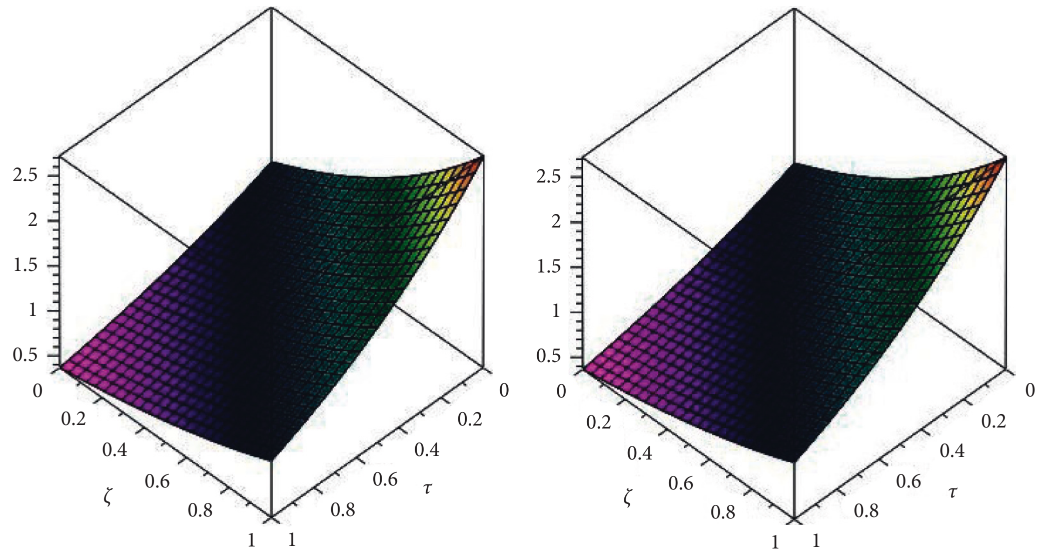

(a) (b)

Figure 3: Graph of (a) exact and (b) analytic solutions of $\beta = 1$ of Example 2.

$$
\begin{aligned}
p^0&: \mathscr{V}_0(\zeta,\tau) = \frac{105}{169}\operatorname{sech}^4\left(\frac{\zeta-\phi}{2\sqrt{13}}\right),\\
p^1&: \mathscr{V}_1(\zeta,\tau) = L_\rho^{-1}\left[\frac{1}{s^\beta}L_\rho\left[(\mathscr{V}_0)_{5\zeta}-(\mathscr{V}_0)_{5\zeta}-H_0(\mathscr{V})\right]\right] = -\frac{100}{377\sqrt{13}}\operatorname{sech}^4\left(\frac{\zeta-\phi}{2\sqrt{13}}\right)\tanh\left(\frac{\zeta-\phi}{2\sqrt{13}}\right)\frac{(\tau^\rho/\rho)^\beta}{\Gamma(\beta+1)},\\
p^2&: \mathscr{V}_2(\zeta,\tau) = L_\rho^{-1}\left[\frac{1}{s^\beta}L_\rho\left[(\mathscr{V}_1)_{5\zeta}-(\mathscr{V}_1)_{3\zeta}-H_1(\mathscr{V})\right]\right]\\
&= -\frac{21687}{10\times10^7\sqrt{13}}\operatorname{sech}^6\left(\frac{\zeta-\phi}{2\sqrt{13}}\right)\left[-3+2\cosh\left(\frac{\zeta-\phi}{2\sqrt{13}}\right)\right]\frac{(\tau^\rho/\rho)^{2\beta}}{\Gamma(2\beta+1)},\\
p^3&: \mathscr{V}_3(\zeta,\tau) = L_\rho^{-1}\left[\frac{1}{s^\beta}L_\rho\left\{(\mathscr{V}_2)_{5\zeta}-(\mathscr{V}_2)_{3\zeta}-H_2(\mathscr{V})\right\}\right]\\
&= -\frac{461962}{10\times10^7\sqrt{13}}\operatorname{sech}^7\left(\frac{\zeta-\phi}{2\sqrt{13}}\right)\times\left[-13\sinh\left(\frac{\zeta-\phi}{2\sqrt{13}}\right)+2\sinh\left(\frac{3(\zeta-t\phi)}{2\sqrt{`13}}\right)\right]\frac{(\tau^\rho/\rho)^{3\beta}}{\Gamma(3\beta+1)},\\
p^4&: \mathscr{V}_4(\zeta,\tau) = L_\rho^{-1}\left[\frac{1}{s^\beta}L_\rho\left[(\mathscr{V}_3)_{5\zeta}-(\mathscr{V}_3)_{3\zeta}-H_3(\mathscr{V})\right]\right]\\
&= -\frac{3784854}{10\times10^7\sqrt{13}}\operatorname{sech}^8\left(\frac{\zeta-\phi}{2\sqrt{13}}\right)\times\left[-49s\cosh\left(\frac{\zeta-\phi}{2\sqrt{13}}\right)+4\cosh\left(\frac{2(\zeta-t\phi)}{2\sqrt{`13}}\right)+52\right]\frac{(\tau^\rho/\rho)^{4\beta}}{\Gamma(4\beta+1)},\\
p^5&: \mathscr{V}_5(\zeta,\tau) = L_\rho^{-1}\left[\frac{1}{s^\beta}L_\rho\left[(\mathscr{V}_4)_{5\zeta}-(\mathscr{V}_4)_{3\zeta}-H_4(\mathscr{V})\right]\right]\\
&= -\frac{3.22496310\times10^7}{\sqrt{13}}\operatorname{sech}^9\left(\frac{\zeta-\phi}{2\sqrt{13}}\right)\times\left[171\sinh\left(\frac{3(\zeta-\phi)}{2\sqrt{13}}\right)-8\sinh\left(\frac{5(\zeta-\phi)}{2\sqrt{`13}}\right)\right.\\
&\quad\left.-661\sinh\left(\frac{5(\zeta-t\phi)}{2sqrt13}\right)\right]\frac{(\tau^\rho/\rho)^{5\beta}}{\Gamma(5\beta+1)}.\\
&\vdots
\end{aligned}
\tag{44}
$$

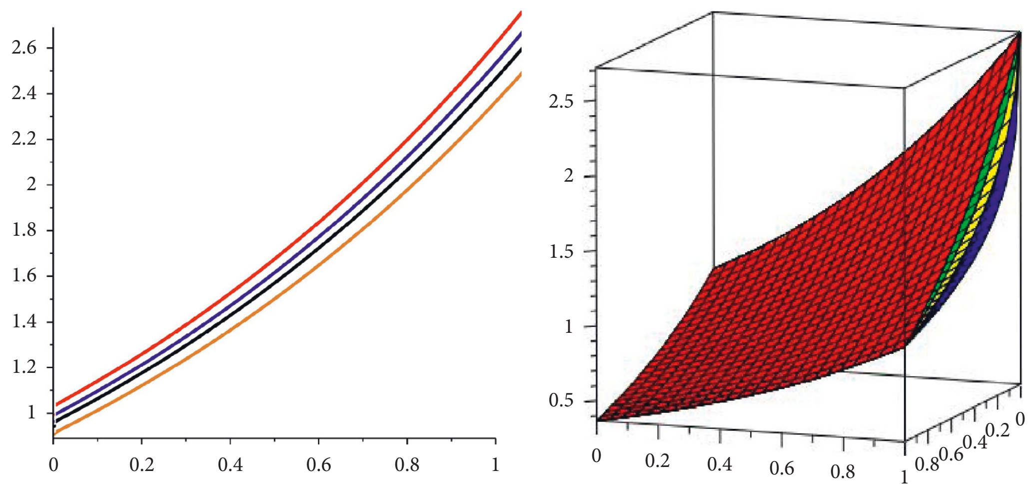

(a) (b)

Figure 4: Figure of (a) and (b) at various fractional-order of Example 2.

The analytic solution $\mathscr{V}(\zeta, \tau)$ is achieved as

$$\mathscr{V}(\zeta,\tau) = \sum_{i=0}^{\infty} \mathscr{V}_i(\zeta,\tau),$$

$$\begin{aligned}
\mathscr{V}(\zeta,\tau) = {} & \frac{105}{169}\operatorname{sech}^4\left(\frac{\zeta-\phi}{2\sqrt{13}}\right) - \frac{100}{377\sqrt{13}}\operatorname{sech}^4\left(\frac{\zeta-\phi}{2\sqrt{13}}\right)\tanh\left(\frac{\zeta-\phi}{2\sqrt{13}}\right)\frac{(\tau^{\rho}/\rho)^{\beta}}{\Gamma(\beta+1)} \\
& - \frac{21687}{10\times 10^{7}\sqrt{13}}\operatorname{sech}^6\left(\frac{\zeta-\phi}{2\sqrt{13}}\right)\left[-3+2\cosh\left(\frac{\zeta-\phi}{2\sqrt{13}}\right)\right]\frac{(\tau^{\rho}/\rho)^{2\beta}}{\Gamma(2\beta+1)} \\
& - \frac{461962}{10\times 10^{7}\sqrt{13}}\operatorname{sech}^7\left(\frac{\zeta-\phi}{2\sqrt{13}}\right)\times\left[-13\sinh\left(\frac{\zeta-\phi}{2\sqrt{13}}\right)+2\sinh\left(\frac{3(\zeta-\phi)}{2\sqrt{13}}\right)\right]\frac{(\tau^{\rho}/\rho)^{3\beta}}{\Gamma(3\beta+1)} \\
& - \frac{3784854}{10\times 10^{7}\sqrt{13}}\operatorname{sech}^8\left(\frac{\zeta-\phi}{2\sqrt{13}}\right)\times\left[-49s\cosh\left(\frac{\zeta-\phi}{2\sqrt{13}}\right)+4\cosh\left(\frac{2(\zeta-\phi)}{2\sqrt{13}}\right)+52\right]\frac{(\tau^{\rho}/\rho)^{4\beta}}{\Gamma(4\beta+1)} \\
& - \frac{3.22496310\times 10^{7}}{\sqrt{13}}\operatorname{sech}^9\left(\frac{\zeta-\phi}{2\sqrt{13}}\right)\times\left[171\sinh\left(\frac{3(\zeta-\phi)}{2\sqrt{13}}\right)-8\sinh\left(\frac{5(\zeta-\phi)}{2\sqrt{13}}\right)\right. \\
& \left. -661\sinh\left(\frac{5(\zeta-\phi)}{2\sqrt{13}}\right)\right]\frac{(\tau^{\rho}/\rho)^{5\beta}}{\Gamma(5\beta+1)} + \cdots.
\end{aligned} \tag{45}$$

The exact solution is $\mathscr{V}(\zeta,\tau) = 105/169\operatorname{sech}^4[1/2\sqrt{13}\,(\zeta + 36\tau/169 - \phi)]$.

In Figure 5, the three-dimensional figures of ρ-HPTM and exact results in graphs (a) and (b) respectively at $\beta = 1$

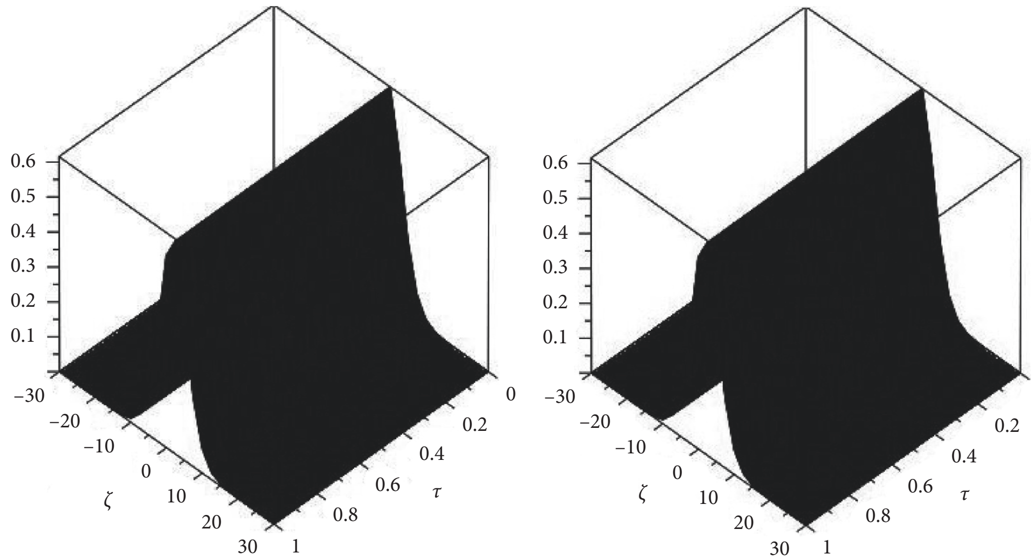

(a) (b)

Figure 5: Graph of (a) exact and (b) analytical results of $\beta = 1$ of Example 3.

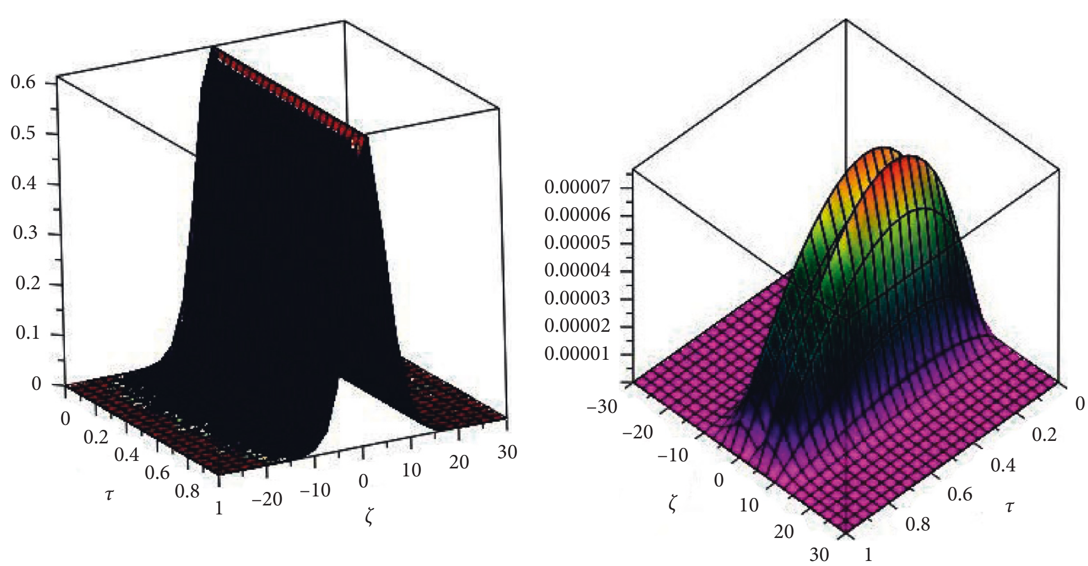

(a) (b)

Figure 6: Figure of (a) at various fractional-order of β and (b) error graph of Example 3.

and the close contact of the exact and ρ-HPTM solutions are investigated. In Figure 6, represent that various fractional order of ρ-HPTM results at $\beta = 1, 0.8, 0.6, 0.4$. The nonclassical results are investigated to be converge to an integer-order result of the given problem.

5. Conclusions

This paper determined the fractional-order Kawahara and fifth-order KdV equations, applying the ρ-homotopy perturbation transform method. The present method is used to describe the results for specific examples. The ρ-HPTM result is highly congruent with the precise solution of the suggested problems. Additionally, the proposed method estimated the results of the cases using fractional-order derivatives. The graphical examination of the resulting fractional-order results proved their convergence to integer-order outcomes. Additionally, the ρ-HPTM technique is straightforward, simple, and computationally efficient; the suggested method can be adapted to solve additional fractional-order partial differential equations.

Data Availability

The numerical data used to support the findings of this study are included within the article.

Conflicts of Interest

The authors declare that there are no conflicts of interest regarding the publication of this article.

Acknowledgments

The authors would like to thank the Deanship of Scientific Research at Umm Al-Qura University for supporting this work (grant code: 22UQU4310396DSR08).

References

[1] N. Iqbal, A. Akgul, R. Shah, A. Bariq, M. Mossa Al-Sawalha, and A. Ali, "On solutions of fractional-order gas dynamics equation by effective techniques," *Journal of Function Spaces*, vol. 2022, 2022.

[2] M. Alesemi, N. Iqbal, and T. Botmart, "Novel analysis of the fractional-order system of non-linear partial differential equations with the exponential-decay kernel," *Mathematics*, vol. 10, no. 4, p. 615, 2022.

[3] M. Alesemi, N. Iqbal, and A. A. Hamoud, "The analysis of fractional-order proportional delay physical models via a novel transform," *Complexity*, vol. 2022, Article ID 2431533, 13 pages, 2022.

[4] M. Areshi, S. A. El-Tantawy, B. M. Alotaibi, and S. Zaland, "Study of fuzzy fractional third-order dispersive KdV equation in a plasma under atangana-baleanu derivative," *Journal of Function Spaces*, vol. 2022, 2022.

[5] P. Sunthrayuth, N. H. Aljahdaly, A. Ali, R. Shah, I. Mahariq, and A. M. Tchalla, "ψ-Haar wavelet operational matrix method for fractional relaxation-oscillation equations containing-caputo fractional derivative," *Journal of Function Spaces*, vol. 2021, 2021.

[6] N. A. Shah, E. R. El-Zahar, and J. D. Chung, "Fractional analysis of coupled Burgers equations within Yang Caputo-Fabrizio operator," *Journal of Function Spaces*, vol. 2022, 2022.

[7] M. Naeem, A. M. Zidan, K. Nonlaopon, M. I. Syam, Z. Al-Zhour, and R. Shah, "A new analysis of fractional-order equal-width equations via novel techniques," *Symmetry*, vol. 13, no. 5, p. 886, 2021.

[8] M. M. Khader and K. M. Saad, "Numerical studies of the fractional Korteweg-de Vries, Korteweg-de Vries-burgers' and burgers' equations," *Proceedings of the National Academy of Sciences, India - Section A*, vol. 91, no. 1, pp. 67–77, 2021.

[9] K. Nonlaopon, A. M. Alsharif, A. M. Zidan, A. Khan, Y. S. Hamed, and R. Shah, "Numerical investigation of fractional-order Swift-Hohenberg equations via a Novel transform," *Symmetry*, vol. 13, no. 7, Article ID 1263, 2021.

[10] K. M. Saad, E. H. F. Al-Shareef, A. K. Alomari, D. Baleanu, and J. F. Gómez-Aguilar, "On exact solutions for time-fractional Korteweg-de Vries and Korteweg-de Vries-Burger's equations using homotopy analysis transform method," *Chinese Journal of Physics*, vol. 63, pp. 149–162, 2020.

[11] R. P. Agarwal, F. Mofarreh, R. Shah, W. Luangboon, and K. Nonlaopon, "An analytical technique, based on natural transform to solve fractional-order parabolic equations," *Entropy*, vol. 23, no. 8, Article ID 1086, 2021.

[12] N. Alam Khan, S. Ahmed, S. Ahmed, T. Hameed, and M. Asif Zahoor Raja, "Expedite homotopy perturbation method based on metaheuristic technique mimicked by the flashing behavior of fireflies," *AIMS Mathematics*, vol. 4, no. 4, pp. 1114–1132, 2019.

[13] N. H. Aljahdaly, R. P. Agarwal, R. Shah, and T. Botmart, "Analysis of the time fractional-order coupled burgers equations with non-singular kernel operators," *Mathematics*, vol. 9, no. 18, Article ID 2326, 2021.

[14] N. A. Shah, I. Dassios, E. R. El-Zahar, and J. D. Chung, "An efficient technique of fractional-order physical models involving ρ-laplace transform," *Mathematics*, vol. 10, no. 5, p. 816, 2022.

[15] K. Nonlaopon, M. Naeem, A. M. Zidan, R. Shah, A. Alsanad, and A. Gumaei, "Numerical investigation of the time-fractional whitham-broer-kaup equation involving without singular kernel operators," *Complexity*, vol. 2021, 2021.

[16] H. Koçak, "A combined meshfree exponential Rosenbrock integrator for the third-order dispersive partial differential equations," *Numerical Methods for Partial Differential Equations*, vol. 37, no. 3, pp. 2458–2468, 2020.

[17] M. K. Alaoui, R. Fayyaz, A. Khan, R. Shah, and M. S. Abdo, "Analytical investigation of noyes-field model for time-fractional belousov-zhabotinsky reaction," *Complexity*, vol. 2021, 2021.

[18] H. Sun and W. Cao, "A fast temporal second-order difference scheme for the time-fractional subdiffusion equation," *Numerical Methods for Partial Differential Equations*, vol. 37, no. 3, pp. 1825–1846, 2020.

[19] M. Kazeminia, S. Soleimani-Amiri, and S. A. Zahedi, "Exact and numerical solutions for nonlinear higher order modified KdV equations by using variational iteration method," *Advanced Studies in Theoretical Physics*, vol. 4, no. 9, pp. 437–447, 2010.

[20] S. Rashid, A. Khalid, S. Sultana, Z. Hammouch, R. Shah, and A. M. Alsharif, "A novel analytical view of time-fractional Korteweg-De Vries equations via a new integral transform," *Symmetry*, vol. 13, no. 7, Article ID 1254, 2021.

[21] A. Goswami, J. Singh, and D. Kumar, "A reliable algorithm for KdV equations arising in warm plasma," *Nonlinear Engineering*, vol. 5, no. 1, pp. 7–16, 2016.

[22] N. A. Shah, H. A. Alyousef, S. A. El-Tantawy, R. Shah, and J. D. Chung, "Analytical investigation of fractional-order korteweg-de-vries-type equations under atangana-baleanu-caputo operator: modeling nonlinear waves in a plasma and fluid," *Symmetry*, vol. 14, no. 4, p. 739, 2022.

[23] M. Alesemi, N. Iqbal, and M. S. Abdo, "Novel investigation of fractional-order cauchy-reaction diffusion equation involving caputo-fabrizio operator," *Journal of Function Spaces*, vol. 2022, 2022.

[24] N. Iqbal, H. Yasmin, A. Rezaiguia, J. Kafle, A. O. Almatroud, and T. S. Hassan, "Analysis of the fractional-order kaup-kupershmidt equation via novel transforms," *Journal of Mathematics*, vol. 2021, 2021.

[25] N. Iqbal, H. Yasmin, A. Ali, A. Bariq, M. M. Al-Sawalha, and W. W. Mohammed, "Numerical methods for fractional-order fornberg-whitham equations in the sense of atangana-baleanu derivative," *Journal of Function Spaces*, vol. 2021, 2021.

[26] P. Sunthrayuth, A. M. Zidan, S.-W. Yao, R. Shah, and M. Inc, "The comparative study for solving fractional-order fornberg-whitham equation via ρ-laplace transform," *Symmetry*, vol. 13, no. 5, p. 784, 2021.

[27] T. Kakutani and H. Ono, "Weak non-linear hydromagnetic waves in a cold collision-free plasma," *Journal of the Physical Society of Japan*, vol. 26, no. 5, pp. 1305–1318, 1969.
[28] R. Shah, H. Khan, D. Baleanu, P. Kumam, and M. Arif, "A novel method for the analytical solution of fractional Zakharov-Kuznetsov equations," *Advances in Difference Equations*, vol. 2019, no. 1, pp. 1–14, 2019.
[29] A. Goswami, J. Singh, and D. Kumar, "Numerical simulation of fifth order KdV equations occurring in magneto-acoustic waves," *Ain Shams Engineering Journal*, vol. 9, no. 4, pp. 2265–2273, 2018.
[30] M. O. Miansari, M. E. Miansari, A. Barari, and D. D. Ganji, "Application of He's variational iteration method to nonlinear helmholtz and fifth-order KdV equations," *Journal of Applied Mathematics, Statistics and Informatics*, vol. 5, no. 1, pp. 5–19, 2009.
[31] S. Abbasbandy and F. S. Zakaria, "Soliton solutions for the fifth-order KdV equation with the homotopy analysis method," *Nonlinear Dynamics*, vol. 51, pp. 83–87, 2008.
[32] A.-M. Wazwaz, "Solitons and periodic solutions for the fifth-order KdV equation," *Applied Mathematics Letters*, vol. 19, no. 11, pp. 1162–1167, 2006.
[33] M. T. Darvishi and F. Khani, "Numerical and explicit solutions of the fifth-order Korteweg-de Vries equations," *Chaos, Solitons & Fractals*, vol. 39, no. 5, pp. 2484–2490, 2009.
[34] H. Wei-Peng and D. Zi-Chen, "Multi-symplectic method for generalized fifth-order KdV equation," *Chinese Physics B*, vol. 17, no. 11, pp. 3923–3929, 2008.
[35] H. Khan, R. Shah, P. Kumam, D. Baleanu, and M. Arif, "Laplace decomposition for solving nonlinear system of fractional order partial differential equations," *Advances in Difference Equations*, vol. 1, pp. 1–18, 2020.
[36] S. Zhang, "Application of Exp-function method to a KdV equation with variable coefficients," *Physics Letters A*, vol. 365, no. 5-6, pp. 448–453, 2007.
[37] F. Jarad and T. Abdeljawad, "A modifi ed Laplace transform for certain generalized fractional operators," *Results in Nonlinear Analysis*, vol. 1, no. 2, pp. 88–98, 2018.
[38] J.-H. He, "Homotopy perturbation method: a new nonlinear analytical technique," *Applied Mathematics and Computation*, vol. 135, no. 1, pp. 73–79, 2003.
[39] J.-H. He, "Homotopy perturbation method for bifurcation of nonlinear problems," *International Journal of Nonlinear Sciences and Numerical Stimulation*, vol. 6, no. 2, pp. 207-208, 2005.
[40] J.-H. He, "Homotopy perturbation method for solving boundary value problems," *Physics Letters A*, vol. 350, no. 1-2, pp. 87-88, 2006.
[41] M. Mahgoub and A. Sedeeg, "A comparative study for solving nonlinear fractional heat -like equations via elzaki transform," *British Journal of Mathematics & Computer Science*, vol. 19, no. 4, pp. 1–12, 2016.
[42] E. M. Elsayed, R. Shah, and K. Nonlaopon, "The analysis of the fractional-order Navier-Stokes equations by a novel approach," *Journal of Function Spaces*, vol. 2022, 2022.
[43] P. Singh and D. Sharma, "Comparative study of homotopy perturbation transformation with homotopy perturbation Elzaki transform method for solving nonlinear fractional PDE," *Nonlinear Engineering*, vol. 9, no. 1, pp. 60–71, 2019.
[44] S. Das and P. K. Gupta, "An approximate analytical solution of the fractional diffusion equation with absorbent term and external force by homotopy perturbation method," *Zeitschrift für Naturforschung A*, vol. 65, no. 3, pp. 182–190, 2010.

Hindawi
Journal of Mathematics
Volume 2022, Article ID 7494049, 18 pages
https://doi.org/10.1155/2022/7494049

Research Article

Persistence of Heteroclinic Cycles Connecting Repellers in Banach Spaces

Zongcheng Li

School of Science, Shandong Jianzhu University, Jinan 250101, China

Correspondence should be addressed to Zongcheng Li; chengzi_0905@163.com

Received 11 December 2021; Accepted 15 February 2022; Published 12 May 2022

Academic Editor: Fairouz Tchier

This paper is concerned with persistence of heteroclinic cycles connecting repellers in Banach spaces. It is proved that if a map with a regular and nondegenerate heteroclinic cycle connecting repellers undergoes a small perturbation, then the perturbed map can still have a regular and nondegenerate heteroclinic cycle connecting repellers. The perturbation rang is given by an explicit positive constant according to the properties of the original map. Hence, the perturbed map and the original map are simultaneously chaotic in the sense of both Devaney and Li-Yorke. Especially, the persistence of heteroclinic cycles connecting repellers is also discussed in the Euclidean space, where the repellers can expand in different norms. Finally, three examples are provided to illustrate the validity of the theoretical results.

1. Introduction

Chaos is a very important kind of dynamical behaviors in nonlinear systems and chaos problems have attracted a lot of attention from many scientists and sgd mathematicians. In 1975, the first mathematical definition of chaos and a famous result that “period three implies chaos” were given by Li and Yorke [1] in studying continuous interval maps. After that, different definitions of chaos from different points of view were proposed by researchers, one can see [2–4] for some related definitions of chaos. Among these mathematical definitions, chaos in the sense of Li-Yorke, Devaney or Wiggins are often used in the literature, see [5–8] for discussions of their relationships. Then, there appeared many works to study chaotic behaviors of multidimensional maps. A very famous work that “a snap-back repeller implies chaos” in the sense of Li-Yorke was proposed by Marotto [9], which is a generalization of Li and Yorke’s result from one-dimensional maps to multidimensional maps. This result shows great power in studying chaos of finite dimensional maps. However, it is clear that there are many systems should be studied in infinite dimensional spaces, such as Banach spaces and metric spaces. Then, a lot of works have been done on chaotic behaviors of infinite dimensional maps. Some of these important results were given by Shi and her cooperators. In 2004, Shi and Chen [10] extended the concept of snap-back repeller to metric spaces and obtained several criteria of chaos. Later, Shi and her cooperators developed the coupled-expansion theory and used it to study chaos, see [11–14] and references therein.

Structural stability of chaotic maps is a very important and interesting question, and many results have been achieved. Marotto first studied perturbations of maps with snap-back repellers in [15, 16], and proved that if a scalar system with a snap-back repeller undergoes a small perturbation, then the perturbation system will have a transversal homoclinic point and thus has chaotic behaviors. Later, there appeared several results about multidimensional perturbations of chaotic systems, see [17–19]. In 2009, Li and Lyu [20] proved that if a map with a snap-back repeller in $\mathbf{R}^n$ undergoes a mall C^1 perturbation, then the perturbed map still has a snap-back repeller and consequently is chaotic in the sense of Li-Yorke. However, all the above perturbations of chaotic systems were made in finite dimensional spaces. In 2011, Chen et al. [21] studied the persistence of snap-back repellers under small C^1 perturbations in Banach spaces. In 2012, Zhang et al. [22] used a different method to study the persistence of snap-back repellers under small Lipschitz perturbations in Banach spaces. Moreover, Zhang and Shi [23] studied the persistence of coupled-expansion for time-varying systems under small time-varying perturbations in Banach spaces, and showed the persistence of snap-back repellers.

In 2006, Lin and Chen [24] gave a result that heteroclinical repellers imply chaos in the sense of Li-Yorke in $\mathbf{R}^n$. In their definition of heteroclinical repellers, there were some conditions given by the Jacobian matrices of a map. However, a map in a metric space may not have derivatives in general. In 2008, based on their work, Li et al. [25] grasped the essential meanings of the definition of heteroclinical repellers to extend it to general metric spaces without needing the continuity or continuous differentiability. For more intuitive to reflect the relationships of the repellers, they redefined it as a heteroclinic cycle connecting repellers and obtained several criteria of chaos. Later, they studied chaos induced by heteroclinic cycles connecting repellers in general Banach spaces [26], and used these results to study existence of chaos or chaotification problems [27]. This shows that the heteroclinic cycle connecting repellers has significant effects on chaos studying. Hence, it is worth studying whether a heteroclinic cycle connecting repellers has the persistence under small perturbations as that for a snap-back repeller. Recently, in 2020, Chen and Wu [28] studied the persistence of heteroclinic repellers in $\mathbf{R}^n$ for C^1 maps under small C^1 perturbations. Chen et al. [29] studied the persistence of heteroclinic repellers in Banach spaces for C^1 maps under small C^1 perturbations. It is noted that the definitions of heteroclinic repellers in [28, 29] both needed the differentiability of a map as that definition in [24]. In 2021, Wu [30] extended the concept of heteroclinic repellers in [24] to heteroclinic cycle connecting expanding periodic points in $\mathbf{R}^n$ and studied the persistence of it for C^1 maps under C^1 perturbations, where the maps needed to be continuously differentiable in the whole space. More recently, Chen and Luo [31] studied the persistence of regular nondegenerate snap-back repellers and heteroclinic cycles for continuous maps under small Lipschitz perturbations, where the maps were continuous in the whole Banach space. On the one hand, it should be pointed out that all the above results needed the maps to be continuous or continuously differentiable in the whole space. However, there are a lot of maps that may not be continuous or continuously differentiable in the whole space. On the other hand, it should be pointed out that all the above results needed the perturbations to be small enough and did not give a relatively explicit expression for the range of small perturbations, which is convenient and useful in applications to quickly check out whether the persistence is maintained. So, it is meaningful to study persistence of heteroclinic cycles connecting repellers for maps which are only continuous or continuously differentiable in some domains of the whole space, and it is also meaningful to study the explicit expression for the range of small perturbations.

The fixed point theory has become an essential tool to resolve some problems in nonlinear analysis, including fractional calculus, see [32, 33] and references therein for more details about this theory. Here, we will apply the Banach contractive mapping principle and the ideas used in [22, 23] to study the persistence of regular and nondegenerate heteroclinic cycles connecting repellers in Banach spaces, where the original maps are only continuous or continuously differentiable in some neighborhoods of points. An important result is that an explicit expression for the range of perturbations is given. It will be proved that if a map with a regular and nondegenerate heteroclinic cycle connecting repellers undergoes a small Lipschitz perturbation, then the perturbed map can still have a regular and nondegenerate heteroclinic cycle connecting repellers. So, the perturbed map and the original map are simultaneously chaotic in the sense of both Devaney and Li-Yorke. Particularly, the persistence of heteroclinic cycles connecting repellers is also discussed in $\mathbf{R}^n$. The significant difference between our result and those obtained in [28, 30] is that the repellers in our result expand in different norms, while the repellers in the latter expand in the single Euclidean norm. It is clear that different fixed points can expand in different norms in $\mathbf{R}^n$. So, our result is more general in practice.

The rest of the paper is organized as follows. Some concepts and lemmas are given in Section 2. Several theorems about perturbations of maps with heteroclinic cycles connecting repellers in general Banach spaces or the Euclidean space are given in Section 3. Three examples are provided to illustrate the validity the theoretical results in Section 4. Finally, conclusions are made in Section 5.

2. Preliminaries

Some definitions and lemmas are given in this section.

Two usually used definitions of chaos in the sense of Li-Yoke or Devaney are first introduced. Then, the concept of a heteroclinic cycle connecting repellers is introduced.

Definition 1 (see [1]). Let (X, d) be a metric space, $f\colon X \longrightarrow X$ be a map, and S be a set of X with at least two distinct points. Then, S is called a scrambled set of f if for any two distinct points $x, y \in S$,

$$\liminf_{n\longrightarrow\infty} d\left(f^n(x), f^n(y)\right) = 0, \quad \limsup_{n\longrightarrow\infty} d\left(f^n(x), f^n(y)\right) > 0. \tag{1}$$

The map f is said to be chaotic in the sense of Li-Yorke if there exists an uncountable scrambled set S of f.

Remark 1. There are three conditions in the original characterization of chaos in Li-Yorke's theorem [1]. Since the third one is not essential, it is removed in Definition 1 in most literature.

Example 1. Consider the following Baker's equation

$$x_{n+1} = \begin{cases} 2x_n, & \text{for } 0 \le x_n \le \dfrac{1}{2}, \\ 2\left(1 - x_n\right), & \text{for } \dfrac{1}{2} < x_n \le 1, \end{cases} \tag{2}$$

which models the mixing of a dye spot on a strip of dough that is repeatedly stretched and folded over on itself. The iterative scheme (2) maps the interval $[0,1]$ into itself. It is easy to check that system (2) has a cycle of period three and hence is chaotic in the sense of Li-Yorke by the Li-Yorke theorem in [1]. This equation has been extensively discussed in the literature [7, 34] and references cited therein.

Definition 2 (see [4]). Let (X,d) be a metric space. A map $f\colon V\subset X\longrightarrow V$ is said to be chaotic on V in the sense of Devaney if

(i) The set of the periodic points of f is dense in V
(ii) f is topologically transitive in V
(iii) f has sensitive dependence on initial conditions in V

Remark 2. In 1992, Banks et al. [5] proved that conditions (i) and (ii) together imply condition (iii) if f is continuous in V. So, condition (iii) is redundant in the above definition in this case. It has been proved by [6] that chaos in the sense of Devaney is stronger than chaos in the sense of Li-Yorke under some conditions.

Example 2. Let

$$\sum\nolimits_2^+ := \left\{s=(s_0,s_1,s_2,\ldots)\colon s_j=0 \text{ or } 1\right\}, \quad (3)$$

with the distance

$$\rho(s,t) := \sum_{i=0}^{\infty}\frac{|s_i-t_i|}{2^i}, \quad (4)$$

where $s=(s_0,s_1,s_2,\ldots)$ and $t=(t_0,t_1,t_2,\ldots)$. Then $(\sum_2^+\rho)$ is a complete metric space and a Cantor set, see Lemma 2.5 in [10]. The shift map $\sigma\colon\Sigma_2^+\longrightarrow\Sigma_2^+$ defined by $\sigma((s_0,s_1,s_2,\ldots))=(s_1,s_2,\ldots)$ is continuous. The dynamical system defined by σ is called a one-sided symbolic dynamical system. It follows from [[4], Part 1, Proposition 6.6] that σ has the following properties:

(i) $\operatorname{Card}\operatorname{Per}_n(\sigma)=2^n$
(ii) $\operatorname{Per}(\sigma)$ is dense in Σ_2^+
(iii) there exists a dense orbit of σ in Σ_2^+

Here, $\operatorname{Card}\operatorname{Per}_n(\sigma)$ denotes the number of periodic points of period n for σ. It is clear that property (iii) implies that σ is transitive. Therefore, the symbolic dynamical system is chaotic in the sense of Devaney. See [3, 4] for more discussions about this symbolic dynamical system.

Definition 3 (see [26], Definition 2.5). Let (X,d) be a metric space and $f\colon X\longrightarrow X$ be a map with $k(\geq 2)$ fixed points $z_1,\ldots,z_k\in X$.

(I) Suppose that, for each $i\,(1\leq i\leq k)$, z_i is an expanding fixed point of f in $\overline{B}_{r_i}(z_i)$, and there exist a point $x_{i0}\in B_{r_i}(z_i)$, $x_{i0}\neq z_i$, and a positive integer $m_i\geq 1$ such that $f^{m_i}(x_{i0})=z_{t(i)}$, and z_i is the limit for the backward orbit of x_{i0}, where $\overline{B}_{r_i}(z_i)$ and $\overline{B}_{r_i}(z_i)$ are the closed and open balls of radius r_i centered at z_i, $t(i)=[i \bmod k]+1$. Then all the points $x_{i0}\,(1\leq i\leq k)$, together with their backward and forward orbits consist of a set, which is called a k-heteroclinic cycle connecting repellers $z_1,\ldots,z_k$.

(II) Suppose that f has a k-heteroclinic cycle connecting repellers $z_1,\ldots,z_k$. For each point x_0 on the cycle, if there exists a positive constant r_0 such that for each positive constant $r\leq r_0$, $f(x_0)$ is an interior point of $f(B_r(x_0))$, then the cycle is called regular; if there exist positive constants r_1 and μ such that $d(f(x),f(y))\geq\mu\, d(x,y),\forall x,y\in\overline{B}_{r_1}(x_0)$, then the cycle is called nondegenerate.

Remark 3. It is pointed out that the necessary and sufficient condition for a heteroclinic cycle connecting repellers is used to give the definition (I) for simplicity, see (1) of Remark 2.2 in [26]. In addition, it does not need the continuity or continuous differentiability in this definition, while some similar definitions need them, see [24–26, 28–31] for more details about this concept.

For convenience, some notations are given in the following. The continuously differentiable maps in a set U of a Banach space X are denoted by $C^1(U,X)$. The derivative of a map f at a point $x\in X$ is denoted by $Df(x)$. In addition, for a linear map $L\colon X\longrightarrow X$, denote

$$\begin{aligned}\|L\| &:= \sup\{\|Lx\|\colon x\in X,\|x\|=1\},\\ \|L\|^0 &:= \inf\{\|Lx\|\colon x\in X,\|x\|=1\}.\end{aligned} \quad (5)$$

If a bounded linear map L has a bounded inverse, then L is said to be an invertible linear map, see Definition 4.17 in [35]. The following four lemmas will be used in the paper.

Lemma 1 (see [22], Lemma 2.4). *Let $(X,\|\cdot\|)$ be a Banach space, $z\in X$, and $f\colon\overline{B}_r(z)\longrightarrow f(\overline{B}_r(z))$ be a continuous map. Assume that $f(B_r(z))$ is an open set of X and*

$$\|f(x)-f(y)\|\geq\mu\|x-y\|,\quad\forall x,y\in\overline{B}_r(z), \quad (6)$$

for some constant $\mu>0$, then

$$B_{(\mu-L)r}(F(z))\subset F(B_r(z)), \quad (7)$$

where $F=f+g$ and g is a Lipschitz map in $\overline{B}_r(z)$ with Lipschitz constant $L<\mu$.

Lemma 2 (see [25], Theorem 3.4). *Let (X,d) be a complete metric space and $f\colon X\longrightarrow X$ be a map. Assume that*

(i) f has a regular and nondegenerate k-heteroclinic cycle connecting repellers $z_1,\ldots,z_k\in X$, $k\geq 2$
(ii) f is continuous in some neighborhood of each point on the cycle

Then there exists an uncountable, perfect, bounded, and closed set V such that $f(V)=V$ and f is chaotic on V in the sense of Devaney as well as in the sense of Li-Yorke.

Lemma 3 (see [26], Lemma 2.2; [22], Lemma 2.3). *Let $(X,\|\cdot\|)$ be a Banach space and $f\colon X\longrightarrow X$ be a map. Assume that f has a heteroclinic cycle connecting repellers*

$z_1, \ldots, z_k \in X$, $k \geq 2$, *and for each point* x_0 *on the cycle* f *is continuously differentiable in some neighborhood of* x_0 *and satisfies that* $Df(x_0)$ *is an invertible linear map, then the cycle is regular and nondegenerate.*

Lemma 4 (see [11], Lemma 2.2). *Let* $(X, \|\cdot\|)$ *be a Banach space. Suppose that a map* $f\colon X \longrightarrow X$ *is continuously differentiable in* $B_{r_0}(x_0)$ *for some* $x_0 \in X$ *and some* $r_0 > 0$, *and satisfies that* $\lambda_0 = \|Df(x_0)\|^0 > 0$, *then for each* $\varepsilon \in (0, \lambda_0)$, *there exists a positive constant* $r_1 < r_0$ *such that*

$$\|f(x) - f(y)\| \geq (\lambda_0 - \varepsilon)\|x - y\|, \quad \forall x, y \in \overline{B}_{r_1}(x_0). \tag{8}$$

3. Persistence of Heteroclinic Cycles Connecting Repellers in Banach Spaces

In this section, we will study persistence of heteroclinic cycles connecting repellers in Banach spaces. Assume that $(X, \|\cdot\|)$ is a Banach space, f, $g\colon X \longrightarrow X$ are two maps, and f has a regular and nondegenerate heteroclinic cycle connecting repellers and is continuous in some neighborhoods of interest points. Here, we study the following system:

$$x_{n+1} = f(x_n) + g(x_n), \quad n \geq 0, \tag{9}$$

where g is viewed as a mall perturbation. It is proved that there still has a regular and nondegenerate heteroclinic cycle connecting repellers in (9) when g satisfies some conditions. Consequently, the perturbed system (9) is chaotic in the sense of both Devaney and Li-Yorke.

Theorem 1. *Suppose that* $(X, \|\cdot\|)$ *is a Banach space and* $f\colon X \longrightarrow X$ *is a map with* $k(\geq 2)$ *different fixed points* $z_1, \ldots, z_k \in X$ *and satisfies the following:*

(i) For each i $(1 \leq i \leq k)$, z_i *is a regular expanding fixed point of* f *in* $\overline{B}_{r_i}(z_i)$ *with expanding coefficient* λ_{i0} *for some constant* $r_i > 0$. *Furthermore, there exist a point* $x_{i0} \in B_{r_i}(z_i)$, $x_{i0} \neq z_i$, *and a positive integer* $m_i \geq 1$ *such that* $f^{m_i}(x_{i0}) = z_{t(i)}$, *where* $t(i) = [i \bmod k] + 1$. *Consequently,* f *has a heteroclinic cycle* Γ *connecting repellers* $z_1, \ldots, z_k$.

(ii) The heteroclinic cycle Γ *connecting repellers is regular and nondegenerate, and* f *is continuous in* $\overline{B}_{r_i}(z_i)$ *and some neighborhood* U_{ij} *of* x_{ij}, *where* $x_{ij} = f^j(x_{i0})$ *for* $1 \leq i \leq k$, $1 \leq j \leq m_i - 1$.

Then, there exists a constant $\varepsilon_0 > 0$ such that for any Lipschitz map g in each set of $\overline{B}_{r_i}(z_i)$ and U_{ij}, $1 \leq i \leq k$, $1 \leq j \leq m_i - 1$, with the Lipschitz constant L satisfying

$$\max\left\{L, \|g(z_i)\|, \left\|g\left(x_{ij}\right)\right\|, 1 \leq i \leq k, 0 \leq j \leq m_i - 1\right\} < \varepsilon_0. \tag{10}$$

The perturbed system (9) also has a regular and nondegenerate heteroclinic cycle Γ' connecting repellers, and consequently there exists an uncountable, perfect, bounded, and closed set V such that system (9) is chaotic on V in the sense of both Devaney and Li-Yorke.

Proof. Without loss of generality and for simplicity, we only show that Theorem 1 is true for $k = 2$. When $k > 2$, one can use a similar method to prove it. For convenience, let $F(x) := f(x) + g(x)$ in the rest of this paper and $i = 1$ or 2 in the rest of this proof.

Without loss of generality, we can suppose that $\overline{B}_{r_1}(z_1) \cap \overline{B}_{r_2}(z_2) = \varnothing$, and $f(x_{i0}) \notin B_{r_i}(z_i)$. Otherwise, one can see the third paragraph in the proof of Theorem 3.1 in [25].

Since z_i is a regular expanding fixed point of f in $\overline{B}_{r_i}(z_i)$ with an expanding coefficient λ_{i0}, we get that

$$\|f(x) - f(y)\| \geq \lambda_{i0}\|x - y\|, \quad \forall x, y \in \overline{B}_{r_i}(z_i), \tag{11}$$

$f\colon \overline{B}_{r_i}(z_i) \longrightarrow f(\overline{B}_{r_i}(z_i))$ is a homeomorphism and $f(B_{r_i}(z_i))$ is open, $f(D)$ is open for any open set $D \subset B_{r_i}(z_i)$. Take a constant

$$\delta_{i0} < \frac{r_i - \|z_i - x_{i0}\|}{2}, \tag{12}$$

such that $\overline{B}_{\delta_{i0}}(x_{i0}) \subset B_{r_i}(z_i)$. Then, it follows form (11) that $f\colon B_{\delta_{i0}}(x_{i0}) \longrightarrow f(B_{\delta_{i0}}(x_{i0}))$ is also a homeomorphism.

From assumption (ii), it follows that there exist positive constants μ_{ij} and δ_{ij} such that

$$\|f(x) - f(y)\| \geq \mu_{ij}\|x - y\|, \quad \forall x, y \in \overline{B}_{\delta_{ij}}\left(x_{ij}\right), \tag{13}$$

$f\colon B_{\delta_{ij}}(x_{ij}) \longrightarrow f(B_{\delta_{ij}}(x_{ij}))$ is homeomorphic, and $f(B_{\delta_{ij}}(x_{ij}))$ is open for $1 \leq j \leq m_i - 1$, where δ_{ij} satisfies the following conditions

$$\delta_{i1} < \lambda_{i0}\delta_{i0}, \quad \delta_{i,j+1} < \mu_{ij}\delta_{ij}, \quad \text{for } 1 \leq j \leq m_i - 2, \tag{14}$$

$\overline{B}_{\delta_{ij}}(x_{ij})$ are disjoint subsets of U_{ij} and $\overline{B}_{\delta_{ij}}(x_{ij}) \cap B_{r_i}(z_i) = \varnothing$ for fixed i and $1 \leq j \leq m_i - 1$.

In the following, we will show that the map F satisfies the conditions in Lemma 2. It will be finished by the following three steps. □

Step 1. It is to prove that F has two regular expanding fixed points z_1^* and z_2^* when g satisfies some conditions.

For proving the existence of z_1^*, we take two positive constants δ_{2,m_2} and ε_1 such that

$$\delta_{2,m_2} < \begin{cases} \min\left\{\lambda_{20}\delta_{20}, \dfrac{r_1 - \|z_1 - x_{10}\|}{2} - \delta_{10}\right\}, & \text{if } m_2 = 1; \\ \min\left\{\mu_{2,m_2-1}\delta_{2,m_2-1}, \dfrac{r_1 - \|z_1 - x_{10}\|}{2} - \delta_{10}\right\}, & \text{if } m_2 > 1. \end{cases}$$

$$\varepsilon_1 = \frac{(\lambda_{10} - 1)\delta_{2,m_2}}{1 + \delta_{2,m_2}}. \tag{15}$$

Consider the following equation

$$F(x) = x, \quad x \in \overline{B}_{\delta_{2,m_2}}(z_1), \tag{16}$$

which is equivalent to the following equation:

$$f(x) = x - g(x), \quad x \in \overline{B}_{\delta_{2,m_2}}(z_1). \tag{17}$$

It follows from the first relation of (15) that $\overline{B}_{\delta_{2,m_2}}(z_1) \subset B_{r_1}(z_1)$. By assumption (i) and (11), we get that $f: \overline{B}_{\delta_{2,m_2}}(z_1) \longrightarrow f(\overline{B}_{\delta_{2,m_2}}(z_1))$ is homeomorphic. Then we obtain that $f(B_{\delta_{2,m_2}}(z_1))$ is an open set and the inverse map $f^{-1}: f(\overline{B}_{\delta_{2,m_2}}(z_1)) \longrightarrow \overline{B}_{\delta_{2,m_2}}(z_1)$ satisfies the following:

$$\|f^{-1}(x) - f^{-1}(y)\| \le \lambda_{10}^{-1}\|x - y\|, \quad \forall x, y \in f\left(\overline{B}_{\delta_{2,m_2}}(z_1)\right). \tag{18}$$

Hence, equation (17) is translated into the following:

$$f^{-1}(x - g(x)) = x. \tag{19}$$

Here, it should prove that

$$x - g(x) \in f\left(\overline{B}_{\delta_{2,m_2}}(z_1)\right), \quad \forall x \in \overline{B}_{\delta_{2,m_2}}(z_1). \tag{20}$$

On the one hand, for any $x \in \overline{B}_{\delta_{2,m_2}}(z_1)$, we have

$$\begin{aligned}\|g(x)\| &= \left\|g(x) - g(z_1) + g(z_1)\right\| \le \left\|g(x) - g(z_1)\right\| \\ &\quad + \left\|g(z_1)\right\| \le L\delta_{2,m_2} + \left\|g(z_1)\right\|.\end{aligned} \tag{21}$$

Suppose that the map g satisfies

$$\max\left\{L, \left\|g(z_1)\right\|\right\} < \varepsilon_1, \tag{22}$$

then,

$$L\delta_{2,m_2} + \left\|g(z_1)\right\| < \varepsilon_1\delta_{2,m_2} + \varepsilon_1 = (\lambda_{10} - 1)\delta_{2,m_2}. \tag{23}$$

Therefore, it follows from (21) and (23) that, for any $x \in \overline{B}_{\delta_{2,m_2}}(z_1)$,

$$\left\|x - g(x) - z_1\right\| \le \|g(x)\| + \left\|x - z_1\right\| < (\lambda_{10} - 1)\delta_{2,m_2} + \delta_{2,m_2} = \lambda_{10}\delta_{2,m_2}. \tag{24}$$

On the other hand, for any $x \in \partial B_{\delta_{2,m_2}}(z_1)$,

$$\left\|f(x) - z_1\right\| = \left\|f(x) - f(z_1)\right\| \ge \lambda_{10}\left\|x - z_1\right\| = \lambda_{10}\delta_{2,m_2}. \tag{25}$$

Since $z_1 \in f(B_{\delta_{2,m_2}}(z_1))$ and $f(B_{\delta_{2,m_2}}(z_1))$ is an open set, it follows from (24) and (25) that (20) is true.

According to the above discussion, we can define a map

$$h_1(x) = f^{-1}(x - g(x)), \quad x \in \overline{B}_{\delta_{2,m_2}}(z_1). \tag{26}$$

For any $x \in \overline{B}_{\delta_{2,m_2}}(z_1)$, it follows from (18) and (24) that

$$\left\|h_1(x) - z_1\right\| = \left\|f^{-1}(x - g(x)) - f^{-1}(z_1)\right\| \le \lambda_{10}^{-1}\left\|x - g(x) - z_1\right\| < \delta_{2,m_2}, \tag{27}$$

which implies that h_1 maps $\overline{B}_{\delta_{2,m_2}}(z_1)$ into itself. Moreover, for any $x, y \in \overline{B}_{\delta_{2,m_2}}(z_1)$, we get from (18) that

$$\begin{aligned}\left\|h_1(x) - h_1(y)\right\| &= \left\|f^{-1}(x - g(x)) - f^{-1}(y - g(y))\right\| \\ &\le \lambda_{10}^{-1}[\|g(x) - g(y)\| + \|x - y\|] \\ &\le \lambda_{10}^{-1}(L + 1)\|x - y\|.\end{aligned} \tag{28}$$

It follows from the second relation of (15) and (22) that

$$\lambda_{10} > L + 1, \tag{29}$$

which together with (28) yields that h_1 is contractive in $\overline{B}_{\delta_{2,m_2}}(z_1)$. It follows from the Banach contractive mapping principle and (27) that there exists a unique point $z_1^* \in B_{\delta_{2,m_2}}(z_1)$ satisfying $h_1(z_1^*) = z_1^*$. Consequently, $F(z_1^*) = z_1^*$, that is, z_1^* is a fixed point of F in $B_{\delta_{2,m_2}}(z_1)$.

It should prove that z_1^* is a regular expanding fixed point of F in some neighborhood of z_1^*. To do this, take

$$r_1^* = \frac{r_1 + \left\|z_1 - x_{10}\right\|}{2}. \tag{30}$$

Then, it follows from $z_1^* \in B_{\delta_{2,m_2}}(z_1)$ and the first relation of (15) that

$$\begin{aligned}\left\|x_{10} - z_1^*\right\| &= \left\|x_{10} - z_1 + z_1 - z_1^*\right\| \\ &\le \left\|x_{10} - z_1\right\| + \left\|z_1 - z_1^*\right\| \\ &\le \left\|x_{10} - z_1\right\| + \delta_{2,m_2} \\ &< \left\|x_{10} - z_1\right\| + \frac{r_1 - \left\|z_1 - x_{10}\right\|}{2} \\ &\quad - \delta_{10} = r_1^* - \delta_{10},\end{aligned} \tag{31}$$

which implies that $\overline{B}_{\delta_{10}}(x_{10}) \subset B_{r_1^*}(z_1^*)$. For any $x \in B_{r_1^*}(z_1^*)$,

$$\begin{aligned}\left\|x - z_1\right\| &= \left\|x - z_1^* + z_1^* - z_1\right\| \le \left\|x - z_1^*\right\| + \left\|z_1^* - z_1\right\| \\ &< r_1^* + \delta_{2,m_2} < \frac{r_1 + \left\|z_1 - x_{10}\right\|}{2} + \frac{r_1 - \left\|z_1 - x_{10}\right\|}{2} - \delta_{10} \\ &= r_1 - \delta_{10},\end{aligned} \tag{32}$$

which implies that $\overline{B}_{r_1^*}(z_1^*) \subset B_{r_1}(z_1)$. Consequently, $f(B_{r_1^*}(z_1^*))$ is an open set. For any $x, y \in \overline{B}_{r_1^*}(z_1^*)$,

$$\|F(x)-F(y)\| = \|f(x)+g(x)-f(y)-g(y)\| \geq \|f(x)-f(y)\| - \|g(x)-g(y)\| \geq (\lambda_{10}-L)\|x-y\|. \tag{33}$$

Then, it follows from (29) and (33) that z_1^* is an expanding fixed point of F in $\overline{B}_{r_1^*}(z_1^*)$ with expanding coefficient $\lambda_{10}-L>1$. Since $f(B_{r_1^*}(z_1^*))$ is an open set, it follows from Lemma 1 that

$$B_{(\lambda_{10}-L)r_1^*}(z_1^*) = B_{(\lambda_{10}-L)r_1^*}(F(z_1^*)) \subset F\left(B_{r_1^*}(z_1^*)\right). \tag{34}$$

which implies that z_1^* is an interior point of $F(B_{r_1^*}(z_1^*))$. Hence, z_1^* is a regular fixed point of F in $\overline{B}_{r_1^*}(z_1^*)$.

Here, it is to show that $F(B_{r_1^*}(z_1^*))$ is an open set. For each given point $y \in F(B_{r_1^*}(z_1^*))$, there is a point $x \in B_{r_1^*}(z_1^*)$ satisfying $F(x)=y$. Then, there is a constant $\overline{r}_1>0$ satisfying $B_{\overline{r}_1}(x) \subset B_{r_1^*}(z_1^*)$. From the third paragraph of the proof, it is easy to see that $f(B_{\overline{r}_1}(x))$ is an open set because of $B_{r_1^*}(z_1^*) \subset B_{r_1}(z_1)$. It also follows from Lemma 1 again that

$$B_{(\lambda_{10}-L)\overline{r}_1}(y) = B_{(\lambda_{10}-L)\overline{r}_1}(F(x)) \subset F\left(B_{\overline{r}_1}(x)\right) \subset F\left(B_{r_1^*}(z_1^*)\right), \tag{35}$$

which implies that y is an interior point of $F(B_{r_1^*}(z_1^*))$ and then $F(B_{r_1^*}(z_1^*))$ is an open set.

With a similar argument to the existence of z_1^*, we can obtain the following positive constants

$$\delta_{1,m_1} < \begin{cases} \min\left\{ \lambda_{10}\delta_{10}, \dfrac{r_2-\|z_2-x_{20}\|}{2}-\delta_{20} \right\}, & \text{if } m_1 = 1; \\ \min\left\{ \mu_{1,m_1-1}\delta_{1,m_1-1}, \dfrac{r_2-\|z_2-x_{20}\|}{2}-\delta_{20} \right\}, & \text{if } m_1 > 1. \end{cases}$$
$$\varepsilon_2 = \frac{(\lambda_{20}-1)\delta_{1,m_1}}{1+\delta_{1,m_1}},$$
$$r_2^* = \frac{r_2+\|z_2-x_{20}\|}{2}, \tag{36}$$

such that when

$$\max\left\{L, \|g(z_2)\|\right\} < \varepsilon_2, \tag{37}$$

there exists a point $z_2^* \in B_{\delta_{1,m_1}}(z_2)$ satisfying that z_2^* is a regular expanding fixed point of F in $(\overline{B}_{r_2^*}(z_2^*))$ with expanding coefficient $\lambda_{20}-L>1$ and $F(B_{r_2^*}(z_2^*))$ is an open set.

A summary for this step is given as follows. When the following condition holds

$$\max\left\{L, \|g(z_1)\|, \|g(z_2)\|\right\} < \min\{\varepsilon_1, \varepsilon_2\}, \tag{38}$$

the map F will have two regular expanding fixed points $z_1^* \in B_{r_1^*}(z_1^*)$ and $z_2^* \in B_{\delta_{1,m_1}}(z_2)$, and $F(B_{r_i^*}(z_i^*))$ is an open set for $i=1,2$.

Step 2. It is to show that for each $i\,(1 \leq i \leq 2)$ there exists a point y_{i0} in $B_{r_i^*}(z_i^*)$ such that $F^{m_i}(y_{i0}) = z_{t(i)}^*$, where $t(i) = [i \bmod 2]+1$.

We first prove that there exist m_1 points $y_{1j} \in B_{\delta_{1j}}(x_{1j})$, $0 \leq j \leq m_1-1$ such that

$$F\left(y_{1j}\right) = y_{1,j+1}, \quad \text{for } 0 \leq j \leq m_1-2,$$
$$F\left(y_{1,m_1-1}\right) = z_2^*. \tag{39}$$

That is, there exists a point $y_{10} \in B_{\delta_{10}}(x_{10}) \subset B_{r_1^*}(z_1^*)$ such that $F^{m_1}(y_{10}) = z_2^*$.

In order to do that, we first prove the existence of y_{1,m_1-1} by solving the following equation:

$$F(x) = z_2^*, \quad x \in \overline{B}_{\delta_{1,m_1-1}}\left(x_{1,m_1-1}\right), \tag{40}$$

which can be translated into the following:

$$f(x) = z_2^* - g(x), \quad x \in \overline{B}_{\delta_{1,m_1-1}}\left(x_{1,m_1-1}\right). \tag{41}$$

It follows from assumption (ii) and (13) that $f\colon \overline{B}_{\delta_{1,m_1-1}}(x_{1,m_1-1}) \longrightarrow f(\overline{B}_{\delta_{1,m_1-1}}(x_{1,m_1-1}))$ is homeomorphic with the inverse map $f^{-1}\colon f(\overline{B}_{\delta_{1,m_1-1}}(x_{1,m_1-1})) \longrightarrow \overline{B}_{\delta_{1,m_1-1}}(x_{1,m_1-1})$ satisfying

$$\left\|f^{-1}(x) - f^{-1}(y)\right\| \leq \mu_{1,m_1-1}^{-1}\|x-y\|, \quad \forall x, y \in f\left(\overline{B}_{\delta_{1,m_1-1}}\left(x_{1,m_1-1}\right)\right). \tag{42}$$

Then, equation (41) can be translated into the following:

$$f^{-1}(z_2^* - g(x)) = x, \quad x \in \overline{B}_{\delta_{1,m_1-1}}\left(x_{1,m_1-1}\right). \tag{43}$$

Here, it needs to prove that

$$z_2^* - g(x) \in f\left(\overline{B}_{\delta_{1,m_1-1}}\left(x_{1,m_1-1}\right)\right), \quad x \in \overline{B}_{\delta_{1,m_1-1}}\left(x_{1,m_1-1}\right). \tag{44}$$

Suppose that g also satisfies

$$\max\left\{L, \left\|g\left(x_{1j}\right)\right\|, 0 \le j \le m_1 - 1\right\} < \varepsilon_3, \quad (45)$$

where

$$\varepsilon_3 = \min\left\{\varepsilon_1, \varepsilon_2, \frac{\min\left\{\lambda_{10}\delta_{10} - \delta_{11}, \mu_{1j}\delta_{1j} - \delta_{1,j+1}, \quad \text{for } 1 \le j \le m_1 - 1\right\}}{1 + \max\left\{\delta_{1j}, 0 \le j \le m_1 - 1\right\}}\right\}. \quad (46)$$

From (14) and (36), we get that $\varepsilon_3 > 0$. On the one hand, for any $x \in \overline{B}_{\delta_{1,m_1-1}}(x_{1,m_1-1})$, it follows from (45) and (46) that

$$\begin{aligned}\left\|z_2^* - g(x) - z_2\right\| &= \left\|g\left(x_{1,m_1-1}\right) - g(x) - g\left(x_{1,m_1-1}\right) + z_2^* - z_2\right\| \\ &\le L\left\|x - x_{1,m_1-1}\right\| + \left\|g\left(x_{1,m_1-1}\right)\right\| + \left\|z_2^* - z_2\right\| \\ &< \varepsilon_3\delta_{1,m_1-1} + \varepsilon_3 + \delta_{1,m_1} = \left(1 + \delta_{1,m_1-1}\right)\varepsilon_3 + \delta_{1,m_1} \\ &\le \left(1 + \delta_{1,m_1-1}\right)\frac{\mu_{1,m_1-1}\delta_{1,m_1-1} - \delta_{1,m_1}}{1 + \delta_{1,m_1-1}} + \delta_{1,m_1} = \mu_{1,m_1-1}\delta_{1,m_1-1}.\end{aligned} \quad (47)$$

On the other hand, for any $x \in \partial B_{\delta_{1,m_1-1}}(x_{1,m_1-1})$, it follows from (13) that

$$\left\|f(x) - z_2\right\| = \left\|f(x) - f\left(x_{1,m_1-1}\right)\right\| \ge \mu_{1,m_1-1}\left\|x - x_{1,m_1-1}\right\| = \mu_{1,m_1-1}\delta_{1,m_1-1}. \quad (48)$$

Since $z_2 \in f(B_{\delta_{1,m_1-1}}(x_{1,m_1-1}))$ and $f(B_{\delta_{1,m_1-1}}(x_{1,m_1-1}))$ is open, it follows from (47) and (48) that (44) is true. So, we can define a map

$$h_2(x) = f^{-1}\left(z_2^* - g(x)\right), \quad x \in \overline{B}_{\delta_{1,m_1-1}}\left(x_{1,m_1-1}\right). \quad (49)$$

It follows from (45) and (46) that

$$L < \varepsilon_3 < \frac{\mu_{1,m_1-1}\delta_{1,m_1-1} - \delta_{1,m_1}}{1 + \delta_{1,m_1-1}} < \mu_{1,m_1-1}\frac{\delta_{1,m_1-1}}{1 + \delta_{1,m_1-1}} < \mu_{1,m_1-1}. \quad (50)$$

Then, for any $x \in \overline{B}_{\delta_{1,m_1-1}}(x_{1,m_1-1})$, it follows from (42) and (47) that

$$\begin{aligned}\left\|h_2(x) - x_{1,m_1-1}\right\| &= \left\|f^{-1}\left(z_2^* - g(x)\right) - f^{-1}(z_2)\right\| \\ &\le \mu_{1,m_1-1}^{-1}\left\|z_2^* - g(x) - z_2\right\| < \delta_{1,m_1-1}.\end{aligned} \quad (51)$$

That is, h_2 maps $\overline{B}_{\delta_{1,m_1-1}}(x_{1,m_1-1})$ into itself. Moreover, for any $x, y \in \overline{B}_{\delta_{1,m_1-1}}(x_{1,m_1-1})$, it follows from (42) that

$$\begin{aligned}\left\|h_2(x) - h_2(y)\right\| &= \left\|f^{-1}\left(z_2^* - g(x)\right) - f^{-1}\left(z_2^* - g(y)\right)\right\| \\ &\le \mu_{1,m_1-1}^{-1}\|g(x) - g(y)\| \le L\mu_{1,m_1-1}^{-1}\|x - y\|,\end{aligned} \quad (52)$$

which together with (50) implies that h_2 is contractive in $\overline{B}_{\delta_{1,m_1-1}}(x_{1,m_1-1})$. It follows from the Banach contractive mapping principle and (51) that there exists a unique point $y_{1,m_1-1} \in B_{\delta_{1,m_1-1}}(x_{1,m_1-1})$ such that $h(y_{1,m_1-1}) = z_2^*$. Consequently, $F(y_{1,m_1-1}) = z_2^*$, that is, equation (40) has a unique solution $y_{1,m_1-1} \in B_{\delta_{1,m_1-1}}(x_{1,m_1-1})$.

Using a similar method as above, we can prove that there exist $m_1 - 1$ unique points $y_{1j} \in B_{\delta_{1j}}(x_{1j})$ for $0 \le j \le m_1 - 2$ such that $F(y_{1j}) = y_{1,j+1}$. Then, we get that $y_{10} \in B_{\delta_{10}}(x_{10}) \subset B_{r_1^*}(z_1^*)$ such that $F^{m_1}(y_{10}) = z_2^*$.

Next, set g also to satisfy

$$\max\left\{L, \left\|g\left(x_{2j}\right)\right\|, 0 \le j \le m_2 - 1\right\} < \varepsilon_4, \quad (53)$$

where

$$\varepsilon_4 = \min\left\{\varepsilon_1, \varepsilon_2, \frac{\min\left\{\lambda_{20}\delta_{20} - \delta_{21}, \mu_{2j}\delta_{2j} - \delta_{2,j+1}, \quad \text{for } 1 \le j \le m_2 - 1\right\}}{1 + \max\left\{\delta_{2j}, 0 \le j \le m_2 - 1\right\}}\right\}. \quad (54)$$

It follows from (14) and (15) that $\varepsilon_4 > 0$.

Repeating a similar discussion as above, we can get when g satisfies (53), there exist m_2 unique points $y_{2j} \in B_{\delta_{2j}}(x_{2j})$, $0 \le j \le m_2 - 1$, such that $F(y_{2j}) = y_{2,j+1}$ for $0 \le j \le m_2 - 2$, and $F(y_{2,m_2-1}) = z_1^*$. That is, there exists a point $y_{20} \in B_{\delta_{20}}(x_{20}) \subset B_{r_2^*}(z_2^*)$ such that $F^{m_2}(y_{20}) = z_1^*$.

Let $\varepsilon_0 = \min\{\varepsilon_j, 1 \le j \le 4\}$. If g satisfies the following condition

$$\max\left\{L, \|g(z_i)\|, \|g(x_{ij})\|, 1 \le i \le 2, 0 \le j \le m_i - 1\right\} < \varepsilon_0, \tag{55}$$

then the statements in Step 2 hold. Consequently, F has a heteroclinic cycle Γ' connecting repellers z_1^* and z_2^*.

Step 3. It is to show that the heteroclinic cycle Γ' connecting repellers z_1^* and z_2^* of F is regular and nondegenerate.

When the map g satisfies (55), it follows from the discussions in Step 2 that $y_{ij} \in B_{\delta_{ij}}(x_{ij})$ for $1 \le i \le 2$, $0 \le j \le m_i - 1$. Hence, for $1 \le i \le 2$, $0 \le j \le m_i - 1$, we can take positive constants $\delta'_{ij} < \delta_{ij}$ such that

$$y_{ij} \in B_{\delta'_{ij}}(y_{ij}) \subset B_{\delta_{ij}}(x_{ij}). \tag{56}$$

It follows from (11), (13), and (56) that for $1 \le i \le 2$, $1 \le j \le m_i - 1$,

$$\|F(x) - F(y)\| \ge \|f(x) - f(y)\| - \|g(x) - g(y)\| \ge (\lambda_{i0} - L)\|x - y\|, \quad \forall x, y \in \overline{B}_{r_i^*}(z_i^*), \tag{57}$$

$$\|F(x) - F(y)\| \ge \|f(x) - f(y)\| - \|g(x) - g(y)\| \ge (\mu_{ij} - L)\|x - y\|, \quad \forall x, y \in \overline{B}_{\delta'_{ij}}(y_{ij}), \tag{58}$$

where $\lambda_{i0} > L + 1$ and $\mu_{ij} > L$ can be derived from (45), (46), (53), and (54).

For each $i\,(1 \le i \le 2)$, since z_i^* is a regular expanding fixed point of F and $F(B_{r_i^*}(z_i^*))$ is an open set, the backward orbit of y_{i0} lies in $B_{r_i^*}(z_i^*)$ and (57) holds in some neighborhood of each point on the backward orbit. The forward orbit of y_{i0} consists of y_{ij} for $1 \le j \le m_i - 1$ and (58) holds for each y_{ij} in $\overline{B}_{\delta'_{ij}}(y_{ij})$. Therefore, the heteroclinic cycle Γ' connecting repellers z_1^* and z_2^* is nondegenerate. In addition, it is clear that F is continuous in $B_{r_i^*}(z_i^*)$ and $B_{\delta'_{ij}}(y_{ij})$ for $1 \le i \le 2$, $1 \le j \le m_i - 1$. It follows from (3) of Remark 2.2 in [25] that if we prove that for each point y_0 on the cycle Γ', there exists a positive constant r_0 such that $F(y_0)$ is an interior point of $F(B_{r_0}(y_0))$, then this cycle Γ' is regular.

Firstly, for each point y_0 on Γ' lying in $B_{r_i^*}(z_i^*)$, there exists a constant r_0 such that $\overline{B}_{r_0}(y_0) \subset B_{r_i^*}(z_i^*)$. It follows from (57) and Lemma 1, by using F to replace f and making $g = 0$, that

$$B_{(\lambda_{i0}-L)r_0}(F(y_0)) \subset F(B_{r_0}(y_0)), \tag{59}$$

which implies that $F(y_0)$ is an interior point of $F(B_{r_0}(y_0))$.

Secondly, for each point y_{ij}, $1 \le j \le m_i - 1$, on Γ' lying out $B_{r_i^*}(z_i^*)$, it follows from (58) and Lemma 1, by using F to replace f and making $g = 0$ again, that

$$B_{(\mu_{ij}-L)\delta'_{ij}}(F(y_{ij})) \subset F(B_{\delta'_{ij}}(y_{ij})), \tag{60}$$

which implies that $F(y_{ij})$ is an interior point of $F(B_{\delta'_{ij}}(y_{ij}))$.

Hence, the cycle Γ' is regular. That is, the heteroclinic cycle Γ' connecting repellers z_1^* and z_2^* of F is regular and nondegenerate. Consequently, it follows form Lemma 2 that there exists an uncountable, perfect, bounded, and closed set V such that system (9) is chaotic on V in the sense of both Devaney and Li-Yorke. This completes the proof.

Remark 4. Theorem 1 gives a relatively explicit range of the Lipschitz perturbation g which is characterized by a constant ε_0 determined by the properties of the original map f. From (10), we see that it only needs L and the values of g at z_i, x_{ij} are less than ε_0, and it does not need to compute all the values of g in some domains. Hence, the conditions about g in Theorem 1 are relatively easy to check out in practice. In addition, it only needs the original map f to be continuous near some points of interest without having to be continuous in the whole space.

Remark 5. From the proof of Theorem 1, it is easy to see that the perturbed map F will have a regular and nondegenerate heteroclinic cycle Γ' connecting repellers if the unperturbed map f with a regular and nondegenerate heteroclinic cycle Γ connecting repellers undergoes a small perturbation, and the cycle Γ' is near to Γ. The perturbed range of g is characterized by ε_0 determined in Theorem 1. Thus, this result can be viewed as persistence of regular and nondegenerate heteroclinic cycles connecting repellers in Banach spaces.

When the original map f is continuously differentiable in some domains of interest, using a similar method to Theorem 1, we can get the following result.

Theorem 2. *Let $(X, \|\cdot\|)$ be a Banach space and $f: X \longrightarrow X$ be a map with $k(\ge 2)$ different fixed points $z_1, \ldots, z_k \in X$. Assume that*

(i) For each $i\,(1 \le i \le k)$, f is continuously differentiable in $B_{r'_i}(z_i)$ for some constant $r'_i > 0$ and $Df(z_i)$ is an invertible linear map satisfying $\|Df(z_i)\|^0 > 1$, which is equivalent to that there exists a positive constant $r_i \le r'_i$ such that z_i is a regular expanding fixed point of f in $\overline{B}_{r_i}(z_i)$.

(ii) f has a heteroclinic cycle Γ connecting repellers $z_1, \ldots, z_k$.

(iii) f is continuously differentiable in some neighborhood U_{x_0} of each point x_0 on the cycle Γ, and $Df(x_0)$ is an invertible linear map.

Then, there exists a constant $\varepsilon_0 > 0$ such that for any Lipschitz map g in each set of $\overline{B}_{r_i}(z_i)$ and U_{x_0} for $x_0 \in \Gamma$, with the Lipschitz constant L satisfying

$$\max\left\{L, \left\|g(x_0)\right\| \text{ for } x_0 \in \Gamma\right\} < \varepsilon_0, \tag{61}$$

the results of Theorem 1 hold.

Proof. It follows from the assumptions in Theorem 2 and Lemma 3 that f has a regular and nondegenerate heteroclinic cycle Γ connecting repellers $z_1, \ldots, z_k$. For each $i (1 \le i \le k)$, since z_i is a regular expanding fixed point of f, there exist a point $x_{i0} \in B_{r_i}(z_i)$ and a positive integer $m_i \ge 1$ such that $f(x_{i0}) \notin B_{r_i}(z_i)$ and $f^{m_i}(x_{i0}) = z_{t(i)}$, where $t(i) = [i \bmod k] + 1$. The rest of the proof is similar to that of Theorem 1, so it is omitted.

For a function $f \in C^1(U, X)$, the following norm is often used

$$\|f\|_{C^1,U} := \sup\{\|f(x)\|, \|Df(x)\|, x \in U \subset X\}. \tag{62}$$

Therefore, if the conditions in Theorems 1 and 2 about g are replaced by those based on the above norm, then we can obtain two consequences of Theorems 1 and 2. For convenience, we list them as the following theorems. □

Theorem 3. *Suppose that* $(X, \|\cdot\|)$ *is a Banach space,* $f: X \longrightarrow X$ *is a map with* $k(\ge 2)$ *different fixed points* $z_1, \ldots, z_k \in X$ *and satisfies the conditions (i) and (ii) in Theorem 1. Then, there exists a constant* $\varepsilon_0 > 0$ *such that for any* $g \in C^1(U, X)$ *with* $\|g\|_{C^1,U} < \varepsilon_0$*, the results of Theorem 1 hold, where* $U = B_{r_i}(z_i) \cup (\cup_{j=1}^{m_i-1} U_{ij}), 1 \le i \le k$.

Theorem 4. *Suppose that* $(X, \|\cdot\|)$ *is a Banach space,* $f: X \longrightarrow X$ *is a map with* $k(\ge 2)$ *different fixed points* $z_1, \ldots, z_k \in X$ *and satisfies the conditions (i)–(iii) in Theorem 2. Then, there exists a constant* $\varepsilon_0 > 0$ *such that for any* $g \in C^1(U, X)$ *with* $\|g\|_{C^1,U} < \varepsilon_0$*, the results of Theorem 1 hold, where* $U = \cup_{x_0 \in \Gamma} U_{x_0}$.

At the last of this section, we discuss a usually used Banach space $\mathbf{R}^n$, which is the Euclidean space. As is well known, there are many different norms in $\mathbf{R}^n$. A map in $\mathbf{R}^n$ can expand in different norms, see [11, 26] and references therein. It is natural to ask whether there is the persistence of heteroclinic cycles connecting repellers in $\mathbf{R}^n$, where the repellers expand in different norms. The following Theorem 5 will answer this question.

The usually used Euclidean norm is denoted by

$$\|x\| = \left(\sum_{j=1}^{n} \left|x_j\right|^2\right)^{1/2}, \quad x = (x_1, \ldots, x_n)^T \in \mathbf{R}^n. \tag{63}$$

In the following, we will use the neighborhood of a point $x \in \mathbf{R}^n$ in different norms. For convenience, let $\overline{B}_r(x)$ and $B_r(x)$ denote the closed and open balls of x with radius r in the Euclidean norm $\|\cdot\|$, let $\overline{N}_r(x)$ and $N_r(z)$ denote the closed and open balls of x with radius r in any other norm $\|\cdot\|'$.

Now, we establish a result on persistence of heteroclinic cycles connecting repellers in $\mathbf{R}^n$, where the repellers expand in different norms.

Theorem 5. *Suppose that a map* $f: \mathbf{R}^n \longrightarrow \mathbf{R}^n$ *has* $k(\ge 2)$ *different fixed points* $z_1, \ldots, z_k \in \mathbf{R}^n$ *and satisfies the following conditions:*

(i) for each $i (1 \le i \le k)$*,* f *is continuously differentiable in some neighborhood of* z_i *and all the eigenvalues of* $Df(z_i)$ *have absolute values larger than 1, which implies that there exist a constant* $r_i > 0$ *and a norm* $\|\cdot\|_i$ *in* $\mathbf{R}^n$ *such that* f *is continuously differentiable in* $\overline{N}_{r_i}(z_i)$*, and* z_i *is a regular expanding fixed point of* f *in* $\overline{N}_{r_i}(z_i)$.

(ii) for each $i (1 \le i \le k)$*, there exist a point* $x_{i0} \in N_{r_i}(z_i)$*,* $x_{i0} \ne z_i$*, and a positive integer* $m_i \ge 1$ *such that* $f^{m_i}(x_{i0}) = z_{t(i)}$*, where* $t(i) = [i \mod k] + 1$*. Furthermore,* f *is continuously differentiable in some neighborhood* U_{ij} *of* x_{ij} *and satisfies that* $\det Df(x_{ij}) \ne 0$*, where* $x_{ij} = f^j(x_{i0})$ *for* $1 \le j \le m_i - 1$.

Then, for any Lipschitz map g with Lipschitz constant L in the Euclidean norm $\|\cdot\|$ in each set of $\overline{N}_{r_i}(z_i)$ and U_{ij}, $1 \le i \le k$, $1 \le j \le m_i - 1$, there exists a constant $\varepsilon_0 > 0$ satisfying

$$\max\left\{L, \left\|g(z_i)\right\|, \left\|g\left(x_{ij}\right)\right\|, \quad 1 \le i \le k,\ 0 \le j \le m_i - 1\right\} < \varepsilon_0, \tag{64}$$

such that the perturbed system (9) is chaotic in the sense of both Devaney and Li-Yorke on a compact and perfect set which contains a Cantor set.

Proof. Without loss of generality and for simplicity, we also only show that Theorem 5 holds for $k = 2$.

For convenience, let $i = 1$ or 2 in the rest of proof. As pointed in the second paragraph of the proof in Theorem 1, we can also suppose that $N_{r_1}(z_1) \cap N_{r_2}(z_2) = \varnothing$ and $f(x_{i0}) \notin N_{r_i}(z_i)$.

Since all the norms on $\mathbf{R}^n$ are equivalent by Corollary 3.14 of Chapter II in [36], there exist positive constants b_{11}, b_{12}, c_{i1} and c_{i2} such that

$$\begin{aligned} b_{11}\|\cdot\|_1 &\le \|\cdot\|_2 \le b_{12}\|\cdot\|_1, \\ c_{i1}\|\cdot\|_i &\le \|\cdot\| \le c_{i2}\|\cdot\|_i. \end{aligned} \tag{65}$$

Since g is a Lipschitz map with Lipschitz constant L in the Euclidean norm $\|\cdot\|$ in $\overline{N}_{r_i}(z_i)$ and U_{ij}, for any $x, y \in \overline{N}_{r_i}(z_i)$ and any $x, y \in U_{ij}$, $1 \le j \le m_i - 1$, it follows from (65) that

$$\|g(x) - g(y)\|_i \le c_{i1}^{-1}\|g(x) - g(y)\| \le c_{i1}^{-1}L\|x - y\| \le c_{i1}^{-1}c_{i2}L\|x - y\|_i \le L'\|x - y\|_i, \tag{66}$$

where

$$L' = \max\left\{c_{i1}^{-1}c_{i2}L, \quad i = 1, 2\right\}. \tag{67}$$

Then it follows from (66) that g is also a Lipschitz map with Lipschitz constant L' in the norm $\|\cdot\|_i$ in $\overline{N}_{r_i}(z_i)$ and U_{ij}.

It follows from assumption (i) that there exists a constant $\lambda_{i0} > 1$ such that

$$\|f(x) - f(y)\|_i \geq \lambda_{i0}\|x - y\|_i, \quad \forall x, y \in \overline{N}_{r_i}(z_i), \tag{68}$$

$f\colon \overline{N}_{r_i}(z_i) \longrightarrow f(\overline{N}_{r_i}(z_i))$ is a homeomorphism and $f(N_{r_i}(z_i))$ is open, $f(D)$ is open for any open set $D \subset N_{r_i}(z_i)$. Take a constant

$$\delta_{i0} < \frac{r_i - \|z_i - x_{i0}\|_i}{2}, \tag{69}$$

such that $\overline{N}_{\delta_{i0}}(x_{i0}) \subset N_{r_i}(z_i)$. Then, it follows form (68) that $f\colon N_{\delta_{i0}}(x_{i0}) \longrightarrow f(N_{\delta_{i0}}(x_{i0}))$ is also a homeomorphism.

In addition, it follows from $\det Df(x_{ij}) \neq 0$, $1 \leq j \leq m_i - 1$, that none of the eigenvalues of $Df(x_{ij})$ is 0. Therefore, $(Df(x_{ij}))^T Df(x_{ij})$ is positive definite. Then,

$$\| Df(x_{ij})\|^0 = \left(\inf_{\|x\|=1}\left(x^T\left(Df(x_{ij})\right)^T Df(x_{ij})x\right)\right)^{\frac{1}{2}} > 0, \tag{70}$$

where $x \in \mathbf{R}^n$. It follows from (65) and (70) that

$$\begin{aligned}\left\|Df(x_{ij})\right\|_i^0 &= \inf_{x\neq 0}\frac{\left\|Df(x_{ij})x\right\|_i}{\|x\|_i} \geq c_{i1}c_{i2}^{-1}\inf_{x\neq 0}\frac{\left\|Df(x_{ij})x\right\|}{\|x\|} \\ &= c_{i1}c_{i2}^{-1}\left\|Df(x_{ij})\right\|^0 > 0,\end{aligned} \tag{71}$$

Hence, it follows from (71) and Lemma 4 that there exist positive constants μ_{ij} and δ_{ij} such that

$$\|f(x) - f(y)\|_i \geq \mu_{ij}\|x - y\|_i, \quad \forall x, y \in \overline{N}_{\delta_{ij}}(x_{ij}), \tag{72}$$

which implies that $f\colon N_{\delta_{ij}}(x_{ij}) \longrightarrow f(N_{\delta_{ij}}(x_{ij}))$ is homeomorphic, and $f(N_{\delta_{ij}}(x_{ij}))$ is open for $1 \leq j \leq m_i - 1$, where δ_{ij} satisfies the following conditions:

$$\begin{aligned}&\delta_{i1} < \lambda_{i0}\delta_{i0}, \\ &\delta_{i,j+1} < \mu_{ij}\delta_{ij}, \quad \text{for } 1 \leq j \leq m_i - 2,\end{aligned} \tag{73}$$

$\overline{N}_{\delta_{ij}}(x_{ij})$ are disjoint subsets of U_{ij} and $\overline{N}_{\delta_{ij}}(x_{ij}) \cap N_{r_i}(z_i) = \varnothing$ for fixed i and $1 \leq j \leq m_i - 1$.

The rest of the proof is almost exactly the same to Steps 1–3 in the proof of Theorem 1 except for three aspects. One is that L is replaced by L' and the domains in the norm $\|\cdot\|$ are replaced by those in the norms $\|\cdot\|_1$ or $\|\cdot\|_2$, respectively. In brief, in the representations of the domains, the alphabet B is replaced by the alphabet N through the proof of Theorem 1. The second is that some values in the norm $\|\cdot\|$ are replaced by those in the norms $\|\cdot\|_1$ or $\|\cdot\|_2$, respectively. It is pointed out that (18) and (42) take the values in the norm $\|\cdot\|_1$, the remainders follow the following rule: if the independent variables of functions are taken from $N_{r_i}(z_i)$ or $N_{\delta_{ij}}(x_{ij})$, then the values in the norm $\|\cdot\|$ are replaced by those in the norm $\|\cdot\|_i$. The third is that some related constants used in the proof are slightly modified since the norm $\|\cdot\|$ is replaced by the norms $\|\cdot\|_1$ or $\|\cdot\|_2$. For convenience, we list them as follows.

$$\delta_{1,m_1} < \begin{cases} \min\left\{\begin{array}{c} b_{11}\lambda_{10}\delta_{10}, \\ \dfrac{r_2 - \|z_2 - x_{20}\|_2}{2} - \delta_{20} \end{array}\right\}, & \text{if } m_1 = 1; \\ \min\left\{\begin{array}{c} b_{11}\mu_{1,m_1-1}\delta_{1,m_1-1}, \\ \dfrac{r_2 - \|z_2 - x_{20}\|_2}{2} - \delta_{20} \end{array}\right\}, & \text{if } m_1 > 1, \end{cases}$$

$$\delta_{2,m_2} < \begin{cases} \min\left\{\begin{array}{c} b_{12}^{-1}\lambda_{20}\delta_{20}, \\ \dfrac{r_1 - \|z_1 - x_{10}\|_1}{2} - \delta_{10} \end{array}\right\}, & \text{if } m_2 = 1; \\ \min\left\{\begin{array}{c} b_{12}^{-1}\mu_{2,m_2-1}\delta_{2,m_2-1}, \\ \dfrac{r_1 - \|z_1 - x_{10}\|_1}{2} - \delta_{10} \end{array}\right\}, & \text{if } m_2 > 1, \end{cases}$$

$$
\begin{aligned}
r_1^* &= \frac{r_1 + \|z_1 - x_{10}\|_1}{2},\\
r_2^* &= \frac{r_1 + \|z_2 - x_{20}\|_2}{2},\\
\varepsilon_1 &= \frac{(\lambda_{10} - 1)\delta_{2,m_2}}{1 + \delta_{2,m_2}},\\
\varepsilon_2 &= \frac{(\lambda_{20} - 1)\delta_{1,m_1}}{1 + \delta_{1,m_1}},\\
\varepsilon_3 &= \min\left\{\varepsilon_1, \varepsilon_2, \frac{\min\left\{\lambda_{10}\delta_{10} - \delta_{11}, \mu_{1,m_1-1}\delta_{1,m_1-1} - b_{11}^{-1}\delta_{1,m_1}, \mu_{1j}\delta_{1j} - \delta_{1,j+1}, \quad \text{for } 1 \le j \le m_1 - 2\right\}}{1 + \max\left\{\delta_{1j}, 0 \le j \le m_1 - 1\right\}}\right\},\\
\varepsilon_4 &= \min\left\{\varepsilon_1, \varepsilon_2, \frac{\min\left\{\lambda_{20}\delta_{20} - \delta_{21}, \mu_{2,m_2-1}\delta_{2,m_2-1} - b_{12}\delta_{2,m_2}, \mu_{2j}\delta_{2j} - \delta_{2,j+1}, \quad \text{for } 1 \le j \le m_2 - 2\right\}}{1 + \max\left\{\delta_{2j}, 0 \le j \le m_2 - 1\right\}}\right\}.
\end{aligned}
\tag{74}
$$

It follows from (73) and the above conditions that $\varepsilon_j > 0$ for $1 \le j \le 4$. Here, it should explain how to take the values of the numerators in terms of m_1 and m_2 in ε_3 and ε_4. We only explain the values in terms of m_1, while that for m_2 is similar. For the numerator of the fraction at the right side of ε_3, when $m_1 = 1$, it only takes the first term; when $m_1 = 2$, it only takes the first two terms; when $m_1 \ge 3$, it takes all of the terms.

Set

$$
\varepsilon_0' = \min\left\{\varepsilon_j,\ 1 \le j \le 4\right\}, \quad \varepsilon_0 = \min\left\{\frac{\varepsilon_0'}{\max\left\{c_{11}^{-1}c_{12}, c_{21}^{-1}c_{22}\right\}}, c_{11}\varepsilon_0', c_{21}\varepsilon_0'\right\}. \tag{75}
$$

If g satisfies condition (64) in the Euclidean norm $\|\cdot\|$, that is the following:

$$
\max\left\{L, \|g(z_i)\|, \left\|g(x_{ij})\right\|, 1 \le i \le 2, 0 \le j \le m_i - 1\right\} < \varepsilon_0, \tag{76}
$$

then it follows from (65), (75) and (76) that g also satisfies the following condition in the norms $\|\cdot\|_1$ and $\|\cdot\|_2$

$$
\max\left\{L', \|g(z_i)\|_i, \left\|g(x_{ij})\right\|_i, 1 \le i \le 2, 0 \le j \le m_i - 1\right\} < \varepsilon_0', \tag{77}
$$

Therefore, repeating the Steps 1–3 in the proof of Theorem 1, we can get that if g satisfies (76), consequently (77), then F has a regular and nondegenerate heteroclinic cycle Γ' connecting repellers z_1^* and z_2^* in different norms $\|\cdot\|_1$ and $\|\cdot\|_2$. It follows from the proof of Theorem 4.1 in [26] that there exists a positive integer p such that F^p has a heteroclinic cycle Γ^* connecting repellers z_1^* and z_2^* in the unified Euclidean norm $\|\cdot\|$. Since all the points on the cycle Γ^* of F^p also lie on the cycle Γ' of F, it is easy to prove that the cycle Γ^* of F^p is also regular and nondegenerate. Consequently, F is chaotic on a compact and perfect set which contains a Cantor set in the sense of both Devaney and Li-Yorke. This completes the proof. □

Remark 6. From the proof of Theorem 5, we obtain that F^p has a regular and nondegenerate heteroclinic cycle connecting repellers in the unified Euclidean norm $\|\cdot\|$ for some positive integer p. Hence, Theorem 5 can also be regarded as the persistence of a regular and nondegenerate heteroclinic cycle connecting repellers in $\mathbf{R}^n$. In the special case that all the norms $\|\cdot\|_i$, $1 \le i \le k$, in assumption (i) become a unified norm, such as the Euclidean norm $\|\cdot\|$, then the positive integer p becomes 1. Hence, this special case of Theorem 5 is consistent with Theorem 1.

The following result is a direct consequence of Theorem 5.

Theorem 6. *Suppose that a map $f\colon \mathbf{R}^n \longrightarrow \mathbf{R}^n$ has $k(\ge 2)$ different fixed points $z_1, \ldots, z_k \in \mathbf{R}^n$ and satisfies the following conditions*

(i) For each $i\,(1 \le i \le k)$, z_i is an expanding fixed point of f in some norm $\|\cdot\|_i$;

(ii) f has a k-heteroclinic cycle Γ connecting fixed points $z_1, \ldots, z_k$ and is continuously differentiable in some neighborhood U_{x_0} of each point $x_0 \in \Gamma$ satisfying $\det Df(x_0) \ne 0$.

Then, there exists a constant $\varepsilon_0 > 0$ such that for any Lipschitz map g in each set of $\cup_{x_0 \in \Gamma} U_{x_0}$ with Lipchitz constant L in the Euclidean norm $\|\cdot\|$ satisfying

$$
\max\left\{L, \|g(x_0)\|, \quad \text{for } x_0 \in \Gamma\right\} < \varepsilon_0, \tag{78}
$$

the results in Theorem 5 hold.

Remark 7. [28] studied the persistence of heteroclinic repellers in $\mathbf{R}^n$ for C^1 maps with C^1 perturbations, where the maps needed to be continuously differentiable in the whole space. Here, it only needs the maps to be continuously differentiable in some neighborhoods of points. The main differences between the above two theorems and the result in [28] are as follows. One is that Theorems 5 and 6 studied the Lipschitz perturbations, while the latter considered the C^1 perturbations. The second is that Theorems 5 and 6 give an explicit expression for the range of perturbations, which are determined by the properties of the original maps, while the latter did not give such a range for perturbations. The third is that Theorems 5 and 6 use different norms for expansions of fixed points which are more general in practice, while the latter only used a single norm for expansions of fixed points.

Remark 8. Just as Theorems 3 and 4, if the perturbed term g is continuously differentiable, then the conditions about g in Theorems 5 or 6 can be replaced by that $g \in C^1(U, X)$ with $\|g\|_{C^1,U} < \varepsilon_0$, where U is taken the corresponding domains used in Theorems 5 or 6, respectively, then the results in Theorems 5 or 6 hold.

4. Examples

In this section, three examples are given to illustrate the validity of the theoretical results.

Example 3. The original map f is taken as the following map on $\mathbf{R}$:

$$f(x) = \begin{cases} 2x, & \text{if } x \in [-2, 2] \\ 5x - 9, & \text{if } x \in (2, 2.5) \\ 0.1x - 0.2875, & \text{else.} \end{cases} \tag{79}$$

The perturbed map g is taken as $g(x) = \gamma|x|$, where $x \in \mathbf{R}$ and γ is a positive real number. It is obvious that f is piecewise continuous on $\mathbf{R}$, g is a Lipschitz map with a Lipschitz constant $L = \gamma$ and it is not differentiable on $\mathbf{R}$.

It is easy to see that $z_1 = 0$ and $z_2 = 2.25$ are two regular expanding fixed points of f. Set $x_{10} = 1.125 \in (-2, 2)$, then $f(x_{10}) = z_2$. Set $x_{20} = 2.375 \in (2, 2.5)$, then $x_{21} = f(x_{20}) = 2.875$ and $f(x_{21}) = z_1$, that is, $f^2(x_{20}) = z_1$. So, f has a 2-heteroclinic cycle Γ connecting repellers z_1 and z_2. It is clear that the cycle is regular and nondegenerate, and assumptions (i) and (ii) in Theorem 1 holds with $k = 2$, $r_1 = 2$, $r_2 = 0.25$, $\lambda_{10} = 2$, $\lambda_{20} = 5$, $m_1 = 1$, $m_2 = 2$, x_{10} and x_{20} as the above.

Some constants that appear in the proof of Theorem 1 are taken as follows: $\mu_{21} = 0.1$, $\delta_{10} = 0.43 < (r_1 - |z_1 - x_{10}|)/2) = 0.4375$, $\delta_{20} = 0.06 < ((r_2 - |z_2 - x_{20}|/2) = 0.0625$, $\delta_{11} = 0.002 < \min\{\lambda_{10}\delta_{10}, ((r_2 - |z_2 - x_{20}|)/2) - \delta_{20}\} = 0.0025$, $\delta_{21} = 0.28 < \lambda_{20}\delta_{20} = 0.3$, $\delta_{22} = 0.007 < \min\{\mu_{21}\delta_{21}, ((r_1 - |z_1 - x_{10}|)/2) - \delta_{10}\} = 0.0075$, $\varepsilon_1 = ((\lambda_{10} - 1)\delta_{22}/1 + \delta_{22}) \approx 0.006951$, $\varepsilon_2 = (((\lambda_{20} - 1)\delta_{11})/1 + \delta_{11}) \approx 0.007984$, $\varepsilon_3 = \min\{\varepsilon_1, \varepsilon_2, ((\delta_{10}\lambda_{10} - \delta_{11})/ \ 1 + \delta_{10})\} = 0.006951$, $\varepsilon_4 = \min \{\varepsilon_1, \varepsilon_2, ((\min \{\lambda_{20}\delta_{20} - \delta_{21}, \mu_{21}\delta_{21} - \delta_{22}\})/1 + \max\{\delta_{20}, \delta_{21}\})\} = 0.006951$, $\varepsilon_0 = \min\left\{\varepsilon_j, 1 \le j \le 4\right\} = 0.006951$. It is easy to check that the perturbation g satisfies condition (10) for $\gamma \le 0.0024$. Then, it follows from the result of Theorem 1 that the perturbed system $F = f + g$ also has a regular and nondegenerate heteroclinic cycle Γ' connecting repellers which is near to Γ. Consequently, F and f are chaotic in the sense of both Devaney and Li-Yorke. For illustrating the persistence of a heteroclinic cycle connecting repellers, we take $\gamma = 0.002$ for example. It is easy to calculate the following results. The perturbed map F has two regular expanding fixed pints $z_1^* = 0$ and $z_2^* = (1500/667) \approx 2.248876$. There exist two points $x_{10}^* = (750000/667667) \approx 1.123314$ and $x_{20}^* = (301375/127551) \approx 2.362780$ such that $F(x_{10}^*) = z_2^*$, $x_{21}^* = F(x_{20}^*) = (575/204) \approx 2.818627$ and $F(x_{21}^*) = z_1^*$. Then, F has a 2-heteroclinic cycle Γ' connecting repellers $z_1^* = 0$ and $z_2^* = 0$. It is clear that Γ' is near to Γ. With the increase of γ, the heteroclinic cycle Γ' will gradually run away from Γ until it breaks or disappears. Since f and F are chaotic on some intervals of $\mathbf{R}$ and the computer simulations of them are on intervals, we omit the computer simulations.

Example 4. The original map f is taken as the following map on $\mathbf{R}^2$

$$f(x, y) = \begin{cases} 8(x, y), & \text{if } (x, y) \in \overline{B}_1(0, 0), \\ (2x - 2, 2y - 2), & \text{if } (x, y) \in \overline{B}_4(0, 0)/\overline{B}_1(0, 0), \\ \left(\sin\left[x - 2 - \frac{\pi}{2} + \left(y - 2 - \frac{\pi}{2}\right)^2\right], \right. & \\ \left. \sin\left[\left(x - 2 - \frac{\pi}{2}\right)^2 + y - 2 - \frac{\pi}{2}\right]\right), & \text{if } (x, y) \notin \overline{B}_4(0, 0). \end{cases} \tag{80}$$

This map is used as an example in [25] for illustrating chaos induced by a heteroclinic cycle connecting repellers. The perturbed map g is taken as $g(x, y) = \gamma(x, y)$, where $(x, y) \in \mathbf{R}^2$ and γ is a real number. It is obvious that f is only continuously differentiable in some domains of $\mathbf{R}^2$, g is continuously differentiable in $\mathbf{R}^2$ and has a Lipschitz constant $L = |\gamma|$.

On the one hand, it is clear that $z_1 = (0, 0)$ and $z_2 = (2, 2)$ are two fixed points of f, f is continuously differentiable in $\overline{B}_1(z_1)$, $\overline{B}_{1.171}(z_2)$, and satisfies that

$$\begin{aligned} Df(z_1) &= 8I_2, \\ Df(z_2) &= 2I_2, \end{aligned} \tag{81}$$

where I_2 is the identity matrix. So, the eigenvalues of $Df(z_1)$ and $Df(z_2)$ have absolute values larger than 1, which implies that z_1 and z_2 are two regular expanding expanding fixed points of f in $\overline{B}(z_1)$ and $\overline{B}_{1.171}(z_2)$ in the Euclidean norm $\|\cdot\|$ with $\lambda_{10} = 8$, $\lambda_{20} = 2$, respectively. It is obvious that $\overline{B}_1(z_1) \cap \overline{B}_{1.171}(z_2) = \varnothing$ and both lie in $B_4(z_1)$. Set $x_{10} = ((1/4), (1/4)) \in B_1(z_1)$, then $f(x_{10}) = z_2$. Set $x_{20} = (2 + (\pi/8), 2 + (\pi/8)) \in B_{1.171}(z_2)$, then $x_{21} = f(x_{20}) = (2 + (\pi/4), 2 + (\pi/4)) \in B_4(z_1) \backslash B_1(z_1)$, $x_{22} = f(x_{21}) = (2 + (\pi/2), 2 + (\pi/2)) \notin \overline{B}_4(z_1)$ and $f(x_{22}) = z_1$, that is, $f^3(x_{20}) = z_1$.

On the other hand, it is also obvious that f is continuously differentiable in some neighborhoods of x_{10}, x_{20}, x_{21}, and x_{22} and satisfies

$$\begin{aligned} Df(x_{10}) &= 8I_2, \\ Df(x_{20}) &= Df(x_{21}) \\ &= 2I_2, \\ Df(x_{22}) &= I_2. \end{aligned} \tag{82}$$

Then, it follows from (82) that

$$\begin{aligned} \|Df(x_{10})\|^0 &= 8, \\ \|Df(x_{20})\|^0 &= \|Df(x_{21})\|^0 \\ &= 2, \\ \|Df(x_{22})\|^0 &= 1, \end{aligned} \tag{83}$$

which together with Lemma 4 imply that the cycle Γ is nondegenerate. Furthermore, it follows from (4) of Remark 2.2 in [25] that the cycle Γ is also regular. Consequently, f has a regular and nondegenerate 2-heteroclinic cycle Γ connecting the repellers z_1 and z_2.

Therefore, assumptions (i) and (ii) in Theorem 5 hold with $k = 2$, $r_1 = 1$, $r_2 = 1.171$, $\lambda_{10} = 8$, $\lambda_{20} = 2$, $m_1 = 1$, $m_2 = 3$, x_{10} and x_{20} as the above. Consequently, f has a 2-heteroclinic cycle Γ connecting repellers z_1 and z_2. As is pointed out in Remark 6, when the norms used in Theorem 5 become a unified norm, the special case of Theorem 5 is consistent with Theorem 1. So, we can take some constants that appear in the proof of Theorem 1 as follows:

$$\begin{aligned}
\mu_{21} &= 2, \\
\mu_{22} &= 1, \\
\delta_{10} &= 0.2 < \frac{r_1 - \|z_1 - x_{10}\|}{2} \approx 0.323223, \\
\delta_{20} &= 0.175 < \frac{r_2 - \|z_2 - x_{20}\|}{2} \approx 0.307820, \\
\delta_{11} &= 0.1328 < \min\left\{\lambda_{10}\delta_{10}, \frac{r_2 - \|z_2 - x_{20}\|}{2} - \delta_{20}\right\} \\
&= 0.132820, \\
\delta_{21} &= 0.2 < \lambda_{20}\delta_{20} \\
&= 0.35, \\
\delta_{22} &= 0.2 < \mu_{21}\delta_{21} \\
&= 0.4, \\
\delta_{23} &= 0.025 < \min\left\{\mu_{22}\delta_{22}, \frac{r_1 - \|z_1 - x_{10}\|}{2} - \delta_{10}\right\} \\
&= 0.123223, \\
\varepsilon_1 &= \frac{(\lambda_{10} - 1)\delta_{23}}{1 + \delta_{23}} \approx 0.170732, \\
\varepsilon_2 &= \frac{(\lambda_{20} - 1)\delta_{11}}{1 + \delta_{11}} \approx 0.117232, \\
\varepsilon_3 &= \min\left\{\varepsilon_1, \varepsilon_2, \frac{\delta_{10}\lambda_{10} - \delta_{11}}{1 + \delta_{10}}\right\} \\
&= 0.117232, \\
\varepsilon_4 &= \min\left\{\varepsilon_1, \varepsilon_2, \frac{\min\{\lambda_{20}\delta_{20} - \delta_{21}, \mu_{21}\delta_{21} - \delta_{22}, \mu_{22}\delta_{22} - \delta_{23}\}}{1 + \max\{\delta_{20}, \delta_{21}, \delta_{22}\}}\right\} \\
&= 0.117232,
\end{aligned} \tag{84}$$

$\varepsilon_0 = \min\{\varepsilon_j, 1 \le j \le 4\} = 0.117232$. It is easy to check that the perturbation g satisfies condition (10) for $|\gamma| \le 0.0297$. Then, it follows from the result of Theorem 5 that the perturbed system $F = f + g$ also has a regular and nondegenerate heteroclinic cycle Γ' connecting repellers which is near to Γ. Consequently, F and f are chaotic in the sense of both Devaney and Li-Yorke.

As is done in Example 3, for a given γ, one can also directly calculate the heteroclinic cycle Γ' of F to check whether it is near to Γ of f. However, it is not easy to directly calculate such a cycle for high-dimensional maps. If there is the persistence of a heteroclinic cycle connecting repellers, then the computer simulations of them will not change very much. The behaviors of the unperturbed map f with an initial point $(x, y) = (0.1, 0.1)$ are illustrated in Figure 1. We do some computers simulations of F as γ increases from -0.0297 to 0 or from 0 to 0.0297, and find that all the simulations are similar with that of the original map f in Figure 1. Here, we give one simulation of F with an initial point $(x, y) = (0.1, 0.1)$ for $\gamma = 0.0297$, see Figure 2. We can see that Figure 2 is a small change to Figure 1, which shows that the heteroclinic cycle Γ' of F is near to Γ of f. When we let $|\gamma|$ continuous to increase, we find that the computer simulations gradually change until there is a big difference from that of the original map. This shows that the heteroclinic cycle Γ breaks or disappears. Are there new heteroclinic cycles connecting repellers not near Γ or new snap-back repellers to make the perturbed system still chaotic? It is an interesting question, while it is out of the scope of this paper and will be our further study.

Example 5. The original map f is taken as the following map on $\mathbf{R}^3$

$$f(x,y,z) = \begin{cases} (6x, 6y, 6z), & \text{if } (x,y,z) \in \overline{B}_1(O), \\ (4x-9, 4y-9, 4z-9), & \text{if } (x,y,z) \in \overline{B}_8(O)/\overline{B}_1(O), \\ \left(\sin\left[x-5+(y-5)^2\right], \right. & \sin\left[y-5+(z-5)^2\right], \\ \left. \sin\left[(x-5)^2+z-5\right]\right), & \text{if } (x,y,z) \notin \overline{B}_8(O), \end{cases} \tag{85}$$

where $O = (0,0,0)$ is the origin. The perturbed map g is taken as $g(x,y,z) = \gamma(x,y,z)$, where $(x,y,z) \in \mathbf{R}^3$ and γ is a real number. It is obvious that f is only continuously differentiable in some domains of $\mathbf{R}^3$, g is continuously differentiable in $\mathbf{R}^3$ and has a Lipschitz constant $L = |\gamma|$.

Theorem 5 is also used to verify the persistence of a heteroclinic cycle connecting repellers, and the process is similar to that of Example 4. So, we omit some details and only give some main results as follows. Assumptions (i) and (ii) in Theorem 5 hold with $k = 2$, $z_1 = (0,0,0)$, $z_2 = (3,3,3)$, $r_1 = 1$, $r_2 = 2.8$, $\lambda_{10} = 6$, $\lambda_{20} = 4$, $m_1 = 1$, $m_2 = 2$, $x_{10} = (0.5, 0.5, 0.5) \in B_1(z_1)$ and $x_{20} = (3.5, 3.5, 3.5) \in B_{2.8}(z_2) \subset B_8(O)$. The points z_1 and z_2 are two regular expanding fixed points of f in the Euclidean norm $\|\cdot\|$. In addition, $f(x_{10}) = z_2$, $x_{21} = f(x_{20}) = (5,5,5) \notin \overline{B}_8(O)$ and $f(x_{21}) = z_1$, that is, $f^2(x_{20}) = z_1$. Then f has a regular and nondegenerate 2-heteroclinic cycle

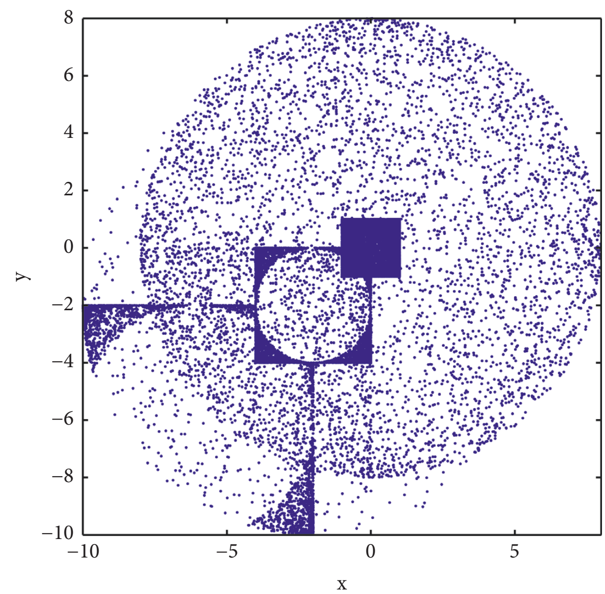

FIGURE 1: Complex behaviors of the original map f in the (x, y) space, where the initial point is take as $(0.1, 0.1)$ and $n = 0, 1, 2, \ldots, 20000$.

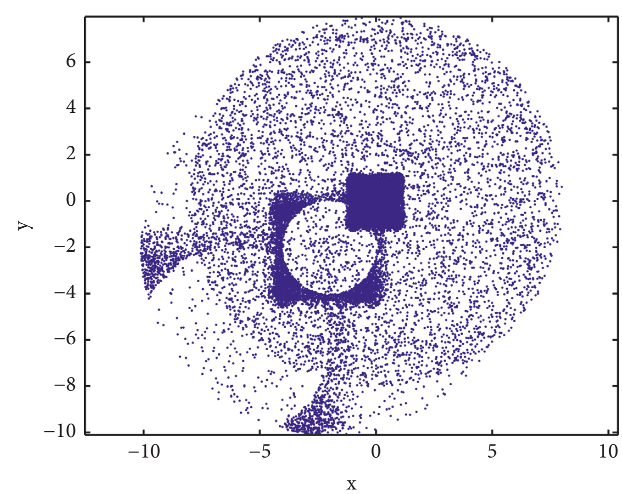

FIGURE 2: Complex behaviors of the perturbed map F in the (x, y) space, where $\gamma = 0.0297$, the initial point is taken as $(0.1, 0.1)$ and $n = 0, 1, 2, \ldots, 20000$.

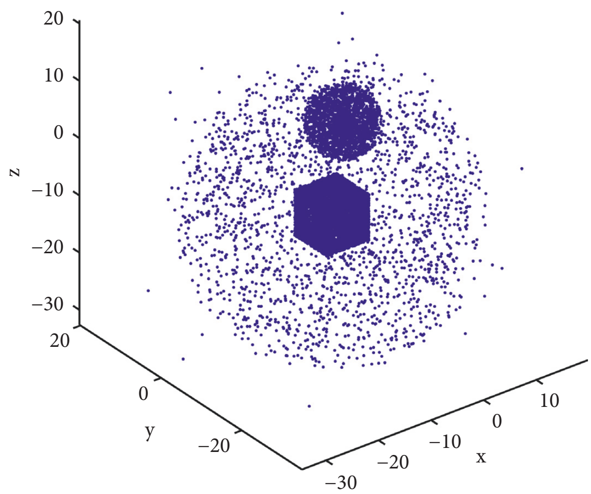

Figure 3: Complex behaviors of the original map f in the (x, y, z) space, where the initial point is take as $(0.1, 0.1, 0.1)$ and $n = 0, 1, 2, \ldots, 20000$.

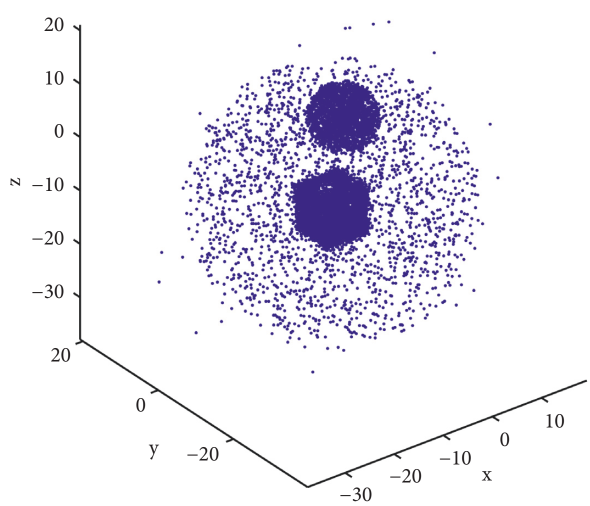

Figure 4: Complex behaviors of the perturbed map F in the (x, y, z) space, where $\gamma = 0.0133$, the initial point is taken as $(0.1, 0.1, 0.1)$ and $n = 0, 1, 2, \ldots, 20000$.

Γ connecting the repellers z_1 and z_2. Some constants that used to determine the range of perturbations are taken as follows:

$$\begin{aligned}
\mu_{21} &= 1,\\
\delta_{10} &= 0.03 < \frac{r_1 - \|z_1 - x_{10}\|}{2} \approx 0.066987,\\
\delta_{20} &= 0.2 < \frac{r_2 - \|z_2 - x_{20}\|}{2} \approx 0.966987,\\
\delta_{11} &= 0.04 < \min\left\{\lambda_{10}\delta_{10}, \frac{r_2 - \|z_2 - x_{20}\|}{2} - \delta_{20}\right\}\\
&= 0.18,\\
\delta_{21} &= 0.2 < \lambda_{20}\delta_{20}\\
&= 0.8,\\
\delta_{22} &= 0.03 < \min\left\{\mu_{21}\delta_{21}, \frac{r_1 - \|z_1 - x_{10}\|}{2} - \delta_{10}\right\}\\
&= 0.036987,\\
\varepsilon_1 &= \frac{(\lambda_{10} - 1)\delta_{22}}{1 + \delta_{22}} \approx 0.145631,\\
\varepsilon_2 &= \frac{(\lambda_{20} - 1)\delta_{11}}{1 + \delta_{11}} \approx 0.115385,\\
\varepsilon_3 &= \min\left\{\varepsilon_1, \varepsilon_2, \frac{\delta_{10}\lambda_{10} - \delta_{11}}{1 + \delta_{10}}\right\}\\
&= 0.115385,\\
\varepsilon_4 &= \min\left\{\varepsilon_1, \varepsilon_2, \frac{\min\{\lambda_{20}\delta_{20} - \delta_{21}, \mu_{21}\delta_{21} - \delta_{22}\}}{1 + \max\{\delta_{20}, \delta_{21}\}}\right\}\\
&= 0.115385,
\end{aligned} \tag{86}$$

$\varepsilon_0 = \min\{\varepsilon_j, 1 \le j \le 4\} = 0.115385$. It is also easy to check that the perturbation g satisfies condition (10) for $|\gamma| \le 0.0133$. Then, it follows from the result of Theorem 5 that the perturbed system $F = f + g$ also has a regular and nondegenerate heteroclinic cycle Γ' connecting repellers which is near to Γ. Consequently, F and f are chaotic in the sense of both Devaney and Li-Yorke.

The behaviors of the unperturbed map f with an initial point $(x, y, z) = (0.1, 0.1, 0.1)$ are illustrated in Figure 3. We also do some computers simulations of F as γ increases from -0.0133 to 0 or from 0 to 0.0133, and find that all the simulations are also similar with that of the original map f in Figure 3. Here, we give one simulation of F with an initial point $(x, y, z) = (0.1, 0.1, 0.1)$ for $\gamma = 0.0133$, see Figure 4. We can see that Figure 4 is also a small change to Figure 3, which shows that the heteroclinic cycle Γ' of F is near to Γ of f. When we let $|\gamma|$ continuous to increase, we also find that the computer simulations gradually change until there is a big difference from that of the original map. This shows that the heteroclinic cycle Γ breaks or disappears.

Remark 9. In the above examples, it only needs the Lipschitz constant L and the values of g at z_i, x_{ij} for $1 \le i \le 2$, $0 \le j \le m_i - 1$ to satisfy condition (10), and does not need to compute the values of g at any other points. This is very easy to check out and is very convenient in applications. Since there are few literature giving concrete methods to identify an exact expanding area of a fixed point, it is very hard to get the largest perturbation range. But we think that the results obtained in this paper are also useful in practice. Because when a perturbation range ε_0 is determined as in the above examples, it can ensure that the persistence is maintained for a large range of parameters. The perturbation range obtained in these examples may not be the largest one for the persistence to be maintained. A more precise perturbed range is needed in practice and this will also be our further research.

5. Conclusions

In this paper, we studied persistence of heteroclinic cycles connecting repellers in Banach spaces. We proved that if a map with a regular and nondegenerate heteroclinic cycle connecting repellers undergoes a small Lipschitz perturbation, then the perturbed map still has a regular and nondegenerate heteroclinic cycle connecting repellers. Consequently, the perturbed map and the original map are simultaneously chaotic in the sense of both Devaney and Li-Yorke. We believe that the results obtained in the paper will be useful for studying the existence of chaos and will provide certain theoretical basis for practical applications of heteroclinic cycles of connecting repellers. Compared with some related papers, three major achievements on the persistence are summarized as follows. One is that the maps discussed in the paper only need to be continuous or continuously differentiable in some domains instead of the whole space. Since a lot of maps may not be continuous or continuously differentiable in the whole space, our results are more general in practice than those in some related papers. The second is that an explicit expression for the range of perturbations is given, while most related papers did not give such an expression. The expression is determined by some properties of the original maps. It only needs to check out some values of the perturbation map at certain points in practice. This is very convenient and has great potential in applications. The third is that different repellers are allowed to expand in different norms in $\mathbf{R}^n$, while some related papers only used the single Euclidean norm to do that. This is very meaningful since it is more general in practice for some fixed points to expand in different norms. To show the validity of the theoretical results, we give some illustrative examples. However, the range of perturbations obtained in this paper is only a sufficient condition for the persistence to be maintained, and it may not be the largest one. Since it is hard to determine the exact area of a fixed point and few researches have given concrete methods to do this, it is not easy to find the largest range of perturbations and this will be our further research.

Data Availability

The data in this paper are acquired from the corresponding author.

Conflicts of Interest

The author declares that there are no conflicts of interest.

Acknowledgments

This research was supported by the Horizontal Foundation of Shandong Jianzhu University (Grant H19271Z0101).

References

[1] T. Y. Li and J. A. Yorke, "Period three implies chaos," *The American Mathematical Monthly*, vol. 82, no. 10, pp. 985–992, 1975.

[2] M. Martelli, M. Dang, and T. Seph, "Defining chaos," *Mathematics Magazine*, vol. 71, no. 2, pp. 112–122, 1998.

[3] C. Robinson, *Dynamical Systems: Stability, Symbolic Dynamics and Chaos*, CRC Press, Boca Raton, FL, USA, 1999.

[4] R. L. Devaney, *An Introduction to Chaotic Dynamical Systems*, Addison-Wesley Publishing Company, New York, NY, USA, 1987.

[5] J. Banks, J. Brooks, G. Cairns, G. Davis, and P. Stacey, "On Devaneys definition of chaos," *The American Mathematical Monthly*, vol. 99, no. 4, pp. 332–334, 1992.

[6] W. Huang and X. D. Ye, "Devaney's chaos or 2-scattering implies Li-Yorke's chaos," *Topology and its Applications*, vol. 117, no. 3, pp. 259–272, 2002.

[7] B. Aulbach and B. Kieninger, "On three definitions of chaos," *Nonlinear Dynamics and Systems Theory*, vol. 1, no. 1, pp. 23–37, 2001.

[8] Y. M. Shi and P. Yu, "Chaos induced by regular snap-back repellers," *Journal of Mathematical Analysis and Applications*, vol. 337, no. 2, pp. 1480–1494, 2008.

[9] F. R. Marotto, "Snap-back repellers imply chaos in $\mathbf{R}^n$," *Journal of Mathematical Analysis and Applications*, vol. 63, no. 1, pp. 199–223, 1978.

[10] Y. M. Shi and G. R. Chen, "Chaos of discrete dynamical systems in complete metric spaces," *Chaos, Solitons & Fractals*, vol. 22, no. 3, pp. 555–571, 2004.

[11] Y. M. Shi and G. R. Chen, "Discrete chaos in Banach spaces," *Science in China, Series A: Mathematics. Chinese version*, vol. 34, pp. 595–609, 2004, English version: vol. 48, pp. 222–238, 2005.

[12] H. Shao, Y. M. Shi, and H. Zhu, "Strong Li-Yorke Chaos for time-varying discrete systems with a coupled-expansion," *International Journal of Bifurcation and Chaos*, vol. 25, Article ID 1550186, 2015.

[13] Y. M. Shi and G. R. Chen, "Chaos of time-varying discrete dynamical systems," *Journal of Difference Equations and Applications*, vol. 15, no. 5, pp. 429–449, 2009.

[14] H. Shao, G. R. Chen, and Y. M. Shi, "Some criteria of chaos in non-autonomous discrete dynamical systems," *Journal of Difference Equations and Applications*, vol. 26, no. 3, pp. 295–308, 2020.

[15] F. R. Marotto, "Perturbations of stable and chaotic difference equations," *Journal of Mathematical Analysis and Applications*, vol. 72, pp. 716–729, 1979.

[16] F. R. Marotto, "Some dynamics of second order unimodal difference schemes," *Nonlinear Analysis: Theory, Methods & Applications*, vol. 18, pp. 277–286, 1992.

[17] M. C. Li and M. Malkin, "Topological horseshoes for perturbations of singular difference equations," *Nonlinearity*, vol. 19, pp. 795–811, 2006.

[18] M. C. Li, M. J. Lyu, and P. Zgliczynski, "Topological entropy for multidimensional perturbations of snap-back repellers and one-dimensional maps," *Nonlinearity*, vol. 21, no. 11, pp. 2555–2567, 2008.

[19] J. Juang, M. C. Li, and M. Malkin, "Chaotic difference equations in two variables and their multidimensional perturbations," *Nonlinearity*, vol. 21, pp. 1019–1040, 2008.

[20] M. C. Li and M. J. Lyu, "A simple proof for persistence of snap-back repellers," *Journal of Mathematical Analysis and Applications*, vol. 352, no. 2, pp. 669–671, 2009.

[21] Y. L. Chen, Y. Huang, and L. L. Li, "The persistence of snap-back repeller under small C^1 perturbations in Banach spaces," *International Journal of Bifurcation and Chaos*, vol. 21, pp. 703–710, 2011.

[22] L. J. Zhang, Y. M. Shi, X. Zhang, and W. Liang, "Structure stability of maps with snap-back repellers in Banach spaces," *Journal of Difference Equations and Applications*, vol. 18, pp. 1817–1842, 2012.

[23] L. J. Zhang and Y. M. Shi, "Time-varying perturbations of chaos discrete systems," *International Journal of Bifurcation and Chaos*, vol. 22, Article ID 1250066, 2012.

[24] W. Lin and G. R. Chen, "Heteroclinical repellers imply chaos," *International Journal of Bifurcation and Chaos*, vol. 16, no. 5, pp. 1471–1489, 2006.

[25] Z. C. Li, Y. M. Shi, and C. Zhang, "Chaos induced by heteroclinic cycles connecting repellers in complete metric spaces," *Chaos, Solitons & Fractals*, vol. 36, no. 3, pp. 746–761, 2008.

[26] Z. C. Li, Y. M. Shi, and W. Liang, "Discrete chaos induced by heteroclinic cycles connecting repellers in Banach spaces," *Nonlinear Analysis: Theory, Methods & Applications*, vol. 72, no. 2, pp. 757–770, 2010.

[27] Z. C. Li and Y. M. Shi, "Chaotification of a class of discrete systems based on heteroclinic cycles connecting repellers in Banach spaces," *Chaos, Solitons & Fractals*, vol. 42, no. 3, pp. 1933–1941, 2009.

[28] Y. L. Chen and X. Y. Wu, "The C^1 persistence of heteroclinic repellers in R^n," *Journal of Mathematical Analysis and Applications*, vol. 485, no. 2, Article ID 123823, 2020.

[29] Y. L. Chen, L. L. Li, X. Y. Wu, and F. Wang, "The structural stability of maps with heteroclinic repellers," *International Journal of Bifurcation and Chaos*, vol. 30, no. 14, Article ID 2050207, 2020.

[30] X. Y. Wu, "Heteroclinic cycles imply chaos and are structurally stable," *Discrete Dynamics in Nature and Society*, vol. 2021, Article ID 6647132, 7 pages, 2021.

[31] Y. L. Chen and S. G. Luo, "The Lipschitz perturbations of regular nondegenrate heteroclinic cycles in Banach spaces (in Chinese)," *Acta Mathematica Sinica Chinese Series*, vol. 64, no. 3, pp. 485–492, 2021.

[32] S. U. Rehman and H. Aydi, "Rational fuzzy cone contractions on fuzzy cone metric spaces with an application to Fredholm integral equations," *Journal of Function Spaces*, vol. 2021, Article ID 5527864, 13 pages, 2021.

[33] H. A. Hammad, H. Aydi, and Y. U. Gaba, "Exciting fixed point results on a novel space with supportive applications," *Journal of Function Spaces*, vol. 2021, Article ID 6613774, 12 pages, 2021.

[34] P. Kloeden and Z. Li, "Li-Yorke Chaos in higher dimensions: a review," *Journal of Difference Equations and Applications*, vol. 12, no. 3-4, pp. 247–269, 2006.

[35] W. Rudin, *Functional Analysis*, McGraw-Hill, New York, NY, USA, 1973.

[36] S. Lang, *Real and Functional Analysis*, Springer-Verlag, New York, NY, USA, 1973.

Hindawi
Journal of Mathematics
Volume 2022, Article ID 7188118, 17 pages
https://doi.org/10.1155/2022/7188118

Research Article

Bifurcation Analysis and Exact Wave Solutions for the Double-Chain Model of DNA

Taher S. Hassan,[1,2] **A.A. Elmandouh**,[2] **Adel A. Attiya**,[1,2] **and Ahmed Y. Khedr**[3,4]

[1]*Department of Mathematics, College of Science, University of Ha'il, Ha'il 2440, Saudi Arabia*
[2]*Department of Mathematics, Faculty of Science, Mansoura University, Mansoura 35516, Egypt*
[3]*Department of Computer Science, University of Ha'il, Ha'il, Saudi Arabia*
[4]*Systems and Computer Engineering Department, Al-Azhar University, Cairo, Egypt*

Correspondence should be addressed to A.A. Elmandouh; aelmandouh@kfu.edu.sa

Received 20 December 2021; Revised 26 January 2022; Accepted 1 April 2022; Published 11 May 2022

Academic Editor: Fairouz Tchier

This work aims to study analytically the nonlinear model for deoxyribonucleic acid (DNA). Based on the complete discrimination and direct method, some new wave solutions are introduced. These solutions are sorted into solitary, periodic, kink (antikink), and singular solutions. Moreover, a part of them is illustrated graphically. Based on Hamilton concepts, we study the bifurcation and phase portrait for the Hamilton system corresponding to the model under consideration.

1. Introduction

Deoxyribonucleic acid (DNA) molecule carries the information for living beings that is required to live and propagate themselves. The nonlinear model for deoxyribonucleic acid (DNA) is attractive for the study because its properties can be investigated precisely by experiments gathering both the physical methods and biological tools [1]. In 1953, Watson and Crick [2] initially discovered the double helix construction of DNA; in spite of that, it is not easy until now to find a specific mathematical model that involved all its characteristics. The reason is its complicated structure and the existence of several motions such as the torsional, transverse, and longitudinal motions [3]. However, the existence of several motions of the DNA on thoroughly distinct time scales becomes aidable to model a few of these that predominate in the given time scale range. The idea that was introduced by Davydov [4] in his pioneer works related to the theoretical studies of the nonlinear characteristics of DNA has been firstly utilized by Englander and coauthors in 1980 to investigate dynamics of DNA regarding the nitrogen rational motion [5]. This idea has been further developed in several subsequent works. For instance, Yomosa proposed a model of the dynamics plane of the base rotator [6], and this study was followed by Takeno and Homma who got better this model by considering the degree of freedom describing base rotations in the plane perpendicular to the helical axis around the structure of the backbone [7]. The denaturation process in which the base transverse motion along the hydrogen bond is regarded was investigated by Peyrard and Bishop [8]. Two kinds of internal motions, which have been proposed by Muto et al., contribute mainly to the denaturation process of DNA. These motions are longitudinal motions over the backbone and transverse motions over the hydrogen bond [9]. This model has been developed and improved in several works in order to study distinct motions and construct solitary wave-type solutions [10–14]. These waves acquire their significance from their ability to transmit energy without losing, i.e., the energy is conserved [8, 15], and moreover, they explicate the long-range interaction of kink solitons in the double chain [16, 17] and transcription regulation [18].

Taking into account some acceptable approximations from the point of biological science, the two equations describe a DNA model with double chains consisting of elastic two long homogeneous strands. These strands characterize two polynucleotide chains of DNA molecules attached by an elastic membrane which represents the hydrogen bonds between the base pair of two chains. The dynamical nonlinear system characterizing the double-chain model of DNA takes the form [19, 20]

$$\begin{aligned} I_{tt} - e_1^2 I_{xx} &= a_1 I + b_1 IJ + c_1 I^3 + d_1 IJ^2, \\ J_{tt} - e_2^2 I_{xx} &= a_2 J + b_2 I^2 + c_2 I^2 J + d_2 J^3 + m_0, \end{aligned} \tag{1}$$

where I refers to the longitudinal displacement difference between the top and bottom wires, while J indicates the transverse displacements between the upper and lower strands, and e_i, a_i, b_i, c_i, d_i, and m_0, $i = 1, 2$, are constants given by

$$\begin{aligned} e_1 &= \pm \frac{R_1}{\rho}, \\ e_2 &= \pm \frac{R_2}{\rho}, \\ a_1 &= \pm \frac{2\mu}{\rho\sigma h}\left(h - l_0\right), \\ a_2 &= \pm \frac{2\mu}{\rho\sigma}, \\ b_1 &= 2b_2 = \frac{2\sqrt{2}\mu l_0}{\rho\sigma h^2}, \\ c_1 &= c_2 = \frac{-2\mu l_0}{h^3 \rho\sigma}, \\ d_1 &= d_2 = \frac{4\mu l_0}{h^3 \rho\sigma}, \\ m_0 &= \frac{\mu\sqrt{2}}{\rho\sigma}\left(h - l_0\right), \end{aligned} \tag{2}$$

where ρ, σ, R_1, and R_2 refer to density of mass, area of cross section, Young's modulus, and density of the tension of each strand, μ indicates the stiffness of the elastic membrane, h is the distance between the two strands, and l_0 is the height of membrane in the equilibrium.

To transform the nonlinear system (1) into a single partial differential equation, we present

$$J = \alpha I + \beta, \tag{3}$$

where α and β are two arbitrary constants, and furthermore, we assume $\beta = h/\sqrt{2}$ and $R_1 = R_2$. Thus, the linear system (1) is reduced to

$$I_{tt} - e_1^2 I_{xx} = f_3 I^3 + f_2 I^2 + f_1 I, \tag{4}$$

where f_i are arbitrary constants introduced for suitability, and they are given by

$$\begin{aligned} f_3 &= \frac{\omega_0}{h^3}\left(4\alpha^2 - 2\right), \\ f_2 &= \frac{6\sqrt{2}\alpha\omega_0}{h^2}, \\ f_1 &= \frac{6\omega_0}{h} - \frac{2\omega_0}{l_0}, \\ \omega_0 &= \frac{l_0\mu}{\sigma\rho}. \end{aligned} \tag{5}$$

The nonlinear model (1) has been investigated in several works. Riccati parameterized factorization method has been applied in [20] to construct some solitary wave solutions for the DNA model (1). The Φ^6- model expansion method has been utilized in [21] to construct some solutions which are assorted into solitary, kink, and singular waves. Some solitary wave solutions for the double-chain model of DNA have been introduced and discussed [19]. Some exact wave solutions of this model have been constructed by using Conte's Painlevé truncation expansion and Pickering's truncation expansion [22]. Some bounded wave solutions for this model such as bell-shaped solitary waves and periodic waves have been formulated based on the method of the dynamical systems [23]. The generalized exponential rational function method has been applied to introduce exact form solutions and solitonic structures for this model [24].

Despite the wide variety of methods used to find wave solutions to nonlinear PDEs, the problem under study has a simple history, for instance, the bifurcation analysis [25–34], sine-Gordon expansion method [35, 36], Hirota bilinear technique [37], G'/G method [38–40], differential transform method (DTM), homotopy perturbation method (HPM) [41], Lie symmetry method [42], homotopic analysis method [43], trigonometric function series method [44], modified mapping method and extended mapping method [45], modified trigonometric function series method [46], tanh-coth expansion method and Jacobi function expansion method [47], and Jacobi elliptic function expansion method [48], and for more different techniques, see [49–53].

In this work, we are interested in constructing some traveling wave solutions for the nonlinear model (1) which is equivalent to building a wave solution for the reduced equation (1). We apply the complete discriminant system in addition to determining the intervals of permitted real propagations. The significance of finding these intervals enables us to construct only real wave solutions, and furthermore, for the same constraints on the system's parameters, there are several intervals of possible real wave propagations. Hence, the missing of such study in previous works leads to missing some wave solutions and the appearance of complex solutions. The bifurcation analysis is introduced which plays an important role in determining the types of the solutions before constructing them. We are also interested in studying the influence of the system's parameters on the solutions.

This work is organized as follows: Section 2 involves the reduction of the DNA model to ordinary differential equations and using the complete discrimination method to construct some traveling wave solutions for equation (1). Section 3 contains the study of some dynamical properties of equation (1) by employing the complete discrimination and Hamiltonian concepts. Section 4 is a graphic representation of some of the obtained solutions. Furthermore, it examines the influence of the one-parameter changing on the solutions keeping the other parameters fixed. Section 4 is a collection and the summary of the obtained results.

2. Exact Wave Solutions

Applying the wave transformation $I(x,t) = u(\zeta)$, $\zeta = kx - \omega t$, to equation (4), we obtain

$$u'' = \frac{f_3}{\omega^2 - k^2 e_1^2} u^3 + \frac{f_2}{\omega^2 - k^2 e_1^2} u^2 + \frac{f_1}{\omega^2 - k a^2 e_1^2} u, \quad (6)$$

where k is a constant that specifies the cosine of angle of propagation with ζ−axis and ω is an arbitrary constant that characterizes the speed of the wave and $\omega^2 - k^2 e_1^2 \neq 0$. For simplicity, we insert

$$u(\zeta) = p(\zeta) - \frac{f_2}{3 f_3}, \quad (7)$$

into equation (6), and we get

$$p''(\zeta) = 2 n_4 p^3(\zeta) + n_2 p(\zeta) + \frac{n_1}{2}, \quad (8)$$

where $'$ indicates derivatives with respect to ζ and n_i, $i = 2, 3, 4$, are constants introduced for suitability and they are given by

$$\begin{aligned} n_4 &= \frac{f_3}{2(\omega^2 - k^2 e_1^2)}, \\ n_2 &= \frac{f_2^2 - 3 f_3 f_1}{3 f_3 (k^2 e_1^2 - \omega^2)}, \\ n_1 &= \frac{2 f_3 (9 f_1 f_2 - 2 f_2^2)}{27 f_3^2 (k^2 e_1^2 - \omega^2)}. \end{aligned} \quad (9)$$

Integrating both sides of equation (8) with respect to p, we obtain

$$p'^2 = n_4 (p^4 + \gamma_2 p^2 + \gamma_1 p + \gamma_0), \quad (10)$$

where γ_i are arbitrary parameters. Separating the variables, we obtain the differential form

$$d\zeta = \frac{dp}{\sqrt{n_4 F_4(p)}}, \quad (11)$$

where

$$F_4(p) = p^4 + \gamma_2 p^2 + \gamma_1 p + \gamma_0, \quad (12)$$

in which

$$\begin{aligned} \gamma_2 &= \frac{n_2}{n_4}, \\ \gamma_1 &= \frac{n_1}{n_4}. \end{aligned} \quad (13)$$

To integrate both sides of equation (11), the range of the parameters is required to be determined. The cause for this is that different values of the parameters imply different solutions to the integral. Hence, the key steps are to find the range of these parameters and consequently integrate both sides of equation (11). There are many tools utilized to find these ranges of parameters. In this work, we will apply a complete discrimination system for a polynomial. This method is a natural generalization of the discrimination $\Delta = b^2 - 4ac$ for the quadratic polynomial $ax^2 + bx + c$, but it becomes difficult to calculate it for the higher degree polynomials. This problem had been solved with aid of computer algebra programs by Yang et al. by presenting an algorithm to compute the complete discrimination system for polynomial [54]. The complete discrimination system for the quartic polynomial $F_4(p) = p^4 + \gamma_2 p^2 + \gamma_1 p + \gamma_0$ is given in [55], and it admits the form

$$\begin{aligned} D_1 &= 4, \\ D_2 &= -\gamma_2, \\ D_3 &= -2\gamma_2^3 + 8\gamma_2\gamma_0 - 9\gamma_1^2, \\ E_2 &= 9\gamma_2^2 - 32\gamma_2\gamma_0, \\ D_4 &= -\gamma_2^3\gamma_1^2 + 4\gamma_0\gamma_2^4 + 36\gamma_2\gamma_1^2 - 32\gamma_2^2\gamma_0^2 - \frac{27}{4}\gamma_1^4 + 64\gamma_0^4. \end{aligned} \quad (14)$$

We study eight cases that describe different types of the roots for polynomial (12). To avoid confounding, we collect the classification of all the different types of the roots of the polynomial $F_4(p)$ by utilizing the discriminant system in Table 1. Furthermore, we integrate only on certain intervals for p in which $n_4 F_4(p)$ is positive in order to get real solutions.

2.1. Case 1. Polynomial (12) has four real roots which are equal to zero if $D_2 = D_3 = D_4 = 0$. Hence, it is written as $F_4(p) = p^4$. Assuming $-\infty < p < 0$ and $p(\zeta_0) = -\infty$ and integrating (11), we obtain

$$I(x,t) = -\frac{1}{\sqrt{n_4}(kx + \omega t - \zeta_0)} - \frac{\sqrt{2} a h}{2a^2 - 1}, \quad (15)$$

and consequently, we have

$$J(x,t) = \alpha \left[-\frac{1}{\sqrt{n_4}(kx + \omega t - \zeta_0)} - \frac{\sqrt{2} a h}{2a^2 - 1} \right] + \beta. \quad (16)$$

Solutions (15) and (16) are singular solutions, and their singularity points lie on the plane $kx + ct - \zeta_0 = 0$.

Table 1: Types of the roots of the polynomial $F_4(p)$.

No.	Conditions on the discriminant system	Types of the roots for $F_4(p)$
1	$D_2 = D_3 = D_4 = 0$	All roots are equal to zero
2	$D_3 = D_4 = E_2 = 0$	Two real roots: one is triple and the other is simple
3	$D_3 = D_4 = 0,\ E_2 > 0$	Two double roots
4	$D_2 > 0,\ D_3 > 0,\ D_4 > 0$	Four real roots
5	$D_4 = 0,\ D_2D_3 < 0$	One double root and two complex conjugate roots
6	$D_4 < 0,\ D_2D_3 > 0$	Two real roots and two complex conjugate roots
7	$D_2D_3 \le 0,\ D_4 > 0$	Two conjugate complex roots
8	$D_2 > 0,\ D_3 > 0,\ D_4 = 0$	Four real roots: one double and others simple

2.2. Case 2. If $D_3 = D_4 = E_2 = 0$, then the quartic polynomial (12) has two real roots: one is simple and the other is triple. Hence, it can be expressed as $F_4(p) = (p - p_1)^3(p + 3p_1)$, where p_1 is assumed to be positive, i.e., $p_1 > 0$. We consider two subcases according to n_4 is positive or negative:

(i) For $n_4 > 0$, the possible interval for real propagation is $p \in]-\infty, -3p_1[\cup]p_1, \infty[$. Thus, if we choose $p < -3p_1$, assume $p(\zeta_0) = -\infty$, and integrate both sides of equation (11), we obtain

$$\sqrt{n_4}\int_{\zeta_0}^{\zeta} d\zeta = \int_{-\infty}^{p} \frac{dp}{(p - p_1)\sqrt{(p - p_1)(p + 3p_1)}}. \quad (17)$$

It follows

$$p(\zeta) = p_1 - \frac{p_1}{p_1\sqrt{n_4}(\zeta - \zeta_0) + 1} + \frac{1}{\sqrt{n_4}(\zeta - \zeta_0)}. \quad (18)$$

Thus, the solution of equation (1) becomes

$$I(x,t) = p_1 - \frac{p_1}{p_1\sqrt{n_4}(\zeta - \zeta_0) + 1} + \frac{1}{\sqrt{n_4}(\zeta - \zeta_0)} - \frac{f_2}{3f_3},$$
$$J(x,t) = \alpha\left[p_1 - \frac{p_1}{p_1\sqrt{n_4}(\zeta - \zeta_0) + 1} + \frac{1}{\sqrt{n_4}(\zeta - \zeta_0)} - \frac{f_2}{3f_3}\right] + \beta. \quad (19)$$

Similarly, we can calculate the solution if $p \in]p_1, \infty[$.

(ii) If $n_4 < 0$, the possible interval for p to obtain real propagation is $p \in]-3p_1, p_1[$. Thus, we assume $p(\zeta_0) = -3p_1$ and integrate both sides of equation (11), and we get

$$I(x,t) = p_1 - \frac{4p_1}{1 + 4n_4p_1^2(\zeta - \zeta_0)^2} - \frac{f_2}{3f_3},$$
$$J(x,t) = \alpha\left[p_1 - \frac{4p_1}{1 + 4n_4p_1^2(\zeta - \zeta_0)^2} - \frac{f_2}{3f_3}\right] + \beta. \quad (20)$$

Both solutions (19) and (20) are singular solutions for equation (1).

2.3. Case 3. The polynomial $F_4(p)$ has two double real zeros, namely, $\pm p_1$, where $p_1 > 0$, if $D_3 = D_4 = 0$, $E_2 > 0$, $D_2 > 0$. Hence, it can be introduced as $F_4(p) = (p^2 - p_1^2)^2$. We consider the following two cases in which n_4 is either positive or negative.

(i) If $n_4 > 0$, the intervals for real propagation are $p < -p_1$, $-p_1 < p < p_1$, and $p > p_1$. If we consider the case in which $p < -p_1$ and assume $p(\zeta_0) = -\infty$, equation (11) gives

$$\sqrt{n_4}\int_{\zeta_0}^{\zeta} d\zeta = \int_{-\infty}^{p} \frac{\mathrm{d}p}{p^2 - p_1^2}. \quad (21)$$

It follows

$$p = -p_1\coth(p_1\sqrt{n_4}(\zeta - \zeta_0)). \quad (22)$$

Using equations (7) and (3), we obtain a wave solution for equation (1) in the form

$$I(x,t) = -p_1\coth(p_1\sqrt{n_4}(\zeta - \zeta_0)) - \frac{f_2}{3f_3},$$
$$J(x,t) = \alpha\left[-p_1\coth(p_1\sqrt{n_4}(\zeta - \zeta_0)) - \frac{f_2}{3f_3}\right] + \beta. \quad (23)$$

When $p > p_1$, equation (1) has the same solution shown in equation (23) if $p_1 \longrightarrow -p_1$. Similarly, if we choose $p \in]-p_1, p_1[$ and assume $p(\zeta_0) = 0$, equation (1) has a solution in the form

$$I(x,t) = -p_1\tanh(p_1\sqrt{n_4}(\zeta - \zeta_0)) - \frac{f_2}{3f_3},$$
$$J(x,t) = \alpha\left[-p_1\tanh(p_1\sqrt{n_4}(\zeta - \zeta_0)) - \frac{f_2}{3f_3}\right] + \beta. \quad (24)$$

(ii) The case in which $n_4 < 0$ is excluded since $n_4F_4(p) < 0$ for all $p \in \mathbb{R}$.

2.4. Case 4. The polynomial $F_4(p)$ has four real zeros, namely, $p_1, p_2, p_3, -(p_1 + p_2 + p_3)$, where we assumed $0 < p_1 < p_2 < p_3$ if $D_2 > 0$, $D_3 > 0$, $D_4 > 0$. Therefore, it takes the form $F_4(p) = (p - p_1)(p - p_2)\ (p - p_3)(p+$

$p_1 + p_2 + p_3)$. Now, we consider the two cases $n_4 > 0$ and $n_4 > 0$, individually:

(i) When $n_4 > 0$, the possible intervals of p for real propagation are $p < -(p_1 + p_2 + p_3)$, $p_1 < p < p_2$, and $p > p_3$. If we choose $p < -(p_1 + p_2 + p_3)$ and assume $p(\zeta_0) = -(p_1 + p_2 + p_3)$, equation (11) becomes

$$\sqrt{n_4}\int_{\zeta_0}^{\zeta} d\zeta = \int_{-(p_1+p_2+p_3)}^{p} \frac{\mathrm{d}p}{\sqrt{(p-p_1)(p-p_2)(p-p_3)(p+p_1+p_2+p_3)}}. \tag{25}$$

It implies to

$$p = p_1 - \frac{(p_1 - p_3)(2p_1 + p_2 + p_3)}{p_1 - p_3 + (p_1 + p_2 + 2p_3)\mathrm{sn}^2(\Omega_1(\zeta - \zeta_0), k_1)}, \quad \zeta_0 < \zeta < \zeta_1, \tag{26}$$

where $\Omega_1 = 1/2\sqrt{n_4(p_3 - p_1)(p_1 + 2p_2 + p_3)}$, $k_1 = \sqrt{((p_2 - p_1)(p_1 + p_2 + 2p_3))/((p_3 - p_1)(p_1 + 2p_2 + p_3))}$, and $\zeta_1 = (1/\Omega_1)K(k_1)$. $K(k_1)$ is a complete elliptic integral of the first type [56]. Using equations (7) and (3), we obtain a new traveling wave solution for equation (1) in the form

$$\begin{aligned}
\Omega_1(x,t) &= p_1 - \frac{(p_1 - p_3)(2p_1 + p_2 + p_3)}{p_1 - p_3 + (p_1 + p_2 + 2p_3)\mathrm{sn}^2(\Omega_1(\zeta - \zeta_0), k_1)} - \frac{f_2}{3f_3},\\
J(x,t) &= \alpha\left[p_1 - \frac{(p_1 - p_3)(2p_1 + p_2 + p_3)}{p_1 - p_3 + (p_1 + p_2 + 2p_3)\mathrm{sn}^2(\Omega_1(\zeta - \zeta_0), k_1)} - \frac{f_2}{3f_3}\right] + \beta.
\end{aligned} \tag{27}$$

If we select $p_1 < p < p_2$, postulate $p(\zeta_0) = p_1$, and follow the same procedures, we will obtain a new traveling wave solution for equation (1) in the form

$$\begin{aligned}
I(x,t) &= -p_1 - p_2 - 2p_3 + \frac{(p_1 + 2p_2 + p_3)(2p_1 + p_2 + 2p_3)}{p_1 + 2p_2 + p_3 + (p_1 - p_2)\mathrm{sn}^2(\Omega_1(\zeta - \zeta_0), k_1)} - \frac{f_2}{3f_3},\\
J(x,t)&\alpha\left[-p_1 - p_2 - 2p_3 + \frac{(p_1 + 2p_2 + p_3)(2p_1 + p_2 + 2p_3)}{p_1 + 2p_2 + p_3 + (p_1 - p_2)\mathrm{sn}^2(\Omega_1(\zeta - \zeta_0), k_1)} - \frac{f_2}{3f_3}\right] + \beta,
\end{aligned} \tag{28}$$

where $\zeta_0 < \zeta < \zeta_1$. Also, if we elect $p > p_3$ and suppose $p(\zeta_0) = p_3$, we will get a new wave solution for equation (1) in the form

$$\begin{aligned}
I(x,t) &= p_2 + \frac{(p_2 - p_3)(p_1 + 2p_2 + p_3)}{(p_1 + p_2 + 2p_3)\mathrm{sn}^2(\Omega_1(\zeta - \zeta_0), k_1)} - \frac{f_2}{3f_3},\\
J(x,t) &= \alpha\left[p_2 + \frac{(p_2 - p_3)(p_1 + 2p_2 + p_3)}{(p_1 + p_2 + 2p_3)\mathrm{sn}^2(\Omega_1(\zeta - \zeta_0), k_1)} - \frac{f_2}{3f_3}\right] + \beta,
\end{aligned} \tag{29}$$

where $\zeta_0 < \zeta < \zeta_1$.

(ii) If $n_4 < 0$, the allowed intervals of p for real propagation are $-p_1 - p_2 - p_3 < p < p_1$ or $p_2 < p < p_3$.

Thus, if we chose $p_1 < p < p$ and assume $p(\zeta_0) = -p_1 - p_2 - p_3$, equation (11) takes the form

$$\sqrt{-n_4}\int_{\zeta_0}^{\zeta} d\zeta = \int_{-p_1-p_2-p_3}^{p} \frac{\mathrm{d}p}{\sqrt{\sqrt{-(p-p_1)(p_2-p)(p_3-p)(p+p_1+p_2+p_3)}}}. \tag{30}$$

It gives

$$p = p_3 + \frac{(p_1-p_3)(p_1+p_2+2p_3)}{p_3-p_1+(2p_1+p_2+p_3)\mathrm{sn}^2(\Omega_2(\zeta-\zeta_0),k_2)}, \quad \zeta_0 < \zeta < \zeta_2, \tag{31}$$

where $\Omega_2 = 1/2\sqrt{-n_4(p_3-p_1)(2p_2+p_1+p_3)}$, $k_2 = \sqrt{((p_3-p_2)(2p_1+p_2+p_3))/ \quad ((p_3-p_1)(2p_2+p_1}$ $+p_3))$, and $\zeta_2 = (1/\Omega_2)K(k_2)$. Utilizing equations (7) and (3), we obtain a new solution for equation (1):

$$\begin{aligned} I(x,t) &= p_3 + \frac{(p_1-p_3)(p_1+p_2+2p_3)}{p_3-p_1+(2p_1+p_2+p_3)\mathrm{sn}^2(\Omega_2(\zeta-\zeta_0),k_2)} - \frac{f_2}{3f_3},\\ J(x,t) &= \alpha\left[p_3 + \frac{(p_1-p_3)(p_1+p_2+2p_3)}{p_3-p_1+(2p_1+p_2+p_3)\mathrm{sn}^2(\Omega_2(\zeta-\zeta_0),k_2)}\right] + \beta. \end{aligned} \tag{32}$$

Similarly, if we select $p_2 < p < p_3$ and assume $p(\zeta_0) = p_2$, we present a new wave solution for equation (1) in the form

$$\begin{aligned} I(x,t) &= p_1 - \frac{(p_1-p_2)(p_1-p_3)}{p_1-p_3+(p_3-p_2)\mathrm{sn}^2(\Omega_2(\zeta-\zeta_0),k_2)} - \frac{f_2}{3f_3},\\ J(x,t) &= \alpha\left[p_1 - \frac{(p_1-p_2)(p_1-p_3)}{p_1-p_3+(p_3-p_2)\mathrm{sn}^2(\Omega_2(\zeta-\zeta_0),k_2)} - \frac{f_2}{3f_3}\right] + \beta. \end{aligned} \tag{33}$$

2.5. Case 5. The polynomial $F_4(p)$ has one double real root and two conjugate complex roots if $D_4 = 0$ and $D_2D_3 < 0$. Therefore, it takes the form $F_4(p) = (p-p_1)^2(p - p_2)(p-p_2^*)$, where * refers to the complex conjugate and $p_1 = -\mathrm{Re}p_2$. We consider the case in which $n_4 > 0$, and sequentially, the allowed intervals for real propagation are $p < p_1$ or $p > p_1$. Choosing $p > p_1$, assuming $p(\zeta_0) = \infty$, and integrating both sides of equation (11), we obtain

$$p = p_1 + \frac{4p_1^2+\rho^2}{-2p_1+\rho\sinh\left(\sqrt{n_4\left(4p_1^2+\rho^2\right)}\,(\zeta-\epsilon)\right)}, \tag{34}$$

where $\epsilon = \zeta_0 - \mathrm{s}(\mathrm{inh}^{-1}(2p_1/\rho))/\sqrt{n_4(4p_1^2+\rho^2)}$ is a new constant which is introduced for suitability and $\rho = \mathrm{Im}p_2$. Employing equations (7) and (3), we obtain a solution for equation (1) in the form

$$I(x,t) = p_1 + \frac{4p_1^2 + \rho^2}{-2p_1 + \rho\sinh\left(\sqrt{n_4\left(4p_1^2 + \rho^2\right)}\,(\zeta - \epsilon)\right)} - \frac{f_2}{3f_3},$$
$$J(x,t) = \alpha\left[p_1 + \frac{4p_1^2 + \rho^2}{-2p_1 + \rho\sinh\left(\sqrt{n_4\left(4p_1^2 + \rho^2\right)}\,(\zeta - \epsilon)\right)} - \frac{f_2}{3f_3}\right] + \beta. \quad (35)$$

It can be noted that the case in which n_4 is negative does not work because $F_4(p) \geq 0$ for all $p \in \mathbb{R}$.

2.6. Case 6. The polynomial $F_4(P)$ has two real roots and two complex conjugate roots if $D_4 < 0$ and $D_2D_3 > 0$. Hence, it can be written in the form $F_4(p) = (p - p_1)(p - p_2)(p - p_3)(p - p_3^*)$, where $p_1 < p_2$ and $\mathrm{Re}p_3 = (1/2)(p_1 + p_2)$. We consider the following:

(i) If $n_4 > 0$, then the permitted intervals for real propagation are $p > p_2$ and $p < p_1$. Selecting $p < p_2$ and $p(\zeta_0) = p_2$ and integrating both sides of equation (11), we obtain

$$p = \frac{p_2B_1 - p_1A_1 + (p_2B_1 + p_1A_1)\mathrm{cn}\left(\sqrt{n_4A_1B_1}\,(\zeta - \zeta_0), k_2\right)}{(A_1 + B_1)\mathrm{cn}\left(\sqrt{n_4A_1B_1}\,(\zeta - \zeta_0), k_2\right) - (A_1 - B_1)}, \quad (36)$$

where $k_2 = \sqrt{\left(\left(A_1 + B_1\right)^2 - \left(p_2 - p\right)_1{}^2\right)/4A_1B_1}$ and $A_1^2 = B_1^2 = (1/4)(p_1 - p_2)^2 + \mathrm{Im}^2(p_3)$. Taking into account equations (7) and (3), we obtain a novel wave solution for equation (1) in the form

$$I(x,t) = \frac{p_2B_1 - p_1A_1 + (p_2B_1 + p_1A_1)\mathrm{cn}\left(\sqrt{n_4A_1B_1}\,(kx + \omega t - \zeta_0), k_2\right)}{(A_1 + B_1)\mathrm{cn}\left(\sqrt{n_4A_1B_1}\,(\zeta - \zeta_0), k_2\right) - (A_1 - B_1)} - \frac{f_2}{3f_3},$$
$$J(x,t) = \alpha\left[\frac{p_2B_1 - p_1A_1 + (p_2B_1 + p_1A_1)\mathrm{cn}\left(\sqrt{n_4A_1B_1}\,(kx + \omega t), k_2\right)}{(A_1 + B_1)\mathrm{cn}\left(\sqrt{n_4A_1B_1}\,(\zeta - \zeta_0), k_2\right) - (A_1 - B_1)} - \frac{f_2}{3f_3}\right] + \beta. \quad (37)$$

(ii) If $n_4 < 0$, then the allowed intervals of possible propagation are $p_1 < p < p_2$. Assuming $p(\zeta_0) = p_1$ and integrating both sides of equation (11), we obtain

$$p = \frac{p_2B_2 + p_1A_2 + (p_1A_2 - p_2B_2)\mathrm{cn}\left(\sqrt{-n_4A_2B_2}\,(\zeta - \zeta_0), k_3\right)}{B_2 + A_2 - (B_2 - A_2)\mathrm{cn}\left(\sqrt{-n_4A_2B_2}\,(\zeta - \zeta_0), k_3\right)}, \quad (38)$$

where $k_3 = \sqrt{\left(\left(p_2 - p_1\right)^2 - \left(A_2 - B_2\right)^2\right)/4A_2B_2}$, $A_2^2 = (1/4)(p_1 + 3p_2)^2 + \mathrm{Im}^2p_3$, and $B_2^2 = (1/4)(3p_1 + p_2)^2 + \mathrm{Im}^2p_3$. Utilizing equations (7) and (3), we construct a novel wave solution for equation (1) in the form

$$I(x,t) = \frac{p_2B_2 + p_1A_2 + (p_1A_2 - p_2B_2)\mathrm{cn}\left(\sqrt{-n_4A_2B_2}\,(kx + \omega t - \zeta_0), k_3\right)}{B_2 + A_2 - (B_2 - A_2)\mathrm{cn}\left(\sqrt{-n_4A_2B_2}\,(kx + \omega t - \zeta_0), k_3\right)} - \frac{f_2}{3f_3},$$
$$J(x,t) = \alpha\left[\frac{p_2B_2 + p_1A_2 + (p_1A_2 - p_2B_2)\mathrm{cn}\left(\sqrt{-n_4A_2B_2}\,(kx + \omega t - \zeta_0), k_3\right)}{B_2 + A_2 - (B_2 - A_2)\mathrm{cn}\left(\sqrt{-n_4A_2B_2}\,(kx + \omega t - \zeta_0), k_3\right)} - \frac{f_2}{3f_3}\right] + \beta. \quad (39)$$

2.7. Case 7. The polynomial $F_4(p)$ has two conjugate complex roots, namely, $p_1, p_1{}^*, p_2, p_2{}^*$, if $D_2D_3 \leq 0$ and $D_4 > 0$. Therefore, it is expressed as $F_4(p) = (p - p_1)(p - p_1^*)(p - p_2)(p - p_2^*)$, where $\mathrm{Re}.p_1 = -\mathrm{Re}.p_2$. The permitted interval for real propagation for the case $n_4 > 0$ is $p \in \mathbb{R}$. Thus, we follow similar steps as above and obtain a new traveling wave solution for equation (1) as

$$
\begin{aligned}
I(x,t) &= \frac{\mathrm{Re}p_1 + \mathrm{Im}p_1\delta + (\mathrm{Im}p_1 + \mathrm{Re}p_1\delta)\mathrm{tn}\left(\left(\sqrt{n_4}/2\right)(A_2+B_2)(kx+\omega t-\zeta_0), k_4\right)}{\delta + \mathrm{tn}\left(\left(\sqrt{n_4}/2\right)(A_2+B_2)(kx+\omega t-\zeta_0), k_4\right)} - \frac{f_2}{3f_3},\\
J(x,t) &= \alpha\left[\frac{\mathrm{Re}p_1 + \mathrm{Im}p_1\delta + (\mathrm{Im}p_1 + \mathrm{Re}p_1\delta)\mathrm{tn}\left(\left(\sqrt{n_4}/2\right)(A_2+B_2)(kx+\omega t-\zeta_0), k_4\right)}{\delta + \mathrm{tn}\left(\left(\sqrt{n_4}/2\right)(A_2+B_2)(kx+\omega t-\zeta_0), k_4\right)} - \frac{f_2}{3f_3}\right] + \beta,
\end{aligned}
\tag{40}
$$

where $A_2^2 = [\mathrm{Im}p_1 - \mathrm{Im}p_2]^2$, $B_2^2 = [\mathrm{Im}p_1 - \mathrm{Im}p_2]^2 + 4\mathrm{Re}^2 p_1$, $\delta^2 = (4\mathfrak{R}p_1{}^2 - (A_2 - B_2)^2)/((A_2+B_2)^2 - 4\mathfrak{R}p_1{}^2)$, and $k_4 = (2\sqrt{A_2B_2})/A_2 + B_2$. It can be noted that the case in which $n_4 < 0$ does not work because $F_4(p) > 0$ for all $p \in \mathbb{R}$.

2.8. Case 8. The polynomial $F_4(p)$ has four real roots in which one of them is double and the others are simple if $D_2 > 0, D_3 > 0$, and $D_4 = 0$. Hence, it takes the form $F_4(p) = (p-p_1)^2(p-p_2)(p-p_3)$, where $p_1 < p_2 < p_3$ and $p_3 = -(2p_1 + p_2)$. We consider the two cases in which n_4 is either positive or negative:

(i) If $n_4 > 0$, then the possible intervals for real propagation are $p < p_1, p > p_3$, and $p_1 < p < p_2$. With similar computations as in previous cases, we present the solution of equation (1) directly.

If we choose $p > -(2p_1 + p_2)$ and assume $p(\zeta_0) = -(2p_1 + p_2)$, we have a new wave solution for equation (1) in the form

$$
\begin{aligned}
I(x,t) &= -2p_1 - p_2 + 4(p_2 - p_1)\mathrm{sech}\left(\sqrt{n_4(-3p_1 - p_2)}\,(kx+\omega t-\zeta_0\right) - \frac{f_2}{3f_3},\\
J(x,t) &= \alpha\left[-2p_1 - p_2 + 4(p_2 - p_1)\mathrm{sech}\left(\sqrt{n_4(-3p_1 - p_2)}\,(kx+\omega t-\zeta_0\right) - \frac{f_2}{3f_3}\right] + \beta.
\end{aligned}
\tag{41}
$$

In similar calculations, we can calculate the wave solution for $p < p_1$ and $p_1 < p < p_2$.

(ii) If $n_4 < 0$, the allowed interval for real propagation is $p \in \,]p_2, p_3[$, and postulating $p(\zeta_0) = p_2$, we obtain a new wave solution for equation (1) in the form

$$
\begin{aligned}
I(x,t) &= p_1 + \frac{(p_2 - p_1)(3p_1 + p_2)}{2p_1 + (p_1 + p_2)\cosh\sqrt{-n_4(3p_1+p_2)(p_1-p_2)}\,(kx - \omega t - \zeta_0)} - \frac{f_2}{3f_3},\\
J(x,t) &= \alpha\left[p_1 + \frac{(p_2 - p_1)(3p_1 + p_2)}{2p_1 + (p_1 + p_2)\cosh\sqrt{-n_4(3p_1+p_2)(p_1-p_2)}\,(kx - \omega t - \zeta_0)} - \frac{f_2}{3f_3}\right] + \beta.
\end{aligned}
\tag{42}
$$

3. Dynamic Properties

The aim of this section is to investigate some dynamic properties for equation (4) by investigating the bifurcation and phase portrait for the traveling wave system corresponding to equation (8) which takes the form

$$
\begin{aligned}
p' &= z,\\
z' &= 2n_4\left(p^3 + \frac{\gamma_2}{2}p + \frac{\gamma_1}{4}\right).
\end{aligned}
\tag{43}
$$

System (43) is a Hamiltonian system with one degree of freedom related to Hamilton function:

$$\frac{1}{2}z^2 + V(p) = h, \tag{44}$$

where h is an arbitrary constant and

$$V(q) = -\frac{n_4}{2}\left(p^4 + \gamma_2 p^2 + \gamma_1 p\right), \tag{45}$$

is the potential function. It is well known that the equilibrium points for the Hamilton system (43) are also critical points for the potential function (45), i.e., they are the roots of

$$\frac{\mathrm{d}V}{\mathrm{d}p} = -2n_4\left(p^3 + \frac{\gamma_2}{2}p + \frac{\gamma_1}{4}\right). \tag{46}$$

Thus, we use the discrimination of (46) to determine the number of equilibrium points. The discrimination of (46) is

$$\Delta = -\frac{1}{8}\left[\frac{\gamma_1^2}{8} + \frac{\gamma_2^3}{27}\right]. \tag{47}$$

Now, let us determine the number of equilibrium points for the Hamilton system (43) and study the properties of its phase space. Thus, we need to define energy curve corresponding to

$$\mathscr{C}_h = \left\{(p, z) \in \mathbb{R}^2 \colon z^2 = 2(h - V(p))\right\}. \tag{48}$$

It is well known that any orbit for the Hamilton system (43) is an energy curve on a certain level of the energy.

Case 1. The dynamical system (43) *has a unique equilibrium point if* $\mathrm{d}V/\mathrm{d}p = 0$ *has a unique real root. This happens in two cases which are studied individually:*

(i) *If* $\Delta = 0$ *and* $\gamma_2 = 0$, *then* $\mathrm{d}V/\mathrm{d}p = 0$ *has one triple real root, i.e.,* $\mathrm{d}V/\mathrm{d}p = -2n_4 p^3$. *This shows* $(0,0)$ *is a unique equilibrium point for system (43) which is saddle if* $n_4 > 0$, *and it is center if* $n_4 < 0$. *The phase space for this case is outlined by Figures 1(a) and 1(b). The value of the energy at the equilibrium point* $(0,0)$ *is* $h_1 = V(0,0) = 0$. *The following proposition describes* Figure 1.

(ii) *If* $\Delta < 0$, *then* $\mathrm{d}V/\mathrm{d}p = 0$ *has one real zero and two complex conjugate roots, i.e.,*

$$\frac{\mathrm{d}V}{\mathrm{d}p} = -2n_4(p - a)\left[\left(p + \frac{a}{2}\right)^2 + m^2\right]. \tag{49}$$

It is clear that the point $(a,0)$ *is a unique equilibrium point for the Hamilton system (43) and it is saddle if* $n_4 > 0$ *and center if* $n_4 < 0$. *The phase space is clarified by Figures 2(a)* and 2(b).

Proposition 1. *The Hamiltonian system (43) has a unique equilibrium point* $(0,0)$ *if* $\gamma_1 = \gamma_2 = 0$. *If* $n_4 > 0$, *it is a saddle point and all the orbits are unbounded, see Figure 1(a). If* $n_4 < 0$, *system (43) has a family of bounded periodic orbits* $\{\mathscr{C}_h\colon h > h_1\}$ *about the center point* $(0,0)$ *as outlined by Figure 1(b). A similar conclusion can be presented to describe Figure 2.*

Case 2. If $\Delta = 0$ *an d* $\gamma_2 < 0$, *then* $\mathrm{d}V/\mathrm{d}p = 0$ *has two real roots: one is simple and the other is double. Thus, we write* $\mathrm{d}V/\mathrm{d}p = -2n_4(p - a)^2(p + 2a)$ *and so* $(a,0)$ *an d* $(-2a,0)$ *are two equilibrium points for system* (43). *It is clear that* $(a,0)$ *is a cusp while* $(-2a,0)$ *is a center if* $n_4 < 0$ *and saddle if* $n_4 > 0$. *The phase portrait for this case is outlined in Figure 3. The following proposition gives a short description for the phase portrait for this case.*

Proposition 2. *The Hamiltonian system (43) has two equilibrium points* $E_1 = (a,0)$ *and* $E_2(-2a,0)$. *If* $n_4 > 0$, *then* E_1 *is cusp point while* E_2 *is saddle, and furthermore, all the phase space orbits are unbounded as outlined in Figure 3(a). While if* $n_4 < 0$, *E1 is a cusp and* E_2 *is a center. The Hamilton system (43) has two bounded families of periodic orbits which are illustrated in green and blue and separated by the phase curve* $\{\mathscr{C}_h\colon h = V(a,0)\}$ *in red.*

Case 3. If $\Delta > 0$ and $\gamma_2 < 0$, *then* $\mathrm{d}V/\mathrm{d}p$ *has three real roots, i.e., it can be written as* $dV/dp = -2n_4(p - a)(p - b)(p + a + b)$, *where we assumed* $b > a > 0$. *Consequently, the dynamical system (43) has three equilibrium points* $(a,0)$, $(b,0)$, and $(-a-b,0)$. *If* $n_4 > 0$, *then* $(a,0)$ *is center and* $(b,0)$ and $(-a-b,0)$ *are saddle points. While if* $n_4 < 0$, $(a,0)$ *is saddle point and the other two equilibrium points are center. The phase portrait for this case is described in Figures 4(a) and 4(b). We describe the phase portrait for the Hamiltonian system in the following proposition.*

Proposition 3. *If* $\Delta > 0$ *and* $\gamma_2 < 0$, *then the Hamilton system (43) has three equilibrium points* $(a,0)$, $(b,0)$, *and* $(-a-b,0)$. *If* $n_4 > 0$, *there are two families of orbits* $\{\mathscr{C}_h\colon h \in]V(a), V(b)[\}$ *in green in which one of them is bounded and surrounded by the homoclinic orbit* $\{\mathscr{C}_h\colon h = V(2a)\}$ *while the other family is unbounded. Moreover, all the other orbits are unbounded, see Figure 4(a) for more clarification. If* $n_4 < 0$, *system (43) has three equilibrium points in which one is a saddle and the others are centers. It has three bounded families of periodic orbits. Two of them in blue and green are periodic orbits around the two center points* $(2a,0)$ *and* $(-a-b,0)$, *and they are separated by the homoclinic orbit in red* $\{\mathscr{C}_h\colon h = V(a)\}$. *The third one is a family of superperiodic orbits in brown* $\{\mathscr{C}_h\colon h > V(a)\}$ *around the two centers points and lies outside the homoclinic orbit in red. For more details about superperiodic orbits, see, for example, [57].*

The investigation of the type of the phase space orbits is helpful in determining the types of the solutions. For instance, the existence of periodic orbits, homoclinic orbits, and heteroclinic orbits for the traveling wave system (43) indicates the existence of periodic wave solutions, solitary, and kink solutions for equation (1). Furthermore, this analysis can be employed to construct the traveling wave solution by introducing the constraints on the coefficients of function (12). Consequently, we can prove the following theorem.

Theorem 1. *Let* $I(x,t) = u(kx - \omega t)$ *and* $J(x,t) = \alpha I(x,t) + \beta$ *be a solution for the double-chain model of DNA (1), then*

(i) *It is a periodic solution if*

(a) $n_4 < 0, h > 0, \Delta = 0\,(\gamma_1 = \gamma_2 = 0)$,
(b) $n_4 < 0, h > V(a,0), \Delta < 0$,
(c) $n_4 < 0$,
$\Delta = 0, \gamma_2 < 0, h \in]V(-2a), V(a)[\,\cup\,]V(a), \infty[$,
(d) $n_4 > 0, \Delta > 0, \gamma_2 > 0, h \in]V(a), V(b)[$,
(e) $n_4 < 0, \Delta > 0, \gamma_2 > 0, h \in]V(a), \infty[$,
(f) $n_4 < 0, \Delta > 0, \gamma_2 > 0, h \in$
$]V(a), \infty[\,\cup\,]V(b), V(a)[\,\cup\,]V(c), V(b)[$.

(ii) *It is a solitary wave solution if* $n_4 < 0, \Delta > 0, \gamma_2 < 0$, *and* $h = V(a)$.

(iii) *It is a kink (antikink) solution if* $n_4 > 0, \Delta > 0, \gamma_2 < 0$, *and* $h = V(b)$.

4. Graphic Interpretations

This section aims to illustrate some of the obtained solutions graphically. Moreover, we study the influence of the physical parameters on the obtained solutions by considering two

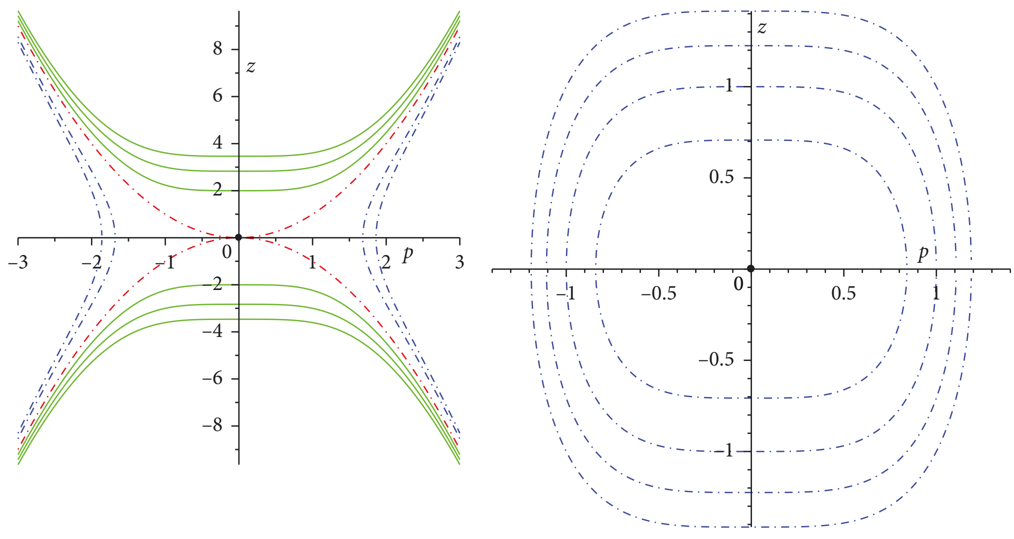

FIGURE 1: Phase portrait for the Hamilton system (43) for $\gamma_1 = 0$ and $\gamma_2 = 0$. (a) $n_4 = 1$ and (b) $n_4 = -1$.

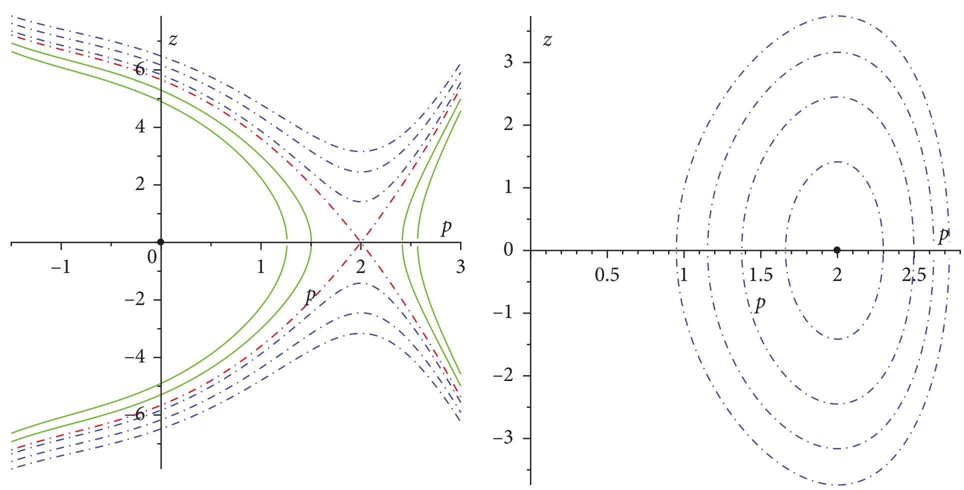

FIGURE 2: Phase portrait for the Hamilton system (43) for $\Delta < 0$. (a) $n_4 = 1$, $\gamma 1 = -16$, and $\gamma 2 = -4$. (b) $n_4 = -1$, $\gamma_1 = -16$, and $\gamma_2 = -4$.

types of solutions: one of them is kink solution and the other is periodic.

Figure 5 and 6 illustrates the kink solution (24) for different aspects. Figures 5(a) and 5(b) clarify the 3D and contour representation for the kink solution (24) when $k = 1$, $\omega = 2$, $\sigma = 0.001$, $\rho = 0.1$, $\mu = 0.0001$, $h = 0.002$, $R_1 = 0.1$, and $l_0 = 0.002$. Now, we illustrate graphically the influence of some parameters on the kink solution while the other parameters are fixed. Figure 6(a) illustrates the effect of the change of the distance between the two strands. It is remarkable the amplitude of solution (24) is decreased when the distance between the two strands is increased. Figure 6(b) clarifies the amplitude of the solution is increased when the stiffness of the elastic membrane is increased. Figure 6(c) clarifies the amplitude of the solution is decreased when the area of the cross section of each strand is increased. Figure 6(d) outlines the amplitude of the kink solution (24) is increased when the height of the membrane in the equilibrium is increased (see Figure 7).

Now, we are going to clarify solution (28) graphically and study the influence of parameter changes on solution (28). Solution (28) is periodic as outlined in Figure 8(a), and its contour is illustrated in Figure 8(b). If the distance between the two strands is increased and the other parameters are fixed, the amplitude of the solution is unchanged but the width of the solution is increased as outlined in Figure 8(a). The amplitude of solution (28) is not affected by the changes in the stiffness of the elastic membrane, while the width of the solution is decreased when the stiffness of the elastic membrane is increased as clarified by Figure 8(d). If the area of the cross section of each strand is increased, then the

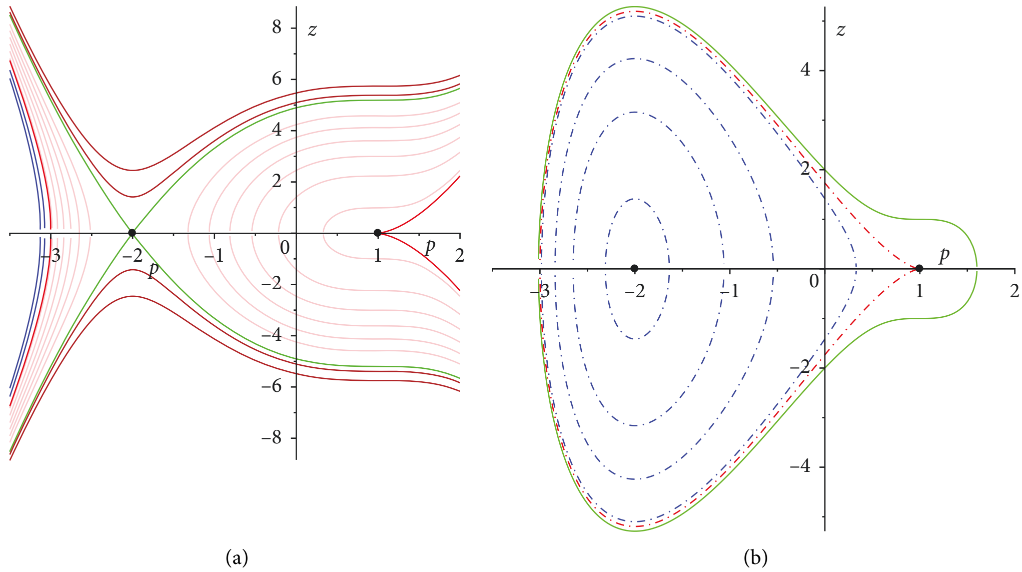

FIGURE 3: Phase portrait for the Hamilton system (43) for $\Delta = 0$ and $\gamma_2 < 0$. (a)$n_4 = 1$, $\gamma_1 = 8$, and $\gamma_2 = -6$. (b)$n_4 = -1$, $\gamma_1 = 8$, and $\gamma_2 = -6$.

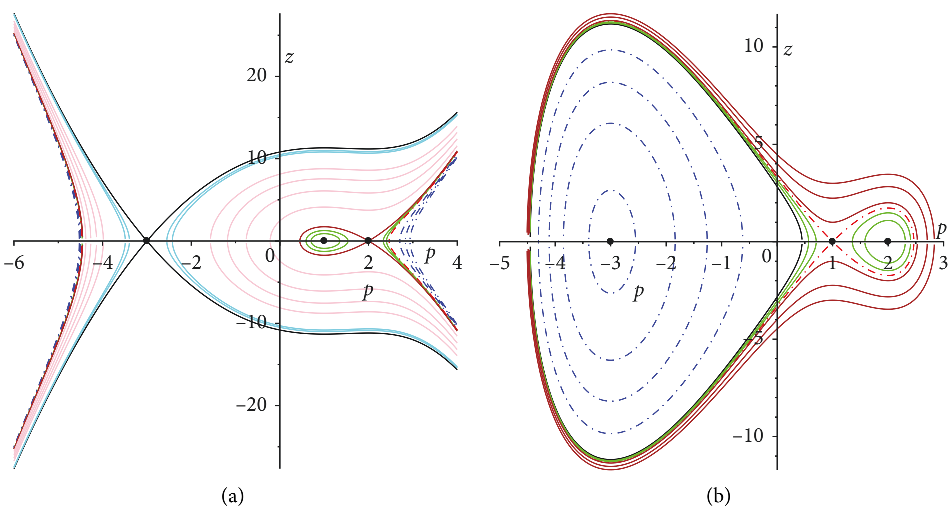

FIGURE 4: Phase portrait for the Hamilton system (43) for $\Delta > 0$ and $\gamma_2 < 0$. (a)$n_4 = 1$, $\gamma_1 = 8$, and $\gamma_2 = -6$. (b)$n_4 = -1$, $\gamma_1 = 8$, and $\gamma_2 = -6$.

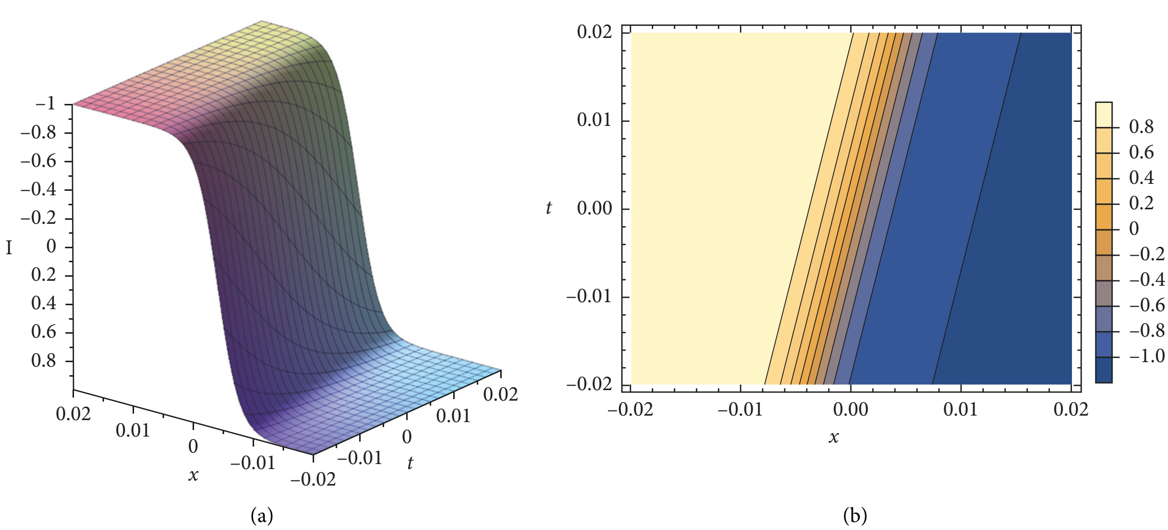

FIGURE 5: Graphic representation of solution (24) for $R_1 = 0.1$, $h = 0.002$, $k = 1$, $l_0 = 0.002$, $\mu = 0.0001$, $\omega = 2$, $\rho = 0.1$, and $\sigma = 0.001$. (a) 3D graphic and (b) 2D contour plot.

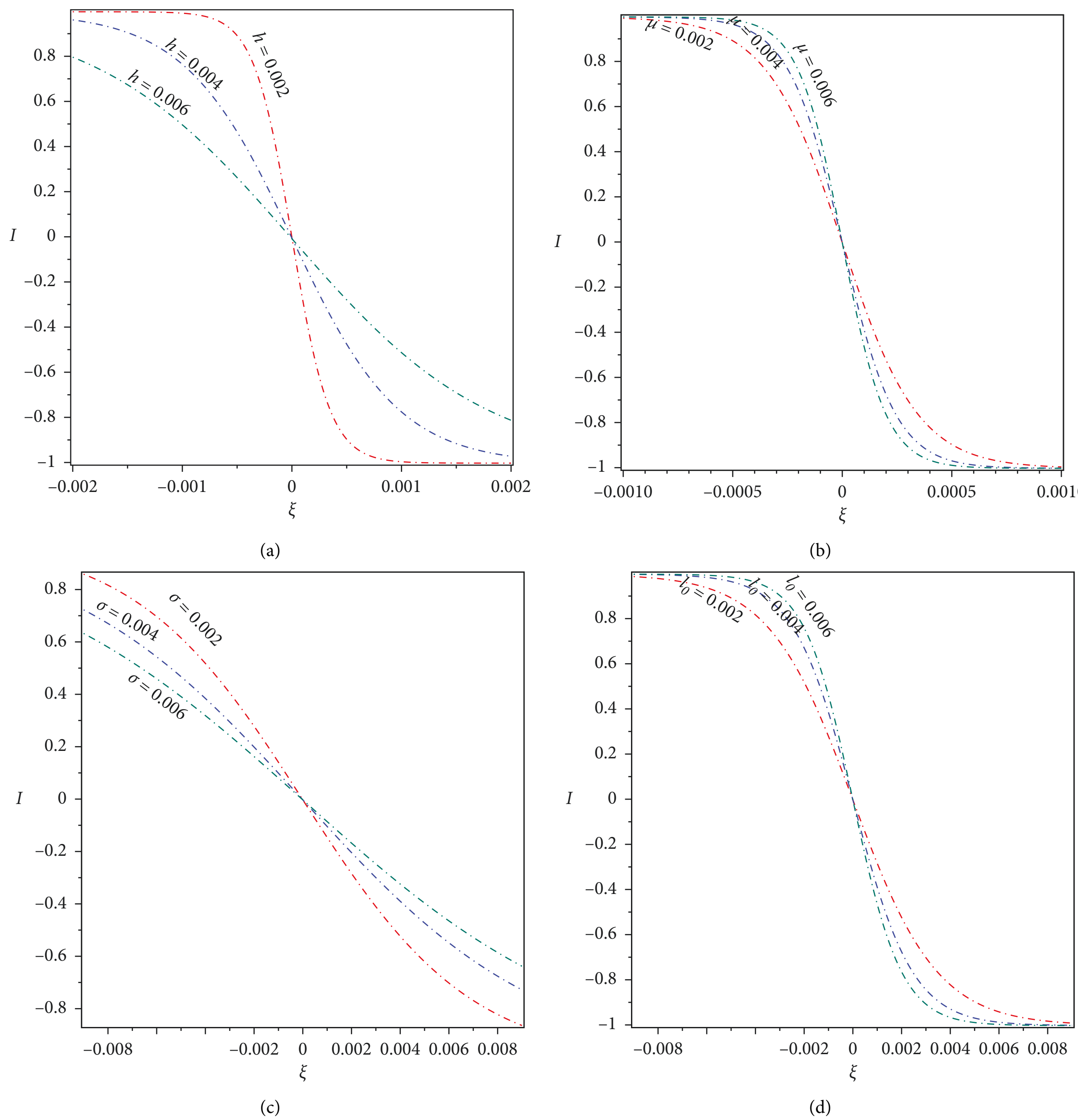

Figure 6: Parameters affecting solution (24): (a) changes in h for $R_1 = 0.1$, $k = 1$, $l_0 = 0.001$, $\mu = 0.002$, $\rho = 0.1$, and $\sigma = 0.0001$, (b) changes in μ for $R_1 = 0.1$, $h = 0.002$, $k = 1$, $l_0 = 0.001$, $\omega = 2$, $\rho = 0.1$, and $\sigma = 0.0001$, (c) changes in σ for $R_1 = 0.1$, $h = 0.002$, $k = 1$, $l_0 = 0.001$, $\mu = 0.0001$, $\omega = 0.1$, and $\rho = 0.1$, and (d) changes in l_0 for $R_1 = 0.1$, $h = 0.002$, $k = 1$, $\sigma = 0.001$, $\rho = 0.1$, $\mu = 0.0001$, and $\omega = 2$.

amplitude keeps fixed while the width is increased, see Figure 8(d). Figure 9(b) outlines the amplitude of the periodic solution (28) is kept unchanged while its width is decreased when the height of the membrane in the equilibrium is increased. Figure 9(a) illustrates the influence of the superperiodic wave solution (39) due the changes in the stiffness of the elastic membrane. If the stiffness of the elastic membrane increases, the amplitude is kept unchanged while the width decreases. Figure 9(b) clarifies the influence of distance between the two strands on the superwave solution (39). If distance between the two strands is increased, then the amplitude and the width of superwave solution (39) are increased.

It is worth mentioning that we can make the same study for the remaining obtained solutions. However, we only give the 3D graphic and the 2D counter for some solutions. The 3D graphic representation and the singularity plane are outlined in Figure 10(a), while Figure 10(b) illustrates the 2D contour of solution (15). Solution (37) is illustrated in Figure 11.

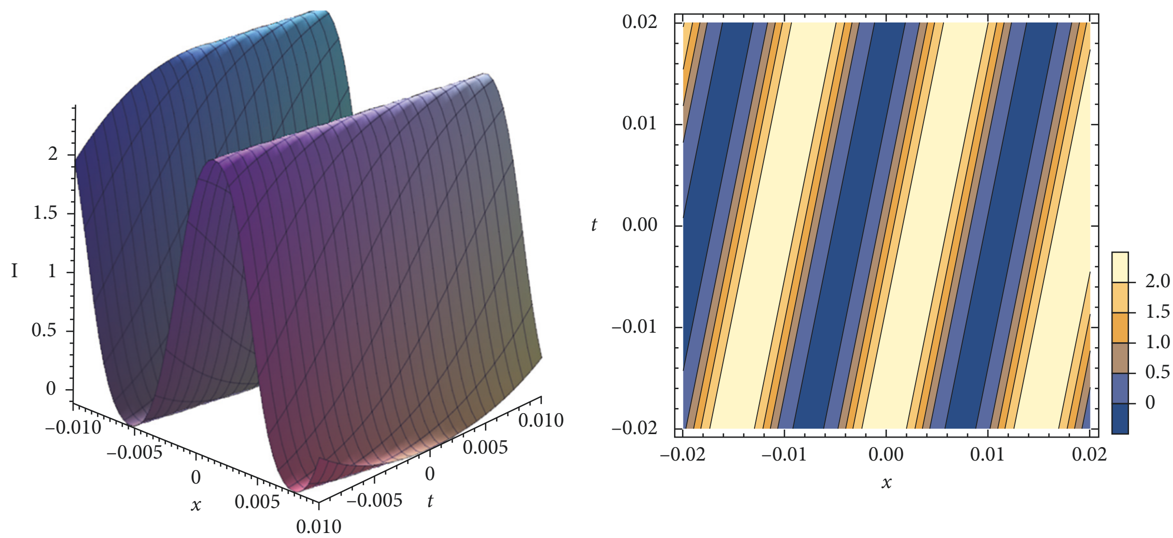

(a) (b)

Figure 7: Graphic representation of solution (28) for $R_1 = 0.1$, $h = 0.002$, $k = 1$, $l_0 = 0.002$, $\mu = 0.0001$, $\omega = 0.2$, $\rho = 0.1$, and $\sigma = 0.001$. (a) 3D graphic and (b) 2D contour plot.

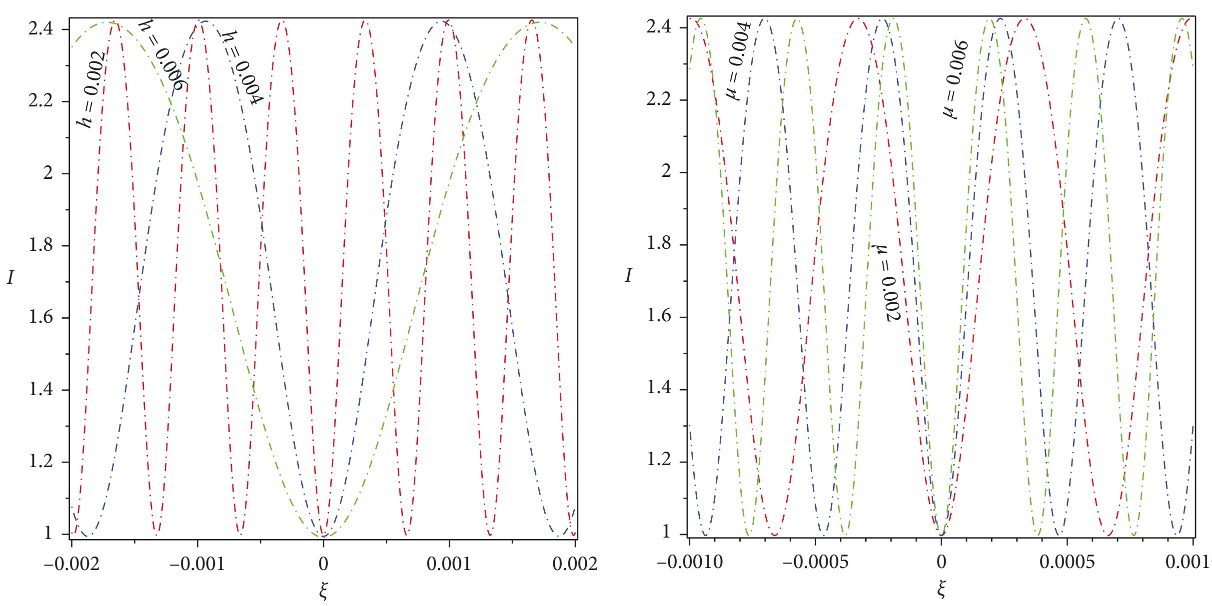

(a) (b)

Figure 8: Continued.

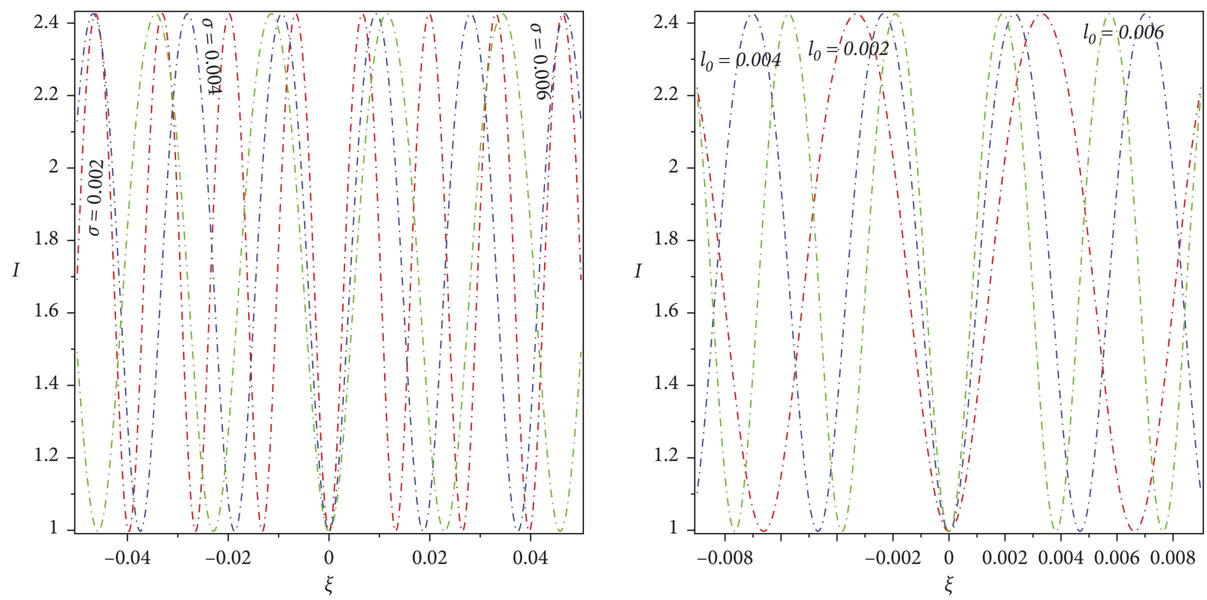

(c) (d)

Figure 8: Parameters affecting solution (28): (a) changes in h for $R_1 = 0.1$, $k = 1$, $l_0 = 0.001$, $\mu = 0.002$, $\omega = 2$, $\rho = 0.1$, and $\sigma = 0.0001$, (b) changes in μ for $R_1 = 0.1$, $h = 0.002$, $k = 1$, $l_0 = 0.001$, $\omega = 2$, $\rho = 0.1$, and $\sigma = 0.0001$, (c) changes in σ for $R_1 = 0.1$, $h = 0.002$, $k = 1$, $l_0 = 0.001$, $\mu = 0.0001$, $\omega = 2$, and $\rho = 0.1$, and (d) changes in l_0 for $R_1 = 0.1$, $h = 0.0002$, $k = 1$, $\mu = 0.0001$, $\omega = 2$, $\rho = 0.1$, and $\sigma = 0.001$.

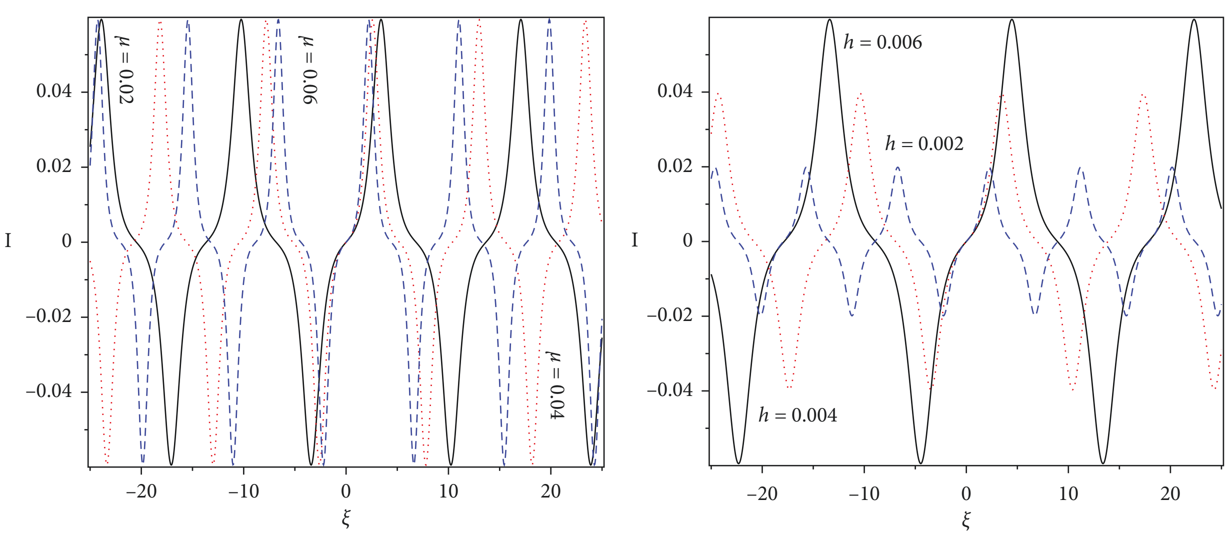

(a) (b)

Figure 9: Parameters affecting the superwave solution (39): (a) changes in μ for $R_1 = 0.01$, $\alpha = 0.8$, $h = 0.006$, $k = 1$, $l_0 = 0.001$, $\rho = 0.00002$, and $\sigma = 0.01$ and (b) changes in h for $R_1 = 0.01$, $\alpha = 0.8$, $h = 0.006$, $k = 1$, $l_0 = 0.001$, $\rho = 0.00002$, and $\sigma = 0.01$.

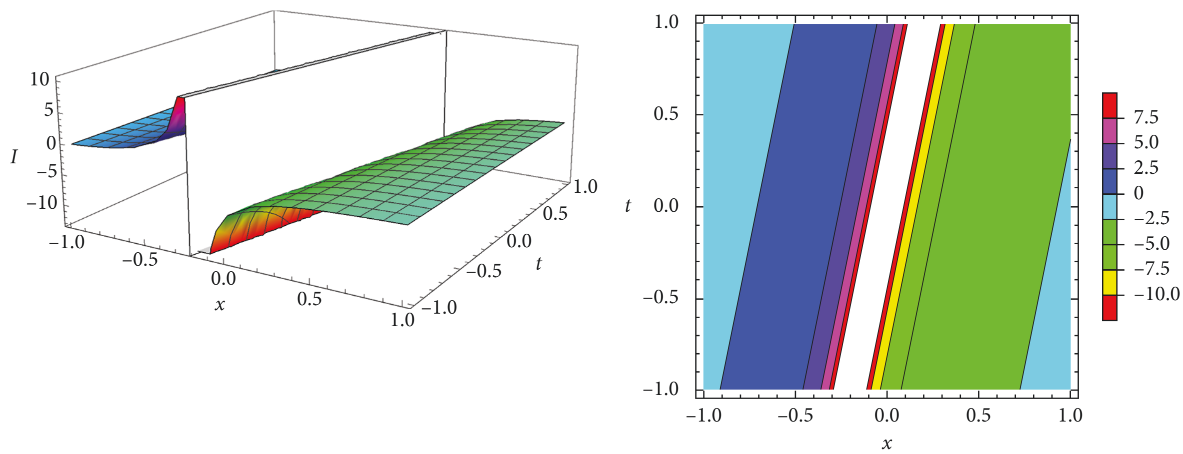

(a) (b)

Figure 10: Graphic representation for the singular wave solution (15). (a) 3D graphic and (b) 2D contour.

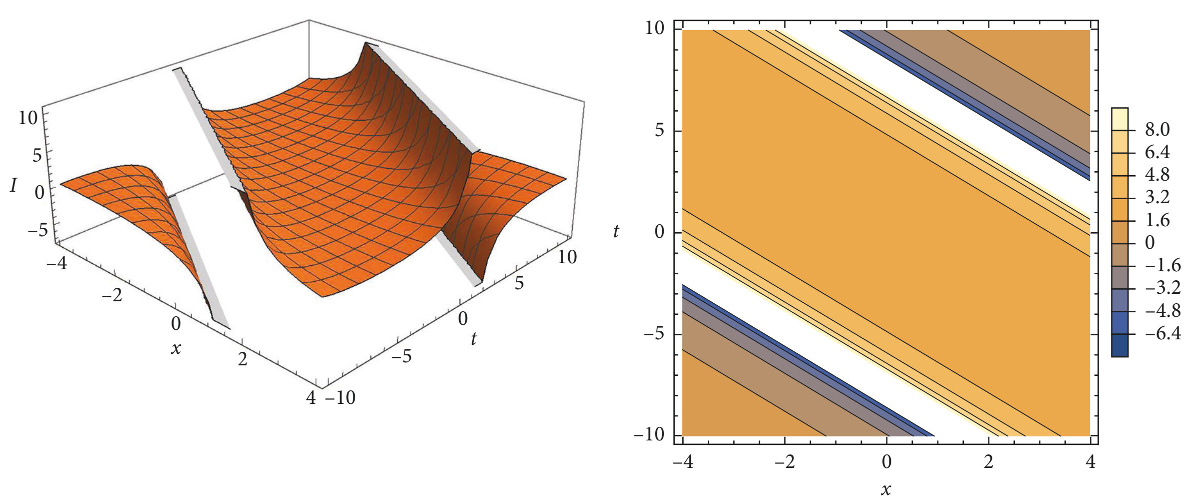

(a) (b)

Figure 11: Graphic representation for the singular wave solution (37). (a) 3D graphic and (b) 2D contour.

5. Conclusion

This work is aimed to study analytically the double-chain model for deoxyribonucleic acid (DNA). A certain wave transformation has been applied to equation (1) to transform it into an ordinary differential equation. The integration of this equation reacquired some studies on the parameters. This study has been performed by applying the complete discrimination of the polynomial $F_4(p)$. Moreover, we have determined the possible interval of real propagations. Such study is more significant because the missing of such study implies to loss some solutions and also, give rise to complex solutions which are undesirable in real problems. For instance, there are several solutions corresponding to the same conditions on the discriminant system as outlined in Case 4. We have introduced new waves' solutions for equation (1). Let us compare the results obtained in the present article with the well-known results obtained by other authors using different methods as follows: our results in a new double-chain model of DNA are new and different from those obtained in references [19–24]. We have studied the influence of some parameters such as the distance between the two strands, the stiffness of the elastic membrane, the area of the cross section of each strand, and the height of the membrane in the equilibrium. We have considered two types of solutions: one is kink (24) and the other is periodic (28). We have shown graphically the amplitude of the kink solution is decreased when the distance between the two strands or the area of the cross section of each strand is increased, while it is increased when the stiffness of the elastic membrane or the height of the membrane in the equilibrium is increased. For more clarification, see Figure 6. The amplitude of the periodic solution remains approximately unchanged when these physical parameters are changed, but the width has been affected. The width is increased due to the increase of the distance between the two strands or the area of the cross section of each strand, while it is decreased as a result of increasing the stiffness of the elastic membrane or the height of the membrane in the equilibrium. For more illustrations, see Figure 10. From another point of view, this ODE has been expressed as a one-dimensional Hamiltonian system that describes the physical motion of a particle with one degree of freedom under the action of potential function $V(p)$ given by (45). Based on the Hamiltonian concepts, we have studied some qualitative analyses such as phase portrait and bifurcation. The description of phase space has been presented through Propositions 1, 2, and 3. Moreover, these propositions contain the conditions for the existence of periodic and solitary wave solutions.

Data Availability

No data were used to support the study.

Conflicts of Interest

The authors declare that they have no conflicts of interest.

Acknowledgments

This research has been funded by the Scientific Research Deanship at University of Ha'il, Saudi Arabia, through project number RG-21008.

References

[1] M. Peyrard, S. Cuesta-López, and G. James, "Modelling DNA at the mesoscale: a challenge for nonlinear science?" *Nonlinearity*, vol. 21, no. 6, pp. T91–T100, 2008.
[2] J. D. Watson and F. H. C. Crick, "Molecular structure of nucleic acids: a structure for deoxyribose nucleic acid," *Nature*, vol. 171, no. 4356, pp. 737-738, 1953.
[3] L. V. Yakushevich, *Nonlinear Physics of DNA*, John Wiley & Sons, Hoboken, NJ, USA, 2006.
[4] A. S. Davydov, "Solitons in molecular systems," *Physica Scripta*, vol. 20, no. 3-4, p. 387, 1979.
[5] S. W. Englander, N. R. Kallenbach, A. J. Heeger, J. A. Krumhansl, and S. Litwin, "Nature of the open state in long polynucleotide double helices: possibility of soliton excitations," *Proceedings of the National Academy of Sciences*, vol. 77, no. 12, pp. 7222–7226, 1980.
[6] S. Yomosa, "Soliton excitations in deoxyribonucleic acid (DNA) double helices," *Physical Review*, vol. 27, no. 4, pp. 2120–2125, 1983.
[7] S. Homma and S. Takeno, "A coupled base-rotator model for structure and dynamics of DNA: local fluctuations in helical twist angles and topological solitons," *Progress of Theoretical Physics*, vol. 72, no. 4, pp. 679–693, 1984.
[8] M. Peyrard and A. R. Bishop, "Statistical mechanics of a nonlinear model for DNA denaturation," *Physical Review Letters*, vol. 62, no. 23, pp. 2755–2758, 1989.
[9] V. Muto, P. S. Lomdahl, and P. L. Christiansen, "Two-dimensional discrete model for DNA dynamics: longitudinal wave propagation and denaturation," *Physical Review*, vol. 42, no. 12, pp. 7452–7458, 1990.
[10] L. V. Yakushevich, A. V. Savin, and L. I. Manevitch, "Nonlinear dynamics of topological solitons in DNA," *Physical review. E, Statistical, nonlinear, and soft matter physics*, vol. 66, no. 1, Article ID 016614, 2002.
[11] D. L. Hien, N. T. Nhan, V. T. Ngo, and N. A. Viet, "Simple combined model for nonlinear excitations in DNA," *Physical review. E, Statistical, nonlinear, and soft matter physics*, vol. 76, no. 2, Article ID 021921, 2007.
[12] M. Daniel and V. Vasumathi, "Perturbed soliton excitations in the DNA double helix," *Physica D: Nonlinear Phenomena*, vol. 231, no. 1, pp. 10–29, 2007.
[13] C. B. Tabi, A. Mohamadou, and T. C. Kofané, "Soliton excitation in the DNA double helix," *Physica Scripta*, vol. 77, no. 4, Article ID 045002, 2008.
[14] S. Zdravković and M. V. Satarić, "Parameter selection in a peyrard–bishop–dauxois model for DNA dynamics," *Physics Letters A*, vol. 373, no. 31, pp. 2739–2745, 2009.
[15] G. Gaeta, C. Reiss, M. Peyrard, and T. Dauxois, "Simple models of non-linearDNA dynamics," *La Rivista Del Nuovo Cimento Series 3*, vol. 17, no. 4, pp. 1–48, 1994.
[16] R. V. Polozov and L. V. Yakushevich, "Nonlinear waves in DNA and regulation of transcription," *Journal of Theoretical Biology*, vol. 130, no. 4, pp. 423–430, 1988.
[17] J. A. González and M. Martín-Landrove, "Long-range interactions of solitons in a double chain," *Physics Letters A*, vol. 292, no. 4-5, pp. 256–262, 2002.
[18] L. V. Yakushevich, "Non-linear DNA dynamics and problems of gene regulation," *Nanobiology*, vol. 1, pp. 343–350, 1992.
[19] K. De-Xing, L. Sen-Yue, and Z. Jin, "Nonlinear dynamics in a new double chain-model of DNA," *Communications in Theoretical Physics*, vol. 36, no. 6, pp. 737–742, 2001.
[20] W. Alka, A. Goyal, and C. Nagaraja Kumar, "Nonlinear dynamics of DNA—riccati generalized solitary wave solutions," *Physics Letters A*, vol. 375, no. 3, pp. 480–483, 2011.
[21] A. R. Seadawy, M. Bilal, M. Younis, S. T. R. Rizvi, S. Althobaiti, and M. M. Makhlouf, "Analytical mathematical approaches for the double-chain model of DNA by a novel computational technique," *Chaos, Solitons & Fractals*, vol. 144, Article ID 110669, 2021.
[22] Q. Xian-Min and L. Sen-Yue, "Exact solutions of nonlinear dynamics equation in a new double-chain model of DNA," *Communications in Theoretical Physics*, vol. 39, no. 4, pp. 501–505, 2003.
[23] Z. Y. Ouyang and S. Zheng, "Travelling wave solutions of nonlinear dynamical equations in a double-chain model of DNA," *Abstract and Applied Analysis*, vol. 2014, Article ID 317543, 5 pages, 2014.
[24] S. Kumar, A. Kumar, and H. Kharbanda, "Abundant exact closed-form solutions and solitonic structures for the double-chain deoxyribonucleic acid (DNA) model," *Brazilian Journal of Physics*, vol. 51, pp. 1–26, 2021.
[25] M. E. Elbrolosy and A. A. Elmandouh, "Dynamical behaviour of nondissipative double dispersive microstrain wave in the microstructured solids," *European Physical Journal Plus*, vol. 136, no. 9, pp. 1–20, 2021.
[26] M. Al Nuwairan and A. A. Elmandouh, "Qualitative analysis and wave propagation of the nonlinear model for low-pass electrical transmission lines," *Physica Scripta*, vol. 96, no. 9, Article ID 095214, 2021.
[27] A. A. Elmandouh, "Integrability, qualitative analysis and the dynamics of wave solutions for Biswas–Milovic equation," *European Physical Journal Plus*, vol. 136, no. 6, pp. 1–17, 2021.

[28] A. A. Elmandouh, "Bifurcation and new traveling wave solutions for the 2D Ginzburg–Landau equation," *European Physical Journal Plus*, vol. 135, no. 8, pp. 1–13, 2020.

[29] M. E. Elbrolosy and A. A. Elmandouh, "Bifurcation and new traveling wave solutions for $(2+1)$-dimensional nonlinear Nizhnik-Novikov-Veselov dynamical equation," *European Physical Journal Plus*, vol. 135, no. 6, p. 533, 2020.

[30] M. E. Elbrolosy, "Qualitative analysis and new soliton solutions for the coupled nonlinear Schrödinger type equations," *Physica Scripta*, vol. 96, no. 12, Article ID 125275, 2021.

[31] Z.-Y. Zhang, Z.-Y. Liu, X.-J. Miao, and Y.-Z. Chen, "Qualitative analysis and traveling wave solutions for the perturbed nonlinear Schrödinger's equation with Kerr law nonlinearity," *Physics Letters A*, vol. 375, no. 10, pp. 1275–1280, 2011.

[32] Q.-S. Liu, Z.-Y. Zhang, R.-G. Zhang, and C.-X. Huang, "Dynamical analysis and exact solutions of a new $(2+1)$-dimensional generalized boussinesq model equation for nonlinear rossby waves*," *Communications in Theoretical Physics*, vol. 71, no. 9, p. 1054, 2019.

[33] P. K. Prasad, A. Abdikian, and A. Saha, "Modeling of nonlinear ion-acoustic solitary, snoidal and superperiodic wave phenomena due to ionospheric escape of Venus," *Advances in Space Research*, vol. 68, no. 10, pp. 4155–4166, 2021.

[34] A. Abdikian, J. Tamang, and A. Saha, "Supernonlinear wave and multistability in magneto-rotating plasma with (r, q) distributed electrons," *Physica Scripta*, vol. 96, no. 9, Article ID 095605, 2021.

[35] K. K. Ali, M. S. Osman, and M. Abdel-Aty, "New optical solitary wave solutions of Fokas-Lenells equation in optical fiber via Sine-Gordon expansion method," *Alexandria Engineering Journal*, vol. 59, no. 3, pp. 1191–1196, 2020.

[36] K. K. Ali, A.-M. Wazwaz, and M. S. Osman, "Optical soliton solutions to the generalized nonautonomous nonlinear Schrödinger equations in optical fibers via the sine-Gordon expansion method," *Optik*, vol. 208, Article ID 164132, 2020.

[37] J.-G. Liu, W.-H. Zhu, M. S. Osman, and W.-X. Ma, "An explicit plethora of different classes of interactive lump solutions for an extension form of 3D-Jimbo-Miwa model," *European Physical Journal Plus*, vol. 135, no. 5, p. 412, 2020.

[38] I. Siddique, M. M. M. Jaradat, A. Zafar, K. Bukht Mehdi, and M. S. Osman, "Exact traveling wave solutions for two prolific conformable M-Fractional differential equations via three diverse approaches," *Results in Physics*, vol. 28, Article ID 104557, 2021.

[39] X.-I. Miao and Z.-Y. Zhang, "The modified $G\prime/G$-expansion method and traveling wave solutions of nonlinear the perturbed nonlinear Schrödinger's equation with Kerr law nonlinearity," *Communications in Nonlinear Science and Numerical Simulation*, vol. 16, no. 11, pp. 4259–4267, 2011.

[40] Z. Zhang, J. Huang, J. Zhong et al., "The extended (G'/G)-expansion method and travelling wave solutions for the perturbed nonlinear Schrödinger's equation with Kerr law nonlinearity," *Pramana*, vol. 82, no. 6, pp. 1011–1029, 2014.

[41] A. Khalid, A. Rehan, K. S. Nisar, and M. S. Osman, "Splines solutions of boundary value problems that arises in sculpturing electrical process of motors with two rotating mechanism circuit," *Physica Scripta*, vol. 96, 2021.

[42] S. Kumar, B. Kour, S.-W. Yao, M. Inc, and M. S. Osman, "Invariance analysis, exact solution and conservation laws of $(2+1)$ dim fractional kadomtsev-petviashvili (KP) system," *Symmetry*, vol. 13, no. 3, p. 477, 2021.

[43] F. S. Bayones, K. S. Nisar, K. A. Khan et al., "Magneto-hydrodynamics (MHD) flow analysis with mixed convection moves through a stretching surface," *AIP Advances*, vol. 11, no. 4, Article ID 045001, 2021.

[44] Z. Zhang, "New exact traveling wave solutions for the nonlinear Klein-Gordon equation," *Turkish Journal of Physics*, vol. 32, no. 5, pp. 235–240, 2008.

[45] Z.-Y. Zhang, Z.-H. Liu, X.-J. Miao, and Y.-Z. Chen, "New exact solutions to the perturbed nonlinear Schrödinger's equation with Kerr law nonlinearity," *Applied Mathematics and Computation*, vol. 216, no. 10, pp. 3064–3072, 2010.

[46] Z.-Y. Zhang, Y.-X. Li, Z.-H. Liu, and X.-J. Miao, "New exact solutions to the perturbed nonlinear Schrödinger's equation with Kerr law nonlinearity via modified trigonometric function series method," *Communications in Nonlinear Science and Numerical Simulation*, vol. 16, no. 8, pp. 3097–3106, 2011.

[47] Z. Y. Zhang, J. Zhong, S. S. Dou, J. I. A. O. Liu, D. Peng, and T. I. N. G. Gao, "First integral method and exact solutions to nonlinear partial differential equations arising in mathematical physics," *Romanian Reports in Physics*, vol. 65, no. 4, pp. 1155–1169, 2013.

[48] Z. Y. Zhang, "Jacobi elliptic function expansion method for the modified Korteweg-de Vries-Zakharov-Kuznetsov and the Hirota equations," *Romanian Journal of Physics*, vol. 60, no. 9-10, pp. 1384–1394, 2015.

[49] K.-J. Wang, "Generalized variational principle and periodic wave solution to the modified equal width-Burgers equation in nonlinear dispersion media," *Physics Letters A*, vol. 419, Article ID 127723, 2021.

[50] K. J. Wang, "Abundant analytical solutions to the new coupled Konno-Oono equation arising in magnetic field," *Results in Physics*, vol. 31, Article ID 104931, 2021.

[51] K.-J. Wang and G.-D. Wang, "Variational theory and new abundant solutions to the $(1+2)$-dimensional chiral nonlinear Schrödinger equation in optics," *Physics Letters A*, vol. 412, Article ID 127588, 2021.

[52] K. J. Wang and G. D. Wang, "Study on the explicit solutions of the Benney-Luke equation via the variational direct method," *Mathematical Methods in the Applied Sciences*, vol. 44, no. 18, pp. 14173–14183, 2021.

[53] K.-J. Wang, "Periodic solution of the time-space fractional complex nonlinear Fokas-Lenells equation by an ancient Chinese algorithm," *Optik*, vol. 243, Article ID 167461, 2021.

[54] L. Yang, X. R. Hou, and Z. B. Zeng, "A complete discrimination system for polynomials," *Science in China, Series A*, vol. 39, no. 6, pp. 628–646, 1996.

[55] L. Cheng-Shi, "Exact travelling wave solutions for $(1+1)$-dimensional dispersive long wave equation," *Chinese Physics*, vol. 14, no. 9, pp. 1710–1715, 2005.

[56] P. F. Byrd and M. D. Fridman, *Handbook of Elliptic Integrals for Engineers and Scientists*, Springer, Berlin, Germany, 1971.

[57] A. Saha and S. Banerjee, *Dynamical Systems and Nonlinear Waves in Plasmas*, CRC Press, Boca Raton, FL, USA, 2021.

Hindawi
Journal of Mathematics
Volume 2022, Article ID 2715767, 10 pages
https://doi.org/10.1155/2022/2715767

Research Article

Some Novel Analytical Approximations to the (Un)damped Duffing–Mathieu Oscillators

Haifa A. Alyousef,[1] Alvaro H. Salas ,[2] Sadah A. Alkhateeb,[3] and S. A. El-Tantawy [4,5]

[1]*Department of Physics, College of Science, Princess Nourah bint Abdulrahman University, P.O. Box 84428, Riyadh 11671, Saudi Arabia*
[2]*Department of Mathematics and Statistics, Universidad Nacional de Colombia, FIZMAKO Research Group, Sede Manizales, Colombia*
[3]*Mathematics Department, Faculty of Science, University of Jeddah, Jeddah, Saudi Arabia*
[4]*Department of Physics, Faculty of Science, Port Said University, Port Said 42521, Egypt*
[5]*Research Center for Physics (RCP), Department of Physics, Faculty of Science and Arts, Al-Mikhwah, Al-Baha University, Saudi Arabia*

Correspondence should be addressed to S. A. El-Tantawy; tantawy@sci.psu.edu.eg

Received 24 December 2021; Accepted 27 March 2022; Published 5 May 2022

Academic Editor: Fairouz Tchier

Some novel exact solutions and approximations to the damped Duffing–Mathieu-type oscillator with cubic nonlinearity are obtained. This work is divided into two parts: in the first part, some exact solutions to both damped and undamped Mathieu oscillators are obtained. These solutions are expressed in terms of the Mathieu functions of the first kind. In the second part, the equation of motion to the damped Duffing–Mathieu equation (dDME) is solved using some effective and highly accurate approaches. In the first approach, the nonintegrable dDME with cubic nonlinearity is reduced to the integrable dDME with linear term having undermined optimal parameter (maybe called reduced method). Using a suitable technique, we can determine the value of the optimal parameter and then an analytical approximation is obtained in terms of the Mathieu functions. In the second approach, the ansatz method is employed for deriving an analytical approximation in terms of trigonometric functions. In the third approach, the homotopy perturbation technique with the extended Krylov–Bogoliubov–Mitropolskii (HKBM) method is applied to find an analytical approximation to the dDME. Furthermore, the dDME is solved numerically using the Runge–Kutta (RK) numerical method. The comparison between the analytical and numerical approximations is carried out. All obtained approximations can help a large number of researchers interested in studying the nonlinear oscillations and waves in plasma physics and many other fields because many evolution equations related to the nonlinear waves and oscillations in a plasma can be reduced to the family of Mathieu-type equation, Duffing-type equation, etc.

1. Introduction

Several physical and natural phenomena related to biology, chemistry, physics, engineering problems, and so on can be modelled by both ordinary differential equations (ODEs) and partial differential equations (PDEs) for studying the nonlinear self-excited oscillators [1–12]. Also, in many real-life problems, some internal and external forces that can affect the system under consideration cannot be neglected. For example, the friction and collisional force and many others that affect on the motion of particles, whether in solid, liquid, gas or plasma physics, cannot be neglected. Therefore, these forces must be included in the mathematical models that will be used for studying the natural and physical problem, such as investigating the nonlinear oscillations in various plasma models [13–23]. Interest in the study of nonlinear oscillations in a plasma is due to its many potential applications. Nowadays, plasma processing is seen as an important and effective technology which has been able to enter into all modern industries. In addition, plasma had a great credit for the modern technology in electronics, medicine, agriculture, biomedicine, automobiles, optics, aerospace, telecommunications, solar energy, polymers, papers, textiles, etc. [16, 24]. Therefore, we focus our attention on the applications of the family of Duffing-type equation for modelling the nonlinear oscillations in a plasma. The Duffing-type oscillator is one of the most popular differential equations that has spread widely due to its ability to explain many nonlinear phenomena in various fields of science and in mechanical systems and engineering. This equation is a mathematical model described by a second order of ODEs with a nonlinear spring force. It is used for describing the motion of (un)damped oscillator rather than simple harmonic motion. Motivated by potential engineering and plasma physics applications in addition to many others applications in electronic circuits and microcontroller, the family of Duffing equation such as (un) damped Duffing equation with lower and higher-order nonlinearities, (un)damped Duffing–Helmholtz equation, and (un)damped Mathieu–Duffing equation have received wide attention due to their ability for investigating the mechanism of a rigid pendulum oscillator, oscillations in different plasma models, and so on. This family of second-order differential equations has provided useful and successful models for investigating the nonlinear oscillations and chaotic nature. The biggest challenge in the study of the dynamics of nonlinear mechanical systems is to find some real solutions (including the analytical and numerical solutions) to the evolution equations that are used for describing the characteristics of nonlinear phenomena under consideration. Accordingly, studying the solutions of many equations of motion to various oscillators is one of the most difficult tasks facing many researchers.

The solutions associated to mentioned evolution equations and many other related equations have been studied extensively due to the fact that such equations arise in a variety of realistic problems. For instance, the fluid equations of electron-ion unmagnetized cold plasma were reduced to Mathieu equation in order to investigate the electron waves [13]. During this study, the authors assumed that the density perturbations of the plasma species are only time-dependent functions and do not depend on space. Also, the basic set of fluid equations to a multicomponent complex plasma consisting of inertial two types of dust grains (both positive and negative charges) as well as inertialess Maxwellian species including electrons and ions were reduced to a Mathieu-type equation for studying the excitation of dust-acoustic oscillations [14]. Moreover, a nonlinear Van der Pol–Mathieu-type equation was derived for the dust grain density in order to investigate the dynamics of dust-acoustic oscillations in a dusty plasma consisting of inertial Boltzmann distributed species (electrons and ions) and inertialess dust grains [15]. A modified Van der Pol–Duffing oscillator with forced term was used in the study and was used in modelling the dynamics of nonlinear oscillations in different plasma models [16]. More recently, the multistage method was used for solving the damping Duffing equation with forced term in order to model the oscillations in a complex unmagnetized plasma [17].

Due to the importance of the family of Duffing-type equation and motivated by the mentioned studies, we focus our attention on the analysis of the so-called (un)damped Mathieu–Duffing oscillator with a twin-well potential [25].

$$\mathbb{R} \equiv \ddot{x} + \left(\alpha - Q_0 \cos(\Omega t)\right)x + \beta x^3 = 0, \tag{1}$$

and

$$\mathbb{R}_1 \equiv \ddot{x} + \varepsilon\dot{x} + \left(\alpha - Q_0 \cos(\Omega t)\right)x + \beta x^3 = 0, \tag{2}$$

for studying the vibrating/oscillating behavior of systems described by (1) and (2), where $(\alpha, \beta) > 0$ are, respectively, the stiffness coefficients of the linear and nonlinear terms and ε represents the coefficients of damping term. The longitudinal loading is periodic, Ω and Q_0 are the frequency and excitation strength of the periodic loading, respectively. The total energy of the undamped Mathieu–Duffing oscillator (DMO) according to (1) is defined by $H = H_0 + H_1$, where $H_0 = 1/2\dot{x}^2 - 1/2\alpha x^2 + 1/4\beta x^4$ and $H_1 = -1/2x^2 Q_0 \cos(\Omega t)$ are, respectively, the unperturbed and perturbation in the Hamiltonian of (1). There is another form to the equation of periodic motion which is called (un)damped Mathieu–Helmholtz oscillator.

$$\begin{cases} \ddot{x} + \left(\alpha - Q_0 \cos(\Omega t)\right)x + \beta x^2 = 0, \\ \ddot{x} + \varepsilon\dot{x} + \left(\alpha - Q_0 \cos(\Omega t)\right)x + \beta x^2 = 0. \end{cases} \tag{3}$$

The analytical solution to the damped Mathieu–Helmholtz oscillator (3) was obtained using the finite Fourier series expansion [26]. Note that in evolution equation (3), the nonlinear term βx^2 is different from the nonlinear term in equations (1) and (2).

The objectives of our study are to find some novel solutions to the (un)damped Duffing–Mathieu-type oscillator, under the initial conditions $x(0) = 0$ and $x'(0) = \dot{x}_0$. Two cases for Duffing–Mathieu-type oscillator will be discussed. In the first case, we will get some exact solutions to (un)damped Mathieu equation in terms of the Mathieu functions of the first kind. In the second case, the damped Duffing–Mathieu oscillator (dDMO) will be solved analytically and numerically using some different approaches. In the first approach, the cubic nonlinear term in equation (1) βx^3 is replaced by the linear term $\beta\kappa x$, where the constant $\kappa \geq 0$ represents an optimal parameter. Then, the nonintegrable dDMO reduces to an integrable one which has an exact solution but with undermined parameter κ. Using a suitable technique, we can determine the value of the optimal parameter κ. Thus, we can get an analytical approximation to the dDMO (2) in terms of the Mathieu functions. For the second approach, the ansatz method with the help of the solution to the undamped Duffing oscillator is employed to derive an analytical approximation to the dDMO (2) in the form of trigonometric functions. Furthermore, the homotopy perturbation technique with the extended Krylov–Bogoliubov–Mitropolskii (KBM) which is called HKBM method is also devoted for solving the dDME (2) for arbitrary physical parameters [27, 28].

2. Mathematical Analysis

Here, we proceed to find some approximate solutions to both undamped and damped Duffing–Mathieu oscillators (1) and (2), respectively. Below we discuss the different approaches for solving the mentioned equations.

2.1. An Exact Solution to (Un)damped Mathieu Equation. Both undamped Mathieu equation, i.e., (1) for $\beta = 0$, and the damped Mathieu equation, i.e., (2) for $\beta = 0$, have exact solutions in the form of Mathieu functions. First, let us find the solution of the following damped Mathieu equation:

$$\ddot{x} + \varepsilon \dot{x} + (\alpha - Q_0 \cos(\Omega t))x = 0, \tag{4}$$

with subjected to the initial conditions (ICs): $x(0) = x_0$ and $x'(0) = \dot{x}_0$.

Using the following MATHEMATICA command

$$\begin{aligned} &g[t\_] := x''[t] + 2\varepsilon\, x'[t] - (\alpha - Q_0 \mathrm{Cos}[\Omega t])x[t] \\ &\quad (\mathrm{NDSolve}[g[t] == 0 \&\& x[0] == x_0 \&\& x'[0] == \dot{x}_0, x[t], t][1,1,2] // \mathrm{FullSimplify})^1, \end{aligned} \tag{5}$$

we can get the exact solution to (4) as follows:

$$x(t) = e^{-\varepsilon t}\left(\frac{x_0 MC_1(t,\varepsilon)}{MC_1(0,\varepsilon)} + \frac{2(\varepsilon x_0 + \dot{x}_0)}{\Omega}\frac{MS_1(t,\varepsilon)}{\mathrm{MathieuSPrime}\left[4\left(\alpha - \varepsilon^2\right)/\Omega^2, 2Q_0/\Omega^2, 0\right]}\right), \tag{6}$$

with

$$\begin{aligned} MC_1(t,\varepsilon) &= \mathrm{MathieuC}\left[\frac{4\left(\alpha - \varepsilon^2\right)}{\Omega^2}, \frac{2Q_0}{\Omega^2}, \frac{\Omega}{2}t\right], \\ MS_1(t,\varepsilon) &= \mathrm{MathieuS}\left[\frac{4\left(\alpha - \varepsilon^2\right)}{\Omega^2}, \frac{2Q_0}{\Omega^2}, \frac{\Omega}{2}t\right], \end{aligned} \tag{7}$$

where MathieuS and MathieuC are the Mathieu functions of the first kind or sometimes called sine-elliptic and cosine-elliptic, respectively. For $\varepsilon = 0$, the damped Mathieu equation (4) reduces to the following undamped Mathieu equation:

$$\ddot{x} - (\alpha + Q_0 \cos(\Omega t))x = 0, \tag{8}$$

and solution (6) reduces to the following one:

$$x(t) = \frac{x_0 MC_1(t,0)}{MC_1(0,0)} + \frac{2\dot{x}_0 MS_1(t,0)}{\Omega \mathrm{MathieuSPrime}\left[4\alpha/\Omega^2, 2Q_0/\Omega^2, 0\right]}. \tag{9}$$

The exact solution (6) is compared with RK numerical solution as shown in Figures 1(a) and 1(b) for different values of x_0.

2.2. Some Analytical Approximations to the Damped Duffing–Mathieu Oscillator. Here, we proceed to discuss two techniques (the hybrid p–expansion method and the ansatz method) for finding some analytical approximations to dDMO (2). For studying dDMO (2), first we rewrite equation (2) in the following new i.v.p.

$$\begin{cases} \mathbb{R}_1 = 0, \\ x(0) = x_0 \;\&\; x'(0) = \dot{x}_0. \end{cases} \tag{10}$$

2.2.1. First Approach: Reduced Method. For $\beta \neq 0$ and $\alpha > 0$, we may obtain simple approximation to the i.v.p. (10) by replacing the cubic term βx^3 by the linear term $\beta \kappa x$, where the constant $\kappa \geq 0$ which is used as an optimal parameter to reduce the residual error. Accordingly, dDMO (2) of cubic nonlinearity reduces to the following dDMO with linear term. Thus, we can replace the i.v.p. (10) by the following new i.v.p.

$$\begin{cases} \ddot{x} + 2\varepsilon \dot{x} + (\alpha - Q_0 \cos(\Omega t))x + \beta\kappa x = 0, \\ x(0) = x_0 \text{ and } x'(0) = \dot{x}_0. \end{cases} \tag{11}$$

Thus, the exact solution to the i.v.p. (11) is expressed by

$$x_\kappa \equiv x_\kappa(t) = e^{-\varepsilon t}\left(\frac{x_0 MC_2(t,\varepsilon,\kappa)}{MC_2(0,\varepsilon,\kappa)} + \frac{2(\varepsilon x_0 + \dot{x}_0)}{\Omega}\frac{MS_2(t,\varepsilon,\kappa)}{\mathrm{MathieuSPrime}\left[4\left(\beta\kappa - \varepsilon^2 + \alpha\right)/\Omega^2, 2Q_0/\Omega^2, 0\right]}\right), \tag{12}$$

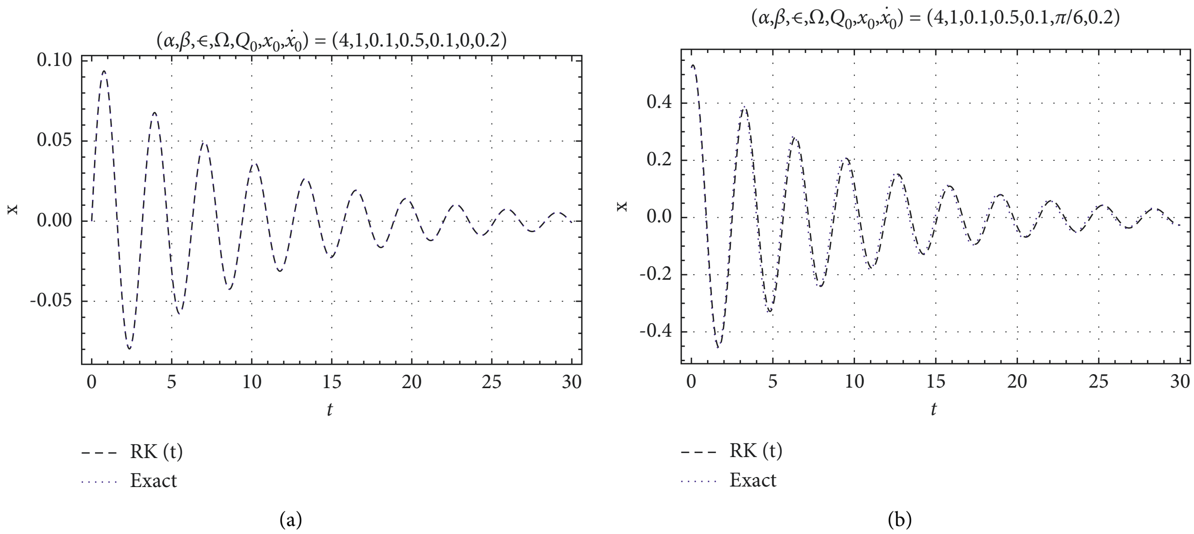

Figure 1: Both exact solution (6) and RK numerical solution to the damped Mathieu equation (4) are compared with each other for different values to the initial amplitude x_0.

with

$$MC_2(t,\varepsilon,\kappa) = \text{MathieuC}\left[\frac{4(\beta\kappa-\varepsilon^2+\alpha)}{\Omega^2}, \frac{2Q_0}{\Omega^2}, \frac{\Omega}{2}t\right],$$
$$MS_2(t,\varepsilon,\kappa) = \text{MathieuS}\left[\frac{4(\beta\kappa-\varepsilon^2+\alpha)}{\Omega^2}, \frac{2Q_0}{\Omega^2}, \frac{\Omega}{2}t\right]. \tag{13}$$

The residual is defined as

$$R_\kappa(t) = \ddot{x}_\kappa + \varepsilon\dot{x}_\kappa + (\alpha - Q_0\cos(\Omega t))x_\kappa + \beta x_\kappa^3. \tag{14}$$

A suitable value of κ can be obtained by solving the equation $R_\kappa(t_0) = 0$ for some $t_0 > 0$, say $t_0 = 1$. Making use of the Padé approximate technique, for $0 < t_0 \le 1$ and $x_0 \approx 0$, we get

$$\kappa_{\text{suitable}} = \frac{Y_1}{Y_2}, \tag{15}$$

with

$$\begin{aligned} Y_1 &= 3x_0^2\left(Q_0t_0x_0^2 - \alpha t_0x_0^2 - 2\varepsilon t_0\dot{x}_0x_0 - 4t_0\dot{x}_0^2 - 2\dot{x}_0x_0\right) \\ &\quad\times\left(4Q_0t_0x_0^2 - 4\alpha t_0x_0^2 + 3\beta t_0x_0^4 - 8\varepsilon t_0\dot{x}_0x_0 - 6t_0\dot{x}_0^2 - 8\dot{x}_0x_0\right), \\ Y_2 &= -26\alpha Q_0t_0^2x_0^4 + 12\beta Q_0t_0^2x_0^6 - 52\varepsilon Q_0t_0^2\dot{x}_0x_0^3 + 13Q_0^2t_0^2x_0^4 \\ &\quad - 52Q_0t_0\dot{x}_0x_0^3 - 30Q_0t_0^2\dot{x}_0^2x_0^2 + 13\alpha^2t_0^2x_0^4 - 12\alpha\beta t_0^2x_0^6 \\ &\quad + 52\alpha\varepsilon t_0^2\dot{x}_0x_0^3 + 52\alpha t_0\dot{x}_0x_0^3 + 30\alpha t_0^2\dot{x}_0^2x_0^2 + 9\beta^2t_0^2x_0^8 \\ &\quad - 24\beta\varepsilon t_0^2\dot{x}_0x_0^5 - 24\beta t_0\dot{x}_0x_0^5 + 12\beta t_0^2\dot{x}_0^2x_0^4 + 52\varepsilon^2t_0^2\dot{x}_0^2x_0^2 \\ &\quad + 104\varepsilon t_0\dot{x}_0^2x_0^2 + 60\varepsilon t_0^2\dot{x}_0^3x_0 + 60t_0\dot{x}_0^3x_0 + 12t_0^2\dot{x}_0^4 + 52\dot{x}_0^2x_0^2. \end{aligned} \tag{16}$$

For a given κ, the residual error $L_R(\kappa)$ of the approximation (12) to the i.v.p. (10) is defined as

$$L_R(\kappa) = \max_{0\le t\le T}\left|R_\kappa(t)\right| = \max_{0\le t\le T}\left|\ddot{x}_\kappa + 2\varepsilon\dot{x}_\kappa + (\alpha - Q_0\cos(\Omega t))x_\kappa + \beta x_\kappa^3\right|. \tag{17}$$

The optimal value of κ_{optimal} for the parameter κ on the interval $0 \le t \le T$ is defined as

$$\kappa_{\text{optimal}} = \min_{\kappa\ge 0} L_R(\kappa). \tag{18}$$

Let us apply the obtained approximation (12) for investigating the properties of the damping oscillations to the dDMO (2) at different values to the physical parameters $(\alpha,\beta,\varepsilon,\Omega,Q_0,x_0,\dot{x}_0)$. The profile of the approximation (12) using the values of κ_{suitable} (given in equation (15)) and κ_{optimal} (given in (18)) is displayed in Figures 2 and 3 at $(\alpha,\beta,\varepsilon,\Omega,Q_0,x_0,\dot{x}_0) = (4,1,0.1,0.5,0.1,0,0.2)$ and $(\alpha,\beta,\varepsilon,\Omega,Q_0,x_0,\dot{x}_0) = (4,1,0.1,0.5,0.1,\pi/6,0.2)$, respectively. The obtained results showed that this approximation gives results with good and acceptable accuracy.

2.2.2. The Ansatz Method for Solving dDMO. Now, we can summarize the main points to get some approximations to the i.v.p. (10) in the following steps.

Step 1. Let us assume the following ansatz:

$$x(t) = y(f(t)), \tag{19}$$

where the time-dependent function $f \equiv f(t)$ can be determined later and the function $y \equiv y(t)$ represents the solution of the following i.v.p.

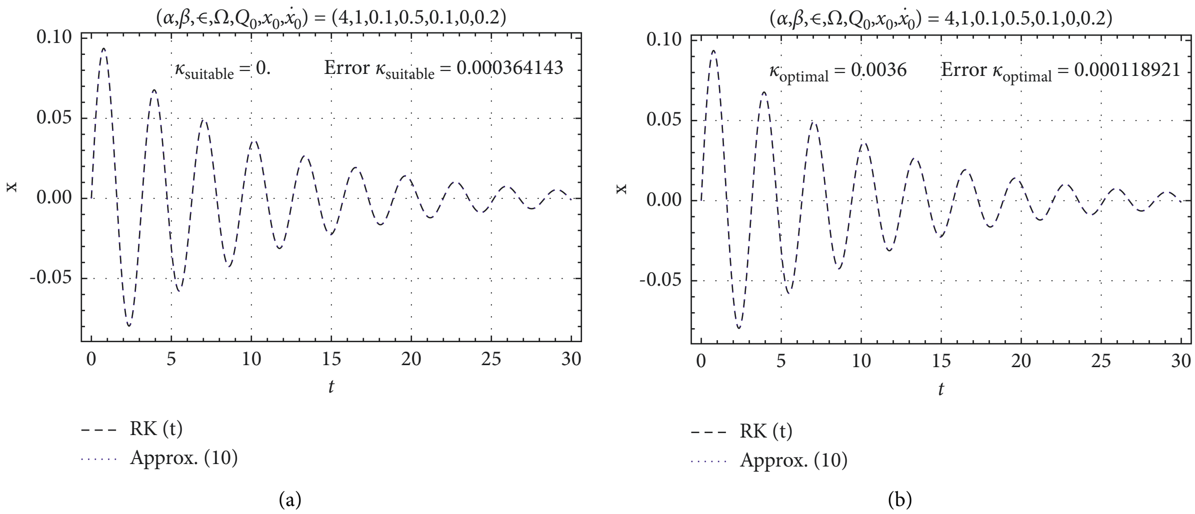

Figure 2: The profile of the approximation (12) using the values of κ_{suitable} (given in equation (15)) and κ_{optimal} (given in (18)) is plotted against t for $(\alpha, \beta, \varepsilon, \Omega, Q_0, x_0, \dot{x}_0) = (4, 1, 0.1, 0.5, 0.1, 0, 0.2)$.

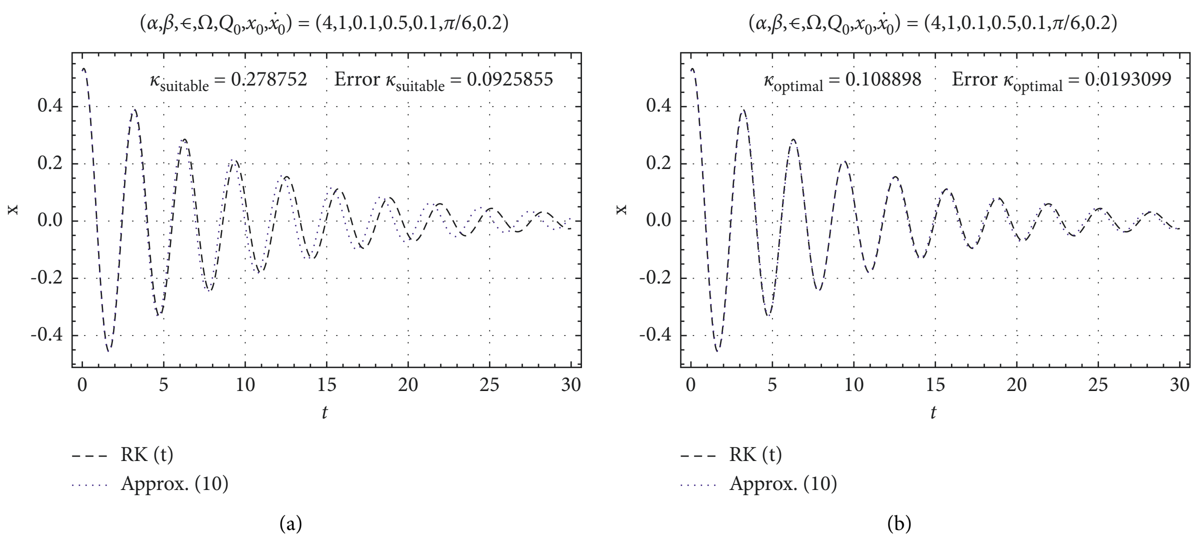

Figure 3: The profile of the approximation (12) using the values of κ_{suitable} (given in equation (15)) and κ_{optimal} (given in (18)) is plotted against t for $(\alpha, \beta, \varepsilon, \Omega, Q_0, x_0, \dot{x}_0) = (4, 1, 0.1, 0.5, 0.1, \pi/6, 0.2)$.

$$\left\{ \ddot{y} + 2\varepsilon \dot{y} + (\alpha - Q_0) y + \beta y^3 = 0, \ y(0) = x_0 \ \& \ y'(0) = \dot{x}_0. \right. \tag{20}$$

Step 2. Inserting ansatz (19) into i.v.p. (10), we get

$$\begin{aligned} \mathbb{R}_1 = {} & y'(f)\left(-2\varepsilon f'^2 + 2\varepsilon f' + f''\right) \\ & + y(f)\left(\alpha - Q_0 \cos(\Omega t) + f'^2 (Q_0 - \alpha)\right) \\ & + \beta y^3(f)\left(1 - f'^2\right). \end{aligned} \tag{21}$$

Step 3. For vanishing the coefficient of $y(f)$ in equation (21), we get

$$f'^2 = \frac{-\alpha + Q_0 \cos(\Omega t)}{(Q_0 - \alpha)}. \tag{22}$$

Step 4. Integrating equation (22) and with the help of $f(0) = 0$, we have

$$f(t) = \frac{2}{\Omega} E\left(\frac{\Omega}{2} t, \frac{2Q_0}{Q_0 - \alpha}\right), \tag{23}$$

where E stands for the EllipticE function.

Now, the value of $f(t)$ has been determined but the solution of the i.v.p. (20) needs to be determined. Thus, we are faced with two things: either we use one of the solutions found in the literature [29] or try to find another solution in the form of trigonometric functions.

Step 5. In this step, we proceed to find a solution to i.v.p. (20) in the form of trigonometric functions. Without loss of generality, i.v.p. (20) can be redefined as

$$\begin{cases} \mathbb{R}_2 = \ddot{v} + 2\varepsilon\dot{v} + pv + qv^3 = 0, \\ v(0) = v_0 \& v'(0) = \dot{v}_0, \end{cases} \tag{24}$$

where i.v.p. (24) is the same as i.v.p. (20) with $p = (\alpha - Q_0)$, $q = \beta$, and $v(t) = y(t)$.

Step 6. Our objective here is to derive another solution that does not involve elliptic functions but an elementary solution. To do that, we assume $\varepsilon > 0$, and for $\lim_{t\longrightarrow\infty} v(t) = 0$, we get

$$v(t) = c_0 e^{-\rho t} \cos\left(h(t) + \arccos\left(\frac{x_0}{c_0}\right)\right), \tag{25}$$

where $h(0) = 0$ and $h(t)$ is undermined function.

Step 7. By substituting solution (25) into i.v.p. (24), we have

$$\begin{aligned} \mathbb{R}_2 &= c_0 \sin(\theta) e^{-\rho t}\left(-2\varepsilon h' + 2\rho h' - h''\right) + \frac{1}{4}c_0^3 q \cos(3\theta) e^{-3\rho t} \\ &\quad + \frac{1}{4}c_0 \cos(\theta) e^{-3\rho t}\left[3c_0^2 q + 4e^{2\rho t}\left(-2\varepsilon\rho - h'^2 + p + \rho^2\right)\right]. \end{aligned} \tag{26}$$

Step 8. For vanishing the coefficient of $\cos(\theta)$ in equation (26): $3c_0^2 q + 4e^{2\rho t}(-2\varepsilon\rho - h'^2 + p + \rho^2) = 0$, we have

$$h' = \pm\frac{1}{2}\sqrt{4p - 8\varepsilon\rho + 4\rho^2 + 3c_0^2 q e^{-2\rho t}}, \tag{27}$$

and by solving (27) with $h(0) = 0$, we get

$$h(t) = H(t) - H(0), \tag{28}$$

with

$$\begin{aligned} H(t) &= \frac{1}{\rho}\left(\sqrt{\Pi}\tanh^{-1}\left(\sqrt{1 + \frac{3c_0^2 q e^{-2\rho t}}{4\Pi}}\right) - \sqrt{\frac{3}{4}c_0^2 q e^{-2\rho t} + \Pi}\right), \\ H(0) &= \frac{1}{\rho}\left(\sqrt{\Pi}\tanh^{-1}\left(\sqrt{1 + \frac{3c_0^2 q}{4\Pi}}\right) - \sqrt{\frac{3}{4}c_0^2 q + \Pi}\right), \end{aligned} \tag{29}$$

where $\Pi = (p - 2\varepsilon\rho + \rho^2)$.

Step 9. The number c_0 is obtained from the condition $v'(0) = \dot{v}_0$ and it is a solution to the quartic

$$\begin{aligned} &3qc_0^4 + \left(4p - 8\varepsilon\rho + 4\rho^2 - 3qv_0^2\right)c_0^2 - 4\left(pv_0^2 - 2\varepsilon\rho v_0^2\right. \\ &\quad \left. + 2\rho^2 v_0^2 + 2\rho v_0 \dot{v}_0 + \dot{v}_0^2\right) = 0, \end{aligned} \tag{30}$$

where the number ρ is a free/optimal parameter that is chosen in order to minimize the residual error. Its default value is $\rho = \varepsilon$.

Step 10. Finally, the trigonometric approximation to i.v.p. (10) is obtained:

$$x(t) = y(f(t)) = c_0 e^{-\rho f(t)} \cos\left(h(f(t)) + \arccos\left(\frac{x_0}{c_0}\right)\right). \tag{31}$$

Step 11. Also, we can solve i.v.p. (20) using RK numerical method and then replacing $t \longrightarrow f(t)$ (given in equation (23)). The following MATHEMATICA command is introduced for this purpose:

$$\begin{aligned} &g[t\_] := y''[t] + 2\,\varepsilon\, y'[t] + (\alpha - Q_0)\, y[t] + \beta\, y[t]^3; \\ &RK[t\_] := \text{NDSolve}[g[t] == 0 \&\& y[0] == x_0 \&\& y'[0] \\ &\qquad == \dot{x}_0, y[t], t][1, 1, 2], \end{aligned} \tag{32}$$

$$x[t\_] := RK[f[t]]. \tag{33}$$

Both analytical and numerical approximations (31) and (33) to i.v.p. (10) are, respectively, plotted against the RK numerical solution as illustrated in Figures 4 and 5. Also, at $(\alpha, \beta, \varepsilon, \Omega, Q_0, \dot{x}_0) = (4, 1, 0.1, 0.5, 0.1, 0.2)$, the maximum global distance of both approximations (31) and (33) is estimated for different values to x_0 as

$$\begin{aligned} L_d(x_0 = 0) &= \max_{0\le t\le 30}\left|RK - x(t)_{\text{Approx.}(26)}\right| = 0.000506901, \\ L_d(x_0 = 0) &= \max_{0\le t\le 30}\left|RK - x(t)_{\text{Approx.}(28)}\right| = 0.000482946, \\ L_d\left(x_0 = \frac{\pi}{6}\right) &= \max_{0\le t\le 30}\left|RK - x(t)_{\text{Approx.}(26)}\right| = 0.00415468, \\ L_d\left(x_0 = \frac{\pi}{6}\right) &= \max_{0\le t\le 30}\left|RK - x(t)_{\text{Approx.}(28)}\right| = 0.00266014. \end{aligned} \tag{34}$$

The obtained results show the high accuracy and efficiency of the obtained approximations (31) and (33). Moreover, these approximations are stable against long time and for arbitrary values of the physical parameters.

2.3. The Homotopy Extended Krylov–Bogoliubov–Mitropolskii Method. The homotopy extended Krylov–Bogoliubov–Mitropolskii (HKBM) method may be used for solving both conservative and nonconservative oscillators. Based on this method (more details can be found in [27, 28]), i.v.p. (10) can be redefined as

$$\begin{cases} \ddot{x} + (\alpha - Q_0)x + p\left[\varepsilon\dot{x} + Q_0(1 - \cos(\Omega t))x + \beta x^3\right] = 0, \\ x(0) = x_0 \text{ and } x'(0) = \dot{x}_0, 0 \le t \le T, \end{cases} \tag{35}$$

where $x_p \equiv x_p(t)$ indicates the solution of i.v.p. (35) while the solution of the dDMO (2) is obtained for $p = 1$. For $\omega_0 = \sqrt{\alpha - Q_0}$, $\phi(t) = Q_0(1 - \cos(\Omega t))$ and $\alpha - Q_0 > 0$, i.v.p. (35) can be written in the following reduced form:

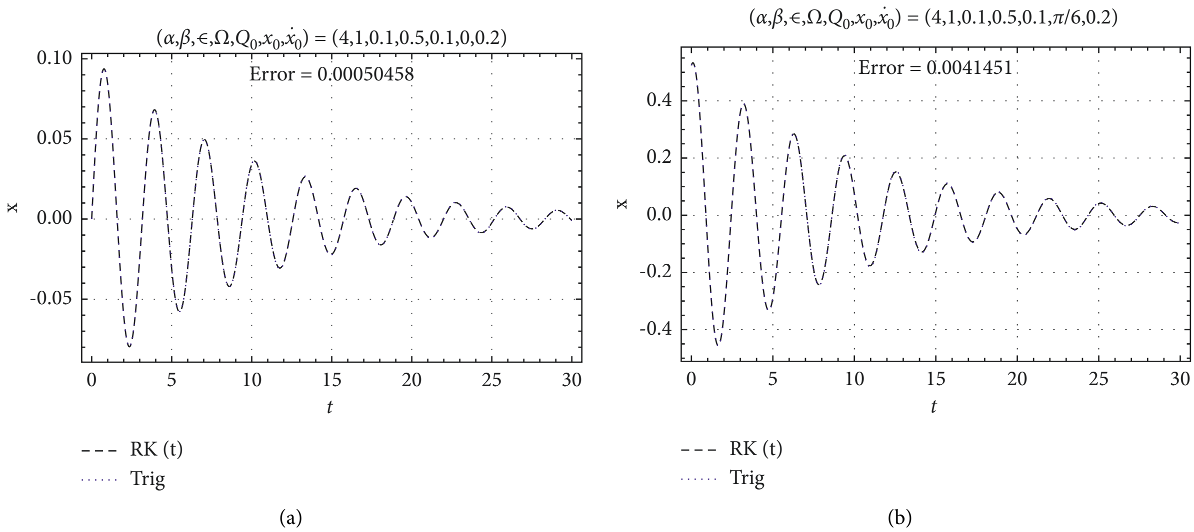

Figure 4: Both trigonometric approximation (31) and RK numerical simulation to the damped Duffing–Mathieu problem (10) are compared with each other for different values to the initial amplitude x_0.

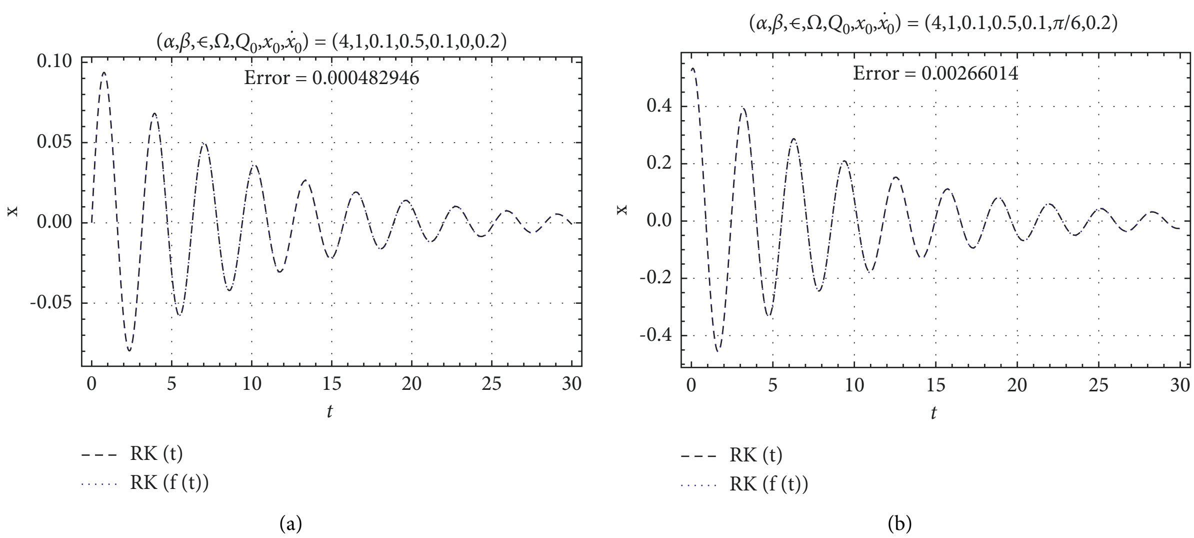

Figure 5: Both RK numerical simulation (32) and RK numerical simulation (33) using the definition of $t \longrightarrow f(t)$ to the damped Duffing–Mathieu problem (10) are compared with each other for different values to the initial amplitude x_0.

$$\begin{cases} \ddot{x} + \omega_0^2 x + p\left(\varepsilon \dot{x} + \phi(t)x + \beta x^3\right) = 0, \\ x(0) = x_0 \text{ and } x'(0) = \dot{x}_0, 0 \leq t \leq T. \end{cases} \tag{36}$$

According to the HKBM method, the following ansatz solution is introduced:

$$x_p = a\cos(\psi) + \sum_{n=1}^{N} p^n u_n(a,\psi) + O\left(p^{N+1}\right), \tag{37}$$

where each $u_n \equiv u_n(a,\psi)$ is a periodic function in ψ, and both amplitude a and phase ψ are assumed to vary with time and subject to the conditions

$$\begin{aligned} \frac{da}{dt} &\equiv \dot{a} = \sum_{n=1}^{N} p^n A_n(a) + O\left(p^{N+1}\right), \\ \frac{d\psi}{dt} &\equiv \dot{\psi} = \omega_0 + \sum_{n=1}^{N} p^n \psi_n(a) + O\left(p^{N+1}\right), \end{aligned} \tag{38}$$

where $a \equiv a(t)$ and $\psi \equiv \psi(t)$.

Inserting ansatz solution (37) and using (38) and after several tedious calculations, we can determine the unknown time-dependent functions (u_n, ψ_n, A_n, a). To avoid the so-called secularity, we choose only the solution that does not contain cos ψ nor sin ψ. For $N = 1$, we get

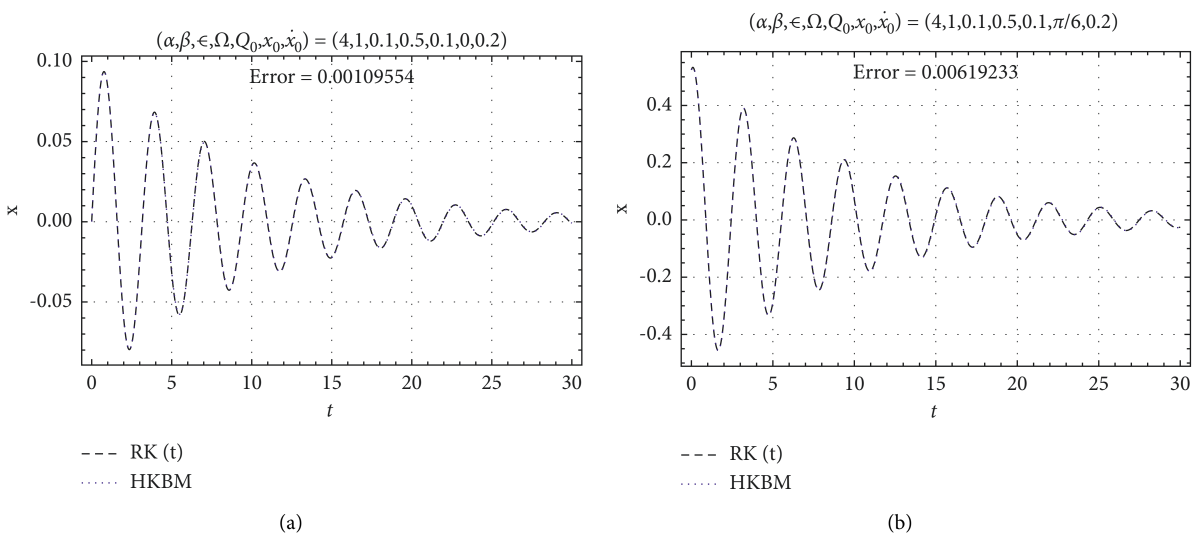

Figure 6: Both HKBM first-order approximate solution (42) and RK numerical simulation are plotted against different values of the initial angle x_0.

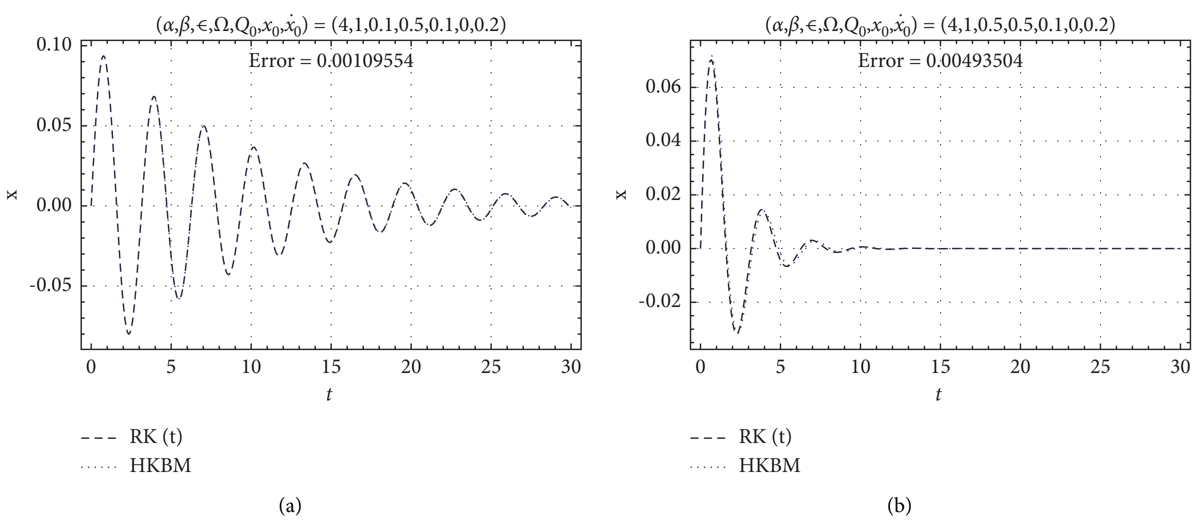

Figure 7: Both HKBM first-order approximate solution (42) and RK numerical simulation are plotted against different values of the damping parameter ε.

$$\begin{aligned} \dot{a} &= -\varepsilon a(t), \\ \dot{\psi} &= \frac{3\beta a(t)^2 + 4\phi(t)}{8\omega_0} + \omega_0, \\ u_1(a,\psi) &= \frac{a^3\beta\cos(3\psi)}{32\omega_0^2}, \end{aligned} \tag{39}$$

and

$$x_p(t) = a\cos(\psi) + p\frac{\beta}{32\omega_0^2}a^3\cos(3\psi). \tag{40}$$

By solving system (39), we have

$$\begin{aligned} a &= c_0 e^{-\varepsilon t}, \\ \psi &= \frac{e^{-2\varepsilon t}}{16\varepsilon\Omega\omega_0}\left[8\varepsilon e^{2\varepsilon t}\left(2c_1\Omega\omega_0 - Q_0(\Omega t + \sin(\Omega t)) + 2\alpha\Omega t\right) + 3\beta c_0^2\Omega\left(e^{2\varepsilon t} - 1\right)\right]. \end{aligned} \tag{41}$$

The first-order approximate solution is obtained for $p = 1$:

$$x(t) = x_1(t) = a\cos(\psi) + \frac{\beta}{32\omega_0^2}a^3\cos(3\psi), \tag{42}$$

where the values of (a, ψ) are defined in (41) while the constants c_0 and c_1 can be obtained from the initial conditions.

The comparison between the HKBM first-order approximate solution (37) and the RK numerical simulation is reported as shown in Figures 6(a) and 6(b) for $x_0 = 0$ and $x_0 = \pi/6$, respectively. Also, both HKBM first-order approximate solution (42) and RK numerical simulation are, respectively, compared with each other for weak $(\varepsilon = 0.1)$ and strong $(\varepsilon = 0.5)$ damping as illustrated in Figures 7(a) and 7(b). Furthermore, at $(\alpha, \beta, \Omega, Q_0, \dot{x}_0) = (4, 1, 0.5, 0.1, 0.2)$ and for different values to (x_0, ε), the maximum global distance error to the HKBM first-order approximate solution (42) is estimated as

$$\begin{aligned} L_d(x_0 = 0) &= \max_{0 \le t \le 30} \left| RK - x(t)_{\mathrm{HKBM}(37)} \right| = 0.00110165, \\ L_d\left(x_0 = \frac{\pi}{6}\right) &= \max_{0 \le t \le 30} \left| RK - x(t)_{\mathrm{HKBM}(37)} \right| = 0.0061929, \\ L_d(\varepsilon = 0.1) &= \max_{0 \le t \le 30} \left| RK - x(t)_{\mathrm{HKBM}(37)} \right| = 0.00110165, \\ L_d(\varepsilon = 0.5) &= \max_{0 \le t \le 30} \left| RK - x(t)_{\mathrm{HKBM}(37)} \right| = 0.00493896. \end{aligned} \tag{43}$$

It is clear that the HKBM first-order approximate solution (42) is characterized by high accuracy and more stability at long time.

3. Conclusion

Given the importance of nonlinear oscillations in plasma physics and engineering and their strong connection to the family of the Duffing-type oscillator, in this work, some exact solutions to the damped and undamped Mathieu equations as well as some analytical approximations to the damped Duffing–Mathieu oscillator (dDMO) using different approaches have been obtained. The exact solutions to both damped and undamped Mathieu equation have been obtained in the terms of Mathieu functions of the first kind. These solutions are numerically compared with the Runge–Kutta (RK) numerical simulation. It was observed that both exact and numerical solutions are completely matched with each other in the whole time interval. On the other hand, the dDMO has been solved using some different approaches. In the first one, the nonintegrable dDMO with cubic nonlinear term (βx^3) has been reduced to an integrable dDMO with linear term $(\beta \kappa x)$ in which κ is undermined optimal parameter. The kappa optimal parameter κ has been determined using a suitable technique as we discussed in the text above. After determining the kappa optimal parameter, a highly accurate analytical approximation has been obtained in terms of the Mathieu functions. In the second approach, a highly accurate analytical approximation has been derived in detail in terms of trigonometric functions using the ansatz method. In the third technique, the homotopy extended Krylov–Bogoliubov–Mitropolskii (HKBM) method was used for getting an effective analytical approximation. Furthermore, the dDMO has been analyzed numerically using the RK numerical method. The comparison between all obtained approximations and the RK numerical solutions has been carried out. Moreover, the maximum global distance error in the whole time interval to all obtained approximations has been estimated. All obtained approximations are characterized by the high accuracy and efficiency in addition to being more stable for a long time.

3.1. Future Work

3.1. Future Work. We may solve the following oscillators using of the methods described in this paper:

3.1.1. Future Idea I. Cubic-quintic Duffing–Mathieu equation:

$$\begin{cases} \ddot{x} + \omega_0^2 x + 2\varepsilon \dot{x} + \phi(t) x + \beta x^3 + \gamma x^5 = 0, \\ x(0) = x_0 \,\&\, x'(0) = x_0, \quad 0 \le t \le T. \end{cases} \tag{44}$$

3.1.2. Future Idea II. Forced damped Duffing–Mathieu equation:

$$\begin{cases} \ddot{x} + \omega_0^2 x + 2\varepsilon \dot{x} + \phi(t) x + \beta x^3 = F(t), \\ x(0) = x_0 \,\&\, x'(0) = x_0, \quad 0 \le t \le T. \end{cases} \tag{45}$$

3.1.3. Future Idea III. The forced Van der Pol–Duffing oscillator:

$$\begin{cases} \ddot{x} - \varepsilon\left(1 - x^2\right)\dot{x} + \omega_0^2 x + \beta x^3 = F(t), \\ x(0) = x_0 \,\&\, x'(0) = x_0, \quad 0 \le t \le T, \end{cases} \tag{46}$$

and many others oscillators.

Data Availability

The data generated or analyzed during this study are included within the article.

Conflicts of Interest

The authors declare that they have no conflicts of interest.

Authors' Contributions

All authors contributed equally to this study and approved the final version of the manuscript.

Acknowledgments

The authors express their gratitude to Princess Nourah bint Abdulrahman University Researchers Supporting Project (grant no. PNURSP2022R17), Princess Nourah bint Abdulrahman University, Riyadh, Saudi Arabia.

References

[1] A.-M. Wazwaz, *Partial Differential Equations and Solitary Waves Theory*, Springer, Berlin, Germany, 2009.

[2] A.-M. Wazwaz, *Partial Differential Equations: Methods and Applications*, A.A.Balkema Publishers, Avereest, Netherlands, 2002.

[3] S. A. Almutlak and S. A. El-Tantawy, "On the approximate solutions of a damped nonplanar modified Korteweg-de Vries equation for studying dissipative cylindrical and spherical solitons in plasmas," *Results in Physics*, vol. 23, Article ID 104034, 2021.

[4] W. Albalawi, A. H. Salas, S. A. El-Tantawy, and A. A. A.-R. Youssef, "Approximate analytical and numerical solutions to the damped pendulum oscillator: Newton-Raphson and moving boundary methods," *Journal of Taibah University for Science*, vol. 15, no. 1, pp. 479–485, 2021.

[5] N. H. Aljahdaly, S. A. El-Tantawy, A.-M. Wazwaz, and H. A. Ashi, "Adomian decomposition method for modelling the dissipative higher-order rogue waves in a superthermal collisional plasma," *Journal of Taibah University for Science*, vol. 15, no. 1, pp. 971–983, 2021.

[6] S. Rajasekar, S. Parthasarathy, and M. Lakshmanan, "Prediction of horseshoe chaos in BVP and DVP oscillators," *Chaos, Solitons & Fractals*, vol. 2, no. 3, pp. 271–280, 1992.

[7] K. Johannessen, "An analytical solution to the equation of motion for the damped nonlinear pendulum," *European Journal of Physics*, vol. 35, no. 3, Article ID 035014, 2014.

[8] E. Esmailzadeh and G. Nakhaie-jazar, "Periodic solution of a Mathieu-Duffing type equation," *International Journal of Non-linear Mechanics*, vol. 32, no. 5, pp. 905–912, 1997.

[9] M. Zamora, "A note on the periodic solutions of a Mathieu–Duffing type equations," *Mathematische Nachrichten*, vol. 290, 2016.

[10] V. Belovodskiy, "About the new periodic solutions of the mathieu-duffing equation in the principal zone of instability," *Mechanics*, vol. 33, pp. 38–42, 2010.

[11] E. Babilio, "The duffing-mathieu equation arising from dynamics of post-buckled beams," *Nonlinear Dynamics of Structures, Systems and Devices*, Springer, Berlin, Germany, pp. 267–275, 2020.

[12] A. Y. T. Leung, Z. Guo, and H. X. Yang, "Transition curves and bifurcations of a class of fractional mathieu-type equations," *International Journal of Bifurcation and Chaos*, vol. 22, no. 11, Article ID 1250275, 2012.

[13] G. Brodin and L. Stenflo, "A simple electron plasma wave," *Physics Letters A*, vol. 381, no. 11, pp. 1033–1035, 2017.

[14] I. Kourakis, M. Momeni, and P. K. Shukla, "A Mathieu equation for dust charge dynamics in multi-component dusty plasmas," in *Proceedings of the 33rd EPS Conference*, vol. 30I, Rome, Italy, June 2006.

[15] M. Momeni, I. Kourakis, M. Moslehi-Fard, and P. K. Shukla, "A Van der Pol-Mathieu equation for the dynamics of dust grain charge in dusty plasmas," *Journal of Physics A: Mathematical and Theoretical*, vol. 40, no. 24, pp. F473–F481, 2007.

[16] C. H. Miwadinou, L. A. Hinviy, A. V. Monwanouz, and J. B. Chabi Orou, "Nonlinear dynamics of plasma oscillations modeled by a forced modified Van der Pol-Duffing oscillator," 2013, http://arxiv.org/abs/1308.6132v1.

[17] N. H. Aljahdaly and S. A. El-Tantawy, "On the multistage differential transformation method for analyzing damping duffing oscillator and its applications to plasma physics," *Mathematics*, vol. 9, no. 4, p. 432, 2021.

[18] A. H. Salas, S. A. El-Tantawy, and E. Jairo, "On the approximate and analytical solutions to the fifth-order Duffing oscillator and its physical applications," *Waves in Random and Complex Media*, pp. 1–21, 2021.

[19] A. H. Salas S, S. A. El-Tantawy, and M. R. Alharthi, "Novel solutions to the (un)damped Helmholtz-Duffing oscillator and its application to plasma physics: moving boundary method," *Physica Scripta*, vol. 96, no. 10, Article ID 104003, 2021.

[20] S. A. El-Tantawy, A. H. Salas, and M. R. Alharthi, "On the analytical and numerical solutions of the damped nonplanar Shamel Korteweg-de Vries Burgers equation for modeling nonlinear structures in strongly coupled dusty plasmas: multistage homotopy perturbation method," *Physics of Fluids*, vol. 33, no. 4, Article ID 043106, 2021.

[21] S. A. El-Tantawy, A. H. Salas, and M. R. Alharthi, "On the analytical solutions of the forced damping duffing equation in the form of weierstrass elliptic function and its applications," *Mathematical Problems in Engineering*, vol. 2021, Article ID 6678102, 9 pages, 2021.

[22] S. A. El-Tantawy, A. H. Salas, and M. R. Alharthi, "A new approach for modelling the damped Helmholtz oscillator: applications to plasma physics and electronic circuits," *Communications in Theoretical Physics*, vol. 73, no. 3, Article ID 035501, 2021.

[23] A. H. Salas, S. A. El-Tantawy, and N. H. Aljahdaly, "An exact solution to the quadratic damping strong nonlinearity duffing oscillator," *Mathematical Problems in Engineering*, vol. 2021, Article ID 8875589, 8 pages, 2021.

[24] J. Proud, *Plasma Processing of Materials: Scientific Opportunities and Technologies Challenges*, National Academy Press, Washington, DC, USA, 1991.

[25] A. C. J. Luo, "Chaotic motion in the generic separatrix band of a Mathieu-Duffing oscillator with a twin-well potential," *Journal of Sound and Vibration*, vol. 248, no. 3, pp. 521–532, 2001.

[26] A. C. J. Luo and B. Yu, "Analytical periodic motions of a parametric oscillator with quadratic nonlinearity," in *Proceedings of the 26th Conference on Mechanical Vibration and Noise*, Buffalo, NY, USA, August 2014.

[27] M. A. Uddin, M. W. Ullah, and R. S. Bipasha, "An approximate analytical technique for solving second order strongly nonlinear generalized duffing equation with small damping," *Journal of Bangladesh Academy of Sciences*, vol. 39, no. 1, pp. 103–114, 2015.

[28] A. H. Salas, "Analytical approximant to a quadratically damped duffing oscillator," *The Scientific World Journal*, vol. 2022, Article ID 3131253, 10 pages, 2022.

[29] A. H. Salas and S. A. El-Tantawy, "On the approximate solutions to a damped harmonic oscillator with higher-order nonlinearities and its application to plasma physics: semi-analytical solution and moving boundary method," *The European Physical Journal Plus*, vol. 135, no. 10, p. 833, 2020.

Hindawi
Journal of Mathematics
Volume 2022, Article ID 2566259, 8 pages
https://doi.org/10.1155/2022/2566259

Review Article

Dynamics of Chinese Export Comparative Advantage: Analysis Based on RSCA Index

Li Wang,[1] Tian-Le Sun ,[2] and Zheng-Qun Cai [3]

[1]*Practical Teaching Department, Anhui Sanlian University, Hefei 230601, China*
[2]*College of Economics, Sichuan Agricultural University, Chengdu 610000, China*
[3]*School of Foreign Studies, Anhui Jianzhu University, Hefei 230601, China*

Correspondence should be addressed to Zheng-Qun Cai; caizhengqun1983@163.com

Received 11 December 2021; Accepted 24 March 2022; Published 15 April 2022

Academic Editor: Fairouz Tchier

Based on RSCA index, using kernel density estimation, Markov chain transition probability matrix, and survival analysis method, this paper analyzes the dynamics of Chinese export comparative advantage from 2001 to 2020 and draws the following conclusions. Firstly, after 20 years of export trade development, although the comparative advantage of a few commodities of China has weakened and comparative disadvantage has increased, the comparative advantage of most commodities is improving, and the overall distribution of comparative advantage remained unchanged. Secondly, the stability of Chinese comparative advantage is higher than liquidity, and liquidity as a whole shows a good trend. In addition, the viability of Chinese commodities with comparative advantage has performed well in the past 20 years. Therefore, China should optimize export mode based on comparative advantage.

1. Introduction

The export mode of country and region has long been one of the research hot-spots in the field of international trade. Although the new trade theory in the 1980s attributed the emergence of trade to two cornerstones, namely, comparative advantage and economies of scale, comparative advantage is still the main theoretical explanation [1]. According to David Ricardo's comparative advantage theory, the difference of relative labor productivity among countries leads to the difference of relative production cost, which leads to the difference of relative export price. Hence, a country should export commodities with comparative advantage and import commodities with comparative disadvantage. Regional relative labor productivity will not always be in a static state, but will continue to change with the passage of time, and then the regional comparative advantage will also change. Therefore, comparative advantage is a dynamic concept and develops endogenously over time [2]. Countries and regions continuously strengthen or weaken the original comparative advantage due to factor endowment, technological progress, industrial policy, and so on and even lead to the reversal of original comparative advantage. In this way, the dynamics of comparative advantage is not only an indirect reflection of the changes of regional factor endowment and technology level, but also an important content to measure the impact of government policies. Hence, how to measure the dynamics of comparative advantage naturally becomes the initial task of researchers.

Since implementation of the strategy of reform and opening up in the late 1970s, China's economy has been fully integrated into the process of economic globalization. Chinese government has vigorously developed open economy, practiced open economic system and mechanism, deepened foreign trade and investment policies adapted to its national conditions, actively developed bilateral and multilateral trade relations, integrated multilateral trade organizations, implemented "going global" strategy, and deepened "The Belt and Road" initiative. These measures have improved Chinese foreign trade development environment, trained a large number of various ownership business entities facing the world market, effectively optimized export commodity structure, and improved international competitiveness. After accession to WTO, although China has experienced the 2008 international financial crisis, trade friction with major countries, rising domestic production cost, fluctuation of exchange rate, COVID-19 virus, etc., its export trade has made remarkable achievements. Chinese commodity exports amounted to US $509.6 billion in 2001. By 2020, its exports reached $2590.6 billion. The export scale has increased more than five times. China has become the largest commodity exporter and the largest foreign trade country in the world, and its import and export trade has become an important engine of global economic growth. With the growth of export scale, China's export commodity structure has also been significantly optimized, gradually reversing the export commodity structure dominated by primary products and labor-intensive products. In 2020, the export volume of manufactured commodities accounted for 95.5% of total exports volume in China, while primary products accounted for only 4.5%. In manufactured commodities, the percentage of mechanical and electrical products and high-tech products representing high technological level in total export is becoming higher and higher. For example, machinery and transportation equipment accounts for 48.6% in 2020, in such commodities, mechanical and electrical products and accessories, telephone communication and audio products, office machinery, and automatic data processing equipment are the main export commodity categories. The optimization of export commodity structure itself is the favorable result of dynamics of export comparative advantage in China. Therefore, it is necessary to conduct in-depth research on the dynamics of Chinese export comparative advantage.

The rest of this paper is organized as follows. The second part summarizes empirical methods of dynamics of comparative advantage, including a brief discussion of comparative advantage index and the statistic methods of index. The third part is the index and research methods used in this paper, including RSCA index and kernel density estimation, Markov chain transition probability matrix, and survival analysis methods. The fourth part presents results of empirical research. The fifth part is main conclusions and suggestions.

2. Literature Review

Analyzing change characteristics of comparative advantage index in certain period is the basic research way of dynamics of comparative advantage. This includes two interrelated aspects of the choice of index and application of statistical methods.

In terms of comparative advantage index, scholars have put forward various types of index since the 1950s, among which Balassa revealed that comparative advantage index (RCA) is most famous [3], but the index is also controversial. The main controversy is that RCA index has inherent defects in both theoretical basis and empirical application. For example, the mean value of RCA index is unstable and its distribution is nonnormal, so the accuracy of measuring comparative advantage is questionable. For this reason, later scholars put forward many alternative indexes with the aim of overcoming one or more shortcomings of the original RCA index. For example, Michaely put forward Michaely Index (MI) [4], Vollrath proposed relative trade advantage (RTS), relative export advantage (RC), and revealed competitiveness (In RCA) [5], Lafay proposed Lafay Index [6], Dalum and Laursen offered revealed symmetric comparative advantage index (RSCA) [7], Heon and Oosterhaven proposed additive (aggregated) revealed comparative advantage index (ARCA) [8], Cai and Yu proposed net export-revealed comparative advantage index (NRCA) [9], Wosiek and Visvizi proposed visviz wosiek RCA index (VWRCA) [10], and Andrey and Vladimir proposed new net trade index (nt RCA) [11]. These alternative indexes can sometimes alleviate some defects of RCA index in some specific cases. However, as Sanidas and Shin said, there is no perfect index [12].

Application of statistical methods on dynamics of comparative advantage is becoming more and more diverse and complex. For example, Benedicits and Tamberi used cumulative distribution, kernel density estimation, Lorentz curve, location index, and other methods based on RCA index [13]. Proudman and Redding and Hinloopen and Marrewijk used Markov chain transition probability matrix of RCA index and liquidity index methods [14, 15]. Laursen and Michele Alessandrini conducted regression analysis of RSCA index and Lafay Index, respectively [16, 17]. Bojnec and Fertö [2] and Olivera kostoska [18] also used regression, Markov chain transition probability matrix and survival analysis method of RCA index.

Application of the above indexes and statistical methods can reflect dynamics of regional comparative advantage to a certain extent; however, the following problems cannot be avoided. Firstly, the choice of index remains unsolved. Some scholars believe that the indexes based on the supply dimension, that is, only export data and no import data, lead to incomplete comparative advantage analysis [19]. Nevertheless, the author believes that if the demand dimension is considered, that is to say, the indexes including import data are adopted, the measurement is more distorted relative to supply dimension due to the influence of government policies, trade relations, and geographical factors. Although these factors can be measured separately, it is actually so challenging. In addition, it is reasonable to use the indexes based on the supply dimension in the current trade environment. After all, export is less affected by trade policies and trade relations than import. Of course, even if the problems related index selection is solved, there are still other straits. For example, using "ex post" trade data to reflect "ex ante" comparative advantage is naturally flawed [11, 20]. Therefore, these all depend on the progress of follow-up index research. Secondly, if we carefully study the specific methods related to dynamics of comparative advantage, we can find that most methods compare the index distribution of discrete time, such as between start time and end time, and ignore complete trend. In addition, the classification level of commodity also has an impact on the research results. For example, according to SITC classification, there may be a phenomenon that commodities with one-digit classification do not have comparative advantage, while commodities with two-digit or three-digit classification may have comparative advantage, and there may also be a phenomenon that commodities with one-digit classification have comparative advantage, but commodities with two-digit or three-digit classification may not have comparative advantage. These are also not conducive to the accurate analysis of comparative advantage. Hence, study on dynamics of comparative advantage may be more accurate when the commodity classification is more detailed. In view of this, referring to SITC three-digit classification, this paper selects RSCA index to carry out research on dynamics of export comparative advantage in China from 2001 to 2020. In addition, this study not only compares discrete years, but also studies the whole trend.

3. Methodology and Data

3.1. RSCARSCA Index, Commodity Classification, and Data

3.1.1. RSCA Index. Revealed symmetric comparative advantage (RSCA) index was proposed by Dalum and Laursen [7]. This index is the modification of the revealed comparative advantage (RCA) index. The RCA index formula is

$$\mathrm{RCA}_{ij} = \frac{X_{ij}/\sum_{i=1}^{m} X_{ij}}{X_{in}/\sum_{i=1}^{m} X_{in}}, \tag{1}$$

where X_{ij} is export volume of region j commodity i. $\sum_{i=1}^{m} X_{ij}$ is total export volume of region j commodity i. X_{in} is export volume of commodity i in reference region n. Then $\sum_{i=1}^{m} X_{in}$ is total export volume of reference region. The value range of RCA_{ij} index is $[0, +\infty)$. When the value of RCA_{ij} index is greater than 1, it indicates that region j has comparative advantage in commodity i; otherwise it is the opposite; when the value of index is equal to 1, it indicates the median point of comparative advantage and represents neutral comparative advantage.

RSCARSCA index is converted from RCA index to alleviate the defect of asymmetric distribution of RCA index. The formula is

$$\mathrm{RSCA}_{ij} = \frac{\mathrm{RCA}_{ij} + 1}{\mathrm{RCA}_{ij} + 1}, \tag{2}$$

where the value of RSCA_{ij} index ranges from $[-1, 1]$. When RSCA_{ij} value is greater than 0, it indicates that region j has comparative advantage in commodity i; otherwise it is the opposite. When the value of index is equal to 0, it represents the median point of comparative advantage and neutral comparative advantage.

3.1.2. Commodity Classification and Data. This paper quotes the three-digit commodity classification in the Standard of International Trade Classification (SITC Rev 3). The classified export data of China and world involved in the index calculation are all from UN COMTRADE database. Due to lack of world's three-digital classified commodity export data in the database, the annual export volume of three digit commodities of each country included in the database is aggregated as the total classified export volume of world. The export data of Chinese classified commodity from 2001 to 2020 are relatively complete in the database, and only two categories of commodities are not included in the analysis due to lack of data of complete years, that is, Ores and concentrates of uranium or thorium (286) and Gold, nonmonetary (excluding gold ores and concentrates (971). A total of 255 commodities are selected finally. In addition, the reason why RSCA index is selected is also due to the consideration of data quality. The quality of export data in the database is better than that of import data. If the selected comparative advantage index contains import data, it will be difficult to have measurement results of 255 categories due to research cycle, commodity classification level, and other reasons.

3.2. Dynamics of Comparative Advantage Method

3.2.1. Kernel Density Estimation. Kernel density estimation is a nonparametric method to estimate the probability density function of continuous random variables without assuming the basic distribution of random variables. Let $(x_1, x_2, \ldots, x_n)$ be a random sample from the same unknown probability density function $f(x)$ and its kernel density estimator is

$$\begin{aligned} f(x) &= \frac{1}{n}\sum_{i=1}^{N} K_h(x - x_i) \\ &= \frac{1}{nh}\sum_{i=1}^{N} K\left(\frac{x - x_i}{h}\right), \end{aligned} \tag{3}$$

where K is kernel function and $h > 0$ is the smoothing parameter (also called the bandwidth). In this paper, the default Epanechnikov kernel function of Stata software is used to obtain the kernel density curve.

After kernel density estimation, two-tailed Wilcoxon signed rank test is also performed. This test is a nonparametric test used to test the difference in the distribution of two samples. The premise of two samples is not independent, or matched samples or paired samples, or repeated measurement of a single sample. Thus, the Wilcoxon signed rank test tests for the null hypothesis of equal distributions through equal means against the alternative hypothesis of unequal distributions through unequal means.

3.2.2. Markov Chain Transition Probability Matrix. Generally, random variables X are considered as a Markov random process. For each n and all states $i_1, \ldots, i_n$,

$$\begin{aligned} &P\left[X_n = i_n \mid X_{n-1} = i_{n-1}, \ldots, X_1 = i_1\right] \\ &\quad = P\left[X_n = i_n \mid X_{n-1} = i_{n-1}\right]. \end{aligned} \tag{4}$$

We use our transition matrices as in a Markovian analysis, as a consequence relative frequencies should be interpreted as probabilities; in practice we utilize the transition matrics as if they had been generated by a stationary Markov process:

$$P[X_n = j|X_{n-1} = i] = P[X_{n+k} = j|X_{n+k-1}]. \tag{5}$$

For all states i and j, $k = (n-1), \ldots, 1, 0, 1, \ldots$.

3.2.3. Survival Analysis. Kaplan–Meier product limit method is used to estimate the survival function. This method is a nonparametric estimation method, which is used to estimate the survival probability beyond a given point in time; that is, the survival distribution is calculated according to the life experience data, and the censored case is considered. In other words, it is a statistical technique for describing and quantifying "time of event" data.

The survival function $S(t)$ is estimated using the Kaplan–Meier product limit method. The specific derivation is as follows: it is assumed that the sample contains n independent observations, expressed as $(t_i; c_i)$, $i = 1, 2, \ldots n$, where t_i is the survival time and c_i is the censored dummy variable C of the observation value i. If the "failure" event occurs, it is taken as 1; otherwise it is taken as 0. In addition, it is assumed that there are $m < n$ recorded failures. Then, the ordered survival time $t(1) < t(2) < \cdots < t(m)$ is defined. Let n_j be the number of failures at $t(j)$, let d_j be the number of failures observed, and the Kaplan–Meier estimate of the survival function is

$$\widehat{S}(t) = \prod_{t(i)<t} \frac{n_j - d_j}{n_j}. \tag{6}$$

By convention, when $t < t(1)$, $\widehat{S}(t) = 1$. Considering that many observations are censored, the estimator is robust to censoring and uses the information of censored and noncensored observations.

4. Empirical Analysis Results

4.1. Kernel Density Estimation. The kernel density of RSCA index in 2001–2002, 2008–2009, and 2019–2020 is estimated, as shown in Figure 1. The two-year average index is used to mitigate the impact of export fluctuations in a single year. At the same time, the reason for choosing the year 2001–2002 is not only the starting year of this study, but also the period of China's entry into WTO. 2008–2009 is a period of international financial crisis and 2019–2020 is the end year of the study. From the distribution pattern, there is an obvious peak on the left of the median point (RSCA = 0) in 2001–2002, indicating that most commodities have no comparative advantage. Actually, the percentages of commodity in the three years are 64.3%, 63.9%, and 62.0%, respectively, and the above results are proved. In 2008–2009, two more flat peaks are formed compared with 2001–2002. The first peak is on the left side of the peak in 2001–2002, which is comparative.

Advantage of some commodities is deteriorating; the second peak is on the right side of the peak in 2001–2002, indicating that comparative advantage of some commodities is improving. In 2019–2020, the left peak moves further to the left, indicating that comparative advantage of some commodities continues to deteriorate. On the right side of the median point (RSCA = 0), the curve in 2008–2009 moves upward relative to that in 2001–2002, indicating that the number of commodities with comparative advantage increases. The curve in 2019–2020 moves further upward, indicating that the number of commodities with comparative advantage is further increased compared with the previous two years, thus forming the highest peak. Obviously, since China's accession to the WTO, although the degree of comparative disadvantage of a few export commodities has increased, it can still be seen that more and more commodities have obtained comparative advantage, and the overall trend is improving. In addition, by observing the tails at both ends of the three curves, it can be seen that the left curve moves up and the right curve moves down, which further shows that the comparative advantage of commodities with strong original advantage decreases and the comparative disadvantage of commodities with weak original disadvantage increases. This phenomenon can be explained to some extent by the calculation of RCA index. Although this study makes analysis based on RSCA index, some defects of RCA index will not be eliminated by conversion to RSCA index. Yeats believes that RCA index calculation result may be more beneficial to small economies [21]. When China joined the WTO, it was not a major exporter in the world, and only a few commodities are exported to the world market. These commodities account for a large share of Chinese total exports, while most other commodities account for a small share, which affects the numerator of RCA index $(X_{ij}/\sum_{i=1}^{m} X_{ij})$. Although Benedicit believes that the value of RCA index depends on the change of numerator and denominator $(X_{in}/\sum_{i=1}^{m} X_{in})$ and the simultaneous change of numerator and denominator [13], the author believes that the numerator influence is greater for China, thus amplifying the comparative advantage of commodities with high export share and weakening the comparative disadvantage of commodities with low export share. More than 20 years after joining WTO, China has become a major exporter. The export commodities with comparative advantage and disadvantage have a lower share compared with more than 20 years ago, which leads to

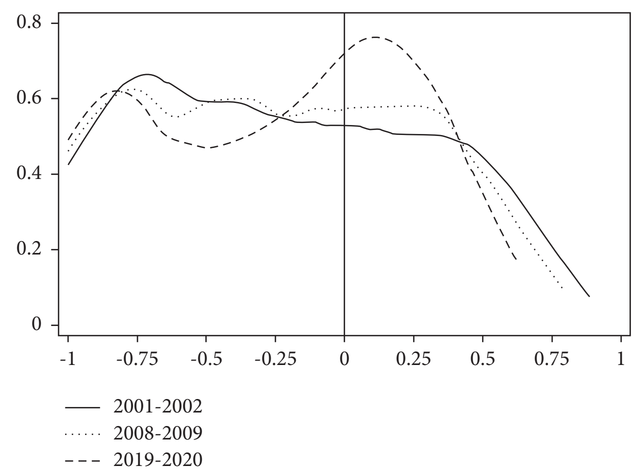

Figure 1: Kernel density estimation of Chinese RSCA index distribution.

decline of advantages of the commodities with strong comparative advantage and enhancement of disadvantages of the commodities with weak comparative advantage.

Wilcoxon signed rank two-tailed test is performed. The test about comparative advantage index distribution can be seen in S. Bodhisattva and D. Kaveri [22]. Here, the original hypothesis (H_0) is that there is no significant difference in the distribution of RSCA index in the above three years, while there is a significant difference in the alternative hypothesis (H_1). The results show that the original hypothesis is not rejected at the 5% significance level, as shown in Table 1. This means that although Chinese RSCA index kernel density curve shows a certain change, the change does not deviate from the original distribution state. That is to say, despite the impact of major external environmental changes such as entry into WTO and the 2008 international financial crisis, the dynamics of Chinese export comparative advantage have changed to a certain extent, but its export specialization mode is still stable.

4.2. Transition Probability Matrix. Taking 2001–2002 as the base year, four intervals, I, II, III, and IV, are divided according to the quartile of RSCA index in 2001–2002. Interval I is between the minimum and lower quartile of RSCA index in 2001–2002, interval II is between the lower quartile and median, III is between the median and upper quartile, and IV is between the upper quartile and maximum. In this way, the transition probability matrices of 2008–2009 and 2019–2020 relative to 2001–2002 are obtained, respectively. Similarly, the other I, II, III, and IV intervals are divided based on the quartile of RSCA index in 2008–2009, and the transition probability matrix in 2019–2020 relative to 2008–2009 is also calculated. All results are shown in Table 2.

Generally speaking, the probability of the diagonal element of the matrix represents stability. When the diagonal probability value is larger, it indicates that the stability is higher. When the probability of each row of elements moves across the interval relative to probability of diagonal elements, it indicates liquidity. When crossing multiple intervals, the liquidity is greater. Since probability values of the matrix are all between [0, 1], the stability and liquidity are evaluated by summing the probability of diagonal elements and nondiagonal elements. Firstly, the transition matrix in 2019–2020 relative to 2001–2002 is analyzed. The sum of probability of diagonal elements and nondiagonal elements is 2.16 and 1.84, respectively, indicating that stability is higher than liquidity. In addition, the probability of the elements in the upper right corner outside the diagonal indicates that the liquidity is in the improving direction, and the probability of the elements in the lower left corner indicates that the liquidity is in the deterioration direction. The sum of probability of the elements in the upper right corner is 0.98, which is greater than the sum of the probability of the elements in the lower left corner which is 0.86, and the overall trend is improving. Secondly, the transition matrix in 2008–2009 relative to 2001–2002 is obtained. The sum of probability value of diagonal elements and nondiagonal elements is 2.5 and 1.5, respectively, and stability is higher than liquidity. Similarly, the total probability values of the upper right corner and lower left corner of the matrix are 0.73 and 0.77, respectively, and there is a deterioration trend as a whole.

Finally, the transition matrix of 2019–2020 relative to 2008–2009 is analyzed. The sum of probability value of diagonal elements is 3.09, and the sum of the probability of nondiagonal elements is 0.91; stability is higher than liquidity. The sum of the probability values in the upper right corner and the sum of the probability value of the elements in the lower left corner of the matrix are 0.52 and 0.39, respectively, showing a good trend as a whole.

From this, it can be concluded that dynamics of Chinese export comparative advantage is stable. Except that Chinese comparative advantage deteriorated slightly during international financial crisis in 2008, the overall comparative advantage has an improving trend, which also verifies the relevant results of kernel density estimation.

4.3. Survival Analysis. The above two methods only use six years' RSCA index distribution information and do not show the complete dynamics of Chinese export comparative advantage. In order to further clarify dynamics of Chinese export comparative advantage, the survival analysis of RSCA index from 2001 to 2020 is carried out. It is defined as 0 when the value of RSCA index is greater than 0 and 1 when the value is less than 0. The Kaplan–Meier method is used to estimate the cumulative survival function. Firstly, find out the uninterrupted sequence with RSCA > 0 from 2001 to 2020, which means that the value of a specific commodity in 20 years is 0. Then consider two cases.

Case 1. If RSCA > 0 turns to RSCA ≤ 0 for a commodity in a certain year, it indicates that an event has occurred and is marked 1 at the end of the time sequences of successive 0's. The minimum length of the sequence is 2. The maximum length of the time sequence is 19.

Case 2. Case I does not occur. This includes two kinds of censored cases. (i) The sequence is 1 from the first year; after multiple consecutive 0's or 1's, it is finally censored with 0 in the 20th year. (ii) The sequence was 1 in 20 years and finally censored with 1.

For Kaplan Meier analysis, here, the censored case (ii) in case II is excluded, so 120 commodities are eliminated and 135 commodities remained. The following situations will happen to 135 commodities: (a) it has been 0 for 20 years; (b) Case 1 occurs; (c) there is also Case 1 and case (i) in Case 2 that occur at the same time. Thus, 173 independent observations were formed, of which 93 commodities are censored with 0, accounting for 53.7%, and 80 commodities are censored with 1, accounting for 46.3%. The survival probability of Chinese survival function in the first year is 1, which decreases to 0.661 after 5 years, 0.578 after 10 years, 0.522 after 15 years, and 0.507 after 16 years and then remains stable (see Table 3).

Table 1: Results for Wilcoxon's signed rank test of Chinese RSCA index.

year	2001-2002 vs. 2008-2009	2008-2009 vs. 2019-2020	2001-2002 vs. 2019-2020
z-value	−0.422	−0.513	−0.506
p-value	0.673	0.595	0.613

Note. Significance level $\alpha = 5\%$.

Table 2: Markov transition probability matrix of Chinese export comparative advantage.

State	2001-2002 vs. 2008-2009				2008-2009 vs. 2019-2020				2001-2002 vs. 2019-2020			
	I	II	III	IV	I	II	III	IV	I	II	III	IV
I	0.734	0.219	0.031	0.016	0.891	0.109	0.000	0.000	0.672	0.219	0.094	0.015
II	0.210	0.500	0.290	0.000	0.143	0.603	0.254	0.000	0.238	0.302	0.429	0.031
III	0.063	0.187	0.578	0.172	0.000	0.110	0.734	0.156	0.063	0.219	0.531	0.187
IV	0.046	0.077	0.185	0.692	0.000	0.000	0.141	0.859	0.094	0.047	0.203	0.656

Table 3: Kaplan–Meier survival analysis of Chinese RSCA index (2001–2020).

Time	Beg. total	Fail	Net lost	Survivor function	Std. error	[95% conf. int.]	
1	173	0	2	1.0000	.	.	.
2	171	23	2	0.8655	0.0261	0.8046	0.9085
3	146	14	2	0.7825	0.0316	0.7126	0.8373
4	130	12	3	0.7103	0.0349	0.6355	0.7725
5	115	8	4	0.6609	0.0366	0.5837	0.7271
6	103	2	0	0.6480	0.0370	0.5704	0.7152
7	101	4	0	0.6224	0.0377	0.5438	0.6913
8	97	3	0	0.6031	0.0381	0.5241	0.6732
9	94	3	0	0.5839	0.0385	0.5045	0.6550
10	91	1	2	0.5775	0.0386	0.4980	0.6489
11	88	2	2	0.5643	0.0388	0.4847	0.6364
13	84	0	4	0.5643	0.0388	0.4847	0.6364
14	80	3	0	0.5432	0.0392	0.4631	0.6163
15	77	3	4	0.5220	0.0396	0.4417	0.5962
16	70	2	3	0.5071	0.0398	0.4266	0.5820
17	65	0	1	0.5071	0.0398	0.4266	0.5820
18	64	0	1	0.5071	0.0398	0.4266	0.5820
19	63	0	2	0.5071	0.0398	0.4266	0.5820
20	61	0	61	0.5071	0.0398	0.4266	0.5820

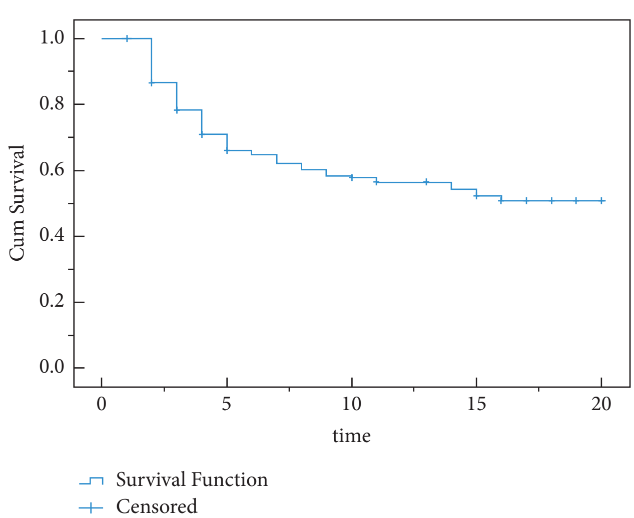

Figure 2: Kaplan–Meier survival analysis of Chinese RSCA index (2001–2020).

Graphically, the period of rapid decline in Chinese survival rate is mainly 1–5 years, the degree of decline decreases in 5–15 years and remains stable after 16 years (see Figure 2). This means that about 50% of China's export commodities with comparative advantage have a chance to survive for more than 16 years. At the 95% confidence level, the mean survival time is 12.84 years and the standard error is 0.61. This shows that, even in the face of fierce international market competition, after excluding the commodities without comparative advantage in the past 20 years, the viability of China's commodities with comparative advantage performs well, which means that China's existing export mode can still support the viability of most commodities.

5. Conclusions and Suggestions

Since entrance to WTO, the development of Chinese foreign trade has significantly improved its position in world trade and become the largest commodity trade country and largest exporter. This is the result of China's continuous optimization of import and export trade mode to meet the needs of world market based on its own comparative advantages. Based on the RSCA index, this paper studies the dynamics of Chinese export comparative advantage from 2001 to 2020; by kernel density estimation method, it is obtained that although China is facing the impact of more fierce international market competition after entrance to WTO, the export comparative advantage of a small number of commodities has weakened, and comparative disadvantage has increased, but most of commodities' comparative advantage has improved, and through Wilcoxon signed rank two-tailed test, it is concluded that the original comparative advantage state of China has not changed. Through analysis of Markov chain transition probability matrix, it is concluded that Chinese export trade mode is relatively stable, the stability of comparative advantage is higher than liquidity, and the liquidity presents an improving trend as a whole. From survival analysis, after excluding the commodities that have not had comparative advantages for 20 years, the viability of China's commodities with comparative advantages performs well, which means that existing export mode can still support viability of most commodities.

As COVID-19 continues to rage, competition between China and major trading partners in trade and other fields will have a greater impact on world trade. Therefore, China needs to be based on the reality and evolution characteristics of export commodities comparative advantage, adapt to the dynamic demand change of international market, actively optimize specialized export mode, and enhance comparative advantage. Specifically, firstly, China should further clarify the status and trend of comparative advantage of various commodities in world market and major export markets, adapt to market dynamic demand, strengthen product innovation, improve the supply chain, improve level of value chain, and further improve added value of export commodities so as to stabilize and develop comparative advantage. Secondly, China should focus on the export of commodities with improved comparative advantages, promote diversification of export markets, and further improve the way of trade organization so as to promote the release of potential of such commodities. Thirdly, China should continue to strengthen the existing export mode and improve the viability of export products continuously in international market based on comparative advantage.

Data Availability

The data used to support the findings of this study are available from the corresponding author upon request.

Conflicts of Interest

The authors declare no conflicts of interest regarding the content and implications of this manuscript.

Acknowledgments

The work of Li Wang was supported by the Academic Support Project for Top-Noth Talents in Disciplines (Majors) of Colleges and Universities in Anhui Province, China, under Grant no. gxjZD55.

References

[1] D. R. Davis, "Critical evidence on comparative advantage? north trade in a multilateral world," *Journal of Political Economy*, vol. 105, no. 1, pp. 1051–1060, 1997.

[2] S. Bojnec and I. Ferto, "European enlargement and agro-food trade," *Canadian Journal of Agricultural Economics*, vol. 56, no. 56, pp. 563–579, 2008.

[3] B. Balassa, "Trade Liberalisation and "Revealed" comparative Advantage," *Manchester School*, Wiley, Hoboken, NJ, USA, 1965.

[4] Y. Michaely, *Trade Preferential Agreements in Latin America*, World Bank Policy Research Working Paper 1583, Africa, 1991.

[5] T. L. Vollrath, "A theoretical evaluation of alternative trade intensity measures of revealed comparative advantage," *Weltwirtschaftliches Archiv*, vol. 127, no. 2, pp. 265–280, 1991.

[6] G. Lafay, "The measurement of revealed comparative advantage," *International Trade Modelling*, Chapman & Hall, NY, USA, 1992.

[7] B. Dalum, K. Laursen, and G. Villumsen, "Structural change in OECD export specialization patterns: de-specialisation and 'stickiness'," *International Review of Applied Economics*, vol. 12, no. 3, pp. 423–443, 1998.

[8] A. R. Hoen and J. Oosterhaven, "On the measurement of comparative advantage," *The Annals of Regional Science*, vol. 40, no. 3, pp. 1–20, 2006.

[9] J. Cai, R. Yu, and P. S. Leung, "The normalized revealed comparative advantage index," *The Annals of Regional Science*, vol. 43, no. 1, pp. 267–282, 2009.

[10] M. Wosiek and A. Visvizi, "Relationship between unemployment and new business registrations at the local level: the case of Poland," *Post-Communist Economies*, vol. 9, no. 2, pp. 1–26, 2021.

[11] A. A. Gnidchenko and V. Salniko, *Trade Intensity, Net Trade, and Revealed Comparative Advantage*, Social Science Electronic Publishing, Rochester, NY, USA, 2021.

[12] E. Sanidas and Y. Shin, "Convergence towards the revealed comparative advantage neutral point for East Asia: similarities and differences between the three countries," *Seoul Journal of Economics*, vol. 24, no. 1, pp. 21–50, 2011.

[13] L. D. Benedicits and M. Tamberi, "Overall specialization empirics: techniques and applications," *Open Economies Review*, vol. 4, pp. 323–346, 2004.

[14] J. Proudman and S. Redding, "Evolving patterns of international trade," *Review of International Economics*, vol. 8, no. 3, pp. 373–396, 2004.

[15] J. Hinloopen and C. V. Marrewijk, *Dynamics of Chinese Comparative Advantage*, pp. 1–70, Social Science Electronic Publishing, Rochester, NY, USA, 2004.

[16] K. Laursen, "Revealed comparative advantage and the alternatives as measures of international specialization," *Eurasian Business Review*, vol. 5, no. 1, pp. 99–115, 2015.

[17] M. Alessandrini, B. Fattouh, and P. Scaramozzino, "The changing pattern of foreign trade specialization in Indian manufacturing," *Oxford Review of Economic Policy*, vol. 23, no. 2, pp. 270–291, 2007.

[18] O. Kostoska and I. Hristoski, "Trade dynamics, revealed comparative advantage, and international competitiveness: evidence from Macedonia," *Economic Annals*, vol. 63, no. 9, pp. 23–59, 2018.

[19] B. Liu and J. Gao, "Understanding the non-Gaussian distribution of revealed comparative advantage index and its alternatives," *International Economics*, vol. 158, no. 8, pp. 1–11, 2019.

[20] E. Leromain and G. Orefice, "New revealed comparative advantage index: dataset and empirical distribution," *International Economics*, vol. 139, pp. 48–70, 2014.

[21] A. J. Yeats, "On the appropriate interpretation of the revealed comparative advantage index: implications of a methodology based on industry sector analysis," *Weltwirtschaftliches Archiv*, vol. 121, no. 1, pp. 61–73, 1985.

[22] S. Bodhisattva and D. Kaveri, "On empirical distribution of RCA indices," 2016, https://mpra.ub.uni-muenchen.de/id/eprint/74087.

Hindawi
Journal of Mathematics
Volume 2022, Article ID 2251623, 8 pages
https://doi.org/10.1155/2022/2251623

Research Article

Pseudospectral Method Based on Müntz–Legendre Wavelets for Solving the Abel Integral Equation

Ioannis Dassios,[1] Fairouz Tchier ,[2] and F. M. O. Tawfiq[2]

[1]AMPSAS, University College Dublin, Dublin 4, Ireland
[2]Department of Mathematics, King Saud University, P.O. Box 22452, Riyadh 11495, Saudi Arabia

Correspondence should be addressed to Fairouz Tchier; ftchier@ksu.edu.sa

Received 17 December 2021; Accepted 14 February 2022; Published 4 March 2022

Academic Editor: Azhar Hussain

This paper deals with the numerical solution of the Abel integral equation based on Müntz–Legendre wavelets. To this end, the Abel integral operator is represented by Müntz–Legendre wavelets as an operational matrix. To find this matrix, we use the similarity between the Abel integral operator and the fractional integral operator. The proposed method can be easily used to solve weakly singular Volterra integral equations. We have proved the convergence of the proposed method. To demonstrate the ability and accuracy of the method, some numerical examples are presented.

1. Introduction

In this paper, we focus our attention on constructing and applying Müntz–Legendre (M-L) wavelets that will be used as the basis in the pseudospectral method to solve the famous Abel integral equation

$$u(x) - \mathscr{A}^{\alpha}(k)(x) = f(x), \tag{1}$$

in which Abel's integral operator $\mathscr{A}^{\alpha}(k)(x)$ of order $0 < \alpha < 1$ is defined in [1] as follows:

$$\mathscr{A}^{\alpha}(k)(x) := \int_0^x k(x, s, u(s))(x-s)^{-\alpha}\mathrm{d}x, \quad x \in [0,1]. \tag{2}$$

Here, given $\Omega = [0,1]$, $f(x)$, and $k(x, s, u(s))$ are assumed to be continuous functions on Ω and S with $S = \{(x, s, u)\colon x, s \in [0,1], u \in \mathbb{R}\}$. Further, we suppose that the kernel function $k(x, s, u(s))$ is equal to the form $g(x, s)u(s)$. In other words, the desired equation is assumed to be linear.

The Abel equation is a special case of the integral equations with the weakly singular kernel that was first introduced by Abel. In investigating the generalization of the tautochrone problem, he introduced this equation [2]. This equation appears widely in modeling many physical problems, such as nuclear physics, X-ray radiography, fluid flow [3], scattering theory, plasma diagnostics, semiconductors, physical electronics, and nonlinear diffusion[1, 4]. Given this equation's wide application, solving this equation is very important. But one cannot always solve the equation analytically, and we need to use numerical methods for it.

Among the many papers that have considered the numerical solution of this equation, we can mention some of them. Saadatmandi and Dehghan [5] utilized the collocation method based on shifted Legendre polynomials. Piessens and Verbaeten [6] introduced a numerical method based on Chebyshev polynomials, and after approximating the unknown solution based on these bases, they obtained the solution as a sum of hypergeometric functions. Using the Bernstein operational matrix, Singh et al. [7] introduced a stable numerical method to solve this problem. In [8], we can find the integrable solution of the Abel integral equation under certain conditions, and also the sufficient and necessary conditions for the existence of this solution are presented. In [9], the authors proposed the Laplace transform method to solve the problem, where they assumed that the solution would be differentiable and continuous. Saray [10] introduced a novel and efficient method based on

Alpert's multiwavelets. In this work, after introducing the sparse representation of the Abel integral operator, the Abel integral equation is reduced to a sparse system of linear algebraic equations in the linear form, and this causes a reduction in time and computational costs. In [11], the unbounded solutions of the nonlinear Abel integral equations are investigated. Li and Zhao [12] used Mikusinski's operator of fractional order to solve the Abel integral equation.

The outline of this article is as follows: the M-L wavelets are constructed in Section 2, and then the Abel integral operator is represented based on these bases. In Section 3, the Abel integral equation is solved by using the pseudospectral method based on M-L wavelets. This section contains the error analysis and the conditions for convergence are investigated. To demonstrate the efficiency and accuracy of the presented method, some numerical examples are given in Section 4.

2. Müntz–Legendre Wavelets

As we know, multiresolution analysis (MRA) is a significant procedure for constructing wavelets. According to MRA, a family of nested subspaces exists such that they satisfy certain circumstances [13]

$$\{0\} \subset \cdots \subset V_{-1} \subset V_0 \subset V_1 \subset \cdots \subset L^2(\Lambda), \tag{3}$$

where Λ is equal to $\mathbb{R}$ or any bounded interval.

Recently, the M-L wavelets have been used to solve some equations, such as fractional optimal control problems [14], fractional pantograph differential equations [15], fractional differential equations [16], and multiorder fractional differential equations [17]. To solve the Abel equation, we first briefly introduce the M-L wavelets as follows.

Given $J \in \mathbb{N}_0$, assume that the subspace $V_J \in L^2(\Lambda)$ is spanned by the scaled and translated version of a set of bases, which are called multiscaling functions, viz.,

$$V_J = \left\{\operatorname{span}\left\{\phi_{J,b}^n \colon b \in \mathscr{B}, n \in \mathscr{R}\right\}\right\}, \tag{4}$$

where $\mathscr{B} := \{0, 1, \ldots, 2^J - 1\}$ and $\mathscr{R} := \{0, 1, \ldots, r-1\}$ with $r \in \mathbb{N}$. The parameter J is called refinement level and r is the multiplicity parameter. In the sequel, we intend to introduce the functions $\phi_{J,b}^n$.

Motivated by [17], we denote the M-L polynomials $L_n(x)$ as

$$L_n(x) = \sum_{k=0}^{n} l_{k,n} x^{\lambda_k}, \quad x \in \Omega, \tag{5}$$

where $\lambda_k := \{k\mu \colon \mu \in \mathbb{R}, k = 0, \ldots, n\}$ and the coefficient $l_{k,n}$ is obtained by

$$l_{k,n} := \frac{\prod_{i=0}^{n-1}(\lambda_k + \lambda_i + 1)}{\prod_{i=0, i\neq k}^{n}(\lambda_k - \lambda_i)}. \tag{6}$$

It can be easily shown that these polynomials satisfy the orthogonality requirements and form an orthogonal system, via

$$\langle L_n(x), L_{n'}(x)\rangle = \int_0^1 L_n(x) L_{n'}(x)\mathrm{d}x = \frac{\delta_{n',n}}{2\lambda_n + 1}, \quad n \geq n', \tag{7}$$

where $\delta_{m\prime,m}$ denotes the Kronecker symbol and is given by

$$\delta_{n',n} := \begin{cases} 1, & n' = n, \\ 0, & n \geq n'. \end{cases} \tag{8}$$

Considering the definition of $L_n(x)$, one can introduce the M-L wavelets [17], via

$$\phi_{J,b}^n = \begin{cases} 2^{J/2}\sqrt{2\lambda_n + 1}\, L_n\left(2^J x - b\right), & \dfrac{b}{2^J} \leq x \leq \dfrac{b+1}{2^J}, \\ 0, & \text{otherwise}. \end{cases} \tag{9}$$

Due to the definition of M-L wavelets, one can introduce the projection operator $\mathscr{P}$ that maps any function $u \in L^2(\Omega)$ onto V_J as follows:

$$u(x) \approx \mathscr{P}(u)(x) = \sum_{b=0}^{2^J-1}\sum_{n=0}^{r-1} u_{b,n}\phi_{J,b}^n(x) = U^T\Phi(x), \tag{10}$$

where and throughout the paper, the superscript T is used for the matrix transpose. Here $\Phi(x)$ is a vector function of dimension $N = 2^J r$ whose $(br + n + 1)$-th element is $\phi_{J,b}^n(x)$, and the $(br + n + 1)$-th element of the vector U is evaluated by

$$u_{b,n} = \langle u, \phi_{J,b}^n\rangle = \int_0^1 u(x)\phi_{J,b}^n(x)\mathrm{d}x. \tag{11}$$

It follows from [15] that one may be able to bound the projection error $\mathscr{P}$ in the sense of Sobolev norms.

Lemma 1 (see [15]). *Given $n \geq 0$, assume that $r > m$. If $u \in H^m(\Omega)$, then*

$$\|u - \mathscr{P}(u)\|_{L_2(\Omega)} \leq c(r-1)^{-m}\left(2^{J-1}\right)^{-m}\left\|u^{(m)}\right\|_{L_2(\Omega)}, \tag{12}$$

and for $s \geq 1$, we have

$$\|u - \mathscr{P}(u)\|_{H^s(\Omega)} \leq c(r-1)^{2s-(1/2)-m}\left(2^{J-1}\right)^{s-m}\left\|u^{(m)}\right\|_{L_2(\Omega)}, \tag{13}$$

in which $H^m(\Omega)$ is the Sobolev space and the related norm is determined by

$$\|u\|_{H^m(\Omega)} = \left(\sum_{j=0}^{m}\left\|u^{(j)}\right\|_{L_2(\Omega)}^2\right)^{1/2}. \tag{14}$$

2.1. Representation of Abel Integral Operator in Müntz–Legendre Wavelets. In this subsection, we consider the Abel operator as a fractional integral operator, and after representing the fractional integral operator in M-L wavelets as an operational matrix, we find a representation of the Abel integral operator in M-L wavelets. To this end, it is necessary to define some concepts about fraction calculation.

Definition 1 (see [18]). Let $u \in L_1[a,b]$. The Riemann–Liouville fractional integral operator $\mathcal{I}_a^\alpha$ of order $\alpha \in \mathbb{R}^+$ is determined by

$$\mathcal{I}_a^\alpha(u)(x) := \frac{1}{\Gamma(\alpha)}\int_a^x (x-s)^{\alpha-1}u(s)\mathrm{d}s, \quad x \in [a,b], \tag{15}$$

where $\Gamma(\alpha)$ represents the gamma function.

Remark 1. It can be verified that the fractional integral of the functions x^κ is given by

$$\mathcal{I}_a^\alpha(x^\kappa) = \frac{\Gamma(\kappa+1)}{\Gamma(\kappa+\alpha+1)}x^{\kappa+\alpha}. \tag{16}$$

Lemma 2 (cf Lemma 2.1(a). see [19]). *The fractional integration operators $\mathcal{I}_a^\alpha$ are bound in $L^p([a,b])$ for $1 \le p \le \infty$ as follows:*

$$\left\|\mathcal{I}_a^\alpha(u)\right\|_p \le K\|u\|_p, \quad K := \frac{(b-a)^\alpha}{\Gamma(\alpha+1)}. \tag{17}$$

It follows from [19] that if $u \in L_1[a,b]$, then the function $\mathcal{I}_a^\alpha u$ itself belongs to $L_1[a,b]$. We recall that the Abel integral operator of order $\alpha \in (0,1)$ is determined by

$$\mathcal{A}^\alpha(u)(x) = \int_0^x (x-s)^{-\alpha}u(s)\mathrm{d}s. \tag{18}$$

There is a similarity between the Abel integral operator $\mathcal{A}^\alpha$ and the Riemann–Liouville fractional integral operator $\mathcal{I}_0^\beta$ $(\beta := 1-\alpha)$, viz,

$$\mathcal{A}^\alpha = \Gamma(\alpha)\mathcal{I}_a^{1-\alpha}. \tag{19}$$

Thus, we can use the Riemann–Liouville fractional integral operator $\mathcal{I}_0^\beta$ instead of the Abel integral operator $\mathcal{A}^\alpha$.

According to the definition of M-L wavelets, the fractional integral operator $\mathcal{I}_0^\beta$ acting on the vector function $\Phi(x)$ may be written as an expansion of M-L wavelets $\Phi(x)$, i.e.,

$$\mathcal{P}\left(\mathcal{I}_0^\beta\right)(\Phi(x)) = I_\beta(x)\Phi(x), \quad \beta \in (0,1), \tag{20}$$

where $I_\beta(x)$ is an $N \times N$ matrix and is famous as the operational matrix of fractional integral for the M-L wavelets.

Before we look at how to calculate the elements of the aforementioned matrix, it is intransitive to introduce the piecewise fractional-order Taylor functions. Let $J \in \mathbb{Z}^+ \cup \{0\}$ be a fixed number, the piecewise fractional-order Taylor functions can be defined in the following form:

$$\psi_{J,b}^n = \begin{cases} t^{\lambda_n}, & \dfrac{b}{2^J} \le x \le \dfrac{b+1}{2^J}, \\ 0, & \text{otherwise.} \end{cases} \quad b \in \mathcal{B},\ n \in \mathcal{M}. \tag{21}$$

By introducing the square matrix T of dimension $N \times N$, whose (i,j)-th element is computed by

$$T_{i,j} = \langle \Phi_i(x), \Psi_j(x)\rangle = \int_0^1 \Phi_i(x), \Psi_j(x)\mathrm{d}x, \quad i,j = 1,\ldots,N. \tag{22}$$

We can expand any elements of vector function $\Phi(x)$ (M-L wavelets) by the piecewise fractional-order Taylor functions $\Psi(x)$, viz,

$$\Phi(x) = T^{-1}\Psi(x). \tag{23}$$

Here the matrix T is a $N \times N$ matrix and it is called the transformation matrix. In the sequel, we assume that Q is a vector of dimension r whose i-th element is x^{λ_i}. Thus, it is easy to show that

$$\Psi(x) = [Q,\ldots,Q]^T. \tag{24}$$

It follows from (16) that one can find the i-th element of $\mathcal{I}_0^\beta(\Psi)(x)$, via

$$\mathcal{I}_0^\beta(\Psi_i)(x) = \frac{\Gamma(\lambda_i+1)}{\Gamma(\lambda_i+\beta+1)}x^{\lambda_i+\beta}. \tag{25}$$

This gives rise to introduce a diagonal matrix $I_{\Phi,\beta}(x)$, such that

$$\mathcal{I}_0^\beta(\Psi)(x) = I_{\Psi,\beta}(x)\Psi(x). \tag{26}$$

It is worth noting that this matrix expresses the fractional integral of functions Ψ as a combination of themselves and has the following form:

$$I_{\Psi,\beta}(x) = \operatorname{diag}\left[P_\beta(x),\ldots,P_\beta(x)\right], \tag{27}$$

where $P_\beta(x) := x^\beta H(\mathcal{I}_0^\beta(Q)(x) = P_\beta(x)Q(x))$ and H is a diagonal matrix of the form

$$(H)_{i,i} = \frac{\Gamma(\lambda_i+1)}{\Gamma(\lambda_i+\beta+1)}. \tag{28}$$

Now, we are able to introduce the operational matrix of fractional integral for the M-L wavelets via

$$\begin{aligned}\mathcal{P}_J\left(\mathcal{I}_0^\beta\right)(\Phi(x)) &= \mathcal{P}_J\left(\mathcal{I}_0^\beta\right)\left(T^{-1}\Psi(x)\right) \\ &= T^{-1}I_{\Psi,\beta}(x)\Psi(x) = T^{-1}I_{\Psi,\beta}(x)T\Phi(x).\end{aligned} \tag{29}$$

Thus, we get

$$I_\beta(x) := T^{-1}I_{\Psi,\beta}(x)T. \tag{30}$$

3. Pseudospectral Method

To derive the numerical solution of the second kind of Abel integral equation based on the pseudospectral method, we can approximate the unknown solution with the projection operator $\mathcal{P}_J$, as follows:

$$u \approx \mathcal{P}_J(u) = U^T\Psi, \tag{31}$$

where U is a vector of dimension N, whose elements should be found. Note that the function $f(x)$ and the kernel function $k(x, s, \mathscr{P}_J(u)(s))$ can be approximated in the same manner, i.e.,

$$\begin{aligned} f(x) &\approx \mathscr{P}_J(u) = F^T\Psi, \\ k\left(x, s, \mathscr{P}_J(u)(s)\right) &\approx \mathscr{P}_J(k)\left(x, s, \mathscr{P}_J(u)(s)\right) \\ &= \Psi^T(x)K\Psi(s), \end{aligned} \tag{32}$$

where $F \in \mathbb{R}^N$ and $K \in \mathbb{R}^{N\times N}$. By substituting (32) into the integral part of the Abel integral equation (1), we obtain

$$\begin{aligned} &\mathscr{P}_J\left(\Psi(x)^T\widetilde{K}\int_0^x (x-s)^{-\alpha}\Psi(s)\mathrm{d}s\right) = \mathscr{P}_J^r\left(\Psi(x)^T\widetilde{K}I_\alpha\Psi(x)\right) \\ &= \widehat{K}\Psi(x). \end{aligned} \tag{33}$$

We now substitute equations (31)–(33) into Abel integral equation (1) and simplify to get

$$r(x) := (U - F + \widehat{K})^T\Psi(x) = 0, \tag{34}$$

where $r(x)$ is the residual function that our goal is to reduce to zero. Let $\{x_i\}$ be a number of points in Ω, we select the solution that satisfies the collocation condition $r(x_i) = 0$, where $\{x_i\}$ are called the collocation points. In this paper, we use the shifted Chebyshev and Legendre polynomials zeros as collocation points. The collocation method gives rise to a system of linear or nonlinear algebraic equations. One can derive the unknown coefficients U after solving this system.

3.1. Error Analysis. We write the Abel integral equation (1) in the form

$$(I - \mathscr{K})u = f, \tag{35}$$

where $\mathscr{K}$ is a compact operator that maps any continuous function onto $C[0,1]$. As we said, our goal is to reduce the residual function $r(x)$ to zero. Symbolically, we have

$$r(x) = (I - \mathscr{K})u_J - f, \tag{36}$$

where $u_J := \mathscr{P}_J(u)$. We note that $\mathscr{P}_J(r)(x) = 0$ if and only if $r(x_i) = 0$ or equivalently,

$$\mathscr{P}_J(I - \mathscr{K})u_J = \mathscr{P}_J(f). \tag{37}$$

Let u_J is a solution of (37), then by applying $\mathscr{P}_J(u_J) = u_J$, equation (37) can be written as follows:

$$\left(I - \mathscr{P}_J\mathscr{K}\right)u_J = \mathscr{P}_J(f). \tag{38}$$

Since both the original equations (1) and (38) are defined on $C[0,1]$, then for the error analysis, we compare them.

Theorem 1. *Let us assume that $I - \mathscr{K}: C[0,1] \longrightarrow C[0,1]$ is a bijections operator. Further, let us assume*

$$\left\|\mathscr{K} - \mathscr{P}_J\mathscr{K}\right\| \longrightarrow 0, \quad \text{as}\, r \longrightarrow \infty. \tag{39}$$

Then for all sufficiently large r $(r \le N)$, the operator $(I - \mathscr{P}_J\mathscr{K})^{-1}$ exists as a bounded operator from $C[0,1]$ to $C[0,1]$. Moreover, it is uniformly bounded

$$\sup_{r\le N}\left\|\left(I - \mathscr{P}_J\mathscr{K}\right)^{-1}\right\| < \infty. \tag{40}$$

For the solutions of (35) and (38)

$$\begin{aligned} u - u_J &= \left(I - \mathscr{P}_J\mathscr{K}\right)^{-1}\left(u - \mathscr{P}_J(u)\right), \\ \frac{1}{\left\|I - \mathscr{P}_J\mathscr{K}\right\|}\left\|u - \mathscr{P}_J(u)\right\| &\le \left\|u - u_J\right\| \\ &\le \left\|\left(I - \mathscr{P}_J\mathscr{K}\right)^{-1}\right\|\left\|u - \mathscr{P}_J(u)\right\|. \end{aligned} \tag{41}$$

Proof. For details, refer to [20].

Since $\mathscr{K}: C[0,1] \longrightarrow C[0,1]$ is a compact operator and $\mathscr{P}_J$ is a bounded projection, such that $\mathscr{P}_J u \longrightarrow 0$ as $r \longrightarrow \infty$. Then motivated by [20] (Lemma 3.1.2), we have

$$\left\|\mathscr{K} - \mathscr{P}_J\mathscr{K}\right\| \longrightarrow 0, \quad \text{as}\, r \longrightarrow \infty. \tag{42}$$

Therefore, the condition of Theorem 1 is held. □

4. Numerical Examples

In this section, some numerical examples are solved to show the validity and efficiency of the method. To do this, we carry out the Maple and MATLAB software simultaneously.

Example 1. For the first example, let us consider the linear Abel integral equation of the second kind with the kernel function $k(t, x, u(x)) := (1/10\Gamma(1-\alpha))u(x)$, and $f(t) = 1$. The exact solution is given in [10] as follows:

$$u(t) = E_{1-\alpha,1}\left(\frac{t^{1-\alpha}}{10}\right), \tag{43}$$

where $E_{\sigma,\beta}$ is the Mittag-Leffler function

$$E_{\sigma,\beta}(z) = \sum_{l=0}^{\infty}\frac{z^l}{\Gamma(\sigma l + \beta)}, \quad \sigma, \beta, z \in \mathbb{R}, \sigma > 0. \tag{44}$$

Table 1 shows the absolute value of errors at different times x_i when the collocation points are chosen to be the Legendre polynomial nodes. As we expected, when the r increases (the degree of the bases as well as the number of collocation points increases) the error will decrease. To show the effect of the parameter μ in the L^2-error, we plot Figure 1 and report Table 2. Figure 2 illustrates the effect of the choosing nodes on the L^2-error and also absolute value of errors at the Chebyshev nodes using different multiplicity r. Also, we can see the effect of the multiplicity parameter r on the L^2-error and absolute error in Figure 2.

Example 2. The second example is devoted to the Abel integral equation (1) with

$$\begin{aligned} f(t) &:= 2\sqrt{t}, \\ k(t, x, u(x)) &:= u(x). \end{aligned} \tag{45}$$

Table 1: The absolute errors at the Legendre nodes for Example 1.

x	$r = 5$	$r = 7$	$r = 9$
0.1	$9.72e-4$	$2.78e-4$	$1.19e-4$
0.2	$2.41e-4$	$2.24e-4$	$1.30e-5$
0.3	$3.15e-4$	$1.22e-6$	$4.64e-5$
0.4	$2.93e-4$	$1.09e-4$	$4.83e-5$
0.5	$1.23e-5$	$7.38e-7$	$1.93e-6$
0.6	$1.94e-4$	$7.95e-6$	$3.14e-5$
0.7	$1.53e-4$	$6.80e-6$	$2.21e-5$
0.8	$7.94e-5$	$6.32e-5$	$6.04e-6$
0.9	$1.89e-4$	$4.44e-5$	$1.60e-5$
1.0	$4.09e-4$	$1.60e-4$	$7.86e-5$

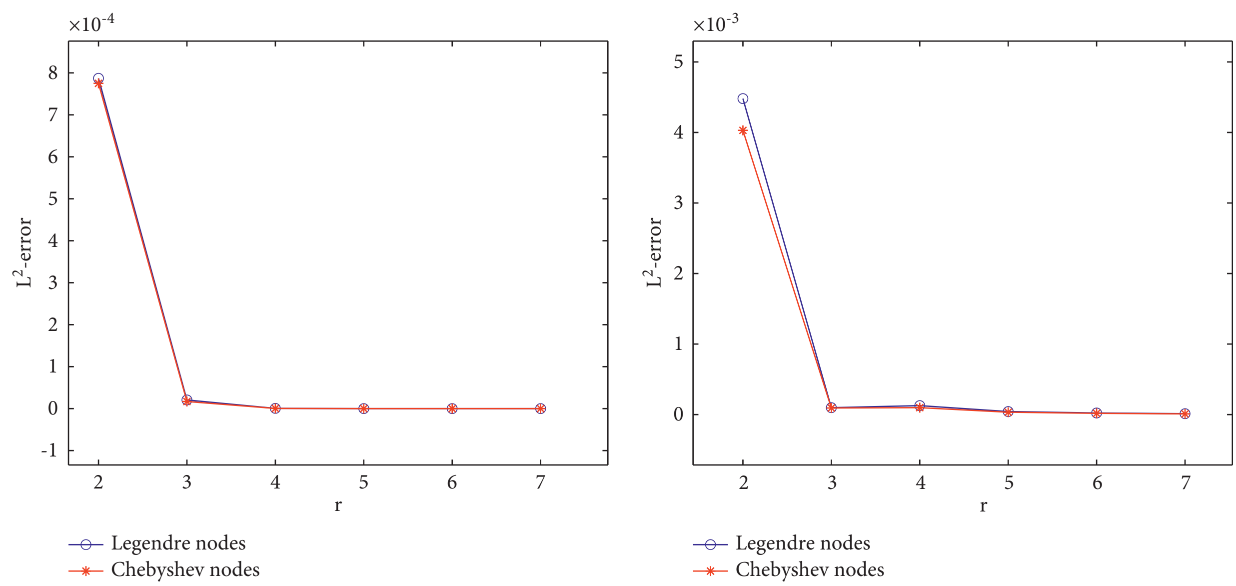

(a) (b)

Figure 1: Plot of the L^2-errors taking $\mu = (1/2)$ (a) and $\mu = (1/3)$ (b) at the Legendre and Chebyshev nodes for Example 1.

Table 2: The L^2-errors at the Legendre and Chebyshev nodes taking different μ for Example 1.

r	$\mu = (1/2)$		$\mu = (1/3)$	
	Chebyshev nodes	Legendre nodes	Chebyshev nodes	Legendre nodes
2	$7.57e-4$	$7.87e-4$	$4.03e-3$	$4.48e-3$
3	$1.69e-5$	$2.06e-5$	$9.34e-5$	$9.79e-5$
4	$3.82e-7$	$5.32e-7$	$9.81e-5$	$1.27e-4$
5	$8.58e-9$	$1.33e-8$	$3.37e-5$	$4.29e-5$
6	$1.89e-10$	$3.16e-10$	$1.76e-5$	$2.26e-5$
7	$4.06e-12$	$7.19e-12$	$9.89e-6$	$1.27e-5$

The exact solution is given by $u(t) = 1 - e^{\pi t} erfc(\sqrt{\pi t})$ [4].

To show the effect of the multiplicity parameter r and choosing the collocation points, we report Table 3. This Table also illustrates the effect of parameter μ on the L^2-error. Due to Table 3, it is obvious that these three parameters have a direct effect on the L^2-error such that when r increases, the error decreases. Also, choosing the Chebyshev nodes gives us a better result than Legendre nodes. In Figure 3, we demonstrate the absolute error when multiplicity parameter r increases taking $\mu = (1/2)$ and different collocation points.

Example 3. Let us consider the following Abel integral equation:

$$f(t) := \sin(x) - \frac{4}{3}x^{3/2}{}_1F_2\left(1; \frac{5}{4}, \frac{7}{4}; -\frac{x^2}{4}\right), \quad k(t, x, u(x)) := u(x), \tag{46}$$

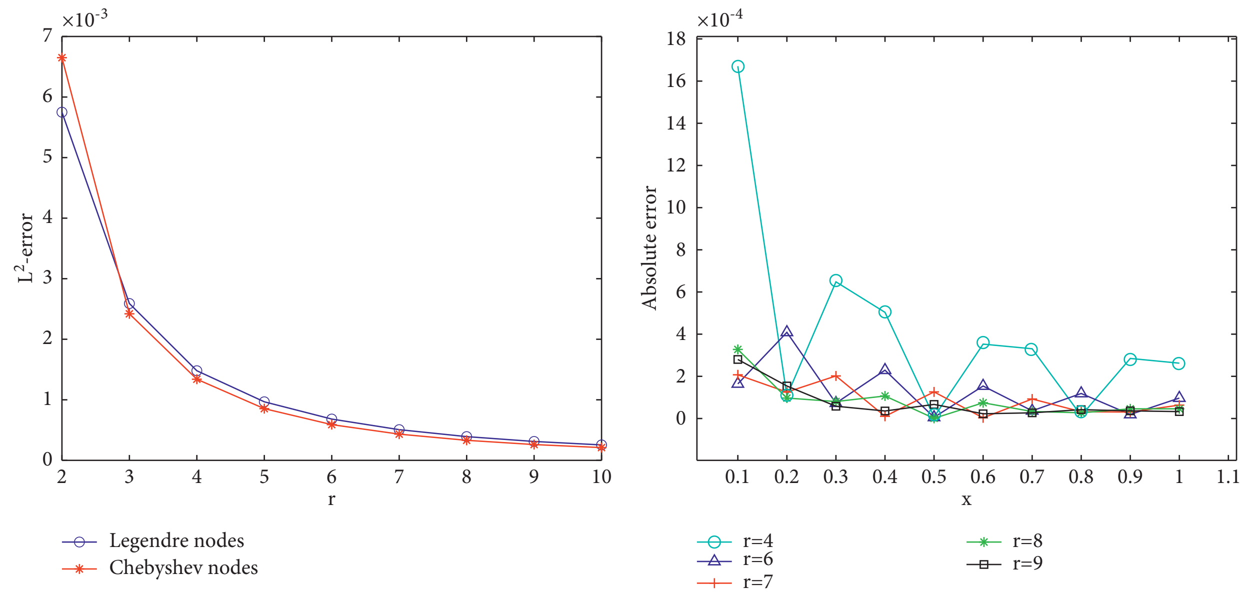

(a) (b)

FIGURE 2: Plot of the L^2-errors (a) taking the Legendre and Chebyshev nodes and the absolute error at the Chebyshev nodes (b) for Example 1.

TABLE 3: The L^2-errors at the Legendre and Chebyshev nodes taking different μ for Example 2.

r	$\mu = (1/2)$		$\mu = 1$	
	Chebyshev nodes	Legendre nodes	Chebyshev nodes	Legendre nodes
2	$3.38e-2$	$3.52e-2$	$5.68e-2$	$5.62e-2$
3	$9.21e-2$	$1.08e-2$	$3.15e-2$	$3.15e-2$
4	$2.57e-3$	$3.36e-3$	$1.95e-2$	$2.00e-2$
5	$7.29e-4$	$1.04e-3$	$1.31e-2$	$1.38e-2$
6	$2.06e-4$	$3.17e-4$	$9.40e-3$	$1.01e-2$
7	$5.77e-5$	$9.40e-5$	$7.04e-3$	$7.73e-3$

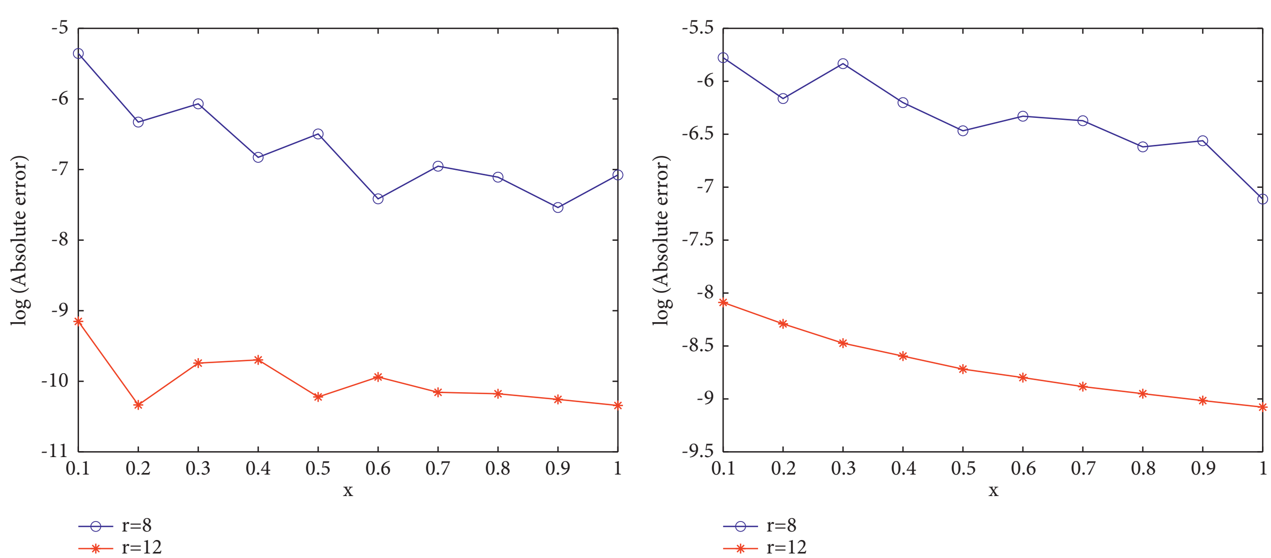

(a) (b)

FIGURE 3: Plot of the absolute error at the Chebyshev nodes (a) and the Legendre nodes (b) taking different r for Example 2.

Table 4: The absolute errors at the Chebyshev nodes for Example 3.

x	$r = 6$	$r = 8$	$r = 10$
0.1	$1.42e-4$	$1.20e-6$	$1.60e-7$
0.2	$6.05e-6$	$2.45e-6$	$1.53e-9$
0.3	$2.39e-6$	$3.44e-7$	$4.50e-8$
0.4	$4.67e-5$	$6.55e-7$	$6.19e-8$
0.5	$8.29e-5$	$1.61e-6$	$7.59e-8$
0.6	$1.03e-4$	$1.87e-6$	$1.08e-7$
0.7	$1.23e-4$	$2.31e-6$	$1.48e-7$
0.8	$1.66e-4$	$3.36e-6$	$2.01e-7$
0.9	$2.40e-4$	$4.64e-6$	$2.76e-7$
1.0	$3.21e-4$	$6.34e-6$	$3.78e-7$

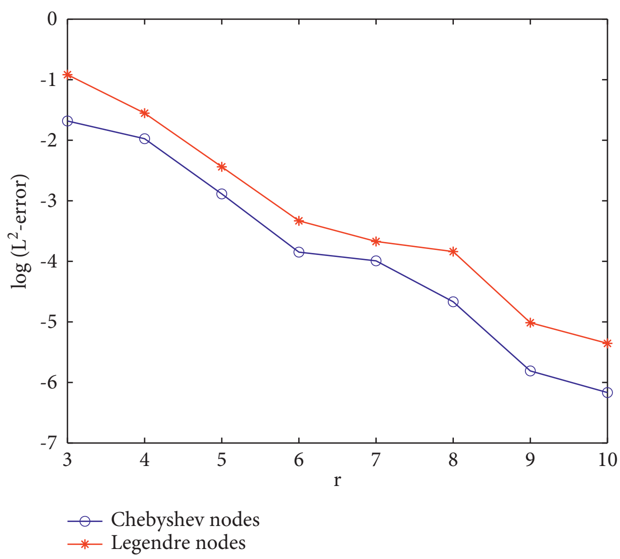

Figure 4: Plot of the L^2-errors taking $\mu = (1/2)$ at the Legendre and Chebyshev nodes for Example 3.

in which ${}_1F_2$ is the hypergeometric function defined in [21]. Also, the exact solution is $u(x) = \sin(x)$.

Table 4 shows the absolute value of errors at different times x_i when the collocation points are chosen to be the Chebyshev polynomials nodes. Figure 4 illustrates the effect of selecting the Chebyshev and Legendre nodes. We can also see the effect of increasing the parameter r. It is observed that by increasing the parameter r, the error decreases.

5. Conclusion

In this paper, we utilize an efficient algorithm based on the wavelet pseudospectral method to solve the well-known Abel integral equation. This method can easily be used to solve weakly singular Volterra integral equations, and this shows the ability of the proposed method. We have compared the method with other methods and shown that this method offers better results. We have proved the convergence of the proposed method. Given the construction of these bases and the role of the parameter μ, which can be polynomials with fractional powers, compared to other bases, if the exact solution or the known functions in the equation are of the fractional type, the proposed method will provide better results.

Data Availability

The data used to support this study are included within this article.

Conflicts of Interest

The authors declare that there are no conflicts of interest with this work.

Authors' Contributions

All authors read and approved the final manuscript. All authors contributed equally and significantly to the writing of this paper.

Acknowledgments

This work is supported by the Researchers Supporting Project Number (RSP-2021/401), King Saud University, Riyadh, Saudi Arabia.

References

[1] R. Gorenflo and S. Vessella, "Abel integral equations, analysis and applications," in *Lecture Notes in Mathematics*Springer, Berlin, Germany, 1991.
[2] G. Simmons, *Differential Equations with Applications and Historical Notes*, McGraw-Hill, New York, NY, USA, 1972.
[3] J. Goncerzewicz, H. Marcinkowska, W. Okrasiński, and K. Tabisz, "On the percolation of water from a cylindrical reservoir into the surrounding soil," *Applicationes Mathematicae*, vol. 16, no. 2, pp. 249–261, 1978.
[4] A. M. Wazwaz, *Linear and Nonlinear Integral Equations: Methods and Applications*, Higher Education Press and Springer, Berlin, Germany, 2011.
[5] A. Saadatmandi and M. Dehghan, "A collocation method for solving Abel's integral equations of first and second kinds," *Zeitschrift für Naturforschung A*, vol. 63, no. 12, pp. 752–756, 2008.
[6] R. Piessens and P. Verbaeten, "Numerical solution of the abel integral equation," *Bit*, vol. 13, no. 4, pp. 451–457, 1973.
[7] O. P. Singh, V. K. Singh, and R. K. Pandey, "A stable numerical inversion of Abel's integral equation using almost Bernstein operational matrix," *Journal of Quantitative Spectroscopy and Radiative Transfer*, vol. 111, no. 1, pp. 245–252, 2010.
[8] J. D. Tamarkin, "On integrable solutions of Abel's integral equation," *Annals of Mathematics*, vol. 31, no. 2, pp. 219–229, 1930.
[9] G. Doetsch, "Integro-differentialgleichungen vom faltungstypus," *Mathematische Annalen*, vol. 89, 1923.
[10] B. N. Saray, "Abel's integral operator: sparse representation based on multiwavelets," *BIT Numerical Mathematics*, vol. 61, pp. 587–606, 2021.
[11] M. R. Arias, R. Benítez, and V. J. Bolós, "Attraction properties of unbounded solutions for a nonlinear Abel integral equation," *Journal of Integral Equations and Applications*, vol. 19, no. 4, pp. 439–452, 2007.
[12] M. Li and W. Zhao, "Solving Abel's type integral equation with Mikusinski's operator of fractional order," *Advances in Mathematical Physics*, vol. 2013, Article ID 806984, 4 pages, 2013.
[13] S. G. Mallat, *A Wavelet Tour of Signal Processing*, Academic Press, Cambridge, MA, USA, 1999.
[14] P. Rahimkhani and Y. Ordokhani, "Numerical solution a class of 2D fractional optimal control problems by using 2D Müntz-Legendre wavelets," *Optimal Control Applications and Methods*, vol. 39, no. 6, pp. 1916–1934, 2018.
[15] P. Rahimkhani, Y. Ordokhani, and E. Babolian, "Müntz-Legendre wavelet operational matrix of fractional-order integration and its applications for solving the fractional pantograph differential equations," *Numerical Algorithms*, vol. 77, pp. 1283–1305, 2018.
[16] P. Mokhtary, F. Ghoreishi, and H. M. Srivastava, "The Müntz-Legendre Tau method for fractional differential equations," *Applied Mathematical Modelling*, vol. 40, no. 2, pp. 671–684, 2016.
[17] H. B. Jebreen and F. Tchier, "A new scheme for solving multiorder fractional differential equations based on Müntz-legendre wavelets," *Complexity*, vol. 2021, Article ID 9915551, 9 pages, 2021.
[18] A. Afarideh, F. Dastmalchi Saei, M. Lakestani, and B. Nemati Saray, "Pseudospectral method for solving fractional Sturm-Liouville problem using Chebyshev cardinal functions," *Physica Scripta*, vol. 96, no. 12, Article ID 125267, 2021.
[19] A. Kilbas, H. M. Srivastava, and J. J. Trujillo, *Theory and Applications of Fractional Differential Equations*, Vol. 24, Elsevier, Amsterdam, Netherlands, 2006.
[20] K. E. Atkinson, *The Numerical Solution of Integral Equations of the Second Kind*, Cambridge University Press, Cambridge, UK, 1997.
[21] R. Beals and R. Wong, *Special Functions*, Cambridge University Press, Cambridge, UK, 2010.

Hindawi
Journal of Mathematics
Volume 2022, Article ID 8876149, 30 pages
https://doi.org/10.1155/2022/8876149

Research Article

A Comparative Analysis of the Fractional-Order Coupled Korteweg–De Vries Equations with the Mittag–Leffler Law

Noufe H. Aljahdaly,[1] **Ali Akgül**,[2] **Rasool Shah**,[3] **Ibrahim Mahariq**,[4] **and Jeevan Kafle**[5]

[1]*Mathematics Department, Faculty of Sciences and Arts, King Abdulaziz University, Rabigh, Saudi Arabia*
[2]*Siirt University, Art and Science Faculty, Department of Mathematics, Siirt 56100, Turkey*
[3]*Department of Mathematics, Abdul Wali Khan University, Mardan 23200, Pakistan*
[4]*College of Engineering and Technology, American University of the Middle East, Egaila 54200, Kuwait*
[5]*Central Department of Mathematics, Tribhuvan University, Kritipur, Kathmandu, Nepal*

Correspondence should be addressed to Jeevan Kafle; jeevan.kafle@cdmath.tu.edu.np

Received 16 September 2021; Accepted 6 January 2022; Published 15 February 2022

Academic Editor: A. Ghareeb

This article applies efficient methods, namely, modified decomposition method and new iterative transformation method, to analyze a nonlinear system of Korteweg–de Vries equations with the Atangana–Baleanu fractional derivative. The nonlinear fractional coupled systems investigated in this current analysis are the system of Korteweg–de Vries and the modified system of Korteweg–de Vries equations applied as a model in nonlinear physical phenomena arising in chemistry, biology, physics, and applied sciences. Approximate analytical results are represented in the form of a series with straightforward components, and some aspects showed an appropriate dependence on the values of the fractional-order derivatives. The convergence and uniqueness analysis is carried out. To comprehend the analytical procedure of both methods, three test examples are provided for the analytical results of the time-fractional KdV equation. Additionally, the efficiency of the mentioned procedures and the reduction in calculations provide broader applicability. It is also illustrated that the findings of the current methodology are in close harmony with the exact solutions. The series result achieved applying this technique is proved to be accurate and reliable with minimal calculations. The numerical simulations for obtained solutions are discussed for different values of the fractional order.

1. Introduction

Many researchers have been working on various aspects of fractional derivatives in recent years. Caputo and Fabrizio modified the existing Caputo derivative to develop the Caputo–Fabrizio fractional derivative [1–5] based on a nonsingular kernel. Because of its advantages, numerous researchers utilized this operator to investigate various types of fractional-order partial differential equations [6–9]. To address this issue, Atangana and Baleanu proposed a new fractional operator called the Atangana–Baleanu derivative, which combines Caputo and Riemann–Liouville derivatives. Because of the existence of the Mittag–Leffler kernel, which is a generalization of the exponential kernel, this new Atangana–Baleanu derivative has a long memory. Moreover, the Atangana–Baleanu operator outperforms other operators, and different scientific models have been successfully solved. Many advances have been made in fractional calculus over the last few years by borrowing ideas from classical calculus, but it does not remain easy. Scholars have the main concern to obtain a numerical solution; for this, numerous efficient methodologies have been constructed for fractional differential equations, such as the Adomian decomposition transform method [10], variational iteration transform method [11, 12], optimal homotopy asymptotic method [13], and homotopy perturbation method [14, 15].

Korteweg and de Vries introduced the Korteweg–de Vries equation in 1895 to model shallow water waves in a canal [16]. The suggested system Korteweg–de Vries equations play a crucial role in diverse engineering and applied sciences such as plasma physics, water waves, hydrodynamics, and theory of the quantum field. The Korteweg–de Vries equations are usually investigated in the analysis of nonlinear dispersive waves [17]. They define the interactions among two long waves with various dispersion relations. Many researchers have been interested in these schemes, and a lot of works have been done. For example, Ghoreishi et al. applied the homotopy analysis method to achieve numerical results of a modified system of Korteweg–de Vries equations [18]. Kaya and Inan in [19] achieved traveling wave results of the system of Korteweg–de Vries and modified system of Korteweg–de Vries equations. The fractional-order system of Korteweg–de Vries equations is defined as follows:

$$\begin{aligned}\frac{\partial^{\gamma}\mathbb{U}}{\partial\mathfrak{I}^{\gamma}} &= -\rho\frac{\partial^{3}\mathbb{U}}{\partial\varphi^{3}} - 6\rho\mathbb{U}\frac{\partial\mathbb{U}}{\partial\varphi} + 6\mathbb{V}\frac{\partial\mathbb{V}}{\partial\varphi},\\ \frac{\partial^{\gamma}\mathbb{V}}{\partial\mathfrak{I}^{\gamma}} &= -\rho\frac{\partial^{3}\mathbb{V}}{\partial\varphi^{3}} - 3\vartheta\mathbb{U}\frac{\partial\mathbb{V}}{\partial\varphi}, \quad \mathfrak{I} > 0, 0 < \gamma \leq 1,\end{aligned} \tag{1}$$

where γ is the fractional-order derivative of $\mathbb{U}(\varphi,\mathfrak{I})$ and $\mathbb{V}(\varphi,\mathfrak{I})$, ϑ, and ρ are constants, respectively. The functions $\mathbb{U}(\varphi,\mathfrak{I})$ and $\mathbb{V}(\varphi,\mathfrak{I})$ are considered as important functions of time and space, disappearing for $\mathfrak{I}$ and φ, respectively. The other method eliminates to the conventional coupled Korteweg–de Vries equations since $\rho = \vartheta = 1$ is implemented.

A classic model in this hierarchy is the modified coupled Korteweg–de Vries system. The following nonlinear partial differential equations govern this model [20]:

$$\begin{aligned}\frac{\partial^{\gamma}\mathbb{U}}{\partial\mathfrak{I}^{\gamma}} &= \frac{1}{2}\frac{\partial^{3}\mathbb{U}}{\partial\mathfrak{I}^{3}} - 3\mathbb{U}^{2}\frac{\partial\mathbb{U}}{\partial\varphi} + \frac{3}{2}\mathbb{W}\frac{\partial^{2}\mathbb{V}}{\partial\varphi^{2}} + 3\frac{\partial\mathbb{V}}{\partial\varphi}\frac{\partial\mathbb{W}}{\partial\varphi}\\ &\quad + \frac{3}{2}\mathbb{V}\frac{\partial^{2}\mathbb{W}}{\partial\varphi^{2}} + 3\mathrm{yx}\frac{\partial\mathbb{U}}{\partial\varphi} + 3\mathrm{zx}\frac{\partial\mathbb{V}}{\partial\varphi} + 3\mathrm{zy}\frac{\partial\mathbb{W}}{\partial\varphi},\\ \frac{\partial^{\gamma}\mathbb{V}}{\partial\mathfrak{I}^{\gamma}} &= -\frac{\partial^{3}\mathbb{V}}{\partial\varphi^{3}} - 3\frac{\partial\mathbb{U}}{\partial\varphi}\frac{\partial\mathbb{V}}{\partial\varphi} - 3\mathbb{V}\frac{\partial^{2}\mathbb{U}}{\partial\varphi^{2}} - 3\mathbb{V}^{2}\frac{\partial\mathbb{W}}{\partial\varphi}\\ &\quad + 6\mathrm{zy}\frac{\partial\mathbb{U}}{\partial\varphi} + 3\mathbb{U}^{2}\frac{\partial\mathbb{V}}{\partial\varphi},\\ \frac{\partial^{\gamma}\mathbb{W}}{\partial\mathfrak{I}^{\gamma}} &= -\frac{\partial^{3}\mathbb{W}}{\partial\varphi^{3}} - 3\frac{\partial\mathbb{U}}{\partial\varphi}\frac{\partial\mathbb{W}}{\partial\varphi} - 3\mathbb{W}\frac{\partial^{2}\mathbb{U}}{\partial\varphi^{2}} - 3\mathbb{W}^{2}\frac{\partial\mathbb{V}}{\partial\varphi}\\ &\quad + 6\mathrm{zx}\frac{\partial\mathbb{U}}{\partial\varphi} + 3\mathbb{U}^{2}\frac{\partial\mathbb{W}}{\partial\varphi}, \quad \mathfrak{I} > 0, 0 < \gamma \leq 1.\end{aligned} \tag{2}$$

The modified Korteweg–de Vries equation in its standard type is simplified by the modified couple Korteweg–de Vries equation (2), with $\mathbb{V} = \mathbb{W} = 0$. Korteweg–de Vries models are a source of nonevolution equations with a wide range of implementations in science and engineering. The Korteweg–de Vries models, for instance, generate ion-acoustic result in fluid mechanics [21, 22]. Long waves characterise geophysical fluid dynamics in shallow and deep oceans [23, 24]. Various studies have suggested numerous systems to overcome the fractional-order Korteweg–de Vries equation employing various methodologies, such as the differential transform method [25], Adomian decomposition method [26], natural decomposition method [27], homotopy analysis method [28], Elzaki projected differential transform method [29], variational iteration method [30], new iterative method [31], modified tanh technique [32], and Lie symmetry analysis [33]. Analogously, same solutions for (2) have been suggested by Inc and Cavlak [34], Fan [35], Lin et al. [36], Inc et al. [37], and Ghoreishi et al. [18].

Daftardar-Gejji and Jafari [38] proposed an innovative iterative method of solving functional equations with approximation solutions. The new iterative approach is constructed on the justification of disappearing the nonlinear functions is identified as the iterative transformation technique [39]. This procedure is quick and accurate, and it avoids the utilization of complicated integrals, unconditioned matrix, and infinite series forms. This technique does not require any expressive parameters for the model. Numerous researchers have analyzed new iterative transformation methods to solve partial differential equations, such as the Fornberg–Whitham equation [40], KdV equation [31], and Klein–Gordon equation [41].

The Adomian decomposition method was firstly introduced by Adomian in 1980 and implemented by several investigators. In recent decades, numerous researchers have investigated the solutions of integral and differential equations by different techniques with the mixed Laplace transform. The Adomian decomposition method was modified with many integral transformations, such as Laplace, ρ-Laplace, Elzaki, Aboodh, and Mohand. Modification of Laplace Adomian decomposition method for solving nonlinear Volterra integral and integro-differential equations based on Newton Raphson formula [42] for solving nonlinear integrodifferential and Volterra integral equations based on the Newton–Raphson method, discrete Adomian decomposition technique [43] applied for investigating the fractional-order Navier–Stokes model, Laplace–Adomian decomposition method [44] study of implicit-impulsive differential equations involving Caputo-Fabrizio fractional derivative.

2. Basic Definitions

Definition 1. The fractional-order Caputo derivative is defined by

$$\begin{aligned}{}^{\mathrm{LC}}D_{\mathfrak{I}}^{\gamma}\{f(\mathfrak{I})\} &= \frac{1}{(n-\gamma)}\int_{0}^{\mathfrak{I}}(\mathfrak{I}-k)^{n-\gamma-1}f^{n}(k)\mathrm{d}k,\\ &\text{where } n < \gamma \leq n+1.\end{aligned} \tag{3}$$

Definition 2. The Laplace transformation connected with fractional Caputo derivative ${}^{\mathrm{LC}}D_{\mathfrak{I}}^{\gamma}\{f(\mathfrak{I})\}$ is expressed by

$$\mathbb{L}\left\{{}^{LC}D_{\mathfrak{I}}^{\gamma}\{f(\mathfrak{I})\}\right\}(s) = \frac{1}{s^{n-\gamma}}\left[s^{n}\mathbb{L}\{f(x,\mathfrak{I})\}(s) - s^{n-1}f(x,0) - \cdots - f^{n-1}(x,0)\right]. \tag{4}$$

Definition 3. In the Caputo sense, the Atangana–Baleanu derivative is defined as

$${}^{ABC}D_{\mathfrak{I}}^{\gamma}\{f(\mathfrak{I})\} = \frac{A(\gamma)}{1-\gamma}\int_{a}^{\mathfrak{I}} f'(k)E_{\gamma}\left[-\frac{\gamma}{1-\gamma}(1-k)^{\gamma}\right]\mathrm{d}k, \tag{5}$$

where $A(\gamma)$ is a normalization function such that $A(0) = A(1) = 1, f \in H^{1}(a,b), b > a, \gamma \in [0,1]$, and E_{γ} represents the Mittag–Leffler function.

Definition 4. The Atangana–Baleanu derivative in the Riemann–Liouville sense is defined as

$${}^{ABC}D_{\mathfrak{I}}^{\gamma}\{f(\mathfrak{I})\} = \frac{A(\gamma)}{1-\gamma}\frac{\mathrm{d}}{\mathrm{d}\mathfrak{I}}\int_{a}^{\mathfrak{I}} f(k)E_{\gamma}\left[-\frac{\gamma}{1-\gamma}(1-k)^{\gamma}\right]\mathrm{d}k. \tag{6}$$

Definition 5. The Laplace transform connected with the Atangana–Baleanu operator is defined as

$${}^{AB}D_{\mathfrak{I}}^{\gamma}\{f(\mathfrak{I})\}(s) = \frac{A(\gamma)s^{\gamma}\mathbb{L}\{f(\mathfrak{I})\}(s) - s^{\gamma-1}f(0)}{(1-\gamma)\left(s^{\gamma} + (\gamma/(1-\gamma))\right)}. \tag{7}$$

Definition 6. Consider $0 < \gamma < 1$, and f is a function of γ; then, the fractional-order integral operator of γ is given as

$${}^{ABC}I_{\mathfrak{I}}^{\gamma}\{f(\mathfrak{I})\} = \frac{1-\gamma}{A(\gamma)}f(\mathfrak{I}) + \frac{\gamma}{A(\gamma)\Gamma(\gamma)}\int_{a}^{\mathfrak{I}} f(k)(\mathfrak{I}-k)^{\gamma-1}\mathrm{d}k. \tag{8}$$

3. The General Implementation of the Modified Decomposition Method

Suppose the nonlinear fractional partial differential equations

$$\mathscr{D}_{\mathfrak{I}}^{\gamma}\mathbb{U}(\varphi,\mathfrak{I}) + \mathscr{L}\mathbb{U}(\varphi,\mathfrak{I}) + \mathscr{N}\mathbb{U}(\varphi,\mathfrak{I}) = \mathscr{H}(\varphi,\mathfrak{I}), \quad \mathfrak{I} > 0, 0 < \gamma \leq 1, \tag{9}$$

with the condition

$$\mathbb{U}(\varphi,0) = \mathscr{G}(\varphi), \tag{10}$$

where $\mathscr{D}_{\mathfrak{I}}^{\gamma} = (\partial^{\gamma}\mathbb{U}(\varphi,\mathfrak{I})/\partial\mathfrak{I}^{\gamma})$ show the fractional-order Caputo derivative operator with $0 < \gamma \leq 1$, while $\mathscr{L}$ is linear, $\mathscr{N}$ are nonlinear functions, and $\mathscr{H}(\varphi,\mathfrak{I})$ defines the source term.

Applying the Laplace transformation to (9), we get

$$\mathbb{L}\left[\mathscr{D}_{\mathfrak{I}}^{\gamma}\mathbb{U}(\varphi,\mathfrak{I}) + \mathscr{L}\mathbb{U}(\varphi,\mathfrak{I}) + \mathscr{N}\mathbb{U}(\varphi,\mathfrak{I})\right] = \mathbb{L}[\mathscr{H}(\varphi,\mathfrak{I})]. \tag{11}$$

Taking the Laplace transformation differentiation, we find

$$\frac{\nu^{\gamma}}{(\nu^{\gamma}(1-\gamma)+\gamma)}\mathscr{U}(\nu,\omega) = \sum_{\kappa=0}^{j-1}\left(\frac{1}{\nu}\right)^{\gamma-\kappa-1}\mathbb{U}^{(\kappa)}(0) + \mathbb{L}[\mathscr{L}\mathbb{U}(\varphi,\mathfrak{I}) + \mathscr{N}\mathbb{U}(\varphi,\mathfrak{I})] + \mathbb{L}[\mathscr{H}(\varphi,\mathfrak{I})]. \tag{12}$$

The inverse Laplace transformation of (12) gives

$$\mathbb{U}(\varphi,\mathfrak{I}) = \mathbb{L}^{-1}\left[\sum_{\kappa=0}^{j-1}\left(\frac{1}{\nu}\right)^{\gamma-\kappa-1}\mathbb{U}^{(\kappa)}(0) + \frac{(\nu^{\gamma}(1-\gamma)+\gamma)}{\nu^{\gamma}}\mathbb{L}[\mathscr{H}(\varphi,\mathfrak{I})]\right] - \mathbb{L}^{-1}\left[\frac{(\nu^{\gamma}(1-\gamma)+\gamma)}{\nu^{\gamma}}\mathbb{L}[\mathscr{L}\mathbb{U}(\varphi,\mathfrak{I}) + \mathscr{N}\mathbb{U}(\varphi,\mathfrak{I})]\right]. \tag{13}$$

The adomain decomposition method series form solution is defined as

$$\mathbb{U}(\varphi,\mathfrak{I}) = \sum_{j=0}^{\infty}\mathbb{U}_{j}(\varphi,\mathfrak{I}). \tag{14}$$

Thus, the nonlinear function $\mathscr{N}(\varphi,\mathfrak{I})$ can be calculated by the Adomian polynomials defined as

$$\mathscr{N}\mathbb{U}(\varphi,\mathfrak{I}) = \sum_{j=0}^{\infty}\widetilde{A}_{j}(\mathbb{U}_{0},\mathbb{U}_{1},\ldots), \quad j = 0,1,\ldots, \tag{15}$$

where

$$\widetilde{A}_{j}(\mathbb{U}_{0},\mathbb{U}_{1},\ldots) = \frac{1}{j!}\left[\frac{\mathrm{d}^{j}}{\mathrm{d}\lambda^{j}}\mathscr{N}\left(\sum_{J=0}^{\infty}\lambda^{J}\mathbb{U}_{J}\right)\right]_{\lambda=0}, \quad j > 0. \tag{16}$$

Putting (14) and (15) into (13), we have

$$\sum_{j=0}^{\infty}\mathbb{U}_{j}(\varphi,\mathfrak{I}) = \mathscr{G}(\varphi) + \widetilde{\mathscr{G}}(\varphi) - \mathbb{L}^{-1}\left[\frac{(\nu^{\gamma}(1-\gamma)+\gamma)}{\nu^{\gamma}}\mathbb{L}\left[\mathscr{L}\mathbb{U}(\varphi,\mathfrak{I}) + \sum_{j=0}^{\infty}\widetilde{A}_{j}\right]\right]. \tag{17}$$

Lastly, the iterative methodology for (17) is achieved as

$$\mathbb{U}_0(\varphi,\mathfrak{F}) = \mathcal{G}(\varphi) + \widetilde{\mathcal{G}}(\varphi), \quad j = 0,$$
$$\mathbb{U}_{j+1}(\varphi,\mathfrak{F}) = -\mathbb{L}^{-1}\left[\frac{(\nu^\gamma(1-\gamma)+\gamma)}{\nu^\gamma}\mathbb{L}\left[\mathcal{L}\mathbb{U}(\varphi,\mathfrak{F}) + \sum_{j=0}^{\infty}\widetilde{A}_j\right]\right], \quad j \geq 1. \tag{18}$$

4. The General Discussion of the New Iterative Transformation Method

Let us assume the following general fractional partial differential equation

$$\mathcal{D}_{\mathfrak{F}}^{\gamma}\mathbb{U}(\varphi,\mathfrak{F}) + \mathcal{L}\mathbb{U}(\varphi,\mathfrak{F}) + \mathcal{N}\mathbb{U}(\varphi,\mathfrak{F}) = \mathcal{H}(\varphi,\mathfrak{F}),$$
$$\mathfrak{F} > 0,\ j-1 < \gamma \leq j,\ j \in \mathbb{N}, \tag{19}$$

with the condition

$$\mathbb{U}^{(\kappa)}(\varphi,0) = \mathcal{G}_\kappa(\varphi), \quad \kappa = 0,1,2,\ldots,j-1, \tag{20}$$

where $\mathcal{L}$ and $\mathcal{N}$ are linear and nonlinear terms and $\mathcal{H}(\varphi,\mathfrak{F})$ shows the source term.

Using the Laplace transformation to (19), we get

$$\mathbb{L}\left[\mathcal{D}_{\mathfrak{F}}^{\gamma}\mathbb{U}(\varphi,\mathfrak{F}) + \mathcal{L}\mathbb{U}(\varphi,\mathfrak{F}) + \mathcal{N}\mathbb{U}(\varphi,\mathfrak{F})\right] = \mathbb{L}[\mathcal{H}(\varphi,\mathfrak{F})]. \tag{21}$$

Taking the Laplace transformation differentiation property, we get

$$\frac{\nu^\gamma}{(\nu^\gamma(1-\gamma)+\gamma)}\mathcal{U}(\nu,\omega) = \sum_{\kappa=0}^{j-1}\left(\frac{1}{\nu}\right)^{\gamma-\kappa-1}\mathbb{U}^{(\kappa)}(0) + \mathbb{L}[\mathcal{L}\mathbb{U}(\varphi,\mathfrak{F}) + \mathcal{N}\mathbb{U}(\varphi,\mathfrak{F})] + \mathbb{L}[\mathcal{H}(\varphi,\mathfrak{F})]. \tag{22}$$

The inverse Laplace transformation of (22) gives

$$\mathbb{U}(\varphi,\mathfrak{F}) = \mathbb{L}^{-1}\left[\sum_{\kappa=0}^{j-1}\left(\frac{1}{\nu}\right)^{\gamma-\kappa-1}\mathbb{U}^{(\kappa)}(0) + \frac{(\nu^\gamma(1-\gamma)+\gamma)}{\nu^\gamma}\mathbb{L}[\mathcal{H}(\varphi,\mathfrak{F})]\right] - \mathbb{L}^{-1}\left[\frac{(\nu^\gamma(1-\gamma)+\gamma)}{\nu^\gamma}\mathbb{L}[\mathcal{L}\mathbb{U}(\varphi,\mathfrak{F}) + \mathcal{N}\mathbb{U}(\varphi,\mathfrak{F})]\right]. \tag{23}$$

From the iterative connection, we achieve

$$\mathbb{U}(\varphi,\mathfrak{F}) = \sum_{j=0}^{\infty}\mathbb{U}_j(\varphi,\mathfrak{F}). \tag{24}$$

Also, the linear operator is $\mathcal{L}$; therefore,

$$\mathcal{L}\left(\sum_{j=0}^{\infty}\mathbb{U}_j(\varphi,\mathfrak{F})\right) = \sum_{j=0}^{\infty}\mathcal{L}\left[\mathbb{U}_j(\varphi,\mathfrak{F})\right], \tag{25}$$

and $\mathcal{N}$ defines the nonlinear term as in [38].

$$\mathcal{N}\left(\sum_{j=0}^{\infty}\mathbb{U}_j(\varphi,\mathfrak{F})\right) = \mathcal{N}(\mathbb{U}_0(\varphi,\mathfrak{F})) + \sum_{j=0}^{\infty}\left[\mathcal{N}\left(\sum_{k=0}^{\infty}\mathbb{U}_\kappa(\varphi,\mathfrak{F})\right) - \mathcal{N}\left(\sum_{k=1}^{\infty}\mathbb{U}_\kappa(\varphi,\mathfrak{F})\right)\right] = \mathcal{N}(\mathbb{U}_0) + \sum_{k=1}^{\infty}D_j, \tag{26}$$

where $D_j = \mathcal{N}(\sum_{\kappa=0}^{j}\mathbb{U}_\kappa) - \mathcal{N}(\sum_{\kappa=0}^{j-1}\mathbb{U}_\kappa)$.

By putting (24), (25), and (??) into (23), we obtain

$$\sum_{j=0}^{\infty}\mathbb{U}_j(\varphi,\mathfrak{F})\mathbb{L}^{-1}\left[\sum_{\kappa=0}^{j-1}\left(\frac{1}{\nu}\right)^{\gamma-\kappa-1}\mathbb{U}^{(\kappa)}(0) + \frac{(\nu^\gamma(1-\gamma)+\gamma)}{\nu^\gamma}\mathbb{L}[\mathcal{H}(\varphi,\mathfrak{F})]\right] - \mathbb{L}^{-1}\left\{\frac{(\nu^\gamma(1-\gamma)+\gamma)}{\nu^\gamma}\mathbb{L}\left[\mathcal{L}\left(\sum_{\kappa=0}^{\infty}\mathbb{U}_\kappa(\varphi,\mathfrak{F})\right) + \mathcal{N}(\mathbb{U}_0) + \sum_{\kappa=1}^{j}D_j\right]\right\}. \tag{27}$$

As a result, we determine the next iteration

$$\begin{aligned}
\mathbb{U}_0(\varphi,\mathfrak{T}) &= \mathbb{L}^{-1}\left[\sum_{\kappa=0}^{j-1}\left(\frac{1}{\nu}\right)^{\gamma-\kappa-1}\mathbb{U}^{(\kappa)}(0) + \frac{(\nu^{\gamma}(1-\gamma)+\gamma)}{\nu^{\gamma}}\mathbb{L}[\mathscr{H}(\varphi,\mathfrak{T})]\right],\\
\mathbb{U}_1(\varphi,\mathfrak{T}) &= -\mathbb{L}^{-1}\left\{\frac{(\nu^{\gamma}(1-\gamma)+\gamma)}{\nu^{\gamma}}\mathbb{L}\left[\mathscr{L}(\mathbb{U}_0(\varphi,\mathfrak{T})) + \mathscr{N}(\mathbb{U}_0(\varphi,\mathfrak{T}))\right]\right\},\\
&\vdots\\
\mathbb{U}_{j+1}(\varphi,\mathfrak{T}) &= -\mathbb{L}^{-1}\left\{\frac{(\nu^{\gamma}(1-\gamma)+\gamma)}{\nu^{\gamma}}\mathbb{L}\left[\mathscr{L}\left(\mathbb{U}_j(\varphi,\mathfrak{T})\right) + D_j\right]\right\}, \quad m \geq 1.
\end{aligned} \tag{28}$$

Finally, (19) and (20) yield the j-term result in the series form, defined as

$$\begin{aligned}
\mathbb{U}(\varphi,\mathfrak{T}) &\approx \mathbb{U}_0(\varphi,\mathfrak{T}) + \mathbb{U}_1(\varphi,\mathfrak{T}) + \mathbb{U}_2(\varphi,\mathfrak{T})\\
&\quad + \cdots + \mathbb{U}_j(\varphi,\mathfrak{T}), \quad j \in \mathbb{N}.
\end{aligned} \tag{29}$$

5. Uniqueness and Existence Solutions for the Modified Decomposition Method

Theorem 1 (uniqueness theorem). *The unique result of equation (9) provide space whenever* $0 < \varepsilon < 1$, *where* $\varepsilon = (\breve{L}_1 + \breve{L}_2 + \breve{L}_3)((1-\gamma) + (\gamma\mathfrak{T}^{\gamma}/\Gamma(\gamma+1)))$.

Proof. Assume that $J = (\mathscr{C}[I], \|.\|)$ represents all continuous mappings on the Banach space, defined on $I = [0, \mathbb{T}]$ having the norm $\|.\|$. For this, we introduce a mapping $W\colon M \mapsto M$, and we have

$$\begin{aligned}
\mathbb{U}_{n+1}(\varphi,\mathfrak{T}) = \mathbb{U}(\varphi,\mathfrak{T}) + \mathbb{L}^{-1}\Bigg[\frac{(\nu^{\gamma}(1-\gamma)+\gamma)}{\nu^{\gamma}}\mathbb{L}\big[\mathscr{L}[\mathbb{U}_n(\varphi,\mathfrak{T})]\\
+ \mathscr{R}[\mathbb{U}_n(\varphi,\mathfrak{T})] + \mathscr{N}[\mathbb{U}_n(\varphi,\mathfrak{T})]\big]\Bigg], \quad n \geq 0,
\end{aligned} \tag{30}$$

when $\mathscr{L}[\mathbb{U}(\varphi,\mathfrak{T})] \equiv (\partial^3\mathbb{U}(\varphi,\mathfrak{T})/\partial\varphi^2)$ and $\mathscr{R}[\mathbb{U}(\varphi,\mathfrak{T})] \equiv (\partial\mathbb{U}(\varphi,\mathfrak{T})/\partial\varphi)$. Suppose that $\mathscr{L}[\mathbb{U}(\varphi,\mathfrak{T})]$ and $\mathscr{M}[\mathbb{U}(\varphi,\mathfrak{T})]$ are also Lipschitzian with $|\mathscr{R}z - \mathscr{R}\breve{\mathbb{U}}| < \breve{L}_1|\mathbb{U} - \breve{\mathbb{U}}|$ and $|\mathscr{L}\mathbb{U} - \mathscr{L}\breve{\mathbb{U}}| < \breve{L}_2|\mathbb{U} - \breve{\mathbb{U}}|$ where $\breve{L}_1$ and $\breve{L}_2$ are Lipschitz constants, respectively, and $\mathbb{U}, \breve{\mathbb{U}}$ are various values of the mapping.

$$\begin{aligned}
\|W\mathbb{U} - W\breve{\mathbb{U}}\| &= \max_{\mathfrak{T}\in I}\left|\begin{array}{l}
\mathbb{L}^{-1}\left[\dfrac{(\nu^{\gamma}(1-\gamma)+\gamma)}{\nu^{\gamma}}\mathbb{L}[\mathscr{L}[\mathbb{U}(\varphi,\mathfrak{T})] + \mathscr{R}[\mathbb{U}(\varphi,\mathfrak{T})] + \mathscr{N}[\mathbb{U}(\varphi,\mathfrak{T})]]\right]\\
-\mathbb{L}^{-1}\left[\dfrac{(\nu^{\gamma}(1-\gamma)+\gamma)}{\nu^{\gamma}}\mathbb{L}[\mathscr{L}[\breve{\mathbb{U}}(\varphi,\mathfrak{T})] + \mathscr{R}[\breve{\mathbb{U}}(\varphi,\mathfrak{T})] + \mathscr{N}[\breve{\mathbb{U}}(\varphi,\mathfrak{T})]]\right]
\end{array}\right|\\
&\leq \max_{\mathfrak{T}\in I}\left|\begin{array}{l}
\mathbb{L}^{-1}\left[\dfrac{(\nu^{\gamma}(1-\gamma)+\gamma)}{\nu^{\gamma}}\mathbb{L}[\mathscr{L}[\mathbb{U}(\varphi,\mathfrak{T})] - \mathscr{L}[\breve{\mathbb{U}}(\varphi,\mathfrak{T})]]\right]\\
+\mathbb{L}^{-1}\left[\dfrac{(\nu^{\gamma}(1-\gamma)+\gamma)}{\nu^{\gamma}}\mathbb{L}[\mathscr{R}[\mathbb{U}(\varphi,\mathfrak{T})] - \mathscr{R}[\breve{\mathbb{U}}(\varphi,\mathfrak{T})]]\right]\\
+\mathbb{L}^{-1}\left[\dfrac{(\nu^{\gamma}(1-\gamma)+\gamma)}{\nu^{\gamma}}\mathbb{L}[\mathscr{N}[\mathbb{U}(\varphi,\mathfrak{T})] - \mathscr{N}[\breve{\mathbb{U}}(\varphi,\mathfrak{T})]]\right]
\end{array}\right|
\end{aligned}$$

$$\leq \max_{\mathfrak{I}\in I}\begin{bmatrix} \breve{L}_1\mathbb{L}^{-1}\left[\dfrac{(\nu^{\gamma}(1-\gamma)+\gamma)}{\nu^{\gamma}}\mathbb{L}|\mathbb{U}(\varphi,\mathfrak{I})-\breve{\mathbb{U}}(\varphi,\mathfrak{I})|\right] \\ +\breve{L}_2\mathbb{L}^{-1}\left[\dfrac{(\nu^{\gamma}(1-\gamma)+\gamma)}{\nu^{\gamma}}\mathbb{L}|\mathbb{U}(\varphi,\mathfrak{I})-\breve{\mathbb{U}}(\varphi,\mathfrak{I})|\right] \\ +\breve{L}_3\mathbb{L}^{-1}\left[\dfrac{(\nu^{\gamma}(1-\gamma)+\gamma)}{\nu^{\gamma}}\mathbb{L}|\mathbb{U}(\varphi,\mathfrak{I})-\breve{\mathbb{U}}(\varphi,\mathfrak{I})|\right] \end{bmatrix}$$
$$\leq \max_{\mathfrak{I}\in I}\left(\breve{L}_1+\breve{L}_2+\breve{L}_3\right)\mathbb{L}^{-1}\left[\dfrac{(\nu^{\gamma}(1-\gamma)+\gamma)}{\nu^{\gamma}}\mathbb{L}|\mathbb{U}(\varphi,\mathfrak{I})-\breve{\mathbb{U}}(\varphi,\mathfrak{I})|\right]$$
$$\leq \left(\breve{L}_1+\breve{L}_2+\breve{L}_3\right)\mathbb{L}^{-1}\left[\dfrac{(\nu^{\gamma}(1-\gamma)+\gamma)}{\nu^{\gamma}}\mathbb{L}\|\mathbb{U}(\varphi,\mathfrak{I})-\breve{\mathbb{U}}(\varphi,\mathfrak{I})\|\right]$$
$$=\left(\breve{L}_1+\breve{L}_2+\breve{L}_3\right)\left((1-\gamma)+\dfrac{\gamma\mathfrak{I}^{\gamma}}{\Gamma(\gamma+1)}\right)\|\mathbb{U}(\varphi,\mathfrak{I})-\breve{\mathbb{U}}(\varphi,\mathfrak{I})\|. \quad (31)$$

The mapping is a contraction under the assumption $0<\varepsilon<1$. As a result of the Banach contraction fixed point theorem, there is a unique solution to (9). As a result, the proof is complete. □

Theorem 2 (convergence analysis). *The solution general form of (9) will be convergent.*

Proof. Suppose $\widehat{S}_n$ is the nth partial sum; that is, $\widehat{W}_n=\sum_{j=0}^{n}\mathbb{U}_j(\varphi,\mathfrak{I})$. Firstly, we define that $\{\widehat{W}_n\}$ is a Banach space Cauchy sequence in M. Using into consideration of Adomian polynomials, we achieve

$$\overline{R}\left(\widehat{W}_n\right)=\breve{H}_n+\sum_{p=0}^{n-1}\breve{H}_p,$$
$$\overline{N}\left(\widehat{W}_n\right)=\breve{H}_n+\sum_{c=0}^{n-1}\breve{H}_c. \quad (32)$$

Now,

$$\left\|\widehat{W}_n-\widehat{W}_q\right\|=\max_{\mathfrak{I}\in I}\left|\widehat{W}_n-\widehat{W}_q\right|$$
$$=\max_{\mathfrak{I}\in I}\left|\sum_{j=q+1}^{n}\breve{\mathbb{U}}(\varphi,\mathfrak{I})\right|,\ (j=1,2,3,\ldots)$$
$$\leq \max_{\mathfrak{I}\in I}\begin{vmatrix} \mathbb{L}^{-1}\left[\dfrac{(\nu^{\gamma}(1-\gamma)+\gamma)}{\nu^{\gamma}}\mathbb{L}\left[\sum_{j=q+1}^{n}\mathscr{L}[\mathbb{U}_{n-1}(\varphi,\mathfrak{I})]\right]\right] \\ +\mathbb{L}^{-1}\left[\dfrac{(\nu^{\gamma}(1-\gamma)+\gamma)}{\nu^{\gamma}}\mathbb{L}\left[\sum_{j=q+1}^{n}\mathscr{R}[\mathbb{U}_{n-1}(\varphi,\mathfrak{I})]\right]\right] \\ +\mathbb{L}^{-1}\left[\dfrac{(\nu^{\gamma}(1-\gamma)+\gamma)}{\nu^{\gamma}}\mathbb{L}\left[\sum_{j=q+1}^{n}\breve{H}_{n-1}(\varphi,\mathfrak{I})\right]\right] \end{vmatrix}$$
$$=\max_{\mathfrak{I}\in I}\begin{vmatrix} \mathbb{L}^{-1}\left[\dfrac{(\nu^{\gamma}(1-\gamma)+\gamma)}{\nu^{\gamma}}\mathbb{L}\left[\sum_{j=q}^{n-1}\mathscr{L}[\mathbb{U}_{n}(\varphi,\mathfrak{I})]\right]\right] \\ +\mathbb{L}^{-1}\left[\dfrac{(\nu^{\gamma}(1-\gamma)+\gamma)}{\nu^{\gamma}}\mathbb{L}\left[\sum_{j=q}^{n-1}\mathscr{R}[\mathbb{U}_{n}(\varphi,\mathfrak{I})]\right]\right] \\ +\mathbb{L}^{-1}\left[\dfrac{(\nu^{\gamma}(1-\gamma)+\gamma)}{\nu^{\gamma}}\mathbb{L}\left[\sum_{j=q}^{n-1}\breve{H}_{n}(\varphi,\mathfrak{I})\right]\right] \end{vmatrix}$$
$$\leq \max_{\mathfrak{I}\in I}\begin{vmatrix} \mathbb{L}^{-1}\left[\dfrac{(\nu^{\gamma}(1-\gamma)+\gamma)}{\nu^{\gamma}}\mathbb{L}\left[\sum_{j=q}^{n-1}\mathscr{L}\left(\widehat{W}_{n-1}\right)-\mathscr{L}\left(\widehat{W}_{q-1}\right)\right]\right] \\ +\mathbb{L}^{-1}\left[\dfrac{(\nu^{\gamma}(1-\gamma)+\gamma)}{\nu^{\gamma}}\mathbb{L}\left[\sum_{j=q}^{n-1}\mathscr{R}\left(\widehat{W}_{n-1}\right)-\mathscr{R}\left(\widehat{W}_{q-1}\right)\right]\right] \\ +\mathbb{L}^{-1}\left[\dfrac{(\nu^{\gamma}(1-\gamma)+\gamma)}{\nu^{\gamma}}\mathbb{L}\left[\sum_{j=q}^{n-1}\mathscr{N}\left(\widehat{W}_{n-1}\right)-\mathscr{N}\left(\widehat{W}_{q-1}\right)\right]\right] \end{vmatrix}$$
$$\leq \max_{\mathfrak{I}\in I}\begin{vmatrix} \mathbb{L}^{-1}\left[\dfrac{(\nu^{\gamma}(1-\gamma)+\gamma)}{\nu^{\gamma}}\mathbb{L}\left[\mathscr{L}\left(\widehat{W}_{n-1}\right)-\mathscr{L}\left(\widehat{W}_{q-1}\right)\right]\right] \\ +\mathbb{L}^{-1}\left[\dfrac{(\nu^{\gamma}(1-\gamma)+\gamma)}{\nu^{\gamma}}\mathbb{L}\left[\mathscr{R}\left(\widehat{W}_{n-1}\right)-\mathscr{R}\left(\widehat{W}_{q-1}\right)\right]\right] \\ +\mathbb{L}^{-1}\left[\dfrac{(\nu^{\gamma}(1-\gamma)+\gamma)}{\nu^{\gamma}}\mathbb{L}\left[\mathscr{N}\left(\widehat{W}_{n-1}\right)-\mathscr{N}\left(\widehat{W}_{q-1}\right)\right]\right] \end{vmatrix}$$
$$\leq \breve{L}_1\max_{\mathfrak{I}\in I}\mathbb{L}^{-1}\left|\left[\dfrac{(\nu^{\gamma}(1-\gamma)+\gamma)}{\nu^{\gamma}}\mathbb{L}\left[\left(\widehat{W}_{n-1}\right)-\left(\widehat{W}_{q-1}\right)\right]\right]\right|$$
$$+\breve{L}_2\max_{\mathfrak{I}\in I}\left|\left[\dfrac{(\nu^{\gamma}(1-\gamma)+\gamma)}{\nu^{\gamma}}\mathbb{L}\left[\left(\widehat{W}_{n-1}\right)-\left(\widehat{W}_{q-1}\right)\right]\right]\right|$$

$$+\breve{L}_3 \max_{\mathfrak{I}\in I}\left\|\left[\frac{(\nu^{\gamma}(1-\gamma)+\gamma)}{\nu^{\gamma}}\mathbb{L}\left[\left(\widehat{W}_{n-1}\right)-\left(\widehat{W}_{q-1}\right)\right]\right]\right\|$$
$$=\left(\breve{L}_1+\breve{L}_2+\breve{L}_3\right)\left((1-\gamma)+\frac{\gamma\mathfrak{I}^{\gamma}}{\Gamma(\gamma+1)}\right)\left\|\widehat{W}_{n-1}-\widehat{W}_{q-1}\right\|. \tag{33}$$

Consider $n=q+1$; then,

$$\left\|\widehat{W}_{q+1}-\widehat{W}_q\right\|\leq\varepsilon\left\|\widehat{W}_q-\widehat{W}_{q-1}\right\|$$
$$\leq\varepsilon^2\left\|\widehat{W}_{q-1}-\widehat{W}_{q-2}\right\|\leq\cdots\leq\varepsilon^q\left\|\widehat{W}_1-\widehat{W}_0\right\|, \tag{34}$$

where $((\breve{L}_1+\breve{L}_2+\breve{L}_3)\mathfrak{I}^{(\gamma-1)}/\gamma!)$. Similarly, we have the triangular inequality

$$\left\|\widehat{W}_n-\widehat{W}_q\right\|\leq\left\|\widehat{W}_{q+1}-\widehat{W}_q\right\|+\left\|\widehat{W}_{q+2}-\widehat{W}_{q+1}\right\|$$
$$+\cdots+\left\|\widehat{W}_n-\widehat{W}_{n-1}\right\|$$
$$\leq\left[\varepsilon^q+\varepsilon^{q+1}+\cdots+\varepsilon^{n-1}\right]\left\|\widehat{W}_1-\widehat{W}_0\right\| \tag{35}$$
$$\leq\varepsilon^q\left(\frac{1-\varepsilon^{n-q}}{\varepsilon}\right)\left\|\mathbb{U}_1\right\|,$$

and since $0<\varepsilon<1$, we get $(1-\varepsilon^{n-q})<1$; then,

$$\left\|\widehat{W}_n-\widehat{W}_q\right\|\leq\frac{\varepsilon^q}{1-\varepsilon}\max_{\mathfrak{I}\in I}\left\|\mathbb{U}_1\right\|. \tag{36}$$

However, $|\mathbb{U}_1|<\infty$ (since $\mathbb{U}(\varphi,\mathfrak{I})$ is bounded). Thus, as $q\mapsto\infty$, $\|\widehat{W}_n-\widehat{W}_q\|\mapsto 0$. Hence, $\{\widehat{W}_1\}$ is a Cauchy sequence in K. As a solution, the series $\sum_{n=0}^{\infty}\mathbb{U}_n$ converges, and this completes the proof. □

Theorem 3 (error estimate). *The maximum absolute truncation error of series solution (9) to (??) is computed as*

$$\max_{\mathfrak{I}\in I}\left|\mathbb{U}(\varphi,\mathfrak{I})\sum_{n=1}^{q}\mathbb{U}_n(\varphi,\mathfrak{I})\right|\leq\frac{\varepsilon^q}{1-\varepsilon}\max_{\mathfrak{I}\in I}\left\|\mathbb{U}_1\right\|. \tag{37}$$

6. Numerical Results

This section describes several test examples by applying two novel techniques, modified decomposition technique and new iterative transformation technique, via the Atangana–Baleanu derivative operator. Also, the stability and convergence of the technique are discussed.

Example 1 (see [31]). Consider the fractional-order nonlinear system of Korteweg–de Vries equation (1) with $\vartheta=\rho=1$, with the initial conditions

$$\mathbb{U}(\varphi,0)=\varrho^2\sec h^2\left(\frac{\delta}{2}+\frac{\varrho\varphi}{2}\right),$$
$$\mathbb{V}(\varphi,0)=\sqrt{\frac{\rho}{2}}\varrho^2\sec h^2\left(\frac{\delta}{2}+\frac{\varrho\varphi}{2}\right). \tag{38}$$

Case I: first, we apply the modified decomposition technique for Example 1.

Applying the Laplace transform to (1), we get

$$\frac{\nu^{\gamma}}{(\nu^{\gamma}(1-\gamma)+\gamma)}\left\{\mathscr{U}(\varphi,\nu)-\sum_{\kappa=0}^{j-1}\left(\frac{1}{\nu}\right)^{\gamma-\kappa-1}\mathbb{U}^{(\kappa)}(0)\right\}$$
$$=\mathbb{L}\left[-\rho\frac{\partial^3\mathbb{U}}{\partial\varphi^3}-6\rho\mathbb{U}\frac{\partial\mathbb{U}}{\partial\varphi}+6\mathbb{V}\frac{\partial\mathbb{V}}{\partial\varphi}\right],$$
$$\frac{\nu^{\gamma}}{(\nu^{\gamma}(1-\gamma)+\gamma)}\left\{\mathscr{V}(\varphi,\nu)-\sum_{\kappa=0}^{j-1}\left(\frac{1}{\nu}\right)^{\gamma-\kappa-1}\mathbb{V}^{(\kappa)}(0)\right\}$$
$$=\mathbb{L}\left[-\rho\frac{\partial^3\mathbb{V}}{\partial\varphi^3}-3\rho\mathbb{U}\frac{\partial\mathbb{V}}{\partial\varphi}\right]. \tag{39}$$

In view of (38) and analytical method procedure as follows:

$$\mathscr{U}(\varphi,\nu)=\frac{1}{\nu}\mathbb{U}^{(0)}(\varphi,0)+\frac{(\nu^{\gamma}(1-\gamma)+\gamma)}{\nu^{\gamma}}\mathbb{L}$$
$$\cdot\left[-\rho\frac{\partial^3\mathbb{U}}{\partial\varphi^3}-6\rho\mathbb{U}\frac{\partial\mathbb{U}}{\partial\varphi}+6\mathbb{V}\frac{\partial\mathbb{V}}{\partial\varphi}\right],$$
$$\mathscr{V}(\varphi,\nu)=\frac{1}{\nu}\mathbb{V}^{(0)}(\varphi,0)+\frac{(\nu^{\gamma}(1-\gamma)+\gamma)}{\nu^{\gamma}}\mathbb{L} \tag{40}$$
$$\cdot\left[-\rho\frac{\partial^3\mathbb{V}}{\partial\varphi^3}-3\rho\mathbb{U}\frac{\partial\mathbb{V}}{\partial\varphi}\right].$$

Using the inverse Laplace transformation, we get

$$\mathbb{U}(\varphi,\mathfrak{I})=\mathbb{L}^{-1}\left[\frac{1}{\nu}\mathbb{U}(\varphi,0)\right]+\mathbb{L}^{-1}\left[\frac{(\nu^{\gamma}(1-\gamma)+\gamma)}{\nu^{\gamma}}\mathbb{L}\right.$$
$$\left.\cdot\left[-\rho\frac{\partial^3\mathbb{U}}{\partial\varphi^3}-6\rho\mathbb{U}\frac{\partial\mathbb{U}}{\partial\varphi}+6\mathbb{V}\frac{\partial\mathbb{V}}{\partial\varphi}\right]\right],$$
$$\mathbb{V}(\varphi,\mathfrak{I})=\mathbb{L}^{-1}\left[\frac{1}{\nu}\mathbb{V}(\varphi,0)\right]+\mathbb{L}^{-1}$$
$$\cdot\left[\frac{(\nu^{\gamma}(1-\gamma)+\gamma)}{\nu^{\gamma}}\mathbb{L}\left[-\rho\frac{\partial^3\mathbb{V}}{\partial\varphi^3}-3\rho\mathbb{U}\frac{\partial\mathbb{V}}{\partial\varphi}\right]\right]. \tag{41}$$

By morality of the modified decomposition technique, we get

$$\begin{aligned}
\mathbb{U}_0(\varphi,\mathfrak{T}) &= \mathbb{L}^{-1}\left[\frac{\omega}{\nu}\mathbb{U}(\varphi,0)\right]\\
&= \mathbb{L}^{-1}\left[\frac{1}{\nu}\varrho^2\sec h^2\left(\frac{\delta}{2}+\frac{\varrho\varphi}{2}\right)\right]\\
&= \varrho^2\sec h^2\left(\frac{\delta}{2}+\frac{\varrho\varphi}{2}\right),\\
\mathbb{V}_0(\varphi,\mathfrak{T}) &= \mathbb{L}^{-1}\left[\frac{\omega}{\nu}\mathbb{V}(\varphi,0)\right]\\
&= \sqrt{\frac{\rho}{2}}\varrho^2\sec h^2\left(\frac{\delta}{2}+\frac{\varrho\varphi}{2}\right),\\
\sum_{j=0}^{\infty}\mathbb{U}_{j+1}(\varphi,\mathfrak{T}) &= \mathbb{L}^{-1}\left[\frac{(\nu^\gamma(1-\gamma)+\gamma)}{\nu^\gamma}\mathbb{L}\right.\\
&\quad\left.\cdot\left[-\rho\sum_{j=0}^{\infty}\left(\mathbb{U}_{\varphi\varphi\varphi}\right)_j-6\rho\sum_{j=0}^{\infty}\mathscr{A}_j+6\sum_{j=0}^{\infty}\mathscr{B}_j\right]\right],\\
\sum_{j=0}^{\infty}\mathbb{V}_{j+1}(\varphi,\mathfrak{T}) &= \mathbb{L}^{-1}\left[\frac{(\nu^\gamma(1-\gamma)+\gamma)}{\nu^\gamma}\mathbb{L}\right.\\
&\quad\left.\cdot\left[-\rho\sum_{j=0}^{\infty}\left(\mathbb{V}_{\varphi\varphi\varphi}\right)_j-3\rho\sum_{j=0}^{\infty}\mathscr{C}_j\right]\right],\\
&\quad j=0,1,2,\ldots.
\end{aligned} \tag{42}$$

The Adomian polynomials' some terms are defined as follows:

$$\begin{aligned}
\mathscr{A}_0\left(\mathbb{U}\mathbb{U}_\varphi\right) &= \mathbb{U}_0\mathbb{U}_{0\varphi},\\
\mathscr{A}_1\left(\mathbb{U}\mathbb{U}_\varphi\right) &= \mathbb{U}_0\mathbb{U}_{1\varphi}+\mathbb{U}_1\mathbb{U}_{0\varphi},\\
\mathscr{A}_2\left(\mathbb{U}\mathbb{U}_\varphi\right) &= \mathbb{U}_1\mathbb{U}_{2\varphi}+\mathbb{U}_1\mathbb{U}_{1\varphi}+\mathbb{U}_2\mathbb{U}_{0\varphi},\\
\mathscr{B}_0\left(\mathbb{V}\mathbb{V}_\varphi\right) &= \mathbb{V}_0\mathbb{V}_{0\varphi},\\
\mathscr{B}_1\left(\mathbb{V}\mathbb{V}_\varphi\right) &= \mathbb{V}_0\mathbb{V}_{1\varphi}+\mathbb{V}_1\mathbb{V}_{0\varphi},\\
\mathscr{B}_2\left(\mathbb{V}\mathbb{V}_\varphi\right) &= \mathbb{V}_1\mathbb{V}_{2\varphi}+\mathbb{V}_1\mathbb{V}_{1\varphi}+\mathbb{V}_2\mathbb{V}_{0\varphi},\\
\mathscr{C}_0\left(\mathbb{U}\mathbb{V}_\varphi\right) &= \mathbb{U}_0\mathbb{V}_{0\varphi},\\
\mathscr{C}_1\left(\mathbb{U}\mathbb{V}_\varphi\right) &= \mathbb{U}_0\mathbb{V}_{1\varphi}+\mathbb{U}_1\mathbb{V}_{0\varphi},\\
\mathscr{C}_2\left(\mathbb{U}\mathbb{V}_\varphi\right) &= \mathbb{U}_1\mathbb{V}_{2\varphi}+\mathbb{U}_1\mathbb{V}_{1\varphi}+\mathbb{U}_2\mathbb{V}_{0\varphi}.
\end{aligned} \tag{43}$$

For $j=0,1,2,3,\ldots,$

$$\begin{aligned}
\mathbb{U}_1(\varphi,\mathfrak{T}) &= \mathbb{L}^{-1}\left[\frac{(\nu^\gamma(1-\gamma)+\gamma)}{\nu^\gamma}\mathbb{L}\left[-\rho\left(\mathbb{U}_{\varphi\varphi\varphi}\right)_0-6\rho\mathscr{A}_0+6\mathscr{B}_0\right]\right]\\
&= \mathbb{L}^{-1}\left[\frac{\omega^{\gamma+2}}{\nu^{\gamma+2}}\varrho^5\rho\tanh\left(\frac{\delta}{2}+\frac{\varrho\varphi}{2}\right)\sec h^2\left(\frac{\delta}{2}+\frac{\varrho\varphi}{2}\right)\right]\\
&= \varrho^5\rho\tanh\left(\frac{\delta}{2}+\frac{\varrho\varphi}{2}\right)\sec h^2\left(\frac{\delta}{2}+\frac{\varrho\varphi}{2}\right)\left((1-\gamma)+\frac{\gamma\mathfrak{T}^\gamma}{\Gamma(\gamma+1)}\right)\\
\mathbb{V}_1(\varphi,\mathfrak{T}) &= \mathbb{L}^{-1}\left[\frac{(\nu^\gamma(1-\gamma)+\gamma)}{\nu^\gamma}\mathbb{L}\left[-\rho\left(\mathbb{V}_{\varphi\varphi\varphi}\right)_0-3\rho\mathscr{C}_0\right]\right]\\
&= \frac{\varrho^5\rho^{3/2}}{\sqrt{2}}\tanh\left(\frac{\delta}{2}+\frac{\varrho\varphi}{2}\right)\sec h^2\left(\frac{\delta}{2}+\frac{\varrho\varphi}{2}\right)\left((1-\gamma)+\frac{\gamma\mathfrak{T}^\gamma}{\Gamma(\gamma+1)}\right)\\
\mathbb{U}_2(\varphi,\mathfrak{T}) &= \mathbb{L}^{-1}\left[\frac{(\nu^\gamma(1-\gamma)+\gamma)}{\nu^\gamma}\mathbb{L}\left[-\rho\left(\mathbb{U}_{\varphi\varphi\varphi}\right)_1-6\rho\mathscr{A}_1+6\mathscr{B}_1\right]\right]
\end{aligned}$$

$$\begin{aligned}
&= \mathbb{L}^{-1}\left[\frac{\omega^{2\gamma+2}}{\nu^{2\gamma+2}}\frac{\varrho^8\rho^2}{2}\left[2\cosh^2\left(\frac{\rho}{2}+\frac{\varrho\varphi}{2}\right)-3\right]\sec h^4\left(\frac{\rho}{2}+\frac{\varrho\varphi}{2}\right)\right]\\
&= \frac{\varrho^8\rho^2}{2}\left[2\cosh^2\left(\frac{\rho}{2}+\frac{\varrho\varphi}{2}\right)-3\right]\sec h^4\left(\frac{\rho}{2}+\frac{\varrho\varphi}{2}\right)\left((1-\gamma)^2+\frac{\gamma^2\mathfrak{T}^{2\gamma}}{\Gamma(2\gamma+1)}+\frac{2(1-\gamma)\gamma\mathfrak{T}^{\gamma}}{\Gamma(\gamma+1)}\right)\\
\mathbb{V}_2(\varphi,\mathfrak{T}) &= \mathbb{L}^{-1}\left[\frac{(\nu^{\gamma}(1-\gamma)+\gamma)}{\nu^{\gamma}}\mathbb{L}\left[-\rho\left(\mathbb{V}_{\varphi\varphi\varphi}\right)_1-3\rho\mathscr{C}_1\right]\right]\\
&= \frac{\varrho^5\rho^{5/2}}{2\sqrt{2}}\left[2\cosh^2\left(\frac{\rho}{2}+\frac{\varrho\varphi}{2}\right)-3\right]\sec h^4\left(\frac{\rho}{2}+\frac{\varrho\varphi}{2}\right)\left((1-\gamma)^2+\frac{\gamma^2\mathfrak{T}^{2\gamma}}{\Gamma(2\gamma+1)}+\frac{2(1-\gamma)\gamma\mathfrak{T}^{\gamma}}{\Gamma(\gamma+1)}\right)\\
&\vdots\,.
\end{aligned} \tag{44}$$

The modified decomposition technique result for Example 1 is shown as

$$\begin{aligned}
\mathbb{U}(\varphi,\mathfrak{T}) &= \mathbb{U}_0(\varphi,\mathfrak{T})+\mathbb{U}_1(\varphi,\mathfrak{T})+\mathbb{U}_2(\varphi,\mathfrak{T})+\mathbb{U}_3(\varphi,\mathfrak{T})+\cdots\\
&= \varrho^2\sec h^2\left(\frac{\delta}{2}+\frac{\varrho\varphi}{2}\right)+\varrho^5\rho\tanh\left(\frac{\delta}{2}+\frac{\varrho\varphi}{2}\right)\sec h^2\left(\frac{\delta}{2}+\frac{\varrho\varphi}{2}\right)\left((1-\gamma)+\frac{\gamma\mathfrak{T}^{\gamma}}{\Gamma(\gamma+1)}\right)\\
&\quad+\frac{\varrho^8\rho^2}{2}\left[2\cosh^2\left(\frac{\rho}{2}+\frac{\varrho\varphi}{2}\right)-3\right]\sec h^4\left(\frac{\rho}{2}+\frac{\varrho\varphi}{2}\right)\left((1-\gamma)^2+\frac{\gamma^2\mathfrak{T}^{2\gamma}}{\Gamma(2\gamma+1)}+\frac{2(1-\gamma)\gamma\mathfrak{T}^{\gamma}}{\Gamma(\gamma+1)}\right)+\cdots.
\end{aligned} \tag{45}$$

Similarly, we get

$$\begin{aligned}
\mathbb{V}(\varphi,\mathfrak{T}) = {}& \sqrt{\frac{\rho}{2}}\varrho^2\sec h^2\left(\frac{\delta}{2}+\frac{\varrho\varphi}{2}\right)+\frac{\varrho^5\rho^{3/2}}{\sqrt{2}}\tanh\left(\frac{\delta}{2}+\frac{\varrho\varphi}{2}\right)\sec h^2\left(\frac{\delta}{2}+\frac{\varrho\varphi}{2}\right)\left((1-\gamma)+\frac{\gamma\mathfrak{T}^{\gamma}}{\Gamma(\gamma+1)}\right)\\
&+\frac{\varrho^5\rho^{5/2}}{2\sqrt{2}}\left[2\cosh^2\left(\frac{\rho}{2}+\frac{\varrho\varphi}{2}\right)-3\right]\sec h^4\left(\frac{\rho}{2}+\frac{\varrho\varphi}{2}\right)\left((1-\gamma)^2+\frac{\gamma^2\mathfrak{T}^{2\gamma}}{\Gamma(2\gamma+1)}+\frac{2(1-\gamma)\gamma\mathfrak{T}^{\gamma}}{\Gamma(\gamma+1)}\right)+\cdots.
\end{aligned} \tag{46}$$

By putting $\gamma = 1$, we achieve the exact result of the system of Korteweg–de Vries equation (1):

$$\begin{aligned}
\mathbb{U}(\varphi,\mathfrak{T}) &= \varrho^2\sec h^2\left(\frac{\delta}{2}+\frac{\varrho\varphi}{2}-\frac{\rho\varrho^3\mathfrak{T}}{2}\right),\\
\mathbb{V}(\varphi,\mathfrak{T}) &= \sqrt{\frac{\rho}{2}}\varrho^2\sec h^2\left(\frac{\delta}{2}+\frac{\varrho\varphi}{2}-\frac{\rho\varrho^3\mathfrak{T}}{2}\right).
\end{aligned} \tag{47}$$

Case II: now, we apply the new iterative transformation technique on Example 1.

Using the suggested analytical method, we have

$$\begin{aligned}
\mathbb{U}_0(\varphi,\mathfrak{T}) &= \mathbb{L}^{-1}\left[\frac{1}{\nu}\mathbb{U}(\varphi,0)\right] = \mathbb{L}^{-1}\left[\frac{1}{\nu}\varrho^2 \sec h^2\left(\frac{\delta}{2}+\frac{\varrho\varphi}{2}\right)\right]\\
&= \varrho^2 \sec h^2\left(\frac{\delta}{2}+\frac{\varrho\varphi}{2}\right)\\
\mathbb{V}_0(\varphi,\mathfrak{T}) &= \mathbb{L}^{-1}\left[\frac{1}{\nu}\mathbb{V}(\varphi,0)\right]\\
\mathbb{U}_1(\varphi,\mathfrak{T}) &= \mathbb{L}^{-1}\left[\frac{(\nu^\gamma(1-\gamma)+\gamma)}{\nu^\gamma}\mathbb{L}\left[-\rho\frac{\partial^3\mathbb{U}_0}{\partial\varphi^3}-6\rho\mathbb{U}_0\frac{\partial\mathbb{U}_0}{\partial\varphi}+6\mathbb{V}_0\frac{\partial\mathbb{V}_0}{\partial\varphi}\right]\right]\\
&= \mathbb{L}^{-1}\left[\frac{(\nu^\gamma(1-\gamma)+\gamma)}{\nu^\gamma}\varrho^5\rho\tanh\left(\frac{\delta}{2}+\frac{\varrho\varphi}{2}\right)\sec h^2\left(\frac{\delta}{2}+\frac{\varrho\varphi}{2}\right)\right]\\
&= \varrho^5\rho\tanh\left(\frac{\delta}{2}+\frac{\varrho\varphi}{2}\right)\sec h^2\left(\frac{\delta}{2}+\frac{\varrho\varphi}{2}\right)\left((1-\gamma)+\frac{\gamma\mathfrak{T}^\gamma}{\Gamma(\gamma+1)}\right)\\
\mathbb{V}_1(\varphi,\mathfrak{T}) &= \mathbb{L}^{-1}\left[\frac{(\nu^\gamma(1-\gamma)+\gamma)}{\nu^\gamma}\mathbb{L}\left[-\rho\frac{\partial^3\mathbb{V}_0}{\partial\varphi^3}-3\rho\mathbb{U}_0\frac{\partial\mathbb{V}_0}{\partial\varphi}\right]\right]\\
&= \frac{\varrho^5\rho^{3/2}}{\sqrt{2}}\tanh\left(\frac{\delta}{2}+\frac{\varrho\varphi}{2}\right)\sec h^2\left(\frac{\delta}{2}+\frac{\varrho\varphi}{2}\right)\left((1-\gamma)+\frac{\gamma\mathfrak{T}^\gamma}{\Gamma(\gamma+1)}\right)\\
\mathbb{U}_2(\varphi,\mathfrak{T}) &= \mathbb{L}^{-1}\left[\frac{(\nu^\gamma(1-\gamma)+\gamma)}{\nu^\gamma}\mathbb{L}\left[-\rho\frac{\partial^3\mathbb{U}_1}{\partial\varphi^3}-6\rho\mathbb{U}_1\frac{\partial\mathbb{U}_1}{\partial\varphi}+6\mathbb{V}_1\frac{\partial\mathbb{V}_1}{\partial\varphi}\right]\right]\\
&= \mathbb{L}^{-1}\left[\frac{\omega^{2\gamma+2}}{\nu^{2\gamma+2}}\frac{\varrho^8\rho^2}{2}\left[2\cosh^2\left(\frac{\rho}{2}+\frac{\varrho\varphi}{2}\right)-3\right]\sec h^4\left(\frac{\rho}{2}+\frac{\varrho\varphi}{2}\right)\right]\\
&= \frac{\varrho^8\rho^2}{2}\left[2\cosh^2\left(\frac{\rho}{2}+\frac{\varrho\varphi}{2}\right)-3\right]\sec h^4\left(\frac{\rho}{2}+\frac{\varrho\varphi}{2}\right)\left((1-\gamma)^2+\frac{\gamma^2\mathfrak{T}^{2\gamma}}{\Gamma(2\gamma+1)}+\frac{2(1-\gamma)\gamma\mathfrak{T}^\gamma}{\Gamma(\gamma+1)}\right)\\
\mathbb{V}_2(\varphi,\mathfrak{T}) &= \mathbb{L}^{-1}\left[\frac{(\nu^\gamma(1-\gamma)+\gamma)}{\nu^\gamma}\mathbb{L}\left[-\rho\frac{\partial^3\mathbb{V}_1}{\partial\varphi^3}-3\rho\mathbb{U}_1\frac{\partial\mathbb{V}_1}{\partial\varphi}\right]\right]\\
&= \frac{\varrho^5\rho^{5/2}}{2\sqrt{2}}\left[2\cosh^2\left(\frac{\rho}{2}+\frac{\varrho\varphi}{2}\right)-3\right]\sec h^4\left(\frac{\rho}{2}+\frac{\varrho\varphi}{2}\right)\left((1-\gamma)^2+\frac{\gamma^2\mathfrak{T}^{2\gamma}}{\Gamma(2\gamma+1)}+\frac{2(1-\gamma)\gamma\mathfrak{T}^\gamma}{\Gamma(\gamma+1)}\right)\\
&\vdots\\
\mathbb{U}_n(\varphi,\mathfrak{T}) &= \mathbb{L}^{-1}\left[\frac{(\nu^\gamma(1-\gamma)+\gamma)}{\nu^\gamma}\mathbb{L}\left[-\rho\frac{\partial^3\mathbb{U}_{j-1}}{\partial\varphi^3}-6\rho\mathbb{U}_{j-1}\frac{\partial\mathbb{U}_{j-1}}{\partial\varphi}+6\mathbb{V}_{j-1}\frac{\partial\mathbb{V}_{j-1}}{\partial\varphi}\right]\right]\\
\mathbb{V}_j(\varphi,\mathfrak{T}) &= \mathbb{L}^{-1}\left[\frac{(\nu^\gamma(1-\gamma)+\gamma)}{\nu^\gamma}\mathbb{L}\left[-\rho\frac{\partial^3\mathbb{V}_{j-1}}{\partial\varphi^3}-3\rho\mathbb{U}_{j-1}\frac{\partial\mathbb{V}_{j-1}}{\partial\varphi}\right]\right].
\end{aligned}\tag{48}$$

The series of solutions for Example 1 is expressed as

$$\begin{aligned}\mathbb{U}(\varphi,\mathfrak{J}) &= \mathbb{U}_0(\varphi,\mathfrak{J}) + \mathbb{U}_1(\varphi,\mathfrak{J}) + \mathbb{U}_2(\varphi,\mathfrak{J}) \\ &\quad + \mathbb{U}_3(\varphi,\mathfrak{J}) + \cdots \mathbb{U}_j(\varphi,\mathfrak{J}), \\ \mathbb{V}(\varphi,\mathfrak{J}) &= \mathbb{V}_0(\varphi,\mathfrak{J}) + \mathbb{V}_1(\varphi,\mathfrak{J}) + \mathbb{V}_2(\varphi,\mathfrak{J}) \\ &\quad + \mathbb{V}_3(\varphi,\mathfrak{J}) + \cdots \mathbb{V}_j(\varphi,\mathfrak{J}).\end{aligned} \tag{49}$$

Consequently, we have

$$\begin{aligned}\mathbb{U}(\varphi,\mathfrak{J}) &= \varrho^2 \sec h^2\left(\frac{\delta}{2}+\frac{\varrho\varphi}{2}\right) + \varrho^5\rho \tanh\left(\frac{\delta}{2}+\frac{\varrho\varphi}{2}\right)\sec h^2\left(\frac{\delta}{2}+\frac{\varrho\varphi}{2}\right)\left((1-\gamma)+\frac{\gamma\mathfrak{J}^\gamma}{\Gamma(\gamma+1)}\right) \\ &\quad + \frac{\varrho^8\rho^2}{2}\left[2\cosh^2\left(\frac{\rho}{2}+\frac{\varrho\varphi}{2}\right)-3\right]\sec h^4\left(\frac{\rho}{2}+\frac{\varrho\varphi}{2}\right)\left((1-\gamma)^2+\frac{\gamma^2\mathfrak{J}^{2\gamma}}{\Gamma(2\gamma+1)}+\frac{2(1-\gamma)\gamma\mathfrak{J}^\gamma}{\Gamma(\gamma+1)}\right)+\cdots, \\ \mathbb{V}(\varphi,\mathfrak{J}) &= \sqrt{\frac{\rho}{2}}\varrho^2\sec h^2\left(\frac{\delta}{2}+\frac{\varrho\varphi}{2}\right) + \frac{\varrho^5\rho^{3/2}}{\sqrt{2}}\tanh\left(\frac{\delta}{2}+\frac{\varrho\varphi}{2}\right)\sec h^2\left(\frac{\delta}{2}+\frac{\varrho\varphi}{2}\right)\left((1-\gamma)+\frac{\gamma\mathfrak{J}^\gamma}{\Gamma(\gamma+1)}\right) \\ &\quad + \frac{\varrho^5\rho^{5/2}}{2\sqrt{2}}\left[2\cosh^2\left(\frac{\rho}{2}+\frac{\varrho\varphi}{2}\right)-3\right]\sec h^4\left(\frac{\rho}{2}+\frac{\varrho\varphi}{2}\right)\left((1-\gamma)^2+\frac{\gamma^2\mathfrak{J}^{2\gamma}}{\Gamma(2\gamma+1)}+\frac{2(1-\gamma)\gamma\mathfrak{J}^\gamma}{\Gamma(\gamma+1)}\right)+\cdots.\end{aligned} \tag{50}$$

By putting $\gamma = 1$, we get the exact result of the system of Korteweg–de Vries equation (1):

$$\begin{aligned}\mathbb{U}(\varphi,\mathfrak{J}) &= \varrho^2\sec h^2\left(\frac{\delta}{2}+\frac{\varrho\varphi}{2}-\frac{\rho\varrho^3\mathfrak{J}}{2}\right), \\ \mathbb{V}(\varphi,\mathfrak{J}) &= \sqrt{\frac{\rho}{2}}\varrho^2\sec h^2\left(\frac{\delta}{2}+\frac{\varrho\varphi}{2}-\frac{\rho\varrho^3\mathfrak{J}}{2}\right).\end{aligned} \tag{51}$$

In Figures 1 and 2, the actual and analytical solutions of $\mathbb{U}(\varphi,\mathfrak{J})$ and $\mathbb{V}(\varphi,\mathfrak{J})$ are proved at $\delta = 2$, $\rho = 0.5$, and $\varrho = 1$. In Figures 3 and 4, the surface and two-dimensional figure for $\mathbb{U}(\varphi,\mathfrak{J})$ and $\mathbb{V}(\varphi,\mathfrak{J})$ for numerous fractional orders are described which demonstrate that the modified decomposition technique and new iterative transformation technique obtained series form solutions are in close contact with the analytical and the exact results. This comparison shows a strong connection among the modified decomposition method and actual solutions. Consequently, the modified decomposition technique and new iterative transformation technique are accurate innovative techniques which need less calculation time and are very simple and more flexible than the homotopy analysis technique and homotopy perturbation technique.

Example 2 (see [31]). Consider the fractional-order nonlinear system of Korteweg–de Vries equation given as

$$\begin{aligned}\frac{\partial^\gamma\mathbb{U}}{\partial\mathfrak{J}^\gamma} &= -\frac{\partial\mathbb{V}}{\partial\varphi}-\frac{1}{2}\frac{\partial\mathbb{U}^2}{\partial\varphi}, \\ \frac{\partial^\gamma\mathbb{V}}{\partial\mathfrak{J}^\gamma} &= -\frac{\partial\mathbb{U}}{\partial\varphi}-\frac{\partial^3\mathbb{U}}{\partial\varphi^3}-\frac{\partial zy}{\partial\varphi}, \quad \mathfrak{J}>0, 0<\gamma\le 1,\end{aligned} \tag{52}$$

with the conditions

$$\begin{aligned}\mathbb{U}(\varphi,0) &= \rho\left[\tanh\left(\frac{\varrho}{2}+\frac{\rho\varphi}{2}\right)+1\right], \\ \mathbb{V}(\varphi,0) &= \frac{\rho^2}{2}\sec h^2\left(\frac{\varrho}{2}+\frac{\rho\varphi}{2}\right)-1.\end{aligned} \tag{53}$$

Case I: first, we apply the modified decomposition technique for Example 2.

Applying the Laplace transform to (52), we find

$$\begin{aligned}\frac{\nu^\gamma}{(\nu^\gamma(1-\gamma)+\gamma)}\mathscr{U}(\varphi,\nu) - \sum_{\kappa=0}^{j-1}\left(\frac{1}{\nu}\right)^{\gamma-\kappa-1}\mathbb{U}^{(\kappa)}(0) &= \mathbb{L}\left[-\frac{\partial\mathbb{V}}{\partial\varphi}-\frac{1}{2}\frac{\partial\mathbb{U}^2}{\partial\varphi}\right], \\ \frac{\nu^\gamma}{(\nu^\gamma(1-\gamma)+\gamma)}\mathscr{V}(\varphi,\nu) - \sum_{\kappa=0}^{j-1}\left(\frac{1}{\nu}\right)^{\gamma-\kappa-1}\mathbb{V}^{(\kappa)}(0) &= \mathbb{L}\left[-\frac{\partial\mathbb{U}}{\partial\varphi}-\frac{\partial^3\mathbb{U}}{\partial\varphi^3}-\frac{\partial zy}{\partial\varphi}\right].\end{aligned} \tag{54}$$

In view of (29) and straightforward approximate achieve

$$\mathscr{U}(\varphi, \nu) = \frac{1}{\nu}\mathbb{U}^{(0)}(\varphi, 0) + \frac{(\nu^{\gamma}(1-\gamma)+\gamma)}{\nu^{\gamma}}\mathbb{L}\left[-\frac{\partial \mathbb{V}}{\partial \varphi} - \frac{1}{2}\frac{\partial \mathbb{U}^2}{\partial \varphi}\right],$$

$$\mathscr{V}(\varphi, \nu) = \frac{1}{\nu}\mathbb{V}^{(0)}(\varphi, 0) + \frac{(\nu^{\gamma}(1-\gamma)+\gamma)}{\nu^{\gamma}}\mathbb{L} \cdot \left[-\frac{\partial \mathbb{U}}{\partial \varphi} - \frac{\partial^3 \mathbb{U}}{\partial \varphi^3} - \frac{\partial \text{zy}}{\partial \varphi}\right]. \tag{55}$$

Using the inverse Laplace transformation, we get

$$\mathbb{U}(\varphi, \mathfrak{I}) = \mathbb{L}^{-1}\left[\frac{1}{\nu}\mathbb{U}(\varphi, 0)\right] + \mathbb{L}^{-1}\left[\frac{(\nu^{\gamma}(1-\gamma)+\gamma)}{\nu^{\gamma}}\mathbb{L} \cdot \left[-\frac{\partial \mathbb{V}}{\partial \varphi} - \frac{1}{2}\frac{\partial \mathbb{U}^2}{\partial \varphi}\right]\right],$$

$$\mathbb{V}(\varphi, \mathfrak{I}) = \mathbb{L}^{-1}\left[\frac{1}{\nu}\mathbb{V}(\varphi, 0)\right] + \mathbb{L}^{-1}\left[\frac{(\nu^{\gamma}(1-\gamma)+\gamma)}{\nu^{\gamma}}\mathbb{L} \cdot \left[-\frac{\partial \mathbb{U}}{\partial \varphi} - \frac{\partial^3 \mathbb{U}}{\partial \varphi^3} - \frac{\partial \text{zy}}{\partial \varphi}\right]\right]. \tag{56}$$

By the consequence of the modified decomposition technique, we get

$$\begin{aligned}\mathbb{U}_0(\varphi, \mathfrak{I}) &= \mathbb{L}^{-1}\left[\frac{1}{\nu}\mathbb{U}(\varphi, 0)\right] \\ &= \mathbb{L}^{-1}\left[\frac{1}{\nu}\rho\left(\tanh\left(\frac{\varrho}{2} + \frac{\rho\varphi}{2}\right) + 1\right)\right] \\ &= \rho\left(\tanh\left(\frac{\varrho}{2} + \frac{\rho\varphi}{2}\right) + 1\right),\end{aligned} \tag{57}$$

$$\mathbb{V}_0(\varphi, \mathfrak{I}) = \mathbb{L}^{-1}\left[\frac{1}{\nu}\mathbb{V}(\varphi, 0)\right]$$

It follows that

$$\sum_{j=0}^{\infty}\mathbb{U}_{j+1}(\varphi, \mathfrak{I}) = \mathbb{L}^{-1}\left[\frac{(\nu^{\gamma}(1-\gamma)+\gamma)}{\nu^{\gamma}}\mathbb{L} \cdot \left[-\rho\sum_{j=0}^{\infty}\left(\mathbb{V}_{\varphi}\right)_j - \frac{1}{2}\sum_{j=0}^{\infty}\mathscr{D}_j\right]\right],$$

$$\sum_{j=0}^{\infty}\mathbb{V}_{j+1}(\varphi, \mathfrak{I}) = \mathbb{L}^{-1}\left[\frac{(\nu^{\gamma}(1-\gamma)+\gamma)}{\nu^{\gamma}}\mathbb{L} \cdot \left[-\sum_{j=0}^{\infty}\left(\mathbb{U}_{\varphi}\right)_j - \sum_{j=0}^{\infty}\left(\mathbb{V}_{\varphi\varphi\varphi}\right)_j - \sum_{j=0}^{\infty}\left(\mathbb{U}\mathbb{V}_{\varphi}\right)_j\right]\right],$$

$$j = 0, 1, 2, \ldots. \tag{58}$$

The Adomian polynomials' some terms are expressed as

$$\begin{aligned}\mathscr{D}_0\left(\mathbb{U}^2\right) &= \mathbb{U}_0^2, \\ \mathscr{D}_1\left(\mathbb{U}^2\right) &= 2\mathbb{U}_0\mathbb{U}_1, \\ \mathscr{D}_2\left(\mathbb{U}^2\right) &= 2\mathbb{U}_0\mathbb{U}_2 + \mathbb{U}_1^2.\end{aligned} \tag{59}$$

For $j = 0, 1, 2, \ldots,$

$$\begin{aligned}\mathbb{U}_1(\varphi, \mathfrak{I}) &= \mathbb{L}^{-1}\left[\frac{(\nu^{\gamma}(1-\gamma)+\gamma)}{\nu^{\gamma}}\mathbb{L}\left[-\rho\left(\mathbb{V}_{\varphi}\right)_0 - \frac{1}{2}\mathscr{D}_0\right]\right] \\ &= -\frac{\rho^2}{2}\mathbb{L}^{-1}\left[\frac{\omega^{\gamma+2}}{\nu^{\gamma+2}}\sec h^2\left(\frac{\varrho}{2} + \frac{\rho\varphi}{2}\right)\right] \\ &= -\frac{\rho^2}{2}\sec h^2\left(\frac{\varrho}{2} + \frac{\rho\varphi}{2}\right)\left((1-\gamma) + \frac{\gamma\mathfrak{I}^{\gamma}}{\Gamma(\gamma+1)}\right)\end{aligned}$$

$$\mathbb{V}_1(\varphi, \mathfrak{I}) = \mathbb{L}^{-1}\left[\frac{(\nu^{\gamma}(1-\gamma)+\gamma)}{\nu^{\gamma}}\mathbb{L}\left[-\left(\mathbb{U}_{\varphi}\right)_0 - \left(\mathbb{V}_{\varphi\varphi\varphi}\right)_0 - \left((\text{zy})_{\varphi}\right)_0\right]\right]$$

$$
\begin{aligned}
&= \frac{\rho^3}{2}\sinh\left(\frac{\varrho}{2}+\frac{\rho\varphi}{2}\right)\sec h^3\left(\frac{\varrho}{2}+\frac{\rho\varphi}{2}\right)\left((1-\gamma)+\frac{\gamma\mathfrak{I}^\gamma}{\Gamma(\gamma+1)}\right)\\
\mathbb{U}_2(\varphi,\mathfrak{I}) &= \mathbb{L}^{-1}\left[\frac{(\nu^\gamma(1-\gamma)+\gamma)}{\nu^\gamma}\mathbb{L}\left[-\rho(\mathbb{V}_\varphi)_1-\frac{1}{2}\mathscr{D}_1\right]\right]\\
&= \mathbb{L}^{-1}\left[-\frac{\rho^5}{4}\sec h^2\left(\frac{\varrho}{2}+\frac{\rho\varphi}{2}\right)+\frac{3\rho^5}{4}\frac{\omega^{2\gamma+2}}{\nu^{2\gamma+2}}\sinh^2\left(\frac{\varrho}{2}+\frac{\rho\varphi}{2}\right)\sec h^4\left(\frac{\varrho}{2}+\frac{\rho\varphi}{2}\right)\right]\\
&\quad+\frac{\rho^7}{4}\mathbb{L}^{-1}\left[\frac{\Gamma(2\gamma+1)}{\Gamma^2(\gamma+1)}\frac{\omega^{3\gamma+2}}{\nu^{3\gamma+2}}\sinh\left(\frac{\varrho}{2}+\frac{\rho\varphi}{2}\right)\sec h^5\left(\frac{\varrho}{2}+\frac{\rho\varphi}{2}\right)\right]\\
&= \left[-\frac{\rho^5}{4}\sec h^2\left(\frac{\varrho}{2}+\frac{\rho\varphi}{2}\right)+\frac{3\rho^5}{4}\sinh^2\left(\frac{\varrho}{2}+\frac{\rho\varphi}{2}\right)\sec h^4\left(\frac{\varrho}{2}+\frac{\rho\varphi}{2}\right)\right]\left((1-\gamma)+\frac{\gamma\mathfrak{I}^\gamma}{\Gamma(\gamma+1)}\right)\\
&\quad+\frac{2(1-\gamma)\gamma\mathfrak{I}^\gamma}{\Gamma(\gamma+1)}+\frac{\rho^7}{4}\sinh\left(\frac{\varrho}{2}+\frac{\rho\varphi}{2}\right)\sec h^5\left(\frac{\varrho}{2}+\frac{\rho\varphi}{2}\right)\frac{\Gamma(2\gamma+1)\mathfrak{I}^{3\gamma}}{\Gamma^2(\gamma+1)\Gamma(3\gamma+1)}\\
\mathbb{V}_2(\varphi,\mathfrak{I}) &= \mathbb{L}^{-1}\left[\frac{(\nu^\gamma(1-\gamma)+\gamma)}{\nu^\gamma}\left[-(\mathbb{U}_\varphi)_1-(\mathbb{V}_{\varphi\varphi\varphi})_1-((\mathrm{zy})_\varphi)_1\right]\right]\\
&= \frac{\rho^6}{4}\left[2\cosh^2\left(\frac{\varrho}{2}+\frac{\rho\varphi}{2}\right)-3\right]\sec h^4\left(\frac{\varrho}{2}+\frac{\rho\varphi}{2}\right)\left((1-\gamma)^2+\frac{\gamma^2\mathfrak{I}^{2\gamma}}{\Gamma(2\gamma+1)}+\frac{2(1-\gamma)\gamma\mathfrak{I}^\gamma}{\Gamma(\gamma+1)}\right)\\
&\ \vdots .
\end{aligned}
\tag{60}
$$

The modified decomposition technique result for Example 2 is represented as

$$
\begin{aligned}
\mathbb{U}(\varphi,\mathfrak{I}) &= \mathbb{U}_0(\varphi,\mathfrak{I})+\mathbb{U}_1(\varphi,\mathfrak{I})+\mathbb{U}_2(\varphi,\mathfrak{I})+\cdots,\\
&= \rho\left(\tanh\left(\frac{\varrho}{2}+\frac{\rho\varphi}{2}\right)+1\right)-\frac{\rho^2}{2}\sec h^2\left(\frac{\varrho}{2}+\frac{\rho\varphi}{2}\right)\left((1-\gamma)+\frac{\gamma\mathfrak{I}^\gamma}{\Gamma(\gamma+1)}\right)\\
&\quad+\left[-\frac{\rho^5}{4}\sec h^2\left(\frac{\varrho}{2}+\frac{\rho\varphi}{2}\right)+\frac{3\rho^5}{4}\sinh^2\left(\frac{\varrho}{2}+\frac{\rho\varphi}{2}\right)\sec h^4\left(\frac{\varrho}{2}+\frac{\rho\varphi}{2}\right)\right]\left((1-\gamma)+\frac{\gamma\mathfrak{I}^\gamma}{\Gamma(\gamma+1)}\right)\\
&\quad+\frac{2(1-\gamma)\gamma\mathfrak{I}^\gamma}{\Gamma(\gamma+1)}+\frac{\rho^7}{4}\sinh\left(\frac{\varrho}{2}+\frac{\rho\varphi}{2}\right)\sec h^5\left(\frac{\varrho}{2}+\frac{\rho\varphi}{2}\right)\frac{\Gamma(2\gamma+1)\mathfrak{I}^{3\gamma}}{\Gamma^2(\gamma+1)\Gamma(3\gamma+1)}+\cdots.
\end{aligned}
\tag{61}
$$

Consequently, we get

$$
\begin{aligned}
\mathbb{V}(\varphi,\mathfrak{I}) &= -1+\frac{\rho^2}{2}\sec h^2\left(\frac{\varrho}{2}+\frac{\rho\varphi}{2}\right)+\frac{\rho^3}{2}\sinh\left(\frac{\varrho}{2}+\frac{\rho\varphi}{2}\right)\sec h^3\left(\frac{\varrho}{2}+\frac{\rho\varphi}{2}\right)\left((1-\gamma)+\frac{\gamma\mathfrak{I}^\gamma}{\Gamma(\gamma+1)}\right)\\
&\quad+\frac{\rho^6}{4}\left[2\cosh^2\left(\frac{\varrho}{2}+\frac{\rho\varphi}{2}\right)-3\right]\sec h^4\left(\frac{\varrho}{2}+\frac{\rho\varphi}{2}\right)\left((1-\gamma)^2+\frac{\gamma^2\mathfrak{I}^{2\gamma}}{\Gamma(2\gamma+1)}+\frac{2(1-\gamma)\gamma\mathfrak{I}^\gamma}{\Gamma(\gamma+1)}\right)+\cdots.
\end{aligned}
\tag{62}
$$

By putting $\gamma=1$, we achieve the exact result of the system of Korteweg–de Vries equation:

$$\begin{aligned}
\mathbb{U}(\varphi,\mathfrak{J}) &= \rho\left(\tanh\left(\frac{\varrho}{2}+\frac{\rho\varphi}{2}-\frac{\rho^2\mathfrak{J}}{2}\right)+1\right),\\
\mathbb{V}(\varphi,\mathfrak{J}) &= \frac{\rho^2}{2}\sec h^2\left(\frac{\varrho}{2}+\frac{\rho\varphi}{2}-\frac{\rho^2\mathfrak{J}}{2}\right)-1.
\end{aligned} \tag{63}$$

Case II: now, we implement the new iterative transformation technique on Example 2.

By using the suggested analytical technique, we get

$$\begin{aligned}
\mathbb{U}_0(\varphi,\mathfrak{J}) &= \mathbb{L}^{-1}\left[\frac{1}{\nu}\mathbb{U}(\varphi,0)\right] = \mathbb{L}^{-1}\left[\frac{1}{\nu}\rho\left(\tanh\left(\frac{\varrho}{2}+\frac{\rho\varphi}{2}\right)+1\right)\right]\\
&= \rho\left(\tanh\left(\frac{\varrho}{2}+\frac{\rho\varphi}{2}\right)+1\right)\\
\mathbb{V}_0(\varphi,\mathfrak{J}) &= \mathbb{L}^{-1}\left[\frac{1}{\nu}\mathbb{V}(\varphi,0)\right]\\
\mathbb{U}_1(\varphi,\mathfrak{J}) &= \mathbb{L}^{-1}\left[\frac{(\nu^\gamma(1-\gamma)+\gamma)}{\nu^\gamma}\mathbb{L}\left[-\frac{\partial\mathbb{V}_0}{\partial\varphi}-\frac{1}{2}\frac{\partial\mathbb{U}_0^2}{\partial\varphi}\right]\right]\\
&= -\frac{\rho^2}{2}\mathbb{L}^{-1}\left[\frac{\omega^{\gamma+2}}{\nu^{\gamma+2}}\sec h^2\left(\frac{\varrho}{2}+\frac{\rho\varphi}{2}\right)\right]\\
&= -\frac{\rho^2}{2}\sec h^2\left(\frac{\varrho}{2}+\frac{\rho\varphi}{2}\right)\left((1-\gamma)+\frac{\gamma\mathfrak{J}^\gamma}{\Gamma(\gamma+1)}\right)\\
\mathbb{V}_1(\varphi,\mathfrak{J}) &= \mathbb{L}^{-1}\left[\frac{(\nu^\gamma(1-\gamma)+\gamma)}{\nu^\gamma}\mathbb{L}\left[-\frac{\partial\mathbb{U}_0}{\partial\varphi}-\frac{\partial^3\mathbb{U}_0}{\partial\varphi^3}-\frac{\partial\mathbb{U}_0\mathbb{V}_0}{\partial\varphi}\right]\right]\\
&= \frac{\rho^3}{2}\sinh\left(\frac{\varrho}{2}+\frac{\rho\varphi}{2}\right)\sec h^3\left(\frac{\varrho}{2}+\frac{\rho\varphi}{2}\right)\left((1-\gamma)+\frac{\gamma\mathfrak{J}^\gamma}{\Gamma(\gamma+1)}\right)\\
\mathbb{U}_2(\varphi,\mathfrak{J}) &= \mathbb{L}^{-1}\left[\frac{(\nu^\gamma(1-\gamma)+\gamma)}{\nu^\gamma}\mathbb{L}\left[-\frac{\partial\mathbb{V}_1}{\partial\varphi}-\frac{1}{2}\frac{\partial\mathbb{U}_1^2}{\partial\varphi}\right]\right]\\
&= \mathbb{L}^{-1}\left[-\frac{\rho^5}{4}\sec h^2\left(\frac{\varrho}{2}+\frac{\rho\varphi}{2}\right)+\frac{3\rho^5}{4}\frac{\omega^{2\gamma+2}}{\nu^{2\gamma+2}}\sinh^2\left(\frac{\varrho}{2}+\frac{\rho\varphi}{2}\right)\sec h^4\left(\frac{\varrho}{2}+\frac{\rho\varphi}{2}\right)\right]\\
&\quad+\frac{\rho^7}{4}\mathbb{L}^{-1}\left[\frac{\Gamma(2\gamma+1)}{\Gamma^2(\gamma+1)}\frac{\omega^{3\gamma+2}}{\nu^{3\gamma+2}}\sinh\left(\frac{\varrho}{2}+\frac{\rho\varphi}{2}\right)\sec h^5\left(\frac{\varrho}{2}+\frac{\rho\varphi}{2}\right)\right]\\
&= \left[-\frac{\rho^5}{4}\sec h^2\left(\frac{\varrho}{2}+\frac{\rho\varphi}{2}\right)+\frac{3\rho^5}{4}\sinh^2\left(\frac{\varrho}{2}+\frac{\rho\varphi}{2}\right)\sec h^4\left(\frac{\varrho}{2}+\frac{\rho\varphi}{2}\right)\right]\left((1-\gamma)+\frac{\gamma\mathfrak{J}^\gamma}{\Gamma(\gamma+1)}\right)\\
&\quad+\frac{2(1-\gamma)\gamma\mathfrak{J}^\gamma}{\Gamma(\gamma+1)}+\frac{\rho^7}{4}\sinh\left(\frac{\varrho}{2}+\frac{\rho\varphi}{2}\right)\sec h^5\left(\frac{\varrho}{2}+\frac{\rho\varphi}{2}\right)\frac{\Gamma(2\gamma+1)\mathfrak{J}^{3\gamma}}{\Gamma^2(\gamma+1)\Gamma(3\gamma+1)}\\
\mathbb{V}_2(\varphi,\mathfrak{J}) &= \mathbb{L}^{-1}\left[\frac{(\nu^\gamma(1-\gamma)+\gamma)}{\nu^\gamma}\left[-\frac{\partial\mathbb{U}_1}{\partial\varphi}-\frac{\partial^3\mathbb{U}_1}{\partial\varphi^3}-\frac{\partial\mathbb{U}_1\mathbb{V}_1}{\partial\varphi}\right]\right]\\
&= \frac{\rho^6}{4}\left[2\cosh^2\left(\frac{\varrho}{2}+\frac{\rho\varphi}{2}\right)-3\right]\sec h^4\left(\frac{\varrho}{2}+\frac{\rho\varphi}{2}\right)\left((1-\gamma)^2+\frac{\gamma^2\mathfrak{J}^{2\gamma}}{\Gamma(2\gamma+1)}+\frac{2(1-\gamma)\gamma\mathfrak{J}^\gamma}{\Gamma(\gamma+1)}\right)\\
&\vdots\\
\mathbb{U}_j(\varphi,\mathfrak{J}) &= \mathbb{L}^{-1}\left[\frac{(\nu^\gamma(1-\gamma)+\gamma)}{\nu^\gamma}\mathbb{L}\left[-\frac{\partial\mathbb{V}_{j-1}}{\partial\varphi}-\frac{1}{2}\frac{\partial\mathbb{U}_{j-1}^2}{\partial\varphi}\right]\right]\\
\mathbb{V}_j(\varphi,\mathfrak{J}) &= \mathbb{L}^{-1}\left[\frac{(\nu^\gamma(1-\gamma)+\gamma)}{\nu^\gamma}\left[-\frac{\partial\mathbb{U}_{j-1}}{\partial\varphi}-\frac{\partial^3\mathbb{U}_{j-1}}{\partial\varphi^3}-\frac{\partial\mathbb{U}_{j-1}\mathbb{V}_{j-1}}{\partial\varphi}\right]\right].
\end{aligned} \tag{64}$$

The series of results for Example 2 is expressed as

$$\mathbb{U}(\varphi,\mathfrak{I}) = \mathbb{U}_0(\varphi,\mathfrak{I}) + \mathbb{U}_1(\varphi,\mathfrak{I}) + \mathbb{U}_2(\varphi,\mathfrak{I}) + \cdots \mathbb{U}_j(\varphi,\mathfrak{I}),$$
$$\mathbb{V}(\varphi,\mathfrak{I}) = \mathbb{V}_0(\varphi,\mathfrak{I}) + \mathbb{V}_1(\varphi,\mathfrak{I}) + \mathbb{V}_2(\varphi,\mathfrak{I}) + \cdots \mathbb{V}_j(\varphi,\mathfrak{I}). \quad (65)$$

Consequently, we have

$$\mathbb{U}(\varphi,\mathfrak{I}) = \rho\left(\tanh\left(\frac{\varrho}{2}+\frac{\rho\varphi}{2}\right)+1\right) - \frac{\rho^2}{2}\sec h^2\left(\frac{\varrho}{2}+\frac{\rho\varphi}{2}\right)\left((1-\gamma)+\frac{\gamma\mathfrak{I}^\gamma}{\Gamma(\gamma+1)}\right)$$
$$+\left[-\frac{\rho^5}{4}\sec h^2\left(\frac{\varrho}{2}+\frac{\rho\varphi}{2}\right)+\frac{3\rho^5}{4}\sinh^2\left(\frac{\varrho}{2}+\frac{\rho\varphi}{2}\right)\sec h^4\left(\frac{\varrho}{2}+\frac{\rho\varphi}{2}\right)\right]\left((1-\gamma)+\frac{\gamma\mathfrak{I}^\gamma}{\Gamma(\gamma+1)}\right)$$
$$+\frac{2(1-\gamma)\gamma\mathfrak{I}^\gamma}{\Gamma(\gamma+1)}+\frac{\rho^7}{4}\sinh\left(\frac{\varrho}{2}+\frac{\rho\varphi}{2}\right)\sec h^5\left(\frac{\varrho}{2}+\frac{\rho\varphi}{2}\right)\frac{\Gamma(2\gamma+1)\mathfrak{I}^{3\gamma}}{\Gamma^2(\gamma+1)\Gamma(3\gamma+1)}+\cdots \quad (66)$$
$$\mathbb{V}(\varphi,\mathfrak{I}) = -1+\frac{\rho^2}{2}\sec h^2\left(\frac{\varrho}{2}+\frac{\rho\varphi}{2}\right)+\frac{\rho^3}{2}\sinh\left(\frac{\varrho}{2}+\frac{\rho\varphi}{2}\right)\sec h^3\left(\frac{\varrho}{2}+\frac{\rho\varphi}{2}\right)\left((1-\gamma)+\frac{\gamma\mathfrak{I}^\gamma}{\Gamma(\gamma+1)}\right)$$
$$\frac{\rho^6}{4}\left[2\cosh^2\left(\frac{\varrho}{2}+\frac{\rho\varphi}{2}\right)-3\right]\sec h^4\left(\frac{\varrho}{2}+\frac{\rho\varphi}{2}\right)\left((1-\gamma)^2+\frac{\gamma^2\mathfrak{I}^{2\gamma}}{\Gamma(2\gamma+1)}+\frac{2(1-\gamma)\gamma\mathfrak{I}^\gamma}{\Gamma(\gamma+1)}\right)+\cdots.$$

By putting $\gamma = 1$, we obtain the actual result of the system of Korteweg–de Vries equation (??):

$$\mathbb{U}(\varphi,\mathfrak{I}) = \rho\left(\tanh\left(\frac{\varrho}{2}+\frac{\rho\varphi}{2}-\frac{\rho^2\mathfrak{I}}{2}\right)+1\right),$$
$$\mathbb{V}(\varphi,\mathfrak{I}) = \frac{\rho^2}{2}\sec h^2\left(\frac{\varrho}{2}+\frac{\rho\varphi}{2}-\frac{\rho^2\mathfrak{I}}{2}\right)-1. \quad (67)$$

In Figures 5 and 6, the actual and analytical solutions of $\mathbb{U}(\varphi,\mathfrak{I})$ and $\mathbb{V}(\varphi,\mathfrak{I})$ are proved at $\delta = 2$, $\rho = 0.5$, and $\varrho = 1$. In Figures 7 and 8, the surface and two-dimensional figure for $\mathbb{U}(\varphi,\mathfrak{I})$ and $\mathbb{V}(\varphi,\mathfrak{I})$ for numerous fractional orders are described which demonstrate that the modified decomposition technique and new iterative transformation technique approximated obtained results are in close contact with the analytical and the exact results. This comparison shows a strong connection among the modified decomposition method and actual solutions. Consequently, the modified decomposition technique and new iterative transformation technique are accurate innovative techniques which need less calculation time and are very simple and more flexible than the homotopy analysis technique and homotopy perturbation technique.

Example 3. (see [31]). Consider the fractional-order nonlinear system of modified Korteweg–de Vries equations given as (2) with the conditions

$$\mathbb{U}(\varphi,0) = \frac{2+\tanh\varphi}{2},$$
$$\mathbb{V}(\varphi,0) = \frac{2-\tanh\varphi}{4}, \quad (68)$$
$$\mathbb{W}(\varphi,0) = 2-\tanh\varphi.$$

Case I: first, we apply the modified decomposition technique for Example 3.

Using the Laplace transformation to (2), we have

$$\frac{\nu^\gamma}{(\nu^\gamma(1-\gamma)+\gamma)}\mathcal{U}(\varphi,\nu) - \sum_{\kappa=0}^{j-1}\left(\frac{1}{\nu}\right)^{\gamma-\kappa-1}\mathbb{U}^{(\kappa)}(0) = \mathbb{L}\left[\frac{1}{2}\frac{\partial^3\mathbb{U}}{\partial\mathfrak{I}^3} - 3\mathbb{U}^2\frac{\partial\mathbb{U}}{\partial\varphi}+\frac{3}{2}\mathbb{W}\frac{\partial^2\mathbb{V}}{\partial\varphi^2}+3\frac{\partial\mathbb{V}}{\partial\varphi}\frac{\partial\mathbb{W}}{\partial\varphi}+\frac{3}{2}\mathbb{V}\frac{\partial^2\mathbb{W}}{\partial\varphi^2}\right.$$
$$\left.+3yx\frac{\partial\mathbb{U}}{\partial\varphi}+3zx\frac{\partial\mathbb{V}}{\partial\varphi}+3zy\frac{\partial\mathbb{W}}{\partial\varphi}\right],$$

$$\frac{\nu^{\gamma}}{(\nu^{\gamma}(1-\gamma)+\gamma)}\mathscr{V}(\varphi,\nu)-\sum_{\kappa=0}^{j-1}\left(\frac{1}{\nu}\right)^{\gamma-\kappa-1}\mathbb{V}^{(\kappa)}(0)=\mathbb{L}\left[-\frac{\partial^3\mathbb{V}}{\partial\varphi^3}-3\frac{\partial\mathbb{U}}{\partial\varphi}\frac{\partial\mathbb{V}}{\partial\varphi}-3\mathbb{V}\frac{\partial^2\mathbb{U}}{\partial\varphi^2}-3\mathbb{V}^2\frac{\partial\mathbb{W}}{\partial\varphi}+6zy\frac{\partial\mathbb{U}}{\partial\varphi}+3\mathbb{U}^2\frac{\partial\mathbb{V}}{\partial\varphi}\right],$$
$$\frac{\nu^{\gamma}}{(\nu^{\gamma}(1-\gamma)+\gamma)}\mathscr{W}(\varphi,\nu)-\sum_{\kappa=0}^{j-1}\left(\frac{1}{\nu}\right)^{\gamma-\kappa-1}\mathbb{W}^{(\kappa)}(0)=\mathbb{L}\left[-\frac{\partial^3\mathbb{W}}{\partial\varphi^3}-3\frac{\partial\mathbb{U}}{\partial\varphi}\frac{\partial\mathbb{W}}{\partial\varphi}-3\mathbb{W}\frac{\partial^2\mathbb{U}}{\partial\varphi^2}-3\mathbb{V}^2\frac{\partial\mathbb{W}}{\partial\varphi}+6zy\frac{\partial\mathbb{U}}{\partial\varphi}+3\mathbb{U}^2\frac{\partial\mathbb{V}}{\partial\varphi}\right]. \tag{69}$$

In view of (68) and straightforward calculations,

$$\mathscr{U}(\varphi,\nu)=\frac{1}{\nu}\mathbb{U}^{(0)}(\varphi,0)+\frac{(\nu^{\gamma}(1-\gamma)+\gamma)}{\nu^{\gamma}}\mathbb{L}\left[\frac{1}{2}\frac{\partial^3\mathbb{U}}{\partial\mathfrak{F}^3}-3\mathbb{U}^2\frac{\partial\mathbb{U}}{\partial\varphi}+\frac{3}{2}\mathbb{W}\frac{\partial^2\mathbb{V}}{\partial\varphi^2}+3\frac{\partial\mathbb{V}}{\partial\varphi}\frac{\partial\mathbb{W}}{\partial\varphi}+\frac{3}{2}\mathbb{V}\frac{\partial^2\mathbb{W}}{\partial\varphi^2}\right.$$
$$\left.+3yx\frac{\partial\mathbb{U}}{\partial\varphi}+3zx\frac{\partial\mathbb{V}}{\partial\varphi}+3zy\frac{\partial\mathbb{W}}{\partial\varphi}\right],$$
$$\mathscr{V}(\varphi,\nu)=\frac{1}{\nu}\mathbb{V}^{(0)}(\varphi,0)+\frac{(\nu^{\gamma}(1-\gamma)+\gamma)}{\nu^{\gamma}}\mathbb{L}\left[-\frac{\partial^3\mathbb{V}}{\partial\varphi^3}-3\frac{\partial\mathbb{U}}{\partial\varphi}\frac{\partial\mathbb{V}}{\partial\varphi}-3\mathbb{V}\frac{\partial^2\mathbb{U}}{\partial\varphi^2}-3\mathbb{V}^2\frac{\partial\mathbb{W}}{\partial\varphi}+6zy\frac{\partial\mathbb{U}}{\partial\varphi}+3\mathbb{U}^2\frac{\partial\mathbb{V}}{\partial\varphi}\right],$$
$$\mathscr{W}(\varphi,\nu)=\frac{1}{\nu}\mathbb{W}^{(0)}(\varphi,0)+\frac{(\nu^{\gamma}(1-\gamma)+\gamma)}{\nu^{\gamma}}\mathbb{L}\left[-\frac{\partial^3\mathbb{W}}{\partial\varphi^3}-3\frac{\partial\mathbb{U}}{\partial\varphi}\frac{\partial\mathbb{W}}{\partial\varphi}-3\mathbb{W}\frac{\partial^2\mathbb{U}}{\partial\varphi^2}-3\mathbb{W}^2\frac{\partial\mathbb{V}}{\partial\varphi}+6zx\frac{\partial\mathbb{U}}{\partial\varphi}+3\mathbb{U}^2\frac{\partial\mathbb{W}}{\partial\varphi}\right]. \tag{70}$$

Applying the Laplace transform, we have

$$\mathbb{U}(\varphi,\mathfrak{F})=\mathbb{L}^{-1}\left[\frac{1}{\nu}\mathbb{U}(\varphi,0)\right]+\mathbb{L}^{-1}\left[\frac{(\nu^{\gamma}(1-\gamma)+\gamma)}{\nu^{\gamma}}\mathbb{L}\left[\frac{1}{2}\frac{\partial^3\mathbb{U}}{\partial\mathfrak{F}^3}-3\mathbb{U}^2\frac{\partial\mathbb{U}}{\partial\varphi}+\frac{3}{2}\mathbb{W}\frac{\partial^2\mathbb{V}}{\partial\varphi^2}+3\frac{\partial\mathbb{V}}{\partial\varphi}\frac{\partial\mathbb{W}}{\partial\varphi}+\frac{3}{2}\mathbb{V}\frac{\partial^2\mathbb{W}}{\partial\varphi^2}+3yx\frac{\partial\mathbb{U}}{\partial\varphi}\right.\right.$$
$$\left.\left.+3zx\frac{\partial\mathbb{V}}{\partial\varphi}+3zy\frac{\partial\mathbb{W}}{\partial\varphi}\right]\right],$$
$$\mathbb{V}(\varphi,\mathfrak{F})=\mathbb{L}^{-1}\left[\frac{1}{\nu}\mathbb{V}(\varphi,0)\right]+\mathbb{L}^{-1}\left[\frac{(\nu^{\gamma}(1-\gamma)+\gamma)}{\nu^{\gamma}}\mathbb{L}\left[-\frac{\partial^3\mathbb{V}}{\partial\varphi^3}-3\frac{\partial\mathbb{U}}{\partial\varphi}\frac{\partial\mathbb{V}}{\partial\varphi}-3\mathbb{V}\frac{\partial^2\mathbb{U}}{\partial\varphi^2}-3\mathbb{V}^2\frac{\partial\mathbb{W}}{\partial\varphi}+6zy\frac{\partial\mathbb{U}}{\partial\varphi}+3\mathbb{U}^2\frac{\partial\mathbb{V}}{\partial\varphi}\right]\right],$$
$$\mathbb{W}(\varphi,\mathfrak{F})=\mathbb{L}^{-1}\left[\frac{1}{\nu}\mathbb{W}(\varphi,0)\right]+\mathbb{L}^{-1}\left[\frac{(\nu^{\gamma}(1-\gamma)+\gamma)}{\nu^{\gamma}}\mathbb{L}\left[-\frac{\partial^3\mathbb{W}}{\partial\varphi^3}-3\frac{\partial\mathbb{U}}{\partial\varphi}\frac{\partial\mathbb{W}}{\partial\varphi}-3\mathbb{W}\frac{\partial^2\mathbb{U}}{\partial\varphi^2}-3\mathbb{W}^2\frac{\partial\mathbb{V}}{\partial\varphi}+6zx\frac{\partial\mathbb{U}}{\partial\varphi}+3\mathbb{U}^2\frac{\partial\mathbb{W}}{\partial\varphi}\right]\right]. \tag{71}$$

By the consequence of the modified decomposition technique, we get

$$\mathbb{U}_0(\varphi,\mathfrak{F})=\mathbb{L}^{-1}\left[\frac{1}{\nu}\mathbb{U}(\varphi,0)\right]=\frac{1}{2}\mathbb{L}^{-1}\left[\frac{1}{\nu}(2+\tanh\varphi)\right]$$
$$\mathbb{V}_0(\varphi,\mathfrak{F})=\mathbb{L}^{-1}\left[\frac{1}{\nu}\mathbb{V}(\varphi,0)\right]=\frac{1}{4}(2-\tanh\varphi),$$
$$\mathbb{W}_0(\varphi,\mathfrak{F})=\mathbb{L}^{-1}\left[\frac{1}{\nu}\mathbb{W}(\varphi,0)\right]=(2-\tanh\varphi). \tag{72}$$

It follows that

$$\sum_{j=0}^{\infty}\mathbb{U}_{j+1}(\varphi,\mathfrak{T})=\mathbb{L}^{-1}\left[\frac{(\nu^{\gamma}(1-\gamma)+\gamma)}{\nu^{\gamma}}\mathbb{L}\left[\frac{1}{2}\sum_{j=0}^{\infty}\left(\mathbb{U}_{\varphi\varphi\varphi}\right)_j-3\sum_{j=0}^{\infty}\mathscr{E}_j+\frac{3}{2}\sum_{j=0}^{\infty}\mathscr{F}_j+3\sum_{j=0}^{\infty}\mathscr{G}_j+\frac{3}{2}\sum_{j=0}^{\infty}\mathscr{H}_j+3\sum_{j=0}^{\infty}I_j+3\sum_{j=0}^{\infty}\mathscr{J}_j+3\sum_{j=0}^{\infty}\mathscr{K}_j\right]\right],\quad j$$

$$\sum_{j=0}^{\infty}\mathbb{V}_{j+1}(\varphi,\mathfrak{T})=\mathbb{L}^{-1}\left[\frac{(\nu^{\gamma}(1-\gamma)+\gamma)}{\nu^{\gamma}}\mathbb{L}\left[-\sum_{j=0}^{\infty}\left(\mathbb{V}_{\varphi\varphi\varphi}\right)_j-3\sum_{j=0}^{\infty}\mathscr{M}_j-3\sum_{j=0}^{\infty}\mathscr{N}_j-3\sum_{j=0}^{\infty}\mathscr{O}_j+6\sum_{j=0}^{\infty}\mathrm{x}_j+3\sum_{j=0}^{\infty}\mathscr{Q}_j\right]\right], \tag{73}$$

$$\sum_{j=0}^{\infty}\mathbb{W}_{j+1}(\varphi,\mathfrak{T})=\mathbb{L}^{-1}\left[\frac{(\nu^{\gamma}(1-\gamma)+\gamma)}{\nu^{\gamma}}\mathbb{L}\left[-\sum_{j=0}^{\infty}\left(\mathbb{W}_{\varphi\varphi\varphi}\right)_j-3\sum_{j=0}^{\infty}\mathscr{R}_j-3\sum_{j=0}^{\infty}W_j-3\sum_{j=0}^{\infty}\mathscr{T}_j+6\sum_{j=0}^{\infty}\mathscr{X}_j+3\sum_{j=0}^{\infty}\mathscr{Y}_j\right]\right].$$

The Adomian polynomials' some terms are defined as

$$\mathscr{E}_J\left(\mathbb{U}^2\mathbb{U}_{\varphi}\right)=\begin{cases}\mathbb{U}_0^2\mathbb{U}_{0\varphi}, & \text{for } J=0,\\ (2\mathbb{U}_0\mathbb{U}_1)\mathbb{U}_{0\varphi}+\mathbb{U}_0^2\mathbb{U}_{1\varphi}, & \text{for } J=1,\\ \left(2\mathbb{U}_0\mathbb{U}_2+\mathbb{U}_1^2\right)\mathbb{U}_{0\varphi}+(2\mathbb{U}_0\mathbb{U}_1)\mathbb{U}_{1\varphi}+\mathbb{U}_0^2\mathbb{U}_{2\varphi}, & \text{for } J=2,\end{cases}$$

$$\mathscr{F}_J\left(\mathbb{W}\mathbb{V}_{\varphi\varphi}\right)=\begin{cases}\mathbb{W}_0\mathbb{V}_{0\varphi\varphi}, & \text{for } J=0,\\ \mathbb{W}_1\mathbb{V}_{0\varphi\varphi}+\mathbb{W}_0\mathbb{V}_{1\varphi\varphi}, & \text{for } J=1,\\ \mathbb{W}_2\mathbb{V}_{0\varphi\varphi}+\mathbb{W}_1\mathbb{V}_{1\varphi\varphi}+\mathbb{W}_0\mathbb{V}_{2\varphi\varphi}, & \text{for } J=2,\end{cases}$$

$$\mathscr{G}_J\left(\mathbb{V}_{\varphi}\mathbb{W}_{\varphi}\right)=\begin{cases}\mathbb{V}_{0\varphi}\mathbb{W}_{0\varphi}, & \text{for } J=0,\\ \mathbb{V}_{0\varphi}\mathbb{W}_{1\varphi}+\mathbb{V}_{1\varphi}\mathbb{W}_{0\varphi}, & \text{for } J=1,\\ \mathbb{V}_{2\varphi}\mathbb{W}_{0\varphi}+\mathbb{V}_{1\varphi}\mathbb{W}_{1\varphi}+\mathbb{V}_{0\varphi}\mathbb{W}_{2\varphi}, & \text{for } J=2,\end{cases}$$

$$\mathscr{H}_J\left(\mathbb{V}_{\varphi}\mathbb{W}_{\varphi\varphi}\right)=\begin{cases}\mathbb{V}_{0\varphi}\mathbb{W}_{0\varphi\varphi}, & \text{for } J=0,\\ \mathbb{V}_{0\varphi}\mathbb{W}_{1\varphi\varphi}+\mathbb{V}_{1\varphi}\mathbb{W}_{0\varphi\varphi}, & \text{for } J=1,\\ \mathbb{V}_{2\varphi}\mathbb{W}_{0\varphi\varphi}+\mathbb{V}_{1\varphi}\mathbb{W}_{1\varphi\varphi}+\mathbb{V}_{0\varphi}\mathbb{W}_{2\varphi\varphi}, & \text{for } J=2,\end{cases}$$

$$I_J\left(\mathbb{V}z\mathbb{U}_{\varphi}\right)=\begin{cases}(\mathrm{yx})_0\mathbb{U}_{0\varphi}, & \text{for } J=0,\\ (\mathrm{yx})_0\mathbb{U}_{1\varphi}+(\mathrm{yx})_1\mathbb{U}_{0\varphi}, & \text{for } J=1,\\ (\mathrm{yx})_0\mathbb{U}_{2\varphi}+(\mathrm{yx})_1\mathbb{U}_{1\varphi}+(\mathrm{yx})_2\mathbb{U}_{0\varphi}, & \text{for } J=2,\end{cases}$$

$$\mathscr{J}_J\left(\mathbb{U}z\mathbb{V}_{\varphi}\right)=\begin{cases}(\mathrm{zx})_0\mathbb{U}_{0\varphi}, & \text{for } J=0,\\ (\mathrm{zx})_0\mathbb{U}_{1\varphi}+(\mathrm{zx})_1\mathbb{U}_{0\varphi}, & \text{for } J=1,\\ (\mathrm{zx})_0\mathbb{U}_{2\varphi}+(\mathrm{zx})_1\mathbb{U}_{1\varphi}+(\mathrm{zx})_2\mathbb{U}_{0\varphi}, & \text{for } J=2,\end{cases}$$

$$\mathscr{K}_J\left(\mathrm{zy}\mathbb{W}_{\varphi}\right)=\begin{cases}(\mathrm{zy})_0\mathbb{U}_{0\varphi}, & \text{for } J=0,\\ (\mathrm{zy})_0\mathbb{U}_{1\varphi}+(\mathrm{zy})_1\mathbb{U}_{0\varphi}, & \text{for } J=1,\\ (\mathrm{zy})_0\mathbb{U}_{2\varphi}+(\mathrm{zy})_1\mathbb{U}_{1\varphi}+(\mathrm{zy})_2\mathbb{U}_{0\varphi}, & \text{for } J=2,\end{cases}$$

$$\mathscr{M}_J\left(\mathbb{U}_{\varphi}\mathbb{V}_{\varphi}\right)=\begin{cases}\mathbb{U}_{0\varphi}\mathbb{V}_{0\varphi}, & \text{for } J=0,\\ \mathbb{U}_{0\varphi}\mathbb{V}_{1\varphi}+\mathbb{U}_{\varphi}\mathbb{V}_{0\varphi}, & \text{for } J=1,\\ \mathbb{U}_{2\varphi}\mathbb{V}_{0\varphi}+\mathbb{U}_{1\varphi}\mathbb{V}_{1\varphi}+\mathbb{U}_{0\varphi}\mathbb{V}_{1\varphi}, & \text{for } J=2,\end{cases}$$

$$\begin{aligned}
\mathcal{N}_J\left(\mathbb{V}\mathbb{U}_{\varphi\varphi}\right) &= \begin{cases} \mathbb{V}_0\mathbb{U}_{0\varphi\varphi}, & \text{for } J=0,\\ \mathbb{V}_0\mathbb{U}_{1\varphi\varphi}+\mathbb{V}_1\mathbb{U}_{0\varphi\varphi}, & \text{for } J=1,\\ \mathbb{V}_2\mathbb{U}_{0\varphi\varphi}+\mathbb{V}_1\mathbb{U}_{1\varphi\varphi}+\mathbb{V}_0\mathbb{U}_{2\varphi\varphi}, & \text{for } J=2,\end{cases}\\
\mathcal{O}_J\left(\mathbb{V}^2\mathbb{W}_{\varphi}\right) &= \begin{cases} \mathbb{V}_0^2\mathbb{W}_{0\varphi}, & \text{for } J=0,\\ (2\mathbb{V}_0\mathbb{V}_1)\mathbb{W}_{0\varphi}+\mathbb{V}_0^2\mathbb{W}_{1\varphi}, & \text{for } J=1,\\ \left(2\mathbb{V}_0\mathbb{V}_2+\mathbb{V}_1^2\right)\mathbb{W}_{0\varphi}+(2\mathbb{V}_0\mathbb{V}_1)\mathbb{W}_{1\varphi}+\mathbb{V}_0^2\mathbb{W}_{2\varphi}, & \text{for } J=2,\end{cases}\\
\mathrm{x}_J\left(\mathrm{zy}\mathbb{W}_{\varphi}\right) &= \begin{cases} (\mathrm{zy})_0\mathbb{U}_{0\varphi}, & \text{for } J=0,\\ (\mathrm{zy})_0\mathbb{U}_{1\varphi}+(\mathrm{zy})_0\mathbb{U}_{1\varphi}, & \text{for } J=1,\\ (\mathrm{zy})_0\mathbb{U}_{2\varphi}+(\mathrm{zy})_1\mathbb{U}_{1\varphi}+(\mathrm{zy})_2\mathbb{U}_{0\varphi}, & \text{for } J=2,\end{cases}\\
\mathcal{Q}_J\left(\mathbb{U}^2\mathbb{V}_{\varphi}\right) &= \begin{cases} \mathbb{U}_0^2\mathbb{V}_{0\varphi}, & \text{for } J=0,\\ (2\mathbb{U}_0\mathbb{U}_1)\mathbb{V}_{0\varphi}+\mathbb{U}_0^2\mathbb{V}_{1\varphi}, & \text{for } J=1,\\ \left(2\mathbb{U}_0\mathbb{U}_2+\mathbb{U}_1^2\right)\mathbb{V}_{0\varphi}+(2\mathbb{U}_0\mathbb{U}_1)\mathbb{V}_{1\varphi}+\mathbb{U}_0^2\mathbb{V}_{2\varphi} & \text{for } J=2,\end{cases}\\
\mathcal{R}_0\left(\mathbb{U}_{\varphi}\mathbb{V}_{\varphi}\right) &= \begin{cases} \mathbb{U}_{0\varphi}\mathbb{V}_{0\varphi}, & \text{for } J=0,\\ \mathbb{U}_{0\varphi}\mathbb{V}_{1\varphi}+\mathbb{U}_{1\varphi}\mathbb{V}_{0\varphi}, & \text{for } J=1,\\ \mathbb{U}_{2\varphi}\mathbb{V}_{0\varphi}+\mathbb{U}_{1\varphi}\mathbb{V}_{1\varphi}+\mathbb{U}_{0\varphi}\mathbb{V}_{2\varphi}, & \text{for } J=2,\end{cases}\\
S_J\left(\mathbb{W}\mathbb{U}_{\varphi\varphi}\right) &= \begin{cases} \mathbb{W}_0\mathbb{U}_{0\varphi\varphi}, & \text{for } J=0,\\ \mathbb{W}_0\mathbb{U}_{1\varphi\varphi}+\mathbb{W}_1\mathbb{U}_{0\varphi\varphi}, & \text{for } J=1,\\ \mathbb{W}_2\mathbb{U}_{0\varphi\varphi}+\mathbb{W}_1\mathbb{U}_{1\varphi\varphi}+\mathbb{W}_0\mathbb{U}_{2\varphi\varphi}, & \text{for } J=2,\end{cases}\\
\mathcal{T}_J\left(\mathbb{W}^2\mathbb{V}_{\varphi}\right) &= \begin{cases} \mathbb{W}_0^2\mathbb{V}_{0\varphi}, & \text{for } J=0,\\ (2\mathbb{W}_0\mathbb{W}_1)\mathbb{V}_{0\varphi}+\mathbb{W}_0^2\mathbb{V}_{1\varphi}, & \text{for } J=1,\\ \left(2\mathbb{W}_0\mathbb{W}_2+\mathbb{W}_1^2\right)\mathbb{V}_{0\varphi}+(2\mathbb{W}_0\mathbb{W}_1)\mathbb{V}_{1\varphi}+\mathbb{W}_0^2\mathbb{V}_{2\varphi}, & \text{for } J=2,\end{cases}\\
\mathcal{X}_J\left(\mathbb{U}\mathbb{W}_1\mathbb{U}_{\varphi}\right) &= \begin{cases} (\mathrm{zx})_0\mathbb{U}_{0\varphi}, & \text{for } J=0,\\ (\mathrm{zx})_0\mathbb{U}_{1\varphi}+(\mathrm{zx})_1\mathbb{U}_{0\varphi}, & \text{for } J=1,\\ (\mathrm{zx})_2\mathbb{U}_{0\varphi}+(\mathrm{zx})_1\mathbb{U}_{1\varphi}+(\mathrm{zx})_2\mathbb{U}_{0\varphi}, & \text{for } J=2,\end{cases}\\
\mathcal{Y}_J\left(\mathbb{U}^2\mathbb{W}_{\varphi}\right) &= \begin{cases} \mathbb{U}_0^2\mathbb{W}_{0\varphi}, & \text{for } J=0,\\ (2\mathbb{U}_0\mathbb{U}_1)\mathbb{W}_{0\varphi}+\mathbb{U}_0^2\mathbb{W}_{1\varphi}, & \text{for } J=1,\\ \left(2\mathbb{U}_0\mathbb{U}_2+\mathbb{U}_1^2\right)\mathbb{W}_{0\varphi}+(2\mathbb{U}_0\mathbb{U}_1)\mathbb{W}_{1\varphi}+\mathbb{U}_0^2\mathbb{W}_{2\varphi}, & \text{for } J=2.\end{cases}
\end{aligned} \tag{74}$$

For $j = 0, 1, 2, 3, \ldots,$

$$\begin{aligned}
\mathbb{U}_1(\varphi,\mathfrak{J}) &= \mathbb{L}^{-1}\left[\frac{(\nu^{\gamma}(1-\gamma)+\gamma)}{\nu^{\gamma}}\mathbb{L}\left[\frac{1}{2}\left(\mathbb{U}_{\varphi\varphi\varphi}\right)_0 - 3\mathcal{E}_0 + \frac{3}{2}\mathcal{F}_0 + 3\mathcal{G}_0 + \frac{3}{2}\mathcal{H}_0 + 3I_0 + 3\mathcal{J}_0 + 3\mathcal{K}_0\right]\right]\\
&= \frac{11}{2}\sec h^2(\varphi)\left((1-\gamma)+\frac{\gamma\mathfrak{J}^{\gamma}}{\Gamma(\gamma+1)}\right)\\
\mathbb{V}_1(\varphi,\mathfrak{J}) &= \mathbb{L}^{-1}\left[\frac{(\nu^{\gamma}(1-\gamma)+\gamma)}{\nu^{\gamma}}\mathbb{L}\left[\left(\mathbb{V}_{\varphi\varphi\varphi}\right)_0 - 3\mathcal{M}_0 - 3\mathcal{N}_0 - 3\mathcal{O}_0 + 6\mathrm{x}_0 + 3\mathcal{Q}_0\right]\right]\\
&= -\frac{11}{8}\sec h^2(\varphi)\left((1-\gamma)+\frac{\gamma\mathfrak{J}^{\gamma}}{\Gamma(\gamma+1)}\right)
\end{aligned}$$

$$
\begin{aligned}
\mathbb{W}_1(\varphi,\mathfrak{T}) &= \mathbb{L}^{-1}\left[\frac{(v^{\gamma}(1-\gamma)+\gamma)}{v^{\gamma}}\mathbb{L}\left[\left(\mathbb{W}_{\varphi\varphi\varphi}\right)_0 - 3\mathscr{R}_0 - 3\widehat{\mathbb{S}}_0 - 3\mathscr{T}_0 + 6\mathscr{X}_0 + 3\mathscr{Y}_0\right]\right]\\
&= -\frac{11}{2}\operatorname{sec} h^2(\varphi)\left((1-\gamma)+\frac{\gamma\mathfrak{T}^{\gamma}}{\Gamma(\gamma+1)}\right)\\
\mathbb{U}_2(\varphi,\mathfrak{T}) &= \mathbb{L}^{-1}\left[\frac{(v^{\gamma}(1-\gamma)+\gamma)}{v^{\gamma}}\mathbb{L}\left[\frac{1}{2}\left(\mathbb{U}_{\varphi\varphi\varphi}\right)_1 - 3\mathscr{E}_1 + \frac{3}{2}\mathscr{F}_1 + 3\mathscr{G}_1 + \frac{3}{2}\mathscr{H}_1 + 3I_1 + 3\mathscr{J}_1 + 3\mathscr{K}_1\right]\right]\\
&= \frac{-121}{8}\tanh(\varphi)\operatorname{sec} h^2(\varphi)\left((1-\gamma)^2+\frac{\gamma^2\mathfrak{T}^{2\gamma}}{\Gamma(2\gamma+1)}+\frac{2(1-\gamma)\gamma\mathfrak{T}^{\gamma}}{\Gamma(\gamma+1)}\right)\\
\mathbb{V}_2(\varphi,\mathfrak{T}) &= \mathbb{L}^{-1}\left[\frac{(v^{\gamma}(1-\gamma)+\gamma)}{v^{\gamma}}\mathbb{L}\left[\left(\mathbb{V}_{\varphi\varphi\varphi}\right)_1 - 3\mathscr{M}_1 - 3\mathscr{N}_1 - 3\mathscr{O}_1 + 6\mathrm{x}_1 + 3\mathscr{Q}_1\right]\right]\\
&= \frac{121}{8}\tanh(\varphi)\operatorname{sec} h^2(\varphi)\left((1-\gamma)^2+\frac{\gamma^2\mathfrak{T}^{2\gamma}}{\Gamma(2\gamma+1)}+\frac{2(1-\gamma)\gamma\mathfrak{T}^{\gamma}}{\Gamma(\gamma+1)}\right)\\
\mathbb{W}_2(\varphi,\mathfrak{T}) &= \mathbb{L}^{-1}\left[\frac{(v^{\gamma}(1-\gamma)+\gamma)}{v^{\gamma}}\mathbb{L}\left[\left(\mathbb{W}_{\varphi\varphi\varphi}\right)_1 - 3\mathscr{R}_1 - 3\widehat{\mathbb{S}}_1 - 3\mathscr{T}_1 + 6\mathscr{X}_1 + 3\mathscr{Y}_1\right]\right]\\
&= \frac{242}{8}anh(\varphi)\operatorname{sec} h^2(\varphi)\left((1-\gamma)^2+\frac{\gamma^2\mathfrak{T}^{2\gamma}}{\Gamma(2\gamma+1)}+\frac{2(1-\gamma)\gamma\mathfrak{T}^{\gamma}}{\Gamma(\gamma+1)}\right)\\
\mathbb{U}_3(\varphi,\mathfrak{T}) &= \mathbb{L}^{-1}\left[\frac{(v^{\gamma}(1-\gamma)+\gamma)}{v^{\gamma}}\mathbb{L}\left[\frac{1}{2}\left(\mathbb{U}_{\varphi\varphi\varphi}\right)_2 - 3\mathscr{E}_2 + \frac{3}{2}\mathscr{F}_2 + 3\mathscr{G}_2 + \frac{3}{2}\mathscr{H}_2 + 3I_2 + 3\mathscr{J}_2 + 3\mathscr{K}_2\right]\right]\\
&= \frac{1331}{48}\operatorname{sec} h^4(\varphi)[\cosh(2\varphi)-2]\left\{(1-\gamma)^3+\gamma(1-\gamma)\left(1+\gamma+2\gamma^2\right)\frac{\mathfrak{T}^{\gamma}}{\Gamma(\gamma+1)}+\frac{3\gamma^2(1-\gamma)\mathfrak{T}^{2\gamma}}{\Gamma(2\gamma+1)}+\frac{\gamma^3\Gamma(2\gamma+1)\mathfrak{T}^{3\gamma}}{\Gamma(3\gamma+1)}\right\}\\
\mathbb{V}_3(\varphi,\mathfrak{T}) &= \mathbb{L}^{-1}\left[\frac{(v^{\gamma}(1-\gamma)+\gamma)}{v^{\gamma}}\mathbb{L}\left[\left(\mathbb{V}_{\varphi\varphi\varphi}\right)_2 - 3\mathscr{M}_2 - 3\mathscr{N}_2 - 3\mathscr{O}_2 + 6\mathrm{x}_2 + 3\mathscr{Q}_2\right]\right]\\
&= \frac{2662}{96}\operatorname{sec} h^4(\varphi)[\cosh(2\varphi)-2]\left\{(1-\gamma)^3+\gamma(1-\gamma)\left(1+\gamma+2\gamma^2\right)\frac{\mathfrak{T}^{\gamma}}{\Gamma(\gamma+1)}+\frac{3\gamma^2(1-\gamma)\mathfrak{T}^{2\gamma}}{\Gamma(2\gamma+1)}+\frac{\gamma^3\Gamma(2\gamma+1)\mathfrak{T}^{3\gamma}}{\Gamma(3\gamma+1)}\right\}\\
\mathbb{W}_3(\varphi,\mathfrak{T}) &= \mathbb{L}^{-1}\left[\frac{(v^{\gamma}(1-\gamma)+\gamma)}{v^{\gamma}}\mathbb{L}\left[\left(\mathbb{W}_{\varphi\varphi\varphi}\right)_2 - 3\mathscr{R}_2 - 3\widehat{\mathbb{S}}_2 - 3\mathscr{T}_2 + 6\mathscr{X}_2 + 3\mathscr{Y}_2\right]\right]\\
&= \frac{-2662}{48}\operatorname{sec} h^4(\varphi)[\cosh(2\varphi)-2]\left\{(1-\gamma)^3+\gamma(1-\gamma)\left(1+\gamma+2\gamma^2\right)\frac{\mathfrak{T}^{\gamma}}{\Gamma(\gamma+1)}+\frac{3\gamma^2(1-\gamma)\mathfrak{T}^{2\gamma}}{\Gamma(2\gamma+1)}+\frac{\gamma^3\Gamma(2\gamma+1)\mathfrak{T}^{3\gamma}}{\Gamma(3\gamma+1)}\right\}\\
&\vdots .
\end{aligned}
\tag{75}
$$

The modified decomposition technique result for Example 3 is given as

$$
\begin{aligned}
\mathbb{U}(\varphi,\mathfrak{T}) &= \mathbb{U}_0(\varphi,\mathfrak{T}) + \mathbb{U}_1(\varphi,\mathfrak{T}) + \mathbb{U}_2(\varphi,\mathfrak{T}) + \mathbb{U}_3(\varphi,\mathfrak{T}) \ldots,\\
&= \frac{1}{2}(2+\tanh\varphi) + \frac{11}{2}\operatorname{sec} h^2(\varphi)\left((1-\gamma)+\frac{\gamma\mathfrak{T}^{\gamma}}{\Gamma(\gamma+1)}\right)\\
&\quad - \frac{121}{8}\tanh(\varphi)\operatorname{sec} h^2(\varphi)\left((1-\gamma)^2+\frac{\gamma^2\mathfrak{T}^{2\gamma}}{\Gamma(2\gamma+1)}+\frac{2(1-\gamma)\gamma\mathfrak{T}^{\gamma}}{\Gamma(\gamma+1)}\right)\\
&\quad + \frac{1331}{48}\operatorname{sec} h^4(\varphi)[\cosh(2\varphi)-2]\left\{(1-\gamma)^3+\gamma(1-\gamma)\left(1+\gamma+2\gamma^2\right)\frac{\mathfrak{T}^{\gamma}}{\Gamma(\gamma+1)}+\frac{3\gamma^2(1-\gamma)\mathfrak{T}^{2\gamma}}{\Gamma(2\gamma+1)}+\frac{\gamma^3\Gamma(2\gamma+1)\mathfrak{T}^{3\gamma}}{\Gamma(3\gamma+1)}\right\}\\
&\quad + \cdots .
\end{aligned}
\tag{76}
$$

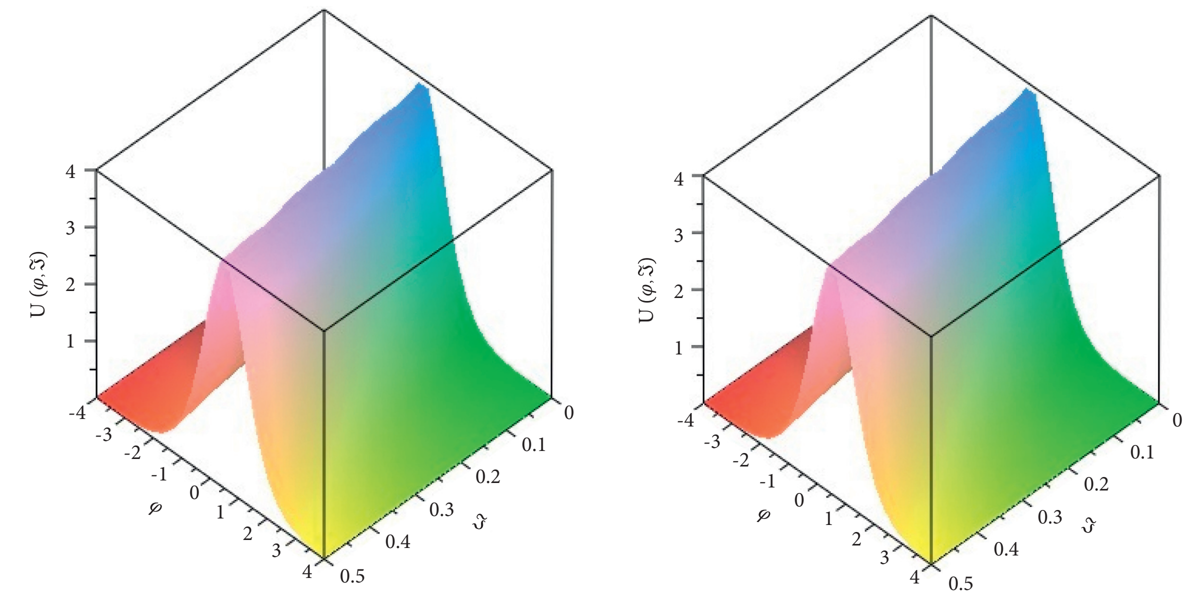

Figure 1: The actual and analytical (MDM/NITM) result figure at $\mathbb{U}(\varphi, \mathfrak{I})$ of Example 1 for $\varrho = 1$, $\rho = 0.5$, and $\delta = 2$.

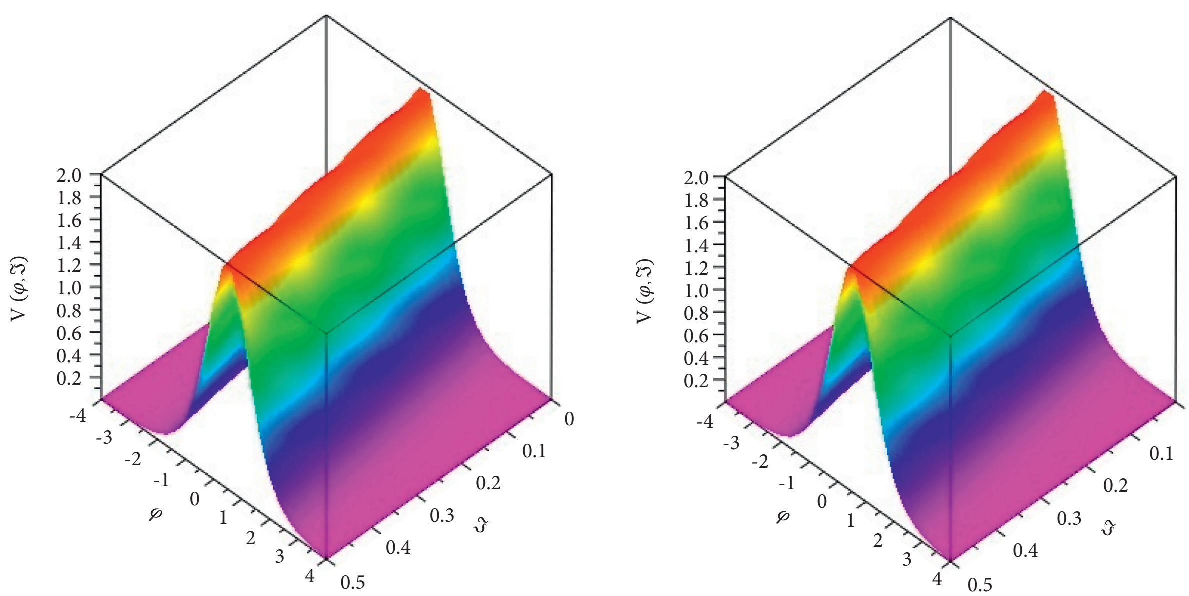

Figure 2: The actual and analytical (MDM/NITM) result figure at $\mathbb{V}(\varphi, \mathfrak{I})$ of Example 1 for $\varrho = 1$, $\rho = 0.5$, and $\delta = 2$.

Consequently, we get

$$\begin{aligned}
\mathbb{V}(\varphi, \mathfrak{I}) &= \frac{1}{4}(2 - \tanh\varphi) - \frac{11}{8}\sec h^2(\varphi)\left((1-\gamma) + \frac{\gamma \mathfrak{I}^{\gamma}}{\Gamma(\gamma+1)}\right) + \frac{121}{8}\tanh(\varphi)\sec h^2(\varphi)\left((1-\gamma)^2 + \frac{\gamma^2 \mathfrak{I}^{2\gamma}}{\Gamma(2\gamma+1)} + \frac{2(1-\gamma)\gamma \mathfrak{I}^{\gamma}}{\Gamma(\gamma+1)}\right) \\
&\quad - \frac{1331}{48}\sec h^4(\varphi)[\cosh(2\varphi) - 2]\left\{(1-\gamma)^3 + \gamma(1-\gamma)\left(1+\gamma+2\gamma^2\right)\frac{\mathfrak{I}^{\gamma}}{\Gamma(\gamma+1)} + \frac{3\gamma^2(1-\gamma)\mathfrak{I}^{2\gamma}}{\Gamma(2\gamma+1)} + \frac{\gamma^3\Gamma(2\gamma+1)\mathfrak{I}^{3\gamma}}{\Gamma(3\gamma+1)}\right\} + \cdots \\
\mathbb{W}(\varphi, \mathfrak{I}) &= (2 - \tanh\varphi) - \frac{11}{2}\sec h^2(\varphi)\left((1-\gamma) + \frac{\gamma \mathfrak{I}^{\gamma}}{\Gamma(\gamma+1)}\right) + \frac{121}{8}\tanh(\varphi)\sec h^2(\varphi)\left((1-\gamma)^2 + \frac{\gamma^2 \mathfrak{I}^{2\gamma}}{\Gamma(2\gamma+1)} + \frac{2(1-\gamma)\gamma \mathfrak{I}^{\gamma}}{\Gamma(\gamma+1)}\right) \\
&\quad - \frac{2662}{96}\sec h^4(\varphi)[\cosh(2\varphi) - 2]\left\{(1-\gamma)^3 + \gamma(1-\gamma)\left(1+\gamma+2\gamma^2\right)\frac{\mathfrak{I}^{\gamma}}{\Gamma(\gamma+1)} + \frac{3\gamma^2(1-\gamma)\mathfrak{I}^{2\gamma}}{\Gamma(2\gamma+1)} + \frac{\gamma^3\Gamma(2\gamma+1)\mathfrak{I}^{3\gamma}}{\Gamma(3\gamma+1)}\right\} + \cdots.
\end{aligned} \tag{77}$$

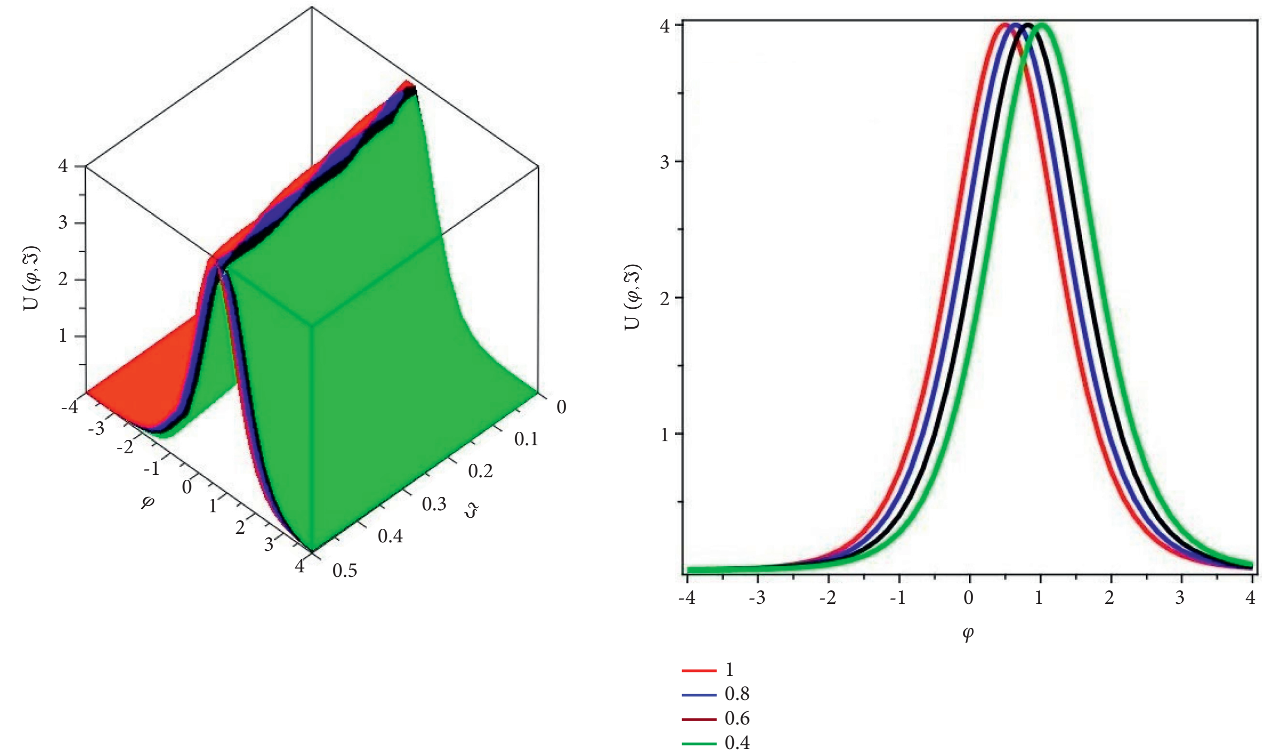

FIGURE 3: Analytical investigation of figure $\mathbb{U}(\varphi, \mathfrak{I})$ for Example 1 for different fractional orders $\gamma = 1.0, 0.8, 0.6, 0.4$, $\rho = 0.5$, $\varrho = 1$, and $\delta = 2$.

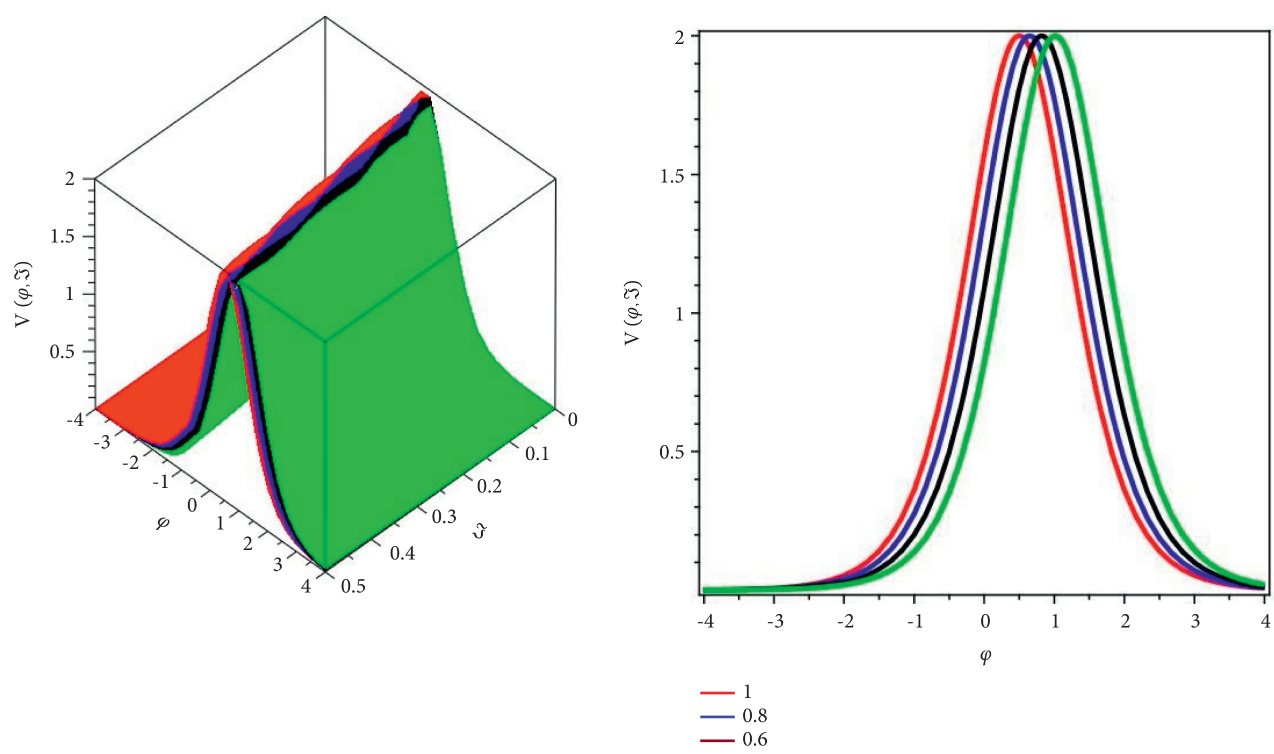

FIGURE 4: Analytical investigation of figure $\mathbb{V}(\varphi, \mathfrak{I})$ for Example 1 for different fractional orders $\gamma = 1.0, 0.8, 0.6, 0.4$, $\rho = 0.5$, $\varrho = 1$, and $\delta = 2$.

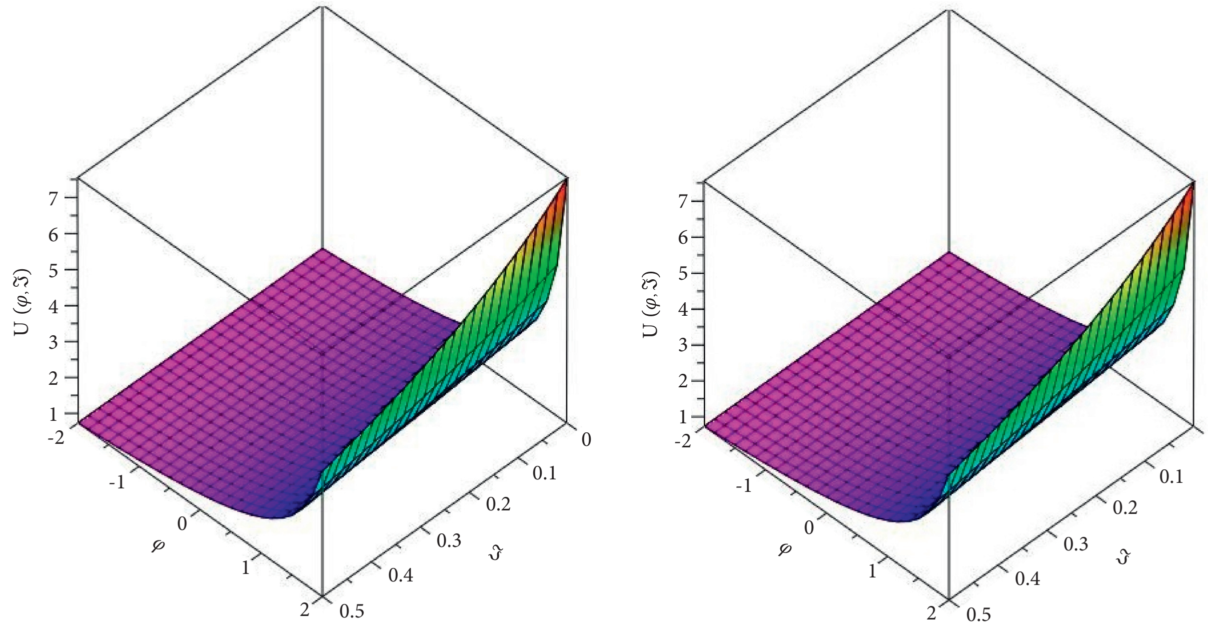

FIGURE 5: The analytical and exact (MDM/NITM) solution plot at $\mathbb{U}(\varphi, \mathfrak{I})$ of Example 2 for $\rho = 0.5$, $\varrho = 1$, and $\delta = 2$.

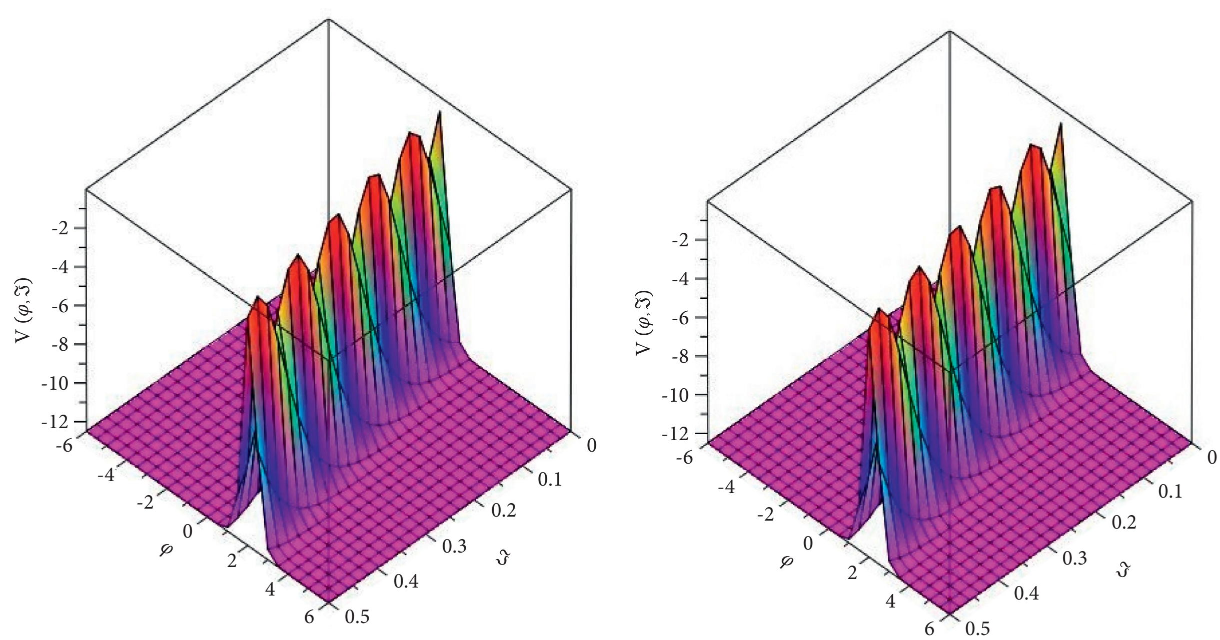

FIGURE 6: The analytical and exact (MDM/NITM) solution plot at $\mathbb{V}(\varphi, \mathfrak{I})$ of Example 2 for $\rho = 0.5$, $\varrho = 1$, and $\delta = 2$.

By putting $\gamma = 1$, we obtain the exact result of the system of Korteweg–de Vries equation (2):

$$\begin{aligned}\mathbb{U}(\varphi, \mathfrak{I}) &= \frac{1}{2}\left(2 + \tanh\left(\varphi - \frac{11\mathfrak{I}}{2}\right)\right),\\ \mathbb{V}(\varphi, \mathfrak{I}) &= \frac{1}{4}\left(2 - \tanh\left(\varphi - \frac{11\mathfrak{I}}{2}\right)\right),\\ \mathbb{W}(\varphi, \mathfrak{I}) &= \left(2 - \tanh\left(\varphi - \frac{11\mathfrak{I}}{2}\right)\right).\end{aligned} \tag{78}$$

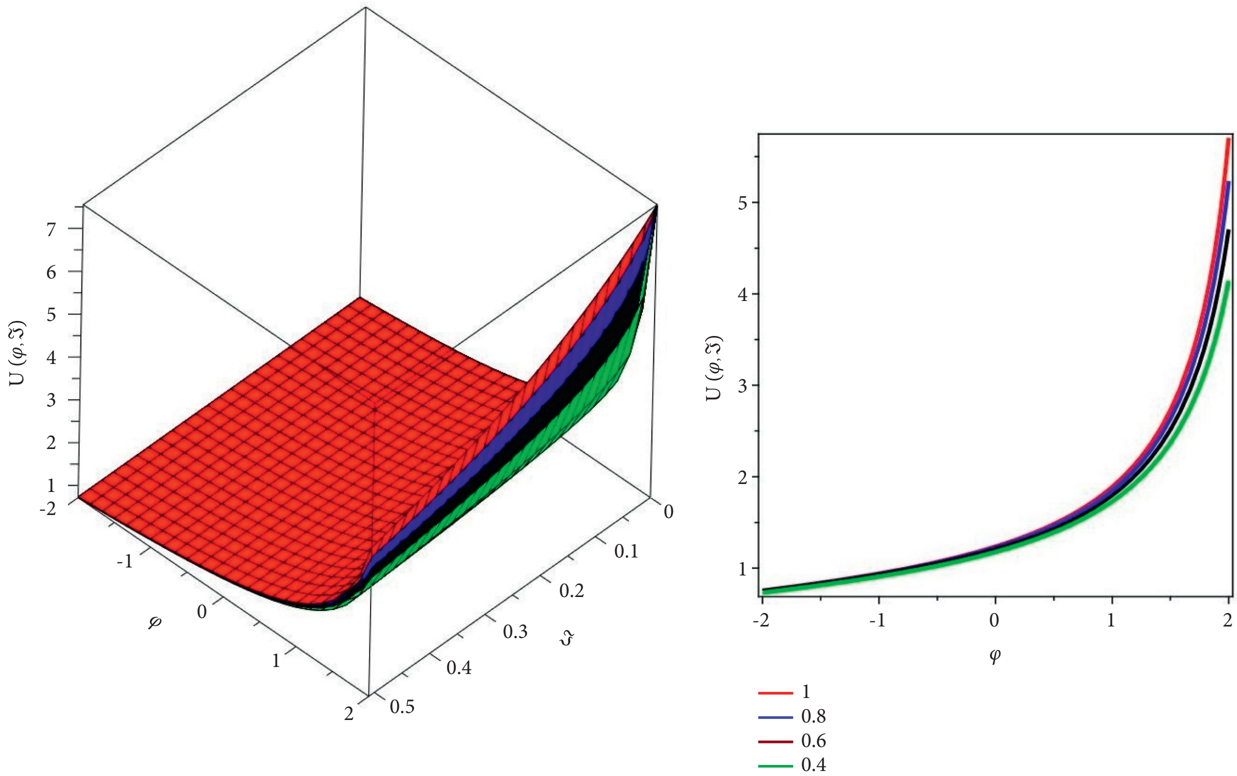

Figure 7: Mathematical analysis of the plot of $\mathbb{V}(\varphi, \mathfrak{I})$ for Example 2 for different fractional orders $\gamma = 1.0, 0.8, 0.6, 0.4$, $\rho = 0.5$, $\varrho = 1$, and $\delta = 2$.

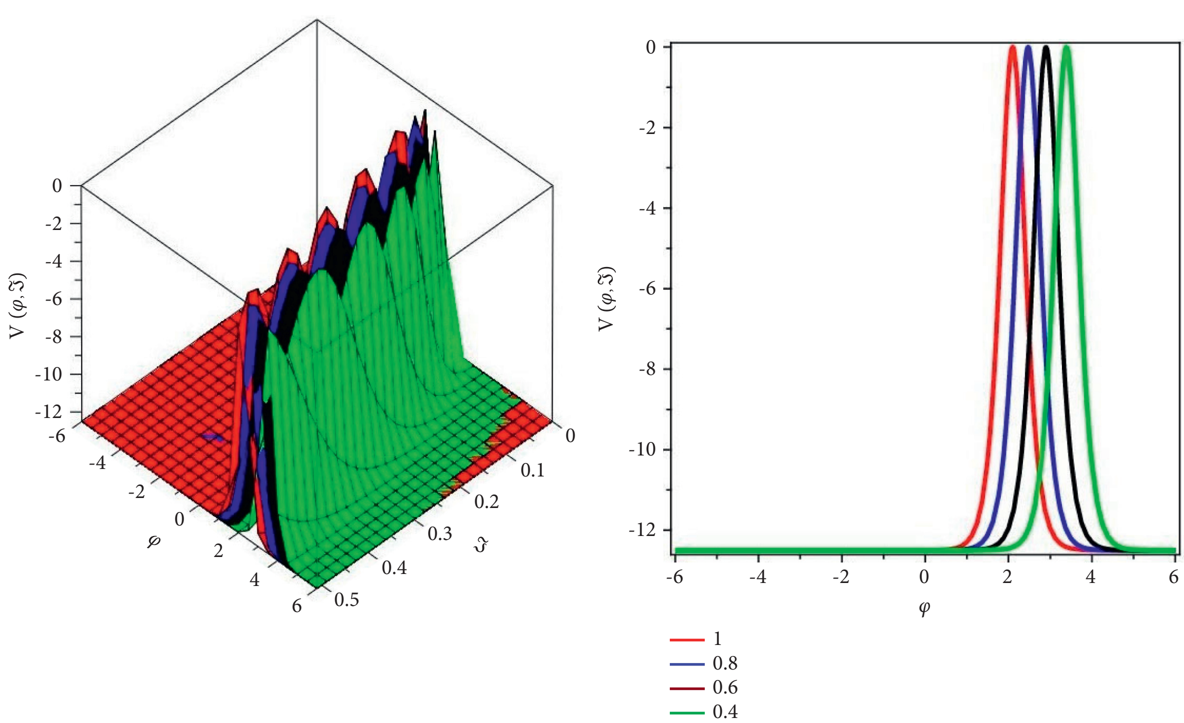

Figure 8: Mathematical analysis of the plot of $\mathbb{V}(\varphi, \mathfrak{I})$ for Example 2 for different fractional orders $\gamma = 1.0, 0.8, 0.6, 0.4 \rho = 0.5$, $\varrho = 1$, and $\delta = 2$.

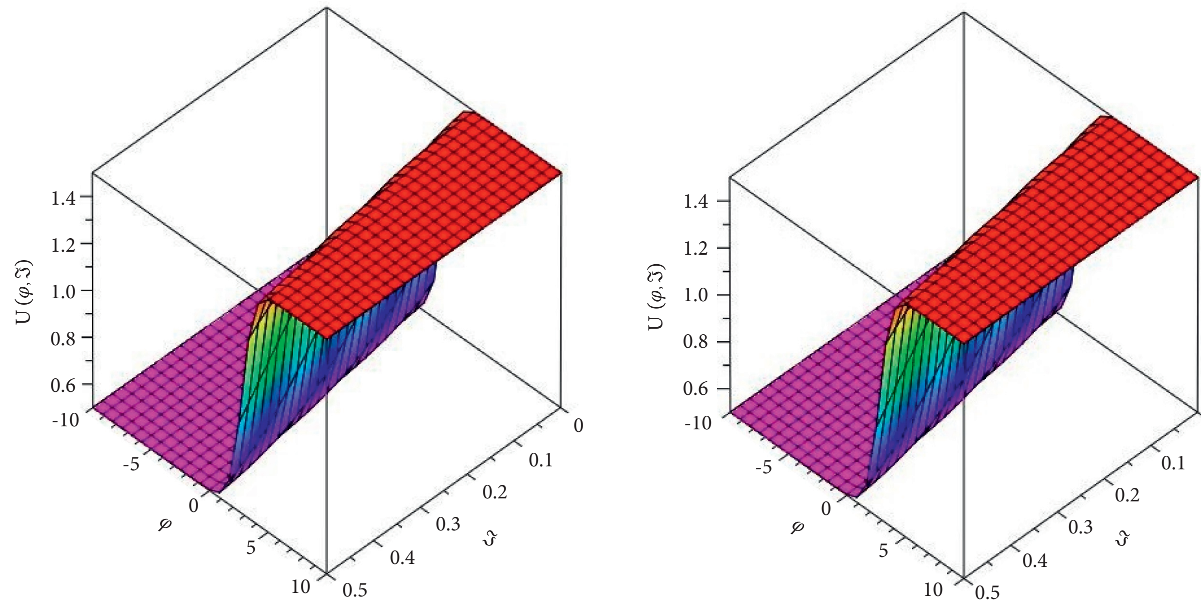

Figure 9: The analytical and exact result plot at $\mathbb{U}(\varphi,\mathfrak{I})$ of Example 3 for $\rho = 0.5$, $\varrho = 1$, and $\delta = 2$.

Case II: now, we apply the new iterative transformation technique for Example 3.

By using the suggested analytical method, we get

$$\mathbb{U}_0(\varphi,\mathfrak{I}) = \frac{1}{2}(2+\tanh\varphi)$$

$$\mathbb{V}_0(\varphi,\mathfrak{I}) = \frac{1}{4}(2-\tanh\varphi)$$

$$\mathbb{W}_0(\varphi,\mathfrak{I}) = (2-\tanh\varphi)$$

$$\mathbb{U}_1(\varphi,\mathfrak{I}) = \mathbb{L}^{-1}\left[\frac{(v^\gamma(1-\gamma)+\gamma)}{v^\gamma}\mathbb{L}\left[\frac{1}{2}\frac{\partial^3\mathbb{U}_0}{\partial\mathfrak{I}^3} - 3\mathbb{U}_0^2\frac{\partial\mathbb{U}_0}{\partial\varphi} + \frac{3}{2}\mathbb{W}_0\frac{\partial^2\mathbb{V}_0}{\partial\varphi^2} + 3\frac{\partial\mathbb{V}_0}{\partial\varphi}\frac{\partial\mathbb{W}_0}{\partial\varphi} + \frac{3}{2}\mathbb{V}_0\frac{\partial^2\mathbb{W}_0}{\partial\varphi^2} + 3\mathbb{V}_0\mathbb{W}_0\frac{\partial\mathbb{U}_0}{\partial\varphi} + 3\mathbb{U}_0\mathbb{W}_0\frac{\partial\mathbb{V}_0}{\partial\varphi} + 3\mathbb{U}_0\mathbb{V}_0\frac{\partial\mathbb{W}_0}{\partial\varphi}\right]\right]$$

$$= \frac{11}{2}\sec h^2(\varphi)\mathbb{L}^{-1}\left[\frac{\omega^{\gamma+2}}{v^{\gamma+2}}\right]$$

$$\mathbb{V}_1(\varphi,\mathfrak{I}) = \mathbb{L}^{-1}\left[\frac{(v^\gamma(1-\gamma)+\gamma)}{v^\gamma}\mathbb{L}\left[-\frac{\partial^3\mathbb{V}_0}{\partial\varphi^3} - 3\frac{\partial\mathbb{U}_0}{\partial\varphi}\frac{\partial\mathbb{V}_0}{\partial\varphi} - 3\mathbb{V}_0\frac{\partial^2\mathbb{U}_0}{\partial\varphi^2} - 3\mathbb{V}_0^2\frac{\partial\mathbb{W}_0}{\partial\varphi} + 6\mathbb{U}_0\mathbb{V}_0\frac{\partial\mathbb{U}_0}{\partial\varphi} + 3\mathbb{U}_0^2\frac{\partial\mathbb{V}_0}{\partial\varphi}\right]\right]$$

$$= -\frac{11}{8}\sec h^2(\varphi)\left((1-\gamma)+\frac{\gamma\mathfrak{I}^\gamma}{\Gamma(\gamma+1)}\right)$$

$$\mathbb{W}_1(\varphi,\mathfrak{I}) = \mathbb{L}^{-1}\left[\frac{(v^\gamma(1-\gamma)+\gamma)}{v^\gamma}\mathbb{L}\left[-\frac{\partial^3\mathbb{W}_0}{\partial\varphi^3} - 3\frac{\partial\mathbb{U}_0}{\partial\varphi}\frac{\partial\mathbb{W}_0}{\partial\varphi} - 3\mathbb{W}_0\frac{\partial^2\mathbb{U}_0}{\partial\varphi^2} - 3\mathbb{W}_0^2\frac{\partial\mathbb{V}_0}{\partial\varphi} + 6\mathbb{U}_0\mathbb{W}_0\frac{\partial\mathbb{U}_0}{\partial\varphi} + 3\mathbb{U}_0^2\frac{\partial\mathbb{W}_0}{\partial\varphi}\right]\right]$$

$$= -\frac{11}{2}\sec h^2(\varphi)\left((1-\gamma)+\frac{\gamma\mathfrak{I}^\gamma}{\Gamma(\gamma+1)}\right)$$

$$\mathbb{U}_2(\varphi,\mathfrak{I}) = \mathbb{L}^{-1}\left[\frac{(v^\gamma(1-\gamma)+\gamma)}{v^\gamma}\mathbb{L}\left[\frac{1}{2}\frac{\partial^3\mathbb{U}_1}{\partial\mathfrak{I}^3} - 3\mathbb{U}_1^2\frac{\partial\mathbb{U}_1}{\partial\varphi} + \frac{3}{2}\mathbb{W}_1\frac{\partial^2\mathbb{V}_1}{\partial\varphi^2} + 3\frac{\partial\mathbb{V}_1}{\partial\varphi}\frac{\partial\mathbb{W}_1}{\partial\varphi} + \frac{3}{2}\mathbb{V}_1\frac{\partial^2\mathbb{W}_1}{\partial\varphi^2} + 3\mathbb{V}_1\mathbb{W}_1\frac{\partial\mathbb{U}_1}{\partial\varphi} + 3\mathbb{U}_1\mathbb{W}_1\frac{\partial\mathbb{V}_1}{\partial\varphi} + 3\mathbb{U}_1\mathbb{V}_1\frac{\partial\mathbb{W}_1}{\partial\varphi}\right]\right]$$

$$= \frac{-121}{8}\tanh(\varphi)\sec h^2(\varphi)\left((1-\gamma)^2+\frac{\gamma^2\mathfrak{I}^{2\gamma}}{\Gamma(2\gamma+1)}+\frac{2(1-\gamma)\gamma\mathfrak{I}^\gamma}{\Gamma(\gamma+1)}\right)$$

$$
\begin{aligned}
\mathbb{V}_2(\varphi,\mathfrak{F}) &= \mathbb{L}^{-1}\left[\frac{(v^{\gamma}(1-\gamma)+\gamma)}{v^{\gamma}}\mathbb{L}\left[-\frac{\partial^3\mathbb{V}_1}{\partial\varphi^3}-3\frac{\partial\mathbb{U}_1}{\partial\varphi}\frac{\partial\mathbb{V}_1}{\partial\varphi}-3\mathbb{V}_1\frac{\partial^2\mathbb{U}_1}{\partial\varphi^2}-3\mathbb{V}_1^2\frac{\partial\mathbb{W}_1}{\partial\varphi}+6\mathbb{U}_1\mathbb{V}_1\frac{\partial\mathbb{U}_1}{\partial\varphi}+3\mathbb{U}_1^2\frac{\partial\mathbb{V}_1}{\partial\varphi}\right]\right]\\
&= \frac{121}{8}\tanh(\varphi)\sec h^2(\varphi)\left((1-\gamma)^2+\frac{\gamma^2\mathfrak{F}^{2\gamma}}{\Gamma(2\gamma+1)}+\frac{2(1-\gamma)\gamma\mathfrak{F}^{\gamma}}{\Gamma(\gamma+1)}\right)\\
\mathbb{W}_2(\varphi,\mathfrak{F}) &= \mathbb{L}^{-1}\left[\frac{(v^{\gamma}(1-\gamma)+\gamma)}{v^{\gamma}}\mathbb{L}\left[-\frac{\partial^3\mathbb{W}_1}{\partial\varphi^3}-3\frac{\partial\mathbb{U}_1}{\partial\varphi}\frac{\partial\mathbb{W}_1}{\partial\varphi}-3\mathbb{W}_1\frac{\partial^2\mathbb{U}_1}{\partial\varphi^2}-3\mathbb{W}_1^2\frac{\partial\mathbb{V}_1}{\partial\varphi}+6\mathbb{U}_1\mathbb{W}_1\frac{\partial\mathbb{U}_1}{\partial\varphi}+3\mathbb{U}_1^2\frac{\partial\mathbb{W}_1}{\partial\varphi}\right]\right]\\
&= \frac{242}{8}\tanh(\varphi)\sec h^2(\varphi)\left((1-\gamma)^2+\frac{\gamma^2\mathfrak{F}^{2\gamma}}{\Gamma(2\gamma+1)}+\frac{2(1-\gamma)\gamma\mathfrak{F}^{\gamma}}{\Gamma(\gamma+1)}\right)\\
\mathbb{U}_3(\varphi,\mathfrak{F}) &= \mathbb{L}^{-1}\left[\frac{(v^{\gamma}(1-\gamma)+\gamma)}{v^{\gamma}}\mathbb{L}\left[\frac{1}{2}\frac{\partial^3\mathbb{U}_2}{\partial\mathfrak{F}^3}-3\mathbb{U}_2^2\frac{\partial\mathbb{U}_2}{\partial\varphi}+\frac{3}{2}\mathbb{W}_2\frac{\partial^2\mathbb{V}_2}{\partial\varphi^2}+3\frac{\partial\mathbb{V}_2}{\partial\varphi}\frac{\partial\mathbb{W}_2}{\partial\varphi}+\frac{3}{2}\mathbb{V}_2\frac{\partial^2\mathbb{W}_2}{\partial\varphi^2}+3\mathbb{V}_2\mathbb{W}_2\frac{\partial\mathbb{U}_2}{\partial\varphi}+3\mathbb{U}_2\mathbb{W}_2\frac{\partial\mathbb{V}_2}{\partial\varphi}+3\mathbb{U}_2\mathbb{V}_2\frac{\partial\mathbb{W}_2}{\partial\varphi}\right]\right]\\
&= \frac{1331}{48}\sec h^4(\varphi)[\cosh(2\varphi)-2]\left\{(1-\gamma)^3+\gamma(1-\gamma)\left(1+\gamma+2\gamma^2\right)\frac{\mathfrak{F}^{\gamma}}{\Gamma(\gamma+1)}+\frac{3\gamma^2(1-\gamma)\mathfrak{F}^{2\gamma}}{\Gamma(2\gamma+1)}+\frac{\gamma^3\Gamma(2\gamma+1)\mathfrak{F}^{3\gamma}}{\Gamma(3\gamma+1)}\right\}\\
\mathbb{V}_3(\varphi,\mathfrak{F}) &= \mathbb{L}^{-1}\left[\frac{(v^{\gamma}(1-\gamma)+\gamma)}{v^{\gamma}}\mathbb{L}\left[-\frac{\partial^3\mathbb{V}_2}{\partial\varphi^3}-3\frac{\partial\mathbb{U}_2}{\partial\varphi}\frac{\partial\mathbb{V}_2}{\partial\varphi}-3\mathbb{V}_2\frac{\partial^2\mathbb{U}_2}{\partial\varphi^2}-3\mathbb{V}_2^2\frac{\partial\mathbb{W}_2}{\partial\varphi}+6\mathbb{U}_2\mathbb{V}_2\frac{\partial\mathbb{U}_2}{\partial\varphi}+3\mathbb{U}_2^2\frac{\partial\mathbb{V}_2}{\partial\varphi}\right]\right]\\
&= \frac{2662}{96}\sec h^4(\varphi)[\cosh(2\varphi)-2]\left\{(1-\gamma)^3+\gamma(1-\gamma)\left(1+\gamma+2\gamma^2\right)\frac{\mathfrak{F}^{\gamma}}{\Gamma(\gamma+1)}+\frac{3\gamma^2(1-\gamma)\mathfrak{F}^{2\gamma}}{\Gamma(2\gamma+1)}+\frac{\gamma^3\Gamma(2\gamma+1)\mathfrak{F}^{3\gamma}}{\Gamma(3\gamma+1)}\right\}\\
\mathbb{W}_3(\varphi,\mathfrak{F}) &= \mathbb{L}^{-1}\left[\frac{(v^{\gamma}(1-\gamma)+\gamma)}{v^{\gamma}}\mathbb{L}\left[-\frac{\partial^3\mathbb{W}_2}{\partial\varphi^3}-3\frac{\partial\mathbb{U}_2}{\partial\varphi}\frac{\partial\mathbb{W}_2}{\partial\varphi}-3\mathbb{W}_2\frac{\partial^2\mathbb{U}_2}{\partial\varphi^2}-3\mathbb{W}_2^2\frac{\partial\mathbb{V}_2}{\partial\varphi}+6\mathbb{U}_2\mathbb{W}_2\frac{\partial\mathbb{U}_2}{\partial\varphi}+3\mathbb{U}_2^2\frac{\partial\mathbb{W}_2}{\partial\varphi}\right]\right]\\
&= \frac{-2662}{48}\sec h^4(\varphi)[\cosh(2\varphi)-2]\left\{(1-\gamma)^3+\gamma(1-\gamma)\left(1+\gamma+2\gamma^2\right)\frac{\mathfrak{F}^{\gamma}}{\Gamma(\gamma+1)}+\frac{3\gamma^2(1-\gamma)\mathfrak{F}^{2\gamma}}{\Gamma(2\gamma+1)}+\frac{\gamma^3\Gamma(2\gamma+1)\mathfrak{F}^{3\gamma}}{\Gamma(3\gamma+1)}\right\}\\
&\vdots\\
\mathbb{U}_j(\varphi,\mathfrak{F}) &= \mathbb{L}^{-1}\left[\frac{v^{\gamma}(1-\gamma)+\gamma}{v^{\gamma}}\mathbb{L}\left[\frac{1}{2}\frac{\partial^3\mathbb{U}_{j-1}}{\partial\mathfrak{F}^3}-3\mathbb{U}_{j-1}^2\frac{\partial\mathbb{U}_{j-1}}{\partial\varphi}+\frac{3}{2}\mathbb{W}_{j-1}\frac{\partial^2\mathbb{V}_{j-1}}{\partial\varphi^2}+3\frac{\partial\mathbb{V}_{j-1}}{\partial\varphi}\frac{\partial\mathbb{W}_{j-1}}{\partial\varphi}+\frac{3}{2}\mathbb{V}_{j-1}\frac{\partial^2\mathbb{W}_{j-1}}{\partial\varphi^2}\right.\right.\\
&\quad\left.\left.+3\mathbb{V}_{j-1}\mathbb{W}_{j-1}\frac{\partial\mathbb{U}_{j-1}}{\partial\varphi}+3\mathbb{U}_{j-1}\mathbb{W}_{j-1}\frac{\partial\mathbb{V}_{j-1}}{\partial\varphi}+3\mathbb{U}_{j-1}\mathbb{V}_{j-1}\frac{\partial\mathbb{W}_{j-1}}{\partial\varphi}\right]\right]\\
\mathbb{V}_j(\varphi,\mathfrak{F}) &= \mathbb{L}^{-1}\left[\frac{v^{\gamma}(1-\gamma)+\gamma}{v^{\gamma}}\mathbb{L}\left[-\frac{\partial^3\mathbb{V}_{j-1}}{\partial\varphi^3}-3\frac{\partial\mathbb{U}_{j-1}}{\partial\varphi}\frac{\partial\mathbb{V}_{j-1}}{\partial\varphi}-3\mathbb{V}_{j-1}\frac{\partial^2\mathbb{U}_{j-1}}{\partial\varphi^2}-3\mathbb{V}_{j-1}^2\frac{\partial\mathbb{W}_{j-1}}{\partial\varphi}+6\mathbb{U}_{j-1}\mathbb{V}_{j-1}\frac{\partial\mathbb{U}_{j-1}}{\partial\varphi}+3\mathbb{U}_{j-1}^2\frac{\partial\mathbb{V}_{j-1}}{\partial\varphi}\right]\right]\\
\mathbb{W}_j(\varphi,\mathfrak{F}) &= \mathbb{L}^{-1}\left[\frac{v^{\gamma}(1-\gamma)+\gamma}{v^{\gamma}}\mathbb{L}\left[-\frac{\partial^3\mathbb{W}_{j-1}}{\partial\varphi^3}-3\frac{\partial\mathbb{U}_{j-1}}{\partial\varphi}\frac{\partial\mathbb{W}_{j-1}}{\partial\varphi}-3\mathbb{W}_{j-1}\frac{\partial^2\mathbb{U}_{j-1}}{\partial\varphi^2}-3\mathbb{W}_{j-1}^2\frac{\partial\mathbb{V}_{j-1}}{\partial\varphi}+6\mathbb{U}_{j-1}\mathbb{W}_{j-1}\frac{\partial\mathbb{U}_{j-1}}{\partial\varphi}+3\mathbb{U}_{j-1}^2\frac{\partial\mathbb{W}_{j-1}}{\partial\varphi}\right]\right].
\end{aligned}
\tag{79}
$$

The series of results for Example 3 is given as

$$
\begin{aligned}
\mathbb{U}(\varphi,\mathfrak{F}) &= \mathbb{U}_0(\varphi,\mathfrak{F})+\mathbb{U}_1(\varphi,\mathfrak{F})+\mathbb{U}_2(\varphi,\mathfrak{F})+\mathbb{U}_3(\varphi,\mathfrak{F})+\cdots\mathbb{U}_j(\varphi,\mathfrak{F})\\
&= \frac{1}{2}(2+\tanh\varphi)+\frac{11}{2}\sec h^2(\varphi)\left((1-\gamma)+\frac{\gamma\mathfrak{F}^{\gamma}}{\Gamma(\gamma+1)}\right)\\
&\quad-\frac{121}{8}\tanh(\varphi)\sec h^2(\varphi)\left((1-\gamma)^2+\frac{\gamma^2\mathfrak{F}^{2\gamma}}{\Gamma(2\gamma+1)}+\frac{2(1-\gamma)\gamma\mathfrak{F}^{\gamma}}{\Gamma(\gamma+1)}\right)\\
&\quad+\frac{1331}{48}\sec h^4(\varphi)[\cosh(2\varphi)-2]\left\{(1-\gamma)^3+\gamma(1-\gamma)\left(1+\gamma+2\gamma^2\right)\frac{\mathfrak{F}^{\gamma}}{\Gamma(\gamma+1)}+\frac{3\gamma^2(1-\gamma)\mathfrak{F}^{2\gamma}}{\Gamma(2\gamma+1)}+\frac{\gamma^3\Gamma(2\gamma+1)\mathfrak{F}^{3\gamma}}{\Gamma(3\gamma+1)}\right\}+\cdots.
\end{aligned}
\tag{80}
$$

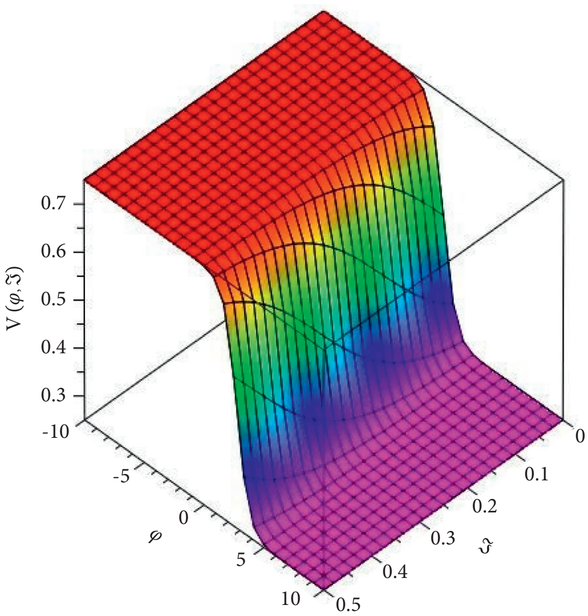

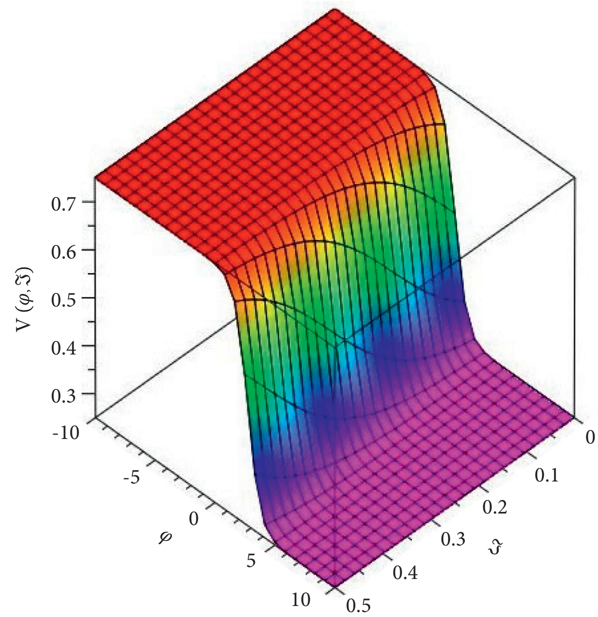

FIGURE 10: The analytical and exact result plot at $\mathbb{V}(\varphi, \mathfrak{J})$ of Example 3 for $\rho = 0.5$, $\varrho = 1$, and $\delta = 2$.

Consequently, we get

$$
\begin{aligned}
\mathbb{V}(\varphi, \mathfrak{J}) &= \frac{1}{4}(2 - \tanh\varphi) - \frac{11}{8}\sec h^2(\varphi)\left((1-\gamma) + \frac{\gamma\mathfrak{J}^{\gamma}}{\Gamma(\gamma+1)}\right) + \frac{121}{8}\tanh(\varphi)\sec h^2(\varphi)\left((1-\gamma)^2 + \frac{\gamma^2\mathfrak{J}^{2\gamma}}{\Gamma(2\gamma+1)} + \frac{2(1-\gamma)\gamma\mathfrak{J}^{\gamma}}{\Gamma(\gamma+1)}\right) \\
&\quad - \frac{1331}{48}\sec h^4(\varphi)[\cosh(2\varphi) - 2]\left\{(1-\gamma)^3 + \gamma(1-\gamma)\left(1+\gamma+2\gamma^2\right)\frac{\mathfrak{J}^{\gamma}}{\Gamma(\gamma+1)} + \frac{3\gamma^2(1-\gamma)\mathfrak{J}^{2\gamma}}{\Gamma(2\gamma+1)} + \frac{\gamma^3\Gamma(2\gamma+1)\mathfrak{J}^{3\gamma}}{\Gamma(3\gamma+1)}\right\} + \cdots, \\
\mathbb{W}(\varphi, \mathfrak{J}) &= (2 - \tanh\varphi) - \frac{11}{2}\sec h^2(\varphi)\left((1-\gamma) + \frac{\gamma\mathfrak{J}^{\gamma}}{\Gamma(\gamma+1)}\right) + \frac{121}{4}\tanh(\varphi)\sec h^2(\varphi)\left((1-\gamma)^2 + \frac{\gamma^2\mathfrak{J}^{2\gamma}}{\Gamma(2\gamma+1)} + \frac{2(1-\gamma)\gamma\mathfrak{J}^{\gamma}}{\Gamma(\gamma+1)}\right) \\
&\quad - \frac{2662}{48}\sec h^4(\varphi)[\cosh(2\varphi) - 2]\left\{(1-\gamma)^3 + \gamma(1-\gamma)\left(1+\gamma+2\gamma^2\right)\frac{\mathfrak{J}^{\gamma}}{\Gamma(\gamma+1)} + \frac{3\gamma^2(1-\gamma)\mathfrak{J}^{2\gamma}}{\Gamma(2\gamma+1)} + \frac{\gamma^3\Gamma(2\gamma+1)\mathfrak{J}^{3\gamma}}{\Gamma(3\gamma+1)}\right\} + \cdots.
\end{aligned}
\tag{81}
$$

By putting $\gamma = 1$, we obtain the exact result of modified couple Korteweg–de Vries equation (2):

$$
\begin{aligned}
\mathbb{U}(\varphi, \mathfrak{J}) &= \frac{1}{2}\left(2 + \tanh\left(\varphi - \frac{11\mathfrak{J}}{2}\right)\right), \\
\mathbb{V}(\varphi, \mathfrak{J}) &= \frac{1}{4}\left(2 - \tanh\left(\varphi - \frac{11\mathfrak{J}}{2}\right)\right), \\
\mathbb{W}(\varphi, \mathfrak{J}) &= \left(2 - \tanh\left(\varphi - \frac{11\mathfrak{J}}{2}\right)\right).
\end{aligned}
\tag{82}
$$

In Figures 9–11, the actual and analytical solutions of $\mathbb{U}(\varphi, \mathfrak{J}), \mathbb{V}(\varphi, \mathfrak{J})$, and $\mathbb{W}(\varphi, \mathfrak{J})$ are proved at $\delta = 2$, $\rho = 0.5$, and $\varrho = 1$. In Figures 12–14, the surface and two-dimensional figure for $\mathbb{U}(\varphi, \mathfrak{J}), \mathbb{V}(\varphi, \mathfrak{J})$, and $\mathbb{W}(\varphi, \mathfrak{J})$ for numerous fractional orders are described which demonstrate that the modified decomposition technique and

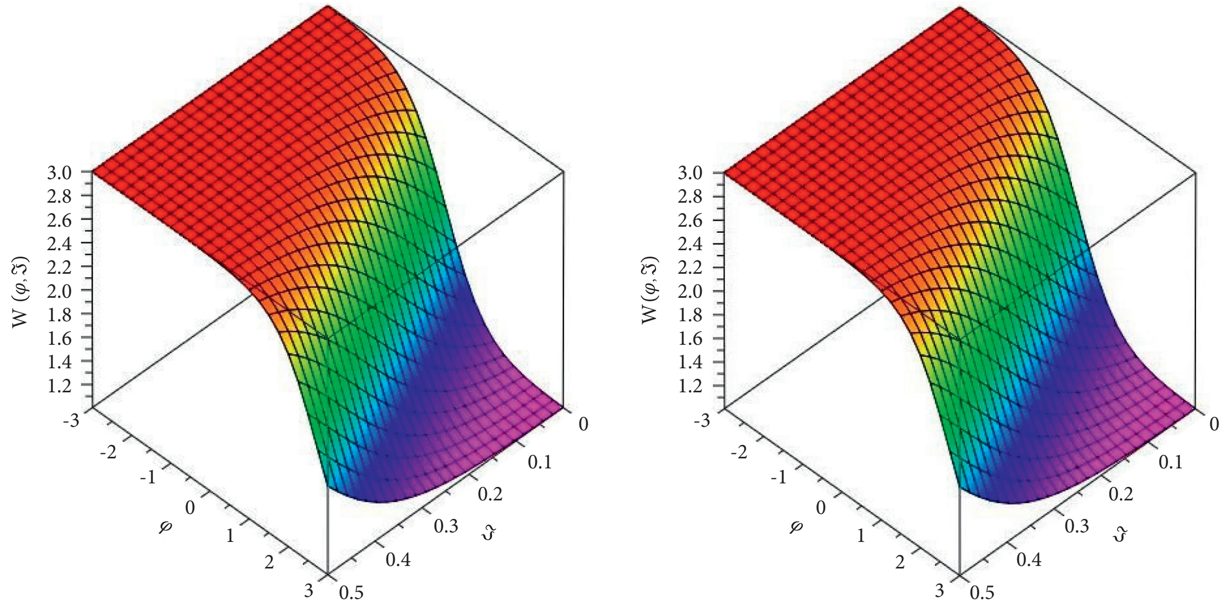

Figure 11: The analytical and exact result plot at $\mathbb{W}(\varphi, \mathfrak{J})$ of Example 3 for $\rho = 0.5$, $\varrho = 1$, and $\delta = 2$.

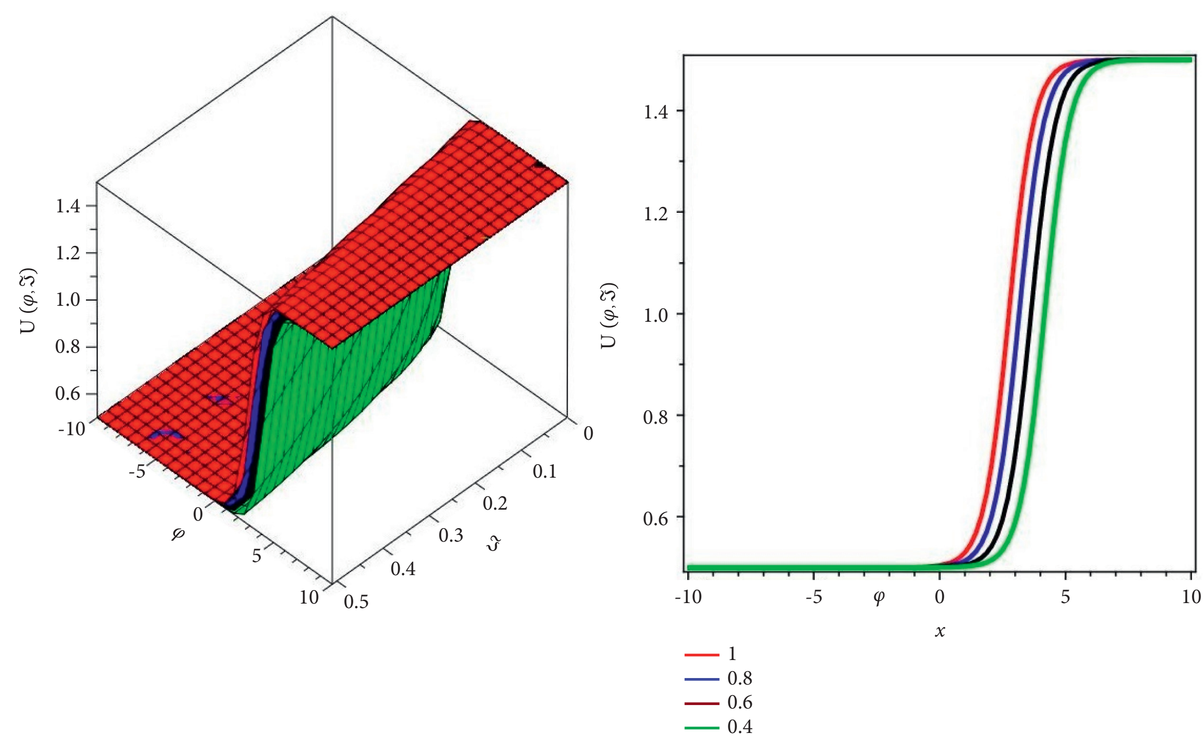

Figure 12: The three and two dimensional different fractional order of Example 3 with respect to $U(\varphi, \mathfrak{J})$.

new iterative transformation technique approximated obtained results are in close contact with the analytical and the exact results. This comparison shows a strong connection among the modified decomposition method and actual solutions. Consequently, the modified decomposition technique and new iterative transformation technique are accurate innovative techniques which need less calculation time and are very simple and more flexible than the homotopy analysis technique and homotopy perturbation technique.

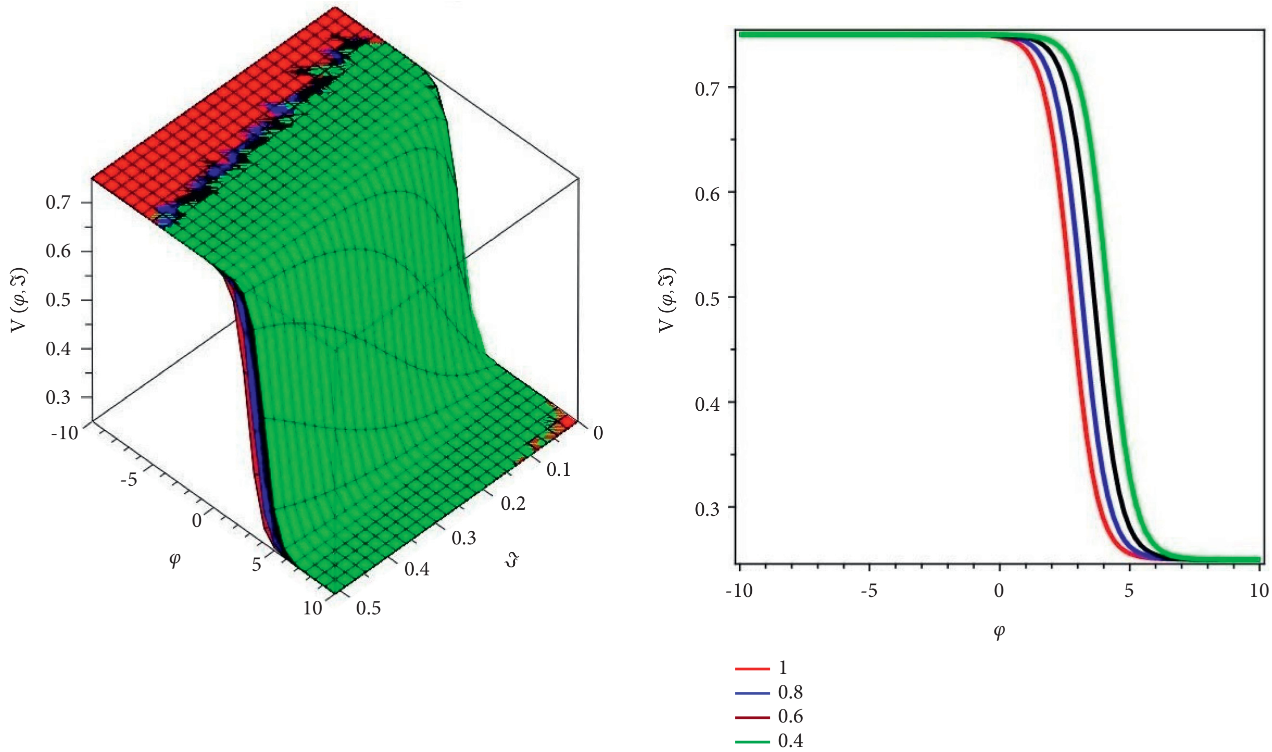

Figure 13: The three and two dimensional different fractional order of Example 3 with respect to V (φ, 𝔍).

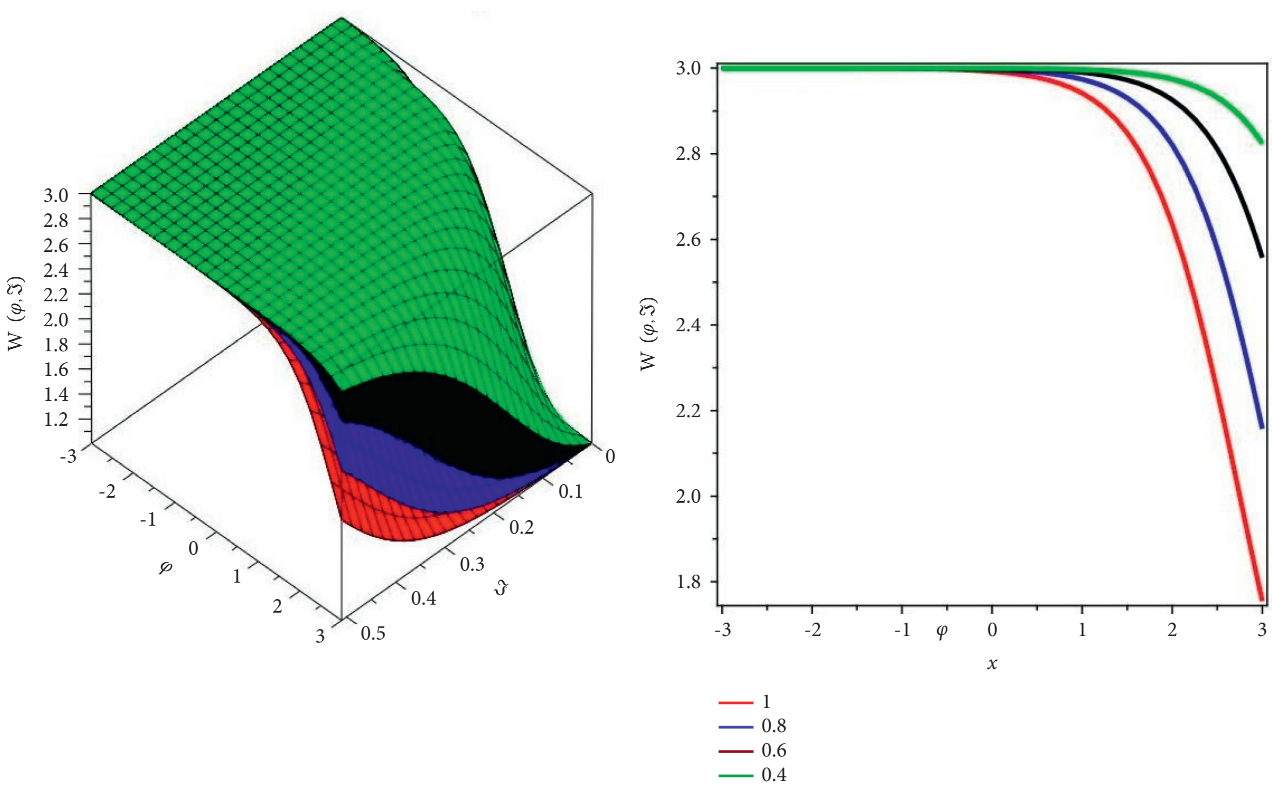

Figure 14: The three and two dimensional different fractional order of Example 3 with respect to W (φ, 𝔍).

7. Conclusion

In this article, we have considered the nonlinear fractional-order Korteweg–de Vries equations in the sense of the Atangana–Baleanu derivative which is able to perform more extensive analysis due to the nonsingular kernel in its structure. The mathematical solutions are obtained with the help of the modified decomposition method and new iterative transformation method associated with the Atangana–Baleanu derivative. The present analysis illuminates the effectiveness of the considered derivative operator. We can conclude from the analytical results that these are very reliable, simple, and powerful methods for finding approximate results of many fractional physical models which arise in applied sciences. In this approach, we do not need the Lagrange multiplier, correction functional, and stationary conditions or to calculate heavy integrals because the results established are noise free, which overcomes the shortcomings of existing methods. It is remarkable that the projected approaches are well-organized analytical methods for finding approximate analytical solutions to complex nonlinear partial differential equations. Finally, we conclude that this scheme, in future, will be taken into account in order to cope with other complex nonlinear fractional-order systems of equations.

Data Availability

The numerical data used to support the findings of this study are included within the article.

Conflicts of Interest

The authors declare that there are no conflicts of interest regarding the publication of this article.

References

[1] M. Caputo and M. Fabrizio, “A new definition of fractional derivative without singular kernel,” *Progress in Fractional Differentiation and Applications*, vol. 1, no. 2, pp. 1–13, 2015.

[2] M. Caputo and M. Fabrizio, “Applications of new time and spatial fractional derivatives with exponential kernels,” *Progress in Fractional Differentiation and Applications*, vol. 2, no. 2, pp. 1–11, 2016.

[3] P. Sunthrayuth, R. Ullah, A. Khan et al., “Numerical analysis of the fractional-order nonlinear system of Volterra integro-differential equations,” *Journal of Function Spaces*, vol. 2021, Article ID 1537958, 10 pages, 2021.

[4] P. Veeresha, E. Ilhan, D. G. Prakasha, H. Mehmet Baskonus, and W. Gao, “Regarding on the fractional mathematical model of tumour invasion and metastasis,” *Computer Modeling in Engineering & Sciences*, vol. 127, no. 3, pp. 1013–1036, 2021.

[5] J. Xu, K. Hassan, S. Rasool, A. A. Alderremy, A. Shaban, and B. Dumitru, “The analytical analysis of nonlinear fractional-order dynamical models,” *AIMS Mathematics*, vol. 6, no. 6, pp. 6201–6219, 2021.

[6] A. Atangana and D. Baleanu, “New fractional derivatives with nonlocal and non-singular kernel: theory and application to heat transfer model,” *Thermal Science*, vol. 20, 2016.

[7] P. Sunthrayuth, N. H. Aljahdaly, A. Ali, R. Shah, I. Mahariq, and A. M. Tchalla, “ψ-haar wavelet operational matrix method for fractional relaxation-oscillation equations containing-caputo fractional derivative,” *Journal of Function Spaces*, vol. 2021, Article ID 7117064, 14 pages, 2021.

[8] O. A. Arqub, M. S. Osman, A.-H. Abdel-Aty, A.-B. A. Mohamed, and S. Momani, “A numerical algorithm for the solutions of ABC singular Lane-Emden type models arising in astrophysics using reproducing kernel discretization method,” *Mathematics*, vol. 8, no. 6, p. 923, 2020.

[9] C. Park, R. I. Nuruddeen, K. K. Ali, L. Muhammad, M. S. Osman, and D. Baleanu, “Novel hyperbolic and exponential ansatz methods to the fractional fifth-order Korteweg-de Vries equations,” *Advances in Difference Equations*, vol. 627, pp. 1–12, 2020.

[10] A. A. Alderremy, H. Khan, R. Shah, S. Aly, and D. Baleanu, “The analytical analysis of time-fractional Fornberg-Whitham equations,” *Mathematics*, vol. 8, no. 6, p. 987, 2020.

[11] J.-H. He, “A short remark on fractional variational iteration method,” *Physics Letters A*, vol. 375, no. 38, pp. 3362–3364, 2011.

[12] R. Shah, H. Khan, D. Baleanu, P. Kumam, and M. Arif, “A semi-analytical method to solve family of Kuramoto-Sivashinsky equations,” *Journal of Taibah University for Science*, vol. 14, no. 1, pp. 402–411, 2020.

[13] S. Sarwar, S. Alkhalaf, S. Iqbal, and M. A. Zahid, “A note on optimal homotopy asymptotic method for the solutions of fractional order heat- and wave-like partial differential equations,” *Computers & Mathematics with Applications*, vol. 70, no. 5, pp. 942–953, 2015.

[14] R. Shah, H. Khan, and D. Baleanu, “Fractional Whitham-Broer-Kaup equations within modified analytical approaches,” *Axioms*, vol. 8, no. 4, p. 125, 2019.

[15] J. Wang, A. Jamal, and X. Li, “Numerical solution of fractional-order fredholm integrodifferential equation in the sense of atangana-baleanu derivative,” *Mathematical Problems in Engineering*, vol. 2021, Article ID 6662808, 8 pages, 2021.

[16] Y. Wu, X. Geng, X. Hu, and S. Zhu, “A generalized Hirota-Satsuma coupled Korteweg-de Vries equation and miura transformations,” *Physics Letters A*, vol. 255, no. 4-6, pp. 259–264, 1999.

[17] D. J. Korteweg and G. De Vries, “XLI. On the change of form of long waves advancing in a rectangular canal, and on a new type of long stationary waves,” *The London, Edinburgh, and Dublin Philosophical Magazine and Journal of Science*, vol. 39, no. 240, pp. 422–443, 1895.

[18] M. Ghoreishi, A. M. Ismail, and A. Rashid, “The solution of coupled modified KdV system by the homotopy analysis method,” *TWMS Journal of Pure and Applied Mathematics*, vol. 3, no. 1, pp. 122–134, 2012.

[19] D. Kaya and I. E. Inan, “Exact and numerical traveling wave solutions for nonlinear coupled equations using symbolic computation,” *Applied Mathematics and Computation*, vol. 151, no. 3, pp. 775–787, 2004.

[20] L. Akinyemi and S. N. Huseen, “A powerful approach to study the new modified coupled Korteweg-de Vries system,” *Mathematics and Computers in Simulation*, vol. 177, pp. 556–567, 2020.

[21] C. O. K. Chen and S. H. Ho, “Solving partial differential equations by two-dimensional differential transform method,” *Applied Mathematics and Computation*, vol. 106, no. 2-3, pp. 171–179, 1999.

[22] Y.-T. Gao and B. Tian, "Ion-acoustic shocks in space and laboratory dusty plasmas: two-dimensional and non-traveling-wave observable effects," *Physics of Plasmas*, vol. 8, no. 7, pp. 3146–3149, 2001.
[23] A. R. Osborne, "The inverse scattering transform: tools for the nonlinear fourier analysis and filtering of ocean surface waves," *Chaos, Solitons & Fractals*, vol. 5, no. 12, pp. 2623–2637, 1995.
[24] L. A. Ostrovsky and Y. A. Stepanyants, "Do internal solitions exist in the ocean?" *Reviews of Geophysics*, vol. 27, no. 3, pp. 293–310, 1989.
[25] A. Gokdogan, A. Yildirim, and M. Merdan, "Solving coupled-KdV equations by differential transformation method," *World Applied Sciences Journal*, vol. 19, no. 12, pp. 1823–1828, 2012.
[26] K. Nonlaopon, A. M. Alsharif, A. M. Zidan, A. Khan, Y. S. Hamed, and R. Shah, "Numerical investigation of fractional-order Swift-Hohenberg equations via a novel transform," *Symmetry*, vol. 13, no. 7, p. 1263, 2021.
[27] H. Khan, R. Shah, P. Kumam, D. Baleanu, and M. Arif, "Laplace decomposition for solving nonlinear system of fractional order partial differential equations," *Advances in Difference Equations*, vol. 375, pp. 1–18, 2020.
[28] H. Jafari and M. A. Firoozjaee, "Homotopy analysis method for solving KdV equations," *Surveys in Mathematics and its Applications*, vol. 5, pp. 89–98, 2010.
[29] M. A. Mohamed and M. S. Torky, "Numerical solution of nonlinear system of partial differential equations by the Laplace decomposition method and the pade approximation," *American Journal of Computational Mathematics*, vol. 3, no. 3, p. 175, 2013.
[30] D. Lu, M. Suleman, M. Ramzan, and J. Ul Rahman, "Numerical solutions of coupled nonlinear fractional KdV equations using He's fractional calculus," *International Journal of Modern Physics B*, vol. 35, no. 02, Article ID 2150023, 2021.
[31] W. He, N. Chen, I. Dassios, N. A. Shah, and J. D. Chung, "Fractional system of korteweg-de Vries equations via Elzaki transform," *Mathematics*, vol. 9, no. 6, p. 673, 2021.
[32] A. R. Seadawy and K. El-Rashidy, "Water wave solutions of the coupled system Zakharov-Kuznetsov and generalized coupled KdV equations," *The Scientific World Journal*, vol. 2014, Article ID 724759, 6 pages, 2014.
[33] R. de la Rosa, E. Recio, T. M. Garrido, and M. S. Bruzon, "Lie symmetry analysis of $(2+1)$-dimensional KdV equations with variable coefficients," *International Journal of Computer Mathematics*, vol. 97, no. 1-2, pp. 330–340, 2020.
[34] M. Inc and E. Cavlak, "On numerical solutions of a new coupled MKdV system by using the adomian decomposition method and He's variational iteration method," *Physica Scripta*, vol. 78, no. 4, Article ID 045008, 2008.
[35] E. Fan, "Using symbolic computation to exactly solve a new coupled MKdV system," *Physics Letters A*, vol. 299, no. 1, pp. 46–48, 2002.
[36] G. Lin, L. Grinberg, and G. E. Karniadakis, "Numerical studies of the stochastic Korteweg-de Vries equation," *Journal of Computational Physics*, vol. 213, no. 2, pp. 676–703, 2006.
[37] M. Inc, M. Parto-Haghighi, M. A. Akinlar, and Y.-M. Chu, "New numerical solutions of fractional-order Korteweg-de Vries equation," *Results in Physics*, vol. 19, Article ID 103326, 2020.
[38] V. Daftardar-Gejji and H. Jafari, "An iterative method for solving nonlinear functional equations," *Journal of Mathematical Analysis and Applications*, vol. 316, no. 2, pp. 753–763, 2006.
[39] H. Jafari, M. Nazari, D. Baleanu, and C. M. Khalique, "A new approach for solving a system of fractional partial differential equations," *Computers & Mathematics with Applications*, vol. 66, no. 5, pp. 838–843, 2013.
[40] M. Ramadan and M. S. Al-luhaibi, "New iterative method for solving the fornberg-whitham equation and comparison with homotopy perturbation transform method," *British Journal of Mathematics & Computer Science*, vol. 4, no. 9, pp. 1213–1227, 2014.
[41] A. A. Alderremy, T. M. Elzaki, and M. Chamekh, "New transform iterative method for solving some Klein-Gordon equations," *Results in Physics*, vol. 10, pp. 655–659, 2018.
[42] D. Rani and V. Mishra, "Modification of Laplace Adomian decomposition method for solving nonlinear Volterra integral and integro-differential equations based on Newton Raphson formula," *European Journal of Pure and Applied Mathematics*, vol. 11, no. 1, pp. 202–214, 2018.
[43] G. A. Birajdar, "Numerical solution of time fractional Navier-Stokes equation by discrete Adomian decomposition method," *Nonlinear Engineering*, vol. 3, no. 1, pp. 21–26, 2014.
[44] T. Sitthiwirattham, R. Gul, K. Shah, I. Mahariq, J. Soontharanon, and K. J. Ansari, "Study of implicit-impulsive differential equations involving Caputo-Fabrizio fractional derivative," *AIMS Mathematics*, vol. 7, no. 3, pp. 4017–4037, 2022.

Hindawi
Journal of Mathematics
Volume 2022, Article ID 3237815, 12 pages
https://doi.org/10.1155/2022/3237815

Research Article

Analysis of Metallic Nanoparticles (Cu, Al_2O_3, and SWCNTs) on Magnetohydrodynamics Water-Based Nanofluid through a Porous Medium

P. K. Pattnaik,[1] S. K. Parida,[2] S. R. Mishra,[3] M. Ali Abbas,[4] and M. M. Bhatti[5]

[1]*Department of Mathematics, Odisha University of Technology and Research, Bhubaneswar 751029, Odisha, India*
[2]*Department of Physics, Siksha 'O' Anusandhan Deemed to be University, Bhubaneswar 751030, Odisha, India*
[3]*Department of Mathematics, Siksha 'O' Anusandhan Deemed to be University, Bhubaneswar 751030, Odisha, India*
[4]*Department of Mathematics, University of Baltistan Skardu, Gilgit-Baltistan 16100, Pakistan*
[5]*College of Mathematics and Systems Science, Shandong University of Science and Technology, Qingdao, Shandong 266590, China*

Correspondence should be addressed to M. M. Bhatti; mmbhatti@sdust.edu.cn

Received 15 October 2021; Revised 29 December 2021; Accepted 7 January 2022; Published 14 February 2022

Academic Editor: Fairouz Tchier

In this communication, the effect of the addition of the copper (Cu), aluminum oxide (Al_2O_3), and single-wall carbon nanotubes (SWCNTs) metallic nanoparticles on the magnetohydrodynamics (MHD) water-based flow over a porous elastic surface is explored. The objective of the work is to include the radiative effect that interacts with the metallic nanoparticles due to permeability of the surface. The significance of this study stems from the fact that the design of various equipment, such as nuclear power plants, gas turbines, propulsion devices for aircraft, and missiles, is dependent on radiative heat transfer. To formulate the mathematical modelling, similarity transformations were used, and nonlinear differential equations were obtained. To solve the formulated nonlinear differential equations, the Runge–Kutta fourth-order numerical scheme is used in conjunction with the shooting technique. The behavior of velocity profile and temperature profile has been discussed in detail and also engineering quantities such as Nusselt and Sherwood number which are calculated. Furthermore, the addition of metallic nanoparticles enhanced the nanofluid properties for energy transfer enrichment and found many applications in various fields of science and technology.

1. Introduction

Choi introduced a new type of fluid called nanofluid in 1995, which has amazing thermal conductivity properties. The goal of the concept is to saturate nanosized particles in conventional fluids known as base fluids. Nanofluids are extremely important in thermal conductivity, heat transfer enhancement, energy, and other thermos-physical properties for industrial applications [1–5]. The heat transfer capacity of a nanofluid after the addition of metallic and nonmetallic nanoparticles in a conventional base fluid was of particular interest to the researchers. Mohebbi et al. [6] investigated the mathematical model of the Heat Transfer Augmentation Associated with Cu/Water Nanofluid in a Channel with Surface Mounted Blocks by using Lattice Boltzmann Method. The numerical method is applied for the forced convection flow and heat transfer of a nanofluid flowing inside a straight circular pipe by Saryazdi et al. [7]. Moreover, Baag and Mishra [8] discussed heat and mass transfer analysis on MHD 3D water-based nanofluid. The prominent examples of nanofluids are ethylene glycols, kerosene, and water. It has been observed that conducting nanofluids presents their special attention because of their use in diversified areas such as biomedical solicitation as tuneable optical filters, drug delivery, and cancer therapy. Watanabe and Pop [9] deliberately presented the magnetohydrodynamic flow of particular fluid for the occurrence of applied magnetic field through a flat plate. Numerical treatment is depicted by Armaghani et al. [10] for the mixed convective flow phenomena of nanofluid within open C-shaped enclosures. For the enhanced properties, they have used CuO nanoparticles which are dispersed within the base fluid water and the enclosure is imposed with constant magnetic field. Furthermore, the influential behavior of the characterizing parameters such as Richardson number and volume concentration affects the flow phenomena as well. The work of Ibrahim and Terbeche [11] leads to bring out the effective properties of the non-Newtonian power-law fluid with due occurrence of the magnetic field. Analytical approach is employed for the solution of the designed problem and numerical methods are useful for the validation of the current result and the convergence criterion.

Fluid flow and heat transfer with non-Newtonian fluids, for example, are a challenge in the modern revolution, particularly in the oil industry, bubble columns and absorption, zymosis, boiling, plastic foam processing [12], etc. However, the possible applications relating to this type of flow can be observed in various industries. The generation of electric power in the corresponding electric power industry is one of the examples that uses the extraction of energy. The governing equations for different non-Newtonian fluid models are amid the utmost complex equations so that the development in mathematical modelling is of great interest nowadays. A time-dependent flow characterized by the several parameters for the nanofluids past an expanding sheet is presented by Andersson et al. [13]. Furthermore, similarity approach for the complex unsteady flow problem past over an expanding sheet is carried out by Elbashbeshy and Bazid [14]. Thermophoresis and Brownian motion effect on the flow of nanofluid through a vertical plate has been studied by Kuznetsov and Nield [15]. They pointed out that the cooling rate of the plate decreases due to decrement in strengthens of thermophoresis and Brownian motion. Heidary and Kermani [16] studied the effect of solid volume fraction of nanofluid and magnetic strength. They examined that existence of magnetic field and nanofluid could significantly enhance heat transfers properties of the flow phenomena. The thermal properties of the base fluids change appreciable after addition of the metallic nanoparticles and calculate the thermos-physical parameters [17]. Masuda et al. [18] reported that, after addition of ultrafine nanoparticles, there is an alteration in the thermal conductivities and viscosities. Mishra et al. [19] recently studied a chemically reactive nano-micropolar fluid with variable heat sink/source and slip conditions. Shutaywi and Shah [20] proposed a numerical and mathematical model of a nanofluid that includes entropy formation.

The application of electrically conductive fluid currents is encircled in the field of nanocomposite and metallurgy. The flows of several fluids under the action of magnetic field such as MHD generators, oil exploration, energy extraction, and boundary layer control have attracted many researchers. Metallurgical requirements consist of continuous cooling belts or filaments such as hardening, disperse, and sketching processes for copper wires. It has been noticed that the effects of Coriolis force are larger than those of viscosity and inertia forces in the hydro-magnetic equations of motion in a rotating environment. Several researchers have been investigated on MHD with various kinds of fluid and geometries. For example, Ibrahim and Negera [21] investigated the upper-convected Maxwell nanofluid flow with slip and MHD effects through a stretching sheet and chemical reaction. Abdal et al. [22] examine the thermo-diffusion with magnetized mixed convection unsteady nanofluid flow through stretching/shrinking surface with heat source and thermal radiation. Ghasemi and Hatami [23] described the solar radiation effects on magnetized stagnation point nanofluid flow through a stretching surface. Some important references related to the proposed topic can be found in [24–28] and several therein. Recently, Upreti et al. [29, 30] considered carbon nanotube nanofluids for the behavior of various physical quantities in different geometries. They have projected the effect of drag force with an interaction of Joule heating and nonuniform heat source/sink. Also, binary chemical reaction with the impact of radiative heat on the flow phenomena over an expanding surface is considered. Sabu et al. [31] investigated the enhancement of heat transfer caused by a thermal and space dependent heat source, magnetic field, and nanoparticles propagating over an elastic spinning disk. Mahanthesh et al. [32] investigated Reiner–Rivlin nanofluid flow through a rotating disk with multiple slips and a distinct heat source.

Therefore, the primary goal of this research is to determine the presence of three metallic nanoparticles (Cu, Al_2O_3, and SWCNTs) in an electrically conducting water-based nanofluid propagating through a porous medium. Thermal radiation is important in industrial applications. As a matter of fact, the study's novelty stems from the incorporation of thermal radiation as well as an additional heat source/sink within a permeable medium. The mathematical modelling was developed using similarity transformations. The nonlinear differential equations are solved using the Runge–Kutta and shooting techniques. When compared to other similar methods used for nonlinear problems, the current numerical method yields promising results [33, 34]. The graphical interpretation of the velocity and temperature profiles have been discussed in detail and expected results show the excellent industrial applications.

2. Problem Formulation

The time-dependent electrically conducting flow of nanofluids through a permeable medium is presented in this article. For the enhanced feature in heat transfer attempt is made to consider SWCNTs in the water-based nanofluid along with Cu and Al_2O_3 nanoparticles. Moreover, the novelty of the study arises for the inclusion of radiative heat transfer with additional external heat source/sink that enriches the energy profile. The flow through porous elastic surface along the x-direction and the transverse magnetic field of uniform strength B_0 is proposed along the normal direction of the surface, i.e., y-direction, as given in Figure 1. Due to permeability of the surface, the occurrence of suction/injection has its immense use on the flow phenomena. Following Zhang et al. [35], the proposed assumptions lead to design the model with the boundary conditions as

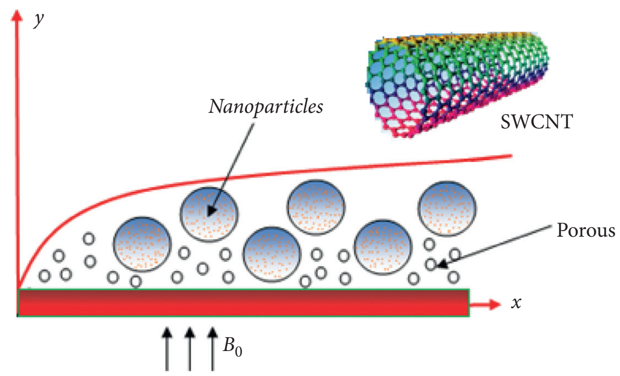

Figure 1: Flow configuration.

$$\frac{\partial u}{\partial x}+\frac{\partial v}{\partial y}=0,$$
$$\rho_{nf}\left(\frac{\partial u}{\partial t}+u\frac{\partial u}{\partial x}+v\frac{\partial u}{\partial y}\right)=-\frac{\partial p}{\partial x}+\mu_{nf}\frac{\partial^2 u}{\partial y^2}-\left(\frac{\mu_{nf}}{K}+\sigma_{nf}B_0^2\right)u,$$
$$\left(\rho c_p\right)_{nf}\left(\frac{\partial T}{\partial t}+u\frac{\partial T}{\partial x}+v\frac{\partial T}{\partial y}\right)=k_{nf}\frac{\partial^2 T}{\partial y^2}-\frac{\partial q_r}{\partial y}+Q_0\left(T-T_\infty\right), \tag{1}$$

with boundary conditions,

$$\left.\begin{aligned} &u(x,0,t)=0,\\ &v(x,0,t)=v_0(t),\\ &-k_{nf}\frac{\partial T(x,0,t)}{\partial t}=q(x),\\ &u(x,\infty,t)=U(x,t),\\ &T(x,\infty,t)=T_\infty. \end{aligned}\right\} \tag{2}$$

Here, u and v, are the components of velocities along $x-$ and $y-$ direction, T is the temperature of the nanofluid, t is the time taken, p is the fluid pressure, v_0 is a constant, and σ_s and σ_f are the electrical conductivity of the base and nanofluid, respectively.

The physical properties relating to nanofluid such as viscosity, specific heat, density, and conductivity are presented as follows [36]:

$$\left.\begin{aligned} &\mu_{nf}=\frac{\mu_f}{(1-\phi)^{2.5}}, \quad \rho_{nf}=(1-\phi)\rho_f+\phi\rho_s, \left(\rho c_p\right)_{nf}=(1-\phi)\left(\rho c_p\right)_f+\phi\left(\rho c_p\right)_s,\\ &\sigma_{nf}=(1-\phi)\sigma_f+\phi\sigma_s, \quad \frac{k_{nf}}{k_f}=\frac{k_s+2k_f-2\phi\left(k_f-k_s\right)}{k_s+2k_f+\phi\left(k_f-k_s\right)}, \end{aligned}\right\} \tag{3}$$

where ϕ is the particle concentration, μ_f is the dynamics viscosity, ρ_f and ρ_s are the densities, k_f and k_s are the thermal conductivities, and the subscripts f and s are for the base fluid and the solid nanoparticles.

$$\rho_{nf}\left(\frac{\partial u}{\partial t}+u\frac{\partial u}{\partial x}+v\frac{\partial u}{\partial y}\right)=\frac{\partial U}{\partial t}+U\frac{\partial U}{\partial x}+\mu_{nf}\frac{\partial^2 u}{\partial y^2}-\left(\frac{\mu_{nf}}{K}+\sigma_{nf}B_0^2\right)(u-U), \tag{4}$$

where

$$-\frac{\partial p}{\partial x}=\frac{\partial U}{\partial t}+U\frac{\partial U}{\partial x}-\left(\frac{v_{nf}}{K}+\frac{\sigma_{nf}}{\rho_{nf}}B_0^2\right)U, \tag{5}$$

Here, K is the permeability of the given medium and B_0 is an external magnetic field strength.

The stream function as well as variables for the problem is expressed as (see [36])

$$u = \frac{\partial \psi}{\partial y},$$
$$v = -\frac{\partial \psi}{\partial x},$$
$$\eta = y\sqrt{\frac{a}{v_f}},$$
$$\psi = \sqrt{a v_f}\, x f(\eta), \tag{6}$$
$$a = \frac{1}{s + bt},$$
$$T = T_\infty + \frac{q_0 x}{k_f}\sqrt{\frac{v_f}{a}}\theta(\eta),$$
$$q(x) = q_0 x,$$
$$v_0(t) = v_i(t).$$

Using the aforesaid functional expressions, the governing equations are presented as

$$f''' + A_1\left[\left(f + \frac{b\eta}{2}\right)f'' - f'^2 + b\left(f'^2 - 1\right) + 1\right] + (MA_2 + Da)(1 - f') = 0, \tag{7}$$

$$\frac{1}{A_3 Pr}\left(\frac{k_{nf}}{k_f} + Nr\right)\theta'' + \left(f + \frac{b\eta}{2}\right)\theta' - \left(f' + \frac{b}{2} + \frac{\delta}{A_3}\right)\theta = 0, \tag{8}$$

where $M = (\sigma_f/\rho_f b)B_0^2$ is the magnetic parameter, $\Pr = \upsilon_f/\kappa$ is the Prandtl number, $Nr = 16\sigma_1 T_\infty^3/3\kappa k_f$ is the thermal radiation parameter, $Da = \upsilon_f/aK$ is the Darcy number with boundary condition, b is the unsteadiness parameter, and $\delta = q_0 x/(\rho c_p)_f U$ is the heat source parameter.

$$\left.\begin{aligned} f(0) &= fw,\\ f'(0) &= 0,\\ \theta'(0) &= -\frac{k_f}{k_{nf}},\\ f'(\infty) &\longrightarrow 1,\\ \theta(\infty) &\longrightarrow 0, \end{aligned}\right\} \tag{9}$$

where

$$A_1 = (1-\phi)^{2.5}\left(1 - \phi + \phi\frac{\rho_s}{\rho_f}\right),$$
$$A_2 = (1-\phi)^{2.5}\left(1 - \phi + \phi\frac{\sigma_s}{\sigma_f}\right), \tag{10}$$
$$A_3 = 1 - \phi + \phi\frac{(\rho c p)_s}{(\rho c p)_f}.$$

The physical quantities are as follows: $C_f = \tau_w/\rho_f U^2$ is called as skin friction coefficient and $Nu_x = q_w x/k_f(T_w - T_\infty)$ is called local Nusselt number:

$$C_f \mathrm{Re}_x^{0.5} = \frac{f''(0)}{(1-\phi)^{2.5}},$$
$$Nu_x \mathrm{Re}_x^{-0.5} = -\left(\frac{k_{nf}}{k_f} + Nr\right)\theta'(0). \tag{11}$$

3. Numerical Methodology

For solving equations (10)–(12), a multistep integration method, i.e., the Runge–Kutta method, with shooting technique has been deployed. In this process, equations (7) and (8) are reduced to a set of ordinary differential equations as defined below:

$$f = y_1, f' = y_2, f'' = y_3, f''' = -A_1\left[\left(y_1 + \frac{b\eta}{2}\right)y_3 - y_2^2 + b\left(y_1^2 - 1\right) + 1\right] - (MA_2 + Da)(1 - y_1),$$
$$\theta = y_4, \theta' = y_5, \theta'' = A_3\Pr\left(-\left(y_1 + \frac{b\eta}{2}\right)y_5 + \left(y_2 + \frac{b}{2} + \frac{\delta}{A_3}\right)y_4\right)\left(\frac{k_{nf}}{k_f} + Nr\right)^{-1}, \tag{12}$$

under the boundary condition,

$$\left.\begin{aligned} y_1 &= fw,\\ y_2 &= 0,\\ y_5 &= -\frac{k_f}{k_{nf}},\\ y_2 &\longrightarrow 1,\\ y_4 &\longrightarrow 0. \end{aligned}\right\}. \tag{13}$$

Now, it uses only the initial conditions, i.e., for $\eta = 0$. However, due to the unavailability of initial conditions, the assumed initial conditions y_3 and y_4 are to be determined. Therefore, some initial guesses are incorporated to both these values in order to satisfy the boundary conditions at $\eta \longrightarrow \infty (\eta = 4)$. These corrections are taken care by a corrective procedure that follows a self-iterative process. This procedure is used to implement a more accurate method, i.e., the RK method, with shooting numerical technique. For the computational purpose, the step size is assumed as $h = 0.01$. Therefore, the accuracy of computation and the convergence criteria are followed.

4. Results and Discussion

An unsteady two-dimensional flow of metallic water-based nanofluids is considered which past a permeable medium for the action of transverse magnetic field is presented. Interaction of Cu and Al_2O_3 nanoparticles along with SWCNTs in base fluid water is dispersed to prepare nanofluid. Incorporation of radiative heat energy enriches the profile in conjunction to the permeable surface. Numerical technique is used to find the solution of the set of equations for the suitable choice of the pertinent parameters. Table 1 displays all the physical properties of both the particles as well as the base fluid. Table 2 present the validation of the present outcomes for the shear rate considering the case of pure fluid as well as the case of nanofluid with the work of Rizwan et al. [36], and this shows a good corroboration. The graphical illustration shows the significant behavior of these parameters associated with the flow phenomena. Furthermore, the tabular simulated results indicate the rate coefficients, i.e., shear rate and Nusselt number. However, throughout the computation, the following values of the parameters are considered as fixed whereas the variation of particular parameters are presented in the corresponding figures, and these are $\phi = 0.2$, $b = 0.1$, $M = 1$, $Da = 1$, $fw = 0.5$, and $\delta = 1$.

The role of particle concentration due to its appearance through the thermo-physical properties is a vital part of this investigation. Figure 2 describes the significance of particle concentration on the velocity for the Cu, Al_2O_3, and SWCNT-water-based nanofluids. Several characteristics of the suction/injection on each profile are displayed. Here, the parameter $fw > 0$ represents the role of suction whereas $fw < 0$ indicates the injection and $fw = 0$ characterizes the behavior when the flow through impermeable region. The decelerating nature of the profiles shows the increasing width of the bounding surface thickness for the increasing particle concentration. The range of the concentration is treated within $\phi = [0.0, 0.2]$. The impermeability region for the pure fluid is similar to the results obtained by Mishra et al. [19], and it can be obtained by considering $fw = 0$ and $\phi = 0$. Furthermore, the increasing suction enriches the profiles, but the thickness of the bounding surface decreases; however, injection reveals opposite impact on the profile. It reveals the density of the Cu particles and diminishes the profile width in comparison to the particles of Al_2O_3 and SWCNTs. Figure 3 illustrates the behavior of the unsteadiness parameter in association with the suction/injection on the nanofluid velocity profiles. Here, $b \neq 0$ indicates the unsteady case on the velocity of the three different water-based nanofluid. An augmentation in the profiles is rendered for the increasing unsteadiness that causes a deceleration in the bounding surface thickness. The profiles of SWCNT nanofluid are lesser than the other nanoparticles of Al_2O_3 and Cu, respectively. Also, for each of the profiles, interestingly, the thickness decelerates more in case of injection in comparison to impermeable and the case of suction successively. Figure 4 portrays the role of magnetic parameter on the nanofluid velocity profiles with the interaction suction/injection. The magnetic field expresses the influence of moving electric charges along with electric current and magnetic materials. In modern technology, there are various applications of magnetic field such as in both the electric motors and generators; the use of rotating magnetic field is important. The profile augments lead to decelerate the thickness of the velocity-bounding surface for the augmented magnetic parameter. This is due to the resistance offered by the resistive force produced with the interaction of magnetic parameter, i.e., the Lorentz force. It is seen that SWCNTs have greater retardation than that of Al_2O_3 and Cu-water nanofluid. However, suction also favors to decelerate the profile significantly than that of injection. Furthermore, Figure 5 examines the significance of the permeability parameter on the nanofluid velocity distribution. Similar to the magnetic parameter, resistive force offered by porosity also causes a similar behavior on the velocity profiles for each of the nanofluids. The influence of the suction/injection has the same tendency on the profiles as described in the earlier description. The control of suction/injection due to the permeable surface is shown in Figure 6 for the velocity distribution of nanofluids. Generally, the pressure differential occurs by the elimination of air from the space. Therefore, the limited pressure is exerted

Table 1: Thermos-physical properties of base fluid and nanoparticles.

	ρ (kg/m^3)	c_p (J/kg K)	k (W/mK)
Pure water	997.1	4179	0.613
Copper (Cu)	8933	385	401
Aluminum oxide (Al_2O_3)	3970	765	40
SWCNTs	2600	425	6600

Table 2: Validation of shear rate.

Nanofluids	ϕ	$f''(0)$ Rizwan et al. [36]	$f''(0)$ Present
Cu-H_2O	0.0	1.48113419	1.481021
	0.1	1.71105504	1.711003
	0.2	1.75138728	1.751128
Al_2O_3-H_2O	0.0	1.48113419	1.481021
	0.1	1.43438455	1.431625
	0.2	1.33096758	1.330727
SWCNT-H_2O	0.0	1.48113419	1.481021
	0.1	1.45088235	1.450122
	0.2	1.35571879	1.355526

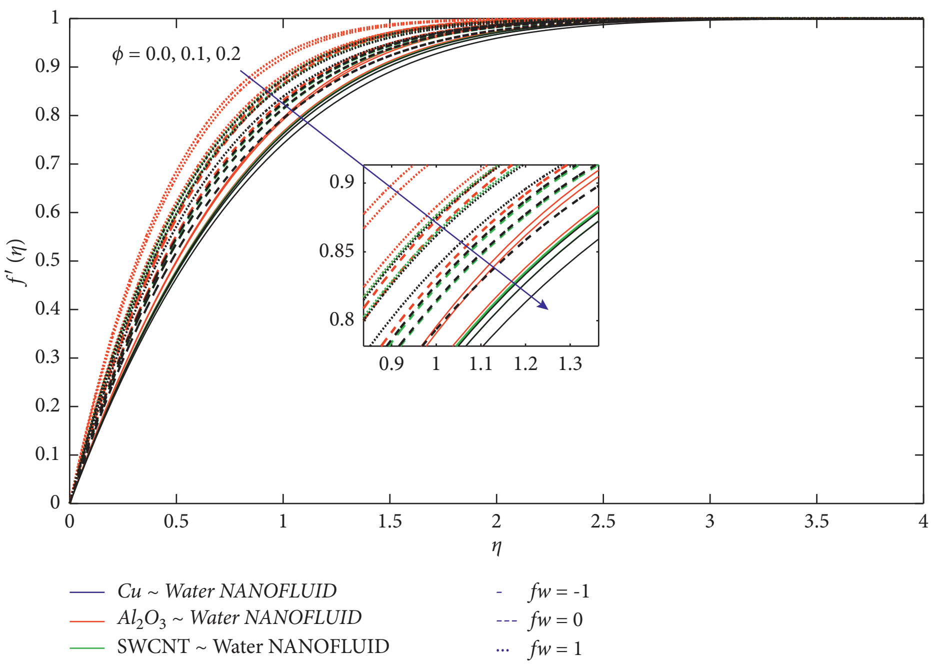

Figure 2: Variation of ϕ on velocity profile.

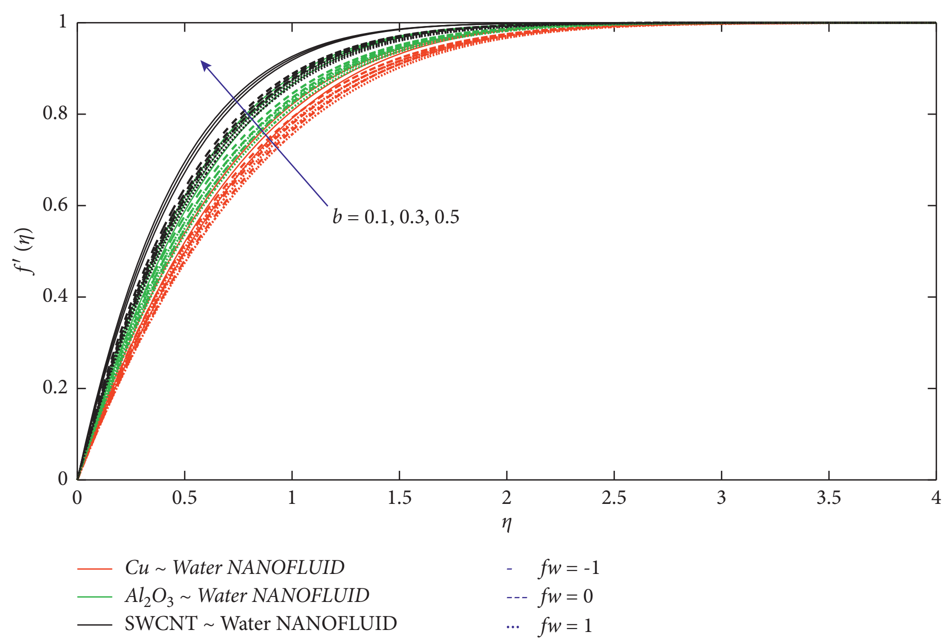

Figure 3: Variation of b on velocity profile.

by the external air. The pressure in one part of the system is reduced in comparison to another; there will be force exerts from the fluid of higher pressure region to lower. However, with escalating suction, the pressure increases, and this leads to decelerate the surface thickness, whereas impact is reversed for the case of injection. The case of impermeability is a particular case which validates with the earlier result. The significant characteristics of the controlling parameters on the fluid temperature is observed and presented. The role of these parameters enhances the thermos-physical properties significantly. Therefore, the current study discloses the properties of particle concentration, magnetic and porosity parameters, suction/injection, and unsteadiness parameter. Figure 7 displays the role of particle concentration on the nanofluid temperature with an interaction of suction/injection. The three-layer variation explains the distribution of different parameters on the Cu, Al_2O_3, and SWCNT-water-based nanofluids, respectively. Furthermore, the fluid temperature boosts its maximum trend in case of Cu-water nanofluid since it is well known that Cu is a good conductor

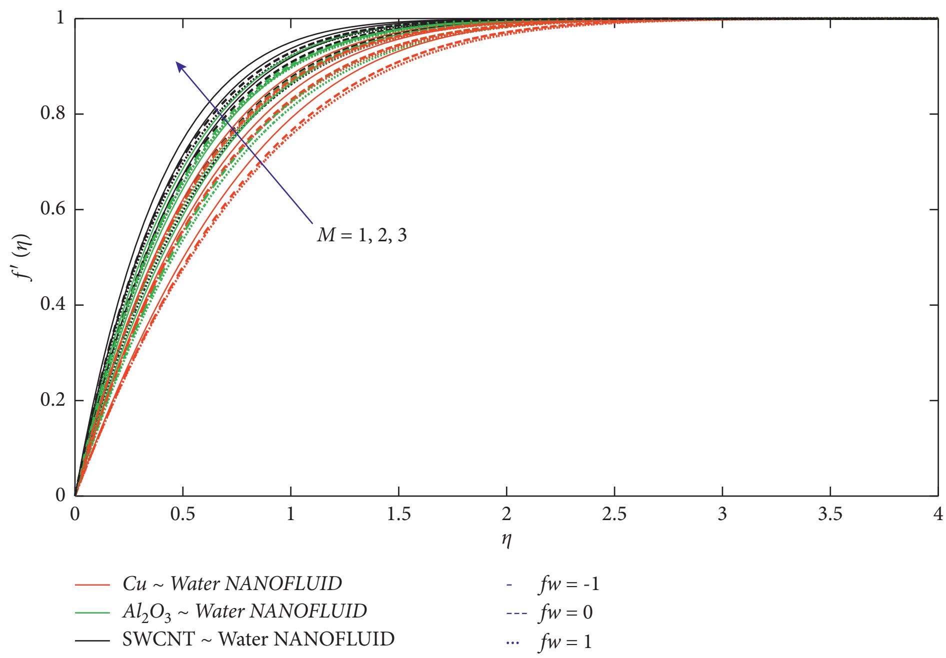

FIGURE 4: Variation of M on velocity profile.

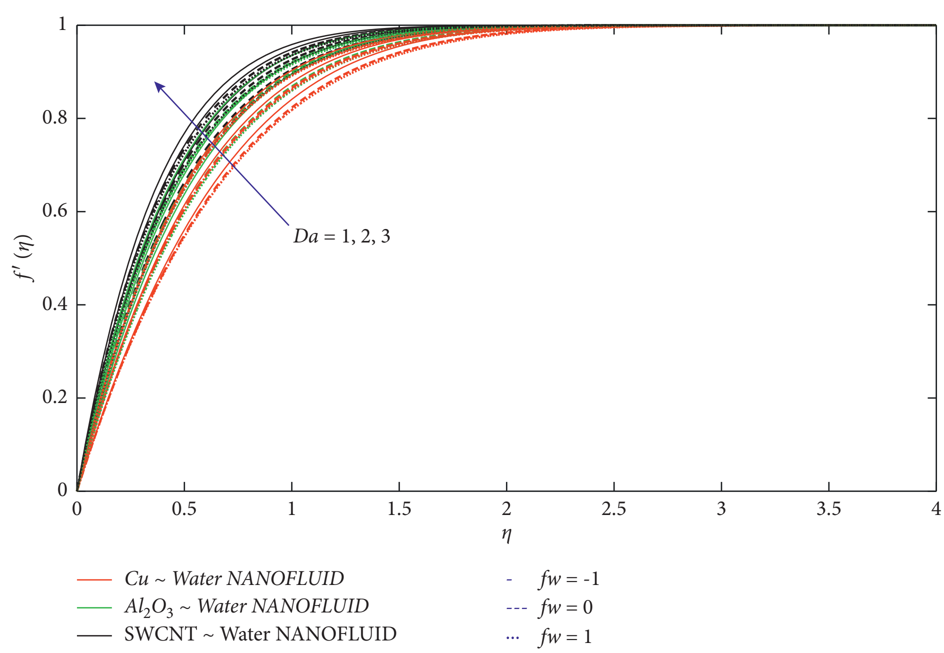

FIGURE 5: Variation of Da on velocity profile.

of heat. Furthermore, with the increase in volume fraction, the profile decelerates significantly. Moreover, suction produces more energy to boost the profile rather than the impermeability of the surface and the case of injection. Figure 8 demonstrates the role of unsteadiness parameter that has important characteristics on the nanofluid temperature. Again, increasing unsteadiness, the fluid temperature decelerates in an order of preference such as Cu, Al_2O_3, and SWCNT-water nanofluid. Therefore, it suggests that effectiveness of the Cu nanoparticle is higher than that of other nanoparticles presented in this study. This gives a suggestive measure for the increasing thermal properties of the Cu-water nanofluid since the proposed thermal conductivity of the nanofluid enhances due to increase in particle concentration. Figure 9 exhibits the effects of the heat source on the nanofluid temperature distribution for different suctions/injections. The inclusion of additional heat suppresses the fluid temperature. In a comparative analysis, it is marked that the Cu-water nanofluid exhibits its maximum strength than other nanofluids. However, no

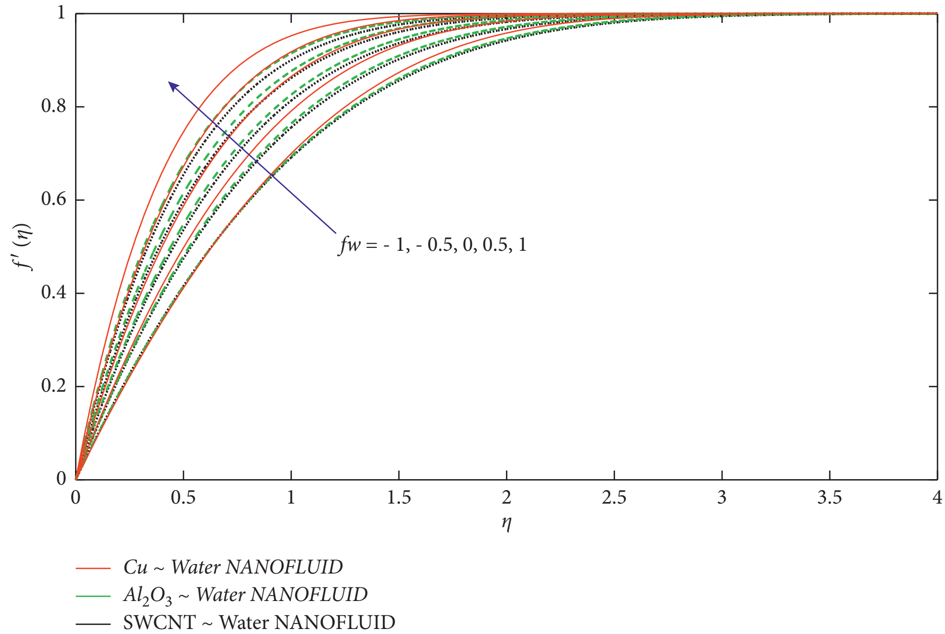

Figure 6: Variation of fw on velocity profile.

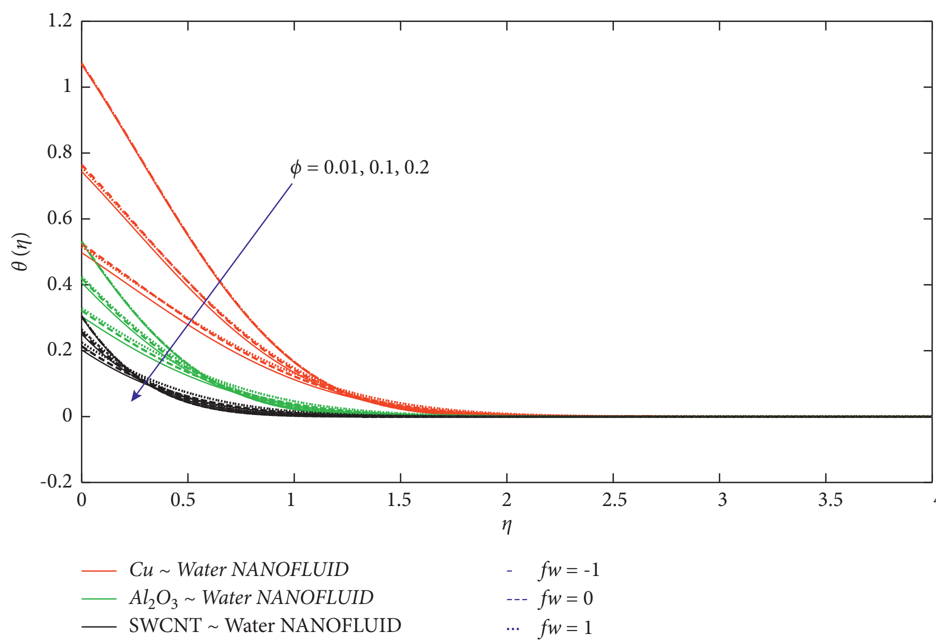

Figure 7: Variation of ϕ on temperature profile.

significant change is marked for the variation of suction/injection. Figure 10 depicts the behavior of the thermal radiation in conjunction to the other contributing parameters on the temperature distributions of the nanofluids. Thermal radiation is due to the release of the electromagnetic waves from the fluid particles that is nothing but the renovation of thermal energy into the electromagnetic energy. With an increase in thermal radiation, the profile rises up and therefore the fluid temperature boosts up. This is because most of the solids and fluids are considered to be the surface phenomena and the interior molecules help to emit the radiations.

Finally, the simulated results of the rate coefficients for several contributing parameters are obtained and presented in Table 3. The nanoparticle concentration enhances the shear rate coefficients whereas heat transfer rate decreases in magnitude. From the tabular results, it is quite clear to see that the rate coefficients are much higher in case of Cu-water nanofluid in comparison to other nanofluids. Furthermore, the resistive forces such as magnetic and porosity of the

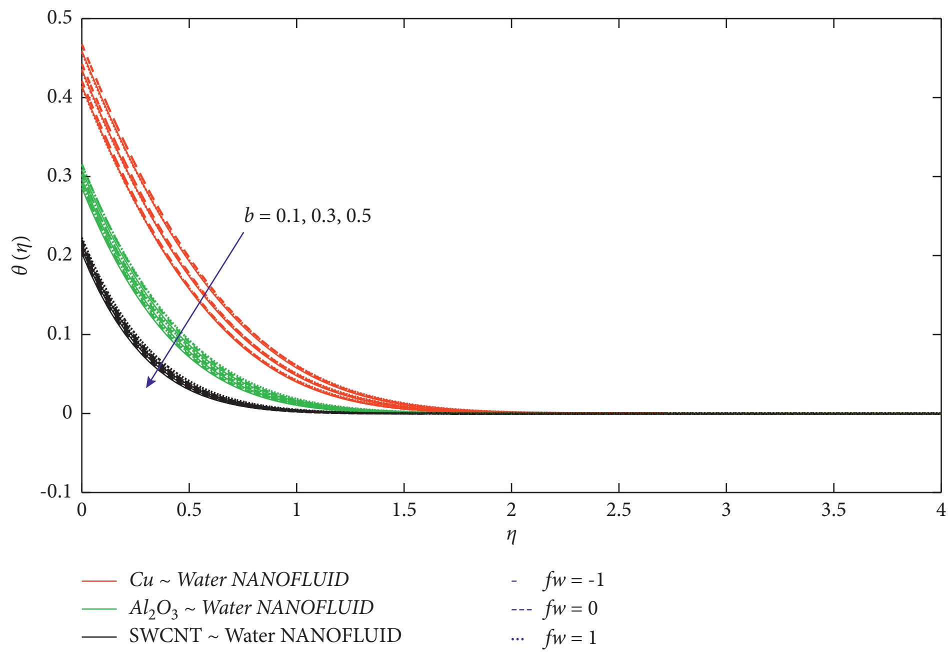

Figure 8: Variation of b on temperature profile.

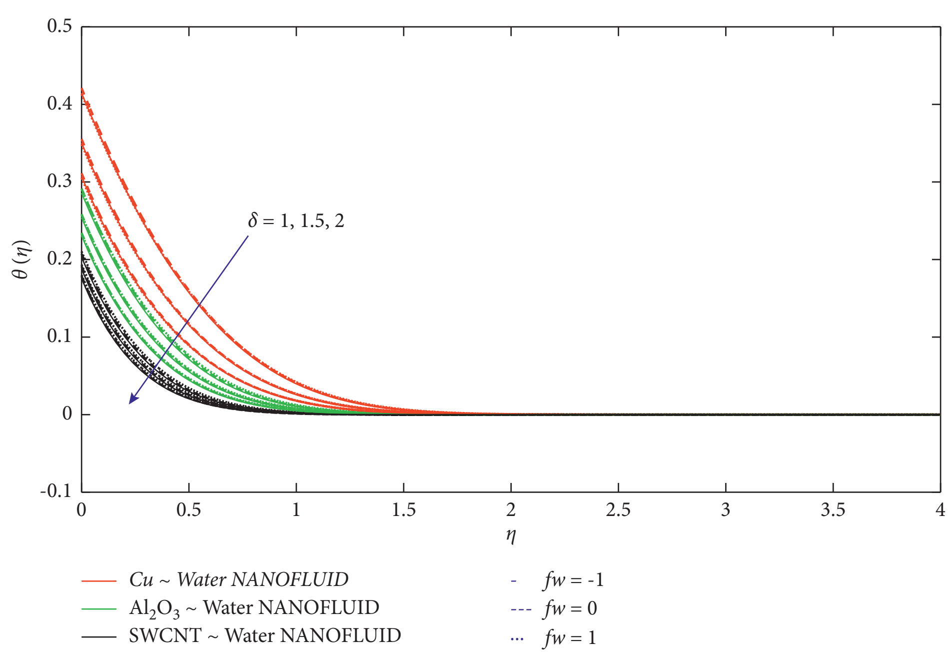

Figure 9: Variation of δ on temperature profile.

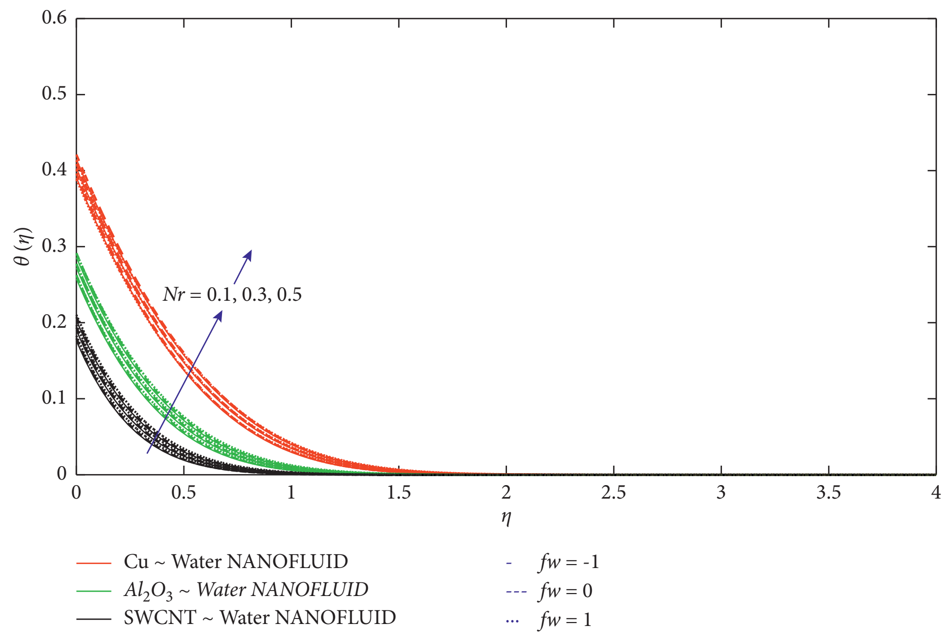

Figure 10: Variation of Nr on temperature profile.

Table 3: Numerical computations of physical quantities used in engineering applications.

ϕ	M	Da	b	fw	Pr	δ	Nr	Cu-water C_f	Cu-water Nu_x	Al_2O_3-water C_f	Al_2O_3-water Nu_x	SWCNTs-water C_f	SWCNTs-water Nu_x
0.1	1	0.1	0.5	0.5	6.2	1	0.5	2.6073	−4.3891	2.2782	−4.3874	2.1858	−4.2266
0.15								3.0849	−3.7691	2.5915	−3.7728	2.4523	−3.5700
0.2								3.6065	−3.2190	2.9466	−3.2312	2.7597	−3.0029
0.1	2							2.9684	−4.4195	2.6735	−4.4239	2.5920	−4.2637
	3							3.2863	−4.4443	3.0137	−4.4528	2.9387	−4.2927
	1	0.2						2.6450	−4.3924	2.3200	−4.3914	2.2290	−4.2308
		0.3						2.6820	−4.3956	2.3610	−4.3953	2.2713	−4.2348
		0.1	0.1					2.8167	−4.1521	2.4481	−4.1439	2.3432	−3.9932
			0.3					2.7139	−4.2726	2.3645	−4.2678	2.2657	−4.1119
			0.5	−0.5				1.5958	−2.1490	1.5570	−2.1602	1.5442	−2.1508
				0				2.0563	−3.1186	1.8913	−3.1214	1.8433	−3.0520
				0.5	1			2.6073	−1.5644	2.2782	−1.5587	2.1858	−1.5107
					2			2.6073	−2.2670	2.2782	−2.2602	2.1858	−2.1872
					6.2	2		2.6073	−5.0817	2.2782	−5.0971	2.1858	−4.9396
						3		2.6073	−5.6848	2.2782	−5.7129	2.1858	−5.5553
						1	0.1	2.6073	−4.0441	2.2782	−4.0408	2.1858	−3.8926
							0.3	2.6073	−4.2204	2.2782	−4.2180	2.1858	−4.0634

medium favors to enhance the shear rate and opposite trend is rendered for the heat transfer rate. An increase in suction enriches the rate coefficients significantly.

5. Conclusion

The radiative heat transport phenomenon on the two-dimensional flow of water-based nanofluids over an elastic surface is carried out in the current investigation. Here, the electrically conducting nanofluid past a porous surface embedding with porous matrix is presented. The effect of heat source is also included to examine the heat transfer properties. Numerical approach is employed for the solution of the flow phenomena designed by the proposed model. Furthermore, the important characteristics of the physical parameters are laid down here:

(i) Comparative analysis shows a pathway for the further investigation of the current problem under study for the behavior of several nanoparticles in the water-based fluid with the interaction of various characterizing parameters.

(ii) Particle concentration decelerates the velocity distributions causing a special effect to enhance the bounding surface thickness whereas the thermal bounding surface behaves in the reverse order, and it clarifies that Cu nanoparticle has a greater role in both the profile in comparison to Al_2O_3 and SWCNT nanoparticles.

(iii) The unsteadiness overshoots the velocity profiles for which the thickness of the bounding surface thickness retards; moreover, similar trend is marked for the temperature distribution. However, steady state conditions preserve maximum magnitude for both the profiles.

(iv) An augmentation in suction enriches the profiles of velocity in comparison to injection, whereas heat source diminishes the fluid temperature significantly.

(v) The shear rate coefficient rises with increase in particle concentration, whereas heat transfer rate shows its opposite impact.

Data Availability

No data were used to support this study.

Conflicts of Interest

The authors declare that they have no conflicts of interest.

References

[1] Z. H. Khan, S. T. Hussain, and Z. Hammouch, "Flow and heat transfer analysis of water and ethylene glycol-based Cu nanoparticles between two parallel disks with suction/injection effects," *Journal of Molecular Liquids*, vol. 221, pp. 298–304, 2016.

[2] K. R. V. Subramanian, T. N. Rao, and A. Balakrishnan, *Nanofluids and Their Engineering Applications*, CRC Press, Boca Raton, FL, USA, 2019.

[3] Y. Ma, M. M. Rashidi, R. Mohebbi, and Z. Yang, "Investigation of magnetohydrodynamics in Ag-TiO2/water hybrid nanofluid in a Shamse knot shaped cavity," *International Journal of Numerical Methods for Heat and Fluid Flow*, vol. 31, no. 1, pp. 251–272, 2020.

[4] A. Riaz, T. Abbas, A. Zeeshan, and M. H. Doranehgard, "Entropy generation and MHD analysis of a nanofluid with peristaltic three dimensional cylindrical enclosures," *International Journal of Numerical Methods for Heat and Fluid Flow*, vol. 31, no. 8, pp. 2698–2714, 2021.

[5] J. Tu, C. Qi, Z. Tang, Z. Tian, and L. Chen, "Experimental study on the influence of bionic channel structure and nanofluids on power generation characteristics of waste heat utilisation equipment," *Applied Thermal Engineering*, vol. 202, Article ID 117893, 2021.

[6] R. Mohebbi, H. Lakzayi, N. A. C. Sidik, and W. M. A. A. Japar, "Lattice Boltzmann method based study of the heat transfer augmentation associated with Cu/water nanofluid in a channel with surface mounted blocks," *International Journal of Heat and Mass Transfer*, vol. 117, pp. 425–435, 2018.

[7] A. B. Saryazdi, F. Talebi, T. Armaghani, and I. Pop, "Numerical study of forced convection flow and heat transfer of a nanofluid flowing inside a straight circular pipe filled with a saturated porous medium," *The European Physical Journal Plus*, vol. 131, no. 4, pp. 1–11, 2016.

[8] S. Baag and S. R. Mishra, "Heat and mass transfer analysis on MHD 3-D water-based nanofluid," *Journal of Nanofluids*, vol. 4, no. 3, pp. 352–361, 2015.

[9] T. Watanabe and I. Pop, "Thermal boundary layers in magnetohydrodynamic flow over a flat plate in the presence of a transverse magnetic field," *Acta Mechanica*, vol. 105, no. 1, pp. 233–238, 1994.

[10] T. Armaghani, H. Esmaeili, Y. A. Mohammadpoor, and I. Pop, "MHD mixed convection flow and heat transfer in an open C-shaped enclosure using water-copper oxide nanofluid," *Heat and Mass Transfer*, vol. 54, no. 6, pp. 1791–1801, 2018.

[11] F. N. Ibrahim and M. Terbeche, "Solutions of the laminar boundary layer equations for a conducting power law non-Newtonian fluid in a transverse magnetic field," *Journal of Physics D: Applied Physics*, vol. 27, no. 4, pp. 740–747, 1994.

[12] M. Y. Malik, I. Khan, A. Hussain, and T. Salahuddin, "Mixed convection flow of MHD Eyring-Powell nanofluid over a stretching sheet: a numerical study," *AIP Advances*, vol. 5, no. 11, Article ID 117118, 2015.

[13] H. I. Andersson, J. B. Aarseth, and B. S. Dandapat, "Heat transfer in a liquid film on an unsteady stretching surface," *International Journal of Heat and Mass Transfer*, vol. 43, no. 1, pp. 69–74, 2000.

[14] E. M. A. Elbashbeshy and M. A. A. Bazid, "Heat transfer over an unsteady stretching surface with internal heat generation," *Applied Mathematics and Computation*, vol. 138, no. 2-3, pp. 239–245, 2003.

[15] A. V. Kuznetsov and D. A. Nield, "Natural convective boundary-layer flow of a nanofluid past a vertical plate," *International Journal of Thermal Sciences*, vol. 49, no. 2, pp. 243–247, 2010.

[16] H. Heidary and M. J. Kermani, "Heat transfer enhancement in a channel with block(s) effect and utilizing Nano-fluid," *International Journal of Thermal Sciences*, vol. 57, pp. 163–171, 2012.

[17] S. U. Choi and J. A. Eastman, *Enhancing Thermal Conductivity of Fluids with Nanoparticles (No. ANL/MSD/CP-84938*, Argonne National Lab., IL, USA, 1995.

[18] H. Masuda, A. Ebata, K. Teramae, and N. Hishinuma, "Alteration of thermal conductivity and viscosity of liquid by dispersing ultra-fine particles. Dispersion of Al_2O_3, SiO_2 and TiO_2 ultra-fine particles," *Netsu Bussei*, vol. 7, no. 4, pp. 227–233, 1993.

[19] A. K. Mishra, P. K. Pattnaik, S. R. Mishra, and N. Senapati, "Dissipative heat energy on Cu and Al2O3 ethylene-glycol-based nanofluid flow over a heated semi-infinite vertical plate," *Journal of Thermal Analysis and Calorimetry*, vol. 145, no. 1, pp. 129–137, 2021.

[20] M. Shutaywi and Z. Shah, "Mathematical Modeling and numerical simulation for nanofluid flow with entropy optimization," *Case Studies in Thermal Engineering*, vol. 26, Article ID 101198, 2021.

[21] W. Ibrahim and M. Negera, "The investigation of MHD williamson nanofluid over stretching cylinder with the effect of activation energy," *Advances in Mathematical Physics*, vol. 2020, no. 1, pp. 1–16, 2020.

[22] S. Abdal, B. Ali, S. Younas, L. Ali, and A. Mariam, "Thermo-diffusion and multislip effects on MHD mixed convection unsteady flow of micropolar nanofluid over a shrinking/stretching sheet with radiation in the presence of heat source," *Symmetry*, vol. 12, no. 1, p. 49, 2020.

[23] S. E. Ghasemi and M. Hatami, "Solar radiation effects on MHD stagnation point flow and heat transfer of a nanofluid over a stretching sheet," *Case Studies in Thermal Engineering*, vol. 25, Article ID 100898, 2021.

[24] F. Saba, N. Ahmed, S. Hussain, U. Khan, S. Mohyud-Din, and M. Darus, "Thermal analysis of nanofluid flow over a curved stretching surface suspended by carbon nanotubes with internal heat generation," *Applied Sciences*, vol. 8, no. 3, p. 395, 2018.
[25] S. Z. A. Adnan, U. Khan, N. Ahmed, S. T. Mohyud-Din, and I. Khan, "Heat transfer enhancement in H2O suspended by aluminium alloy nanoparticles over a convective stretching surface," *Advances in Mechanical Engineering*, vol. 12, no. 9, Article ID 1687814020942342, 2020.
[26] G. Rasool, A. Shafiq, M. S. Alqarni, A. Wakif, I. Khan, and M. S. Bhutta, "Numerical scrutinization of Darcy-Forchheimer relation in convective magnetohydrodynamic nanofluid flow bounded by nonlinear stretching surface in the perspective of heat and mass transfer," *Micromachines*, vol. 12, no. 4, p. 374, 2021.
[27] N. S. Wahid, N. Md Arifin, M. Turkyilmazoglu, M. E. H. Hafidzuddin, and N. A. Abd Rahmin, "MHD hybrid Cu-Al2O3/water nanofluid flow with thermal radiation and partial slip past a permeable stretching surface: analytical solution," *Journal of Nano Research*, vol. 64, pp. 75–91, 2020.
[28] R. Kalaivanan, N. Vishnu Ganesh, and Q. M. Al-Mdallal, "An investigation on Arrhenius activation energy of second grade nanofluid flow with active and passive control of nanomaterials," *Case Studies in Thermal Engineering*, vol. 22, Article ID 100774, 2020.
[29] H. Upreti, A. K. Pandey, S. K. Rawat, and M. Kumar, "Modified Arrhenius and thermal radiation effects on three-dimensional magnetohydrodynamic flow of carbon nanotubes nanofluids over bi-directional stretchable surface," *Journal of Nanofluids*, vol. 10, no. 4, pp. 538–551, 2021.
[30] H. Upreti, A. K. Pandey, M. Kumar, and O. D. Makinde, "Ohmic heating and non-uniform heat source/sink roles on 3D Darcy-forchheimer flow of CNTs nanofluids over a stretching surface," *Arabian Journal for Science and Engineering*, vol. 45, no. 9, pp. 7705–7717, 2020.
[31] A. S. Sabu, J. Mackolil, B. Mahanthesh, and A. Mathew, "Reiner-Rivlin nanomaterial heat transfer over a rotating disk with distinct heat source and multiple slip effects," *Applied Mathematics and Mechanics*, vol. 42, no. 10, pp. 1495–1510, 2021.
[32] B. Mahanthesh, N. S. Shashikumar, and G. Lorenzini, "Heat transfer enhancement due to nanoparticles, magnetic field, thermal and exponential space-dependent heat source aspects in nanoliquid flow past a stretchable spinning disk," *Journal of Thermal Analysis and Calorimetry*, vol. 145, pp. 3339–3347, 2020.
[33] K. A. Al-Utaibi, A. Sohail, Z. Yu et al., "Dynamical analysis of the delayed immune response to cancer," *Results in Physics*, vol. 26, Article ID 104282, 2021.
[34] A. Riaz, E. Bobescu, K. Ramesh, and R. Ellahi, "Entropy analysis for cilia-generated motion of Cu-blood flow of nanofluid in an annulus," *Symmetry*, vol. 13, no. 12, p. 2358, 2021.
[35] L. Zhang, M. M. Bhatti, E. E. Michaelides, M. Marin, and R. Ellahi, "Hybrid nanofluid flow towards an elastic surface with tantalum and nickel nanoparticles, under the influence of an induced magnetic field," *The European Physical Journal - Special Topics*, vol. 45, 2021.
[36] Ul H. Rizwan, S. Nadeem, Z. H. Khan, and N. F. M. Noor, "MHD squeezed flow of water functionalized metallic nanoparticles over a sensor surface," *Physica E*, vol. 73, pp. 45–53, 2015.

Hindawi
Journal of Mathematics
Volume 2022, Article ID 5658680, 11 pages
https://doi.org/10.1155/2022/5658680

Research Article

Suppressing Chaos for a Fractional-Order Chaotic Chemical Reaction Model via PD$^\zeta$ Controller

Hui Wang

Department of Finance and Insurance, School of Business Nanjing University, Nanjing 210093, China

Correspondence should be addressed to Hui Wang; hwangcn1@sina.com

Received 27 November 2021; Revised 19 December 2021; Accepted 10 January 2022; Published 4 February 2022

Academic Editor: Fairouz Tchier

In this work, based on the earlier publications, we build a new fractional-order chemical reaction model. Computer simulations manifest that the fractional-order chemical reaction model presents chaotic behavior under a certain parameter condition. To eliminate the chaotic dynamical property, a suitable fractional-order PD$^\zeta$ controller with time delay is designed. Regarding the time delay as a bifurcation parameter, we set up a novel delay-independent stability and bifurcation criterion guaranteeing the stability and the creation of Hopf bifurcation of the controlled fractional-order chemical reaction model. The influence of time delay on the stability and Hopf bifurcation of the controlled fractional-order chemical reaction model is revealed. At last, numerical simulations are performed to sustain the rationality of the designed PD$^\zeta$ controller. The obtained conclusions of this work are completely novel and have immense application prospects in the chaos control of chemical reaction systems. Furthermore, the research idea can also be utilized to suppress the chaos of a lot of fractional-order chaotic models.

1. Introduction

Chaos exists widely in many areas such as climate, physics, chemistry, engineering, economy and finance, complex networks, and population systems [1–6]. The chaotic phenomenon depends on the initial condition of the original system. The chaotic behavior occurring in the nonlinear dynamical systems owns the very complex property and unpredictability. In many cases, chaotic behavior is not what we want in our practical life. Thus, a natural problem arises: how to suppress the chaotic behavior of the original system has been an important theme in many disciplines. During the past several decades, suppressing chaos has received great attention from many scholars. For example, Chen [7] controlled the chaos via a simple adaptive feedback control technique. Du et al. [8] applied the phase space compression method to control the chaos of an economic model. In 1990, Yorke [9] utilized Ott, Grebogi, and Yorke (OGY) control approach to control the chaos of a chaotic model. Paula and Savi [10] designed an extended time-delayed feedback control approach to suppress the chaos of a nonlinear pendulum. For more detailed literature on this aspect, one can refer [11–14].

In 1996, Geysermans and Baras [15] proposed a homogeneous chaotic Wilamowski–Rossler model. The balance equations of this model have a well-defined microscopic counterpart and all the reaction follows the following "elementary" steps:

$$\begin{cases} \mathscr{A}_1 + \mathscr{X} \xrightarrow{\kappa_1} 2\mathscr{X}, \mathscr{A}_1 + \mathscr{X} \xleftarrow{\kappa_{-1}} 2\mathscr{X}, \\ \mathscr{X} + \mathscr{Y} \xrightarrow{\kappa_2} 2\mathscr{Y}, \\ \mathscr{A}_5 + \mathscr{Y} \xrightarrow{\kappa_3} \mathscr{A}_2, \\ \mathscr{X} + \mathscr{Z} \xrightarrow{\kappa_4} \mathscr{A}_3, \\ \mathscr{A}_4 + \mathscr{Z} \xrightarrow{\kappa_5} 2\mathscr{Z}, \mathscr{A}_4 + \mathscr{Z} \xleftarrow{\kappa_{-5}} 2\mathscr{Z}. \end{cases} \tag{1}$$

System (1) includes two autocatalytic steps involving constituents $\mathscr{X}$ and $\mathscr{Z}$, coupled via three other steps involving the three constituents $\mathscr{X}$, $\mathscr{Z}$, and $\mathscr{Y}$. The initial $(\mathscr{A}_1, \mathscr{A}_4, \mathscr{A}_5)$ and final $(\mathscr{A}_2, \mathscr{A}_3)$ product concentrations remain fixed. The distance from thermodynamic equilibrium is controlled by the values of $\mathscr{A}_1, \mathscr{A}_2, \mathscr{A}_3, \mathscr{A}_4, \mathscr{A}_5$. $\kappa_{\pm i}$ $(i = 1, 2, 3, 4, 5)$ stands for the rate constant. In model (1), there are 15 free parameters. To reduce the number of free parameters, Geysermans and Baras [15] selected the rate coefficients $\kappa_{-2}=0, \kappa_{-3}=0$, and $\kappa_{-4}=0$. Note that the last two relations imply that $\mathscr{A}_2$ and $\mathscr{A}_3$ are continuously removed from the reactor [15, 16].

Assuming that there exists an ideal mixture and a well-stirred reactor, then the macroscopic rate equations of model (1) can be expressed as follows:

$$\begin{cases} \dfrac{du_1(t)}{dt} = \beta_1 u_1(t) - \kappa_{-1} u_1^2(t) - u_1(t)u_2(t) - u_1(t)u_3(t), \\ \dfrac{du_2(t)}{dt} = u_1(t)u_2(t) - \beta_5 u_2(t), \\ \dfrac{du_3(t)}{dt} = \beta_4 u_3(t) - u_1(t)u_3(t) - k_{-5} u_3^2(t), \end{cases} \tag{2}$$

where $u_1(t), u_2(t)$, and $u_3(t)$ stand for the mole fractions of $\mathscr{X}, \mathscr{Y}$, and $\mathscr{Z}$ at the time t. The rate constants κ_1, κ_3, and κ_5 are incorporated in the parameters β_1, β_5, and β_4 (e.g., $\beta_1 = \kappa_1[\mathscr{A}_1], \ldots, o$) and $\beta_1 > 0, \beta_4 > 0, \beta_5 > 0, \kappa_{-1} > 0, \kappa_{-5} > 0$ stand for the constants. In detail, one can refer [15, 16]. In 2015, Xu and Wu [17] dealt with the bifurcation control of chaos for model (2) via three-time delay feedback controllers. Namely, they considered the following controller chemical model:

$$\begin{cases} \dfrac{du_1(t)}{dt} = \beta_1 u_1(t) - \kappa_{-1} u_1^2(t) - u_1(t)u_2(t) - u_1(t)u_3(t) + \mu_1[u_1(t) - u_1(t-\theta)], \\ \dfrac{du_2(t)}{dt} = u_1(t)u_2(t) - \beta_5 u_2(t) + \mu_2[u_2(t) - u_2(t-\theta)], \\ \dfrac{du_3(t)}{dt} = \beta_4 u_3(t) - u_1(t)u_3(t) - k_{-5} u_3^2(t) + \mu_3[u_3(t) - u_3(t-\theta)], \end{cases} \tag{3}$$

where $\mu_i (i = 1, 2, 3)$ stands for a real constant and θ is a delay.

It is worth mentioning that all the literature above (see [15–17]) are only concerned with the integer-order chemical models and they are not concerned with the fractional-order chemical models. Recent studies have shown that fractional-order differential equation is deemed as a more effective tool to portray natural phenomena than the classical integer-order ones since it has great advantages in memory trait and hereditary property of numerous materials and development processes [18–20]. Recently, fractional-order dynamical systems have displayed great application in lots of areas such as network systems, intelligent control, physical science, biological engineering, chemistry, finance, and so on [21–26]. Rich achievements on fractional-order dynamical models have been obtained. For example, Ke [27] dealt with the Mittag–Leffler stability and asymptotic ω-periodicity for a class of fractional-order inertial delayed neural networks. Du and Lu [28] focused on the finite-time stability for fractional-order fuzzy delayed cellular neural networks. Xiao et al. [29] probed into the bifurcation control problem for fractional-order small-world networks; Huang et al. [30] studied the bifurcation problem of fractional-order delayed neural networks. In detail, we refer the readers to [31–34].

Inspired by the exploration above and on the basis of system (2), in order to describe the continuous change process of the mole fractions of $\mathscr{X}, \mathscr{Y}$, and $\mathscr{Z}$ and characterize the memory trait and hereditary property of the variables $\mathscr{X}, \mathscr{Y}$, and $\mathscr{Z}$, we modify system (2) as the following fractional-order form:

$$\begin{cases} \dfrac{d^\zeta u_1(t)}{dt^\zeta} = \beta_1 u_1(t) - \kappa_{-1} u_1^2(t) - u_1(t)u_2(t) - u_1(t)u_3(t), \\ \dfrac{d^\zeta u_2(t)}{dt^\zeta} = u_1(t)u_2(t) - \beta_5 u_2(t), \\ \dfrac{d^\zeta u_3(t)}{dt^\zeta} = \beta_4 u_3(t) - u_1(t)u_3(t) - k_{-5} u_3^2(t), \end{cases} \tag{4}$$

where $\zeta \in (0, 1]$. The research indicates that when $\zeta = 0.97, \beta_1 = 30, \kappa_{-1} = 0.55, \beta_5 = 9.5, \beta_4 = 16.5, \kappa_{-5} = 0.5$, then there is a chaotic phenomenon in system (3). The software simulation figures are presented in Figure 1.

In this current work, we are to deal with the chaos control of system (4) by virtue of a fractional-order PD^ζ controller. The key contributions of this study are as follows:

(i) On the basis of the earlier studies, a new fractional-order chaotic chemical reaction model is set up

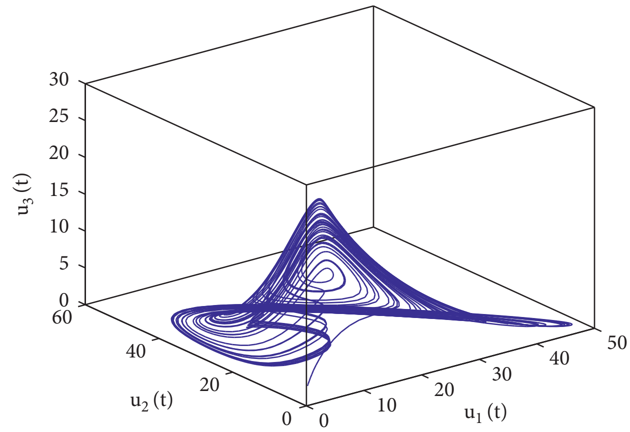

Figure 1: Software simulation figures of system (4) with $\zeta = 0.97, \beta_1 = 30, \kappa_{-1} = 0.55, \beta_5 = 9.5, \beta_4 = 16.5, \kappa_{-5} = 0.5$.

(ii) The chaotic phenomenon of system (4) is suppressed by means of an appropriate fractional-order PD^{ζ} controller

(iii) The study approach can be utilized to suppress the chaos of lots of fractional-order dynamical models in many subjects

This manuscript can be arranged as follows: some prerequisite theory on the fractional-order differential equation is prepared in Section 2; in Section 3, we prove the existence and uniqueness of the solution of system (4); in Section 4, the chaos of system (4) is suppressed via fractional-order PD^{ζ} controller and a delay-independent sufficient condition that ensures the stability and the creation of Hopf bifurcation of the fractional-order controlled chaotic chemical reaction model is built; in Section 5, software simulation results are presented to sustain the established conclusions; and Section 6 completes this article.

2. Preliminary Knowledge

In this part, we present some indispensable theories on a fractional-order differential equation.

Definition 1 (see [35]). The fractional type integral of the order ζ of the function $u(\xi)$ is given by

$$\mathcal{I}^{\zeta} u(\xi) = \frac{1}{\Gamma(\zeta)} \int_{\xi_0}^{\xi} (\xi - \nu)^{\zeta - 1} u(\nu) d\nu, \tag{5}$$

where $\xi > \xi_0, \zeta > 0$ and $\Gamma(\nu) = \int_0^{\infty} s^{\nu-1} e^{-s} ds$.

Definition 2 (see [35]). The Caputo fractional order derivative of the order ζ of the function $u(\nu) \in ([\nu_0, \infty), R)$ is defined as follows:

$$\mathcal{D}^{\zeta} u(\nu) = \frac{1}{\Gamma(\kappa - \zeta)} \int_{\nu_0}^{\nu} \frac{u^{(\kappa)}(s)}{(\nu - s)^{\zeta - \kappa + 1}} ds, \tag{6}$$

where $\nu \geq \nu_0$ and κ represents a positive integer ($\zeta \in [\kappa - 1, \kappa)$). In particular, if $\zeta \in (0, 1)$, then

$$\mathcal{D}^{\zeta} u(\nu) = \frac{1}{\Gamma(1 - \zeta)} \int_{\nu_0}^{\nu} \frac{u'(s)}{(\nu - s)^{\zeta}} ds. \tag{7}$$

Lemma 1 (see [36]). *Consider the fractional-order system $\mathcal{D}^{\zeta} w = \mathcal{F} w, w(0) = w_0$ where $\zeta \in (0,1), w \in R^l, \mathcal{F} \in R^{l \times l}$. Assuming that $\chi_i (i = 1, 2, \ldots, l)$ is the root of the characteristic equation of $\mathcal{D}^{\zeta} w = \mathcal{F} w$, then the equilibrium point of the system $\mathcal{D}^{\zeta} w = \mathcal{F} w$ is locally asymptotically stable if $|arg(\chi_i)| > (\zeta\pi/2) (i = 1, 2, \ldots, l)$ and the equilibrium point of the system $\mathcal{D}^{\zeta} w = \mathcal{F} w$ is stable if $|arg(\chi_i)| > (\zeta\pi/2) (i = 1, 2, \ldots, l)$ and all critical eigenvalues that satisfy $|arg(\chi_i)| = (\zeta\pi/2) (i = 1, 2, \ldots, l)$ own geometric multiplicity one.*

3. Existence and Uniqueness of the Solution of System (4)

In this section, we will prove the existence and uniqueness of the solution of system (4).

Theorem 1. *Let $\Lambda = \{(u_1, u_2, u_3) \in R^3\colon \max\{|u_1|, |u_2|, |u_3|\} \leq A\}$, where $A > 0$ is a constant. $\forall (u_{10}, u_{20}, u_{30}) \in \Lambda$, system (4) with the initial value (u_{10}, u_{20}, u_{30}) has a unique solution $U = (u_1, u_2, u_3) \in \Lambda$.*

Proof. Define the following mapping:

$$f(U) = (f_1(U), f_2(U), f_3(U)), \tag{8}$$

where

$$\begin{cases} f_1(U) = \beta_1 u_1(t) - \kappa_{-1} u_1^2(t) - u_1(t) u_2(t) - u_1(t) u_3(t), \\ f_2(U) = u_1(t) u_2(t) - \beta_5 u_2(t), \\ f_3(U) = \beta_4 u_3(t) - u_1(t) u_3(t) - k_{-5} u_3^2(t). \end{cases} \tag{9}$$

$\forall U, \overline{U} \in \Lambda$, one obtains

$$
\begin{aligned}
&\|f(U)-f(\widetilde{U})\| \\
&= |\beta_1 u_1(t) - \kappa_{-1}u_1^2(t) - u_1(t)u_2(t) - u_1(t)u_3(t) \\
&\quad - \left[\beta_1 \overline{u}_1(t) - \kappa_{-1}\overline{u}_1^2(t) - \overline{u}_1(t)\overline{u}_2(t) - \overline{u}_1(t)\overline{u}_3(t)\right]| \\
&\quad + \left|u_1(t)u_2(t) - \beta_5 u_2(t) - \left[\overline{u}_1(t)\overline{u}_2(t) - \beta_5\overline{u}_2(t)\right]\right| \\
&\quad + |\beta_4 u_3(t) - u_1(t)u_3(t) - k_{-5}u_3^2(t) \\
&\quad - \left[\beta_4\overline{u}_3(t) - \overline{u}_1(t)\overline{u}_3(t) - k_{-5}\overline{u}_3^2(t)\right]| \\
&\le \left(\beta_1 + 2\kappa_{-1}A + A\right)\left|u_1(t)-\overline{u}_1(t)\right| + A\left|u_2(t)-\overline{u}_2(t)\right| + A\left|u_3(t)-\overline{u}_3(t)\right| + A\left|u_1(t)-\overline{u}_1(t)\right| \\
&\quad + \left(A+\beta_5\right)\left|u_2(t)-\overline{u}_2(t)\right| + A\left|u_1(t)-\overline{u}_1(t)\right| \\
&\quad + \left(\beta_4 + A + 2\kappa_{-5}A\right)\left|u_3(t)-\overline{u}_3(t)\right| \\
&= A_1\left|u_1(t)-\overline{u}_1(t)\right| + A_2\left|u_2(t)-\overline{u}_2(t)\right| + A_3\left|u_3(t)-\overline{u}_3(t)\right| \\
&\le A_0\|U-\overline{U}\|,
\end{aligned}
\tag{10}
$$

where

$$
\begin{cases}
A_1 = \beta_1 + 2\kappa_{-1}A + 3A, \\
A_2 = 2A + \beta_5, \\
A_3 = \beta_4 + 2A + 2\kappa_{-5}A,
\end{cases}
\tag{11}
$$

$$
A_0 = \max\{A_1, A_2, A_3\}. \tag{12}
$$

Then $f(U)$ satisfies Lipschitz condition with respect to U (see [39, 40]). According to Banach fixed point theorem, we know that Theorem 1 is true. □

4. Suppressing Chaos via Fractional-Order PD$^\zeta$ Controller

In this part, we are to apply a suitable controller to eliminate the chaotic phenomenon of system (4). By virtue of the idea of Tang et al. [37], the fractional-order PD$^\zeta$ controller can be designed as follows:

$$
\psi(t) = \varrho_p u_1(t-\theta) + \varrho_d \frac{d^\zeta u_1(t)}{dt^\zeta}, \tag{13}
$$

where ϱ_p and $\varrho_d \neq 1$ present the proportional control parameter and the derivative control parameter, respectively, and θ denotes a delay. Adding (13) to the first equation of system (4), we get

$$
\begin{cases}
\dfrac{d^\zeta u_1(t)}{dt^\zeta} = \beta_1 u_1(t) - \kappa_{-1}u_1^2(t) - u_1(t)u_2(t) - u_1(t)u_3(t) + \psi(t), \\[2ex]
\dfrac{d^\zeta u_2(t)}{dt^\zeta} = u_1(t)u_2(t) - \beta_5 u_2(t), \\[2ex]
\dfrac{d^\zeta u_3(t)}{dt^\zeta} = \beta_4 u_3(t) - u_1(t)u_3(t) - k_{-5}u_3^2(t).
\end{cases}
\tag{14}
$$

That is

$$\begin{cases} \dfrac{d^{\zeta}u_1(t)}{dt^{\zeta}} = \beta_1 u_1(t) - \kappa_{-1}u_1^2(t) - u_1(t)u_2(t) - u_1(t)u_3(t) \\ + \varrho_p u_1(t-\theta) + \varrho_d \dfrac{d^{\zeta}u_1(t)}{dt^{\zeta}}, \\ \dfrac{d^{\zeta}u_2(t)}{dt^{\zeta}} = u_1(t)u_2(t) - \beta_5 u_2(t), \\ \dfrac{d^{\zeta}u_3(t)}{dt^{\zeta}} = \beta_4 u_3(t) - u_1(t)u_3(t) - k_{-5}u_3^2(t). \end{cases} \tag{15}$$

System (15) can be rewritten as the following form:

$$\begin{cases} \dfrac{d^{\zeta}u_1(t)}{dt^{\zeta}} = \dfrac{\beta_1}{1-\varrho_d}u_1(t) - \dfrac{\kappa_{-1}}{1-\varrho_d}u_1^2(t) - \dfrac{1}{1-\varrho_d}u_1(t)u_2(t) \\ - \dfrac{1}{1-\varrho_d}u_1(t)u_3(t) + \dfrac{\varrho_p}{1-\varrho_d}u_1(t-\theta), \\ \dfrac{d^{\zeta}u_2(t)}{dt^{\zeta}} = u_1(t)u_2(t) - \beta_5 u_2(t), \\ \dfrac{d^{\zeta}u_3(t)}{dt^{\zeta}} = \beta_4 u_3(t) - u_1(t)u_3(t) - k_{-5}u_3^2(t). \end{cases} \tag{16}$$

It is not difficult to obtain that if the following condition

$$(\mathcal{Q}_1)\ \beta_4 > \beta_5,\ (\beta_1 - \kappa_{-1})\kappa_{-5} > \kappa_4 - \kappa_5, \tag{17}$$

holds, then system (16) owns the following unique positive equilibrium $\mathcal{U}(u_1^*, u_2^*, u_3^*)$, where

$$\begin{cases} u_1^* = \beta_5, \\ u_2^* = \dfrac{(\beta_1 - \kappa_{-1}\beta_5)\kappa_{-5} - \beta_4 + \beta_5}{\kappa_{-5}}, \\ u_3^* = \dfrac{\beta_4 - \beta_5}{\kappa_{-5}}. \end{cases} \tag{18}$$

The linear system of (16) around the positive equilibrium $\mathcal{U}(u_1^*, u_2^*, u_3^*)$ takes the following form:

$$\begin{cases} \dfrac{d^{\zeta}u_1(t)}{dt^{\zeta}} = a_1 u_1(t) + a_2 u_2(t) + a_2 u_3(t) + a_3 u_1(t-\theta), \\ \dfrac{d^{\zeta}u_2(t)}{dt^{\zeta}} = a_4 u_1(t) + a_5 u_2(t), \\ \dfrac{d^{\zeta}u_3(t)}{dt^{\zeta}} = a_6 u_1(t) + a_7 u_3(t), \end{cases} \tag{19}$$

where

$$\begin{cases} a_1 = \dfrac{\beta_1 - 2\kappa_{-1}u_1^* - u_2^* - u_3^*}{1-\varrho_d}, \\ a_2 = -\dfrac{u_1^*}{1-\varrho_d}, \\ a_3 = \dfrac{\varrho_p}{1-\varrho_d}, \\ a_4 = u_2^*, \\ a_5 = u_1^* - \beta_5, \\ a_6 = -u_3^*, \\ a_7 = \beta_4 - u_1^* - 2\kappa_5 u_3^*. \end{cases} \tag{20}$$

The characteristic equation of system (19) takes the form

$$\det\begin{bmatrix} s^{\zeta} - a_1 - a_3 e^{-s\theta} & -a_2 & -a_2 \\ -a_4 & s^{\zeta} - a_5 & 0 \\ -a_6 & 0 & s^{\zeta} - a_7 \end{bmatrix} = 0. \tag{21}$$

Then,

$$s^{3\zeta} + b_1 s^{2\zeta} + b_2 s^{\zeta} + b_3 + \left(c_1 s^{2\zeta} + c_2 s^{\zeta} + c_3\right)e^{-s\theta} = 0, \tag{22}$$

where

$$\begin{cases} b_1 = -(a_1 + a_5 + a_7), \\ b_2 = a_5 a_7 + a_1 a_5 + a_1 a_7 - a_2 a_6 - a_2 a_4, \\ b_3 = a_2 a_5 a_6 + a_2 a_4 a_7 - a_1 a_5 a_7, \\ c_1 = -a_3, \\ c_2 = a_3 (a_5 + a_7), \\ c_3 = -a_3 a_5 a_7. \end{cases} \tag{23}$$

When $\theta = 0$, then (22) becomes

$$\lambda^3 + (b_1 + c_1)\lambda^2 + (b_2 + c_2)\lambda + b_3 + c_3 = 0. \tag{24}$$

Assuming that

$$(\mathcal{Q}_2)\begin{cases} b_1 + c_1 > 0, \\ (b_1 + c_1)(b_2 + c_2) > b_3 + c_3, \\ (b_3 + c_3)[(b_1 + c_1)(b_2 + c_2) - (b_3 + c_3)] > 0, \end{cases} \tag{25}$$

is true, then the three roots $\lambda_1, \lambda_2, \lambda_3$ of (24) satisfy $|\arg(\lambda_1)| > (\zeta\pi/2)$, $|\arg(\lambda_2)| > (\zeta\pi/2)$, and $|\arg(\lambda_3)| > (\zeta\pi/2)$. By virtue of Lemma 1, we can conclude that the positive equilibrium point $\mathcal{U}(u_1^*, u_2^*, u_3^*)$ of system (14) is locally asymptotically stable when $\theta = 0$.

Assume that $s = i\rho = \rho(\cos(\zeta\pi/2) + i\sin(\pi/2))$ is the root of equation (22). It follows from (22) that

$$\begin{aligned} &\rho^{3\zeta}\left(\cos\frac{3\zeta\pi}{2} + i\sin\frac{3\zeta\pi}{2}\right) + b_1\rho^{2\zeta}(\cos\zeta\pi + i\sin\zeta\pi) \\ &+ b_2\rho^{\zeta}\left(\cos\frac{\zeta\pi}{2} + i\sin\frac{\zeta\pi}{2}\right) + b_3 \\ &+ \left[c_1\rho^{2\zeta}(\cos\zeta\pi + i\sin\zeta\pi) + c_2\rho^{\zeta}\left(\cos\frac{\zeta\pi}{2} + i\sin\frac{\zeta\pi}{2}\right) + c_3\right] \\ &\times(\cos\rho\theta - i\sin\rho\theta) = 0. \end{aligned} \tag{26}$$

Then,

$$\begin{cases} \mathcal{G}_1\cos\rho\theta + \mathcal{G}_2\sin\rho\theta = \mathcal{H}_1, \\ \mathcal{G}_2\cos\rho\theta - \mathcal{G}_1\sin\rho\theta = \mathcal{H}_2, \end{cases} \tag{27}$$

where

$$\begin{cases} \mathcal{G}_1 = d_1\rho^{2\zeta} + d_2\rho^{\zeta} + d_3, \\ \mathcal{G}_2 = d_4\rho^{2\zeta} + d_5\rho^{\zeta}, \\ \mathcal{H}_1 = e_1\rho^{3\zeta} + e_2\rho^{2\zeta} + e_3\rho^{\zeta} + e_4, \\ \mathcal{H}_2 = e_5\rho^{3\zeta} + e_6\rho^{2\zeta} + e_7\rho^{\zeta}, \end{cases} \tag{28}$$

where

$$\begin{cases} d_1 = c_1\cos\zeta\pi, \\ d_2 = c_2\cos\dfrac{\zeta\pi}{2}, \\ d_3 = c_3, \\ d_4 = c_1\sin\zeta\pi, \\ d_5 = c_2\sin\dfrac{\zeta\pi}{2}, \\ e_1 = -\cos\dfrac{\zeta\pi}{2}, \\ e_2 = -b_1\cos\zeta\pi, \\ e_3 = -b_2\cos\dfrac{\zeta\pi}{2}, \\ e_4 = -b_3, \\ e_5 = -\sin\dfrac{\zeta\pi}{2}, \\ e_6 = -b_1\sin\zeta\pi, \\ e_7 = -b_2\sin\dfrac{\zeta\pi}{2}. \end{cases} \tag{29}$$

It follows from (27) that

$$\cos\rho\theta = \frac{\mathcal{H}_1\mathcal{G}_1 + \mathcal{H}_2\mathcal{G}_2}{\mathcal{G}_1^2 + \mathcal{G}_2^2}, \tag{30}$$

$$\mathcal{G}_1^2 + \mathcal{G}_2^2 = \mathcal{H}_1^2 + \mathcal{H}_2^2. \tag{31}$$

By virtue of (28) and (31), one gets

$$\begin{aligned} &\left(d_1\rho^{2\zeta} + d_2\rho^{\zeta} + d_3\right)^2 + \left(d_4\rho^{2\zeta} + d_5\rho^{\zeta}\right)^2 = \\ &\left(e_1\rho^{3\zeta} + e_2\rho^{2\zeta} + e_3\rho^{\zeta} + e_4\right)^2 + \left(e_5\rho^{3\zeta} + e_6\rho^{2\zeta} + e_7\rho^{\zeta}\right)^2, \end{aligned} \tag{32}$$

which leads to

$$\epsilon_1\rho^{6\zeta} + \epsilon_2\rho^{5\zeta} + \epsilon_3\rho^{4\zeta} + \epsilon_4\rho^{3\zeta} + \epsilon_5\rho^{2\zeta} + \epsilon_6\rho^{\zeta} + \epsilon_7 = 0, \tag{33}$$

where

$$\begin{cases} \epsilon_1 = e_1^2 + e_5^2, \\ \epsilon_2 = 2(e_1e_2 + e_5e_6), \\ \epsilon_3 = e_2^2 + e_6^2 - d_1^2 - d_4^2 + 2(e_1e_3 + e_5e_7), \\ \epsilon_4 = 2(e_1e_4 + e_2e_3 + e_6e_7 - d_1d_2 - d_4d_5), \\ \epsilon_5 = e_3^2 + e_7^2 - d_2^2 - d_5^2 + 2(e_2e_4 - d_1d_3), \\ \epsilon_6 = 2(e_3e_4 - d_2d_3), \\ \epsilon_7 = e_4^2 - d_3^2. \end{cases} \quad (34)$$

Set

$$\Theta(\rho) = \epsilon_1\rho^{6\zeta} + \epsilon_2\rho^{5\zeta} + \epsilon_3\rho^{4\zeta} + \epsilon_4\rho^{3\zeta} + \epsilon_5\rho^{2\zeta} + \epsilon_6\rho^{\zeta} + \epsilon_7. \quad (35)$$

Assuming that

$$(\mathcal{Q}_3)\ |e_4| < |d_3| \quad (36)$$

is true, since $\lim_{\rho\longrightarrow\infty}\Theta(\rho) = +\infty$, then equation (33) owns at least one real positive root. So equation (22) has at least one pair of pure roots. Making use of Sun et al. [38], one can easily establish the conclusion as follows.

Lemma 2. *(a) Supposing that $\epsilon_k > 0\,(k = 1,2,3,4,5,6)$, equation (22) owns no root with zero real parts for $\theta \geq 0$. (b) Supposing that $(\mathcal{Q}_3)$ holds and $\epsilon_k > 0\,(k = 1,2,3,4,5)$, then equation (22) owns a pair of purely imaginary roots $\pm i\rho_0$ if $\theta = \theta_0^{(l)}\,(l = 1,2,\ldots,)$ where*

$$\theta_0^{(l)} = \frac{1}{\rho_0}\left[\arccos\left(\frac{\mathcal{H}_1\mathcal{G}_1 + \mathcal{H}_2\mathcal{G}_2}{\mathcal{G}_1^2 + \mathcal{G}_2^2}\right) + 2l\pi\right], \quad (37)$$

where $l = 0,1,\ldots$, and $\rho_0 > 0$ represents the unique zero of $\Theta(\rho)$.

Denote $\theta_0 = \theta_0^{(0)}$. Now the following hypothesis is given:

$$(\mathcal{Q}_4)\ \mathcal{C}_{1R}\mathcal{C}_{2R} + \mathcal{C}_{1I}\mathcal{C}_{2I} > 0, \quad (38)$$

where

$$\begin{cases} \mathcal{C}_{1R} = 3\zeta\rho_0^{3\zeta-1}\cos\frac{(3\zeta-1)\pi}{2} + 2\zeta c_1\rho_0^{2\zeta-1}\cos\frac{(2\zeta-1)\pi}{2} \\ +\zeta c_2\rho_0^{\zeta-1}\cos\frac{(\zeta-1)\pi}{2} + \left[2\zeta c_1\rho_0^{2\zeta-1}\cos\frac{(2\zeta-1)\pi}{2} + \zeta c_2\rho_0^{\zeta-1}\cos\frac{(\zeta-1)\pi}{2}\right]\cos\rho_0\theta_0 + \sin\rho_0\theta_0 \\ \times\left[2\zeta c_1\rho_0^{2\zeta-1}\sin\frac{(2\zeta-1)\pi}{2} + \zeta c_2\rho_0^{\zeta-1}\sin\frac{(\zeta-1)\pi}{2}\right], \\ \mathcal{C}_{1I} = 3\zeta\rho_0^{3\zeta-1}\sin\frac{(3\zeta-1)\pi}{2} + 2\zeta c_1\rho_0^{2\zeta-1}\sin\frac{(2\zeta-1)\pi}{2} \\ +\zeta c_2\rho_0^{\zeta-1}\sin\frac{(\zeta-1)\pi}{2} - \left[2\zeta c_1\rho_0^{2\zeta-1}\cos\frac{(2\zeta-1)\pi}{2} + \zeta c_2\rho_0^{\zeta-1}\cos\frac{(\zeta-1)\pi}{2}\right]\sin\rho_0\theta_0 + \cos\rho_0\theta_0 \\ \times\left[2\zeta c_1\rho_0^{2\zeta-1}\sin\frac{(2\zeta-1)\pi}{2} + \zeta c_2\rho_0^{\zeta-1}\sin\frac{(\zeta-1)\pi}{2}\right], \\ \mathcal{C}_{2R} = \left(c_1\rho_0^{2\zeta}\cos\zeta\pi + c_2\rho_0^{\zeta}\cos\frac{\zeta\pi}{2} + c_3\right)\rho_0\sin\rho_0\theta_0 \\ -\left(c_1\rho_0^{2\zeta}\sin\zeta\pi + c_2\rho_0^{\zeta}\sin\frac{\zeta\pi}{2} + c_3\right)\rho_0\cos\rho_0\theta_0, \\ \mathcal{C}_{2I} = \left(c_1\rho_0^{2\zeta}\cos\zeta\pi + c_2\rho_0^{\zeta}\cos\frac{\zeta\pi}{2} + c_3\right)\rho_0\cos\rho_0\theta_0 \\ +\left(c_1\rho_0^{2\zeta}\sin\zeta\pi + c_2\rho_0^{\zeta}\sin\frac{\zeta\pi}{2} + c_3\right)\rho_0\sin\rho_0\theta_0. \end{cases} \quad (39)$$

Lemma 3. *Let $s(\theta) = \phi_1(\theta) + i\phi_2(\theta)$ be the root of (22) at $\theta = \theta_0$ satisfying $\phi_1(\theta_0) = 0, \phi_2(\theta_0) = \rho_0$, then $Re(ds/d\theta)|_{\theta=\theta_0,\rho=\rho_0} > 0$.*

Proof. Making use of (22), we get

$$\begin{aligned}&\left(3\zeta s^{3\zeta-1} + 2\zeta b_1 s^{2\zeta-1} + \zeta b_2 s^{\zeta-1}\right)\frac{\mathrm{d}s}{\mathrm{d}\theta}\\&+\left(2\zeta c_1 s^{2\zeta-1} + \zeta c_2 s^{\zeta-1}\right)e^{-s\theta}\frac{\mathrm{d}s}{\mathrm{d}\theta}\\&- e^{-s\theta}\left(\frac{\mathrm{d}s}{\mathrm{d}\theta}\theta + s\right)\left(c_1 s^{2\zeta} + c_2 s^{\zeta} + c_3\right) = 0,\end{aligned}\tag{40}$$

which leads to

$$\begin{aligned}&\left[3\zeta s^{3\zeta-1} + 2\zeta b_1 s^{2\zeta-1} + \zeta b_2 s^{\zeta-1} + \left(2\zeta c_1 s^{2\zeta-1} + \zeta c_2 s^{\zeta-1}\right)e^{-s\theta} - \theta e^{-s\theta}\left(c_1 s^{2\zeta} + c_2 s^{\zeta} + c_3\right)\right]\frac{\mathrm{d}s}{\mathrm{d}\theta}\\&= s e^{-s\theta}\left(c_1 s^{2\zeta} + c_2 s^{\zeta} + c_3\right).\end{aligned}\tag{41}$$

Then,

$$\left(\frac{\mathrm{d}s}{\mathrm{d}\theta}\right)^{-1} = \frac{\mathscr{C}_1(s)}{\mathscr{C}_2(s)} - \frac{\theta}{s},\tag{42}$$

where

$$\begin{cases}\mathscr{C}_1(s) = 3\zeta s^{3\zeta-1} + 2\zeta b_1 s^{2\zeta-1} + \zeta b_2 s^{\zeta-1}\\ +\left(2\zeta c_1 s^{2\zeta-1} + \zeta c_2 s^{\zeta-1}\right)e^{-s\theta},\\ \mathscr{C}_2(s) = s e^{-s\theta}\left(c_1 s^{2\zeta} + c_2 s^{\zeta} + c_3\right).\end{cases}\tag{43}$$

Then,

$$\begin{aligned}\mathrm{Re}\left[\left(\frac{\mathrm{d}s}{\mathrm{d}\theta}\right)^{-1}\right]_{\theta=\theta_0,\rho=\rho_0} &= \mathrm{Re}\left[\frac{\mathscr{C}_1(s)}{\mathscr{C}_2(s)}\right]_{\theta=\theta_0,\rho=\rho_0}\\&= \frac{\mathscr{C}_{1R}\mathscr{C}_{2R} + \mathscr{C}_{1I}\mathscr{C}_{2I}}{\mathscr{C}_{2R}^2 + \mathscr{C}_{2I}^2}.\end{aligned}\tag{44}$$

In view of $(\mathscr{Q}_4)$, we have

$$\mathrm{Re}\left[\left(\frac{\mathrm{d}s}{\mathrm{d}\theta}\right)^{-1}\right]_{\theta=\theta_0,\rho=\rho_0} > 0,\tag{45}$$

which completes the proof.

Making use of Lemma 1, we can easily obtain the following conclusion. □

Theorem 2. *Supposing that $(\mathscr{Q}_1)$–$(\mathscr{Q}_4)$ hold, then the positive equilibrium point $\mathscr{U}(u_1^*, u_2^*, u_3^*)$ of system (16) is locally asymptotically stable if the time delay θ lies in the interval $[0, \theta_0)$ and the Hopf bifurcation phenomenon of system (16) will arise near the positive equilibrium point $\mathscr{U}(u_1^*, u_2^*, u_3^*)$ if $\theta = \theta_0$.*

Remark 1. Xu and Wu [17] dealt with the chaos control for an integer-order chaotic chemical reaction model by time-delay feedback control technique. This manuscript deals with the chaos control issue for a fractional-order chaotic chemical reaction model via a fractional-order PD^ζ controller. The model and the research approach is very different from those in [17]. From this viewpoint, we think that the obtained results and the research method of this manuscript supplement the work of [17] and promote the development of the chaos control theory of fractional-order differential equation to some degree.

Remark 2. In this paper, we use the fractional-order PD^ζ controller to control the chaos of the fractional-order chaotic chemical reaction model (4). Compared with the time delay feedback controller, the fractional-order PD^ζ controller has more adjustable parameters and then can control the chaos of model (4) neatly.

5. Example

Consider the following controlled fractional-order chaotic chemical reaction model:

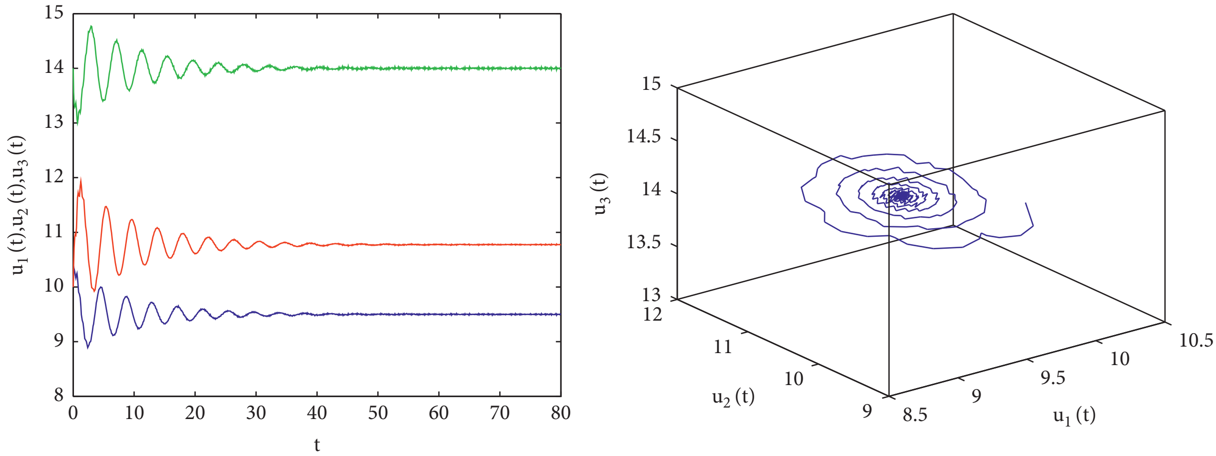

Figure 2: Computer simulation figures of the controlled fractional-order chaotic chemical reaction model (46) with $\theta = 0.20 < \theta_0 = 0.25$. The blue line represents $u_1(t)$, the red line represents $u_2(t)$, and the green line represents $u_3(t)$.

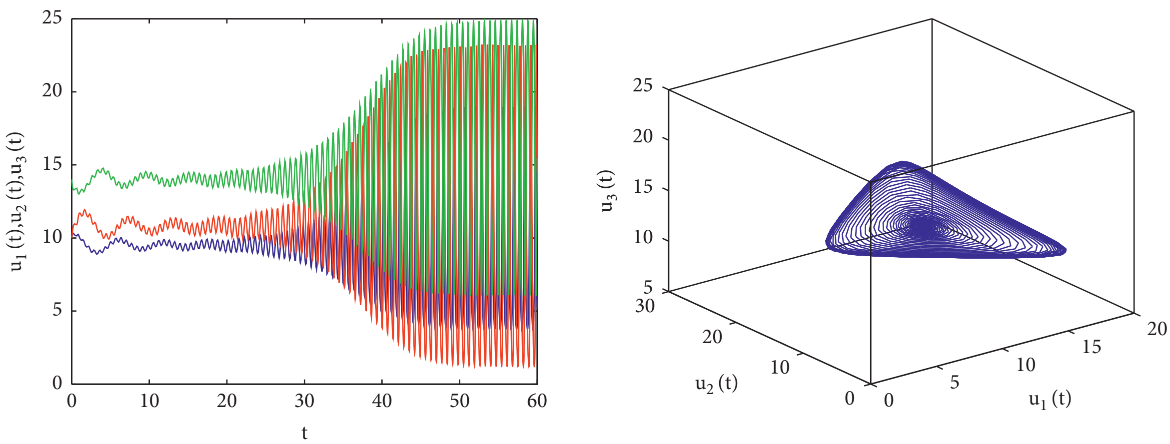

Figure 3: Computer simulation figures of the controlled fractional-order chaotic chemical reaction model (46) with $\theta = 0.28 > \theta_0 = 0.25$. The blue line represents $u_1(t)$, the red line represents $u_2(t)$, and the green line represents $u_3(t)$.

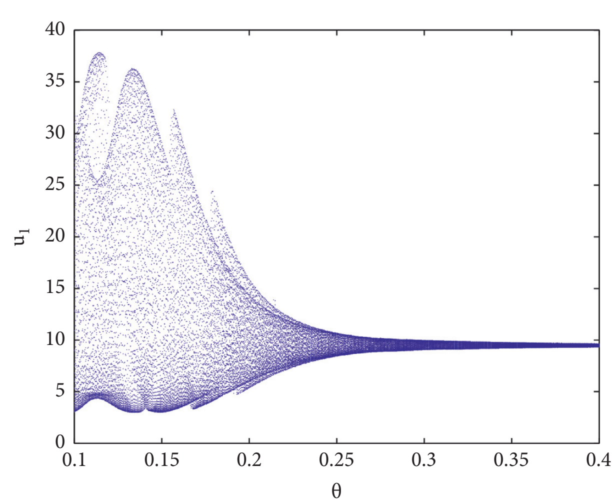

Figure 4: Bifurcation plot of the controlled fractional-order chaotic chemical reaction model (46): θ-u_1.

$$\begin{cases} \frac{d^{\zeta}u_1(t)}{dt^{\zeta}} = \beta_1 u_1(t) - \kappa_{-1}u_1^2(t) - u_1(t)u_2(t) - u_1(t)u_3(t) \\ + \varrho_p u_1(t-\theta) + \varrho_d \frac{d^{\zeta}u_1(t)}{dt^{\zeta}}, \\ \frac{d^{\zeta}u_2(t)}{dt^{\zeta}} = u_1(t)u_2(t) - \beta_5 u_2(t), \\ \frac{d^{\zeta}u_3(t)}{dt^{\zeta}} = \beta_4 u_3(t) - u_1(t)u_3(t) - k_{-5}u_3^2(t), \end{cases} \tag{46}$$

where ζ=0.97,β_1=30,κ_{-1}=0.55,β_5=9.5,β_4=16.5,κ_{-5}= 0.5. Let ϱ_p=0.5,ϱ_d=0.9. It is not difficult to obtain the unique positive equilibrium point of system (46) is $\mathscr{U}$(9.5,10.775,14). By direct computation via MATLAB software, we can easily get ρ_0=4.0239 and θ_0=0.25. The three assumptions ($\mathscr{Q}_1$)–($\mathscr{Q}_4$) of Theorem 2 are easily verified to be right. So we can conclude that the positive equilibrium point $\mathscr{U}$(9.5, 10.775,14) of system (46) is locally asymptotically stable if the time delay θ lies in the interval [0,0.25) and the Hopf bifurcation phenomenon for system (46) will arise near the positive equilibrium point $\mathscr{U}$(9.5,10.775,14) if θ=0.25. In this paper, we use the predictor-correctors approach [39, 41, 42] to discretize system (46) and by virtue of the MATLAB software to carry out numerical simulations. In order to display these results, we select two sets of different delay parameters. Firstly, we choose θ=0.20<θ_0=0.25, and the software simulation plots are presented in Figure 2, which implies that $u_1\longrightarrow 9.5, u_2\longrightarrow 10.775, u_3\longrightarrow 14$ as the time t tends to infinity. From the chemical point of view, the mole fraction of the constituent $\mathscr{X}$ will be close to 9.5, the mole fraction of the constituent $\mathscr{Y}$ will be close to 10.775, and the mole fraction of the constituent $\mathscr{Z}$ will be close to 14. Secondly, we choose θ=0.28>θ_0=0.25, and the software simulation plots are presented in Figure 3, which implies that a Hopf bifurcation periodic solution of system (46) will arise near the positive equilibrium point $\mathscr{U}$(9.5,10.775,14) as the time t tends to infinity. From the chemical point of view, the mole fraction of the constituent $\mathscr{X}$, the mole fraction of the constituent $\mathscr{Y}$, and the mole fraction of the constituent $\mathscr{Z}$ will remain periodically oscillatory situations near the values 9.5, 10.775, 14, respectively. Furthermore, we give the bifurcation plot, which can be seen in Figure 4, to indicate that the bifurcation value of system (46) is 0.25.

6. Conclusions

Suppressing the chaotic behavior of nonlinear dynamical systems has been a significant and classic issue in many disciplines. For a long time, the suppression of chaos has attracted much attention from many scholars in mathematics, physics, chemistry, engineering, and numerous other areas. In the present manuscript, based on the earlier publications, we set up a novel fractional-order chaotic chemical reaction model. Taking advantage of an appropriate fractional-order PD$^{\zeta}$ controller, we can effectively eliminate the chaotic phenomenon of the involved fractional-order chaotic chemical reaction model. A delay-independent sufficient condition to guarantee the stability and the creation of Hopf bifurcation of the fractional-order controlled chaotic chemical reaction model is built. The exploration manifests that the delay occurring in fractional-order PD$^{\zeta}$ controller is the key factor in suppressing the chaotic phenomenon of the fractional-order chaotic chemical reaction model. The derived conclusions of this manuscript are entirely new and the exploration approach of this manuscript can also be utilized to inquire into numerous chaos control problem of lots of fractional-order chaotic dynamical systems.

Data Availability

No data were used to support this study.

Conflicts of Interest

The authors declare that they have no conflicts of interest.

References

[1] C. T. Dhanya and D. Nagesh Kumar, "Multivariate nonlinear ensemble prediction of daily chaotic rainfall with climate inputs," *Journal of Hydrology*, vol. 403, no. 3-4, pp. 292–306, 2011.
[2] S. Kumar, R. Kumar, C. Cattani, and B. Samet, "Chaotic behaviour of fractional predator-prey dynamical system," *Chaos, Solitons & Fractals*, vol. 135, Article ID 109811, 2020.
[3] K. P. Harikrishnan, R. Misra, and G. Ambika, "Quantifying information loss on chaotic attractors through recurrence networks," *Physics Letters A*, vol. 383, no. 27, Article ID 125854, 2019.
[4] A. M. Wojtusiak, A. G. Balanov, and S. E. Savel'ev, "Intermittent and metastable chaos in a memristive artificial neuron with inertia," *Chaos, Solitons & Fractals*, vol. 142, Article ID 110383, 2021.
[5] I. Ahmad, A. Ouannas, M. Shafiq, V.-T. Pham, and D. Baleanu, "Finite-time stabilization of a perturbed chaotic finance model," *Journal of Advanced Research*, vol. 32, pp. 1–14, 2021.
[6] S. Harshavarthini, R. Sakthivel, Y.-K. Ma, and M. Muslim, "Finite-time resilient fault-tolerant investment policy scheme for chaotic nonlinear finance system," *Chaos, Solitons & Fractals*, vol. 132, Article ID 109567, 2020.
[7] G. Chen, "A simple adaptive feedback control method for chaos and hyper-chaos control," *Applied Mathematics and Computation*, vol. 217, no. 17, pp. 7258–7264, 2011.
[8] J. Du, T. Huang, Z. Sheng, and H. Zhang, "A new method to control chaos in an economic system," *Applied Mathematics and Computation*, vol. 217, no. 6, pp. 2370–2380, 2010.
[9] E. Ott, C. Grebogi, and J. A. Yorke, "Controlling chaos," *Physical Review Letters*, vol. 64, no. 11, pp. 1196–1199, 1990.
[10] A. S. de Paula and M. A. Savi, "Controlling chaos in a nonlinear pendulum using an extended time-delayed feedback control method," *Chaos, Solitons & Fractals*, vol. 42, no. 5, pp. 2981–2988, 2009.
[11] H. Sadeghian, H. Salarieh, A. Alasty, and A. Meghdari, "On the control of chaos via fractional delayed feedback method,"

Computers & Mathematics with Applications, vol. 62, no. 3, pp. 1482–1491, 2011.

[12] Y. Han, J. Ding, L. Du, and Y. Lei, "Control and anti-control of chaos based on the moving largest Lyapunov exponent using reinforcement learning," *Physica D: Nonlinear Phenomena*, vol. 428, Article ID 133068, 2021.

[13] X. Yin, J. She, Z. Liu, M. Wu, and O. Kaynak, "Chaos suppression in speed control for permanent-magnet-synchronous-motor drive system," *Journal of the Franklin Institute*, vol. 357, no. 18, pp. 13283–13303, 2020.

[14] X. Chen and J. Zhou, "The complexity analysis and chaos control in omni-channel supply chain with consumer migration and advertising cost sharing," *Chaos, Solitons & Fractals*, vol. 146, Article ID 110884, 2021.

[15] P. Geysermans and F. Baras, "Particle simulation of chemical chaos," *The Journal of Chemical Physics*, vol. 105, no. 4, pp. 1402–1408, 1996.

[16] P. Geysermans and G. Nicolis, "Thermodynamic fluctuations and chemical chaos in a well-stirred reactor: a master equation analysis," *The Journal of Chemical Physics*, vol. 99, no. 11, pp. 8964–8969, 1993.

[17] C. Xu and Y. Wu, "Bifurcation and control of chaos in a chemical system," *Applied Mathematical Modelling*, vol. 39, no. 8, pp. 2295–2310, 2015.

[18] C. J. Xu, W. Zhang, C. Aouiti, Z. X. Liu, M. X. Liao, and P. L. Li, "Further investigation on bifurcation and their control of fractional-order BAM neural networks involving four neurons and multiple delays," *Mathematical Methods in the Applied Sciences*, 2021.

[19] C. Xu, Z. Liu, L. Yao, and C. Aouiti, "Further exploration on bifurcation of fractional-order six-neuron bi-directional associative memory neural networks with multi-delays," *Applied Mathematics and Computation*, vol. 410, Article ID 126458, 2021.

[20] F. B. Yousef, A. Yousef, and C. Maji, "Effects of fear in a fractional-order predator-prey system with predator density-dependent prey mortality," *Chaos, Solitons & Fractals*, vol. 145, Article ID 110711, 2021.

[21] C. Huang, H. Liu, X. Chen et al., "Dynamic optimal control of enhancing feedback treatment for a delayed fractional order predator-prey model," *Physica A: Statistical Mechanics and its Applications*, vol. 554, Article ID 124136, 2020.

[22] C. Xu, M. Liao, P. Li, Y. Guo, and Z. Liu, "Bifurcation properties for fractional order delayed BAM neural networks," *Cognitive Computation*, vol. 13, no. 2, pp. 322–356, 2021.

[23] F. A. Rihan and C. Rajivganthi, "Dynamics of fractional-order delay differential model of prey-predator system with Holling-type III and infection among predators," *Chaos, Solitons & Fractals*, vol. 141, Article ID 110365, 2020.

[24] X. Nie, P. Liu, J. Liang, and J. Cao, "Exact coexistence and locally asymptotic stability of multiple equilibria for fractional-order delayed Hopfield neural networks with Gaussian activation function," *Neural Networks*, vol. 142, pp. 690–700, 2021.

[25] F. Zhang, T. Huang, Q. Wu, and Z. Zeng, "Multistability of delayed fractional-order competitive neural networks," *Neural Networks*, vol. 140, pp. 325–335, 2021.

[26] C. Xu, Z. Liu, M. Liao, P. Li, Q. Xiao, and S. Yuan, "Fractional-order bidirectional associate memory (BAM) neural networks with multiple delays: the case of Hopf bifurcation," *Mathematics and Computers in Simulation*, vol. 182, pp. 471–494, 2021.

[27] L. Ke, "Mittag-Leffler stability and asymptotic ω-periodicity of fractional-order inertial neural networks with time-delays," *Neurocomputing*, vol. 465, pp. 53–62, 2021.

[28] F. F. Du and J. G. Lu, *Finite-Time Stability of Fractional-Order Fuzzy Cellular Neural Networks with Time Delays, Fuzzy Sets and Systems*, 2021.

[29] M. Xiao, W. X. Zheng, J. Lin, G. Jiang, L. Zhao, and J. Cao, "Fractional-order PD control at Hopf bifurcations in delayed fractional-order small-world networks," *Journal of the Franklin Institute*, vol. 354, no. 17, pp. 7643–7667, 2017.

[30] C. Huang, H. Liu, X. Shi et al., "Bifurcations in a fractional-order neural network with multiple leakage delays," *Neural Networks*, vol. 131, pp. 115–126, 2020.

[31] J. Alidousti and E. Ghafari, "Dynamic behavior of a fractional order prey-predator model with group defense," *Chaos, Solitons & Fractals*, vol. 134, Article ID 109688, 2020.

[32] W. Wang and M. A. Khan, "Analysis and numerical simulation of fractional model of bank data with fractal-fractional Atangana-Baleanu derivative," *Journal of Computational and Applied Mathematics*, vol. 369, Article ID 112646, 2020.

[33] C. Xu, M. Liao, P. Li, and S. Yuan, "Impact of leakage delay on bifurcation in fractional-order complex-valued neural networks," *Chaos, Solitons & Fractals*, vol. 142, Article ID 110535, 2021.

[34] C. Xu, W. Zhang, W. Zhang et al., "Bifurcation dynamics in a fractional-order Oregonator model including time delay," *MATCH Communications in Mathematical and in Computer Chemistry*, vol. 87, no. 2, pp. 397–414, 2022.

[35] I. Podlubny, *Fractional Differential Equations*, Academic Press, New York, NY, USA, 1999.

[36] D. Matignon, "Stability results for fractional differential equations with applications to control processing, Computational engineering in systems and application multi-conference, IMACS," *IEEE-SMC Proceedings, Lille*, vol. 2, pp. 963–968, 1996.

[37] Y. Tang, M. Xiao, G. Jiang, J. Lin, J. Cao, and W. X. Zheng, "Fractional-order PD control at Hopf bifurcations in a fractional-order congestion control system," *Nonlinear Dynamics*, vol. 90, no. 3, pp. 2185–2198, 2017.

[38] Q. Sun, M. Xiao, and B. Tao, "Local bifurcation analysis of a fractional-order dynamic model of genetic regulatory networks with delays," *Neural Processing Letters*, vol. 47, no. 3, pp. 1285–1296, 2018.

[39] A. M. Sayed, A. E. Matouk, S. Kumar, V. Ali, and L. Bachioua, "Chaotic dynamics and chaos control in a fractional-order satellite model and its time-delay counterpart," *Discrete Dynamics in Nature and Society*, vol. 2021, Article ID 5542908, 11 pages, 2021.

[40] H.-L. Li, L. Zhang, C. Hu, Y.-L. Jiang, and Z. Teng, "Dynamical analysis of a fractional-order predator-prey model incorporating a prey refuge," *Journal of Applied Mathematics and Computing*, vol. 54, no. 1-2, pp. 435–449, 2017.

[41] K. Diethelm, "An algorithm for the numerical solution of differential equations of fractional order," *Electronic Transactions on Numerical Analysis*, vol. 5, pp. 1–6, 1997.

[42] K. Diethelm, N. J. Ford, and A. D. Freed, "A predictor-corrector approach for the numerical solution of fractional differential equations," *Nonlinear Dynamics*, vol. 29, no. 1/4, pp. 3–22, 2002.

Hindawi
Journal of Mathematics
Volume 2022, Article ID 2681789, 13 pages
https://doi.org/10.1155/2022/2681789

Research Article

On q-Convex Functions Defined by the q-Ruscheweyh Derivative Operator in Conic Regions

Mehwish Jabeen,[1] **Sarfraz Nawaz Malik**,[1] **Shahid Mahmood**,[2] **S. M. Jawwad Riaz**,[1] **and Md. Shajib Ali**[3]

[1]*Department of Mathematics, COMSATS University Islamabad, Wah Campus, Wah Cantt 47040, Pakistan*
[2]*Department of Mechanical Engineering, Sarhad University of Science & I. T Landi Akhun Ahmad, Hayatabad Link. Ring Road, Peshawar, Pakistan*
[3]*Department of Mathematics, Islamic University, Kushtia-7003, Bangladesh*

Correspondence should be addressed to Md. Shajib Ali; shajib_301@yahoo.co.in

Received 20 December 2021; Accepted 10 January 2022; Published 1 February 2022

Academic Editor: Fairouz Tchier

The core objective of this article is to introduce and investigate a new class $\beta - \mathrm{UCV}_q^\lambda[A, B]$ of convex functions associated with the conic domain defined by the Ruscheweyh q-differential operator. Many interesting properties such as sufficiency criteria, coefficient bounds, partial sums, and radius of convexity of order α for the functions of the said class are investigated here.

1. Introduction

Quantum calculus has emerged as one of the most vibrant areas of research in recent years. Researchers have discussed and found its applications in numerous dimensions, such as hypergeometric series, complex analysis, and applied physics. It has developed techniques to be used in q-calculus, time scales, partitions, and continued fractions. Jackson, for the first time, in the beginning of the 20th century, introduced quantum calculus, where he developed and standardized it. For more details about quantum calculus, see [1–14]. To make a good pace and understanding of the results presented in this article, we are going to give below some primary definitions and relevant details of quantum calculus. Suppose $\mathcal{F}$ represents the class of holomorphic functions of type

$$y(z) = z + \sum_{n=2}^{\infty} b_n z^n. \tag{1}$$

in open unit disk $\mathscr{E} = \{z\colon z \in \mathbb{C} \text{ and } |z| < 1\}$ and normalized by the conditions $y'(0) = 1$ and $y(0) = 0$. Moreover, $\mathcal{S}$ represents the class of all functions in $\mathcal{F}$ which are univalent in $\mathscr{E}$; see [15].

A domain $\mathscr{D}$ is starlike with respect to a point $z_0 \in \mathscr{D}$ if all possible lines which are confined by two points, connecting z_0 to any other point, lie entirely within $\mathscr{D}$. Correspondingly, a domain $\mathscr{E}$ is convex if all possible lines which are obtained by connecting any two points in $\mathscr{D}$ lie thoroughly within $\mathscr{D}$. More clearly, we can say that if the domain is starlike with respect to each of its points in $\mathscr{D}$, then it is convex. If $y(\mathscr{E})$ is starlike for $y \in \mathcal{S}$ with respect to the origin, then it is called a starlike function, whereas if $y(\mathscr{E})$ is convex, then it is called a convex function. The class of all convex functions is represented by C, and the class of all starlike functions is represented by S^*. Analytically, these are defined as follows:

$$\begin{aligned} S^*\colon &= \left\{ y \in \mathcal{S}\colon \Re\left\{\frac{zy'(z)}{y(z)}\right\} > 0, \quad z \in \mathscr{E} \right\}, \\ C\colon &= \left\{ y \in \mathcal{S}\colon \Re\left\{1 + \frac{zy''(z)}{y'(z)}\right\} > 0, \quad z \in \mathscr{E} \right\}. \end{aligned} \tag{2}$$

For $\alpha \in [0,1)$, suppose that $S^*(\alpha)$ and $C(\alpha)$ are subclasses of $\mathcal{S}$ consisting of α-starlike functions and α-convex functions, respectively, defined analytically as follows:

$$\begin{aligned} S^*(\alpha):&=\left\{y\in\mathcal{S}:\ \mathfrak{R}\left\{\frac{zy'(z)}{y(z)}\right\}>\alpha,\quad z\in\mathscr{E}\right\},\\ C(\alpha):&=\left\{y\in\mathcal{S}:\ \mathfrak{R}\left\{1+\frac{zy''(z)}{y'(z)}\right\}>\alpha,\quad z\in\mathscr{E}\right\}.\end{aligned}\tag{3}$$

For $\alpha=0$, the class $S^*(\alpha)\Rightarrow S^*$ and the class $C(\alpha)\Rightarrow C$. Moreover, the following two classes are closely related with their functions defined, respectively.

$$\begin{aligned} S^*_\alpha:&=\left\{y\in\mathcal{S}:\ \left|\frac{zy'(z)}{y(z)}-1\right|<1-\alpha,\quad z\in\mathscr{E}\right\},\\ C_\alpha:&=\left\{y\in\mathcal{S}:\ \left|\frac{zy''(z)}{y'(z)}\right|<1-\alpha,\quad z\in\mathscr{E}\right\}.\end{aligned}\tag{4}$$

Note that $S^*_\alpha\subseteq S^*(\alpha)$ and $C_\alpha\subseteq C(\alpha)$. The k^{th} partial sum of the function y, denoted by y_k, is the polynomial, defined by

$$y_k(z)=z+\sum_{n=2}^{k}b_nz^n.\tag{5}$$

Generally, lower bounds on ratios such as $\mathfrak{R}\{y(z)/y_k(z)\}$ or $\mathfrak{R}\{y_k(z)/y(z)\}$ have been found to be sharp only when $k=1$, but Silverman determined sharpness $\forall n\in\mathbb{N}$; see [16, 17]. He investigated that lower bounds are strictly increasing functions of k. In the present article, by using Silverman's technique [16], we will find the function's ratio having Taylor series (1) to its sequence of partial sums $y_k(z)=z+\sum_{n=2}^{k}b_nz^n$ when the coefficients of y are sufficiently small to fulfill the necessary and sufficient condition. In more details to clarify, we will find sharp lower bounds for $y(z)/y_k(z)$, $y'(z)/y_k'(z)$, $y_k(z)/y(z)$, and $y_k'(z)/y'(z)$. Indeed, we will use the familiar result, i.e., $\mathfrak{R}\{w(z)-1/w(z)+1\}>0$, $z\in\mathscr{E}$, if and only if $w(z)=\sum_{n=1}^{\infty}c_nz^n$ satisfies $|w(z)|\le|z|$. Unless otherwise stated, we will presume that y has form (1) and that its sequence of partial sums is represented by (5).

For $\alpha\in[0,1)$, Ravichandran gave the sharp radius of starlike and convex functions of order α with form (1) whose Taylor series coefficients b_n satisfy the conditions $|b_2|=2\,d$, $d\in[0,1]$, and $|b_n|\le n$; M or M/n $(M>0)$ for $n\ge3$.

Consider that y_1 and y_2 are holomorphic functions in $\mathscr{E}$ with $w(0)=0$ and $|w(z)\le1|$, $\forall z\in\mathscr{E}$, so that $y_1(z)=y_2(w(z))$; y_1 will be subordinated by y_2 and denoted by $y_1\prec y_2$. If y_2 is holomorphic, then $y_1\prec y_2$ iff $y_1(0)=y_2(0)$ and $y_1(\mathscr{E})\subseteq y_2(\mathscr{E})$.

For two holomorphic functions

$$y_1(z)=\sum_{k=0}^{\infty}a_kz^k \text{ and } y_2(z)=\sum_{k=0}^{\infty}b_kz^k\ (z\in\mathrm{E}),\tag{6}$$

the Hadamard product of $y_1(z)$ and $y_2(z)$ is defined as

$$y_1(z)*y_2(z)=\sum_{k=0}^{\infty}a_kb_kz^k.\tag{7}$$

We will define some notations and concepts of quantum calculus which are to be used in this article. All results can be found in [2, 3, 18]. For $n\in\mathbb{N}$, $0<q<1$, we see the classical q-theory begins with the q-extension of the positive numbers. The expression

$$\lim_{q\longrightarrow1}\frac{1-q^n}{1-q}=n.\tag{8}$$

proposes that we define the q-generalization of n, which is also called the q-bracket of n, given as

$$[n,q]=[n]_q=\frac{1-q^n}{1-q},\tag{9}$$

and the q-generalization of the factorial which is called q-factorial given by

$$[n]_q!=\begin{cases}[n]_q[n-1]_q\ldots[1]_q, & n=1,2,\ldots,\\ 1, & n=0.\end{cases}\tag{10}$$

The q-difference operator for $y\in\mathcal{F}$ is defined as

$$\partial_qy(z)=\frac{y(qz)-y(z)}{z(q-1)},\quad(z\in\mathrm{E}),\tag{11}$$

and we can see that, for $n\in\mathbb{N}$ and $z\in\mathrm{E}$,

$$\begin{aligned}\partial_qz^n&=[n]_qz^{n-1},\\ \partial_q\left\{\sum_{n-1}^{\infty}b_nz^n\right\}&=\sum_{n-1}^{\infty}[n]_qb_nz^{n-1}.\end{aligned}\tag{12}$$

For $y(z)\in\mathcal{F}$, the q-analogue of the Ruscheweyh differential operator is defined as

$$\begin{aligned}R_q^\lambda y(z)&=\varphi(q,\lambda+1;z)*y(z)\\ &=z+\sum_{n=2}^{\infty}\psi_{n-1}b_nz^n,\ (z\in\mathrm{E}\text{ and }\lambda>-1),\end{aligned}\tag{13}$$

where

$$\varphi(q,\lambda+1;z)=z+\sum_{n=2}^{\infty}\psi_{n-1}z^n,\tag{14}$$

and

$$\psi_{n-1}=\frac{\Gamma_q(\lambda+n)}{[n-1]_q!\Gamma_q(\lambda+1)}=\frac{[\lambda+1,q]_{n-1}}{[n-1]_q!},\quad(\psi_0=1),\tag{15}$$

where $[\lambda+1,q]_{n-1}$ is a Pochhammer symbol, which is defined as follows:

$$[n,q]_m = \begin{cases} 1, & n=0, \\ [n,q][n+1,q][n+2,q][n+3,q]\dots[m+n-1,q], & n\in\mathbb{N}. \end{cases} \tag{16}$$

From (13), it is clear that

$$\begin{aligned} &R_q^0 y(z) = y(z) \text{ and } R_q^1 y(z) = z\partial_q y(z),\\ &R_q^m y(z) = \frac{z\partial_q^m\left(z^{m-1}y(z)\right)}{[m]_q!}, \quad (m\in\mathbb{N}),\\ &\lim_{q\longrightarrow 1^-}\varphi(q,\lambda+1;z) = \frac{z}{(1-z)^{\lambda+1}},\\ &\lim_{q\longrightarrow 1^-} R_q^\lambda y(z) = y(z) * \frac{z}{(1-z)^{\lambda+1}}. \end{aligned} \tag{17}$$

It follows that $q\longrightarrow 1^-$, and the Ruscheweyh q-differential operator converts into the Ruscheweyh differential operator $D^\delta(y(z))$; for more details, see [19]. Using (13),

$$z\partial R_q^\lambda y(z) = \left(1+\frac{[\lambda]_q}{q^\lambda}\right)R_q^{\lambda+1}y(z) - \frac{[\lambda]_q}{q^\lambda}R_q^\lambda y(z). \tag{18}$$

If $q\longrightarrow 1^-$, then

$$z\left(R^\lambda y(z)\right)' = (1+\lambda)R^{\lambda+1}y(z) - \lambda R^\lambda y(z). \tag{19}$$

Definition 1. The function $p(z)$ will lie in the class $\beta - P_q[A,B]$ if and only if

$$p(z) \prec \frac{(A(1+q)+(3-q))\widetilde{p}_\beta(z) - (A(1+q)-(3-q))}{(B(1+q)+(3-q))\widetilde{p}_\beta(z) - (B(1+q)-(3-q))}, \quad \beta\geq 0, \tag{20}$$

where

$$\widetilde{p}_\beta(z) = \begin{cases} \dfrac{1+z}{1-z}, & \beta=0,\\ 1+\dfrac{2}{\pi^2}\left(\log\dfrac{1+\sqrt{z}}{1-\sqrt{z}}\right)^2, & \beta=1,\\ 1+\dfrac{2}{1-\beta^2}\sinh^2\left[\left(\dfrac{2}{\pi}\arccos\beta\right)\arctan\ y\sqrt{z}\right], & 0<\beta<1,\\ 1+\dfrac{1}{\beta^2-1}\sin\left(\dfrac{\pi}{2R(n)}\displaystyle\int_0^{u(z)/\sqrt{t}}\dfrac{1}{\sqrt{1-x^2}\sqrt{1-(tx)^2}}dx\right)+\dfrac{1}{\beta^2-1}, & \beta>1. \end{cases} \tag{21}$$

For more details, see [20–24]. If $\widetilde{p}_\beta(z) = 1+\delta_\beta z+\cdots$, then it is shown in [25] that, from (46), one can have

$$\delta_\beta = \begin{cases} \dfrac{8(\arccos\beta)^2}{\pi^2(1-\beta^2)}, & 0 \le \beta < 1, \\ \dfrac{8}{\pi^2}, & \beta = 1, \\ \dfrac{\pi^2}{4(\beta^2-1)\sqrt{t}\,(1+t)R^2(t)}, & \beta > 1. \end{cases} \quad (22)$$

Definition 2. A function $y(z) \in \mathscr{F}$ will lie in the class $\beta - \mathrm{UCV}_q[A,B]$, $\beta \ge 0$, $-1 \le B < A \le 1$, if and only if

$$\Re\left[\frac{(B(1+q)-(3-q))D_q(zD_q y(z))/D_q y(z)-(A(1+q)-(3-q))}{(B(1+q)+(3-q))D_q(zD_q y(z))/D_q y(z)-(A(1+q)+(3-q))}\right] > \beta\left|\frac{(B(1+q)-(3-q))D_q(zD_q y(z))/D_q y(z)-(A(1+q)-(3-q))}{(B(1+q)+(3-q))D_q(zD_q y(z))/D_q y(z)-(A(1+q)+(3-q))}-1\right|, \quad (23)$$

or equivalently,

$$\frac{D_q(zD_q y(z))}{D_q y(z)} \in \beta - P_q[A,B]. \quad (24)$$

For more details about the above classes and conic domain, we refer the readers to [20, 25–28]. Using the q-Ruscheweyh differential operator, we now define the following more general class $\beta - \mathrm{UCV}_q^\lambda[A,B]$ of functions associated with the conic domain defined by Janowski functions.

Definition 3. A function $y(z) \in \mathscr{F}$ will lie in the class $\beta - \mathrm{UCV}_q^\lambda[A,B]$, $\beta \ge 0, -1 \le B < A \le 1$, if and only if

$$\Re\left[\frac{(B(1+q)-(3-q))\partial_q(z\partial_q R_q^\lambda y(z))/\partial_q R_q^\lambda y(z)-(A(1+q)-(3-q))}{(B(1+q)+(3-q))\partial_q(z\partial_q R_q^\lambda y(z))/\partial_q R_q^\lambda y(z)-(A(1+q)+(3-q))}\right] > \beta\left|\frac{(B(1+q)-(3-q))\partial_q(z\partial_q R_q^\lambda y(z))/\partial_q R_q^\lambda y(z)-(A(1+q)-(3-q))}{(B(1+q)+(3-q))\partial_q(z\partial_q R_q^\lambda y(z))/\partial_q R_q^\lambda y(z)-(A(1+q)+(3-q))}-1\right|, \quad (25)$$

or equivalently,

$$\frac{\partial_q(z\partial_q R_q^\lambda y(z))}{\partial_q R_q^\lambda y(z)} \in \beta - P[A,B]. \quad (26)$$

The above defined class $\beta - \mathrm{UCV}_q^\lambda[A,B]$ generalizes many known classes which can be obtained by setting suitable particular values to the parameters as follows.

Special cases:

(1) $\beta - \mathrm{UCV}_{1^-}^0[A,B] = \beta - \mathrm{UCV}[A,B]$, the well-known class of β-uniformly Janowski convex functions, introduced by Noor and Malik [27]

(2) $0 - \mathrm{UCV}_{1^-}^0[A,B] = C[A,B]$, the well-known class of Janowski convex functions, introduced by Janowski [20]

(3) $\beta - \mathrm{UCV}_{1^-}^0[1-2\alpha,-1] = \mathrm{KD}(\beta,\alpha)$, see [29]

(4) $0 - \mathrm{UCV}_{1^-}^0[1-2\alpha,-1] = C(\alpha)$, see [15]

Lemma 1 (see [30]). *Let $g(z) = 1 + \sum_{n=1}^{\infty} c_n z^n$ be subordinate to $G(z) = 1 + \sum_{n=1}^{\infty} C_n z^n$. If $G(z)$ is holomorphic in $\mathscr{E}$ and $G(\mathscr{E})$ is convex, then*

$$|c_n| \le |C_1|, \quad n \ge 1. \quad (27)$$

2. Main Results

Theorem 1. *A function $y(z) \in \mathscr{F}$ with form (1) will lie in class $\beta - UCV_q^\lambda[A,B]$, $\beta \ge 0$, $-1 \le B < A \le 1$, if it satisfies the condition*

$$\sum_{n=2}^{\infty} \frac{\mathbb{E}_n}{\varepsilon}|b_n| < 1, \quad (28)$$

where

$$\mathbb{E}_n = [n]_q\left\{2(3-q)(\beta+1)q[n-1]_q + \left|(B(1+q)+(3-q))[n]_q - (A(1+q)+(3-q))\right|\right\}\psi_{n-1}, \tag{29}$$

and

$$\varepsilon = (1+q)|B-A|. \tag{30}$$

Proof. Suppose that (28) holds; then, it is enough to show that

$$\beta\left|\frac{(B(1+q)-(3-q))\partial_q\left(z\partial_q R_q^{\lambda} y(z)\right)/\partial_q R_q^{\lambda} y(z) - (A(1+q)-(3-q))}{(B(1+q)+(3-q))\partial_q\left(z\partial_q R_q^{\lambda} y(z)\right)/\partial_q R_q^{\lambda} y(z) - (A(1+q)+(3-q))} - 1\right| - \Re\left[\frac{(B(1+q)-(3-q))\partial_q\left(z\partial_q R_q^{\lambda} y(z)\right)/\partial_q R_q^{\lambda} y(z) - (A(1+q)-(3-q))}{(B(1+q)+(3-q))\partial_q\left(z\partial_q R_q^{\lambda} y(z)\right)/\partial_q R_q^{\lambda} y(z) - (A(1+q)+(3-q))} - 1\right] < 1. \tag{31}$$

We consider

$$\begin{aligned}
&\beta\left|\frac{(B(1+q)-(3-q))\partial_q\left(z\partial_q R_q^{\lambda} y(z)\right)/\partial_q R_q^{\lambda} y(z) - (A(1+q)-(3-q))}{(B(1+q)+(3-q))\partial_q\left(z\partial_q R_q^{\lambda} y(z)\right)/\partial_q R_q^{\lambda} y(z) - (A(1+q)+(3-q))} - 1\right| \\
&\quad - \Re\left[\frac{(B(1+q)-(3-q))\partial_q\left(z\partial_q R_q^{\lambda} y(z)\right)/\partial_q R_q^{\lambda} y(z) - (A(1+q)-(3-q))}{(B(1+q)+(3-q))\partial_q\left(z\partial_q R_q^{\lambda} y(z)\right)/\partial_q R_q^{\lambda} y(z) - (A(1+q)+(3-q))} - 1\right] \\
&\le (\beta+1)\left|\frac{(B(1+q)-(3-q))\partial_q\left(z\partial_q R_q^{\lambda} y(z)\right) - (A(1+q)-(3-q))\partial_q R_q^{\lambda} y(z)}{(B(1+q)+(3-q))\partial_q\left(z\partial_q R_q^{\lambda} y(z)\right) - (A(1+q)+(3-q))\partial_q R_q^{\lambda} y(z)} - 1\right| \\
&= 2(3-q)(\beta+1)\left|\frac{\partial_q R_q^{\lambda} y(z) - \partial_q\left(z\partial_q R_q^{\lambda} y(z)\right)}{(B(1+q)+(3-q))\partial_q\left(z\partial_q R_q^{\lambda} y(z)\right) - (A(1+q)+(3-q))\partial_q R_q^{\lambda} y(z)}\right| \\
&= 2(3-q)(\beta+1)\left|\frac{\sum_{n=2}^{\infty}\left(1-[n]_q\right)\psi_{n-1}[n]_q b_n z^n}{z(B-A)(1+q) + \sum_{n=2}^{\infty}\begin{pmatrix}(B(1+q)+(3-q))[n]_q \\ -(A(1+q)+(3-q))\end{pmatrix}\psi_{n-1}[n]_q b_n z^n}\right| \\
&\le \frac{2(3-q)(\beta+1)\sum_{n=2}^{\infty} q[n-1]_q[n]_q\left|b_n\right|}{(1+q)|B-A|1/\psi_{n-1} - \sum_{n=2}^{\infty}\left|(B(1+q)+(3-q))[n]_q - (A(1+q)+(3-q))\right|[n]_q\left|b_n\right|}.
\end{aligned} \tag{32}$$

The last expression is bounded above by 1 if

$$2(3-q)(\beta+1)\sum_{n=2}^{\infty} q[n-1]_q[n]_q|b_n| < (1+q)|B-A|\frac{1}{\psi_{n-1}}$$
$$-\sum_{n=2}^{\infty}\left|(B(1+q)+(3-q))[n]_q-(A(1+q)+(3-q))\right|[n]_q|b_n|, \tag{33}$$

which reduces to

$$\sum_{n=2}^{\infty}[n]_q\left\{2(3-q)(\beta+1)q[n-1]_q+\left|\begin{matrix}(B(1+q)+(3-q))[n]_q\\ -(A(1+q)+(3-q))\end{matrix}\right|\right\}\psi_{n-1}|b_n|<(1+q)|B-A|. \tag{34}$$

This finalizes the proof. □ □

For $q \longrightarrow 1^-$ and $\lambda = 0$, we have the following known result, proved in [27].

Corollary 1. *A function $y(z) \in \mathscr{F}$ with form (1) will lie in class $\beta - UCV[A,B]$, $\beta \geq 0$, $-1 \leq B < A \leq 1$, if it satisfies the condition*

$$\sum_{n=2}^{\infty} n\{2(\beta+1)(n-1)+|n(B+1)-(A+1)|\}|b_n|<|B-A|. \tag{35}$$

For $q \longrightarrow 1^-$, $\lambda = 0$, and $A = 1-2\alpha$ and $B=-1$, we have the following known result, proved in [29].

Corollary 2. *A function $y(z) \in \mathscr{F}$ with form (1) will lie in class $KD(\beta,\alpha)$, $\beta \geq 0$, $0 \leq \alpha < 1$, if it satisfies the condition*

$$\sum_{n=2}^{\infty} n\{n(\beta+1)-(\beta+\alpha)\}|b_n|<(1-\alpha). \tag{36}$$

Theorem 2. *Let $y(z) \in \beta - UCV_q^{\lambda}[A,B]$, $\beta \geq 0$, $-1 \leq B < A \leq 1$, and be of form (1); then, for $n \geq 2$,*

$$|b_n| \leq \frac{1}{[n]_q}\prod_{j=0}^{n-2}\frac{\left|(A-B)(q+1)\delta_\beta\psi_j-4Bq[j]_q\psi_j\right|}{4q[j+1]_q\psi_{j+1}}, \tag{37}$$

where ψ is defined by (15).

Proof. By the definition for $y(z) \in \beta - \mathrm{UCV}_q^{\lambda}[A,B]$, we have

$$\frac{\partial_q\left(z\partial_q R_q^{\lambda} y(z)\right)}{\partial_q R_q^{\lambda} y(z)} = p(z), \tag{38}$$

where

$$p(z) \prec \frac{(A(1+q)+(3-q))\widetilde{p}_\beta(z)-(A(1+q)-(3-q))}{(B(1+q)+(3-q))\widetilde{p}_\beta(z)-(B(1+q)-(3-q))}. \tag{39}$$

If $\widetilde{p}_\beta(z) = 1+\delta_\beta z+\ldots$, then

$$\frac{(A(1+q)+(3-q))\widetilde{p}_\beta(z)-(A(1+q)-(3-q))}{(B(1+q)+(3-q))\widetilde{p}_\beta(z)-(B(1+q)-(3-q))} = 1+\frac{1}{4}(A-B)(q+1)\delta_\beta+$$
$$\frac{1}{4}\left[\left(-\frac{1}{4}Aq-\frac{1}{4}A+\frac{1}{4}Bq+\frac{1}{4}B\right)((B+1)(1+q)+2-2q)\right]\delta_\beta^2+\cdots. \tag{40}$$

Now, if $p(z) = 1+\sum_{n=1}^{\infty} c_n z^n$, then by (27) and (39), we have

$$|c_n| \leq \frac{1}{4}(A-B)(q+1)|\delta_\beta|, \quad n \geq 1. \tag{41}$$

Now, from (38), we have

$$\partial_q\left(z\partial_q R_q^{\lambda} y(z)\right) = p(z)\partial_q R_q^{\lambda} y(z). \tag{42}$$

Let $p(z) = 1+\sum_{n=1}^{\infty} c_n z^n$, and using the Cauchy product formula, we obtain

$$\begin{aligned}1+\sum_{n=2}^{\infty}[n]_q[n]_q\psi_{n-1}b_nz^{n-1} &= \left(1+\sum_{n=1}^{\infty}c_nz^n\right)\left(1+\sum_{n=2}^{\infty}[n]_q\psi_{n-1}b_nz^{n-1}\right)\\ \sum_{n=2}^{\infty}[n]_q[n]_q\psi_{n-1}b_nz^{n-1} &= \sum_{n=2}^{\infty}c_{n-1}z^{n-1}+\sum_{n=2}^{\infty}[n]_q\psi_{n-1}b_nz^{n-1}+\left(\sum_{n=2}^{\infty}[n]_q\psi_{n-1}b_nz^{n-1}\right).\left(\sum_{n=2}^{\infty}c_{n-1}z^{n-1}\right).\end{aligned} \tag{43}$$

This implies that

$$\sum_{n=2}^{\infty}\left([n]_q-1\right)[n]_q\psi_{n-1}b_nz^{n-1}=\left(\sum_{n=2}^{\infty}c_{n-1}+\sum_{n=2}^{\infty}\sum_{j=2}^{n}[j]_q\psi_{j-1}b_jc_{n-j}\right)z^{n-1}. \tag{44}$$

Comparison of coefficients of z^{n-1} gives us

$$\left([n]_q-1\right)[n]_q\psi_{n-1}b_n=\left(c_{n-1}+\sum_{j=2}^{n}[j,q]\psi_{j-1}b_jc_{n-j}\right)(b_1=1), \tag{45}$$

or

$$b_n=\frac{1}{\left([n]_q-1\right)[n]_q\psi_{n-1}}\left(c_{n-1}+\sum_{j=2}^{n}[j]_q\psi_{j-1}b_jc_{n-j}\right). \tag{46}$$

Using (41), we have

$$\left|b_n\right|\leq\frac{(A-B)(q+1)\left|\delta_\beta\right|}{4q[n-1]_q[n]_q\psi_{n-1}}\left(1+\sum_{j=2}^{n-1}[j]_q\psi_{j-1}\left|b_j\right|\right), \tag{47}$$

or

$$\left|b_n\right|\leq\frac{(A-B)(q+1)\left|\delta_\beta\right|}{4q[n-1]_q[n]_q\psi_{n-1}}\left(\sum_{j=1}^{n-1}[j]_q\psi_{j-1}\left|b_j\right|\right). \tag{48}$$

Now, we prove that

$$\frac{(A-B)(q+1)\left|\delta_\beta\right|}{4q[n-1]_q[n]_q\psi_{n-1}}\left(\sum_{j=1}^{n-1}[j]_q\psi_{j-1}\left|b_j\right|\right)\leq\frac{1}{[n]_q}\prod_{j=0}^{n-2}\frac{\left|(A-B)(q+1)\delta_\beta\psi_j-4Bq[n]_q\psi_j\right|}{4q[j+1]_q\psi_{j+1}}. \tag{49}$$

For this, we use the induction technique. For $n=2$, we have from (46),

$$\left|b_2\right|\leq\frac{\left|\delta_\beta\right|(q+1)(A-B)}{4q[1]_q[2]_q\psi_1}\sum_{j=1}^{2-1}[j]_q\psi_{j-1}\left|b_j\right|, \tag{50}$$

or

$$\left|b_2\right|\leq\frac{\left|\delta_\beta\right|(A-B)(q+1)}{4q[1]_q[2]_q\psi_1},\quad \psi_0=1. \tag{51}$$

For $n=3$, we have from (46),

$$\begin{aligned}\left|b_3\right| &\leq\frac{\left|\delta_\beta\right|(A-B)(q+1)}{4q[2]_q[3]_q\psi_2}\sum_{j=1}^{2}[j]_q\psi_{j-1}\left|b_j\right|\\ &=\frac{\left|\delta_\beta\right|(A-B)(q+1)}{4q[2]_q[3]_q\psi_2}\left([1]_q\psi_0\left|b_1\right|+[2]_q\psi_1\left|b_2\right|\right)\\ &\leq\frac{\left|\delta_\beta\right|(A-B)(q+1)}{4q[2]_q[3]_q\psi_2}\left(1+\frac{(A-B)(q+1)\left|\delta_\beta\right|}{4q[1]_q}\right).\end{aligned} \tag{52}$$

From (37), we have

$$\begin{aligned}\left|b_3\right| &\leq \frac{1}{[3]_q}\prod_{j=0}^{1}\frac{\left|(A-B)(q+1)\delta_\beta\psi_j - 4Bq[j]_q\psi_j\right|}{4q[j+1]_q\psi_{j+1}}\\ &= \frac{1}{[3]_q}\frac{(A-B)(q+1)\left|\delta_\beta\right|}{4q[1]_q\psi_1}\left(\frac{(A-B)(q+1)\left|\delta_\beta\right|\psi_1 + 4q[1]_q\psi_1}{4q[2]_q\psi_2}\right)\\ &= \frac{\left|\delta_\beta\right|(A-B)(q+1)}{4q[2]_q[3]_q\psi_2}\left(1+\frac{(A-B)(q+1)\left|\delta_\beta\right|}{4q[1]_q}\right).\end{aligned} \tag{53}$$

Let the assumption be true for $n = m+1$. From (46), we have

$$\left|b_m\right| \leq \frac{\left|\delta_\beta\right|(A-B)(q+1)}{4q[m-1]_q[m]_q\psi_{m-1}}\left(\sum_{j=1}^{m-1}[j]_q\psi_{j-1}\left|b_j\right|\right). \tag{54}$$

From (37), we have

$$\left|b_m\right| \leq \frac{1}{[m]_q}\prod_{j=0}^{m-2}\frac{\left|(A-B)(q+1)\delta_\beta\psi_j - 4Bq[j]_q\psi_j\right|}{4q[j+1]_q\psi_{j+1}}. \tag{55}$$

By the induction hypothesis,

$$\frac{1}{[m]_q}\prod_{j=0}^{m-2}\frac{\left|(A-B)(q+1)\delta_\beta\psi_j - 4Bq[j]_q\psi_j\right|}{4q[j+1]_q\psi_{j+1}} \geq \frac{\left|\delta_\beta\right|(A-B)(q+1)}{4q[m-1]_q[m]_q\psi_{m-1}}\sum_{j=1}^{m-1}[j]_q\psi_{j-1}\left|b_j\right|. \tag{56}$$

Multiplying both sides by $1/[m]_q(A-B)(q+1)|\delta_\beta|\psi_{m-1} + 4q[m-1]_q\psi_{m-1}/4q[m]_q\psi_m$, we have

$$\begin{aligned}&\frac{1}{[m]_q}\prod_{j=0}^{m-2}\frac{\left|(A-B)(q+1)\delta_\beta\psi_j - 4Bq[j]_q\psi_j\right|}{4q[j+1]_q\psi_{j+1}}\\ &\geq \left(\frac{1}{[m]_q}\frac{(A-B)(q+1)\left|\delta_\beta\right|\psi_{m-1} + 4q[m-1]_q\psi_{m-1}}{4q[m]_q\psi_m}\right)\times\\ &\cdot\left(\frac{\left|\delta_\beta\right|(A-B)(q+1)}{4q[m-1]_q\psi_{m-1}}\sum_{j=1}^{m-1}\psi_{j-1}\left|b_j\right|\right)\\ &= \frac{\left|\delta_\beta\right|(A-B)(q+1)}{4q[m]_q\psi_m}\times\\ &\cdot\left(\psi_{m-1}\frac{\left|\delta_\beta\right|(A-B)(q+1)}{4q[m-1]_q[m]_q\psi_{m-1}}\sum_{j=1}^{m-1}\psi_{j-1}\left|b_j\right| + \frac{1}{[m]_q}\sum_{j=1}^{m-1}\psi_{j-1}\left|b_j\right|\right)\\ &\geq \frac{\left|\delta_\beta\right|(A-B)(q+1)}{4q[m]_q\psi_m}\left(\psi_{m-1}\left|b_m\right| + \frac{1}{[m]_q}\sum_{j=1}^{m-1}\psi_{j-1}\left|b_j\right|\right)\\ &= \frac{\left|\delta_\beta\right|(A-B)(q+1)}{4q[m]_q[m]_q\psi_m}\sum_{j=1}^{m}\psi_{j-1}\left|b_j\right|.\end{aligned} \tag{57}$$

That is,

$$\frac{\left|\delta_\beta\right|(A-B)(q+1)}{4q[m-1]_q[m]_q\psi_{m-1}}\sum_{j=1}^{m-1}\psi_{j-1}\left|b_j\right|\leq\frac{1}{[m]_q}\prod_{j=0}^{m-2}\frac{\left|(A-B)(q+1)\delta_\beta\psi_j-4Bq[j]_q\psi_j\right|}{4q[j+1]_q\psi_{j+1}}. \tag{58}$$

Hence, the consequence is true for $n=m+1$. Therefore, using mathematical induction, we have proved that (37) is true $\forall n$, $n\geq 2$. □ □

For $q\longrightarrow 1^-$ and $\lambda=0$, we have the following known result, proved in [27].

Corollary 3. *Let $y(z)\in\beta-UCV[A,B]$, $\beta\geq 0$, $-1\leq B<A\leq 1$, and be of form (1); then, for $n\geq 2$,*

$$\left|b_n\right|\leq\frac{1}{n}\prod_{j=0}^{n-2}\frac{\left|(A-B)\delta_\beta-2Bj\right|}{2(j+1)}. \tag{59}$$

For $q\longrightarrow 1^-$, $\lambda=0$, and $A=1-2\alpha$ and $B=-1$, we have the following known result, proved in [29].

Corollary 4. *Let $y(z)\in KD(\beta,\alpha)$, $\beta\geq 0$, $0\leq\alpha<1$, and be of form (1); then, for $n\geq 2$,*

$$\left|b_n\right|\leq\frac{1}{n}\prod_{j=0}^{n-2}\frac{\left|(1-\alpha)\delta_\beta+j\right|}{(j+1)}. \tag{60}$$

Using the already proven results of Silverman [16] and Silvia [17] on partial sums of holomorphic functions, we will find the fraction of (1) to its sequence of partial sums $y_k(z)=z+\sum_{n=2}^k b_n z^n$ when the function $y(z)$ has coefficients small enough to satisfy condition (28). We will investigate sharp lower bounds for $\Re\{y(z)/y_k(z)\}$, $\Re\{y'(z)/y_k'(z)\}$, $\Re\{y_k(z)/y(z)\}$, and $\Re\{y_k'(z)/y'(z)\}$ in the class $\beta-\mathrm{UCV}_q^\lambda[A,B]$.

Theorem 3. *If $y(z)\in\beta-UCV_q^\lambda[A,B]$, then*

$$\Re\left\{\frac{y(z)}{y_k(z)}\right\}\geq 1-\frac{\varepsilon}{\mathbb{E}_{k+1}}, \tag{61}$$

where $\mathbb{E}_{k+1}$ is defined by (29) and $\varepsilon=(1+q)|B-A|$. The extremal function

$$y(z)=z+\frac{\varepsilon}{\mathbb{E}_{k+1}}z^{k+1}. \tag{62}$$

gives the sharp result.

Proof. Define a function $w(z)$:

$$w(z)=\frac{\mathbb{E}_{k+1}}{\varepsilon}\cdot\left[\frac{y(z)}{y_k(z)}-\left(1-\frac{\varepsilon}{\mathbb{E}_{k+1}}\right)\right], \tag{63}$$

and this will reduce to

$$\begin{aligned}&=\frac{\mathbb{E}_{k+1}\left(1+\sum_{n=2}^{\infty}b_n z^{n-1}\right)}{\varepsilon\left(1+\sum_{n=2}^{k}b_n z^{n-1}\right)}-\frac{\mathbb{E}_{k+1}}{\varepsilon}+1\\ w(z)&=\frac{1+\sum_{n=2}^{k}b_n z^{n-1}+\mathbb{E}_{k+1}/\varepsilon\sum_{n=k+1}^{\infty}b_n z^{n-1}}{1+\sum_{n=2}^{k}b_n z^{n-1}}.\end{aligned} \tag{64}$$

We have

$$\left|\frac{w(z)-1}{w(z)+1}\right|\leq\frac{\mathbb{E}_{k+1}/\varepsilon\sum_{n=k+1}^{\infty}\left|b_n\right|}{2-2\sum_{n=2}^{k}\left|b_n\right|-\mathbb{E}_{k+1}/\varepsilon\sum_{n=k+1}^{\infty}\left|b_n\right|}. \tag{65}$$

Now,

$$\left|\frac{w(z)-1}{w(z)+1}\right|\leq 1 \tag{66}$$

if

$$\sum_{n=2}^{k}\left|b_n\right|+\frac{\mathbb{E}_{k+1}}{\varepsilon}\sum_{n=k+1}^{\infty}\left|b_n\right|\leq 1. \tag{67}$$

It is sufficient to show that the left hand side of (28) is bounded above by $\sum_{n=2}^{\infty}\mathbb{E}_n/\varepsilon\left|b_n\right|$ if

$$\sum_{n=2}^{k}\left|b_n\right|+\frac{\mathbb{E}_{k+1}}{\varepsilon}\sum_{n=k+1}^{\infty}\left|b_n\right|\leq\sum_{n=2}^{\infty}\frac{\mathbb{E}_n}{\varepsilon}\left|b_n\right|. \tag{68}$$

This leads to the following expression:

$$\sum_{n=2}^{k}\left(\frac{\mathbb{E}_n-\varepsilon}{\varepsilon}\right)\left|b_n\right|+\left(\frac{\mathbb{E}_n-\mathbb{E}_{k+1}}{\varepsilon}\right)\sum_{n=k+1}^{\infty}\left|b_n\right|\geq 0. \tag{69}$$

To ensure that the function defined by (62) gives the sharp outcome, we note that, for $z=re^{i\pi/n}$,

$$\begin{aligned}\frac{y(z)}{y_k(z)}&=1+\frac{\varepsilon}{\mathbb{E}_{k+1}}z^n\\ &=1+\frac{\varepsilon}{\mathbb{E}_{k+1}}r^n e^{\frac{i\pi}{n}}\\ &=1+\frac{\varepsilon r^n}{\mathbb{E}_{k+1}}\left(\cos\frac{\pi}{n}+i\sin\frac{\pi}{n}\right)\\ &=1-\frac{\varepsilon r^n}{\mathbb{E}_{k+1}}\\ \frac{y(z)}{y_k(z)}&=\frac{\mathbb{E}_{k+1}-\varepsilon}{\mathbb{E}_{k+1}}\ \text{when}\ r\longrightarrow 1.\end{aligned} \tag{70}$$

□

Theorem 4. *If* $y(z) \in \beta - UCV_q^{\lambda}[A,B]$, *then*

$$\Re\left\{\frac{y_k(z)}{y(z)}\right\} \geq \frac{\mathbb{E}_{k+1}}{\mathbb{E}_{k+1}+\varepsilon}, \tag{71}$$

where $\mathbb{E}_{k+1}$ *is defined by (29) and* $\varepsilon = (1+q)|B-A|$. *The result (71) is sharp with the function given by (62).*

Proof. Define the function $w(z)$:

$$\begin{aligned} w(z) &= \frac{\mathbb{E}_{k+1}+\varepsilon}{\varepsilon}.\left[\frac{y_k(z)}{y(z)} - \frac{\mathbb{E}_{k+1}}{\mathbb{E}_{k+1}+\varepsilon}\right] \\ &= \frac{1+\sum_{n=2}^{k} b_n z^{n-1} - \mathbb{E}_{k+1}/\varepsilon \sum_{n=k+1}^{\infty} b_n z^{n-1}}{1+\sum_{n=2}^{\infty} b_n z^{n-1}}. \end{aligned} \tag{72}$$

This will become

$$\begin{aligned} \frac{w(z)-1}{w(z)+1} &= \frac{\sum_{n=2}^{k} b_n z^{n-1} - \sum_{n=2}^{\infty} b_n z^{n-1} - \mathbb{E}_{k+1}/\varepsilon \sum_{n=k+1}^{\infty} b_n z^{n-1}}{2+\sum_{n=2}^{k} b_n z^{n-1} + \sum_{n=2}^{\infty} b_n z^{n-1} - \mathbb{E}_{k+1}/\varepsilon \sum_{n=k+1}^{\infty} |b_n| z^{k-1}} \\ &= \frac{-(1+\mathbb{E}_{k+1}/\varepsilon)\sum_{n=k+1}^{\infty} b_n z^{n-1}}{2+2\sum_{n=2}^{k} b_n z^{n-1} + (1-\mathbb{E}_{k+1}/\varepsilon)\sum_{n=k+1}^{\infty} |b_n| z^{k-1}}. \end{aligned} \tag{73}$$

This implies that

$$\left|\frac{w(z)-1}{w(z)+1}\right| \leq \frac{(1+\mathbb{E}_{k+1}/\varepsilon)\sum_{n=k+1}^{\infty}|b_n|}{2-2\sum_{n=2}^{k}|b_n| - (1-\mathbb{E}_{k+1}/\varepsilon)\sum_{n=k+1}^{\infty}|b_n|}. \tag{74}$$

Now,

$$\left|\frac{w(z)-1}{w(z)+1}\right| \leq 1 \tag{75}$$

if

$$\sum_{n=2}^{k}|b_n| + \sum_{n=k+1}^{\infty}|b_n| \leq 1. \tag{76}$$

It would be enough to show that the left side of (28) is bounded above by $\sum_{n=2}^{\infty}\mathbb{E}_n/\varepsilon|b_n|$ if

$$\sum_{n=2}^{k}|b_n| + \sum_{n=k+1}^{\infty}|b_n| \leq \sum_{n=2}^{\infty}\frac{\mathbb{E}_n}{\varepsilon}|b_n|, \tag{77}$$

which leads to the following expression:

$$\sum_{n=2}^{k}\left(\frac{\mathbb{E}_n}{\varepsilon}-1\right)|b_n| + \sum_{n=k+1}^{\infty}\left(\frac{\mathbb{E}_n}{\varepsilon}-1\right)|b_n| \geq 0 \tag{78}$$

or

$$\sum_{n=2}^{\infty}\left(\frac{\mathbb{E}_n}{\varepsilon}-1\right)|b_n| \geq 0. \tag{79}$$

Consequently, the equality holds for the extreme function $y(z)$ given by (62). □ □

We now turn to fractions related to the derivatives.

Theorem 5. *If* $y(z) \in \beta - UCV_q^{\lambda}[A,B]$, *then*

$$\Re\left\{\frac{y'(z)}{y_k'(z)}\right\} \geq \frac{\mathbb{E}_{k+1} - \varepsilon(k+1)}{\mathbb{E}_{k+1}}, \tag{80}$$

where $\mathbb{E}_{k+1}$ *is defined by (29) and* $\varepsilon = (1+q)|B-A|$. *The result (80) is sharp with the function given by (62).*

Proof. Define the function $w(z)$:

$$\begin{aligned} w(z) &= \frac{\mathbb{E}_{k+1}}{\varepsilon(k+1)}.\left[\frac{y'(z)}{y_k'(z)} - \frac{\mathbb{E}_{k+1}-\varepsilon(k+1)}{\mathbb{E}_{k+1}}\right] \\ &= \frac{\mathbb{E}_{k+1}\left(1+\sum_{n=2}^{\infty} n b_n z^{n-1}\right)}{\varepsilon(k+1)\left(1+\sum_{n=2}^{k} n b_n z^{n-1}\right)} - \frac{(\mathbb{E}_{k+1}-\varepsilon(k+1))}{\varepsilon(k+1)}, \end{aligned} \tag{81}$$

and this will reduce to

$$w(z) = \frac{1+\sum_{n=2}^{k} n b_n z^{n-1} + \mathbb{E}_{k+1}/\varepsilon(k+1)\sum_{n=k+1}^{\infty} n b_n z^{n-1}}{1+\sum_{n=2}^{k} n b_n z^{n-1}}. \tag{82}$$

Now, we have

$$\frac{w(z)-1}{w(z)+1} = \frac{\mathbb{E}_{k+1}/\varepsilon(k+1)\sum_{n=k+1}^{\infty} n b_n z^{n-1}}{2+2\sum_{n=2}^{k} n b_n z^{n-1} + \mathbb{E}_{k+1}/\varepsilon(k+1)\sum_{n=k+1}^{\infty} n b_n z^{n-1}}. \tag{83}$$

This implies that

$$\left|\frac{w(z)-1}{w(z)+1}\right| \leq \frac{\mathbb{E}_{k+1}/\varepsilon(k+1)\sum_{n=k+1}^{\infty} n|b_n|}{2-2\sum_{n=2}^{k} n|b_n| - \mathbb{E}_{k+1}/\varepsilon(k+1)\sum_{n=k+1}^{\infty} n|b_n|}. \tag{84}$$

Now,

$$\left|\frac{w(z)-1}{w(z)+1}\right| \leq 1 \tag{85}$$

if

$$\sum_{n=2}^{k} n|b_n| + \frac{\mathbb{E}_{k+1}}{\varepsilon(k+1)} \sum_{k=n+1}^{\infty} n|b_n| \leq 1. \tag{86}$$

It would be enough to show that the left side of (28) is bounded above by $\sum_{n=2}^{\infty}\mathbb{E}_n/\varepsilon|b_n|$ if

$$\sum_{n=2}^{k} n|b_n| + \frac{\mathbb{E}_{k+1}}{\varepsilon(k+1)} \sum_{n=k+1}^{\infty} n|b_n| \leq \sum_{n=2}^{\infty} \frac{\mathbb{E}_k}{\varepsilon}|b_n|, \tag{87}$$

which leads to the following expression:

$$\sum_{n=2}^{k}\left(\frac{\mathbb{E}_n}{\varepsilon} - n\right)|b_n| + \sum_{n=k+1}^{\infty}\left(\frac{\mathbb{E}_n}{\varepsilon} - \frac{n\mathbb{E}_{k+1}}{\varepsilon(k+1)}\right)|b_n| \geq 0. \tag{88}$$

The result (80) is sharp with respect to the function given by (62). □ □

Theorem 6. *If $y(z) \in \beta - UCV_q^{\lambda}[A,B]$, then*

$$\Re\left\{\frac{y_k'(z)}{y'(z)}\right\} \geq \frac{\mathbb{E}_{k+1}}{\varepsilon(k+1) + \mathbb{E}_{k+1}}, \tag{89}$$

where $\mathbb{E}_{k+1}$ is defined by (29) and $\varepsilon = (1+q)|B-A|$. The result (89) is sharp with respect to the function given by (62).

Proof. Define the function $w(z)$:

$$w(z) = \frac{\varepsilon(k+1) + \mathbb{E}_{k+1}}{\varepsilon(k+1)} \cdot \left[\frac{y_k'(z)}{y'(z)} - \frac{\mathbb{E}_{k+1}}{\varepsilon(k+1) + \mathbb{E}_{k+1}}\right] = \frac{\left(\varepsilon(k+1) + \mathbb{E}_{k+1}\right)\left(1 + \sum_{n=2}^{k} nb_n z^{n-1}\right)}{\varepsilon(k+1)\left(1 + \sum_{n=2}^{\infty} nb_n z^{n-1}\right)} - \frac{\mathbb{E}_{k+1}}{\varepsilon(k+1)}. \tag{90}$$

This will become

$$w(z) = \frac{1 + \sum_{n=2}^{k} nb_n z^{n-1} - \mathbb{E}_{k+1}/\varepsilon(k+1)\sum_{n=k+1}^{\infty} nb_n z^{n-1}}{\left(1 + \sum_{n=2}^{\infty} nb_n z^{n-1}\right)}. \tag{91}$$

This leads us to

$$\frac{w(z)-1}{w(z)+1} = \frac{-\sum_{n=k+1}^{\infty}\left(1 + \mathbb{E}_{k+1}/\varepsilon(k+1)\right) nb_n z^{n-1}}{2 + 2\sum_{n=2}^{k} nb_n z^{n-1} + \sum_{n=k+1}^{\infty}\left(1 - \mathbb{E}_{k+1}/\varepsilon(k+1)\right) nb_n z^{n-1}}, \tag{92}$$

which reduces to

$$\left|\frac{w(z)-1}{w(z)+1}\right| \leq \frac{\left(1 + \mathbb{E}_{k+1}/\varepsilon(k+1)\right)\sum_{n=k+1}^{\infty} n|b_n|}{2 - 2\sum_{n=2}^{k} n|b_n| - \left(1 - \mathbb{E}_{k+1}/\varepsilon(k+1)\right)\sum_{n=k+1}^{\infty} n|b_n|}. \tag{93}$$

Now,

$$\left|\frac{w(z)-1}{w(z)+1}\right| \leq 1. \tag{94}$$

if

$$\sum_{n=2}^{k} n|b_n| + \sum_{n=k+1}^{\infty} n|b_n| \leq 1. \tag{95}$$

It is sufficient to show that the left hand side of (28) is bounded above by $\sum_{n=2}^{\infty}\mathbb{E}_n/\varepsilon|b_n|$ if

$$\sum_{n=2}^{k} n|b_n| + \sum_{n=k+1}^{\infty} n|b_n| \leq \sum_{n=2}^{\infty} \frac{\mathbb{E}_n}{\varepsilon}|b_n|, \tag{96}$$

which leads to the following expression:

$$\sum_{n=2}^{\infty}\left(\frac{\mathbb{E}_n}{\varepsilon} - n\right)|b_n| \geq 0. \tag{97}$$

The result (89) is sharp with respect to the function given by (62). □ □

In the next theorem, we will find the radii of starlikeness for the class $\beta - \mathrm{UCV}_q^{\lambda}[A,B]$.

Theorem 7. *Let $y(z) \in \beta - UCV_q^{\lambda}[A,B]$. Then, $y(z)$ is a convex function of order $\alpha \in [0,1)$ in $|z| < r = r_1(\alpha)$, where*

$$r_1(\alpha) = \left(\frac{\mathbb{E}_n(1-\alpha)}{\varepsilon\left(q[n-1]_q + (1-\alpha)\right)}\right)^{1/n-1}, \quad n = 2, 3, \ldots, \tag{98}$$

where $\mathbb{E}_n$ is defined by (29) and $\varepsilon = (1+q)|B-A|$.

Proof. Let $y(z) \in \beta - \mathrm{UCV}_q^{\lambda}[A,B]$. Then, by the theorem,

$$\sum_{n=2}^{\infty} \frac{\mathbb{E}_n}{\varepsilon} |b_n| < 1, \tag{99}$$

where $\mathbb{E}_n$ is defined by (29) and $\varepsilon = (1+q)|B-A|$. For $\alpha \in [0,1)$, we need to show that

$$\left| \frac{\partial_q \left(z\partial_q R_q^\lambda y(z) \right)}{\partial_q R_q^\lambda y(z)} \right| < 1 - \alpha, \tag{100}$$

that is,

$$\begin{aligned} \left| \frac{\partial_q \left(z\partial_q R_q^\lambda y(z) \right) - \partial_q R_q^\lambda y(z)}{\partial_q R_q^\lambda y(z)} \right| &= \left| -\frac{\sum_{n=2}^{\infty} q[n-1]_q [n]_q \psi_{n-1} b_n z^{n-1}}{1 - \sum_{n=2}^{\infty} [n]_q \psi_{n-1} b_n z^{n-1}} \right| \\ &\le \frac{\sum_{n=2}^{\infty} q[n-1]_q [n]_q \psi_{n-1} |b_n| |z|^{n-1}}{1 - \sum_{n=2}^{\infty} [n]_q \psi_{n-1} |b_n| |z|^{n-1}} \\ &< 1 - \alpha. \end{aligned} \tag{101}$$

Thus, $|\partial_q (z\partial_q R_q^\lambda y(z)) - \partial_q R_q^\lambda y(z)/\partial_q R_q^\lambda y(z)| \le 1 - \alpha$ if

$$\left(\frac{q[n-1]_q}{1-\alpha} + 1 \right) [n]_q \psi_{n-1} |b_n| |z|^{n-1} \le 1. \tag{102}$$

According to theorem (99), inequality (102) will be true if

$$\left(\frac{q[n-1]_q}{1-\alpha} + 1 \right) |z|^{n-1} \le \frac{\mathbb{E}_n}{\varepsilon}. \tag{103}$$

Solving (103) for $|z|$, we obtain

$$|z|^{n-1} \le \frac{\mathbb{E}_n (1-\alpha)}{\varepsilon \left(q[n-1]_q + (1-\alpha) \right)}. \tag{104}$$

Setting $|z| = r(\alpha)$ in (104), we have

$$r(\alpha) = \left(\frac{\mathbb{E}_n (1-\alpha)}{\varepsilon \left(q[n-1]_q + (1-\alpha) \right)} \right)^{1/n-1}, \tag{105}$$

which is the required result. □ □

3. Conclusion

In this article, we have applied the q-Ruscheweyh differential operator to define and study a new class $\beta - \mathrm{UCV}_q^\lambda [A,B]$ of q-convex functions associated with the conic domain. This class generalizes the classes $\beta - \mathrm{UCV}[A,B]$, $C[A,B]$, $K(\beta,\alpha)$, $C(\alpha)$, and C which have been defined and studied earlier. This fact has been illustrated above with details and proper referencing. The results presented include sufficiency criteria related to Taylor series coefficients, the coefficient bounds, and the ratios of partial sums to their infinite sum for functions of the class $\beta - \mathrm{UCV}_q^\lambda [A,B]$.

Data Availability

No data were used in this article.

Conflicts of Interest

The authors declare that there are no conflicts of interest regarding the publication of this article.

Authors' Contributions

All authors contributed equally and approved the final manuscript.

References

[1] A. Aral, V. Gupta, and R. P. Agarwal, *Applications of q-Calculus in Operator Theory*, Springer, Berlin, Germany, 2013.

[2] F. H. Jackson, "On q-functions and certain difference operator," *Transactions of the Royal Society of Edinburgh*, vol. 46, pp. 253–281, 1908.

[3] F. H. Jackson, "On q-definite integrals," *Quarterly Journal of Pure and Applied Mathematics*, vol. 41, pp. 193–203, 1910.

[4] V. Kac and P. Cheung, *Quantum Calculus*, Springer Science & Business Media, Berlin, Germay, 2001.

[5] H. M. Srivastava, "Operators of basic (or q-) calculus and fractional q-calculus and their applications in geometric function theory of complex analysis. Iran," *Iranian Journal of Science and Technology Transaction A-Science*, vol. 44, no. 1, pp. 327–344, 2020.

[6] H. M. Srivastava, Q. Z. Ahmad, N. Khan, N. Khan, and B. Khan, "Hankel and Toeplitz determinants for a subclass of q-starlike functions associated with a general conic domain," *Mathematics*, vol. 7, Article ID 181, 2019.

[7] H. M. Srivastava, M. K. Aouf, and A. O. Mostafa, "Some properties of analytic functions associated with fractional q-calculus operators," *Miskolc Mathematical Notes*, vol. 20, no. 2, pp. 1245–1260, 2019.

[8] H. M. Srivastava, M. Arif, and M. Raza, "Convolution properties of meromorphically harmonic functions defined by a generalized convolution q-derivative operator," *AIMS Math*, vol. 6, pp. 5869–5885, 2021.

[9] H. M. Srivastava, S. Arjika, and A. S. Kelil, "Some homogeneous q-difference operators and the associated generalized

Hahn polynomials," *Applied Set-Valued Analysis and Optimization*, vol. 1, pp. 187–201, 2019.

[10] H. M. Srivastava and D. Bansal, "Close-to-convexity of a certain family of q-Mittag-Leffler functions," *Journal of Nonlinear and Variational Analysis*, vol. 1, pp. 61–69, 2017.

[11] H. M. Srivastava, J. Cao, and S. Arjika, "A note on generalized q-difference equations and their applications involving q-hypergeometric functions," *Symmetry*, vol. 12, Article ID 1816, 2020.

[12] H. M. Srivastava and S. Arjika, "A general family of q-hypergeometric polynomials and associated generating functions," *Mathematics*, vol. 9, Article ID 1161, 2021.

[13] H. M. Srivastava, B. Khan, N. Khan, and Q. Z. Ahmad, "Coefficient inequalities for q-starlike functions associated with the Janowski functions," *Hokkaido Mathematical Journal*, vol. 48, pp. 407–425, 2019.

[14] H. M. Srivastava, B. Khan, N. Khan, M. Tahir, S. Ahmad, and N. Khan, "Upper bound of the third Hankel determinant for a subclass of q-starlike functions associated with the q-exponential function," *Bulletin des Sciences Mathematiques*, vol. 167, Article ID 102942, 2021.

[15] A. W. Goodman, *Univalent Functions*, Polygonal Publishing House, New Jersey, NJ, USA, 1983.

[16] H. Silverman, "Partial sums of starlike and convex functions," *Journal of Mathematical Analysis and Applications*, vol. 209, no. 1, pp. 221–227, 1997.

[17] E. M. Silvia, "Partial sums of convex functions of order %," *Houston Journal of Mathematics*, vol. 11, no. 3, pp. 397–404, 1985.

[18] H. Al dweby and M. Darus, "On harmonic holomorphic functions associated with basic hypergeometric functions," *The Scientific World Journal*, vol. 2013, Article ID 164287, 7 pages, 2013.

[19] S. Ruscheweyh, "New criteria for univalent functions," *Proceedings of the American Mathematical Society*, vol. 49, pp. 109–115, 1975.

[20] W. Janowski, "Some extremal problems for certain families of analytic functions," *Annales Polonici Mathematici*, vol. 28, no. 3, pp. 297–326, 1973.

[21] S. Kanas and A. Wiśniowska, "Conic domains and starlike functions," *Revue Roumaine de Mathématique Pures et Appliquées*, vol. 45, pp. 647–657, 2000.

[22] S. Kanas and A. Wisniowska, "Conic regions and k-uniform convexity," *Journal of Computational and Applied Mathematics*, vol. 105, no. 1-2, pp. 327–336, 1999.

[23] S. Mahmood, M. Arif, and S. N. Malik, "Janowski type close-to-convex functions associated with conic regions," *Journal of Inequalities and Applications*, vol. 2017, no. 1, p. 259, 2017.

[24] S. N. Malik, M. Raza, M. Arif, and S. Hussain, "Coefficients estimates of some subclasses of analytic functions related with conic domain," *Analele Universitatii "Ovidius" Constanta-Seria Matematica*, vol. 21, no. 2, pp. 181–188, 2013.

[25] S. Kanas, "Coefficient estimates in subclasses of the Caratheodory class related to conical domains," *Acta Mathematica Universitatis Comenianae*, vol. 74, no. 2, pp. 149–161, 2005.

[26] S. Mahmood, M. Jabeen, S. N. Malik, H. M. Srivastava, R. Manzoor, and S. M. J. Riaz, "Some coefficient inequalities of q-starlike functions associated with conic domain defined by q-derivative," *Journal of Function Spaces*, vol. 2018, Article ID 8492072, 13 pages, 2018.

[27] K. I. Noor and S. N. Malik, "On coefficient inequalities of functions associated with conic domains," *Computers & Mathematics with Applications*, vol. 62, no. 5, pp. 2209–2217, 2011.

[28] S. Malik, S. Mahmood, M. Raza, S. Farman, and S. Zainab, "Coefficient inequalities of functions associated with petal type domains," *Mathematics*, vol. 6, no. 12, p. 298, 2018.

[29] S. Shams, S. R. Kulkarni, and J. M. Jahangiri, "Classes of uniformly starlike and convex functions," *International Journal of Mathematics and Mathematical Sciences*, vol. 2004, no. 55, pp. 2959–2961, 2004.

[30] W. Rogosinski, "On the coefficients of subordinate functions," *Proceedings of the London Mathematical Society*, vol. 48, pp. 48–82, 1943.

Hindawi
Journal of Mathematics
Volume 2021, Article ID 2567927, 13 pages
https://doi.org/10.1155/2021/2567927

Research Article

Analysis of the Fractional-Order Kaup–Kupershmidt Equation via Novel Transforms

Naveed Iqbal,[1] **Humaira Yasmin**,[2] **Ali Rezaiguia**,[1,3] **Jeevan Kafle**,[4]
A. Othman Almatroud,[1] **and Taher S. Hassan**[1,5]

[1]*Department of Mathematics, Faculty of Science, University of Ha'il, Ha'il 2440, Saudi Arabia*
[2]*Department of Basic Sciences, Preparatory Year Deanship, King Faisal University, Al-Ahsa 31982, Saudi Arabia*
[3]*Department of Computer Science and Mathematics, Mouhamed Cherif Messadia University, Souk Ahras, Algeria*
[4]*Central Department of Mathematics, Tribhuvan University Kritipur, Kathmandu, Nepal*
[5]*Department of Mathematics, Faculty of Science, Mansoura University, Mansoura 35516, Egypt*

Correspondence should be addressed to Naveed Iqbal; n.iqbal@uoh.edu.sa and Jeevan Kafle; jeevan.kafle@cdmath.tu.edu.np

Received 27 September 2021; Revised 2 November 2021; Accepted 8 December 2021; Published 26 December 2021

Academic Editor: Fairouz Tchier

In this article, we develop a technique to determine the analytical result of some Kaup–Kupershmidt equations with the aid of a modified technique called the new iteration transform method. This technique is a mixture of the novel integral transformation Elzaki transformation and the new iteration technique. The nonlinear term can be handled easily by a new iteration technique. The results show that the combination of the Elzaki transformation and the new iteration technique is quite capable and basically well suited for applying in such problems and that it can be implemented to other nonlinear models. This technique is viewed as an effective alternative approach to certain existing approaches for such accurate models.

1. Introduction

Fractional calculus is regarded as an important branch of science, particularly for phenomena that cannot be defined by basic nonlinear ordinary differential equations or partial differential equations with integer-order operators. The use of memory is one of the main advantages of fractional-order derivatives over standard derivatives. In recent years, there have been numerous applications of fractional-order ordinary and partial differential equations in many fields of physics and engineering. There have been several key works discovered, particularly in genetic mechanics and in the viscoelasticity concept, where fractional-order derivatives are utilized for a good explanation of the properties of materials. This is the main benefit of fractional derivatives compared with traditional integer-order models in which such effects are neglected. The computational modeling and analysis of structures and procedures, based on the explanation of their properties in concepts of fractional derivatives, obviously result in differential equations of fractional order and the requirement of finding solutions such as mathematical equations [1–10].

The fractional-order Kaup–Kupershmidt equation is used to investigate the analysis of capillary gravity waves' attitude and nonlinear dispersive waves. The extensive fifth-order nonlinear development equation is written as

$$D_{\tau}^{\rho}\mu(\zeta,\tau) + \alpha\mu\mu_{\zeta\zeta\zeta} + \beta p\mu_{\zeta}\mu_{\zeta\zeta} + \gamma\mu^{2}\mu_{\zeta} + \mu_{\zeta\zeta\zeta\zeta\zeta} = 0, \quad (1)$$

with the initial condition

$$\mu(\zeta,0) = g(\zeta), \quad (2)$$

where α, β, and γ are real constants and $0 < \rho \leq 1$ is the parameter symbolizing the order of the fractional-order derivative. By considering different values for α, β, and γ, the overload nonlinear fifth-order development model can be scaled down to the fifth-order fractional-order Kaup–Kupershmidt equation.

For $\alpha = -15, \beta = -15$, and $\gamma = 45$, the above equation simplifies to

$$D^{\rho}_{\tau}\mu(\zeta,\tau) - 15\mu\mu_{\zeta\zeta\zeta} - 15p\mu_{\zeta}\mu_{\zeta\zeta} + 45\mu^2\mu_{\zeta} + \mu_{\zeta\zeta\zeta\zeta\zeta} = 0, \tag{3}$$

with the initial condition

$$\mu(\zeta,0) = g(\zeta). \tag{4}$$

In 1980, Kaup [11] first introduced a significant dispersive basic Kaup–Kupershmidt equation, and then it was improved by Kupershmidt [12] in 1994. This study is concerned with the analysis of the modified fractional-order Kaup–Kupershmidt (KK) equation. In recent decades, excellent scientific work has been devoted to the analysis of the classical KK equation. The modern KK equation can be integrated at $p = 5/2$ [13] and is considered to have bilinear representation [14]. Soliton and solitary wave results can be obtained for general nonlinear development problems by importing four diverse techniques autonomously. Nonlaopon et al. [15] used the inverse scattering approach to establish soliton results to analyze nonlinear equations with physical implications. Two integrable differential-difference equations exhibit soliton solutions of the Kaup-Kupershmidt equation type [16]. Musette introduced the fifth-order KK equation, and Verhoeven was one of the combined instances of the Henon–Heiles method; see [17] for more details. Prakasha et al. [18] used the q-homotopy analysis transform method which is implemented to obtain the result for the fractional-order KK equation.

Daftardar-Gejji and Jafari [19] introduced a new iterative methodology for investigating nonlinear equations in 2006. Jafari [20] was the first to use the Laplace transform in an iterative technique. In [21], Jafari et al. suggested a modified straightforward methodology, named iterative Laplace transformation technique, to look for the numerical effects of the fractional partial differential equation system. Iterative Laplace transformation technique is used to solve linear and nonlinear partial differential equations such as time-fractional Zakharov–Kuznetsov equation [22], fractional-order Fokker–Planck equation [23], and Fornberg–Whitham equation [24].

This article modified the iterative method with the Elzaki transform; the novel approach is named the iterative transformation technique. The new iterative transformation technique is implemented to evaluate the fractional order of the system of the KK equation. The outcome of several illustrative cases is described to demonstrate the effectiveness of the proposed technique. The present method is used to obtain the results of fractional-order and integral-order models. The new method reduces computing costs while increasing rate convergence. The proposed method is also helpful in dealing with other fractional-order linear and nonlinear partial differential equations.

2. Basic Definitions

Definition 1 (see [25–27]). The fractional-order Riemann–Liouville operator D^{ρ} of order ρ is defined as

$$D^{\rho}\nu(\zeta) = \begin{cases} \dfrac{d^{\kappa}}{d\zeta^{\kappa}}\nu(\zeta), & \text{for } \rho = \kappa, \\ \dfrac{1}{\Gamma(\kappa-\rho)}\dfrac{d}{d\zeta^{\kappa}}\displaystyle\int_0^{\zeta}\dfrac{\nu(\zeta)}{(\zeta-\psi)^{\rho-\kappa+1}}d\psi, & \text{for } \kappa-1<\rho<\kappa, \end{cases} \tag{5}$$

where $\kappa \in \mathbb{Z}^{+}, \rho \in \mathbb{R}^{+}$, and

$$D^{-\rho}\nu(\zeta) = \frac{1}{\Gamma(\rho)}\int_0^{\zeta}(\zeta-\psi)^{\rho-1}\nu(\psi)d\psi, \quad 0<\rho\leq 1. \tag{6}$$

Definition 2 (see [25–27]). The Riemann–Liouville fractional integral operator J^{ρ} is given as

$$J^{\rho}\nu(\zeta) = \frac{1}{\Gamma(\rho)}\int_0^{\zeta}(\zeta-\psi)^{\rho-1}\nu(\zeta)d\zeta, \quad \zeta>0,\ \rho>0. \tag{7}$$

Some properties of the operator are as follows:

$$\begin{aligned} J^{\rho}\zeta^{\kappa} &= \frac{\Gamma(\kappa+1)}{\Gamma(\kappa+\rho+1)}\zeta^{\kappa+\psi}, \\ D^{\rho}\zeta^{\kappa} &= \frac{\Gamma(\kappa+1)}{\Gamma(\kappa-\rho+1)}\zeta^{\kappa-\psi}. \end{aligned} \tag{8}$$

Definition 3 (see [25–27]). The fractional-order Caputo operator ${}^{C}D^{\rho}$ of ρ is given as

$${}^{C}D^{\rho}\nu(\zeta) = \begin{cases} \dfrac{1}{\Gamma(\kappa-\rho)}\displaystyle\int_0^{\zeta}\dfrac{\nu^{\kappa}(\psi)}{(\zeta-\psi)^{\rho-\kappa+1}}d\psi, & \text{for } \kappa-1<\rho<\kappa, \\ \dfrac{d^{\kappa}}{d\zeta^{\kappa}}\nu(\zeta), & \text{for } \kappa = \rho. \end{cases} \tag{9}$$

Definition 4 (see [25–27]).

$$\begin{aligned} &J^{\rho}_{\zeta}D^{\rho}_{\zeta}g(\zeta) = g(\zeta) - \sum_{k=0}^{m} g^{k}(0^{+})\frac{\zeta^{k}}{k!}, \quad \text{for } \zeta>0 \text{ and } \kappa-1<\rho\leq\kappa, \kappa\in\mathbb{N}, \\ &D^{\rho}_{\zeta}J^{\rho}_{\zeta}g(\zeta) = g(\zeta). \end{aligned} \tag{10}$$

Definition 5 (see [25–27]). The Elzaki transformation of the fractional Caputo derivative is expressed as

$$E\left[D^{\rho}_{\zeta}g(\zeta)\right] = s^{-\rho}E[g(\zeta)] - \sum_{k=0}^{\kappa-1} s^{2-\rho+k}g^{(k)}(0), \tag{11}$$

where $\kappa-1<\rho<\kappa$.

Definition 6 (see [25–27]). The inverse Elzaki transform is given as

$$E^{-1}[\mathfrak{T}(s)] = h(\mathfrak{T}) = \frac{1}{2\pi\iota}\int_{\alpha-\iota\infty}^{\alpha+\iota\infty} h\left(\frac{1}{s}\right)e^{s\mathfrak{T}} s ds = \Sigma \text{ residues of } h\left(\frac{1}{s}\right)e^{s\mathfrak{T}} s. \tag{12}$$

The inverse Elzaki transform of some of the functions is given by

$$\begin{aligned}
&\bullet E^{-1}\{s^n\} = \frac{\mathfrak{T}^{n-2}}{(n-2)!}, \; n = 2, 3, 4, \ldots, \\
&\bullet E^{-1}\left(\frac{s^2}{1-as}\right) = e^{a\mathfrak{T}}, \\
&\bullet E^{-1}\left(\frac{s^3}{1+a^2s^2}\right) = \frac{1}{a}\sin a\mathfrak{T}, \\
&\bullet E^{-1}\left(\frac{s^2}{1+a^2s^2}\right) = \frac{1}{a}\cos a\mathfrak{T}.
\end{aligned} \tag{13}$$

3. The General Discussion of the Proposed Method

Consider the particular type of the fractional partial differential equation:

$$D_\tau^\rho v(\zeta,\tau) + Mv(\zeta,\tau) + Nv(\zeta,\tau) = h(\zeta,\tau), \quad n-1 < \rho \le n, \tag{14}$$

where $n \in \mathbb{N}, M$ and N are linear and nonlinear functions, and h is a source function.

The initial condition is

$$v^k(\zeta,0) = g_k(\zeta), \quad k = 0, 1, 2, \ldots, n-1. \tag{15}$$

Applying the Elzaki transform of (14), we obtain as

$$E[D_\tau^\rho v(\zeta,\tau)] + E[Mv(\zeta,\tau) + Nv(\zeta,\tau)] = E[h(\zeta,\tau)]. \tag{16}$$

The differentiation property is defined as

$$E[v(\zeta,\tau)] = \sum_{k=0}^{m} s^{2-\rho+k}u^{(k)}(\zeta,0) + s^\rho E[h(\zeta,\tau)] - s^\rho E[Mv(\zeta,\tau) + Nv(\zeta,\tau)], \tag{17}$$

using the inverse Elzaki transform of equation (17), we have

$$\begin{aligned}
v(\zeta,\tau) = {} & E^{-1}\left[\left(\sum_{k=0}^{m} s^{2-\rho+k}u^k(\zeta,0) + s^\rho E[h(\zeta,\tau)]\right)\right] \\
& - E^{-1}\left[s^\rho E[Mv(\zeta,\tau) + Nv(\zeta,\tau)]\right].
\end{aligned} \tag{18}$$

Through the iterative technique, we have

$$v(\zeta,\tau) = \sum_{m=0}^{\infty} v_m(\zeta,\tau). \tag{19}$$

M is a linear operator:

$$M\left(\sum_{m=0}^{\infty} v_m(\zeta,\tau)\right) = \sum_{m=0}^{\infty} M[v_m(\zeta,\tau)], \tag{20}$$

and N is the nonlinear function; we get

$$\begin{aligned}
N\left(\sum_{m=0}^{\infty} v_m(\zeta,\tau)\right) = {} & v_0(\zeta,\tau) + M\left(\sum_{k=0}^{m} v_k(\zeta,\tau)\right) \\
& - N\left(\sum_{k=0}^{m} v_k(\zeta,\tau)\right).
\end{aligned} \tag{21}$$

Substituting (19)–(21) in (18), we obtain the following solution:

$$\begin{aligned}
\sum_{m=0}^{\infty} v_m(\zeta,\tau) = {} & E^{-1}\left[s^\rho\left(\sum_{k=0}^{m} s^{2-\zeta+k}u^k(\zeta,0) + E[h(\zeta,\tau)]\right)\right] \\
& - E^{-1}\left[s^\rho E\left[M\left(\sum_{k=0}^{m} v_k(\zeta,\tau)\right) - N\left(\sum_{k=0}^{m} v_k(\zeta,\tau)\right)\right]\right].
\end{aligned} \tag{22}$$

Applying the iterative method, we get

$$\begin{aligned}
v_0(\zeta,\tau) &= E^{-1}\left[s^\rho\left(\sum_{k=0}^{m} s^{2-\zeta+k}u^k(\zeta,0) + s^\rho E(g(\zeta,\tau))\right)\right], \\
v_1(\zeta,\tau) &= -E^{-1}\left[s^\rho E[M[v_0(\zeta,\tau)]] + N[v_0(\zeta,\tau)]\right], \\
v_{m+1}(\zeta,\tau) &= -E^{-1}\left[s^\rho E\left[-M\left(\sum_{k=0}^{m} v_k(\zeta,\tau)\right) - N\left(\sum_{k=0}^{m} v_k(\zeta,\tau)\right)\right]\right], \quad m \ge 1.
\end{aligned} \tag{23}$$

Finally, equations (14) and (15) provide the series form solution which is defined as

$$v(\zeta,\tau) \cong v_0(\zeta,\tau) + v_1(\zeta,\tau) + v_2(\zeta,\tau) + \cdots + v_m(\zeta,\tau), \quad m \in \mathbb{N}. \tag{24}$$

3.1. Error Analysis of the Projected Technique. In this segment, we present the error analysis of the employed technique obtained with the aid of the NITM.

Theorem 1. *If we can find a real number $0 < k < 1$ satisfying $\|v_{m+1}(r,s)\| \le k\|v_m(r,s)\|$ for all values of m and, moreover, if* *the truncated series* $\sum_{m=0}^{l} v_m(r,s)$ *is employed as an approximate solution* $v(r,s)$, *then the maximum absolute truncated error can be obtained by*

$$\left\| v(r,s) - \sum_{m=0}^{l} v_m(r,s) \right\| \leq \frac{k^{l+1}}{(1-k)} \left\| v_0(r,s) \right\|. \tag{25}$$

Proof. We have

$$\begin{aligned} \left\| v(r,s) - \sum_{m=0}^{l} v_m(r,s) \right\| &= \left\| \sum_{m=l+1}^{\infty} v_m(r,s) \right\| \leq \sum_{m=l+1}^{\infty} \left\| v_m(r,s) \right\| \leq \sum_{m=l+1}^{\infty} k^m \left\| v_0(r,s) \right\| \\ &\leq (k)^{l+1} \left[1 + (k)^1 + (k)^2 + \ldots \right] \left\| v_0(r,s) \right\| \leq \frac{k^{l+1}}{(1-k)} \left\| v_0(r,s) \right\|, \end{aligned} \tag{26}$$

which proves the theorem. □

4. Numerical Results

Example 1. Consider the following fractional Kaup–Kupershmidt equation which is given as

$$D_\tau^\rho \mu(\zeta,\tau) - 15\mu\mu_{\zeta\zeta\zeta} - 15p\mu_\zeta\mu_{\zeta\zeta} + 45\mu^2\mu_\zeta + \mu_{\zeta\zeta\zeta\zeta\zeta} = 0, \tag{27}$$

with the initial condition

$$\mu(\zeta,0) = \frac{1}{4} w^2 \lambda^2 \sec h^2\left(\frac{w\zeta\lambda}{2}\right) + \frac{w^2\lambda^2}{12}. \tag{28}$$

Using the Elzaki transform to (24), we obtain

$$\begin{aligned} \frac{1}{s^\rho} E[\mu(\zeta,\tau)] &= \mu_{(0)}(\zeta,0)s^{2-\rho} + E\left[-15\mu\mu_{\zeta\zeta\zeta} - 15p\mu_\zeta\mu_{\zeta\zeta} + 45\mu^2\mu_\zeta + \mu_{\zeta\zeta\zeta\zeta\zeta}\right], \\ E[\mu(\zeta,\tau)] &= s^2\mu(\zeta,0) + s^\rho E\left[-15\mu\mu_{\zeta\zeta\zeta} - 15p\mu_\zeta\mu_{\zeta\zeta} + 45\mu^2\mu_\zeta + \mu_{\zeta\zeta\zeta\zeta\zeta}\right]. \end{aligned} \tag{29}$$

Applying the inverse Elzaki transform of (29), we have

$$\begin{aligned} \mu(\zeta,\tau) &= E^{-1}\left[s^2\mu(\zeta,0)\right] \\ &\quad + E^{-1}\left[s^\rho E\left(-15\mu\mu_{\zeta\zeta\zeta} - 15p\mu_\zeta\mu_{\zeta\zeta} + 45\mu^2\mu_\zeta + \mu_{\zeta\zeta\zeta\zeta\zeta}\right)\right]. \end{aligned} \tag{30}$$

Now, by applying the proposed semianalytical technique, we get

$$\begin{aligned} \mu_0(\zeta,\tau) &= \frac{1}{4} w^2\lambda^2 \sec h^2\left(\frac{w\zeta\lambda}{2}\right) + \frac{w^2\lambda^2}{12}, \\ \mu_1(\zeta,\tau) &= E^{-1}\left[s^\rho E\left(-15\mu_{(0)}\mu_{(0)\zeta\zeta\zeta} - 15p\mu_{(0)\zeta}\mu_{(0)\zeta\zeta} + 45\mu_{(0)}^2\mu_{(0)\zeta} + \mu_{(0)\zeta\zeta\zeta\zeta\zeta}\right)\right], \\ \mu_1(\zeta,\tau) &= \left(-\frac{1}{512} w^7\lambda^7 \left(3843 + 480p - 4(209 + 60p)\cosh(w\zeta\lambda) + \cosh(2w\zeta\lambda)\operatorname{sech}^6\left(\frac{w\zeta\lambda}{2}\right)\tanh\left(\frac{w\zeta\lambda}{2}\right)\right)\right. \\ &\quad \frac{\tau^\rho}{\Gamma(1+\rho)}, \end{aligned}$$

$$\mu_2(\zeta,\tau) = E^{-1}\left[s^{\rho}E\left(-15\mu_{(1)}\mu_{(1)\zeta\zeta\zeta} - 15p\mu_{(1)\zeta}\mu_{(1)\zeta\zeta} + 45\mu_{(1)}^2\mu_{(1)\zeta} + \mu_{(1)\zeta\zeta\zeta\zeta\zeta}\right)\right],$$

$$\begin{aligned}\mu_2(\zeta,\tau) = &\big(-733469760p - 3947228724 + 6\left(148082560p + 777305099 + 4358400p^2\right)\cosh(ws\lambda)\\ &- 20736000p^2 - 48\left(3850520p + 18859301 + 124800p^2\right)\cosh(2w\zeta\lambda)\\ &+ 46313277\cosh(3w\zeta\lambda) + 10287360p\cosh(3w\zeta\lambda) + 345600p^2\cosh(3w\zeta\lambda)\\ &- 305756\cosh(4w\zeta\lambda) - 87360p\cosh(4w\zeta\lambda) + \cosh(5w\zeta\lambda)\operatorname{sech}^{12}\left(\frac{w\zeta\lambda}{2}\right)\frac{w^{12}\lambda^{12}\tau^{2\rho}}{524288\Gamma(1+2\rho)}\\ &\vdots\end{aligned} \tag{31}$$

$$\mu_n(\zeta,\tau) = E^{-1}\left[s^{\rho}E\left(-15\mu_{(n)}\mu_{(n)\zeta\zeta\zeta} - 15p\mu_{(n)\zeta}\mu_{(n)\zeta\zeta} + 45\mu_{(n)}^2\mu_{(n)\zeta} + \mu_{(n)\zeta\zeta\zeta\zeta\zeta}\right)\right].$$

The series form result is

$$\begin{aligned}\mu(\zeta,\tau) = &\mu_0(\zeta,\tau) + \mu_1(\zeta,\tau) + \mu_2(\zeta,\tau)\\ &+ \mu_3(\zeta,\tau) + \cdots + \mu_n(\zeta,\tau).\end{aligned} \tag{32}$$

Therefore, we have

$$\begin{aligned}u(\zeta,\tau) = &\frac{1}{4}w^2\lambda^2\sec h^2\left(\frac{w\zeta\lambda}{2}\right) + \frac{w^2\lambda^2}{12} + \Big(-\frac{1}{512}w^7\lambda^7(480p + 3843 - 4(60p + 209)\cosh(w\zeta\lambda)\\ &+ \cosh(2w\zeta\lambda)\sec h^6\left(\frac{w\zeta\lambda}{2}\right)\tanh\left(\frac{w\zeta\lambda}{2}\right)\frac{\tau^{\rho}}{\Gamma(1+\rho)} + (-733469760p - 3947228724\\ &- 20736000p^2 + 6\left(1480925060p + 778300098 + 3358400p^2\right)\cosh(ws\lambda) - 48\\ &\left(3850520 + 18859301 + 124800p^2\right)\cosh(2w\zeta\lambda) + 46313277\cosh(3w\zeta\lambda) + 10287360p\cosh(3w\zeta\lambda)p\\ &+ 345600p^2\cosh(3w\zeta\lambda) - 305756\cosh(4w\zeta\lambda) - 87360p\cosh(4w\zeta\lambda)\\ &+ \cosh(5w\zeta\lambda)\sec h^{12}\left(\frac{w\zeta\lambda}{2}\right)\frac{w^{12}\lambda^{12}\tau^{2\rho}}{524288\Gamma(1+2\rho)} + \cdots.\end{aligned} \tag{33}$$

For $\rho = 1$, the exact results of (27) are given by

$$\mu(\zeta,\tau) = \frac{1}{4}w^2\lambda^2\sec h^2\left(\frac{\lambda}{2}\left(\frac{-w^5\left(-8\lambda^2\nu + 16\nu^2 + \lambda^4\right)}{16\Gamma(1+\rho)}\tau^{\rho} + w\zeta\right)\right) + \frac{w^2\lambda^2}{12}. \tag{34}$$

Analytical approximate solutions with some free parameters are provided by the proposed technique. The analytical findings are extremely useful in deciphering the internal components of acts of nature. Depending on the physical factors, the explicit solutions represented several forms of approximate solutions. Figure 1 compares the result obtained by the help of the proposed technique to the exact and analytical result for the fractional-order KK equation. Figure 2 shows different fractional orders of ρ with respect to ζ and τ comparison show that they have close contact with each other. Figure 3 shows the error plot of three- and two-dimensional graphs.

Example 2. Consider the following fractional Kaup–Kupershmidt equation which is given as

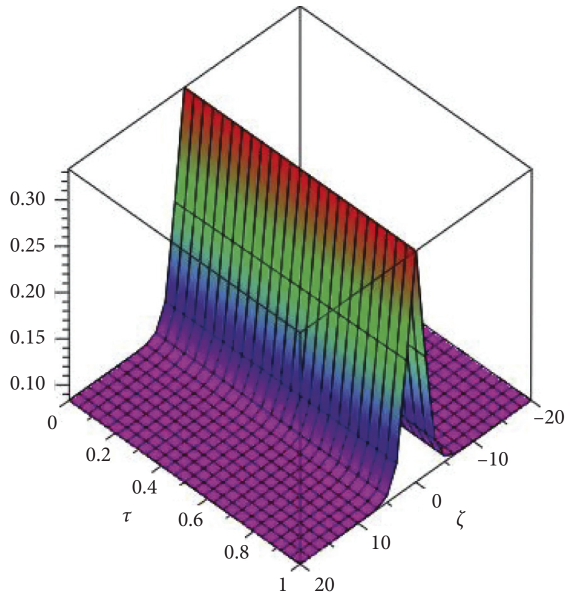

FIGURE 1: The exact and analytical solutions of Example 1.

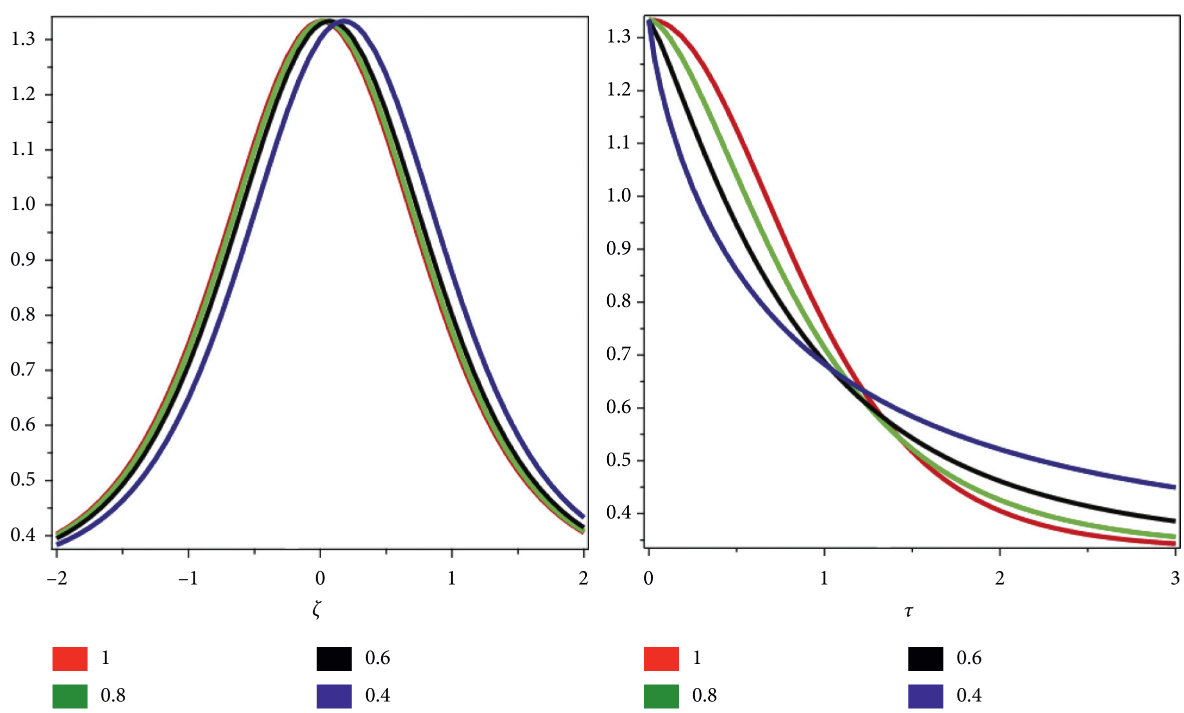

FIGURE 2: The fractional order ρ of Example 1 with respect to ζ and τ.

$$D_\tau^\rho \mu(\zeta,\tau) - 15\mu\mu_{\zeta\zeta\zeta} - 15p\mu_\zeta\mu_{\zeta\zeta} + 45\mu^2\mu_\zeta + \mu_{\zeta\zeta\zeta\zeta\zeta} = 0, \tag{35}$$

with the initial condition

$$\mu(\zeta,0) = \frac{4}{3}c - \frac{4}{p}\operatorname{csc} h^2(\sqrt{c}\zeta). \tag{36}$$

Using the Elzaki transform to (35), we get

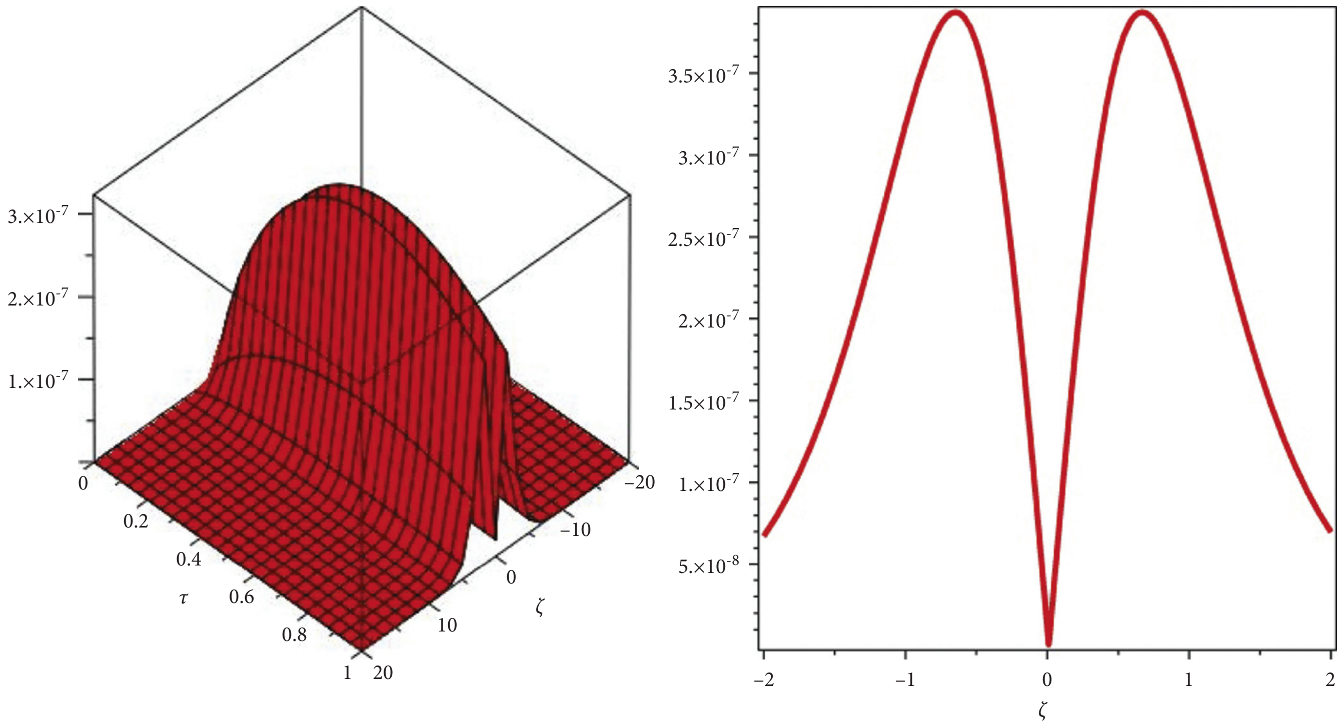

Figure 3: The 2D and 3D error plot of Problem 1.

$$\frac{1}{s^{\rho}}E[\mu(\zeta,\tau)] = \mu_{(0)}(\zeta,0)s^{2-\rho} + E\left[-15\mu\mu_{\zeta\zeta\zeta} - 15p\mu_{\zeta}\mu_{\zeta\zeta} + 45\mu^2\mu_{\zeta} + \mu_{\zeta\zeta\zeta\zeta\zeta}\right], \tag{37}$$

$$E[\mu(\zeta,\tau)] = s^2\mu(\zeta,0) + s^{\rho}E\left[-15\mu\mu_{\zeta\zeta\zeta} - 15p\mu_{\zeta}\mu_{\zeta\zeta} + 45\mu^2\mu_{\zeta} + \mu_{\zeta\zeta\zeta\zeta\zeta}\right]. \tag{38}$$

Applying the inverse Elzaki transform of (38), we have

$$\mu(\zeta,\tau) = E^{-1}\left[s^2\mu(\zeta,0)\right] + E^{-1}\left[s^{\rho}E\left(-15\mu\mu_{\zeta\zeta\zeta} - 15p\mu_{\zeta}\mu_{\zeta\zeta} + 45\mu^2\mu_{\zeta} + \mu_{\zeta\zeta\zeta\zeta\zeta}\right)\right]. \tag{39}$$

Now, by applying the proposed semianalytical technique, we get

$$\begin{aligned}
\mu_0(\zeta,\tau) &= \frac{4}{3}c - \frac{4}{p}\operatorname{csch}^2\left(\sqrt{c\zeta}\right),\\
\mu_1(\zeta,\tau) &= E^{-1}\left[s^{\rho}E\left(-15\mu_{(0)}\mu_{(0)\zeta\zeta\zeta} - 15p\mu_{(0)\zeta}\mu_{(0)\zeta\zeta} + 45\mu_{(0)}^2\mu_{(0)\zeta} + \mu_{(0)\zeta\zeta\zeta\zeta\zeta}\right)\right].\\
\mu_1(\zeta,\tau) &= 63p^2 + 360 - 420p + 4p(16p-15)\cosh\left(2\sqrt{c\zeta}\right)\\
&\quad + p^2\cosh\left(4\sqrt{cx}\right)\operatorname{sech}^6\left(\sqrt{c\zeta}\right)\tanh\left(\sqrt{c\zeta}\right)\frac{16c^{7/2}\tau^{\rho}}{p^3\Gamma(1+\rho)},\\
\mu_2(\zeta,\tau) &= E^{-1}\left[s^{\rho}E\left(-15\mu_{(1)}\mu_{(1)\zeta\zeta\zeta} - 15p\mu_{(1)\zeta}\mu_{(1)\zeta\zeta} + 45\mu_{(1)}^2\mu_{(1)\zeta} + \mu_{(1)\zeta\zeta\zeta\zeta\zeta}\right)\right].
\end{aligned}$$

$$\mu_2(\zeta,\tau) = -306084p^4 - 3110400 + 14515200p - 26369280p^3 - 6\left(2217600p - 432000 + 2656400p^3 - 4451160p^2 + 9181p^4\right) \cosh(2\sqrt{c\zeta}) + 48p\left(41590p^2 + 14400 - 60780p + 4789p^3\right) \cosh(4\sqrt{c\zeta}) - 59040p^3\cosh(6\sqrt{c\zeta}) + 79920p^2\cosh(6\sqrt{c\zeta}) - 20883p^4\cosh(6\sqrt{c\zeta}) - 240p^3\cosh(8\sqrt{c\zeta}) + p^4\cosh(10\sqrt{c\zeta}) + 244p^4\cosh(8\sqrt{c\zeta})\frac{8c^2\tau^{2\rho}\text{sech}^{12}\sqrt{c\zeta}}{p^5\Gamma(1+2\rho)} \tag{40}$$

$$\vdots$$

$$\mu_n(\zeta,\tau) = E^{-1}\left[s^{\rho}E\left(-15\mu_{(n)}\mu_{(n)\zeta\zeta\zeta} - 15p\mu_{(n)\zeta}\mu_{(n)\zeta\zeta} + 45\mu_{(n)}^2\mu_{(n)\zeta} + \mu_{(n)\zeta\zeta\zeta\zeta\zeta}\right)\right].$$

The series form result is

$$\mu(\zeta,\tau) = \mu_0(\zeta,\tau) + \mu_1(\zeta,\tau) + \mu_2(\zeta,\tau) + \mu_3(\zeta,\tau) + \cdots + \mu_n(\zeta,\tau). \tag{41}$$

Therefore, we have

$$u(\zeta,\tau) = \frac{4}{3}c - \frac{4}{p}\csc h^2(\sqrt{c\zeta}) + \left(63p^2 + 360 - 420p + 4p(16p-15)\cosh(2\sqrt{c\zeta}) + p^2\cosh(4\sqrt{cx})\sec h^6(\sqrt{c\zeta})\tanh(\sqrt{c\zeta})\frac{16c^{7/2}\tau^{\rho}}{p^3\Gamma(1+\rho)} + \left\{14515200p - 3110400 - 306084p^4 - 26369280p^3 - 6\left(2656400p^3 + 2217600p - 4451160p^2 - 432000 + 9181p^4\right)\cosh(2\sqrt{c\zeta}) + 48p\left(41590p^2 + 14400 + 4789p^3 - 60780p\right)\cosh(4\sqrt{c\zeta}) + 79920p^2\cosh(6\sqrt{c\zeta}) - 59040p^3\cosh(6\sqrt{c\zeta}) - 20883p^4\cosh(6\sqrt{c\zeta}) - 240p^3\cosh(8\sqrt{c\zeta}) + p^4\cosh(10\sqrt{c\zeta}) + 244p^4\cosh(8\sqrt{c\zeta})\right\}\frac{8c^2\tau^{2\rho}\sec h^{12}\sqrt{c\zeta}}{p^5\Gamma(1+2\rho)} + \cdots. \tag{42}$$

For $\rho = 1$, the exact results of (35) are given by

$$\mu(\zeta,\tau) = \frac{4}{3}c - \frac{4}{p}\text{sech}^2\left(\sqrt{c}\left(\zeta + 8\left(3c^2 - 5\text{pc}\right)\tau\right)\right). \tag{43}$$

Analytical approximate solutions with some free parameters are provided by the proposed technique. The analytical findings are extremely useful in deciphering the internal components of acts of nature. Depending on the physical factors, the explicit solutions represented several forms of approximate solutions. Figure 4 compares the result obtained by the help of the proposed technique to the exact and analytical result for the fractional-order KK equation. Figure 5 shows different fractional orders of ρ with respect to ζ and τ comparison which show that they have close contact with each other.

Example 3. Consider the following fractional Kaup–Kupershmidt equation which is given as

$$D_{\tau}^{\alpha}\mu(\zeta,\tau) = 5\mu\mu_{\zeta\zeta\zeta} + \frac{25}{2}\mu_{\zeta}\mu_{\zeta\zeta} + 5\mu^2\mu_{\zeta} + \mu_{\zeta\zeta\zeta\zeta\zeta}, \tag{44}$$

with the initial condition

$$\mu(\zeta,0) = -2k^2 + \frac{24k^2}{1+e^{k\zeta}}c - \frac{24k^2}{1+ek\zeta}. \tag{45}$$

Using the Elzaki transform to (44), we get

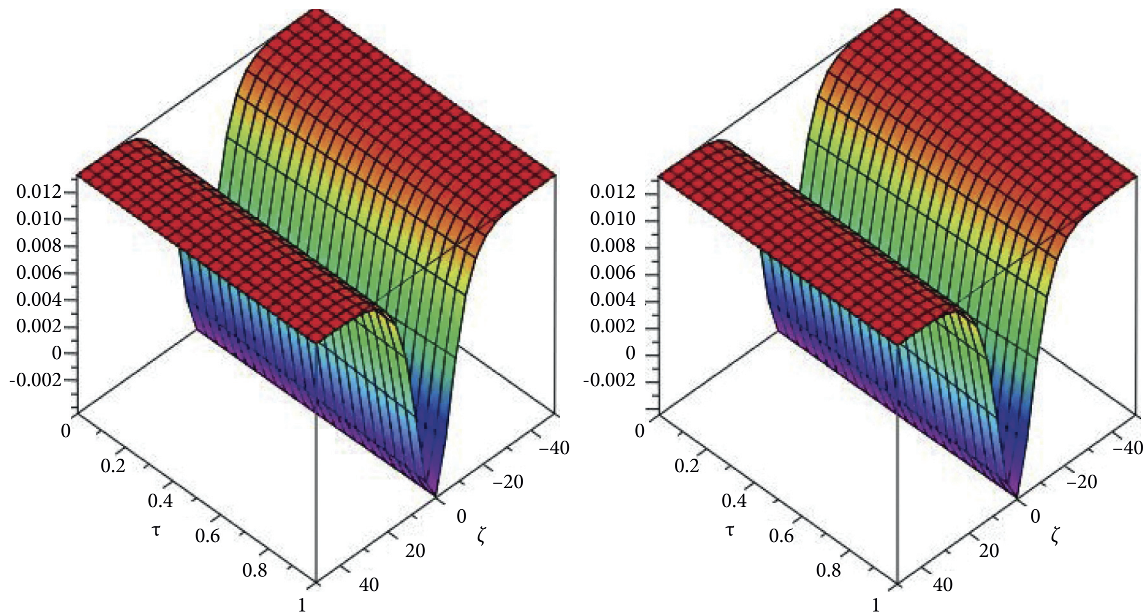

Figure 4: The exact and analytical solutions of Example 2.

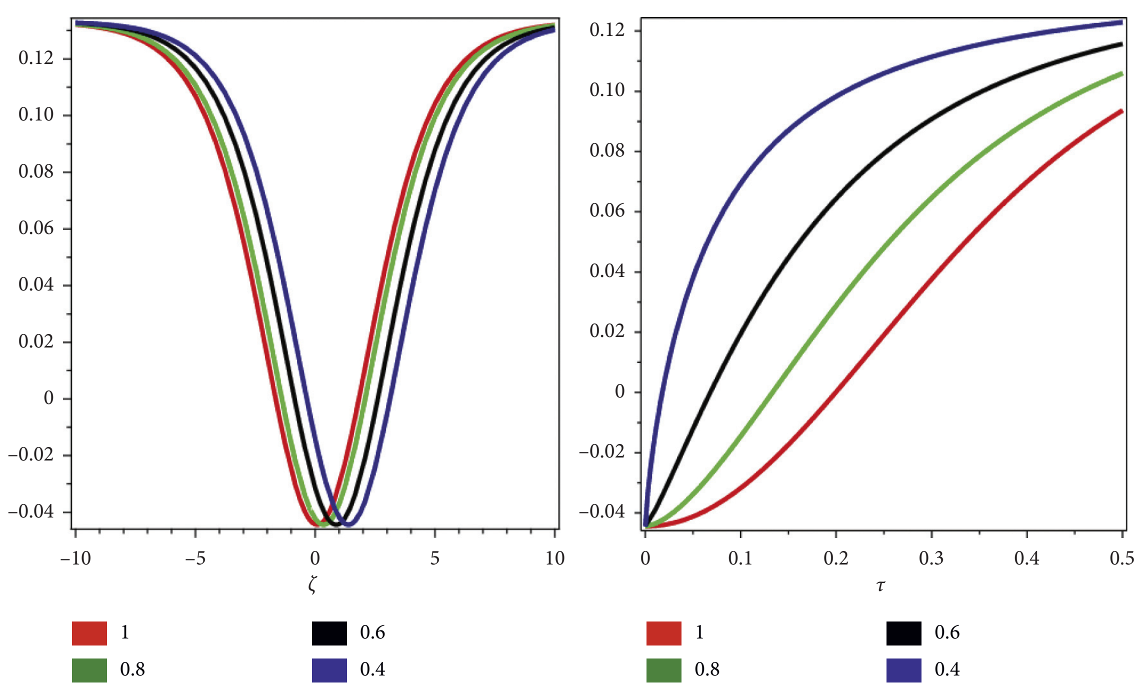

Figure 5: The fractional order ρ of Example 2 with respect to ζ and τ.

$$\frac{1}{s^{\rho}}E[\mu(\zeta,\tau)] = \mu_{(0)}(\zeta,0)s^{2-\rho} + E\left[5\mu\mu_{\zeta\zeta\zeta} + \frac{25}{2}\mu_{\zeta}\mu_{\zeta\zeta} + 5\mu^2\mu_{\zeta} + \mu_{\zeta\zeta\zeta\zeta\zeta}\right], \tag{46}$$

$$E[\mu(\zeta,\tau)] = s^2\mu(\zeta,0) + s^{\rho}E\left[5\mu\mu_{\zeta\zeta\zeta} + \frac{25}{2}\mu_{\zeta}\mu_{\zeta\zeta} + 5\mu^2\mu_{\zeta} + \mu_{\zeta\zeta\zeta\zeta\zeta}\right]. \tag{47}$$

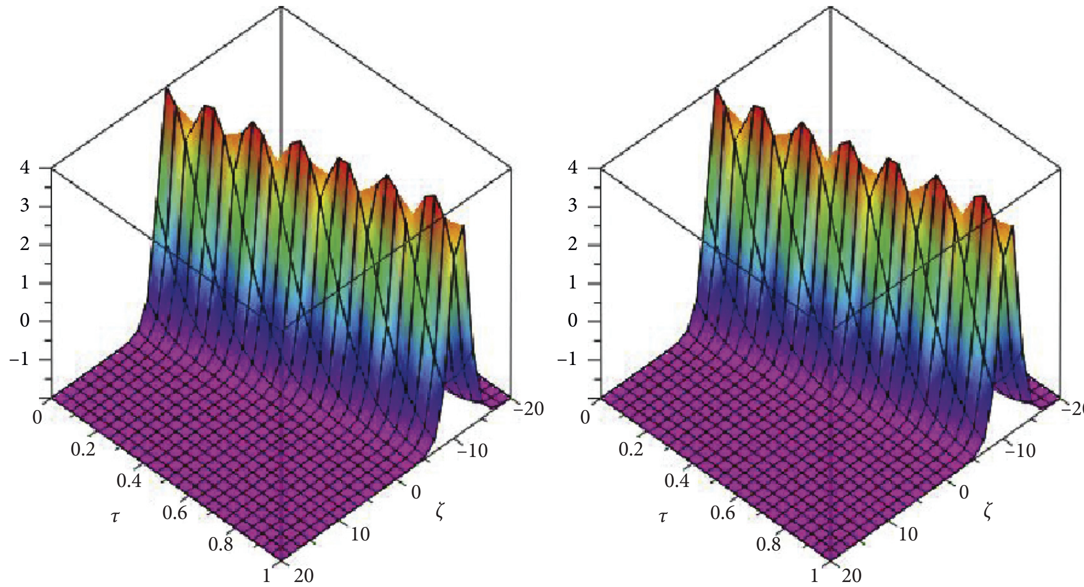

Figure 6: The exact and analytical solutions of Example 3.

Applying the inverse Elzaki transformation of (47), we have

$$mu(\zeta,\tau)=E^{-1}\left[s^2\mu(\zeta,0)\right]+E^{-1}\left[s^\rho E\left(5\mu\mu_{\zeta\zeta\zeta}+\frac{25}{2}\mu_\zeta\mu_{\zeta\zeta}+5\mu^2\mu_\zeta+\mu_{\zeta\zeta\zeta\zeta\zeta}\right)\right]. \tag{48}$$

Now, by applying the proposed semianalytical technique, we get

$$\mu_0(\zeta,\tau)=-2k^2+\frac{24k^2}{1+e^{k\zeta}}c-\frac{24k^2}{1+ek\zeta},$$

$$\mu_1(\zeta,\tau)=E^{-1}\left[s^\rho E\left(5\mu_{(0)}\mu_{(0)\zeta\zeta\zeta}+\frac{25}{2}\mu_{(0)\zeta}\mu_{(0)\zeta\zeta}+5\mu^2_{(0)}\mu_{(0)\zeta}+\mu_{(0)\zeta\zeta\zeta\zeta\zeta}\right)\right].$$

$$\mu_1(\zeta,\tau)=\frac{\tau^\rho}{\Gamma(1+\rho)}\left(\frac{264e^{k\zeta}\left(-1+e^{k\zeta}\right)k^7}{\left(1+e^{k\zeta}\right)^3}\right)$$

$$\mu_2(\zeta,\tau)=E^{-1}\left[s^\rho E\left(5\mu_{(1)}\mu_{(1)\zeta\zeta\zeta}+\frac{25}{2}\mu_{(1)\zeta}\mu_{(1)\zeta\zeta}+5\mu^2_{(1)}\mu_{(1)\zeta}+\mu_{(1)\zeta\zeta\zeta\zeta\zeta}\right)\right].$$

$$\mu_2(\zeta,\tau)=\frac{2904e^{k\zeta}\left(1-4e^{k\zeta}+e^{2k\zeta}\right)k^{12}\tau^{2\rho}}{\left(1+e^{k\zeta}\right)^4\Gamma(1+2\rho)}$$

$$\mu_3(\zeta,\tau)=E^{-1}\left[s^\rho E\left(5\mu_{(2)}\mu_{(2)\zeta\zeta\zeta}+\frac{25}{2}\mu_{(2)\zeta}\mu_{(2)\zeta\zeta}+5\mu^2_{(2)}\mu_{(2)\zeta}+\mu_{(2)\zeta\zeta\zeta\zeta\zeta}\right)\right].$$

$$\mu_3(\zeta,\tau) = 2904e^{k\zeta}\left(-1+e^{k\zeta}\right)k^{17}\tau^{3\rho}\Big(\Big(11+54e^{k\zeta}-4923e^{2k\zeta}+10228e^{3k\zeta}-4923e^{4k\zeta}+54e^{5k\zeta}+11e^{6k\zeta}\Big)$$
$$\Gamma(1+\rho)^2-60e^{k\zeta}\left(1-38e^{k\zeta}+90e^{2k\zeta}-38e^{3k\zeta}+e^{4k\zeta}\right)$$
$$\Gamma(1+2\rho)\div\left(1+e^{k\zeta}\right)^9\Gamma(1+\rho)^2\Gamma(1+3\rho) \tag{49}$$
$$\vdots$$
$$\mu_n(\zeta,\tau) = E^{-1}\left[s^\rho E\left(5\mu_{(n)}\mu_{(n)\zeta\zeta\zeta}+\frac{25}{2}\mu_{(n)\zeta}\mu_{(n)\zeta\zeta}+5\mu_{(n)}^2\mu_{(n)\zeta}+\mu_{(n)\zeta\zeta\zeta\zeta\zeta}\right)\right].$$

The series form result is

$$\mu(\zeta,\tau) = \mu_0(\zeta,\tau)+\mu_1(\zeta,\tau)+\mu_2(\zeta,\tau)+\mu_3(\zeta,\tau)+\cdots+\mu_n(\zeta,\tau). \tag{50}$$

Therefore, we have

$$u(\zeta,\tau) = -2k^2+\frac{24k^2}{1+e^{k\zeta}}c-\frac{24k^2}{1+ek\zeta}+\frac{\tau^\rho}{\Gamma(1+\rho)}\left(\frac{264e^{k\zeta}\left(-1+e^{k\zeta}\right)k^7}{\left(1+e^{k\zeta}\right)^3}\right)$$
$$+\frac{2904e^{k\zeta}\left(1-4e^{k\zeta}+e^{2k\zeta}\right)k^{12}\tau^{2\rho}}{\left(1+e^{k\zeta}\right)^4\Gamma(1+2\rho)}+2904e^{k\zeta}\left(-1+e^{k\zeta}\right)k^{17}\tau^{3\rho}$$
$$\left(11+54e^{k\zeta}-4923e^{2k\zeta}+10228e^{3k\zeta}-4923e^{4k\zeta}+54e^{5k\zeta}+11e^{6k\zeta}\right) \tag{51}$$
$$\Gamma(1+\rho)^2-60e^{k\zeta}\left(1-38e^{k\zeta}+90e^{2k\zeta}-38e^{3k\zeta}+e^{4k\zeta}\right)$$
$$\Gamma(1+2\rho)\div\left(1+e^{k\zeta}\right)^9\Gamma(1+\rho)^2\Gamma(1+3\rho)+\cdots.$$

For $\rho = 1$, the exact results of (44) are given by

$$\mu(\zeta,\tau) = -2k^2+\frac{24k^2}{1+e^{k\zeta+11k^5\tau}}-\frac{24k^2}{\left(1+e^{k\zeta+11k^5\tau}\right)^2}. \tag{52}$$

Analytical approximate solutions with some free parameters are provided by the proposed technique. The analytical findings are extremely useful in deciphering the internal components of acts of nature. Depending on the physical factors, the explicit solutions represented several forms of approximate solutions. Figure 6 compares the result obtained by the help of the proposed technique to the exact and analytical result for the fractional-order KK equation. Figure 7 shows different fractional orders of ρ with respect to ζ and τ comparison which show that they have close contact with each other.

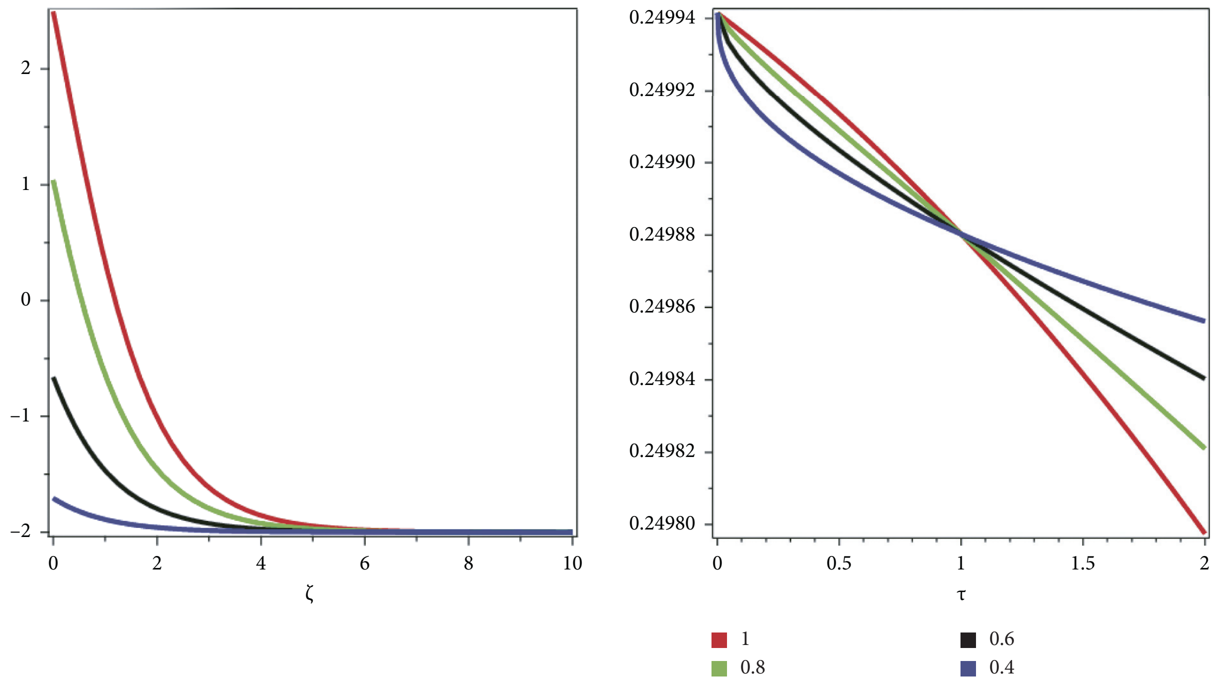

Figure 7: The fractional order ρ of Example 3 with respect to ζ and τ.

5. Conclusion

In this article, the iterative transformation technique is utilized to achieve analytical solutions of the fractional-order Kaup–Kupershmidt equations, which are broadly utilized as problems for spatial effects in applied sciences. The method gave a series type of solutions that converge very quickly in the mathematical model. It is predicted that the results obtained in this paper will be effective for more evaluation of the complicated nonlinear physical models. The analyses of this method are very clear and straightforward. As a result, we conclude that this method can be used to solve a variety of nonlinear fractional-order partial differential equation schemes.

Data Availability

The numerical data used to support the findings of this study are included within the article.

Conflicts of Interest

The authors declare that there are no conflicts of interest regarding the publication of this article.

Acknowledgments

This research was funded by Scientific Research Deanship at the University of Ha'il, Saudi Arabia, through project no. RG-21 005.

References

[1] J. H. He, "Nonlinear oscillation with fractional derivative and its applications," *International conference on vibrating engineering*, vol. 98, pp. 288–291, 1998.

[2] R. Almeida, N. R. O. Bastos, and M. T. T. Monteiro, "Modeling some real phenomena by fractional differential equations," *Mathematical Methods in the Applied Sciences*, vol. 39, no. 16, pp. 4846–4855, 2016.

[3] Y. A. Rossikhin and M. V. Shitikova, "Application of fractional calculus for dynamic problems of solid mechanics: novel trends and recent results," *Applied Mechanics Reviews*, vol. 63, no. 1, 2010.

[4] Y. A. Rossikhin, "Reflections on two parallel ways in the progress of fractional calculus in mechanics of solids," *Applied Mechanics Reviews*, vol. 63, no. 1, 2010.

[5] P. Sunthrayuth, A. M. Zidan, S.-W. Yao, R. Shah, and M. Inc, "The comparative study for solving fractional-order fornberg-whitham equation via ρ-laplace transform," *Symmetry*, vol. 13, no. 5, p. 784, 2021.

[6] R. P. Agarwal, F. Mofarreh, R. Shah, W. Luangboon, and K. Nonlaopon, "An analytical technique, based on natural transform to solve fractional-order parabolic equations," *Entropy*, vol. 23, no. 8, p. 1086, 2021.

[7] Y. Zhang, H. Sun, H. H. Stowell, M. Zayernouri, and S. E. Hansen, "A review of applications of fractional calculus in Earth system dynamics," *Chaos, Solitons & Fractals*, vol. 102, pp. 29–46, 2017.

[8] N. H. Aljahdaly, R. P. Agarwal, R. Shah, and T. Botmart, "Analysis of the time fractional-order coupled burgers equations with non-singular kernel operators," *Mathematics*, vol. 9, no. 18, p. 2326, 2021.

[9] F. Mohammadi, L. Moradi, D. Baleanu, and A. Jajarmi, "A hybrid functions numerical scheme for fractional optimal control problems: application to nonanalytic dynamic systems," *Journal of Vibration and Control*, vol. 24, no. 21, pp. 5030–5043, 2018.

[10] A. Jajarmi and D. Baleanu, "On the fractional optimal control problems with a general derivative operator," *Asian Journal of Control*, vol. 23, 2019.

[11] D. J. Kaup, "On the inverse scattering for cubic eigenvalue problems of the class equations," *Studies in Applied Mathematics*, vol. 62, pp. 183–195, 1980.

[12] B. A. Kupershmidt, "A super Korteweg-de-Vries equations: an integrable system," *Physics Letters A*, vol. 102, pp. 213–218, 1994.

[13] E. Fan, "Uniformly constructing a series of explicit exact solutions to nonlinear equations in mathematical physics," *Chaos, Solitons & Fractals*, vol. 16, no. 5, pp. 819–839, 2003.

[14] M. Inc, "On numerical soliton solution of the Kaup-Kupershmidt equation and convergence analysis of the decomposition method," *Applied Mathematics and Computation*, vol. 172, no. 1, pp. 72–85, 2006.

[15] K. Nonlaopon, A. M. Alsharif, A. M. Zidan, A. Khan, Y. S. Hamed, and R. Shah, "Numerical investigation of fractional-order Swift-Hohenberg equations via a Novel transform," *Symmetry*, vol. 13, no. 7, p. 1263, 2021.

[16] H.-W. Tam and X.-B. Hu, "Two integrable differential-difference equations exhibiting soliton solutions of the Kaup-Kupershmidt equation type," *Physics Letters A*, vol. 272, no. 3, pp. 174–183, 2000.

[17] M. Musette and C. Verhoeven, "Nonlinear superposition formula for the Kaup-Kupershmidt partial differential equation," *Physica D: Nonlinear Phenomena*, vol. 144, no. 1-2, pp. 211–220, 2000.

[18] D. G. Prakasha, N. S. Malagi, P. Veeresha, and B. C. Prasannakumara, "An efficient computational technique for time-fractional Kaup-Kupershmidt equation," *Numerical Methods for Partial Differential Equations*, vol. 37, pp. 1–18, 2020.

[19] V. Daftardar-Gejji and H. Jafari, "An iterative method for solving nonlinear functional equations," *Journal of Mathematical Analysis and Applications*, vol. 316, no. 2, pp. 753–763, 2006.

[20] H. Jafari, *Iterative Methods for Solving System of Fractional Differential Equations*, Ph.D. Thesis, Pune University, Pune, Maharashtra, 2006.

[21] H. Jafari, M. Nazari, D. Baleanu, and C. M. Khalique, "A new approach for solving a system of fractional partial differential equations," *Computers & Mathematics with Applications*, vol. 66, no. 5, pp. 838–843, 2013.

[22] A. Prakash, M. Kumar, and D. Baleanu, "A new iterative technique for a fractional model of nonlinear Zakharov-Kuznetsov equations via Sumudu transform," *Applied Mathematics and Computation*, vol. 334, pp. 30–40, 2018.

[23] K. Nonlaopon, M. Naeem, A. M. Zidan, R. Shah, A. Alsanad, and A. Gumaei, "Numerical investigation of the time-fractional whitham-broer-kaup equation involving without singular kernel operators," *Complexity*, vol. 2021, Article ID 7979365, 21 pages, 2021.

[24] M. Ramadan and M. S. Al-luhaibi, "New iterative method for solving the Fornberg-Whitham equation and comparison with homotopy perturbation transform method," *British Journal of Mathematics & Computer Science*, vol. 4, no. 9, pp. 1213–1227, 2014.

[25] T. M. Elzaki, "The new integral transform Elzaki transform," *Global Journal of Pure and Applied Mathematics*, vol. 7, no. 1, pp. 57–64, 2011.

[26] T. M. Elzaki, "On the connections between Laplace and Elzaki transforms," *Advances in Theoretical and Applied Mathematics*, vol. 6, no. 1, pp. 1–11, 2011.

[27] T. M. Elzaki, "On the new integral transform Elzaki Transform" fundamental properties investigations and applications," *Global Journal of Mathematical Sciences: Theory and Practical*, vol. 4, no. 1, pp. 1–13, 2012.

Hindawi
Journal of Mathematics
Volume 2021, Article ID 5337255, 12 pages
https://doi.org/10.1155/2021/5337255

Research Article

Approximate and Exact Solutions to Fractional Order Cauchy Reaction-Diffusion Equations by New Combine Techniques

Adnan Khan,[1] **Muhammad Imran Liaqat**,[1] **Muhammad Younis**,[2] **and Ashraful Alam**[3]

[1]*National College of Business Administration & Economics, Lahore, Pakistan*
[2]*PUCIT, University of the Punjab, Lahore 54000, Pakistan*
[3]*Department of Mathematics, Jahangirnagar University, Savar, Dhaka, Bangladesh*

Correspondence should be addressed to Ashraful Alam; ashraf_math20@juniv.edu

Received 9 October 2021; Revised 22 November 2021; Accepted 26 November 2021; Published 16 December 2021

Academic Editor: Fairouz Tchier

In this paper, we present a simple and efficient novel semianalytic method to acquire approximate and exact solutions for the fractional order Cauchy reaction-diffusion equations (CRDEs). The fractional order derivative operator is measured in the Caputo sense. This novel method is based on the combinations of Elzaki transform method (ETM) and residual power series method (RPSM). The proposed method is called Elzaki residual power series method (ERPSM). The proposed method is based on the new form of fractional Taylor's series, which constructs solution in the form of a convergent series. As in the RPSM, during establishing the coefficients for a series, it is required to compute the fractional derivatives every time. While ERPSM only requires the concept of the limit at zero in establishing the coefficients for the series, consequently scarce calculations give us the coefficients. The recommended method resolves nonlinear problems deprived of utilizing Adomian polynomials or He's polynomials which is the advantage of this method over Adomain decomposition method (ADM) and homotopy-perturbation method (HTM). To study the effectiveness and reliability of ERPSM for partial differential equations (PDEs), absolute errors of three problems are inspected. In addition, numerical and graphical consequences are also recognized at diverse values of fractional order derivatives. Outcomes demonstrate that our novel method is simple, precise, applicable, and effectual.

1. Introduction

Differential equations (DEs) can be resolved by a diversity of procedures, analytical and numerical. However, there are numerous analytic methods for verdict on the results of DEs; there occur quite a numeral of DEs that cannot be explained analytically. This means that the result cannot be articulated as a summation of a fixed numeral of basic functions.

Numerous DEs arising in applications are so thorny that it is occasionally unreasonable to have result formulations or as a minimum if a result formula is existing, it possibly will comprise integrals that can be premeditated only by means of an algebraic quadrature formulation. In moreover instance, numerical procedures offer an influential substitute means for resolving the DEs under the prearranged preliminary condition.

Earlier, numerous procedures have been offered to resolve fractional order DEs comprising the Bernstein wavelets method [1], Shehu variational iteration method [2], Chebyshev spectral collocation approach [3], Taylor wavelet technique [4], operational matrix approach [5], fractional natural decomposition method [6]. homotopy analysis approach [7], Aboodh decomposition approach [8], Sumudu decomposition method [9], Elzaki decomposition technique [10], residual power series method [11], and generalized pseudospectral method [12]. Numerical method is based on the generalized fractional order of the Chebyshev orthogonal functions (GFCFs) and the collocation method [13].

In this research, an easy and effective novel semianalytical method is initiated. The unexploited method is called ERPSM that is the merger of ETM and RPSM. The process of this efficacious method relies on transforming DE into the Elzaki space and creating a series explanation and subsequently acquiring the consequence of the actual DE by utilizing the inverse ETM.

Reaction-diffusion equation is a mathematical model, characterized by the parabolic PDEs. It is exemplifying in what way chemicals might work to each other, whereas they diffuse by a medium instantaneously. Alan Tuning recognized it in 1952 [14]. Reaction-diffusion is measured immensely by experts in biology, chemistry, physics, and computer science [15].

By a reaction-diffusion, we mean an equation of the following form:

$$\frac{\partial \Phi}{\partial \Upsilon} = \Delta\Phi + \Omega(\Phi, \Delta\Phi, \chi, \Upsilon), \tag{1}$$

where Φ is the diffusion term and $\Omega(\Phi, \Delta\Phi, \chi, \Upsilon)$ is the reaction term.

In this paper, we deliberate the one-dimensional time-fractional CRDEs. The time-fractional CRDEs can be utilized to explicate several categories of linear and nonlinear systems in physics, chemistry, ecology, biology, and engineering [16–18].

The general form of the fractional order CRDE is as follows [19]:

$$\frac{\partial^{\varpi}\Phi(\chi,\Upsilon)}{\partial \Upsilon^{\varpi}} = \lambda \frac{\partial^2 \Phi(\chi,\Upsilon)}{\partial \chi^2} + z(\chi,\Upsilon)\Phi(\chi,\Upsilon), \quad \chi \geq 0,\ \Upsilon \geq 0,\ 0 < \varpi \leq 1. \tag{2}$$

With the initial condition,

$$\Phi(\chi, 0) = g(\chi). \tag{3}$$

Fractional derivative is considered in the Caputo sense.

The term $\lambda\ (\partial^2\Phi(\chi,\Upsilon)/\partial\chi^2)$ represents diffusion and $z(\chi,\Upsilon)\Phi(\chi,\Upsilon)$ represents the reaction, where $z(\chi,\Upsilon)$ is the reaction parameter, $\Phi(\chi,\Upsilon)$ is the concentration, and λ is the diffusion coefficient constant.

Verdict on the results of fractional order CRDEs is a fascinating zone for the researchers. Chowdhury and Hashim applied homotopy-perturbation method (HPM) to acquire estimated analytical explanations for the CRDEs [20]. Ali et al. established estimated results of CRDEs by optimal homotopy asymptotic method (OHAM) [21]. Wang and Liu used a novel evaluating procedure for nonlinear time-fractional CRDE [22]. Kumar et al. applied homotopy analysis transform method (HATM) for cracking CRDEs [23]. Hosseini et al. recognized comparative explanation of CRDEs by Mittag–Leffler law [24]. Lima et al. considered problems of CRDEs by means of finite element approach [25].

Elzaki transform was presented by Elzaki in 2011 [26]. It is a very useful method to resolve the entire natures of DEs.

Elzaki transform was defined for functions of exponential order. We consider functions in the set ξ defined as

$$\xi = \left\{\Phi(\Upsilon) | \exists M,\ \Theta_1,\ \Theta_2 > 0, |\Phi(\Upsilon) < Me^{(|\Upsilon|/\Theta_j)} \text{if } \Upsilon \in (-1)^j X[0,\infty)\right\}. \tag{4}$$

Elzaki transform is defined as

$$E[\Phi(\Upsilon)] = v\int_0^{\infty} \Phi(\Upsilon)e^{-(\Upsilon/v)}d\Upsilon, \quad \Theta_1 \leq v \leq \Theta_2, \tag{5}$$

where E symbolizes Elzaki transform operator.

The framework of this study is as follows. In the next section, a new form of fractional Taylor's series is introduced that will be used in our work in the next sections and further explained and the conditions for convergence of the new form of Taylor's formula were determined. Moreover, we presented some new results. Next, we build Elzaki residual power series solutions for CRDEs. Further, few problems are solved to illustrate the capability, the potentiality, and the simplicity of the proposed method. Eventually, our results are compiled in the conclusion.

2. Some New Results

In this section, we familiarize a novel formula of fractional Taylor's series and elucidate and govern the circumstances for the convergence of the novel formula of fractional Taylor's series and present some expedient outcomes which are pillars for the new effectual method.

Lemma 1 (a new formula of fractional Taylor's series in Elzaki transform). *Suppose that $\Phi(\Upsilon)$ is a piecewise continuous and exponential order; the Elzaki transform of $\Phi(\Upsilon)E[\Phi(\Upsilon)] = \Psi(v)$ has fractional Taylor's series representation as*

$$\Psi(v) = \sum_{n=0}^{\infty} \aleph_n v^{n\varpi+2}, \tag{6}$$

where $\aleph_n$ represents nth coefficient of the new formula of fractional Taylor's series in Elzaki transform.

Proof: Consider the following fractional Taylor's series:

$$\Phi(\Upsilon) = \aleph_0 + \frac{\aleph_1}{\Gamma(\varpi+1)}\Upsilon^{\varpi} + \frac{\aleph_2}{\Gamma(2\varpi+1)}\Upsilon^{2\varpi} + \frac{\aleph_3}{\Gamma(3\varpi+1)}\Upsilon^{3\varpi} + \cdots. \tag{7}$$

Applying Elzaki transform at the both sides of equation (6),

$$E[\Phi(\Upsilon)] = \aleph_0 E[1] + \frac{\aleph_1}{\Gamma(\varpi+1)} E\left[\Upsilon^{\varpi}\right] + \frac{\aleph_2}{\Gamma(2\varpi+1)} E\left[\Upsilon^{2\varpi}\right] + \frac{\aleph_3}{\Gamma(3\varpi+1)} E\left[\Upsilon^{3\varpi}\right] + \frac{\aleph_4}{\Gamma(4\varpi+1)} E\left[\Upsilon^{4\varpi}\right] + \cdots,$$
$$\Psi(v) = \sum_{n=0}^{\infty} \aleph_n v^{n\varpi+2}. \tag{8}$$

which is a new form of fractional Taylor formula in Elzaki transform form. □

Remark 1. The multiple fractional Taylor's series or generalized form of Taylor's series representation at $\Upsilon = 0$ takes the following form in Elzaki transform space:

$$\Psi(\chi, v) = \sum_{n=0}^{\infty} \aleph_n(\chi) v^{n\varpi+2},$$
$$\text{where } \chi = (\chi_1, \chi_2, \chi_3 \ldots \chi_d) \in \mathfrak{R}^d,\ d \in N. \tag{9}$$

Lemma 2. *Assume that the function $E[\Phi(\Upsilon)] = \Psi(v)$ has fractional power series (FPS) representation as follows:*

$$\Psi(v) = \sum_{n=0}^{\infty} \aleph_n v^{n\varpi+2}. \tag{10}$$

Then, $\lim_{v\longrightarrow 0}(1/v^2)\Psi(v) = \aleph_0$.

Proof: From the new form of fractional Taylor's series, we have

$$\frac{1}{v^2}\Psi(v) = \aleph_0 + \aleph_1 v^{\varpi} + \aleph_2 v^{2\varpi} + \aleph_3 v^{3\varpi} + \aleph_4 v^{4\varpi} + \cdots. \tag{11}$$

Taking limit $v \longrightarrow 0$, so the last equation becomes as

$$\lim_{v\longrightarrow 0} \frac{1}{v^2}\Psi(v) = \aleph_0 = \Phi(0). \tag{12}$$

□

Remark 2. In the case of a generalized form of Taylor's series in Elzaki transform space, we have the following:

$$\lim_{v\longrightarrow 0} \frac{1}{v^2}\Psi(\chi, v) = \aleph_0(\chi, 0),$$
$$\text{where } \chi = (\chi_1, \chi_2, \chi_3 \ldots \chi_d) \in \mathfrak{R}^d,\ d \in N. \tag{13}$$

Lemma 3. *Presume that $\Phi(\Upsilon)$ is a piecewise continuous function on $[0,\infty)$ and exponential order, $E[\Phi(\Upsilon)] = \Psi(v)$. Then,*

$$E\left[D_{\Upsilon}^{n\varpi}\Phi(\Upsilon)\right] = \frac{E[\Phi(\Upsilon)]}{v^{n\varpi}} - \sum_{j=0}^{n-1} v^{(j-n)\varpi+2}\left(D_{\Upsilon}^{j\varpi}\Phi\right)(0),$$
$$0 < \varpi \leq 1, \tag{14}$$

where $D_{\Upsilon}^{n\varpi}\Phi = D_{\Upsilon}^{\varpi}.D_{\Upsilon}^{\varpi}.D_{\Upsilon}^{\varpi}\ldots D_{\Upsilon}^{\varpi}$ (n – times).

Proof: To prove, we use the principle of mathematical induction method.

Using $n = 1$ in equation (14),

$$E\left[D_{\Upsilon}^{\varpi}\Phi(\Upsilon)\right] = \frac{E[\Phi(\Upsilon)]}{v^{\varpi}} - v^{-\varpi+2}\Phi(0). \tag{15}$$

Equation (14) is effective for $n = 1$.

Using $n = 2$ in equation (14), we get

$$E\left[D_{\Upsilon}^{2\varpi}\Phi(\Upsilon)\right] = \frac{E[\Phi(\Upsilon)]}{v^{2\varpi}} - v^{-2\varpi+2}\Phi(0) + v^{-\varpi+2}\left(D_{\Upsilon}^{\varpi}\Phi\right)(0),$$
$$\text{L.H.S} = E\left[D_{\Upsilon}^{2\varpi}\Phi(\Upsilon)\right] = E\left[D_{\Upsilon}^{\varpi}\left(D_{\Upsilon}^{\varpi}\Phi(\Upsilon)\right)\right]. \tag{16}$$

Let $D_{\Upsilon}^{\varpi}\Phi(\Upsilon) = z(\Upsilon)$.

So, equation (16) becomes as

$$\text{L.H.S} = E\left[D_{\Upsilon}^{2\varpi}\Phi(\Upsilon)\right] = E\left[D_{\Upsilon}^{\varpi}(z(\Upsilon))\right]. \tag{17}$$

By utilizing Caputo fractional derivative, the last equation becomes as

$$\text{L.H.S} = E\left[D_{\Upsilon}^{2\varpi}\Phi(\Upsilon)\right] = E\left[J_{\Upsilon}^{1-\varpi}z^{(1)}(\Upsilon)\right]. \tag{18}$$

By using Riemann–Liouville integral formula of Elzaki transform,

$$\text{L.H.S} = E\left[D_{\Upsilon}^{2\varpi}\Phi(\Upsilon)\right] = v^{1-\varpi}E\left[z^{(1)}(\Upsilon)\right]. \tag{19}$$

By differential property, the above equation becomes as follows:

$$E\left[D_{\Upsilon}^{2\varpi}\Phi(\Upsilon)\right] = v^{-\varpi}Z(v) - v^{2-\varpi}z(0),$$
$$\text{where } \left(D_{\Upsilon}^{\varpi}\Phi\right)(0) = z(0). \tag{20}$$

From equation (20), we have

$$E\left[D_{\Upsilon}^{2\varpi}\Phi(\Upsilon)\right] = v^{-\varpi}E\left[D_{\Upsilon}^{\varpi}\Phi(\Upsilon)\right] - v^{2-\varpi}\left(D_{\Upsilon}^{\varpi}\Phi\right)(0),$$
$$E\left[D_{\Upsilon}^{2\varpi}\Phi(\Upsilon)\right] = \frac{E[\Phi(\Upsilon)]}{v^{2\varpi}} - v^{2-2\varpi}\Phi(0) - v^{2-\varpi}\left(D_{\Upsilon}^{\varpi}\Phi\right)(0). \tag{21}$$

So, from equation (21), we conclude that formula equation (14) is accurate when $n = 2$. Now, suppose formula is valid for $n = r$. So, we have

$$E\left[D_{\Upsilon}^{r\varpi}\Phi(\Upsilon)\right] = \frac{E[\Phi(\Upsilon)]}{v^{r\varpi}} - \sum_{j=0}^{r-1} v^{(j-r)\varpi+2}\left(D_{\Upsilon}^{j\varpi}\Phi\right)(0). \tag{22}$$

Now, we will prove for $n = r + 1$.

$$E\left[D_{\Upsilon}^{(r+1)\varpi}\Phi(\Upsilon)\right]=\frac{E[\Phi(\Upsilon)]}{v^{r\varpi}}-\sum_{j=0}^{r-1+1}v^{(j-(r+1))\varpi+2}\left(D_{\Upsilon}^{j\varpi}\Phi\right)(0), \tag{23}$$

$$\begin{aligned}\text{L.H.S}&=E\left[D_{\Upsilon}^{(r+1)\varpi}\Phi(\Upsilon)\right],\\ \text{L.H.S}&=E\left[D_{\Upsilon}^{\varpi}\left(D_{\Upsilon}^{r\varpi}\Phi(\Upsilon)\right)\right].\end{aligned} \tag{24}$$

Suppose that

$$D_{\Upsilon}^{r\varpi}\Phi(\Upsilon)=b(\Upsilon). \tag{25}$$

So, equation (24) becomes as

$$\text{L.H.S}=E\left[D_{\Upsilon}^{\varpi}(b(\Upsilon))\right]. \tag{26}$$

By utilizing Caputo fractional derivative, so the last equation becomes as

$$\text{L.H.S}=E\left[J_{\Upsilon}^{1-\varpi}b^{(1)}(\Upsilon)\right]. \tag{27}$$

By utilizing Riemann–Liouville fractional integral formula, equation (27) becomes as follows:

$$\text{L.H.S}=v^{1-\varpi}E\left[b^{(1)}(\Upsilon)\right]. \tag{28}$$

By differential property of E-L, so equation (28) becomes as

$$\text{L.H.S}=v^{\varpi}E\left[D_{\Upsilon}^{r\varpi}\Phi(\Upsilon)\right]-v^{2-\varpi}b(0), \tag{29}$$

where $\left(D_{\Upsilon}^{r\varpi}\Phi\right)(0)=b(0)$.

From equation (29), we get

$$\begin{aligned}\text{L.H.S}&=\frac{E[\Phi(\Upsilon)]}{v^{(r+1)\varpi}}-\sum_{j=0}^{r-1}v^{(j-(r+1))\varpi+2}\left(D_{\Upsilon}^{j\varpi}\Phi\right)(0)-v^{2-\varpi}b(0),\\ \text{L.H.S}&=\frac{E[\Phi(\Upsilon)]}{v^{n\varpi}}-\sum_{j=0}^{n-1}v^{(j-n)\varpi+2}\left(D_{\Upsilon}^{j\varpi}\Phi\right)(0).\end{aligned} \tag{30}$$

So, equation (14) is valid for all integers. Thus, the proof completes. □

Remark 3. By making generalization, the above proved formula takes the following form:

$$E\left[D_{\Upsilon}^{n\varpi}\Phi(\chi,\Upsilon)\right]=\frac{E[\Phi(\chi,\Upsilon)]}{v^{n\varpi}}-\sum_{j=0}^{n-1}v^{(j-n)\varpi+2}\left(D_{\Upsilon}^{j\varpi}\Phi\right)(0),\quad \text{where}\chi=\left(\chi_1,\chi_2,\chi_3,\ldots\chi_d\right)\in\mathfrak{R}^d, d\in N, \tag{31}$$

and $D_{\Upsilon}^{n\varpi}\Phi=D_{\Upsilon}^{\varpi}.D_{\Upsilon}^{\varpi}.D_{\Upsilon}^{\varpi}\ldots D_{\Upsilon}^{\varpi}(n-\text{times})$.

Theorem 1. *Suppose that the function $E[\Phi(\Upsilon)]=\Psi(v)$ has FPS representation as follows:*

$$\Psi(v)=\sum_{n=0}^{\infty}\aleph_n v^{n\varpi+2}, \tag{32}$$

then we have $\aleph_n=\left(D_{\Upsilon}^{n\varpi}\Phi\right)(0)$, where $D_{\Upsilon}^{n\varpi}\Phi=D_{\Upsilon}^{\varpi}.D_{\Upsilon}^{\varpi}.D_{\Upsilon}^{\varpi}\ldots D_{\Upsilon}^{\varpi}(n-\text{times})$.

Proof: Consider new form of Taylor's series.

$$\Psi(v)=\aleph_0v^2+\aleph_1v^{\varpi+2}+\aleph_2v^{2\varpi+2}+\aleph_3v^{3\varpi+2}+\aleph_4v^{4\varpi+2}+\cdots. \tag{33}$$

From the above equation, we have

$$\begin{aligned}\aleph_1=&\frac{1}{v^{\varpi+2}}\Psi(v)-\frac{1}{v^{\varpi+2}}v^2\Psi(0)-\frac{1}{v^{\varpi+2}}\aleph_2v^{2\varpi+2}\\&-\frac{1}{v^{\varpi+2}}\aleph_3v^{3\varpi+2}-\frac{1}{v^{\varpi+2}}\aleph_4v^{4\varpi+2}+\cdots.\end{aligned} \tag{34}$$

Taking $v\longrightarrow 0$ on the above equation,

$$\aleph_1=\lim_{v\longrightarrow 0}\frac{1}{v^2}\left(\frac{1}{v^{\varpi}}\Psi(v)-\frac{1}{v^{\varpi-2}}\Psi(0)\right). \tag{35}$$

By using Lemma 3,

$$\aleph_1=\lim_{v\longrightarrow 0}\frac{1}{v^2}\left(E\left[D_{\Upsilon}^{\varpi}\Phi(\Upsilon)\right](v)\right). \tag{36}$$

By Lemma 2, the above equation becomes as

$$\aleph_1=\left(D_{\Upsilon}^{\varpi}\Phi\right)(0). \tag{37}$$

Again from equation (32),

$$\begin{aligned}\aleph_2=&\frac{1}{v^2}\left(\frac{1}{v^{2\varpi}}\Psi(v)-\frac{1}{v^{2\varpi-2}}\Psi(0)-\frac{1}{v^{\varpi-2}}\aleph_1\right)-\aleph_3v^{\varpi}\\&-\aleph_4v^{2\varpi}+\cdots.\end{aligned} \tag{38}$$

Taking $v\longrightarrow 0$ on the last equation, utilizing Lemma 3, the above equation becomes as

$$\aleph_2=\lim_{v\longrightarrow 0}\frac{1}{v^2}\left(E\left[D_{\Upsilon}^{2\varpi}\Phi(\Upsilon)\right](v)\right). \tag{39}$$

By Lemma 2,

$$\aleph_2=\left(D_{\Upsilon}^{2\varpi}\Phi\right)(0). \tag{40}$$

Again from equation (32), we have

$$\aleph_3=\lim_{v\longrightarrow 0}\frac{1}{v^2}\left(\frac{1}{v^{3\varpi}}\Psi(v)-\Psi(0)\frac{1}{v^{3\varpi-2}}-\aleph_1\frac{1}{v^{2\varpi}}-\aleph_2\frac{1}{v^{\varpi-2}}\right). \tag{41}$$

By Lemma 3,

$$\aleph_3 = \lim_{\upsilon\longrightarrow 0}\left(\frac{1}{\upsilon^2}E\left[D_{\Upsilon}^{3\varpi}\Phi(\Upsilon)\right](\upsilon)\right). \quad (42)$$

By Lemma 2, the last equation becomes as

$$\aleph_3 = \left(D_{\Upsilon}^{3\varpi}\Phi\right)(0). \quad (43)$$

In the same manner, we can obtain the following form by making generalization:

$$\aleph_n = \left(D_{\Upsilon}^{n\varpi}\Phi\right)(0). \quad (44)$$

This completes the proof of the theorem. □

Remark 4. For multiple Taylor's series, the proved result becomes as follows:

$$\aleph_n(\chi) = \left(D_{\Upsilon}^{n\varpi}\Phi\right)(0), \quad \text{where } \chi = (\chi_1, \chi_2, \chi_3, \ldots \chi_d) \in \mathfrak{R}^d, d \in N. \quad (45)$$

The following theorem describes and determines the conditions for convergence of the new form of Taylor's formula that are introduced in Lemma 1.

Theorem 2. *Let $\Psi(\upsilon) = E[\Phi(\Upsilon)]$ be represented as the new form of fractional Taylor's formula as in Elzaki transform:*

$$\Psi(\upsilon) = \sum_{n=0}^{\infty}\aleph_n \upsilon^{n\varpi+2}, \quad (46)$$

if

$$\left|\frac{1}{\upsilon^2}E\left[D_{\Upsilon}^{(n+1)\varpi}\Phi(\Upsilon)\right]\right| \le T. \quad (47)$$

Then, the remainder $R_n(\upsilon)$ of the new form of fractional Taylor's formula satisfies the following inequality:

$$\left|R_n(\upsilon)\right| \le \upsilon^{(n+1)\varpi+2}T. \quad (48)$$

Proof: Consider the following:

$$\Psi_n(\upsilon) = \aleph_0\upsilon^2 + \aleph_1\upsilon^{\varpi+2} + \aleph_2\upsilon^{2\varpi+2} + \aleph_3\upsilon^{3\varpi+2} + \cdots \aleph_n\upsilon^{n\varpi+2}. \quad (49)$$

From equations (46) and (49), we get

$$R_n(\upsilon) = \Psi(\upsilon) - \sum_{k=0}^{n}\aleph_k\upsilon^{k\varpi+2}. \quad (50)$$

By Theorem 1,

$$\begin{aligned} R_n(\upsilon) &= \Psi(\upsilon) - \sum_{k=0}^{n}\upsilon^{k\varpi+2}\left(D_{\Upsilon}^{k\varpi}\Phi\right)(0), \\ \frac{1}{\upsilon^{(n+1)\varpi+2}}R_n(\upsilon) &= \frac{1}{\upsilon^2}\left(\frac{1}{\upsilon^{(n+1)\varpi}}\Psi(\upsilon) - \sum_{k=0}^{n}\frac{1}{\upsilon^{(n+1-k)\varpi-2}}\left(D_{\Upsilon}^{k\varpi}\Phi\right)(0)\right). \end{aligned} \quad (51)$$

By Lemma 3,

$$\begin{aligned} \frac{1}{\upsilon^{(n+1)\varpi+2}}R_n(\upsilon) &= \frac{1}{\upsilon^2}E\left[D_{\Upsilon}^{(n+1)\varpi}\Phi(\Upsilon)\right], \\ \left|\frac{1}{\upsilon^{(n+1)\varpi+2}}R_n(\upsilon)\right| &= \left|\frac{1}{\upsilon^2}E\left[D_{\Upsilon}^{(n+1)\varpi}\Phi(\Upsilon)\right]\right|. \end{aligned} \quad (52)$$

By the given assumption, the above equation becomes as

$$-\upsilon^{(n+1)\varpi+2}T \le R_n(\upsilon) \le \upsilon^{(n+1)\varpi+2}T, \quad (53)$$

$|R_n(\upsilon)| \le \upsilon^{(n+1)\varpi+2}T$. Hence, the required result is proved. □

3. Demonstrating the ERPSM for the CRDEs

We exploit our novel ERPSM to originate the results of the linear and nonlinear CRDEs. The foremost set of rules of this method for resolving the CRDEs can be accumulated by the following steps: employing the Elzaki transform to CRDE and then deploying the novel form of Taylor's series to introduce the solution of CRDE in the novel space. The coefficients of this series are established with a new idea. At the end, employing the inverse Elzaki transform to achieve the solution of the problem in the actual space.

3.1. Elzaki Residual Power Series Solutions for the CRDEs. In this subsection, we systematized the stages for conquering the Elzaki residual power series solution for the linear and nonlinear CRDE by the following procedure.

Step 1. Rewriting equation (2) as demonstrated:

$$\frac{\partial^{\varpi}\Phi(\chi,\Upsilon)}{\partial\Upsilon^{\varpi}} - \lambda\frac{\partial^2\Phi(\chi,\Upsilon)}{\partial\chi^2} - z(\chi,\Upsilon)\Phi(\chi,\Upsilon) = 0. \quad (54)$$

Step 2. Manipulating Elzaki transform at both sides of equation (54), we get in this way

$$E\left[\frac{\partial^{\varpi}\Phi(\chi,\Upsilon)}{\partial\Upsilon^{\varpi}}\right] - \lambda E\left[\frac{\partial^2\Phi(\chi,\Upsilon)}{\partial\chi^2}\right] - E\left[E^{-1}[Z(\chi,\upsilon)]E^{-1}[\Psi(\chi,\upsilon)]\right] = 0, \quad (55)$$

where

$$E^{-1}[Z(\chi, \upsilon)] = z(\chi, \Upsilon),$$
$$E^{-1}[\Psi(\chi, \upsilon)] = \Phi(\chi, \Upsilon), \tag{56}$$
$$E\left[\frac{\partial^{\varpi}\Phi(\chi, \Upsilon)}{\partial \Upsilon^{\varpi}}\right] = \frac{\Psi(\chi, \upsilon)}{\upsilon^{\varpi}} - \upsilon^{-\varpi+2} g(\chi).$$

So, we get the following form:

$$\Psi(\chi, \upsilon) = \upsilon^2 g(\chi) + \lambda \upsilon^{\varpi} D_{\chi\chi}\Psi(\chi, \upsilon) + \upsilon^{\varpi} E\left[E^{-1}[Z(\chi, \upsilon)]E^{-1}[\Psi(\chi, \upsilon)]\right]. \tag{57}$$

Step 3. Considering the solution of equation (57) as the following:

$$\Psi(\chi, \upsilon) = \sum_{n=0}^{\infty} \aleph_n(\chi)\upsilon^{2+n\varpi}. \tag{58}$$

Step 4. Setting $\aleph_0(\chi) = \lim_{\upsilon\longrightarrow\infty}(1/\upsilon^2)\Psi(\chi, \upsilon) = \Phi(\chi, 0)$.
Step 5. Establishing the kth-truncated series of $\Psi(\chi, \upsilon)$ as

$$\Psi_k(\chi, \upsilon) = \sum_{n=0}^{k} \aleph_n(\chi)\upsilon^{2+n\varpi},$$
$$\aleph_0 = \lim_{\upsilon\longrightarrow 0} \frac{1}{\upsilon^2}\Psi(\chi, \upsilon), \tag{59}$$
$$\Psi_k(\chi, \upsilon) = \aleph_0 \upsilon^2 + \sum_{n=1}^{k} \aleph_n(\chi)\upsilon^{2+n\varpi}.$$

Step 6. Considering the Elzaki residual function (ERF) of equation (57) and the kth-truncated ERF separately such that

$$E\mathrm{Res}(\chi, \upsilon) = \Psi(\chi, \upsilon) - \upsilon^2 g(\chi) - \lambda\upsilon^{\varpi} D_{\chi\chi}\Psi(\chi, \upsilon) - \upsilon^{\varpi} E\left[E^{-1}[Z(\chi, \upsilon)]E^{-1}[\Psi(\chi, \upsilon)]\right],$$
$$E\mathrm{Res}_k(\chi, \upsilon) = \Psi_k(\chi, \upsilon) - \upsilon^2 g(\chi) - \lambda\upsilon^{\varpi} D_{\chi\chi}\Psi_k(\chi, \upsilon) - \upsilon^{\varpi} E\left[E^{-1}[Z(\chi, \upsilon)]E^{-1}[\Psi_k(\chi, \upsilon)]\right]. \tag{60}$$

Step 7. Replacing the series form of $\Psi_k(\chi, \upsilon)$ into equation (60).

Step 8. Dividing at both sides of equation (60) with $\upsilon^{k\upsilon+2}$ as follows:

$$\frac{1}{\upsilon^{2+k\varpi}} E\mathrm{Res}_k(\chi, \upsilon) = \frac{1}{\upsilon^{2+k\varpi}}\Psi_k(\chi, \upsilon) - \frac{1}{\upsilon^{2+k\varpi}}\upsilon^2 g(\chi) - \lambda\frac{1}{\upsilon^{2+k\varpi}}\upsilon^{\varpi} D_{\chi\chi}\Psi_k(\chi, \upsilon) - \frac{1}{\upsilon^{2+k\varpi}}\upsilon^{\varpi} E\left[E^{-1}[Z(\chi, \upsilon)]E^{-1}[\Psi_k(\chi, \upsilon)]\right]. \tag{61}$$

Step 9. Taking limit at both sides of equation (61).

$$\lim_{\upsilon\longrightarrow 0}\frac{1}{\upsilon^{2+k\varpi}} E\mathrm{Res}_k(\chi, \upsilon) = \lim_{\upsilon\longrightarrow 0}\frac{1}{\upsilon^{2+k\varpi}}\Psi_k(\chi, \upsilon) - \lim_{\upsilon\longrightarrow 0}\frac{1}{\upsilon^{2+k\varpi}}\upsilon^2 g(\chi) - \lambda\lim_{\upsilon\longrightarrow 0}\frac{1}{\upsilon^{2+k\varpi}}\upsilon^{\varpi} D_{\chi\chi}\Psi_k(\chi, \upsilon) - \lim_{\upsilon\longrightarrow 0}\frac{1}{\upsilon^{2+k\varpi}}\upsilon^{\varpi} E\left[E^{-1}[Z(\chi, \upsilon)]E^{-1}[\Psi_k(\chi, \upsilon)]\right]. \tag{62}$$

Step 10. Solving the following equation for $\aleph_n(\chi)$:

$$\lim_{\upsilon\longrightarrow 0}\left(\frac{1}{\upsilon^{k\varpi+2}} E\mathrm{Res}_k(\chi, \upsilon)\right) = 0, \quad k = 1, 2, 3, \ldots. \tag{63}$$

Step 11. Replacing the attained values of $\aleph_n(\chi)$ into kth-truncated series of $\Psi(\chi, \upsilon)$ to get the kth-approximate solution of equation (57).

Step 12. Manipulating the inverse Elzaki transform on $\Psi_k(\chi, \upsilon)$ to attain the kth-approximate solution of $\Phi_k(\chi, \Upsilon)$ in the real space.

3.2. Applications to Linear and Nonlinear CRDEs. In this subsection, we consider three main problems of CRDEs to illustrate the execution and capability of ERPSM.

3.2.1. Approximate and Closed Form Solutions of Linear CRDEs. Two applications are considered for linear CRDEs.

Problem 1. Consider the time-fractional linear CRDE [19].

$$D_{\Upsilon}^{\varpi}\Phi(\chi, \Upsilon) = \Phi_{\chi\chi}(\chi, \Upsilon) - \Phi(\chi, \Upsilon), \quad \chi, \Upsilon \geq 0, \ 0 < \varpi \leq 1. \tag{64}$$

Subject to initial condition,

$$\Phi(\chi,0)=e^{-\chi}+\chi. \tag{65}$$

Solution. Utilizing Elzaki transform on equation (64),

$$E\left[D_\Upsilon^{\varpi}\Phi(\chi,\Upsilon)\right]=E\left[\Phi_{\chi\chi}(\chi,\Upsilon)\right]-E[\Phi(\chi,\Upsilon)], \tag{66}$$

where $E[\Phi(\chi,\Upsilon)]=\Psi(\chi,\upsilon)$,

$$E\left[D_\Upsilon^{\varpi}\Phi(\chi,\Upsilon)\right]=\frac{\Psi(\chi,\upsilon)}{\upsilon^{\varpi}}-\upsilon^{-\varpi+2}\Phi(\chi,0), \tag{67}$$

so equation (66) becomes as

$$\Psi(\chi,\upsilon)=\upsilon^2\Phi(\chi,0)+\upsilon^{\varpi}D_{\chi\chi}\Psi(\chi,\upsilon)-\upsilon^{\varpi}\Psi(\chi,\upsilon). \tag{68}$$

Initiate a series solution to the algebraic equation (68). Hence, presume that the expansion of $\Psi(\chi,\upsilon)$ is the following:

$$\Psi(\chi,\upsilon)=\sum_{n=0}^{\infty}\aleph_n(\chi)\upsilon^{2+n\varpi}. \tag{69}$$

Assume that $\Psi(\chi,\upsilon)$ has the kth-truncated series as

$$\Psi_k(\chi,\upsilon)=\sum_{n=0}^{k}\aleph_n(\chi)\upsilon^{2+n\varpi}. \tag{70}$$

By Lemma 2, we have

$$\lim_{\upsilon\longrightarrow 0}\frac{1}{\upsilon^2}\Psi(\chi,\upsilon)=\Phi(\chi,0)=e^{-\chi}+\chi. \tag{71}$$

The kth-truncated series becomes as follows:

$$\Psi_k(\chi,\upsilon)=\upsilon^2\left(e^{-\chi}+\chi\right)+\sum_{n=1}^{k}\aleph_n(\chi)\upsilon^{2+n\varpi}. \tag{72}$$

The ERF of the algebraic equation (68) is described as

$$E\text{Res}(\chi,\upsilon)=\Psi(\chi,\upsilon)-\upsilon^2\left(e^{-\chi}+\chi\right)-\upsilon^{\varpi}D_{\chi\chi}\Psi(\chi,\upsilon)+\upsilon^{\varpi}\Psi(\chi,\upsilon). \tag{73}$$

Furthermore, kth-truncated ERF of the algebraic equation (69) is explained as follows:

$$\begin{aligned}E\text{Res}_k(\chi,\upsilon)&=\Psi_k(\chi,\upsilon)-\upsilon^2\left(e^{-\chi}+\chi\right)\\&\quad-\upsilon^{\varpi}D_{\chi\chi}\Psi_k(\chi,\upsilon)+\upsilon^{\varpi}\Psi_k(\chi,\upsilon).\end{aligned} \tag{74}$$

By utilizing equations (72) and (74), we get undefined coefficients in the following form:

$$\begin{aligned}\aleph_1(\chi)&=-\chi,\\ \aleph_2(\chi)&=\chi,\\ \aleph_3(\chi)&=-\chi,\\ \aleph_4(\chi)&=\chi,\\ \aleph_5(\chi)&=-\chi.\end{aligned} \tag{75}$$

So, we get the 5th approximate solution of Elzaki transform of equation (68).

$$\Psi_5(\chi,\upsilon)=\frac{e^{-\chi}+\chi}{\upsilon^2}-\frac{\chi}{\upsilon^{2+\varpi}}+\frac{\chi}{\upsilon^{2+2\varpi}}-\frac{\chi}{\upsilon^{2+3\varpi}}+\frac{\chi}{\upsilon^{2+4\varpi}}-\frac{\chi}{\upsilon^{2+5\varpi}}. \tag{76}$$

Operating inverse Elzaki transform on both sides of equation (76), we get the 5th approximate solution of equation (64).

$$\Phi_5(\chi,\Upsilon)=e^{-\chi}+\chi\left(1-\frac{\Upsilon^{\varpi}}{\Gamma(\varpi+1)}+\frac{\Upsilon^{2\varpi}}{\Gamma(2\varpi+1)}-\frac{\Upsilon^{3\varpi}}{\Gamma(3\varpi+1)}+\frac{\Upsilon^{4\varpi}}{\Gamma(4\varpi+1)}-\frac{\Upsilon^{5\varpi}}{\Gamma(5\varpi+1)}\right). \tag{77}$$

When $\varpi=1$, equation (77) becomes as

$$\Phi_5(\chi,\Upsilon)=e^{-\chi}+\chi\left(1-\frac{\Upsilon}{1!}+\frac{\Upsilon^2}{2!}-\frac{\Upsilon^3}{3!}+\frac{\Upsilon^4}{4!}-\frac{\Upsilon^5}{5!}\right). \tag{78}$$

Equation (78) is coinciding with the six terms of the expansion of the exact solution $\Phi(\chi,\Upsilon)=e^{-\chi}+\chi e^{-\Upsilon}$.

Table 1 demonstrates the values of absolute error of the 5th order approximate and exact solutions at $\varpi=1$ when $\chi=1$ which support the capability and exactness of the novel technique.

Figure 1 displays the evaluations of exact solution at $\varpi=1$ and the 5th approximate solution of Problem 1, at $\chi=1$, for several values of Υ and ϖ. Figure 1 confirms that when values of ϖ approach to "1," the approximate solution approaches to the exact solution, which approves the efficacy and correctness of the new method. Moreover, the approximate solution overlaps with the exact solution at $\varpi=1$ and this once more ratifies the usefulness and correctness of the ERPSM.

Problem 2. Consider the time-fractional linear CRDE [20],

$$\begin{aligned}&D_\Upsilon^{\varpi}\Phi(\chi,\Upsilon)=\Phi_{\chi\chi}(\chi,\Upsilon)-\left(1+4\chi^2\right)\Phi(\chi,\Upsilon),\\&\chi,\Upsilon\geq 0,\ 0<\varpi\leq 1.\end{aligned} \tag{79}$$

With the initial condition,

$$\Phi(\chi,0)=e^{\chi^2}. \tag{80}$$

Solution. Manipulating Elzaki transform on equation (79),

Table 1: Absolute error of ERPS results.

Υ	Exact solution	Approximate solution	Absolute error
0	2.71828182846	2.71828182846	0
0.06	2.88637098927	2.88637098909	1.7766543792 × 10−10
0.12	3.06485420329	3.06485419182	1.1469452055 × 10−8
0.18	3.25437420289	3.2543740711	1.3178722424 × 10−7
0.24	3.45561346476	3.45561271778	7.4698766506 × 10−7
0.30	3.66929666762	3.66929379283	0.00000287478963168
0.36	3.8961933018	3.89618464113	0.00000866066429372
0.42	4.13712044025	4.13709840516	0.0000220350955411
0.48	4.39294568092	4.39289613873	0.044093686996

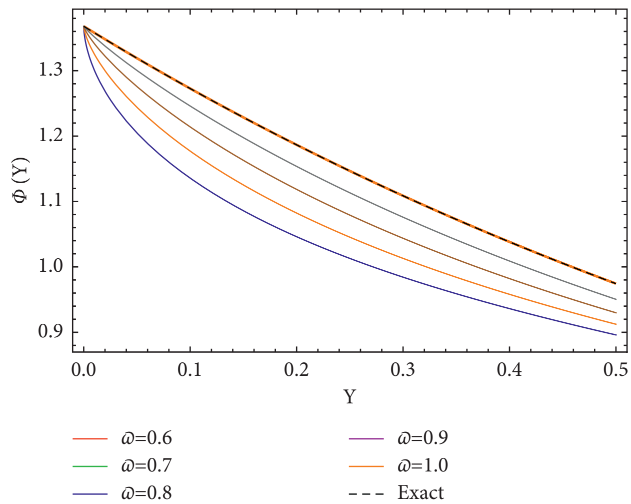

Figure 1: Evaluation of closed form and approximate consequences of Problem 1.

$$E\left[D_{\Upsilon}^{\varpi}\Phi(\chi,\Upsilon)\right] = E\left[\Phi_{\chi\chi}(\chi,\Upsilon)\right] - \left(1+4\chi^2\right)E[\Phi(\chi,\Upsilon)],$$
$$\Psi(\chi,\upsilon) = \upsilon^2 e^{\chi^2} + \upsilon^{\varpi} D_{\chi\chi}\Psi(\chi,\upsilon) - \upsilon^{\varpi}\left(1+4\chi^2\right)\Psi(\chi,\upsilon), \tag{81}$$

where

$$E\left[D_{\Upsilon}^{\varpi}\Phi(\chi,\Upsilon)\right] = \frac{\Psi(\chi,\upsilon)}{\upsilon^{\varpi}} - \upsilon^{-\varpi+2}e^{\chi^2},$$
$$E[\Phi(\chi,\Upsilon)] = \Psi(\chi,\upsilon). \tag{82}$$

Now, establishing a series solution of equation (81), consequently assume that $\Psi(\chi,\upsilon)$ has the expansion as follows:

$$\Psi(\chi,\upsilon) = \sum_{n=0}^{\infty} \aleph_n(\chi)\upsilon^{2+n\varpi}. \tag{83}$$

The kth-truncated series $\Psi(\chi,\upsilon)$ is as follows:

$$\Psi_k(\chi,\upsilon) = \sum_{n=0}^{k} \aleph_n(\chi)\upsilon^{2+n\varpi}. \tag{84}$$

By Lemma 2, we have

$$\lim_{\upsilon\longrightarrow 0}\frac{1}{\upsilon^2}\Psi(\chi,\upsilon) = \Phi(\chi,0) = e^{\chi^2}. \tag{85}$$

So, equation (84) becomes as

$$\Psi_k(\chi,\upsilon) = e^{\chi^2}\upsilon^2 + \sum_{n=1}^{k}\aleph_n(\chi)\upsilon^{2+n\varpi}. \tag{86}$$

The ERF of equation (81) is defined as

$$E\text{Res}(\chi,\upsilon) = \Psi(\chi,\upsilon) - \upsilon^2 e^{\chi^2} - \upsilon^{\varpi}D_{\chi\chi}\Psi(\chi,\upsilon) + \upsilon^{\varpi}\left(1+4\chi^2\right)\Psi(\chi,\upsilon). \tag{87}$$

The kth-ERF is as follows:

$$E\text{Res}_k(\chi,\upsilon) = \Psi_k(\chi,\upsilon) - \upsilon^2 e^{\chi^2} - \upsilon^{\varpi}D_{\chi\chi}\Psi_k(\chi,\upsilon) + \upsilon^{\varpi}\left(1+4\chi^2\right)\Psi_k(\chi,\upsilon). \tag{88}$$

To find unspecified coefficients using equations (86) and (88), so we have

$$\aleph_1(\chi) = e^{\chi^2},$$
$$\aleph_2(\chi) = e^{\chi^2},$$
$$\aleph_3(\chi) = e^{\chi^2}, \tag{89}$$
$$\aleph_4(\chi) = e^{\chi^2},$$
$$\aleph_5(\chi) = e^{\chi^2}.$$

The 5^{th} approximate solution of equation (81) in Elzaki transform form is

$$\Psi_5(\chi, v) = e^{\chi^2}\left(\frac{1}{v^2} + \frac{1}{v^{2+\varpi}} + \frac{1}{v^{2+2\varpi}} + \frac{1}{v^{2+3\varpi}} + \frac{1}{v^{2+4\varpi}} + \frac{1}{v^{2+5\varpi}}\right). \tag{90}$$

By applying inverse Elzaki transform on equation (90), we get the 5^{th} approximate solution of equation (79) as follows:

$$\Phi_5(\chi, \Upsilon) = e^{\chi^2}\left(1 + \frac{\Upsilon^{\varpi}}{\Gamma(\varpi+1)} + \frac{\Upsilon^{2\varpi}}{\Gamma(2\varpi+1)} + \frac{\Upsilon^{3\varpi}}{\Gamma(3\varpi+1)} + \frac{\Upsilon^{4\varpi}}{\Gamma(4\varpi+1)} + \frac{\Upsilon^{5\varpi}}{\Gamma(5\varpi+1)}\right). \tag{91}$$

When $\varpi = 1$, equation (91) becomes as

$$\Phi_5(\chi, \Upsilon) = e^{\chi^2}\left(1 + \frac{\Upsilon}{1!} + \frac{\Upsilon^2}{2!} + \frac{\Upsilon^3}{3!} + \frac{\Upsilon^4}{4!} + \frac{\Upsilon^5}{5!}\right). \tag{92}$$

Equation (92) represents the first six terms of the expansion of $e^{\chi^2+\Upsilon}$, so closed form solution of equation (79) is $e^{\chi^2+\Upsilon}$.

Table 2 demonstrates the values of absolute error of the 5^{th} order approximate and exact solutions at $\varpi = 1$ when $\chi = 1$, which support the capability and accuracy of the new technique.

Figure 2 demonstrates the exploits of exact solution at $\varpi = 1$ and the 5^{th} approximate solution of Problem 2, when $\chi = 1$ for numerous values of Υ and ϖ. The figure endorses that when values of ϖ approach to "1," the approximate solution approaches to exact solution, which supports the ability and precision of the new method. Moreover, the approximate solution overlaps with the exact solution at $\varpi = 1$ and this once more ratifies the usefulness and correctness of the ERPSM.

3.2.2. Approximate and Closed Form Solutions of Nonlinear CRDEs

Problem 3. Consider the nonlinear time-fractional CRDE [21],

$$\begin{aligned} D_{\Upsilon}^{\varpi}\Phi(\chi, \Upsilon) &= \Phi_{\chi\chi}(\chi, \Upsilon) - \Phi_{\chi}(\chi, \Upsilon) + \Phi(\chi, \Upsilon)\Phi_{\chi\chi}(\chi, \Upsilon) \\ &\quad - \Phi^2(\chi, \Upsilon) + \Phi(\chi, \Upsilon), \quad \chi, \Upsilon \geq 0,\ 0 < \varpi \leq 1, \end{aligned} \tag{93}$$

With the initial condition,

$$\Phi(\chi, 0) = e^{\chi}. \tag{94}$$

Solution. By applying Elzaki transform on equation (93), we get

$$\begin{aligned} \Psi(\chi, v) &= v^2 e^{\chi} + v^{\varpi} D_{\chi\chi}\Psi(\chi, v) - v^{\varpi} D_{\chi}\Psi(\chi, v) \\ &\quad + v^{\varpi} E\left[E^{-1}[\Psi(\chi, v)] D_{\chi\chi} E^{-1}[\Psi(\chi, v)]\right] \\ &\quad - v^{\varpi} E\left[\left[E^{-1}\Psi(\chi, v)\right]^2\right] + v^{\varpi}\Psi(\chi, v). \end{aligned} \tag{95}$$

Here,

$$\begin{aligned} E\left[\Phi_{\chi\chi}(\chi, \Upsilon)\right] &= D_{\chi\chi}\Psi(\chi, v), \\ E\left[\Phi_{\chi}(\chi, \Upsilon)\right] &= D_{\chi}\Psi(\chi, v), \\ \Phi(\chi, \Upsilon) &= E^{-1}[\Psi(\chi, v)], \\ \Phi^2(\chi, \Upsilon) &= \left[E^{-1}[\Psi(\chi, v)]\right]^2, \\ \Phi_{\chi\chi}(\chi, \Upsilon) &= D_{\chi\chi}E^{-1}[\Psi(\chi, v)], \\ E\left[D_{\Upsilon}^{\varpi}\Phi(\chi, \Upsilon)\right] &= \frac{\Psi(\chi, v)}{v^{\varpi}} - v^{-\varpi+2}e^{\chi}. \end{aligned} \tag{96}$$

Define a series solution of equation (95) as follows:

$$\Psi(\chi, v) = \sum_{n=0}^{\infty} \aleph_n(\chi) v^{2+n\varpi}. \tag{97}$$

The kth-truncated series is

$$\Psi_k(\chi, v) = \sum_{n=0}^{k} \aleph_n(\chi) v^{2+n\varpi}. \tag{98}$$

By Lemma 2,

$$\lim_{v \longrightarrow 0} \frac{1}{v^2}\Psi(\chi, v) = \Phi(\chi, 0) = e^{\chi}. \tag{99}$$

Therefore, the kth-truncated series becomes as

$$\Psi_k(\chi, v) = e^{\chi}v^2 + \sum_{n=1}^{k} \aleph_n(\chi) v^{2+n\varpi}. \tag{100}$$

Now, define ERF in the following form:

$$\begin{aligned} E\mathrm{Res}(\chi, v) &= \Psi(\chi, v) - v^2 e^{\chi} - v^{\varpi} D_{\chi\chi}\Psi(\chi, v) + v^{\varpi} D_{\chi}\Psi(\chi, v) \\ &\quad - v^{\varpi} E\left[E^{-1}[\Psi(\chi, v)] D_{\chi\chi} E^{-1}[\Psi(\chi, v)]\right] \\ &\quad + v^{\varpi} E\left[\left[E^{-1}\Psi(\chi, v)\right]^2\right] - v^{\varpi}\Psi(\chi, v). \end{aligned} \tag{101}$$

The kth-truncated ERF is

Table 2: Absolute error of ERPS results.

Υ	Exact solution	Approximate solution	Absolute error
0.00	1.36787944117	1.36787944117	0.0
0.06	1.30964397476	1.30964397469	7 × 10−11
0.12	1.25479987789	1.25479987381	4.08 × 10−9
0.18	1.20314965258	1.20314960653	4.605 × 10−8
0.24	1.15450730224	1.15450704565	2.5659 × 10−7
0.30	1.10869766185	1.10869669117	9.7068 × 10−7
0.36	1.06555576724	1.06555289269	0.00000287455
0.42	1.02492626099	1.02491907181	0.00000718918
0.48	0.98666283297	0.98664694453	0.000015888447

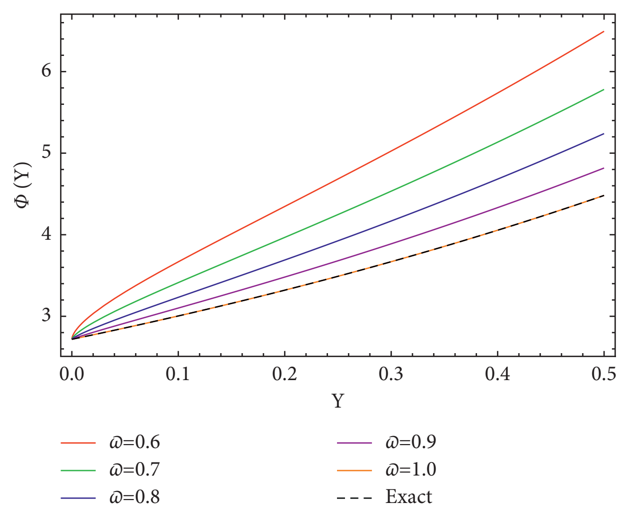

Figure 2: The behavior of exact and approximate outcomes of Problem 2.

$$\begin{aligned} ERes_k(\chi, \upsilon) &= \Psi_k(\chi, \upsilon) - \upsilon^2 e^\chi - \upsilon^\varpi D_{\chi\chi}\Psi_k(\chi, \upsilon) \\ &+ \upsilon^\varpi D_\chi \Psi_k(\chi, \upsilon) \\ &- \upsilon^\varpi E\left[E^{-1}\left[\Psi_k(\chi, \upsilon)\right] D_{\chi\chi} E^{-1}\left[\Psi_k(\chi, \upsilon)\right]\right] \\ &+ \upsilon^\varpi E\left[\left[E^{-1}\Psi_k(\chi, \upsilon)\right]^2\right] - \upsilon^\varpi \Psi_k(\chi, \upsilon). \end{aligned} \tag{102}$$

The undefined coefficients are determined in the following form by utilizing equations (100) and (102).

$$\begin{aligned} \aleph_1(\chi) &= e^\chi, \\ \aleph_2(\chi) &= e^\chi, \\ \aleph_3(\chi) &= e^\chi, \\ \aleph_4(\chi) &= e^\chi, \\ \aleph_5(\chi) &= e^\chi. \end{aligned} \tag{103}$$

The 5$^{\text{th}}$ approximate solution of equation (95) is given as

$$\Psi_5(\chi, \upsilon) = e^\chi \left(\frac{1}{\upsilon^2} + \frac{1}{\upsilon^{2+\varpi}} + \frac{1}{\upsilon^{2+2\varpi}} + \frac{1}{\upsilon^{2+3\varpi}} + \frac{1}{\upsilon^{2+4\varpi}} + \frac{1}{\upsilon^{2+5\varpi}} \right). \tag{104}$$

By applying inverse Elzaki transform on the above equation, we get the 5$^{\text{th}}$ approximate solution of equation (93).

$$\Phi_5(\chi, \Upsilon) = e^\chi \left(1 + \frac{\Upsilon^\varpi}{\Gamma(\varpi + 1)} + \frac{\Upsilon^{2\varpi}}{\Gamma(2\varpi + 1)} + \frac{\Upsilon^{3\varpi}}{\Gamma(3\varpi + 1)} + \frac{\Upsilon^{4\varpi}}{\Gamma(4\varpi + 1)} + \frac{\Upsilon^{5\varpi}}{\Gamma(4\varpi + 1)} \right). \tag{105}$$

For $\varpi = 1$, the last equation becomes as

Table 3: Absolute error of ERPS results.

Υ	Exact solution	Approximate solution	Absolute error
0.00	1.36787944117	1.36787944117	0.0
0.06	1.30964397476	1.30964397469	$7\times 10-11$
0.12	1.25479987789	1.25479987381	$4.08\times 10-9$
0.18	1.20314965258	1.20314960653	$4.605\times 10-8$
0.24	1.15450730224	1.15450704565	$2.5659\times 10-7$
0.30	1.10869766185	1.10869669117	$9.7068\times 10-7$
0.36	1.06555576724	1.06555289269	0.00000287455
0.42	1.02492626099	1.02491907181	0.00000718918
0.48	0.98666283297	0.98664694453	0.000015888447

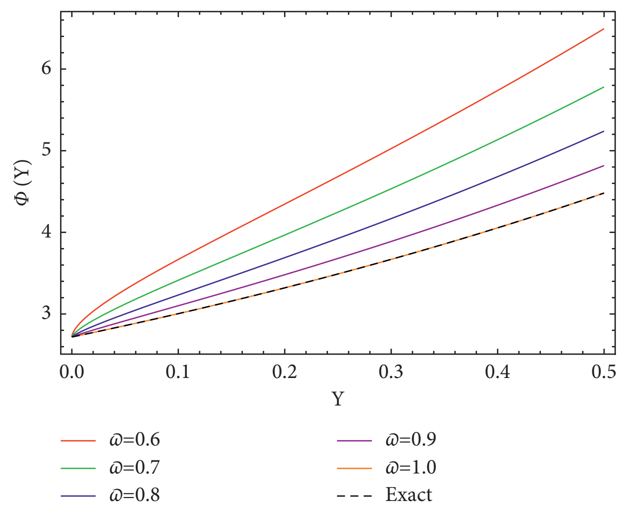

Figure 3: 2D plot of exact and approximate solution of Problem 3.

$$\Phi_5(\chi,\Upsilon) = e^{\chi}\left(1 + \frac{\Upsilon}{1!} + \frac{\Upsilon^2}{2!} + \frac{\Upsilon^3}{3!} + \frac{\Upsilon^4}{4!} + \frac{\Upsilon^5}{5!}\right). \tag{106}$$

Equation (106) coincides with the 1^{st} six terms of the expansion of $e^{\chi+\Upsilon}$, therefore exact solution of equation (93) is $e^{\chi+\Upsilon}$.

Table 3 demonstrates the values of absolute error of the 5^{th} order approximate and exact results at $\varpi = 1$, and $\chi = 1$, which support the ability and accuracy of the novel technique.

Figure 3 establishes the actions of exact solution at $\varpi = 1$ and the 5^{th} approximate solution of Problem 3, when $\chi = 1$ for certain values of Υ and ϖ. The figure recommends that when values of ϖ approach to "1," the approximate solution approaches to exact solution, which supports the capability and exactness of the new method. Moreover, the approximate solution overlaps with the exact solution at $\varpi = 1$ and this once more ratifies the usefulness and correctness of the ERPSM.

4. Conclusions

There are enormous number of numerical and analytical methods for resolving the DEs; there are numerous methods that have superiority over the others. Few of them are precise and operative, but they necessitate mathematical operations that can be problematic and elongated. Our novel method, ERPSM, is considered by accurateness, rapidity, and effortlessness in finding exact and approximate solutions to DEs.

To study the efficiency and reliability of ERPSM for PDEs, absolute errors of three applications are scrutinized. Consequences verify that our novel technique is simple, accurate, applicable, and efficient. The recommended techniques offered us an effortless and quick technique to perceive the coefficients of the suggested series to be a solution to the equation. Dissimilar to the traditional RPS method, while establishing the coefficients for a series, it is required to compute the fractional derivative every time, while ERPSM only requires the concept of the limit at zero in establishing the coefficients for the series.

The gain of the ERPSM is that it decreases considerably the numerical calculations to construct the consequences for this category of equations related to existing methods, for instance, the differential transform method (DTM), perturbation method, and Adomian decomposition method (ADM). Consequently, we can accomplish that the ERPSM is effortless, effective, and practical for solving numerous further fractional order PDEs.

Data Availability

No data were used to support this study.

Conflicts of Interest

The authors declare that they have no conflicts of interest.

References

[1] S. Kumar, A. Ahmadian, R. Kumar et al., "An efficient numerical method for fractional SIR epidemic model of infectious disease by using Bernstein wavelets," *Mathematics*, vol. 8, no. 4, pp. 558–570, 2020.

[2] A. Khalouta and A. Kadem, "A comparative study of Shehu variational iteration method and Shehu decomposition method for solving nonlinear Caputo time-fractional wave-like equations with variable coefficients," *Applications and Applied Mathematics: International Journal*, vol. 15, no. 1, pp. 24–41, 2020.

[3] K. M. Saad, M. M. Khader, J. F. Gómez-Aguilar, and D. Baleanu, "Numerical solutions of the fractional Fisher's type equations with Atangana-Baleanu fractional derivative by using spectral collocation methods," *Chaos: An Interdisciplinary Journal of Nonlinear Science*, vol. 29, no. 2, pp. 101–122, 2019.

[4] P. T. Toan, T. N. Vo, and M. Razzaghi, "Taylor wavelet method for fractional delay differential equations," *Engineering with Computers*, vol. 37, no. 1, pp. 231–240, 2021.

[5] A. Saadatmandi and M. Dehghan, "A new operational matrix for solving fractional-order differential equations," *Computers & Mathematics with Applications*, vol. 59, no. 3, pp. 1326–1336, 2010.

[6] A. Khalouta and A. Kadem, "Fractional natural decomposition method for solving a certain class of nonlinear time-fractional wave-like equations with variable coefficients," *Acta Universitatis Sapientiae, Mathematica*, vol. 11, no. 1, pp. 99–116, 2019.

[7] V. Gupta and S. Gupta, "Application of homotopy analysis method for solving nonlinear Cauchy problem," *Surveys in Mathematics and its Applications*, vol. 7, no. 1, pp. 105–116, 2012.

[8] R. I. Nuruddeen and A. M. Nass, "Aboodh decomposition method and its application in solving linear and nonlinear heat equations," *European Journal of Advances in Engineering and Technology*, vol. 3, no. 7, pp. 34–37, 2016.

[9] H. Eltayeb and E. Abdeldaim, "Sumudu decomposition method for solving fractional delay dierential equations," *Research in Applied Mathematics*, vol. 1, no. 1, pp. 1–13, 2017.

[10] J. Ul Rahman, D. Lu, M. Suleman, J. H. He, and M. Ramzan, "He–Elzaki method for spatial diffusion of biological population," *Fractals*, vol. 27, no. 5, pp. 112–121, 2019.

[11] S. Momani, O. Abu Arqub, M. m. Abu Hammad, and Z. S. Abo-Hammour, "A residual power series technique for solving systems of initial value problems," *Applied Mathematics & Information Sciences*, vol. 10, no. 2, pp. 765–775, 2016.

[12] M. Delkhosh and K. Parand, "Generalized pseudospectral method: theory and applications," *Journal of Computational Science*, vol. 34, pp. 11–32, 2019.

[13] K. Parand and M. Delkhosh, "An effective numerical method for solving the nonlinear singular Lane-Emden type equations of various orders," *Jurnal Teknologi*, vol. 79, no. 1, 2017.

[14] R. Shah, H. Khan, S. Mustafa, P. Kumam, and M. Arif, "Analytical solutions of fractional-order diffusion equations by natural transform decomposition method," *Entropy*, vol. 21, no. 6, pp. 557–570, 2019.

[15] H. Ahmad, T. A. Khan, I. Ahmad, P. S. Stanimirović, and Y. M. Chu, "A new analyzing method for nonlinear time fractional Cauchy reaction-diffusion model equations," *Results in Physics*, vol. 19, no. 8, pp. 462–474, 2020.

[16] N. F. Britton, *Reaction–Diffusion Equations and Their Applications to Biology*, Academic Press, New York, NY, USA, 1998.

[17] R. S. Cantrell and C. Cosner, *Spatial Ecology via Reaction–Diffusion Equations. Wiley Series in Mathematical and Computational Biology*, Wiley, New York, NY, USA, 2003.

[18] P. Grindrod, *The Theory and Applications of Reaction–Diffusion Equations*, Oxford University Press, Oxford, UK, 2nd edition, 1996.

[19] H. Gul, H. Alrabaiah, S. Ali, K. Shah, and S. Muhammad, "Computation of solution to fractional order partial reaction diffusion equations," *Journal of Advanced Research*, vol. 25, no. 19, pp. 31–38, 2020.

[20] M. S. H. Chowdhury and I. Hashim, "Analytical solution for Cauchy reaction-diffusion problems by homotopy perturbation method," *Sains Malaysiana*, vol. 39, no. 3, pp. 495–504, 2010.

[21] S. Ali, S. Bushnaq, K. Shah, and M. Arif, "Numerical treatment of fractional order Cauchy reaction diffusion equations," *Chaos, Solitons & Fractals*, vol. 103, no. 12, pp. 578–587, 2017.

[22] K. Wang and S. Liu, "A new Sumudu transform iterative method for time-fractional Cauchy reaction–diffusion equation," *Springer Plus*, vol. 5, no. 1, pp. 1–20, 2016.

[23] S. Kumar, A. Kumar, S. Abbas, M. Al Qurashi, and D. Baleanu, "A modified analytical approach with existence and uniqueness for fractional Cauchy reaction–diffusion equations," *Advances in Difference Equations*, vol. 2020, no. 1, 13 pages, 2020.

[24] K. Hosseini, M. Ilie, M. Mirzazadeh, and D. Baleanu, "An analytic study on the approximate solution of a nonlinear time-fractional Cauchy reaction-diffusion equation with the Mittag-Leffler law," *Mathematical Methods in the Applied Sciences*, vol. 44, no. 8, pp. 6247–6258, 2021.

[25] S. A. Lima, M. Kamrujjaman, and M. S. Islam, "Numerical solution of convection–diffusion–reaction equations by a finite element method with error correlation," *AIP Advances*, vol. 11, no. 8, pp. 85–98, 2021.

[26] T. M. Elzaki, "The new integral transform Elzaki transform," *Global Journal of Pure and Applied Mathematics*, vol. 7, no. 1, pp. 57–64, 2011.

Hindawi
Journal of Mathematics
Volume 2021, Article ID 3920937, 10 pages
https://doi.org/10.1155/2021/3920937

Research Article

Dynamic Response Analysis of a Forced Fractional Viscoelastic Beam*

Kenan Yildirim [1] **and Sertan Alkan** [2]

[1] *Mus Alparslan University, Merkez, Mus, Turkey*
[2] *Iskenderun Technical University, İskenderun, Hatay, Turkey*

Correspondence should be addressed to Kenan Yildirim; k.yildirim@alparslan.edu.tr

Received 3 September 2021; Revised 12 November 2021; Accepted 4 December 2021; Published 15 December 2021

Academic Editor: Fairouz Tchier

In this paper, dynamic response analysis of a forced fractional viscoelastic beam under moving external load is studied. The beauty of this study is that the effect of values of fractional order, the effect of internal damping, and the effect of intensity value of the moving force load on the dynamic response of the beam are analyzed. Constitutive equations for fractional order viscoelastic beam are constructed in the manner of Euler–Bernoulli beam theory. Solution of the fractional beam system is obtained by using Bernoulli collocation method. Obtained results are presented in the tables and graphical forms for two different beam systems, which are polybutadiene beam and butyl B252 beam.

1. Introduction

Theory and applications of beams are very important research area due to its wide usage areas in applied sciences. Especially after starting the space adventure of the mankind, the demand to more resistant structures has great importance. Beams are generally modeled based on Euler–Bernoulli beam theory, which is called classical beam theory. The background of beam theory goes on Newton's second law and some different aspects of beams, such as modeling, analysis of bending-buckling, and reinforcement and control, are hot topics of research papers since the beginning of the nineteenth century. The books can provide a general overview about the Euler–Bernoulli beam theory, please see [1–3]. Some important studies related to beams modeled in the sense of classical beam theory are also summarized as follows, but not limited to [4–15]. The beam systems in [1–15] have the integer order derivatives of the state function. In the beginning of 1930s, fractional derivative was introduced for describing the constitutive relation of some beam materials [16], and after 1980s, since fractional order equations have good memory and can be used to describe material properties more accurately with fewer parameters, they are considered to be good mathematical models for describing the dynamic mechanical behavior of materials [17]. In [18], the dynamic behavior of the thin plates resting on a fractionally damped viscoelastic foundation subjected to a moving point load is investigated and results show that the damping of the foundation system increases with increasing the order of the fractional derivative, which leads to a decrease in the dynamic response. In [19], the dynamic response spectra of fractionally damped viscoelastic beams subjected to concentrated moving load are presented and results reveal that with an increase in the order of the fractional derivative, the system damping of the system increases and the dynamic amplification factor (DAF) decreases, especially in the dynamic zone of the sweep parameter. In [20], the precise integration method (PIM) is extended to numerically integrate the equation of motion with fractional terms, which offers high accuracy and obtained numerical results indicate the viscoelastic dampers can enhance the seismic performance of structures significantly. In [21], the nonstationary free vibration and nonlinear dynamic behavior of the viscoelastic nanoplates are analyzed. Obtained results show that the viscoelastic model-based vibration is nonstationary unlike the elastic model.

Moreover, the damping mechanism of the viscoelasticity is amplitude dependent and the contribution of the viscoelastic damping terms at higher forcing conditions becomes noticeable. On the other hand, several numerical methods are developed and employed for better analyzing the fractional mechanical systems. Widely used methods for fractional systems are finite element method [22], Galerkin method [23], variational iteration method [24], and multiscale method [25, 26]. Especially, papers existing in the literature, which include a solution method for analyzing the dynamic response of a fractional order beam system, can be shortly listed as [19, 27–30]. In [19], the authors combined Galerkin method and Newton–Raphson method for analyzing the vibration of a fractional beam equation and they compared the results for only seeing the effects of fractional or integer derivatives. In [27], the author considered the dynamic response analyzing of a fractional order viscoelastic beam by means of green function method. In [27], the author only compared the results based on changes on the fractional derivative between $(0, 1)$. In [28], the authors employed the Adomian decomposition method for solving a fractional beam equation and they only observed the effect of the order of fractional derivative. In [29], the authors used the dynamic green function method for analyzing the dynamic response in a fractional beam equation and the beam equation does not include the damping term. Results are simulated for only indicating the effects of order of fractional derivative. In [30], the author employed the green function method for a fractional viscoelastic beam system subjected to a base excitation. After obtaining the solution, the author compared the results corresponding to different fractional order derivative. By comparing the present study with the studies existing in the literature, objectives of the present study are expressed as follows:

(i) In this paper, Bernoulli collocation method is firstly employed for analyzing the fractional viscoelastic beam equation. In the literature, especially for the fractional beam systems, green function method, Galerkin method, Newton–Raphson method, Adomian decomposition method, and Bernoulli collocation method in this paper were used, but by comparing these five methods, it is clear that Bernoulli collocation method is new and has less computational process and less work.

(ii) In the literature, the authors only considered and discussed the effects of order of fractional derivative on the dynamic response. But, we discussed both the effects of the order of fractional order derivative and the effects of damping coefficient term and the effect of density of moving force load. So, it is said that the present study has wider perspective than other studies.

(iii) Also, in the literature, results are obtained for one beam system. In this paper, effects of order of fractional derivative, effects of damping coefficient term, and the effect of density of moving force load are observed and compared for two different beam systems which are polybutadiene beam and butyl B252 beam.

For theoretical and experimental review about the fractional Euler–Bernoulli beams, please see [31]. Specifically, in the present paper, displacement analysis of a forced fractional viscoelastic beam is studied. External moving force load perfectly moves on the beam with the velocity $v(t)$ from the left edge to the right edge of the beam. The solution of the fractional beam system is obtained by means of Bernoulli collocation method. The main advantage of the Bernoulli collocation method is that employing the Bernoulli polynomials is easier than Chebyshev, Bessel polynomials, and Haar wavelets [32–34]. These advantages of Bernoulli polynomials provide us for obtaining the solution by making less computational process in shorter time. In the step of employing the Bernoulli collocation method, some external moving force loads having different load intensities are considered and also the effects of internal damping and fractional order of the derivative are searched for a fractional beam system. In the simulations, two different beam systems, which are polybutadiene beam and butyl B252 beam, are taken into account for being compared each other in the aspects of internal damping effects and resistance to effect of external moving force. Comparison results of the beam systems are presented in tables and graphics. The rest of the paper is organized as follows: in the next section, definition of the displacement analysis problem for a fractional viscoelastic beam is presented and scheme of the beam is overviewed. In the third section, short definition of the fractional derivative in the Caputo sense is introduced. In the fourth section, Bernoulli collocation method is explained and adopted to the present problem. In the fifth section, obtained results are given and discussions are made in the light of employing the Bernoulli collocation method to fractional viscoelastic beam system.

2. Definition of the Problem

The motion equation of the fractional viscoelastic homogeneous beam is obtained by considering the Euler–Bernoulli beam theory by ignoring shear deformation factor and rotary inertia of the beam. The beam is considered as a uniform viscoelastic beam and mechanical energy dissipation inside the beam is modeled by fractional order differential equations. By taking into account the [35], stress-strain constitutive relation of a fractional viscoelastic beam is given as follows:

$$\sigma = E\varepsilon(t) + E'_{\gamma} D_t^{\gamma} [\varepsilon(t)] = E\left(\varepsilon + \mu_{\gamma} \frac{d^{\gamma}\varepsilon(t)}{\mathrm{d}t^{\gamma}}\right), \tag{1}$$

in which E is the Young's modulus of the viscoelastic beam, μ_γ is the damping coefficient, and D_t^γ is the fractional derivative operator with the order γ with respect to t. The simply supported viscoelastic beam initially is at rest and nondeformed. The beam is subjected to a horizontally moving constant force load with the velocity $v(t)$ from the left edge to right edge of the beam, respect to x axis. In the light of [27], let us introduce the formulation of a fractional viscoelastic beam structure illustrated in Figure 1.

$$A\rho \frac{\partial^2 w(t,x)}{\partial t^2} + \mathrm{EI}\mu_\gamma \left[\frac{d^\gamma}{dt^\gamma}\frac{\partial^4 w(t,x)}{\partial x^4}\right] + \mathrm{EI}\frac{\partial^4 w(t,x)}{\partial x^4} = P\delta(x - v(t)), \quad (2)$$

in which w is the deflection of the viscoelastic beam in $\mathscr{C} = \{(t,x): t \in (0,\mathrm{tf}), x \in (0,\ell)\}$, t is the time variable, t_f is the final time observed duration, x is the space variable, ℓ is the length of the viscoelastic beam, A is the cross-section area of the structure, ρ is the material mass density of the viscoelastic beam, I is the axial moment of inertia of the beam, P is a constant showing intensity of the external moving force load, δ is the Dirac-delta function, and $v(t)$ is the velocity of the moving force load with the condition $0 \le v(t) \le \ell$. Equation (2) is subjected to the following boundary conditions:

$$w(t,x) = 0,\ w_{xx}(t,x) = 0 \text{ at } x = 0,\ell, \quad (3)$$

and the following initial conditions:

$$w(t,x) = w_0(x),\ w_t(t,x) = w_1(x) \text{ at } t = 0, \quad (4)$$

in which $w_0(x) \in H^1(0,\ell) = \{w_0(x) \in L^2(0,\ell): \partial w_0(x)/\partial x \in L^2(0,\ell)\}$, $w_1(x) \in L^2(0,\ell)$. $L^2(\mathscr{C})$ means to square-integrable functions space in the manner of Hilbert in the domain $\mathscr{C}$ in the Lebesgue sense with the following norm and inner product:

$$\|\eta\|^2 = <\eta,\eta>, \quad <\eta,\rho>_{\mathscr{C}} = \int_{\mathscr{C}} \rho\eta \, d\mathscr{C}. \quad (5)$$

Let us assume that

$$w(t,x) = \sum_{n=1}^{N} z_n(t)\sqrt{2}\sin\left(\frac{n\pi x}{\ell}\right). \quad (6)$$

After substituting the equations (6) into (2) and multiplying both sides of equation (2) with $\sqrt{2}\sin(n\pi x/\ell)$, integrating on $(0,\ell)$, we obtain the following ordinary differential equation as follows:

$$A\rho z_n''(t) + \mathrm{EI}(n\pi)^4\mu_\gamma\left[\frac{d^\gamma}{\mathrm{d}t^\gamma} z_n(t)\right] + \mathrm{EI}(n\pi)^4 z_n(t) = P\sqrt{2}\sin\left(\frac{n\pi v(t)}{\ell}\right), \quad n = 1,\ldots,N. \quad (7)$$

Equation (7) is subjected to the following initial conditions:

$$z_n(0) = \sqrt{2}\int_0^\ell w_0(x)\sin\left(\frac{n\pi x}{\ell}\right)\mathrm{d}x, \quad z_n'(0) = \sqrt{2}\int_0^\ell w_1(x)\sin\left(\frac{n\pi x}{\ell}\right)\mathrm{d}x. \quad (8)$$

3. The Fractional Derivative in the Caputo Sense

Definition. The Caputo definition of the fractional-order derivative is

$$D^\gamma f(x) = \frac{1}{\Gamma(n-\gamma)}\int_0^x \frac{f^{(n)}(t)}{(x-t)^{\gamma+1-n}}\mathrm{d}t, \quad n-1 < \gamma \le n,\ n \in \mathbb{N}, \quad (9)$$

where $\gamma > 0$ is the order of the derivative and n is the smallest integer greater than γ. For the Caputo derivative, we have

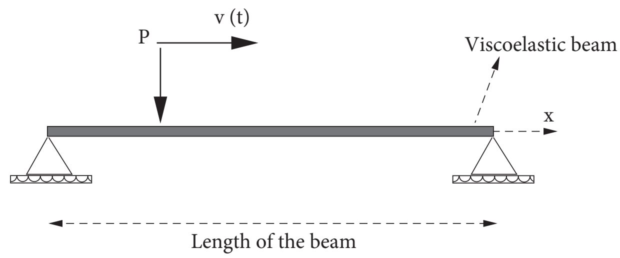

Figure 1: Schematic of the viscoelastic beam under moving force load P with the velocity $v(t)$.

$$D^{\gamma}C = 0, \quad C \text{ is constant},$$
$$D^{\gamma}x^{q} = \begin{cases} 0, & \text{for } q \in \mathbb{N}_0 \text{ and } q < \lceil \gamma \rceil, \\ \dfrac{\Gamma(q+1)}{\Gamma(q+1-\gamma)} x^{q-\gamma}, & \text{for } q \in \mathbb{N}_0 \text{ and } q \geq \lceil \gamma \rceil \text{ or } q \notin \mathbb{N} \text{ and } q > \lfloor \gamma \rfloor. \end{cases} \tag{10}$$

4. Bernoulli Collocation Method

The recurrence relation of the Bernoulli polynomials is defined by

$$B_n(x) = 2xB_{n-1}(x) + B_{n-2}(x). \tag{11}$$

For $n \geq 3.$, $B_1(x) = 1$, $B_2(x) = 2x$. The first few Bernoulli polynomials are

$$B_1(x) = 1, \tag{12}$$

$$\begin{aligned} B_2(x) &= x - \frac{1}{2}, \\ B_3(x) &= x^2 - x - \frac{1}{6}, \\ B_4(x) &= x^3 - \frac{3}{2}x^2 + \frac{x}{2}. \\ &\vdots \end{aligned} \tag{13}$$

Our goal is to get the approximate solution as the truncated Bernoulli series defined by

$$y(x) = \sum_{n=1}^{N+1} c_n B_n(x), \tag{14}$$

where $B_n(x)$ denotes the Bernoulli polynomials; $c_n\,(1 \leq n \leq N+1)$ are the unknown coefficients for Bernoulli polynomial, and N is any positive integer which possess $N \geq m$. Let us assume that linear combination of Bernoulli polynomials equation (14) is an approximate solution of equation (7). Our purpose is to determine the matrix forms of equation (7) by using (14). Firstly, we can write Bernoulli polynomials (12) in the matrix form

$$\mathbf{B}(x) = \mathbf{T}(x)\mathbf{M}, \tag{15}$$

where $B(x) = [B_1(x)\, B_2(x) \cdots B_{N+1}(x)]$, $\mathbf{T}(x) = (1\; x\; x^2\; x^3 \ldots x^N)$, $\mathbf{C} = (c_1\, c_2 \cdots c_{N+1})^T$, and

$$\mathbf{M} = \begin{pmatrix} 1 & -\frac{1}{2} & \frac{1}{6} & 0 & -\frac{1}{30} & 0 & \frac{1}{42} & 0 & -\frac{1}{30} \\ 0 & 1 & -1 & \frac{1}{2} & 0 & -\frac{1}{6} & 0 & \frac{1}{6} & 0 \\ 0 & 0 & 1 & -\frac{3}{2} & 1 & 0 & -\frac{1}{2} & 0 & \frac{2}{3} \\ 0 & 0 & 0 & 1 & -2 & \frac{5}{3} & 0 & -\frac{7}{6} & 0 \\ 0 & 0 & 0 & 0 & 1 & -\frac{5}{2} & \frac{5}{2} & 0 & -\frac{7}{3} \\ 0 & 0 & 0 & 0 & 0 & 1 & -3 & \frac{7}{2} & 0 \\ 0 & 0 & 0 & 0 & 0 & 0 & 1 & -\frac{7}{2} & \frac{14}{3} \\ 0 & 0 & 0 & 0 & 0 & 0 & 0 & 1 & -4 \\ 0 & 0 & 0 & 0 & 0 & 0 & 0 & 0 & 1 \end{pmatrix}. \tag{16}$$

The matrix form of equation (14) by a truncated Bernoulli series is given by

$$y(x) = \mathbf{B}(x)\mathbf{C}. \tag{17}$$

By using equations (15) and (17), the matrix relation is expressed as

$$\begin{aligned} y(x) &\cong y_N(x) = \mathbf{T}(x)\mathbf{MC}, \\ y^{(\gamma)}(x) &\cong y_N^{(\gamma)}(x) = \mathbf{T}(x)\mathbf{X}_{(\gamma)}(x)\mathbf{D}_{(\gamma)}\mathrm{MC}, \\ y''(x) &\cong y_N''(x) = \mathbf{T}(x)\mathbf{D}^2\mathbf{MC}, \end{aligned} \tag{18}$$

where

$$\mathbf{X}_{(\gamma)}(x) = \left[0, x^{1-\gamma}, x^{2-\gamma}, \ldots, x^{N-\gamma}\right], \quad (19)$$

$$\mathbf{D} = \begin{bmatrix} 0 & 1 & 0 & 0 & 0 & 0 & \cdots & 0 \\ 0 & 0 & 2 & 0 & 0 & 0 & \cdots & 0 \\ 0 & 0 & 0 & 3 & 0 & 0 & \cdots & 0 \\ 0 & 0 & 0 & 0 & 4 & 0 & \cdots & 0 \\ 0 & 0 & 0 & 0 & 0 & 5 & \cdots & 0 \\ 0 & 0 & 0 & 0 & 0 & 0 & \cdots & 0 \\ \vdots & \vdots & \vdots & \vdots & \vdots & \ddots & \ddots & N \\ 0 & 0 & 0 & 0 & 0 & 0 & \cdots & 0 \end{bmatrix}, \mathbf{D}^0 = \begin{bmatrix} 1 & 0 & 0 & 0 & 0 & 0 & \cdots & 0 \\ 0 & 1 & 0 & 0 & 0 & 0 & \cdots & 0 \\ 0 & 0 & 1 & 0 & 0 & 0 & \cdots & 0 \\ 0 & 0 & 0 & 1 & 0 & 0 & \cdots & 0 \\ 0 & 0 & 0 & 0 & 1 & 0 & \cdots & 0 \\ 0 & 0 & 0 & 0 & 0 & 1 & \cdots & 0 \\ \vdots & \vdots & \vdots & \vdots & \vdots & \ddots & \ddots & 0 \\ 0 & 0 & 0 & 0 & 0 & 0 & \cdots & 1 \end{bmatrix},$$

$$\mathbf{T} = \begin{bmatrix} \mathbf{T}(x_0) \\ \mathbf{T}(x_1) \\ \vdots \\ \mathbf{T}(x_N) \end{bmatrix} = \begin{bmatrix} 1 & x_0 & \ldots & x_0^N \\ 1 & x_1 & \ldots & x_1^N \\ 1 & \vdots & \ldots & \vdots \\ 1 & x_N & \ldots & x_N^N \end{bmatrix}, \mathbf{D}_{(\gamma)} = \begin{bmatrix} 0 & 0 & 0 & \cdots & 0 \\ 0 & \dfrac{\Gamma(2)}{\Gamma(2-\gamma)} & 0 & \cdots & 0 \\ 0 & 0 & \dfrac{\Gamma(3)}{\Gamma(3-\gamma)} & \cdots & 0 \\ \vdots & \vdots & \vdots & \ddots & \vdots \\ 0 & 0 & 0 & \cdots & \dfrac{\Gamma(N)}{\Gamma(N-\gamma)} \end{bmatrix}. \quad (20)$$

By using equation (18), we obtain the following relation:

$$\mathbf{Y}^{(k)}(x) = \mathbf{T}(x)\mathbf{D}^k\mathbf{MC}. \quad (21)$$

By substituting the Bernoulli collocation points given by

$$x_i = a + \frac{(b-a)i}{N}, \quad i = 0, 1, \ldots, N, \quad (22)$$

into equation (21), we obtain

$$\mathbf{Y}^{(k)}(x_i) = \mathbf{T}(x_i)\mathbf{D}^k\mathbf{MC}, \quad k = 0, \gamma, 2. \quad (23)$$

and the compact form of the relation (23) becomes

$$\mathbf{Y}^{(k)} = \mathbf{TD}^k\mathbf{MC}, \quad k = 0, \gamma, 2. \quad (24)$$

In this way, the unknown Bernoulli coefficients c_n, $n = 1, 2, \ldots, N+1$ are obtained by solving the system. Then, these coefficients are substituted into (14), and the approximate solution is obtained. For more details, see [36].

5. Simulation Results and Discussion

Bernoulli collocation method for obtaining the solution of fractional viscoelastic beam equation is employed. Hence, displacement analysis of a forced fractional viscoelastic beam is investigated by taking into account the different moving force loads, different values of internal damping coefficient, and different values of fractional order of derivative. Obtained results are simulated and presented in the tables and graphical forms. The velocity, from left to right, of the external moving force on beam $v(t)$ is considered as $\sin(\pi t)$. In order to observe the dynamic response of the viscoelastic beams under the different intensity of external moving force, the intensity constant of the external moving force load on the beam is involved to computation as $P = 1, 25, 50$. Also, the values in Tables 1–6 are computed on $x = 0.5$, which is the middle point of the fractional viscoelastic beams. Observed duration of time is $t_f = 1$. In the first case, forced displacement analysis of a polybutadiene beam is observed for different values of moving force load and results are presented in Table 1. The length and material density of the fractional viscoelastic beam are taken into account as $\ell = 1\,m$ and $\rho = 160\,\text{kg/m}^3$, respectively. The cross-sectional area A is $0.72\,\text{m}^2$, moment of inertia J is $(0.1)^4/12$, and Young's modulus E is 8.15×10^5 for a fractional viscoelastic polybutadiene beam. Also, the order of fractional derivative γ is evaluated as 0.528 for the results in Figure 2 and Tables 1 and 3. By observing Figure 2, it is concluded that while the intensity of the external moving load force increases, namely, P is 1 to 25 and 50, the displacement of the fractional viscoelastic polybutadiene beam also increases. Also, parallel observation results to Figure 2 are obtained by taking into account Table 1. For example, on the moment $t = 0.5$, the amount of the displacement of the polybutadiene beam is measured as 0.001 1 for $P = 1$, 0.028 for $P = 25$, and 0.056 for $P = 50$. This observation is valid the entire time interval $t = 0, \ldots, 1$ for polybutadiene beam. Also, the effect of internal damping on the displacement is presented in Table 3 for polybutadiene beam. The internal damping

Table 1: Some values of $w(t, x)$ for $P = 1, 25, 50$ (for a polybutadiene beam).

t	$w_{P=1}$	$w_{P=25}$	$w_{P=50}$
0.1	0.000 025 2	0.000 632 0	0.001 264 0
0.2	0.000 176 1	0.004 402 5	0.008 805 0
0.3	0.000 463 7	0.011 593 4	0.023 186 8
0.4	0.000 805 8	0.020 145 2	0.040 290 4
0.5	0.001 115 0	0.027 877 2	0.055 754 5
0.6	0.001 350 9	0.033 774 5	0.067 549 0
0.7	0.001 529 4	0.038 236 1	0.076 472 1
0.8	0.001 709 4	0.042 735 6	0.085 471 2
0.9	0.001 933 0	0.048 326 2	0.096 652 5
1.0	0.002 026 3	0.050 657 4	0.101 315 0

Table 2: Some values of $w(t, x)$ for $P = 1, 25, 50$ (for a butyl B252 beam).

t	$w_{P=1}$	$w_{P=25}$	$w_{P=50}$
0.1	0.000 020 2	0.000 505 3	0.001 010 7
0.2	0.000 140 7	0.003 517 7	0.007 035 4
0.3	0.000 370 1	0.009 253 1	0.018 506 4
0.4	0.000 642 1	0.016 053 0	0.032 106 1
0.5	0.000 886 5	0.022 164 5	0.044 328 9
0.6	0.001 070 9	0.026 772 4	0.053 544 8
0.7	0.001 207 9	0.030 198 1	0.060 396 2
0.8	0.001 345 0	0.033 624 9	0.067 249 8
0.9	0.001 515 9	0.037 899 2	0.075 798 4
1.0	0.001 581 7	0.039 544 7	0.079 089 3

Table 3: Some values of $w(t, x)$ for different values of μ for $P = 1$ (for a polybutadiene beam).

$t\mu$	0.2	0.4	0.6	0.8	1.0
0.1	0.000 024 90	0.000 024 24	0.000 023 62	0.000 023 03	0.000 022 48
0.2	0.000 170 50	0.000 161 04	0.000 152 42	0.000 144 54	0.000 137 32
0.3	0.000 440 42	0.000 402 52	0.000 369 54	0.000 340 70	0.000 315 37
0.4	0.000 748 72	0.000 659 75	0.000 586 20	0.000 524 91	0.000 473 41
0.5	0.001 011 32	0.000 856 73	0.000 735 83	0.000 640 02	0.000 563 11
0.6	0.001 194 99	0.000 973 52	0.000 810 05	0.000 687 00	0.000 592 56
0.7	0.001 323 26	0.001 044 56	0.000 850 35	0.000 711 06	0.000 608 30
0.8	0.001 459 32	0.001 136 46	0.000 922 48	0.000 774 52	0.000 667 97
0.9	0.001 645 41	0.001 287 75	0.001 058 63	0.000 902 75	0.000 790 71
1.0	0.001 713 62	0.001 340 71	0.001 112 91	0.000 964 62	0.000 862 85

Table 4: Some values of $w(t, x)$ for different values of μ for $P = 1$ (for a butyl B252 beam).

$t\mu$	0.2	0.4	0.6	0.8	1.0
0.1	0.000 019 90	0.000 019 35	0.000 018 85	0.000 018 37	0.000 017 91
0.2	0.000 136 09	0.000 128 33	0.000 121 26	0.000 114 82	0.000 108 94
0.3	0.000 350 96	0.000 319 92	0.000 293 02	0.000 269 58	0.000 249 07
0.4	0.000 595 32	0.000 522 71	0.000 463 02	0.000 413 52	0.000 372 12
0.5	0.000 801 77	0.000 676 17	0.000 578 62	0.000 501 79	0.000 440 45
0.6	0.000 943 91	0.000 764 93	0.000 633 94	0.000 536 04	0.000 461 36
0.7	0.001 040 91	0.000 817 11	0.000 662 68	0.000 552 79	0.000 472 22
0.8	0.001 459 32	0.000 886 19	0.000 717 38	0.000 601 55	0.000 667 97
0.9	0.001 285 91	0.001 002 83	0.000 823 34	0.000 701 97	0.000 518 57
1.0	0.001 333 74	0.001 041 33	0.000 864 75	0.000 750 70	0.000 615 00

coefficient is evaluated from 0.2 to 1 and by examining Table 3; it reveals that when internal damping coefficient increases, the displacement of the polybutadiene beam decreases under the same conditions. The effect of the fractional order to system is observed from Table 5 and it can be concluded that while increasing the values of the

TABLE 5: Some values of $w(t,x)$ for different values of γ for $P = 1$ (for a polybutadiene beam).

$t\gamma$	0.2	0.4	0.6	0.8	1.0
0.1	0.000 025 28	0.000 025 28	0.000 025 28	0.000 025 27	0.000 025 27
0.2	0.000 176 11	0.000 176 10	0.000 176 09	0.000 176 07	0.000 176 04
0.3	0.000 463 79	0.000 463 76	0.000 463 71	0.000 463 63	0.000 463 49
0.4	0.000 805 96	0.000 805 88	0.000 805 75	0.000 805 56	0.000 805 26
0.5	0.001 115 39	0.001 115 23	0.001 114 99	0.001 114 65	0.001 114 16
0.6	0.001 351 46	0.001 351 20	0.001 350 84	0.001 350 34	0.001 349 69
0.7	0.001 530 10	0.001 529 73	0.001 529 25	0.001 528 64	0.001 527 88
0.8	0.001 710 24	0.001 709 78	0.001 709 20	0.001 708 52	0.001 707 72
0.9	0.001 933 99	0.001 933 45	0.001 932 81	0.001 932 09	0.000 790 71
1.0	0.002 027 31	0.002 026 71	0.002 026 06	0.002 025 38	0.001 931 32

TABLE 6: Some values of $w(t,x)$ for different values of γ for $P = 1$ (for a butyl B252 beam).

$t\gamma$	0.2	0.4	0.6	0.8	1.0
0.1	0.000 020 21	0.000 020 21	0.000 020 21	0.000 020 21	0.000 020 21
0.2	0.000 140 71	0.000 140 71	0.000 140 70	0.000 140 69	0.000 140 66
0.3	0.000 370 16	0.000 370 14	0.000 370 11	0.000 370 06	0.000 369 97
0.4	0.000 642 21	0.000 642 16	0.000 642 08	0.000 641 96	0.000 641 77
0.5	0.000 886 76	0.000 886 66	0.000 886 51	0.000 886 29	0.000 885 98
0.6	0.001 071 19	0.001 071 02	0.001 070 79	0.001 070 48	0.001 070 07
0.7	0.001 208 33	0.001 208 09	0.001 207 79	0.001 207 41	0.001 206 93
0.8	0.001 345 49	0.001 345 20	0.001 344 84	0.001 344 41	0.001 343 92
0.9	0.001 516 53	0.001 516 20	0.001 515 80	0.001 515 36	0.001 514 89
1.0	0.001 582 39	0.001 582 02	0.001 581 62	0.001 581 21	0.001 580 82

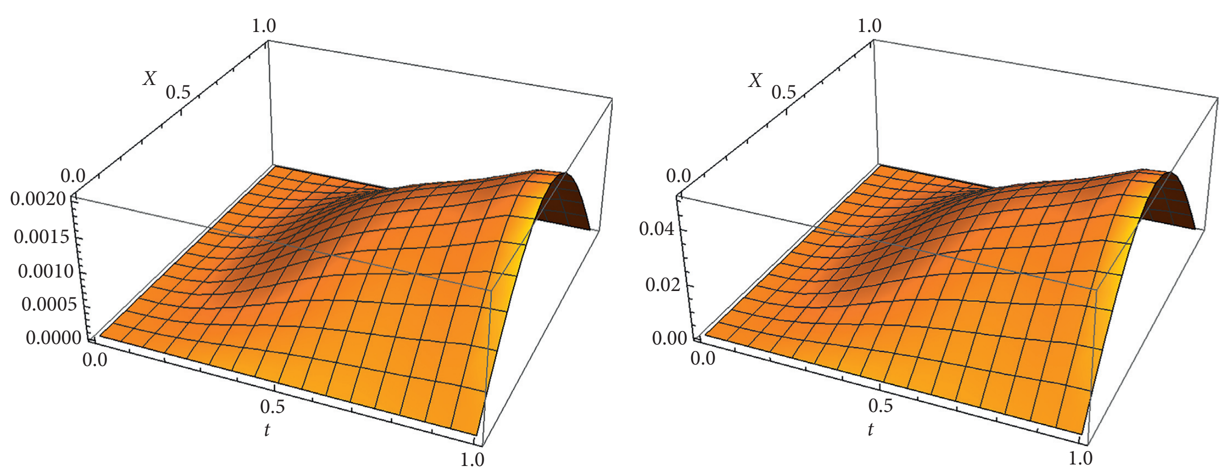

(a) (b)

FIGURE 2: Continued.

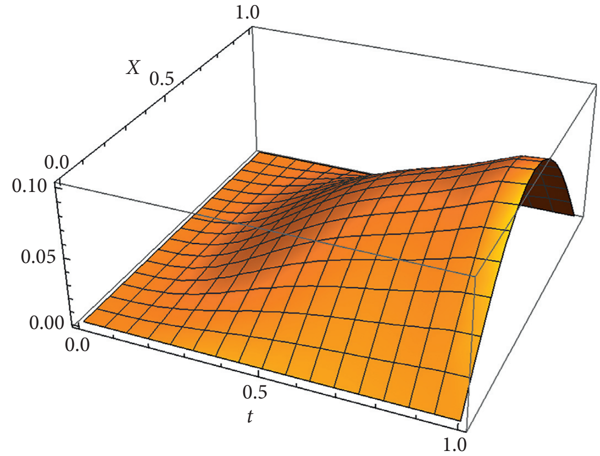

(c)

Figure 2: Displacements of a polybutadiene beam for $P = 1, 25, 50$.

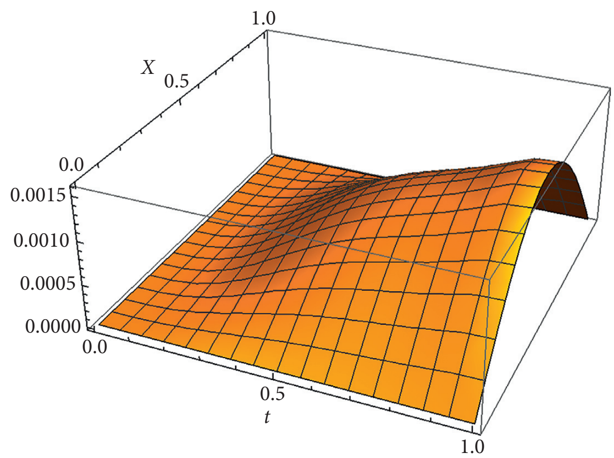

(a)

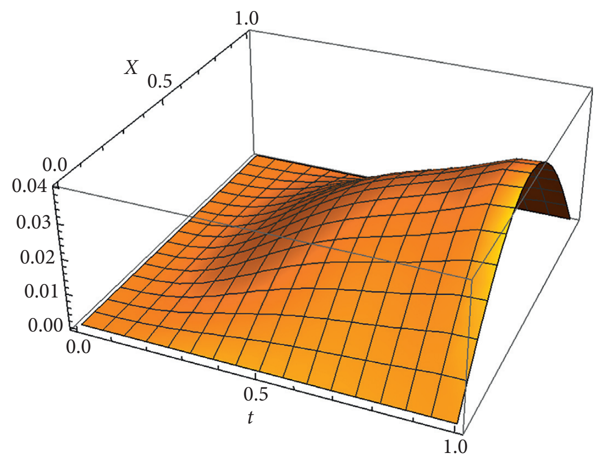

(b)

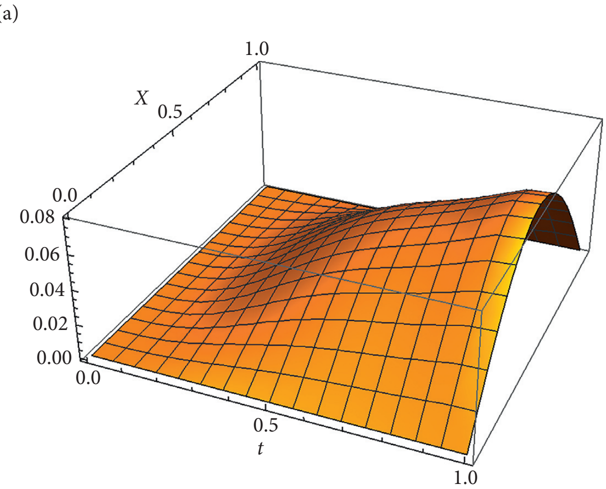

(c)

Figure 3: Displacements of a butyl B252 beam for $P = 1, 25, 50$.

fractional derivative, the value of the displacement is decreasing. In the second case, a butyl B252 beam is taken into account by the coefficients; the cross-sectional area A is $0.72\,\text{m}^2$, moment of inertia J is $(0.1)^4/12$, and Young's modulus E is 1.05×10^6. The order of fractional derivative γ is considered as 0.519 for Figure 3 and Tables 2 and 4. By checking Figure 3, it is easy to see that displacements corresponding to much bigger intensity of moving force load are much bigger. For example, on the moment $t = 0.5$, while $P = 1$ to $P = 25, 50$, corresponding displacements are calculated as 0.00089, 0.022, and 0.044, respectively. This is effective along the observation duration. In Table 4, some results related to the effect of internal damping are presented and internal damping coefficient is included in the computation as 0.2 to 1. After looking at Table 4, it is concluded that while internal damping coefficient decreases, the displacement of the butyl B252 beam increases and relation between the effects of internal damping and displacements is inversely proportional. The relation between the displacement and fractional order in the system is vice versa. As understood from Table 6, while decreasing the values of the fractional derivative, the value of the displacement is increasing. These observation results of the present study are also compatible with the results existing in the literature. By taking into account Tables 1–6 and Figures 2 and 3 and comparing these two kinds of fractional viscoelastic beams, it is seen that the polybutadiene beam has more greater displacements than butyl B252 beam under same conditions. Also, the effect of internal damping coefficient is more visible on the butyl B252 beam according to polybutadiene beam. These observations make clear that butyl B252 beam is stronger and preferable than the polybutadiene beam.

6. Conclusion

In this study, the Bernoulli collocation method as a new solution method for obtaining the approximate solution of a fractional viscoelastic beam model subjected to moving force load is employed. Dynamic response analysis of the fractional viscoelastic beam model is investigated for two different specific beams: polybutadiene beam and butyl B252 beam. Displacement analysis of a point on the fractional viscoelastic beams is studied for different moving force loads and also effect of the internal damping to displacement is observed for different internal damping coefficients. Moreover, dynamic response of the fractional viscoelastic beam is examined for different values of the fractional order. Obtained results are presented in tables and graphics and results reveal that Bernoulli collocation method is very effective and powerful solution method for obtaining the solution of fractional order viscoelastic beam models. After observing Figures 2 and 3, it is easy to conclude that as the moving force load increases, the displacement of a point on the beams also increases. Also, numerical results, presented in Tables 1–4, show that under the same moving force load with the same internal damping effect, the displacement of a point on the polybutadiene beam is greater than that corresponding to butyl B252 beam. Moreover, under the same moving force load, changes in the displacements of a point on the beams are examined in the aspect of different internal damping effects and observations made clear that butyl B252 beam better reflects the effect of internal damping to displacement of a point on the beam. By comparing polybutadiene beam and butyl B252 beam, it is concluded that polybutadiene beam is more open to destructive effects of vibrations under the same conditions with the butyl B252 beam.

Data Availability

The data used to support the findings of this study are included within the article.

Conflicts of Interest

The authors declare that they have no conflicts of interest.

Authors' Contributions

The authors completed this study and wrote and approved the final version of the manuscript.

References

[1] O. A. Bauchau and J. I. Craig, *Structural Analysis*, Springer-Verlag, New York, NY, USA, 2009.

[2] J. Lubliner and P. Papadopoulos, *Introduction to Solid Mechanics:An Integrated Approach*, Springer-Verlag, New York, NY, USA, 2014.

[3] R. Rowland Jr., *Principal of Solid Mechanics*, CRC Press, Boca Raton, FL, USA, 2000.

[4] T. Blaszczyk, J. Siedlecki, and H. Sun, "An exact solution of fractional Euler-Bernoulli equation for a beam with fixed-supported and fixed-free ends," *Applied Mathematics and Computation*, vol. 396, p. 125932, 2021.

[5] G. Radenkovic and A. Borkovic, "On the analytical approach to the linear analysis of an arbitrarily curved spatial Bernoulli Euler beam," *Applied Mathematical Modelling*, vol. 77, pp. 1603–1624, 2020.

[6] E. Pan and P. R. Heyliger, "Free vibrations of simply supported and multilayered magneto-electro-elastic plates," *Journal of Sound and Vibration*, vol. 252, no. 3, pp. 429–442, 2002.

[7] A. R. Annigeri, N. Ganesan, and S. Swarnamani, "Free vibration behaviour of multiphase and layered magneto-electro-elastic beam," *Journal of Sound and Vibration*, vol. 299, no. 1, pp. 44–63, 2007.

[8] G. W. Griffiths and W. E. Schiesser, *Traveling Wave Analysis of Partial Differential Equations*, Academic Press, Cambridge, MA, USA, 2011.

[9] C.-G. Zhang, "Boundary feedback stabilization of the undamped Timoshenko beam with both ends free," *Journal of Mathematical Analysis and Applications*, vol. 326, no. 1, pp. 488–499, 2007.

[10] A. Capsoni, G. Maria Viganò, and K. Bani-Hani, "On damping effects in Timoshenko beams," *International Journal of Mechanical Sciences*, vol. 73, pp. 27–39, 2013.

[11] K. Morfidis, "Vibration of Timoshenko beams on three-parameter elastic foundation," *Computers & Structures*, vol. 88, no. 5-6, pp. 294–308, 2010.

[12] M. Ishaquddin and S. Gopalakrishnan, "A novel weak form quadrature element for gradient elastic beam theories," *Applied Mathematical Modelling*, vol. 77, pp. 1–16, 2020.

[13] B. Martin and A. Salehian, "Techniques for approximating a spatially varying Euler-Bernoulli model with a constant coefficient model," *Applied Mathematical Modelling*, vol. 79, pp. 260–283, 2020.

[14] J. Gahleitner and J. Schoeftne, "An anisotropic beam theory based on the extension of Boleyr's method," *Composite Structures*, vol. 243, pp. 112–149, 2020.

[15] B. Wang, X. Luo, Y. Liu, and Z. Yang, "Thickness-variable composite beams for vibration energy harvesting," *Composite Structures*, vol. 244, p. 112232, 2020.

[16] A. Gemant, "XLV.On fractional differentials," *The London, Edinburgh, and Dublin Philosophical Magazine and Journal of Science*, vol. 25, no. 168, pp. 540–549, 1938.

[17] C. Yu, J. Zhang, Y. Chen, Y. Feng, and A. Yang, "A numerical method for solving fractional-order viscoelastic Euler Bernoulli beams," *Chaos, Solitons & Fractals*, vol. 128, pp. 275–279, 2016.

[18] R. K. Praharaj and N. Datta, "Dynamic response of plates resting on a fractional viscoelastic foundation and subjected to a moving load," *Mechanics Based Design of Structures and Machines*, pp. 1–16, 2020.

[19] R. K. Praharaj and N. Datta, "Dynamic response spectra of fractionally damped viscoelastic beams subjected to moving load," *Mechanics Based Design of Structures and Machines*, vol. 2020, Article ID 1725563, 15 pages, 2020.

[20] J. Xu and J. Li, "Stochastic dynamic response and reliability assessment of controlled structures with fractional derivative model of viscoelastic dampers," *Mechanical Systems and Signal Processing*, vol. 72-73, pp. 865–896, 2016.

[21] M. Ajri, M. M. Fakhrabadi, and A. Rastgoo, "Analytical solution for nonlinear dynamic behavior of viscoelastic nanoplates modeled by consistent couple stress theory," *Latin American Journal of Solids and Structures*, vol. 15, pp. 1–23, 2018.

[22] C. Chazal and R. M. Pitti, "Integral approach for time dependent materials using finite element method," *Journal of Theorical and Applied Mechanics*, vol. 49, pp. 1029–1048, 2011.

[23] Y. Lei, M. I. Friswell, and S. Adhikari, "A Galerkin method for distributed systems with non-local damping," *International Journal of Solids and Structures*, vol. 43, no. 11-12, pp. 3381–3400, 2006.

[24] O. Martin, "A modified variational iteration method for the analysis of viscoelastic beams," *Applied Mathematical Modelling*, vol. 40, no. 17-18, pp. 7988–7995, 2016.

[25] D. D. Demir, N. Bildik, and B. G. Sýnýr, "Linear dynamical analysis of fractionally damped beams and rods," *Journal of Engineering Mathematics*, vol. 85, no. 1, p. 13147, 2014.

[26] S. Mareishi, M. Rafiee, X. Q. He, and K. M. Liew, "Nonlinear free vibration, postbuckling and nonlinear static deflection of piezoelectric fiber-reinforced laminated com- posite beams," *Composites Part B: Engineering*, vol. 59, p. 12332, 2014.

[27] J. K. Freundlich, "Dynamic response of a simply supported viscoelastic beam of a fractional derivative type to a moving force load," *Journal of Theoretical and Applied Mechanics*, vol. 54, no. 4, pp. 1433–1445, 2016.

[28] Z.-F. Liang and X.-Y. Tang, "Analytical solution of fractionally damped beam by Adomian decomposition method," *Applied Mathematics and Mechanics*, vol. 28, no. 2, pp. 219–228, 2007.

[29] M. A. Foda and Z. Abduljabbar, "A dynamic green function formulation for the response of a beam structure to a moving mass," *Journal of Sound and Vibration*, vol. 210, no. 3, pp. 295–306, 1998.

[30] J. Freundlich, "Transient vibrations of a fractional Kelvin-Voigt viscoelastic cantilever beam with a tip mass and subjected to a base excitation," *Journal of Sound and Vibration*, vol. 438, pp. 99–115, 2019.

[31] W. Sumelka, T. Blaszczyk, and C. Liebold, "Fractional Euler-Bernoulli beams: theory, numerical study and experimental validation," *European Journal of Mechanics-A: Solids*, vol. 54, pp. 243–251, 2015.

[32] M. Sameeh and A. Elsaid, "Chebyshev collocation method for parabolic partial integrodifferential equations," *Advances in Mathematical Physics*, vol. 2016, Article ID 7854806, 7 pages, 2016.

[33] F. Toutounian, E. Tohidi, and S. Shateyi, "A collocation method based on the Bernoulli operational matrix for solving high-order linear complex differential equations in a rectangular domain," *Abstract and Applied Analysis*, vol. 2013, Article ID 823098, 12 pages, 2013.

[34] Ö. Oruç, A. Esen, and F. Bulut, "Numerical investigation of dynamic Euler-Bernoulli equation via 3-Scale Haar wavelet collocation method," *Hacettepe Journal of Mathematics and Statistics*, vol. 50, no. 1, pp. 1–21, 2021.

[35] R. L. Bagley and P. J. Torvik, "A theoretical basis for the application of fractional calculus to viscoelasticity," *Journal of Rheology*, vol. 27, no. 3, pp. 201–210, 1983.

[36] B. Zogheib, E. Tohidi, and S. Shateyi, "Bernoulli collocation method for solving linear multidimensional diffusion and wave equations with dirichlet boundary conditions," *Advances in Mathematical Physics*, vol. 2017, Article ID 5691452, 15 pages, 2017.

Hindawi
Journal of Mathematics
Volume 2021, Article ID 9178444, 11 pages
https://doi.org/10.1155/2021/9178444

Research Article

Several Characterizations on Degree-Based Topological Indices for Star of David Network

Nadeem Salamat,[1] Muhammad Kamran,[1] Shahbaz Ali ,[1] Md. Ashraful Alam ,[2] and Riaz Hussain Khan[1]

[1]*Department of Mathematics, Khwaja Fareed University of Engineering & Information Technology Rahim Yar Khan, Punjab 64200, Pakistan*
[2]*Department of Mathematics, Jahangirnagar University, Savar, Dhaka, Bangladesh*

Correspondence should be addressed to Md. Ashraful Alam; ashraf_math20@juniv.edu

Received 28 August 2021; Revised 26 September 2021; Accepted 26 November 2021; Published 11 December 2021

Academic Editor: Fairouz Tchier

In order to make quantitative structure-movement/property/danger relations, topological indices (TIs) are the numbers that are related to subatomic graphs. Some fundamental physicochemical properties of chemical compounds, such as breaking point, protection, and strain vitality, correspond to these TIs. In the compound graph hypothesis, the concept of TIs was developed in view of the degree of vertices. In investigating minimizing exercises of Star of David, these indices are useful. In this study, we explore the different types of Zagreb indices, Randić indices, atom-bond connectivity indices, redefined Zagreb indices, and geometric-arithmetic index for the Star of David. The edge partitions of this network are tabled based on the sum of degrees-of-end vertices and the sum of degree-based edges. To produce closed formulas for some degree-based network TIs, these edge partitions are employed.

1. Introduction

Graph theory is a branch of mathematics in which we use graph parameter methods to precisely expose the compound phenomenon. For example, the graph theory characterizes an area between different disciplines of science when applied to the investigation of molecular structures, which is known as molecular topology or the theory of chemical graphs. A significant part of the analysis was supported by chemical graph theory [1]. Chemist can be performed for the statistical demonstration of chemical marvel by means of graph theory. In quantitative structure activity, researchers tried to figure out what structural characteristics will be developed. Physicochemical features and topological measures are discussed by Wiener. Different types of graph descriptors, such as distance-based, degree-based, spectral, and polynomial-related descriptors, have been well defined and explored extensively in the literature. Vertex degree-based descriptors are the most important of these classes, and they play a crucial role in chemical graph theory. These descriptors are combined to infer physicochemical, biological, and pharmacological qualities such stability, chirality, melting point, boiling point, similarity, connectedness, entropy, enthalpy of formation, surface tension, density, critical temperature, and others. Mathematicians and chemists use a variety of topological indices in these types of studies. The quantitative structure-property relationship (QSPR) and quantitative structure-activity relationship (QSAR) research use the index, the Randic index, the Zagreb indices, and the ABC index to measure by Yang et al. [2] in the bioactivity of chemical compounds [3]. Topological indices provide numerical representations, molecular size, shape, branching, and other properties that are used to compare chemical compounds' topological similarities and in QSPR/QSAR research [4, 5]. There are several properties related to new families of graphs that are discussed in [6–8] such as metric dimensions and indices. The spectral properties, metric dimensions, and indices of different families of graphs are discussed in [9–14]. These include distance-based and degree-based TIs, as well as related polynomials [15] and classified graph indices, among other forms of topological indices. In 2017, Maji and Ghorai introduced new distance-degree-based topological indices, see [16]. In chemical graph theory and notably in chemistry, degree-based TIs are extremely important and serve a critical function. Furthermore, algebraic graph theory results are discussed in [17–21] by using the notion of totient number which was introduced by Shahbaz and Khalid in 2017.

In this paper, we study some degree-based analysis of TIs of the Star of David network. In Hebrew, the Star of David, or "Magen David" ("Shield of David"), consists of two overlaid equilateral triangles that form a six-pointed star. It cannot be traced back to the Bible or the Talmud, but it is said that it comes from the (presumed) similarity to the shape of the shield of King David. It was neither used as a sign of Jewish identity, although it originated in Antiquity, nor was even restricted to Judaism. The seven-branched candelabrum, still one of Israel's emblems today, was the most famous symbol of Judaism at that time.

We arranged our paper as follows. In Section 2, we give some preliminary concepts related to topological indices of different kinds. In Section 3, we construct the Star of David network and proposed their algorithm. In Section 4, we compute several results on topological indices for the proposed network. In Section 5, we give a comparison of topological indices for proposed networks. In Section 6, we give the concluding remarks about our proposed work. In future work, one can compute more indices on proposed Star of David networks.

2. Preliminaries

According to this study, a simple connected graph G is made up of vertices $V(G)$ and edges $E(G)$, with $\aleph(\mu)$ being the degree of each vertex and the number of edges intersecting μ."

Definition 1. Topological index (TI) is derived by Wiener, which was created in 1945 after investigating alkane's boiling point [22]. According to Randić [23] characterization, the earliest degree-based index is the Randić index, which is defined as

$$R(G) = \sum_{\mu\nu\in E(G)} \frac{1}{\left(\sqrt{\aleph(\mu)\aleph(\nu)}\right)}. \quad (1)$$

As a traditional graph-based molecular structure descriptor, the Randić index has been widely used in chemical and pharmaceutical research. Even the mathematical sense of this index is clear for detail of its QSPR/QSAR application, see [24, 25]. Bollobác and Paul [26] presented the general Randić index, which is defined as

$$R_\alpha(G) = \sum_{\mu\nu\in E(G)} (\aleph(\mu)\aleph(\nu))^\alpha \text{ for } \alpha = 1, \frac{1}{2}, -\frac{1}{2}, -1. \quad (2)$$

Definition 2. Gutman and Trinajstić [27] defined the first and second Zagreb indices as follows; also, see [28–30]:

$$\begin{aligned} M_1(G) &= \sum_{\mu\nu\in E(G)} (\aleph(\mu) + \aleph(\nu)), \\ M_2(G) &= \sum_{\mu\nu\in E(G)} (\aleph(\mu)\aleph(\mu)). \end{aligned} \quad (3)$$

Definition 3. Ranjini et al. [31] proposed the redefined version of Zagreb indices

The redefined first Zagreb index of graph G is defined as

$$R_eZG_1(\mathrm{G}) = \sum_{\mu\nu\in E(G)} \frac{(\aleph(\mu) + \aleph(\nu))}{(\aleph(\mu)\cdot\aleph(\nu))}. \quad (4)$$

The redefined second Zagreb index of graph G is defined as

$$R_eZG_2(G) = \sum_{\mu\nu\in E(G)} \frac{(\aleph(\mu)\cdot\aleph(\nu))}{(\aleph(\mu) + \aleph(\nu))}. \quad (5)$$

The redefined third Zagreb index of graph G is defined as

$$R_eZG_3(G) = \sum_{\mu\nu\in E(G)} (\aleph(\mu)\cdot\aleph(\nu))(\aleph(\mu) + \aleph(\nu)). \quad (6)$$

Definition 4. Estrada et al., in [32], proposed degree-based TI ABC and defined it as

$$ABC(G) = \sum_{\mu\nu\in E(G)} \sqrt{\frac{\aleph(\mu) + \aleph(\nu) - 2}{\aleph(\mu)\cdot\aleph(\nu)}}. \quad (7)$$

The atom-bond connectivity index (ABC) is a molecular structural descriptor that has lately found surprising applicability in explaining linear and branched alkane stability, as well as cycloalkane strain energy. It is used for modeling the thermodynamic characteristics in organic chemical molecules.

Definition 5. The GA index is proposed by Vukicevic and Furtula in [33] and defined as

$$GA(G) = \sum_{\mu\nu\in E(G)} 2\frac{\sqrt{\aleph(\mu)\cdot\aleph(\nu)}}{\aleph(\mu) + \aleph(\nu)}. \quad (8)$$

The prediction value of the GA index is slightly greater than the Randić connection index for physicochemical characteristics such as entropy and acentric factor, according to [33].

Definition 6. Furtula and Gutman, in [34], proposed the forgotten TI and stated it as

$$F(G) = \sum_{\mu\nu\in E(G)} (\aleph(\mu))^2 + (\aleph(\nu))^2. \quad (9)$$

For further study, see [35]. The Star of David networks are shown in Figures 1 and 2.

3. Higher Dimension $SD_{(n)}$ Drawing Algorithm for Star of David Network

Step 1 : the Star of David, consists of two equilateral overlapping triangles forming a six-pointed star. Draw David's Star graph G, which is one and two dimensional, as seen in figure ??. Algorithm for Star of David is as given below:

(i)
```
≠inclu de⟨iostream⟩
  using namespace std;, ≠ define n ⟍'n'
    int i, j;, int main()
{
    for (i = 0; i ≤ 1; i + +)
    {
      for (j = 1; j ≤ 5 − i; j + +)
  cout ⟨⟨" ";
⟨⟨" * ";
if (i == 1)
  cout ⟨⟨" * ";
  cout ⟨⟨n;
    }
    for (i = 1; i ≤ ; i + +)
      {
    for (j = 1; j ≤ 11; j + +)
        {
if (i == 2‖i == 3)
        {
if (j == 2‖j == 3‖j == 9‖j == 10)
          {
  cout ⟨⟨" * ";
  }
  else
        cout ⟨⟨" ";
      }
      else
            cout ⟨⟨" * ";
      }
            cout ⟨⟨n;
        }
    for (i = 1; i ≥ 0; i − −)
            {
    for (j = (5 − i); j ≥ 1; j − −)
                cout ⟨⟨" ";
                  cout ⟨⟨" * ";
    if (i == 1)
                    cout ⟨⟨" * ";
                      cout ⟨⟨n;
            }
              }
```

Step 2 : add two David's stars on the upper and lower sides.

Step 3 : adding one more star of David in each step similarly, we proceed up to $n = 5$. We get the sequence at $n = 5$.

4. Results on Indices for Star of David Network

Theorem 1. *The atom-bond connectivity index of Star of David network is*

$$ABC(G) = 3.2n^2 - 10.6n - 10.2. \tag{10}$$

Proof. Let G be the graph of Star of David network. By using Table 1, we apply the formula of the atom-bond connectivity index for G:

$$\begin{aligned}
ABC(G) &= \sum_{\mu\nu \in E(G)} \sqrt{\frac{\aleph(\mu) + \aleph(\nu) - 2}{\aleph(\mu) \cdot \aleph(\nu)}} \\
&= \sum_{\mu\nu \in E\{2,2\}} \sqrt{\frac{\aleph(\mu) + \aleph(\nu) - 2}{\aleph(\mu) \cdot \aleph(\nu)}} + \sum_{\mu\nu \in E\{2,4\}} \sqrt{\frac{\aleph(\mu) + \aleph(\nu) - 2}{\aleph(\mu) \cdot \aleph(\nu)}} + \sum_{\mu\nu \in E\{2,6\}} \sqrt{\frac{\aleph(\mu) + \aleph(\nu) - 2}{\aleph(\mu) \cdot \aleph(\nu)}} \\
&\quad + \sum_{\mu\nu \in E\{4,4\}} \sqrt{\frac{\aleph(\mu) + \aleph(\nu) - 2}{\aleph(\mu) \cdot \aleph(\nu)}} + \sum_{\mu\nu \in E\{4,6\}} \sqrt{\frac{\aleph(\mu) + \aleph(\nu) - 2}{\aleph(\mu) \cdot \aleph(\nu)}} + \sum_{\mu\nu \in E\{6,6\}} \sqrt{\frac{\aleph(\mu) + \aleph(\nu) - 2}{\aleph(\mu) \cdot \aleph(\nu)}} \\
&= 4\sqrt{\frac{2+2-2}{2 \cdot 2}} + 8\sqrt{\frac{2+4-2}{2 \cdot 4}} + (12n - 16)\sqrt{\frac{2+6-2}{2 \cdot 6}} \\
&\quad + (6n - 6)\sqrt{\frac{4+4-2}{4 \cdot 4}} + (12n - 20)\sqrt{\frac{4+6-2}{4 \cdot 6}} + 6(n-2)^2\sqrt{\frac{6+6-2}{6 \cdot 6}}.
\end{aligned} \tag{11}$$

Figure 1: Star of David.

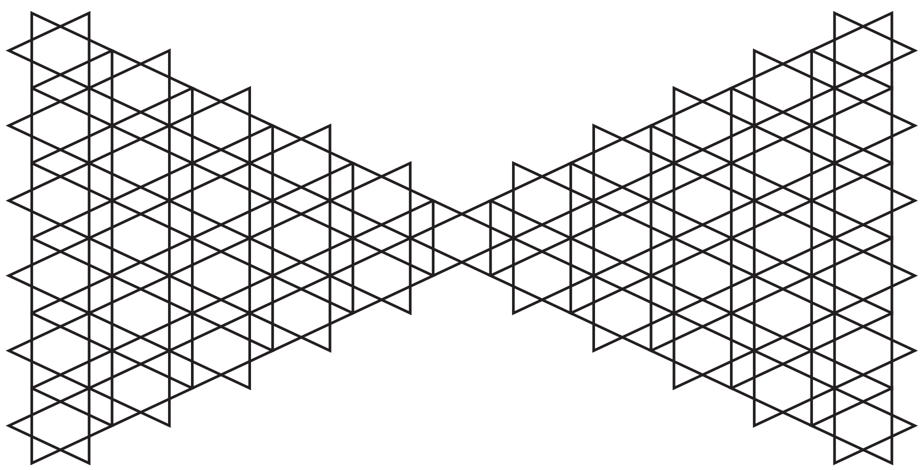

Figure 2: Star of David network.

Table 1: Star of David network edge partition.

Types of edges	$E_{\{2,2\}}$	$E_{\{2,4\}}$	$E_{\{2,6\}}$	$E_{\{4,4\}}$	$E_{\{4,6\}}$	$E_{\{6,6\}}$
Number of edges	$(2,2)$	$(2,4)$	$(2,6)$	$(4,4)$	$(4,6)$	$(6,6)$
Frequency	4	8	$12n-16$	$6n-6$	$12n-20$	$6(n-2)^2$

We get the outcomes after estimates:

$$ABC(G) = 3.2n^2 - 10.6n - 10.2. \tag{12}$$

Theorem 2. *The geometric-arithmetic index of Star of David network is*

$$GA(G) = 6n^2 + 4.2n - 6.46. \tag{13}$$

Proof. Let G be the graph of Star of David network. By using Table 1, we apply the formula of geometric-arithmetic index for G:

$$GA(G) = \sum_{\mu\nu\in E(G)} 2\frac{\sqrt{\aleph(\mu)\cdot\aleph(\nu)}}{\aleph(\mu)+\aleph(\nu)}$$

$$= \sum_{\mu\nu\in E(2,2)} 2\frac{\sqrt{\aleph(\mu)\cdot\aleph(\nu)}}{\aleph(\mu)+\aleph(\nu)} + \sum_{\mu\nu\in E(2,4)} 2\frac{\sqrt{\aleph(\mu)\cdot\aleph(\nu)}}{\aleph(\mu)+\aleph(\nu)} + \sum_{\mu\nu\in E(2,6)} 2\frac{\sqrt{\aleph(\mu)\cdot\aleph(\nu)}}{\aleph(\mu)+\aleph(\nu)}$$

$$
\begin{aligned}
&+\sum_{\mu\nu\in E(4,4)} 2\frac{\sqrt{\aleph(\mu)\cdot\aleph(\nu)}}{\aleph(\mu)+\aleph(\nu)}+\sum_{\mu\nu\in E(4,6)} 2\frac{\sqrt{\aleph(\mu)\cdot\aleph(\nu)}}{\aleph(\mu)+\aleph(\nu)}+\sum_{\mu\nu\in E(6,6)} 2\frac{\sqrt{\aleph(\mu)\cdot\aleph(\nu)}}{\aleph(\mu)+\aleph(\nu)}\\
&= 4\cdot 2\frac{\sqrt{2\cdot 2}}{2+2}+8\cdot 2\frac{\sqrt{2\cdot 4}}{2+4}+(12n-16)\cdot 2\frac{\sqrt{2\cdot 6}}{2+6}\\
&+(6n-6)\cdot 2\frac{\sqrt{4\cdot 4}}{4+4}+(12n-20)\cdot 2\frac{\sqrt{4\cdot 6}}{4+6}+6(n-2)^2\cdot 2\frac{\sqrt{6\cdot 6}}{6+6}\\
&= 6n^2+4.2n-6.46.
\end{aligned} \tag{14}
$$

Theorem 3. *The first Zagreb index of Star of David network is*

$$M_1(G) = 72n^2 - 24n - 24. \tag{15}$$

Proof. Let G be the graph of Star of David network. By using Table 1, we apply the formula of the first Zagreb index for G:

$$
\begin{aligned}
M_1(G) &= \sum_{\mu\nu\in E(G)} (\aleph(\mu)+\aleph(\nu))\\
&= \sum_{\mu\nu\in E(2,2)} (\aleph(\mu)+\aleph(\nu))+\sum_{\mu\nu\in E(2,4)} (\aleph(\mu)+\aleph(\nu))+\sum_{\mu\nu\in E(2,6)} (\aleph(\mu)+\aleph(\nu))\\
&+\sum_{\mu\nu\in E(4,4)} (\aleph(\mu)+\aleph(\nu))+\sum_{\mu\nu\in E(4,6)} (\aleph(\mu)+\aleph(\nu))+\sum_{\mu\nu\in E(6,6)} (\aleph(\mu)+\aleph(\nu))\\
&= 4(2+2)+8(2+4)+(12n-16)(2+6)+(6n-6)(4+4)\\
&+(12n-20)(4+6)+6(n-2)^2(6+6).
\end{aligned} \tag{16}
$$

We get the outcomes after estimates:

$$M_1(G) = 72n^2 - 24n - 24. \tag{17}$$

Theorem 4. *The second Zagreb index of Star of David network is*

$$M_2(G) = 216n^2 - 336n + 176. \tag{18}$$

Proof. Let G be the graph of Star of David network. By using Table 1, we apply the formula of the second Zagreb index for G:

$$
\begin{aligned}
M_2(G) &= \sum_{\mu\nu\in E(G)} (\aleph(\mu)\cdot\aleph(\nu))\\
&= \sum_{\mu\nu\in E(2,2)} (\aleph(\mu)\cdot\aleph(\nu))+\sum_{\mu\nu\in E(2,4)} (\aleph(\mu)\cdot\aleph(\nu))+\sum_{\mu\nu\in E(2,6)} (\aleph(\mu)\cdot\aleph(\nu))\\
&+\sum_{\mu\nu\in E(4,4)} (\aleph(\mu)\cdot\aleph(\nu))+\sum_{\mu\nu\in E(4,6)} (\aleph(\mu)\cdot\aleph(\nu))+\sum_{\mu\nu\in E(6,6)} (\aleph(\mu)\cdot\aleph(\nu))\\
&= 4(2\cdot 2)+8(2\cdot 4)+(12n-16)(2\cdot 6)+(6n-6)(4\cdot 4)+(12n-20)(4\cdot 6)\\
&+6(n-2)^2(6\cdot 6)\\
&= 216n^2-336n+176.
\end{aligned} \tag{19}
$$

Theorem 5. *The redefined first Zagreb index of Star of David network is*

$$R_eZG_1(G) = 2n^2 + 8n - 3.97. \tag{20}$$

Proof. Let G be the graph of Star of David network. By using Table 1, we apply the formula of the redefined first Zagreb index for G:

$$
\begin{aligned}
R_eZG_1(G) &= \sum_{\mu\nu\in E(G)} \frac{\aleph(\mu)+\aleph(\nu)}{\aleph(\mu)\cdot\aleph(\nu)} \\
&= \sum_{\mu\nu\in E(2,2)} \frac{\aleph(\mu)+\aleph(\nu)}{\aleph(\mu)\cdot\aleph(\nu)} + \sum_{\mu\nu\in E(2,4)} \frac{\aleph(\mu)+\aleph(\nu)}{\aleph(\mu)\cdot\aleph(\nu)} + \sum_{\mu\nu\in E(2,6)} \frac{\aleph(\mu)+\aleph(\nu)}{\aleph(\mu)\cdot\aleph(\nu)} \\
&\quad + \sum_{\mu\nu\in E(4,4)} \frac{\aleph(\mu)+\aleph(\nu)}{\aleph(\mu)\cdot\aleph(\nu)} + \sum_{\mu\nu\in E(4,6)} \frac{\aleph(\mu)+\aleph(\nu)}{\aleph(\mu)\cdot\aleph(\nu)} + \sum_{\mu\nu\in E(6,6)} \frac{\aleph(\mu)+\aleph(\nu)}{\aleph(\mu)\cdot\aleph(\nu)} \\
&= 4\cdot\frac{2+2}{2\cdot 2} + 8\cdot\frac{2+4}{2\cdot 4} + (12n-16)\cdot\frac{2+6}{2\cdot 6} + (6n-6)\frac{4+4}{4\cdot 4} \\
&\quad + (12n-20)\frac{4+6}{4\cdot 6} + 6(n-2)^2\frac{6+6}{6\cdot 6}.
\end{aligned} \tag{21}
$$

We get the outcomes after estimates:

$$R_eZG_1(G) = 2n^2 + 8n - 3.97. \tag{22}$$

Theorem 6. *The redefined second Zagreb index of Star of David network is*

$$R_eZG_2(G) = 18n^2 - 13.2n + 2.67. \tag{23}$$

Proof. Let G be the graph of Star of David network. By using Table 1, we apply the formula of the redefined second Zagreb index for G:

$$
\begin{aligned}
R_eZG_2(G) &= \sum_{\mu\nu\in E(G)} \frac{\aleph(\mu)\cdot\aleph(\nu)}{\aleph(\mu)+\aleph(\nu)} \\
&= \sum_{\mu\nu\in E(2,2)} \frac{\aleph(\mu)\cdot\aleph(\nu)}{\aleph(\mu)+\aleph(\nu)} + \sum_{\mu\nu\in E(2,4)} \frac{\aleph(\mu)\cdot\aleph(\nu)}{\aleph(\mu)+\aleph(\nu)} + \sum_{\mu\nu\in E(2,6)} \frac{\aleph(\mu)\cdot\aleph(\nu)}{\aleph(\mu)+\aleph(\nu)} \\
&\quad + \sum_{\mu\nu\in E(4,4)} \frac{\aleph(\mu)\cdot\aleph(\nu)}{\aleph(\mu)+\aleph(\nu)} + \sum_{\mu\nu\in E(4,6)} \frac{\aleph(\mu)\cdot\aleph(\nu)}{\aleph(\mu)+\aleph(\nu)} + \sum_{\mu\nu\in E(6,6)} \frac{\aleph(\mu)\cdot\aleph(\nu)}{\aleph(\mu)+\aleph(\nu)} \\
&= 4\cdot\frac{2\cdot 2}{2+2} + 8\cdot\frac{2\cdot 4}{2+4} + (12n-16)\cdot\frac{2\cdot 6}{2+6} + (6n-6)\frac{4\cdot 4}{4+4} \\
&\quad + (12n-20)\frac{4\cdot 6}{4+6} + 6(n-2)^2\frac{6\cdot 6}{6+6}.
\end{aligned} \tag{24}
$$

We get the outcomes after estimates:

$$R_eZG_2(G) = 18n^2 - 13.2n + 2.67. \tag{25}$$

Theorem 7. *The redefined third Zagreb index of Star of David network is*

$$R_eZG_3(G) = 2592n^2 - 5568n + 3712. \tag{26}$$

Proof. Let G be the graph of Star of David network. By using Table 1, we apply the formula of the redefined third Zagreb index for G:

$$
\begin{aligned}
R_eZG_3(G) &= \sum_{\mu\nu\in E(G)} (\aleph(\mu)\cdot\aleph(\nu))(\aleph(\mu)+\aleph(\nu)) \\
&= \sum_{\mu\nu\in E(2,2)} (\aleph(\mu)\cdot\aleph(\nu))(\aleph(\mu)+\aleph(\nu)) + \sum_{\mu\nu\in E(2,4)} (\aleph(\mu)\cdot\aleph(\nu))(\aleph(\mu)+\aleph(\nu))
\end{aligned}
$$

$$+ \sum_{\mu\nu\in E(2,6)} (\aleph(\mu)\cdot\aleph(\nu))(\aleph(\mu)+\aleph(\nu)) + \sum_{\mu\nu\in E(4,4)} (\aleph(\mu)\cdot\aleph(\nu))(\aleph(\mu)+\aleph(\nu))$$
$$+ \sum_{\mu\nu\in E(4,6)} (\aleph(\mu)\cdot\aleph(\nu))(\aleph(\mu)+\aleph(\nu)) + \sum_{\mu\nu\in E(6,6)} (\aleph(\mu)\cdot\aleph(\nu))(\aleph(\mu)+\aleph(\nu)) \quad (27)$$
$$= 4(2\cdot 2)(2+2) + 8(2\cdot 4)(2+4) + (12n-16)(2\cdot 6)(2+6)$$
$$+ (6n-6)(4\cdot 4)(4+4) + (12n-20)(4\cdot 6)(4+6) + 6(n-2)^2(6\cdot 6)(6+6).$$

We get the outcomes after estimates:

$$R_eZG_3(G) = 2592n^2 - 5568n + 3712. \quad (28)$$

Theorem 8. *The forgotten TI of Star of David network is*

$$F(G) = 432n^2 - 432n + 48. \quad (29)$$

Proof. Let G be the graph of Star of David network. By using Table 1, we apply the formula of forgotten TI for G:

$$F(G) = \sum_{\mu\nu\in E(G)} (\aleph(\mu))^2 + (\aleph(\nu))^2$$
$$= \sum_{\mu\nu\in E(2,2)} (\aleph(\mu))^2 + (\aleph(\nu))^2 + \sum_{\mu\nu\in E(2,4)} (\aleph(\mu))^2 + (\aleph(\nu))^2 + \sum_{\mu\nu\in E(2,6)} (\aleph(\mu))^2 + (\aleph(\nu))^2$$
$$+ \sum_{\mu\nu\in E(4,4)} (\aleph(\mu))^2 + (\aleph(\nu))^2 + \sum_{\mu\nu\in E(4,6)} (\aleph(\mu))^2 + (\aleph(\nu))^2 + \sum_{\mu\nu\in E(6,6)} (\aleph(\mu))^2 + (\aleph(\nu))^2 \quad (30)$$
$$= 4\left(2^2+2^2\right) + 8\left(2^2+4^2\right) + (12n-16)\left(2^2+6^2\right) + (6n-6)\left(4^2+4^2\right)$$
$$+ (12n-20)\left(4^2+6^2\right) + 6(n-2)^2\left(6^2+6^2\right).$$

We get the outcomes after estimates:

$$F(G) = 432n^2 - 432n + 48. \quad (31)$$

Theorem 9. *The Randić indices of Star of David network are*

$$R_1(G) = 216n^2 - 336n + 176,$$
$$R_{1/2}(G) = 36n^2 + 220.4n + 85.4,$$
$$R_{-1/2}(G) = n^2 + 3.4n - 1.4, \quad (32)$$
$$R_{-1}(G) = 0.17n^2 + 1.2n - 0.54.$$

Proof. Let G be the graph of Star of David network. By using Table 1, we apply the formula of the general Randić index for G:

$$R_\alpha(G) = \sum_{\mu\nu\in E(G)} (\aleph(\mu)\cdot\aleph(\nu))^\alpha. \quad (33)$$

For $\alpha = 1$,

$$R_1(G) = \sum_{\mu\nu\in E(G)} (\aleph(\mu)\cdot\aleph(\nu))$$
$$= \sum_{\mu\nu\in E(2,2)} (\aleph(\mu)\cdot\aleph(\nu)) + \sum_{\mu\nu\in E(2,4)} (\aleph(\mu)\cdot\aleph(\nu)) + \sum_{\mu\nu\in E(2,6)} (\aleph(\mu)\cdot\aleph(\nu))$$
$$+ \sum_{\mu\nu\in E(4,4)} (\aleph(\mu)\cdot\aleph(\nu)) + \sum_{\mu\nu\in E(4,6)} (\aleph(\mu)\cdot\aleph(\nu)) + \sum_{\mu\nu\in E(6,6)} (\aleph(\mu)\cdot\aleph(\nu)) \quad (34)$$
$$= 4(2\cdot 2) + 8(2\cdot 4) + (12n-16)(2\cdot 6) + (6n-6)(4\cdot 4)$$
$$+ (12n-20)(4\cdot 6) + 6(n-2)^2(6\cdot 6).$$

We get the outcomes after estimates:

$$R_1(G) = 216n^2 - 336n + 176. \quad (35)$$

For $\alpha = 1/2$,

$$\begin{aligned} R_{1/2}(G) &= \sum_{\mu\nu\in E(G)} (\aleph(\mu)\cdot\aleph(\nu))^{1/2} \\ &= \sum_{\mu\nu\in E(2,2)} (\aleph(\mu)\cdot\aleph(\nu))^{1/2} + \sum_{\mu\nu\in E(2,4)} (\aleph(\mu)\cdot\aleph(\nu))^{1/2} + \sum_{\mu\nu\in E(2,6)} (\aleph(\mu)\cdot\aleph(\nu))^{1/2} \\ &\quad \sum_{\mu\nu\in E(4,4)} (\aleph(\mu)\cdot\aleph(\nu))^{1/2} + \sum_{\mu\nu\in E(4,6)} (\aleph(\mu)\cdot\aleph(\nu))^{1/2} + \sum_{\mu\nu\in E(6,6)} (\aleph(\mu)\cdot\aleph(\nu))^{1/2} \\ &= 4(2\cdot 2)^{1/2} + 8(2\cdot 4)^{1/2} + (12n-16)(2\cdot 6)^{1/2} + (6n-6)(4\cdot 4)^{1/2} \\ &\quad + (12n-20)(4\cdot 6)^{1/2} + 6(n-2)^2(6\cdot 6)^{1/2}. \end{aligned} \quad (36)$$

We get the outcomes after estimates:

$$R_{1/2}(G) = 36n^2 + 220.4n + 85.4. \quad (37)$$

For $\alpha = -1/2$,

$$\begin{aligned} R_{-1/2}(G) &= \sum_{\mu\nu\in E(G)} (\aleph(\mu)\cdot\aleph(\nu))^{-1/2} \\ &= \sum_{\mu\nu\in E(2,2)} (\aleph(\mu)\cdot\aleph(\nu))^{-1/2} + \sum_{\mu\nu\in E(2,4)} (\aleph(\mu)\cdot\aleph(\nu))^{-1/2} + \sum_{\mu\nu\in E(2,6)} (\aleph(\mu)\cdot\aleph(\nu))^{-1/2} \\ &\quad \sum_{\mu\nu\in E(4,4)} (\aleph(\mu)\cdot\aleph(\nu))^{-1/2} + \sum_{\mu\nu\in E(4,6)} (\aleph(\mu)\cdot\aleph(\nu))^{-1/2} + \sum_{\mu\nu\in E(6,6)} (\aleph(\mu)\cdot\aleph(\nu))^{-1/2} \\ &= 4(2\cdot 2)^{-1/2} + 8(2\cdot 4)^{-1/2} + (12n-16)(2\cdot 6)^{-1/2} + (6n-6)(4\cdot 4)^{-1/2} \\ &\quad + (12n-20)(4\cdot 6)^{-1/2} + 6(n-2)^2(6\cdot 6)^{-1/2}. \end{aligned} \quad (38)$$

We get the outcomes after estimates:

$$R_{-1/2}(\mathrm{G}) = n^2 + 3.4n - 1.4. \quad (39)$$

For $\alpha = -1$,

$$\begin{aligned} R_{-1}(G) &= \sum_{\mu\nu\in E(G)} (\aleph(\mu)\cdot\aleph(\nu))^{-1} \\ &= \sum_{\mu\nu\in E(2,2)} (\aleph(\mu)\cdot\aleph(\nu))^{-1} + \sum_{\mu\nu\in E(2,4)} (\aleph(\mu)\cdot\aleph(\nu))^{-1} + \sum_{\mu\nu\in E(2,6)} (\aleph(\mu)\cdot\aleph(\nu))^{-1} \\ &\quad + \sum_{\mu\nu\in E(4,4)} (\aleph(\mu)\cdot\aleph(\nu))^{-1} + \sum_{\mu\nu\in E(4,6)} (\aleph(\mu)\cdot\aleph(\nu))^{-1} + \sum_{\mu\nu\in E(6,6)} (\aleph(\mu)\cdot\aleph(\nu))^{-1} \\ &= 4(2\cdot 2)^{-1} + 8(2\cdot 4)^{-1} + (12n-16)(2\cdot 6)^{-1} + (6n-6)(4\cdot 4)^{-1} \\ &\quad + (12n-20)(4\cdot 6)^{-1} + 6(n-2)^2(6\cdot 6)^{-1}. \end{aligned} \quad (40)$$

We get the outcomes after estimates:

$$R_{-1}(G) = 0.17n^2 + 1.2n - 0.54. \quad (41)$$

4.1. 3D Graphical Representation of Topological Indices for Star of David Networks. The TIs of the Star of David Network are illustrated graphically in Figure 3. The evolution of TIs along various parameters is portrayed in graphs. Despite the fact

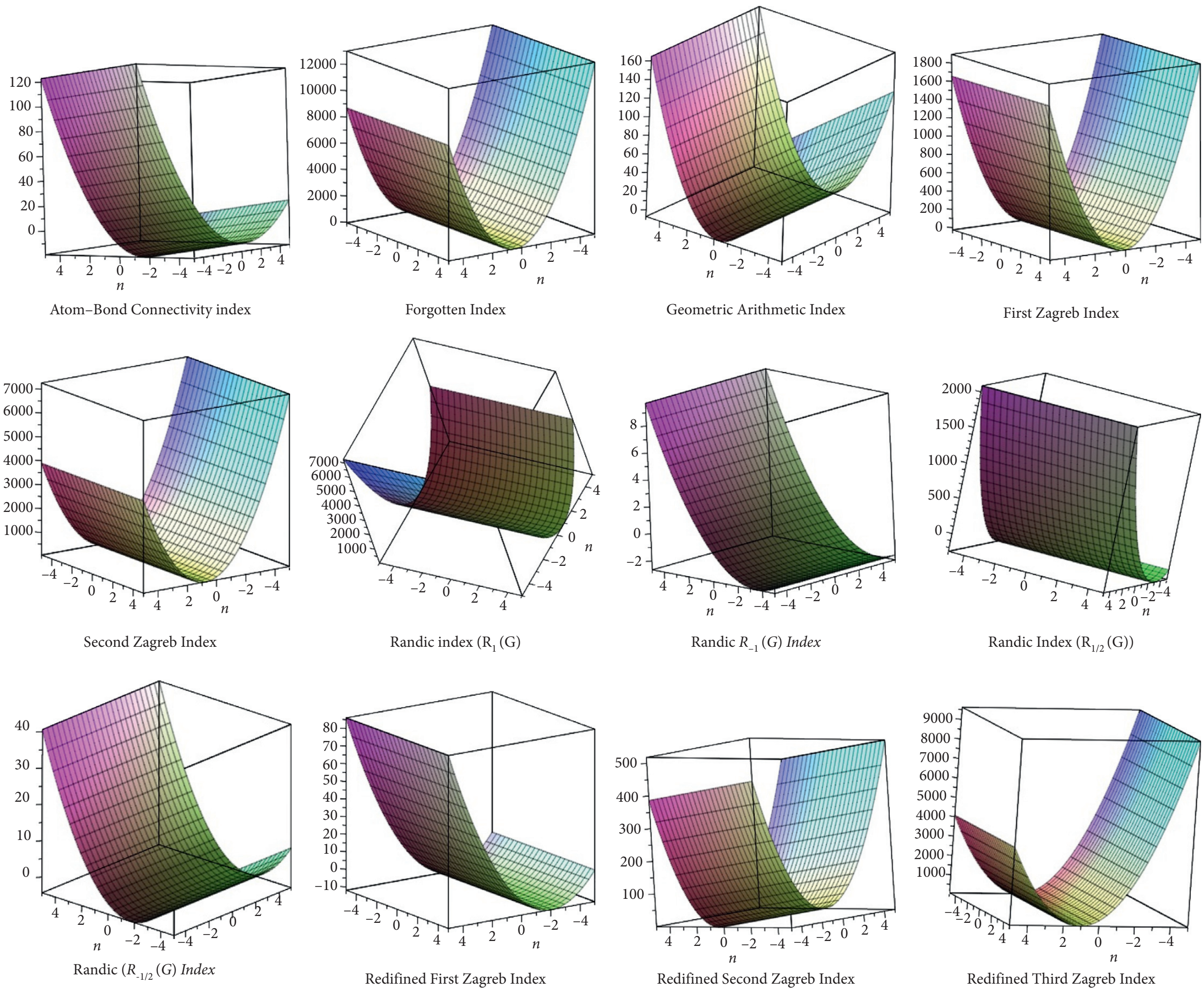

Figure 3: Three-dimensional graphical representation of degree-based topological indices.

Table 2: Numerical comparison of Star of David network.

n	$ABC(G)$	$GA(G)$	$M_1(G)$	$M_2(G)$	$\mathrm{Re}ZG_1(G)$	$\mathrm{Re}ZG_2(G)$	$\mathrm{Re}ZG_3(G)$	$F(G)$
1	−17.6	−21.8	24	56	6.03	7.47	736	48
2	−18.6	−149.6	216	368	20.03	48.27	2944	912
3	−13.2	−553.4	552	1112	38.03	125.07	10 336	2640
4	−1.4	−1377.2	1032	2288	60.03	237.87	22 912	5232
5	16.8	−2765	1656	3896	86.03	386.67	40 672	8688
6	41.4	−4860.8	2424	5936	116.03	571.47	63 616	13 008
7	72.4	−7808.6	3336	8408	150.03	792.27	91 744	18 192
8	109.8	−11 752.4	4392	11 312	188.03	1049.07	125 056	24 240
9	153.6	−16 836.2	5592	14 648	230.03	1341.87	163 552	31 152
10	203.8	−23 204	6936	18 416	276.03	1670.67	207 232	38 928

Table 3: Numerical comparison of Star of David networks.

n	1	2	3	4	5	6	7	8	9	10
$R_1(G)$	56	368	1112	2288	3896	5936	8408	11 312	14 648	18 416
$R_{1/2}(G)$	341.8	670.2	1070.6	1543	2087.4	2703.8	3392.2	4152.6	4985	5889.4
$R_{-1/2}(G)$	3	9.4	17.8	28.2	40.6	55	71.4	89.8	110.2	132.6
$R_{-1}(G)$	0.83	2.54	4.59	6.98	9.71	12.78	16.19	19.94	24.03	28.46

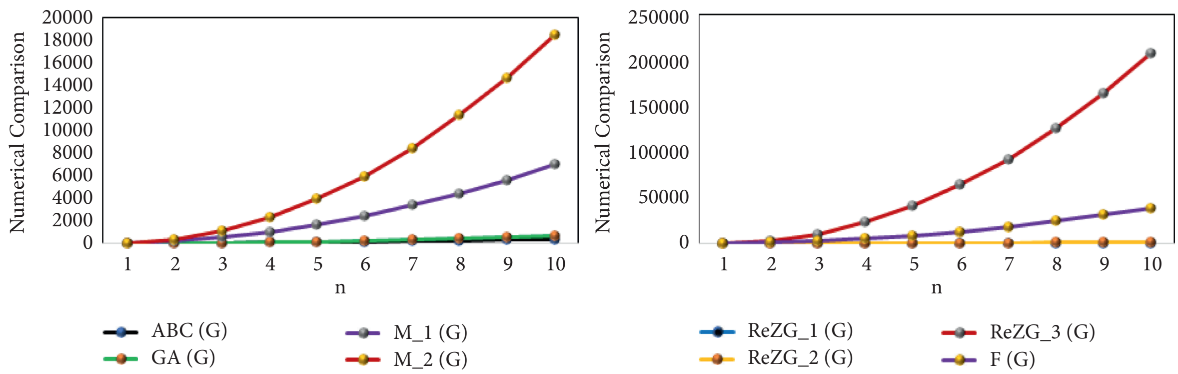

Figure 4: Two-dimensional numerical comparison of Star of David network.

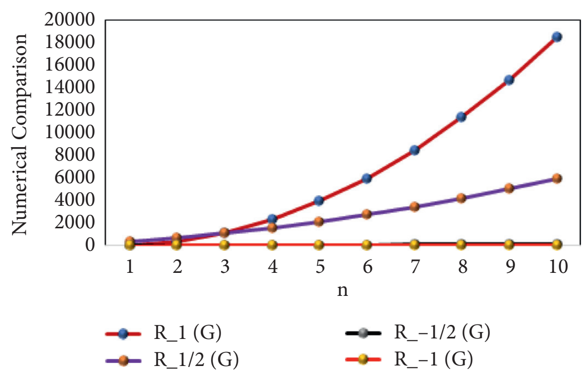

Figure 5: Two-dimensional numerical comparison of Star of David networks.

that the graphs appear to be similar, their gradients differ. In Figures 4 and 5, we give a two-dimensional numerical comparison of Star of David networks. We discuss the numerical comparison of Star of David networks with different degree-based topological indices in Tables 2 and 3.

5. Comparison of Results for Topological Indices of Star of David Networks

6. Conclusion

TIs for Star of David networks are computed in this paper; as well as, the analytic closed algorithms are reviewed and specified for these networks, namely, the general Randić index, the atomic-bond connectivity index, and the geometric-arithmetic index, as well as the first and second Zagreb index and closed formulas of this network were determined that will help network scientists in understanding and exploring the fundamental topologies of such networks. Computer scientists and chemists who work with Hex-derived networks may find these discoveries valuable.

Data Availability

No data were used to support this study.

Conflicts of Interest

The authors declare no conflicts of interest.

Authors' Contributions

All authors contributed equally to this manuscript. All authors have read and agreed to the published version of the manuscript.

Acknowledgments

The authors thank Jahangirnagar University, Savar, Dhaka for funding this reasearch.

References

[1] H. Ali, M. A. Binyamin, M. K. Shafiq, and W. Gao, "On the degree-based topological indices of some derived networks," *Mathematics*, vol. 7, no. 7, p. 612, 2019.

[2] H. Yang, M. Naeem, A. Q. Baig, H. Shaker, and M. K. Siddiqui, "Vertex szeged index of crystal cubic carbon structure," *Journal of Discrete Mathematical Sciences and Cryptography*, vol. 22, no. 7, pp. 1177–1187, 2019.

[3] Z. Raza and E. K. Sukaiti, "M-polynomial and degree based topological indices of some nanostructures," *Symmetry*, vol. 12, no. 5, p. 831, 2020.

[4] A. K. K. Syed, P. Ali, F. Azam, and P. Ahmad Alvi, "On ve-degree and ev-degree topological properties of hyaluronic acid-anticancer drug conjugates with qspr," *Journal of Chemistry*, vol. 2021, Article ID 3860856, 23 pages, 2021.

[5] A. Rani and U. Ali, "Degree-based topological indices of polysaccharides: amylose and blue starch-iodine complex," *Journal of Chemistry*, vol. 2021, Article ID 6652014, 10 pages, 2021.

[6] S. Ali, M. Khalid Mahmmod, and M. K. Mahmmod, "A paradigmatic approach to investigate restricted hyper totient graphs," *AIMS Mathematics*, vol. 6, no. 4, pp. 3761–3771, 2021.

[7] S. Ali, M. K. Mahmood, F. Tchier, and F. M. O. Tawfiq, "Classification of upper bound sequences of local fractional metric dimension of rotationally symmetric hexagonal planar networks," *Journal of Mathematics*, vol. 2021, Article ID 6613033, 24 pages, 2021.

[8] S. Ali, M. K. Mahmood, and K. P. Shum, "Novel classes of integers and their applications in graph labeling," *Hacettepe Journal of Mathematics and Statistics*, vol. XX, pp. 1–17, 2021.

[9] J.-B. Liu and S. Nagy Daoud, "Number of spanning trees in the sequence of some graphs," *Complexity*, vol. 2019, Article ID 4271783, 22 pages, 2019.

[10] J.-B. Liu, X.-F. Pan, and J. Cao, "Some properties on estrada index of folded hypercubes networks," in *Abstract and Applied Analysis*vol. 2014, Hindawi, Article ID 167623, 6 pages, Hindawi, 2014.

[11] J.-B. Liu, Z.-Yu Shi, Y.-H. Pan, J. Cao, M. Abdel-Aty, and U. Al-Juboori, "Computing the laplacian spectrum of linear octagonal-quadrilateral networks and its applications," *Polycyclic Aromatic Compounds*, pp. 1–12, 2020.

[12] J.-B. Liu, C. Wang, S. Wang, and B. Wei, "Zagreb indices and multiplicative zagreb indices of Eulerian graphs," *Bulletin of the Malaysian Mathematical Sciences Society*, vol. 42, no. 1, pp. 67–78, 2019.

[13] J.-B. Liu, J. Zhao, and Z.-Q. Cai, "On the generalized adjacency, laplacian and signless laplacian spectra of the weighted edge corona networks," *Physica A: Statistical Mechanics and its Applications*, vol. 540, Article ID 123073, 2020.

[14] J.-B. Liu, J. Zhao, J. Min, and J. Cao, "The hosoya index of graphs formed by a fractal graph," *Fractals*, vol. 27, no. 8, Article ID 1950135, 2019.

[15] D. Maji and G. Ghorai, "Computing f-index, coindex and zagreb polynomials of the kth generalized transformation graphs," *Heliyon*, vol. 6, 2020.

[16] D. Maji and G. Ghorai, "A novel graph invariant: the third leap zagreb index under several graph operations," *Discrete Mathematics, Algorithms and Applications*, vol. 11, 2019.

[17] S. Ali, R. M. Falcón, and M. K. Mahmood, "Local fractional metric dimension of rotationally symmetric planar graphs arisen from planar chorded cycles," arXiv preprint arXiv: 2105.07808, 2021.

[18] S. Ali and K. Mahmood, "New numbers on euler's totient function with applications," *Journal of Mathematical Extension*, vol. 14, pp. 61–83, 2019.

[19] S. Ali and M. K. Mahmood, "A paradigmatic approach to investigate restricted totient graphs and their indices," *Computer Science*, vol. 16, no. 2, pp. 793–801, 2021.

[20] M. K. Mahmood and S. Ali, "A novel labeling algorithm on several classes of graphs," *Punjab University Journal of Mathematics*, vol. 49, pp. 23–35, 2017.

[21] M. K. Mahmood and S. Ali, "On super totient numbers, with applications and algorithms to graph labeling," *Ars Combinatoria*, vol. 143, pp. 29–37, 2019.

[22] H. Wiener, "Structural determination of paraffin boiling points," *Journal of the American Chemical Society*, vol. 69, no. 1, pp. 17–20, 1947.

[23] M. Randic, "Characterization of molecular branching," *Journal of the American Chemical Society*, vol. 97, no. 23, pp. 6609–6615, 1975.

[24] L. B. Kier and L. H. Hall, "Molecular connectivity vii: specific treatment of heteroatoms," *Journal of Pharmaceutical Sciences*, vol. 65, no. 12, pp. 1806–1809, 1976.

[25] M. Randić, M. Novič, and D. Plavšić, *Solved and Unsolved Problems of Structural Chemistry*, CRC Press, Boca Raton, MA, USA, 2016.

[26] B. Bollobás and E. Paul, "Graph of extremal weights," *Ars Combinatoria*, vol. 50, pp. 225–233, 1998.

[27] I. Gutman and N. Trinajstić, "Graph theory and molecular orbitals. total -electron energy of alternant hydrocarbons," *Chemical Physics Letters*, vol. 17, no. 4, pp. 535–538, 1972.

[28] I. Gutman and K. C. Das, "The first zagreb index 30 years after," *MATCH Communications in Mathematical and in Computer Chemistry*, vol. 50, no. 1, pp. 83–92, 2004.

[29] N. Trinajstić, S. Nikolić, A. Miličević, and I. Gutman, "About the zagreb indices," *Kemija U Industriji: Časopis kemičara i kemijskih inženjera Hrvatske*, vol. 59, no. 12, pp. 577–589, 2010.

[30] D. Maji and G. Ghorai, "The first entire zagreb index of various corona products and their bounds," *Journal of Mathematical and Computational Science*, vol. 11, 2021.

[31] P. S. Ranjini, V. Lokesha, and A. Usha, "Relation between phenylene and hexagonal squeeze using harmonic index," *International Journal of Graph Theory*, vol. 1, no. 4, pp. 116–121, 2013.

[32] E. Estrada, L. Torres, L. Rodriguez, and I. Gutman, "An atom-bond connectivity index: modelling the enthalpy of formation of alkanes," *Indian Journal of Chemistry*, vol. 37A, 1998.

[33] D. Vukičević and B. Furtula, "Topological index based on the ratios of geometrical and arithmetical means of end-vertex degrees of edges," *Journal of Mathematical Chemistry*, vol. 46, no. 4, pp. 1369–1376, 2009.

[34] B. Furtula and I. Gutman, "A forgotten topological index," *Journal of Mathematical Chemistry*, vol. 53, no. 4, pp. 1184–1190, 2015.

[35] W. Gao, M. K. Siddiqui, M. Imran, M. Kamran Jamil, and M. Reza Farahani, "Forgotten topological index of chemical structure in drugs," *Saudi Pharmaceutical Journal*, vol. 24, no. 3, pp. 258–264, 2016.

Hindawi
Journal of Mathematics
Volume 2021, Article ID 5353372, 11 pages
https://doi.org/10.1155/2021/5353372

Research Article

On *q*-ANALOGUE of Differential Subordination Associated with Lemniscate of Bernoulli

Mohsan Raza [1], **Hira Naz** [2], **Sarfraz Nawaz Malik** [2], **and Sahidul Islam** [3]

[1] *Department of Mathematics, Government College University Faisalabad, Faisalabad 38000, Pakistan*
[2] *Department of Mathematics, COMSATS University Islamabad, Wah Campus, Wah Cantt 47040, Pakistan*
[3] *Department of Mathematics, Jahangirnagar University, Savar, Dhaka, Bangladesh*

Correspondence should be addressed to Sahidul Islam; sahidul.sohag@juniv.edu

Received 21 September 2021; Accepted 15 October 2021; Published 1 November 2021

Academic Editor: Fairouz Tchier

This article comprises the study of differential subordination with analogue of q-derivative. It includes the sufficient condition on γ for $1 + (\gamma \partial z_q h(z)/h^n(z))$ to be subordinated by $(1 + Az/1 + Bz)$, $-1 \le B < A \le 1$, and implies that $h(z) \prec \sqrt{1+z}$, where $h(z)$ is the analytic function in the open unit disk. Moreover, certain sufficient conditions for q-starlikeness of analytic functions related with lemniscate of Bernoulli are determined.

1. Introduction

Let a set $\mathscr{A}$ be considered as the class of analytic functions defined in open unit disk $\mathbb{U} = \{\varsigma\colon \varsigma \in \mathbb{C} \text{ and } |\varsigma| < 1\}$ under normalization conditions $f(0) = 0$ and $f'(0) = 1$, having

$$f(\varsigma) = \varsigma + \sum_{n=2}^{\infty} a_n \varsigma^n, \quad \varsigma \in \mathbb{U}, \tag{1}$$

as Taylor series. The class S comprises the normalized univalent functions, defined in $\mathbb{U}$. The major subcategories of class S are C of convex functions and S^* of starlike functions. The class P is another important class of analytic univalent functions whose co-domains are restricted to the right half plane and are used to determine the convexity and starlikeness of univalent functions. For more details, see [1, 2].

Let f and g be two analytic functions in $\mathbb{U}$. Then, f is subordinated by g, denoted as $f \prec g$ if f can be written in the form of composition of g and ϖ as $f(\varsigma) = g(\varpi(\varsigma))$ subject to the existence of analytic function ϖ which satisfies the condition that $\varpi(0) = 0$ and $|\varpi(\varsigma)| < |\varsigma|$. Furthermore, if both f and g are univalent functions in $\mathbb{U}$, then $f \prec g$ implies that $f(0) = g(0)$ and $f(\mathbb{U}) \subset g(\mathbb{U})$.

Subordination plays an important role in univalent function theory, and this concept was first introduced by Lindelöf, but Littlewood [3, 4] contributed remarkably to this field. Differential subordination is actually the generalized version of differential inequalities with real variables. Many researchers contributed in the work related to differential subordinations. Historical developments in the field of differential subordination are briefly described by Miller and Mocanu in [5].

The advancement in the field of differential subordination starts with the usage of univalent functions. It was noticed in an article by Miller et al. [6] in 1974. Furthermore, many developments in this field have been achieved with the usage of differential subordinations in past fifty years. Differential inequality was a very well-known concept of real variables, and to study it in terms of complex variables, Miller and Mocanu [7] in 1981 were the first ones to introduce the idea of differential subordination. The contribution of Ruscheweyh and Singh [8] and Ruscheweyh and Wilken [9] is also of great importance in this field. Well-known Jack's lemma [10] has brought the advancements in differential subordinations. Dziok [11] worked on some of the applications of Jack's lemma. The research work carried out by Ma and Minda [12] in the function theory is worth to mention here, as they introduced the analytic function Φ, which satisfies the conditions of normalization $\Phi(0) = 0$ and $\Phi'(0) > 1$ having real part positive. The authors in [12] utilized the function Φ and introduced the subclass $\mathscr{S}^*(\Phi)$ of starlike functions as follows:

$$\mathcal{S}^*(\Phi) = \left\{ f \in \mathcal{A}: \frac{\varsigma f'(\varsigma)}{f(\varsigma)} \prec \Phi(\varsigma); \quad \varsigma \in \mathbb{U} \right\}. \tag{2}$$

The idea presented in [12] is very useful, and it helped many researchers for further studies in this direction. Ali et al. [13, 14] worked on differential subordination for sufficiency criteria of Janowski starlikeness and evaluated several differential subordinations such as $1 + \gamma\varsigma (p'(\varsigma)/p^n(\varsigma))$ and found $p(\varsigma) \prec \sqrt{1+\varsigma}$. Also, Ravichandran et al. [15] used this concept to find the sufficient conditions for starlikeness of Bernoulli's lemniscate and Janowski functions. Sharma et al. [16] studied the differential subordinations to prove the starlikeness associated with cardioid domain and Halim et al. [17] introduced the concept for limacon domain.

Jackson [18, 19] was the one who introduced the q-derivatives and q-integrals. After Jackson, Srivastava was amongst the pioneers to contribute in the q-calculus for its usage for analytic functions and their subclasses. Not only this, but he also applied q-hypergeometric function in the functions theory. All these contributions are comprised in his book (pp. 347 in [20]). Ismail et al. [21] contributed in the q-calculus for the study of starlike functions. Anastassiu and Gal [22, 23] also played their part in the development of complex variables with q-generalization. Purohit et al. [24] have used fractional q-calculus operators to apply subordination conditions on the class of non-Bazilevic functions. Sahoo and Agrawal [25] worked on starlike functions in q-calculus and extended the idea of q-starlikeness for particular subclasses of starlike functions. The involvement of q-derivative in the class $\mathcal{S}^*(\Phi)$ gave the formation of following subclass $\mathcal{S}_q^*(\Phi)$ of starlike functions which was introduced by Aouf and Seoudy [26].

$$\mathcal{S}_q^*(\Phi) = \left\{ f \in \mathcal{A}: \frac{\varsigma D_q f(\varsigma)}{f(\varsigma)} \prec \Phi(\varsigma); \quad \varsigma \in \mathbb{U} \right\}. \tag{3}$$

The class described above has drawn the attention of many researchers. Replacing $\Phi(\varsigma)$ with different functions such as Janowski, lemniscate of Bernoulli, cardioid, and limacon, the researchers got the new directions to the study. Srivastava et al. [27] studied q-derivatives to find the relation between different classes of q-starlike functions related to Janowski function. Srivastava et al. [28] introduced the class of q-starlike functions by using general conic domains. They also obtained the bounds on Hankel and Toeplitz determinants for q-starlike functions and continued working par excellence. They produced unmatchable results that worked as great motivation for many researchers worldwide. To have an idea of their remarkable work, one can see [29–31], [20, 27, 28, 32–43]. Contributions of Haq et al. [44] and Zainab et al. [45] are also worth to mention. They studied q-analogue of differential subordinations for star-like functions related to limacon and cardioid domains, and Janowski functions. The q-derivative is the foundation of all this work in q-analogue, and it is defined as follows.

The q-derivative of a complex valued function f, defined in the domain $\mathbb{U}$, is given as follows:

$$\left(D_q f\right)(\varsigma) = \begin{cases} \dfrac{f(\varsigma) - f(q\varsigma)}{(1-q)\varsigma}, & \varsigma \neq 0, \\ f'(0), & \varsigma = 0, \end{cases} \tag{4}$$

where $0 < q < 1$. This implies the following:

$$\lim_{q \longrightarrow 1^-} \left(D_q f\right)(\varsigma) = \lim_{q \longrightarrow 1^-} \frac{f(\varsigma) - f(q\varsigma)}{(1-q)\varsigma} = f'(\varsigma), \tag{5}$$

on the assumption that the function f is differentiable in $\mathbb{U}$. The q-derivative $D_q f$ of an analytic function f has Taylor series of the form

$$\left(D_q f\right)(\varsigma) = \sum_{n=0}^{\infty} [n]_q a_n \varsigma^{n-1}, \tag{6}$$

where

$$[n]_q = \begin{cases} \dfrac{1-q^n}{1-q}, & n \in \mathbb{C}, \\ \sum_{k=0}^{n-1} q^k, & n \in \mathbb{N}. \end{cases} \tag{7}$$

For more details about q-derivative and recent work on it, we refer the readers to [29–31], [20, 27, 28, 32–43]. In addition, the q-analogue of Jack's lemma has played a vital role in this paper which states as follows.

Lemma 1 (see [46]). *Let ϖ be an analytic function in $\mathbb{U}$ with $\varpi(0) = 0$. For maximum of ϖ on $|\varsigma| = 1$ at $\varsigma_0 = ae^{i\theta}$, where $\theta \in [-\pi, \pi]$ and $0 < q < 1$, then we have*

$$\varsigma_0 D_q \varpi(\varsigma_0) = m\varpi(\varsigma_0), \tag{8}$$

where $m \in \mathbb{R}$ with $m \geq 1$.

2. Main Results

Theorem 1. *Assume that*

$$|\gamma| \geq \frac{(A-B)(\sqrt{2} + \sqrt{3-q})}{(1-|B|)}, \quad -1 < B < A \leq 1. \tag{9}$$

Consider an analytic function h on $\mathbb{U}$ with $h(0) = 1$ which satisfies

$$1 + \gamma\varsigma D_q h(\varsigma) \prec \frac{1 + A\varsigma}{1 + B\varsigma}, \quad \varsigma \in \mathbb{U}. \tag{10}$$

Also, suppose

$$1 + \gamma\varsigma D_q h(\varsigma) = \frac{1 + A\varpi(\varsigma)}{1 + B\varpi(\varsigma)}, \quad \varsigma \in \mathbb{U}. \tag{11}$$

Here, ϖ is an analytic function in $\mathbb{U}$ such that $\varpi(0) = 0$. Then, we have

$$h(\varsigma) \prec \sqrt{1+\varsigma}. \tag{12}$$

Proof. Suppose that

$$p(\varsigma) = 1 + \gamma\varsigma D_q h(\varsigma), \tag{13}$$

where p is analytic, and we have $p(0) = 1$. Also, consider that

$$h(\varsigma) = \sqrt{1 + \varpi(\varsigma)}. \tag{14}$$

Now, we prove that $|\varpi(\varsigma)| < 1$, where

$$\varpi(\varsigma) = \frac{p(\varsigma) - 1}{A - Bp(\varsigma)}. \tag{15}$$

Using (13) and (14), we obtain

$$p(\varsigma) = 1 + \gamma\varsigma \frac{D_q\varpi(\varsigma)}{\sqrt{1 + \varpi(\varsigma)} + \sqrt{1 + \varpi(\varsigma) - \varsigma D_q\varpi(\varsigma)(1 - q)}}. \tag{16}$$

Also, we have

$$\left|\frac{p(\varsigma) - 1}{A - Bp(\varsigma)}\right| = \left|\frac{\gamma\varsigma D_q\varpi(\varsigma)}{(A - B)\left[\sqrt{1 + \varpi(\varsigma)} + \sqrt{1 + \varpi(\varsigma) - \varsigma D_q\varpi(\varsigma)(1 - q)}\right] - B\gamma\varsigma D_q\varpi(\varsigma)}\right|. \tag{17}$$

Consider a point $\varsigma_0 \in \mathbb{U}$ such that

$$\max_{|\varsigma| \le |\varsigma_0|} |\varpi(\varsigma)| = |\varpi(\varsigma_0)| = 1. \tag{18}$$

Now, by using Lemma 1, we have $\varsigma_0 D_q\varpi(\varsigma_0) = m\varpi(\varsigma_0)$, $m \ge 1$. Now, consider that $\varpi(\varsigma_0) = e^{i\theta}$, $\theta \in [-\pi, \pi]$; then, for $\varsigma_0 \in \mathbb{U}$, we obtain

$$\begin{aligned} \left|\frac{p(\varsigma_0) - 1}{A - Bp(\varsigma_0)}\right| &= \left|\frac{\gamma\varsigma_0 D_q\varpi(\varsigma_0)}{(A - B)\left[\sqrt{1 + \varpi(\varsigma_0)} + \sqrt{1 + \varpi(\varsigma_0) - \varsigma_0 D_q\varpi(\varsigma_0)(1 - q)}\right] - B\gamma\varsigma_0 D_q\varpi(\varsigma_0)}\right|, \\ &\ge \frac{|\gamma|m}{(A - B)\left[\sqrt{|1| + \left|e^{i\theta}\right|} + \sqrt{|1| + \left|e^{i\theta}\right| + \left|me^{i\theta}(1 - q)\right|}\right] + |B||\gamma|m}, \\ &= \frac{|\gamma|m}{(A - B)\left[\sqrt{2} + \sqrt{2 + m(1 - q)}\right] + |B||\gamma|m}. \end{aligned} \tag{19}$$

Consider a new function

$$\Xi(m) = \frac{|\gamma|m}{(A - B)\left[\sqrt{2} + \sqrt{2 + m(1 - q)}\right] + |B||\gamma|m}. \tag{20}$$

Then,

$$\Xi'(m) = \frac{|\gamma|\left[(A - B)\left\{\sqrt{2} + \sqrt{2 + m(1 - q)}\right\}\right] - |\gamma|m\left[\left((A - B)(1 - q)/2\sqrt{2 + m(1 - q)}\right)\right]}{\left[(A - B)\left\{\sqrt{2} + \sqrt{2 + m(1 - q)}\right\} + |B||\gamma|m\right]^2} > 0. \tag{21}$$

Above expression represents that the function Ξ has increasing behavior, so we have its minimum value at $m = 1$ and

$$\Xi(1) = \frac{|\gamma|}{(A - B)\left[\sqrt{2} + \sqrt{3 - q}\right] + |B||\gamma|}. \tag{22}$$

So, we conclude that

$$\left|\frac{p(\varsigma_0) - 1}{A - Bp(\varsigma_0)}\right| \ge \frac{|\gamma|}{(A - B)\left[\sqrt{2} + \sqrt{3 - q}\right] + |B||\gamma|}. \tag{23}$$

Now, from (9), we have

$$\left|\frac{p(\varsigma_0) - 1}{A - Bp(\varsigma_0)}\right| \ge 1, \tag{24}$$

Since this result contradicts (10), therefore, $|\varpi(\varsigma)| < 1$, which completes the proof.

By taking $h(\varsigma) = (\varsigma D_q f(\varsigma)/f(\varsigma))$, we deduce the following result. ☐

Corollary 1. *Let* $|\gamma| \ge ((A - B)(\sqrt{2} + \sqrt{3 - q})/(1 - |B|))$, $-1 < B < A \le 1$ *and* $f \in \mathcal{A}$, *satisfy the subordination*

$$1+\gamma\varsigma D_q\left(\frac{\varsigma D_q f(\varsigma)}{f(\varsigma)}\right)\prec\frac{1+A\varsigma}{1+B\varsigma}. \tag{25}$$

Then, $f\in\mathcal{S}_q^*(\sqrt{1+\varsigma})$.

Theorem 2. *Assume that*

$$|\gamma|\geq\frac{\sqrt{2}(A-B)(\sqrt{2}+\sqrt{3-q})}{(1-|B|)},\quad -1<B<A\leq 1. \tag{26}$$

Consider an analytic function h on $\mathbb{U}$ with $h(0)=1$ which satisfies

$$1+\frac{\gamma\varsigma D_q h(\varsigma)}{h(\varsigma)}\prec\frac{1+A\varsigma}{1+B\varsigma},\quad \varsigma\in\mathbb{U}. \tag{27}$$

Also, suppose

$$1+\frac{\gamma\varsigma D_q h(\varsigma)}{h(\varsigma)}=\frac{1+A\varpi(\varsigma)}{1+B\varpi(\varsigma)},\quad \varsigma\in\mathbb{U}, \tag{28}$$

where ϖ is analytic function on $\mathbb{U}$ with $\varpi(0)=0$. Then,

$$h(\varsigma)\prec\sqrt{1+\varsigma}. \tag{29}$$

Proof. We define a function

$$p(\varsigma)=1+\frac{\gamma\varsigma D_q h(\varsigma)}{h(\varsigma)}, \tag{30}$$

where p is analytic and $p(0)=1$. Now, consider that

$$h(\varsigma)=\sqrt{1+\varpi(\varsigma)}. \tag{31}$$

To obtain the result, we have to show that $|\varpi(\varsigma)|<1$. Using (30) and (31), we obtain the result

$$p(\varsigma)=1+\gamma\varsigma\frac{D_q\varpi(\varsigma)}{\sqrt{1+\varpi(\varsigma)}\left[\sqrt{1+\varpi(\varsigma)}+\sqrt{1+\varpi(\varsigma)-\varsigma D_q\varpi(\varsigma)(1-q)}\right]}. \tag{32}$$

Also, we have

$$\left|\frac{p(\varsigma)-1}{A-Bp(\varsigma)}\right|=\left|\frac{\gamma\varsigma D_q\varpi(\varsigma)}{(A-B)\sqrt{1+\varpi(\varsigma)}\left[\sqrt{1+\varpi(\varsigma)}+\sqrt{1+\varpi(\varsigma)-\varsigma D_q\varpi(\varsigma)(1-q)}\right]-B\gamma\varsigma D_q\varpi(\varsigma)}\right|. \tag{33}$$

Consider a point $\varsigma_0\in\mathbb{U}$ such that

$$\max_{|\varsigma|\leq|\varsigma_0|}|\varpi(\varsigma)|=|\varpi(\varsigma_0)|=1. \tag{34}$$

Now, by using Lemma 1, we have $\varsigma_0 D_q\varpi(\varsigma_0)=m\varpi(\varsigma_0)$, $m\geq 1$. Now, consider that $\varpi(\varsigma_0)=e^{i\theta}$, $\theta\in[-\pi,\pi]$; then, for $\varsigma_0\in\mathbb{U}$, we obtain

$$\begin{aligned}\left|\frac{p(\varsigma_0)-1}{A-Bp(\varsigma_0)}\right|&=\left|\frac{\gamma m e^{i\theta}}{(A-B)\sqrt{1+e^{i\theta}}\left[\sqrt{1+e^{i\theta}}+\sqrt{1+e^{i\theta}-me^{i\theta}(1-q)}\right]-B\gamma me^{i\theta}}\right|,\\ &\geq\frac{|\gamma|m}{(A-B)\sqrt{|1|+|e^{i\theta}|}\left[\sqrt{|1|+|e^{i\theta}|}+\sqrt{|1|+|e^{i\theta}|+|me^{i\theta}(1-q)|}\right]+|B||\gamma|m},\\ &=\frac{|\gamma|m}{(A-B)\sqrt{2}[\sqrt{2}+\sqrt{2+m(1-q)}]+|B||\gamma|m}.\end{aligned} \tag{35}$$

Consider

$$\Xi_1(m) = \frac{|\gamma|m}{(A-B)\sqrt{2}[\sqrt{2} + \sqrt{2+m(1-q)}] + |B||\gamma|m}. \tag{36}$$

Then,

$$\Xi_1'(m) = \frac{|\gamma|[(A-B)\sqrt{2}\{\sqrt{2} + \sqrt{2+m(1-q)}\}] - |\gamma|m[(\sqrt{2}(A-B)(1-q)/2\sqrt{2+m(1-q)})]}{[(A-B)\sqrt{2}\left\{\sqrt{2} + \sqrt{2+m(1-q)}\right\} + |B||\gamma|m]^2} > 0. \tag{37}$$

Above expression represents that function Ξ_1 has increasing behavior, so we have its minimum value at $m = 1$ and

$$\Xi_1(1) = \frac{|\gamma|}{(A-B)\sqrt{2}[\sqrt{2} + \sqrt{3-q}] + |B||\gamma|}. \tag{38}$$

So, we conclude that

$$\left|\frac{p(\varsigma_0)-1}{A-Bp(\varsigma_0)}\right| \geq \frac{|\gamma|}{(A-B)\sqrt{2}[\sqrt{2} + \sqrt{3-q}] + |B||\gamma|}. \tag{39}$$

Now, from (26), we have

$$\left|\frac{p(\varsigma_0)-1}{A-Bp(\varsigma_0)}\right| \geq 1, \tag{40}$$

which contradicts (27), and hence, $|\varpi(\varsigma)| < 1$, which completes the proof.

By taking $h(\varsigma) = (\varsigma D_q f(\varsigma)/f(\varsigma))$,we deduce the following result. □

Corollary 2. *Let* $|\gamma| \geq \sqrt{2}((A-B)(\sqrt{2} + \sqrt{3-q})/(1-|B|))$, $-1 < B < A \leq 1$ *and* $f \in \mathcal{A}$, *which satisfies the subordination*

$$1 + \gamma\varsigma\left(\frac{f(\varsigma)}{\varsigma D_q f(\varsigma)}\right) D_q\left(\frac{\varsigma D_q f(\varsigma)}{f(\varsigma)}\right) \prec \frac{1+A\varsigma}{1+B\varsigma}. \tag{41}$$

Then, $f \in \mathcal{S}_q^*(\sqrt{1+\varsigma})$.

Theorem 3. *Assume that*

$$|\gamma| \geq \frac{2(A-B)(\sqrt{2} + \sqrt{3-q})}{(1-|B|)}, \quad -1 < B < A \leq 1. \tag{42}$$

Consider an analytic function h on $\mathbb{U}$ with $h(0) = 1$ which satisfies

$$1 + \frac{\gamma\varsigma D_q h(\varsigma)}{h^2(\varsigma)} \prec \frac{1+A\varsigma}{1+B\varsigma}, \quad \varsigma \in \mathbb{U}. \tag{43}$$

Also, suppose

$$1 + \frac{\gamma\varsigma D_q h(\varsigma)}{h^2(\varsigma)} = \frac{1+A\varpi(\varsigma)}{1+B\varpi(\varsigma)}, \quad \varsigma \in \mathbb{U}, \tag{44}$$

where ϖ is analytic function on $\mathbb{U}$ with $\varpi(0) = 0$. Then,

$$h(\varsigma) \prec \sqrt{1+\varsigma}. \tag{45}$$

Proof. We define a function

$$p(\varsigma) = 1 + \frac{\gamma\varsigma D_q h(\varsigma)}{h^2(\varsigma)}, \tag{46}$$

where p is analytic, and we have $p(0) = 1$. Now, consider that

$$h(\varsigma) = \sqrt{1+\varpi(\varsigma)}. \tag{47}$$

To obtain the result, we have to show that $|\varpi(\varsigma)| < 1$. Using (46) and (47), we obtain the result

$$p(\varsigma) = 1 + \gamma\varsigma \frac{D_q\varpi(\varsigma)}{\sqrt{1+\varpi(\varsigma)}\left[\sqrt{1+\varpi(\varsigma)} + \sqrt{1+\varpi(\varsigma) - \varsigma D_q\varpi(\varsigma)(1-q)}\right]}. \tag{48}$$

Also, we have

$$\left|\frac{p(\varsigma)-1}{A-Bp(\varsigma)}\right| = \left|\frac{\gamma\varsigma D_q\varpi(\varsigma)}{(A-B)\sqrt{1+\varpi(\varsigma)}\left[\sqrt{1+\varpi(\varsigma)} + \sqrt{1+\varpi(\varsigma) - \varsigma D_q\varpi(\varsigma)(1-q)}\right] - B\gamma\varsigma D_q\varpi(\varsigma)}\right|. \tag{49}$$

Consider a point $\varsigma_0 \in \mathbb{U}$ such that

$$\max_{|\varsigma|\leq|\varsigma_0|} |\varpi(\varsigma)| = |\varpi(\varsigma_0)| = 1. \tag{50}$$

Now, by using Lemma 1, we have $\varsigma_0 D_q \varpi(\varsigma_0) = m\varpi(\varsigma_0)$, $m \geq 1$. Now, consider that $\varpi(\varsigma_0) = e^{i\theta}$, $\theta \in [-\pi, \pi]$; then, for $\varsigma_0 \in \mathbb{U}$, we obtain

$$\begin{aligned}\left|\frac{p(\varsigma_0)-1}{A-Bp(\varsigma_0)}\right| &= \left|\frac{\gamma m e^{i\theta}}{(A-B)\sqrt{1+e^{i\theta}}\left[\sqrt{1+e^{i\theta}} + \sqrt{1+e^{i\theta} - me^{i\theta}(1-q)}\right] - B\gamma m e^{i\theta}}\right|,\\ &\geq \frac{|\gamma| m}{(A-B)\sqrt{|1|+\left|e^{i\theta}\right|}\left[\sqrt{|1|+\left|e^{i\theta}\right|} + \sqrt{|1|+\left|e^{i\theta}\right| + \left|me^{i\theta}(1-q)\right|}\right] + |B||\gamma| m},\\ &= \frac{|\gamma| m}{(A-B)2\left[\sqrt{2} + \sqrt{2+m(1-q)}\right] + |B||\gamma| m}.\end{aligned} \tag{51}$$

Consider a function

$$\Xi_2(m) = \frac{|\gamma| m}{(A-B)2\left[\sqrt{2} + \sqrt{2+m(1-q)}\right] + |B||\gamma| m}. \tag{52}$$

Then,

$$\Xi_2'(m) = \frac{|\gamma|\left[(A-B)2\left\{\sqrt{2} + \sqrt{2+m(1-q)}\right\}\right] - |\gamma| m\left[\left(2(A-B)(1-q)/2\sqrt{2+m(1-q)}\right)\right]}{\left[(A-B)2\left\{\sqrt{2} + \sqrt{2+m(1-q)}\right\} + |B||\gamma| m\right]^2} > 0. \tag{53}$$

Here, Ξ_2 is clearly an increasing function, so we have its minimum value at $m = 1$ and

$$\Xi_2(1) = \frac{|\gamma|}{2(A-B)\left[\sqrt{2} + \sqrt{3-q}\right] + |B||\gamma|}. \tag{54}$$

So, we conclude that

$$\left|\frac{p(\varsigma_0)-1}{A-Bp(\varsigma_0)}\right| \geq \frac{|\gamma|}{2(A-B)\left[\sqrt{2} + \sqrt{3-q}\right] + |B||\gamma|}. \tag{55}$$

Now, from (42), we have

$$\left|\frac{p(\varsigma_0)-1}{A-Bp(\varsigma_0)}\right| \geq 1, \tag{56}$$

which contradict (43), and hence, $|\varpi(\varsigma)| < 1$, which completes the proof.

By taking $h(\varsigma) = (\varsigma D_q f(\varsigma)/f(\varsigma))$, we deduce the following result. ☐

Corollary 3. *Let* $|\gamma| \geq 2\left((A-B)\left(\sqrt{2} + \sqrt{3-q}\right)/(1-|B|)\right)$, $-1 < B < A \leq 1$ *and* $f \in \mathscr{A}$, *satisfies the subordination*

$$1 + \gamma\varsigma\left(\frac{f(\varsigma)}{\varsigma D_q f(\varsigma)}\right)^2 D_q\left(\frac{\varsigma D_q f(\varsigma)}{f(\varsigma)}\right) \prec \frac{1+A\varsigma}{1+B\varsigma}. \tag{57}$$

Then, $f \in \mathcal{S}_q^*\left(\sqrt{1+\varsigma}\right)$.

Theorem 4. *Assume that*

$$|\gamma| \geq \frac{2\sqrt{2}(A-B)\left(\sqrt{2} + \sqrt{3-q}\right)}{(1-|B|)}, \quad -1 < B < A \leq 1. \tag{58}$$

Consider an analytic function h on $\mathbb{U}$ with $h(0) = 1$ which satisfies

$$1 + \frac{\gamma\varsigma D_q h(\varsigma)}{h^3(\varsigma)} \prec \frac{1+A\varsigma}{1+B\varsigma}, \quad \varsigma \in \mathbb{U}. \tag{59}$$

Also, suppose

$$1 + \frac{\gamma\varsigma D_q h(\varsigma)}{h^3(\varsigma)} = \frac{1+A\varpi(\varsigma)}{1+B\varpi(\varsigma)}, \quad \varsigma \in \mathbb{U}, \tag{60}$$

where ϖ is analytic function on $\mathbb{U}$ with $\varpi(0) = 0$. Then,

$$h(\varsigma) \prec \sqrt{1+\varsigma}. \tag{61}$$

Proof. We define a function

$$p(\varsigma) = 1 + \frac{\gamma\varsigma D_q h(\varsigma)}{h^3(\varsigma)}, \tag{62}$$

where p is analytic, and we have $p(0) = 1$. Now, consider that

$$h(\varsigma) = \sqrt{1 + \varpi(\varsigma)}. \tag{63}$$

To obtain the result, we have to show that $|\varpi(\varsigma)| < 1$. Using (62) and (63), we obtain

$$p(\varsigma) = 1 + \gamma\varsigma \frac{D_q\varpi(\varsigma)}{(1 + \varpi(\varsigma))^{(3/2)}\left[\sqrt{1 + \varpi(\varsigma)} + \sqrt{1 + \varpi(\varsigma) - \varsigma D_q\varpi(\varsigma)(1 - q)}\right]}. \tag{64}$$

Also, we have

$$\left|\frac{p(\varsigma) - 1}{A - Bp(\varsigma)}\right| = \left|\frac{\gamma\varsigma D_q\varpi(\varsigma)}{(A - B)(1 + \varpi(\varsigma))^{(3/2)}\left[\sqrt{1 + \varpi(\varsigma)} + \sqrt{1 + \varpi(\varsigma) - \varsigma D_q\varpi(\varsigma)(1 - q)}\right] - B\gamma\varsigma D_q\varpi(\varsigma)}\right|. \tag{65}$$

Consider a point $\varsigma_0 \in \mathbb{U}$ such that

$$\max_{|\varsigma| \le |\varsigma_0|} |\varpi(\varsigma)| = |\varpi(\varsigma_0)| = 1. \tag{66}$$

Now, by using Lemma 1, we have $\varsigma_0 D_q\varpi(\varsigma_0) = m\varpi(\varsigma_0)$, $m \ge 1$. Now, consider that $\varpi(\varsigma_0) = e^{i\theta}$, $\theta \in [-\pi, \pi]$; then, for $\varsigma_0 \in \mathbb{U}$, we obtain

$$\begin{aligned}
\left|\frac{p(\varsigma_0) - 1}{A - Bp(\varsigma_0)}\right| &= \left|\frac{\gamma m e^{i\theta}}{(A - B)\left(1 + e^{i\theta}\right)^{(3/2)}\left[\sqrt{1 + e^{i\theta}} + \sqrt{1 + e^{i\theta} - m e^{i\theta}(1 - q)}\right] - B\gamma m e^{i\theta}}\right|, \\
&\ge \frac{|\gamma| m}{(A - B)\left(|1| + \left|e^{i\theta}\right|\right)^{(3/2)}\left[\sqrt{|1| + \left|e^{i\theta}\right|} + \sqrt{|1| + \left|e^{i\theta}\right| + \left|m e^{i\theta}(1 - q)\right|}\right] + |B||\gamma| m}, \\
&= \frac{|\gamma| m}{(A - B)2^{(3/2)}\left[\sqrt{2} + \sqrt{2 + m(1 - q)}\right] + |B||\gamma| m}.
\end{aligned} \tag{67}$$

Consider a function

$$\Xi_3(m) = \frac{|\gamma| m}{2^{(3/2)}(A - B)\left[\sqrt{2} + \sqrt{2 + m(1 - q)}\right] + |B||\gamma| m}. \tag{68}$$

Then,

$$\Xi_3'(m) = \frac{|\gamma|\left[(A - B)2^{(3/2)}\left\{\sqrt{2} + \sqrt{2 + m(1 - q)}\right\}\right] - |\gamma| m\left[\left(2^{(3/2)}(A - B)(1 - q)/2\sqrt{2 + m(1 - q)}\right)\right]}{\left[(A - B)2^{(3/2)}\left\{\sqrt{2} + \sqrt{2 + m(1 - q)}\right\} + |B||\gamma| m\right]^2} > 0. \tag{69}$$

Above expression represents that function Ξ_3 has increasing behavior, so we have its minimum value at $m = 1$ and

$$\Xi_3(1) = \frac{|\gamma|}{2^{(3/2)}(A-B)[\sqrt{2}+\sqrt{3-q}]+|B||\gamma|}. \tag{70}$$

So, we conclude that

$$\left|\frac{p(\varsigma_0)-1}{A-Bp(\varsigma_0)}\right| \geq \frac{|\gamma|}{2^{(3/2)}(A-B)[\sqrt{2}+\sqrt{3-q}]+|B||\gamma|}. \tag{71}$$

Now, from (58), we have

$$\left|\frac{p(\varsigma_0)-1}{A-Bp(\varsigma_0)}\right| \geq 1, \tag{72}$$

which contradicts (59), and hence, $|\varpi(\varsigma)| < 1$, which completes the proof.

By taking $h(\varsigma) = (\varsigma D_q f(\varsigma)/f(\varsigma))$, we deduce the following result. □

Corollary 5. *Let* $|\gamma| \geq 2\sqrt{2}((A-B)(\sqrt{2}+\sqrt{3-q})/(1-|B|))$, $-1 < B < A \leq 1$ *and* $f \in \mathcal{A}$, *satisfy the subordination*

$$1+\gamma\varsigma\left(\frac{f(\varsigma)}{\varsigma D_q f(\varsigma)}\right)^3 D_q\left(\frac{\varsigma D_q f(\varsigma)}{f(\varsigma)}\right) \prec \frac{1+A\varsigma}{1+B\varsigma}. \tag{73}$$

Then, $f \in \mathcal{S}_q^*(\sqrt{1+\varsigma})$.

Theorem 6. *Assume that*

$$|\gamma| \geq \frac{2^{(n/2)}(A-B)(\sqrt{2}+\sqrt{3-q})}{(1-|B|)}, \quad -1 < B < A \leq 1. \tag{74}$$

Consider an analytic function h on $\mathbb{U}$ with $h(0) = 1$ which satisfies

$$1+\frac{\gamma\varsigma D_q h(\varsigma)}{h^n(\varsigma)} \prec \frac{1+A\varsigma}{1+B\varsigma}, \quad \varsigma \in \mathbb{U}. \tag{75}$$

Also, suppose

$$1+\frac{\gamma\varsigma D_q h(\varsigma)}{h^n(\varsigma)} = \frac{1+A\varpi(\varsigma)}{1+B\varpi(\varsigma)}, \quad \varsigma \in \mathbb{U}, \tag{76}$$

where ϖ is analytic function on $\mathbb{U}$ with $\varpi(0) = 0$. Then,

$$h(\varsigma) \prec \sqrt{1+\varsigma}. \tag{77}$$

Proof. We define a function

$$p(\varsigma) = 1+\frac{\gamma\varsigma D_q h(\varsigma)}{h^n(\varsigma)}, \tag{78}$$

where p is analytic, and we have $p(0) = 1$. Now, consider that

$$h(\varsigma) = \sqrt{1+\varpi(\varsigma)}. \tag{79}$$

To obtain the result, we have to show that $|\varpi(\varsigma)| < 1$. Using (78) and (79), we obtain

$$p(\varsigma) = 1+\gamma\varsigma\frac{D_q\varpi(\varsigma)}{(1+\varpi(\varsigma))^{(n/2)}\left[\sqrt{1+\varpi(\varsigma)}+\sqrt{1+\varpi(\varsigma)-\varsigma D_q\varpi(\varsigma)(1-q)}\right]}. \tag{80}$$

Also, we have

$$\begin{aligned}\left|\frac{p(\varsigma)-1}{A-Bp(\varsigma)}\right| &= \left|\frac{\gamma\varsigma\left(D_q\varpi(\varsigma)/(1+\varpi(\varsigma))^{(n/2)}\left[\sqrt{1+\varpi(\varsigma)}+\sqrt{1+\varpi(\varsigma)-\varsigma D_q\varpi(\varsigma)(1-q)}\right]\right)}{A-B\left[1+\gamma\varsigma\left(D_q\varpi(\varsigma)/(1+\varpi(\varsigma))^{(n/2)}\left[\sqrt{1+\varpi(\varsigma)}+\sqrt{1+\varpi(\varsigma)-\varsigma D_q\varpi(\varsigma)(1-q)}\right]\right)\right]}\right| \\ &= \left|\frac{\gamma\varsigma D_q\varpi(\varsigma)}{(A-B)(1+\varpi(\varsigma))^{(n/2)}\left[\sqrt{1+\varpi(\varsigma)}+\sqrt{1+\varpi(\varsigma)-\varsigma D_q\varpi(\varsigma)(1-q)}\right]-B\gamma\varsigma D_q\varpi(\varsigma)}\right|.\end{aligned} \tag{81}$$

Consider a point $\varsigma_0 \in \mathbb{U}$ such that

$$\max_{|\varsigma|\leq|\varsigma_0|}|\varpi(\varsigma)| = |\varpi(\varsigma_0)| = 1. \tag{82}$$

Now, by using Lemma 1, we have $\varsigma_0 D_q\varpi(\varsigma_0) = m\varpi(\varsigma_0)$, $m \geq 1$. Now, consider that $\varpi(\varsigma_0) = e^{i\theta}$, $\theta \in [-\pi,\pi]$; then, for $\varsigma_0 \in \mathbb{U}$, we obtain

$$\begin{aligned}
\left|\frac{p(\varsigma_0)-1}{A-Bp(\varsigma_0)}\right| &= \frac{\gamma\varsigma_0 D_q\varpi(\varsigma_0)}{(A-B)(1+\varpi(\varsigma_0))^{(n/2)}\left[\sqrt{1+\varpi(\varsigma_0)}+\sqrt{1+\varpi(\varsigma_0)-\varsigma_0 D_q\varpi(\varsigma_0)(1-q)}\right]-B\gamma\varsigma_0 D_q\varpi(\varsigma_0)},\\
&= \left|\frac{\gamma m e^{i\theta}}{(A-B)\left(1+e^{i\theta}\right)^{(n/2)}\left[\sqrt{1+e^{i\theta}}+\sqrt{1+e^{i\theta}-me^{i\theta}(1-q)}\right]-B\gamma m e^{i\theta}}\right|,\\
&\geq \frac{|\gamma|m}{(A-B)\left(1+e^{i\theta}\right)^{(n/2)}\left[\left|\sqrt{1+e^{i\theta}}\right|+\left|\sqrt{1+e^{i\theta}-me^{i\theta}(1-q)}\right|\right]-|B||\gamma|m},\\
&= \frac{|\gamma|m}{(A-B)\left(|1|+\left|e^{i\theta}\right|\right)^{(n/2)}\left[\sqrt{\left|1+e^{i\theta}\right|}+\sqrt{\left|1+e^{i\theta}-me^{i\theta}(1-q)\right|}\right]+|B||\gamma|m},\\
&\geq \frac{|\gamma|m}{(A-B)\left(|1|+\left|e^{i\theta}\right|\right)^{(n/2)}\left[\sqrt{|1|+\left|e^{i\theta}\right|}+\sqrt{|1|+\left|e^{i\theta}\right|+\left|me^{i\theta}(1-q)\right|}\right]+|B||\gamma|m},\\
&= \frac{|\gamma|m}{(A-B)2^{(n/2)}\left[\sqrt{2}+\sqrt{2+m(1-q)}\right]+|B||\gamma|m}.
\end{aligned} \tag{83}$$

Consider

$$\Xi_4(m) = \frac{|\gamma|m}{2^{(n/2)}(A-B)\left[\sqrt{2}+\sqrt{2+m(1-q)}\right]+|B||\gamma|m}. \tag{84}$$

Then,

$$\Xi_4'(m) = \frac{|\gamma|\left[(A-B)2^{(n/2)}\left\{\sqrt{2}+\sqrt{2+m(1-q)}\right\}\right]-|\gamma|m\left[\left(2^{(n/2)}(A-B)(1-q)/2\sqrt{2+m(1-q)}\right)\right]}{\left[(A-B)2^{(n/2)}\left\{\sqrt{2}+\sqrt{2+m(1-q)}\right\}+|B||\gamma|m\right]^2} > 0. \tag{85}$$

Above expression represents that function Ξ_4 has increasing behavior, so we have its minimum value at $m = 1$ and

$$\Xi_4(1) = \frac{|\gamma|}{2^{(n/2)}(A-B)\left[\sqrt{2}+\sqrt{3-q}\right]+|B||\gamma|}. \tag{86}$$

So, we conclude that

$$\left|\frac{p(\varsigma_0)-1}{A-Bp(\varsigma_0)}\right| \geq \frac{|\gamma|}{2^{(n/2)}(A-B)\left[\sqrt{2}+\sqrt{3-q}\right]+|B||\gamma|}. \tag{87}$$

Now, from (74), we have

$$\left|\frac{p(\varsigma_0)-1}{A-Bp(\varsigma_0)}\right| \geq 1, \tag{88}$$

which contradict (75), and hence, $|\varpi(\varsigma)| < 1$, which completes the proof.

By taking $h(\varsigma) = (\varsigma D_q f(\varsigma)/f(\varsigma))$, we deduce the following result. □

Corollary 7. *Let* $|\gamma| \geq (2^{(n/2)}(A-B)(\sqrt{2}+\sqrt{3-q})/(1-|B|))$, $-1 < B < A \leq 1$ *and* $f \in \mathscr{A}$, *satisfy the subordination*

$$1+\gamma\varsigma\left(\frac{f(\varsigma)}{\varsigma D_q f(\varsigma)}\right)^n D_q\left(\frac{\varsigma D_q f(\varsigma)}{f(\varsigma)}\right) \prec \frac{1+A\varsigma}{1+B\varsigma}. \tag{89}$$

Then, $f \in \mathcal{S}_q^*(\sqrt{1+\varsigma})$.

3. Conclusion

In this article, we have investigated the q-differential subordination by using q-version of well-known Jack's Lemma. We have found the condition on γ such that $1 + (\gamma\varsigma D_q h(\varsigma)/h^n(\varsigma)) \prec (1 + A\varsigma/1 + B\varsigma)$ implies that $h(\varsigma) \prec \sqrt{1+\varsigma}$. These results have been utilized to find sufficient conditions for star-like functions related to lemniscate of Bernoulli. This method can further be applied to find sufficient conditions for star-like functions of Ma–Minda type.

Data Availability

No data were used in this article.

Conflicts of Interest

The authors declare that they have no conflicts of interest.

Authors' Contributions

All authors contributed equally and approved the final manuscript.

References

[1] P. L. Duren, *Univalent functions. Grundlehren der Math. Wissenchaften*, Springer-Verlag, New York, NY, USA, 1983.

[2] A. W. Goodman, "Univalent functions," *Mariner Publishing Company*, vol. 1, no. 2, 1983.

[3] J. E. Littlewood, *Lectures on the Theory of Functions*, Oxford University Press, London, UK, 1944.

[4] J. E. Littlewood, "On inequalities in the theory of functions," *Proceedings of the London Mathematical Society*, vol. 2, no. 23, pp. 481–519, 2002.

[5] S. S. Miller and P. T. Mocanu, *Differential Subordinations Theory and Applications*, Marcel Dekker, New York, NY, USA, 2000.

[6] S. S. Miller, P. T. Mocanu, and M. O. Reade, "Bazilevic functions and generalized convexity," *Revue Roumaine de Mathématique Pures et Appliquées*, vol. 19, pp. 213–224, 1974.

[7] S. S. Miller and P. T. Mocanu, "Differential subordinations and univalent functions," *Michigan Mathematical Journal*, vol. 28, pp. 157–171, 1981.

[8] S. Ruscheweyh and V. Singh, "On a Briot-Bouquet equation related to univalent functions," *Revue Roumaine de Mathématique Pures et Appliquées*, vol. 24, pp. 285–290, 1979.

[9] S. Ruscheweyh and D. R. Wilken, "Sharp estimates for certain Briot-Bouquet subordinations," *Revue Roumaine de Mathématique Pures et Appliquées*, vol. 30, pp. 559–569, 1985.

[10] I. S. Jack, "Functions starlike and convex of order α," *Journal of the London Mathematical Society*, vol. 2-3, no. 3, pp. 469–474, 1971.

[11] D. Jacek, "Applications of the Jack lemma," *Acta Mathematica Hungaria*, vol. 105, pp. 93–102, 2004.

[12] W. C. Ma and D. A. Minda, "Unified treatment of some special classes of univalent functions," in *Proceedings of the Conference on Complex Analysis*, pp. 157–169, International Press, Cambridge, MA, USA, 1992.

[13] R. M. Ali, V. Ravichndaran, and N. Seenivasagan, "Sufficient conditions for janoswski starlikeness," *International Journal of Mathematics and Mathematical Sciences*, vol. 23, no. 9, p. 56, 2007.

[14] R. M. Ali, N. E. Cho, V. Ravichandran, and S. S. Kumar, "Differential subordination for functions associated with the lemniscate of Bernoulli. Taiwan," *Jurnal Matematika*, vol. 16, pp. 1017–1026, 2012.

[15] K. Sivaprasad, K. Virendra, V. Ravichandran, and E. C. Nak, "Sufficient conditions for starlike functions associated with the lemniscates of Bernoulli," *Journal of Inequalities and Applications*, vol. 173, 2013.

[16] K. Sharma, N. K. Jain, and V. Ravichandran, "Starlike functions associated with a cardioid," *Afrika Matematika*, vol. 27, no. 5-6, pp. 923–939, 2016.

[17] Y. Yunus, S. A. Halim, and A. B. Akbarally, "Subclass of starlike functions associated with a limacon," *AIP Conference Proceedings*, vol. 1974, Article ID 030023, 2018.

[18] F. H. Jackson, "On q-functions and certain difference operator," *Transactions of the Royal Society of Edinburgh*, vol. 46, pp. 253–281, 1908.

[19] F. H. Jackson, "On q-definite integrals," *Quarterly Journal of Pure and Applied Mathematics*, vol. 41, pp. 193–203, 1910.

[20] H. M. Srivastava, "Univalent functions, fractional calculus, and associated generalized hypergeometric functions in Univalent Functions," in *Fractional Calculus, and Their Applications*, H. M. Srivastava and S. Owa, Eds., pp. 329–354, Wileya, J. and Sons, New York, NY, USA, 1989.

[21] M. E. Ismail, E. Merkes, and D. Styer, "A generalization of Starlike functions," *Theory and Applications*, vol. 14, no. 4, pp. 77–84, 1990.

[22] G. A. Anastassiu and S. G. Gal, "Geometric and approximation properties of some singular integrals in the unit disk," *Journal of Inequalities and Applications*, vol. 1, p. 19, Article ID 17231, 2006.

[23] G. A. Anastassiu and S. G. Gal, "Geometric and approximation properties of generalized singular integrals," *Journal of the Korean Mathematical Society*, vol. 23, no. 2, pp. 425–443, 2006.

[24] S. Abelman, K. A. Selvakumaran, M. M. Rashidi, and S. D. Purohit, "Subordination conditions for a class of non-bazilevič type defined by using fractional Q-calculus operators," *Facta Universitatis – Series: Mathematics and Informatics*, vol. 32, no. 2, pp. 255–267, 2017.

[25] S. Agrawal and S. K. Sahoo, "A generalization of starlike functions of order alpha," *Hokkaido Mathematical Journal*, vol. 46, pp. 15–27, 2017.

[26] T. M. Seoudy and M. K. Aouf, "Coefficient estimates of new classes of q-starlike and q-convex functions of complex order," *Journal of Mathematical Inequalities*, vol. 10, no. 1, pp. 135–145, 2016.

[27] H. M. Srivastava, M. Tahir, B. Khan, Q. Z. Ahmad, and N. Khan, "Some general classes of q-starlike functions associated with the Janowski functions," *Symmetry Plus*, vol. 11, Article ID 292, 2019.

[28] H. M. Srivastava, M. Tahir, B. Khan, Q. Ahmad, and N. Khan, "Some general families of q-starlike functions associated with the Janowski functions," *Filomat*, vol. 33, no. 9, pp. 2613–2626, 2019.

[29] B. Khan, H. M. Srivastava, N. Khan, M. Darus, M. Tahir, and Q. Z. Ahmad, "Coefficient estimates for a subclass of analytic functions associated with a certain leaf-like domain," *Mathematics*, vol. 8, no. 8, p. 1334, 2020.

[30] S. Mahmood, M. Jabeen, S. N. Malik, H. M. Srivastava, R. Manzoor, and S. M. J. Riaz, "Some coefficient inequalities of q-starlike functions associated with conic domain defined by

q-derivative," *Journal of Function Spaces*, vol. 2018, Article ID 8492072, 13 pages, 2018.

[31] M. Shafiq, H. M. Srivastava, N. Khan, Q. Z. Ahmad, M. Darus, and S. Kiran, "An upper bound of the third Hankel determinant for a subclass of q-starlike functions associated with k-fibonacci numbers," *Symmetry Plus*, vol. 12, no. 6, p. 1043, 2020.

[32] H. M. Srivastava, "Operators of basic (or q-) calculus and fractional q-calculus and their applications in geometric function theory of complex analysis," *Iranian Journal of Science and Technology Transaction A-Science*, vol. 44, no. 1, pp. 327–344, 2020.

[33] H. M. Srivastava, Q. Z. Ahmad, N. Khan, N. Khan, and B. Khan, "Hankel and Toeplitz determinants for a subclass of q-starlike functions associated with a general conic domain," *Mathematics*, vol. 7, Article ID 181, 2019.

[34] H. M. Srivastava, M. K. Aouf, and A. O. Mostafa, "Some properties of analytic functions associated with fractional q-calculus operators q-calculus operators," *Miskolc Mathematical Notes*, vol. 20, no. 2, pp. 1245–1260, 2019.

[35] H. M. Srivastava, M. Arif, M. Arif, and M. Raza, "Convolution properties of meromorphically harmonic functions defined by a generalized convolution $ q $-derivative operator," *AIMS Mathematics*, vol. 6, no. 6, pp. 5869–5885, 2021.

[36] H. M. Srivastava, S. Arjika, and A. S. Kelil, "Some homogeneous q-difference operators and the associated generalized Hahn polynomials," *Applied Set-Valued Analysis and Optimization*, vol. 1, pp. 187–201, 2019.

[37] H. M. Srivastava and D. Bansal, "Close-to-convexity of a certain family of q-Mittag-Leffler functions," *Journal of Nonlinear and Variational Analysis*, vol. 1, pp. 61–69, 2017.

[38] H. M. Srivastava, J. Cao, and S. Arjika, "A note on generalized q-difference equations and their applications involving q-hypergeometric functions," *Symmetry Plus*, vol. 12, Article ID 1816, 2020.

[39] H. M. Srivastava and S. Arjika, "A general family of q-hypergeometric polynomials and associated generating functions," *Mathematics*, vol. 9, Article ID 1161, 2021.

[40] H. M. Srivastava, B. Khan, N. Khan, and Q. Z. Ahmad, "Coefficient inequalities for q-starlike functions associated with the Janowski functions," *Hokkaido Mathematical Journal*, vol. 48, pp. 407–425, 2019.

[41] H. M. Srivastava, B. Khan, N. Khan, M. Tahir, S. Ahmad, and N. Khan, "Upper bound of the third Hankel determinant for a subclass of q-starlike functions associated with the q-exponential function," *Bulletin des Sciences Mathematiques*, vol. 167, Article ID 102942, 2021.

[42] H. M. Srivastava, S. Khan, S. Khan, Q. Z. Ahmad, N. Khan, and S. Hussain, "The Faber polynomial expansion method and its application to the general coefficient problem for some subclasses of bi-univalent functions associated with a certain q-integral operator," *Studia Universitatis Babes-Bolyai Matematica*, vol. 63, no. 4, pp. 419–436, 2018.

[43] H. M. Srivastava, N. Raza, E. S. A. AbuJarad, G. Srivastava, and M. H. AbuJarad, "Fekete-Szegö inequality for classes of (p, q)-Starlike and (p, q)-convex functions," *Revista de la Real Academia de Ciencias Exactas, Físicas y Naturales. Serie A. Matemáticas*, vol. 113, no. 4, pp. 3563–3584, 2019.

[44] M. Ul-Haq, M. Raza, M. Arif, Q. Khan, and H. Tang, "Q-analogue of differential subordinations," *Mathematics*, vol. 7, no. 8, p. 724, 2019.

[45] S. Zainab, A. Shakeel, M. Imran et al., "Sufficiency criteria for q-starlike functions associated with cardioid," *Journal of Function Spaces*, vol. 2021, Article ID 9999213, 9 pages, 2021.

[46] A. Çetinkaya and Y. Polatoglu, "q-Harmonic mappings for which analytic part is q-convex functions of complex order," *Hacettepe Journal of Mathematics and Statistics*, vol. 47, pp. 813–820, 2018.